

(NASA-CF-144310) DEVELOPMENT OF
SPACE-STABLE THERMAL CONTROL COATINGS FOR
USE ON LARGE SPACE VEHICLES Final Report, 4
Jan. 1971 - 1 Nov. 1975 (IIT Research Inst.)
466 p HC \$12.00

N76-23584

Unclass
28221

CSCI 11C G3/37

Contract No. NAS8-26791
Report No. IITRI-C6233-57

DEVELOPMENT OF SPACE-STABLE THERMAL CONTROL
COATINGS FOR USE ON LARGE SPACE VEHICLES

Prepared by

J.E. Gilligan and Y. Harada

of

IIT Research Institute
10 West 35th Street
Chicago, Illinois 60616

for

National Aeronautics & Space Administration
George C. Marshall Space Flight Center
Marshall Space Flight Center, Alabama 35812

15 March 1976



FOREWORD

This is IITRI Report No. C6233-57, the Final Report on NASA Contract No. NAS8-26791, "Development of Space-Stable Thermal Control Coatings for Use on Large Space Vehicles." It summarizes the work and accomplishments of IITRI Project No. C6233 spanning the period from Jan. 4, 1971 to Nov. 1, 1975.

During the course of this program many people contributed to its achievements. We acknowledge the following individuals and their contributions. The Project Leader was Mr. J.E. Gilligan, who also acted as Principal Investigator in the Environmental Test studies; Mr. Y. Harada was Principal Investigator for the Pigment Development activities. Dr. C. Giori was responsible for the silicone resin improvement efforts. Responsibility for preparation, characterization, and engineering evaluation of coatings rested with Mr. F.O. Rogers. Assisting the above senior contributors were Dr. N.A. Ashford and Mr. F.A. Jarke in EPR investigations; Mr. W.R. Logan, E.J. Onesto and R. Steuhner, pigment preparation; Ms. Donna Mathe, pigment x-ray evaluations; Mr. R.M. Leas, strippable coatings and general paint studies; and Mr. T. Yamauchi, experimental polymer synthesis. Messrs R.F. Boutin, P. Mencinkas, A. Lackland and J.E. Brzuskiwicz operated the irradiation facilities, made spectral reflectance measurements and performed many other important experimental tasks. We acknowledge the services of Mr. G.A. Zerlaut, initially, as Manager of the Polymer Chemistry Section for administrative management and, later, as a technical consultant; and the services of Dr. A.M. Stake for administrative guidance.

We are pleased to recognize the highly valuable assistance of Mr. D.W. Gates, who represented the National Aeronautics and Space Administration as the NASA Program Manager and as the Contracting Officer's Technical Representative. We are especially indebted to Mr. Gates for performing the extensive SEM investigations of Zn_2TiO_4 pigments. The advice and counsel of Messrs. W.F. Carroll of the Jet Propulsion Laboratory and of Mr. D.R. Wilkes of the Marshall Space Flight Center are also acknowledged and appreciated. Mr. B.G. Achhammer of the office of Advanced Science and Technology (NASA-HQ) also provided valuable assistance.

The work reported herein was performed under the technical direction of the Space Sciences Laboratory of the George C. Marshall Space Flight Center. The contract was funded under the following Codes:

124-09-31-0000-33-1-004-080-2510
114-03-51-0000-33-2-004-080-2510
502-21-27-0000-33-3-004-080-2510
502-21-27-0000-33-3-004-080-2510
502-21-27-0000-33-4-004-W06-2510
506-16-33-0000-59-5-004-300-2510

Respectfully submitted,

IIT RESEARCH INSTITUTE



J.E. Gilligan
Senior Engineer-Group Leader
Polymer Chemistry Research

APPROVED:



A.M. Stake
Manager
Polymer Chemistry Research

JEG:ge

CROSS-REFERENCE OF IITRI TRIANNUAL REPORTS

IITRI Report No. CR No.

C6233-4	CR-143990
-8	121035
-12	123629
-16	127215
-20	124003
-24	131038
-28	133195
-32	136446
-36	143991
-40	120723
-44	120722
-48	143850
-52	143879

Copies of IITRI Triannual reports on this contract can be obtained in microfiche or hardcopy by ordering the appropriate CR No. from:

National Technical Information Service
U.S. Department of Commerce
Springfield, VA 22161

TABLE OF CONTENTS

	<u>Page</u>
1.0 INTRODUCTION	1-1
1.1 TECHNICAL BACKGROUND	1-6
1.1.1 Low α_s/ϵ Requirements	1-6
1.1.2 Basic Approaches	1-8
1.2 SUMMARY OF PREVIOUS PROGRAM RESULTS	1-8
1.3 PROGRAM GOALS	1-10
1.4 BIBLIOGRAPHY	1-12
1.4.1 Cited References	1-12
1.4.2 Uncited Bibliography	1-14
2.0 TECHNICAL DISCUSSIONS	2-1
2.1 LOW α_s/ϵ SURFACES	2-1
2.1.1 General Qualities	2-1
2.1.2 Optical Requirements	2-2
2.1.3 Physical Requirements	2-3
2.1.4 Application Requirements	2-3
2.2 ENVIRONMENTAL STABILITY	2-5
2.3 SUMMARY REMARKS	2-8
2.4 BIBLIOGRAPHY	2-10
2.4.1 Cited References	2-10
3.0 PIGMENT STUDIES	3-1
3.1 ZINC ORTHOTITANATE STUDIES	3-1
3.1.1 Background	3-1
3.1.2 Methods of Evaluation	3-4
3.1.2.1 Gravimetric Analysis	3-4
3.1.2.2 X-Ray Analysis	3-5
3.1.2.3 SEM Analysis	3-5
3.1.2.4 Optical Analysis	3-6

TABLE OF CONTENTS (cont.)

	<u>Page</u>
3.2 SYNTHESIS BY COPRECIPITATION/CALCINATION (COP)	3-6
3.2.1 Precipitation Effects	3-7
3.2.2 Scale-Up Studies	3-12
3.2.3 Sample Designation	3-16
3.2.4 Heat Treatment Studies	3-16
3.2.5 Acid-Leach Studies	3-18
3.2.6 X-Ray Analyses	3-19
3.2.7 SEM Analyses	3-23
3.2.8 COP Materials for Other Laboratories	3-33
3.3 DECOMPOSITION STUDIES	3-34
3.3.1 Zinc Oxalate	3-34
3.3.2 "TiOX"	3-41
3.3.3 Coprecipitated Material	3-44
3.4 SYNTHESIS BY REACTION SINTERING	3-48
3.4.1 Comparison of Mixed Oxalate (MOX) Processing	3-50
3.4.2 Particle Size ("MOX" Process)	3-56
3.4.3 Effect of Ball Milling	3-63
3.4.4 Zinc Oxalate Studies	3-66
3.4.4.1 Preparation Methods	3-67
3.4.4.2 Characterization of ZnOx	3-69
3.4.4.3 Calcination Studies	3-70
3.4.4.4 Zn ₂ TiO ₄ Synthesis	3-75
3.4.5 Use of Precursors Other than Oxalates	3-77
3.5 STOICHIOMETRY STUDIES	3-79
3.5.1	3-79
3.5.1.1 X-Ray Analysis	3-81
3.5.1.2 Gravimetric Analysis	3-83

TABLE OF CONTENTS (cont.)

	<u>Page</u>
3.5.1.3 SEM Analysis	3-83
3.5.1.4 Summary	3-87
3.5.2 Zn/Ti Ratio of 1.90/1 to 2.05/1	3-93
3.5.2.1 X-Ray Analysis	3-93
3.5.2.2 Gravimetric Analysis	3-95
3.5.2.3 SEM Analysis	3-95
3.6 NEW PIGMENT MATERIALS STUDIES	3-96
3.6.1 ZnO - ZrO ₂ Studies	3-96
3.6.2 Ultraviolet-Vacuum Irradiation Studies	3-98
3.6.3 Conclusions	3-100
3.7 REFERENCES	3-101
4.0 ENVIRONMENTAL TESTING	4-1
4.1 INTRODUCTION	4-1
4.2 INTERPRETATION OF SPECTRA	4-2
4.3 EQUIPMENT AND FACILITIES	4-6
4.3.1 Irradiation Facilities	4-6
4.3.2 Ultraviolet Sources	4-7
4.3.3 Test Procedures	4-13
4.3.4 Terminology	4-14
4.3.5 Sample Notation	4-14
4.4 ENVIRONMENTAL TEST DESCRIPTIONS - PART I	4-15
4.4.1 CREF Test No. 5	4-15
4.4.1.1 Purpose/Description	4-15
4.4.1.2 Test Sequence	4-16
4.4.1.3 Discussion	4-16
4.4.1.3.1 Code C-070, Zn ₂ TiO ₄ :K ₂ SiO ₃ (Plasma)/OI-650	4-21
4.4.1.3.2 Code C-068, Zn ₂ TiO ₄ :K ₂ SiF ₆ /PS-7	4-21
4.4.1.3.3 Code C-067, Zn ₂ TiO ₄ :K ₄ Si ₄ W ₁₂ O ₄₀ PS-7	4-21

TABLE OF CONTENTS (cont.)

	<u>Page</u>
4.4.1.3.4 OI-650 "Glass" Resin	4-28
4.4.1.4 Conclusions	4-28
4.4.2 CREF-6	4-30
4.4.2.1 Purpose/Description	4-30
4.4.2.2 Test Sequence	4-30
4.4.2.3 Discussion	4-30
4.4.2.3.1 Code SRI-2, $\text{Zn}_2\text{TiO}_4\text{:K}_2\text{SiF}_6$ (Plasma)/PS-7	4-30
4.4.2.3.2 Codes SRI-I,3 $\text{Zn}_2\text{TiO}_4\text{:K}_2\text{SiF}_6$ (Plasma)/OI	4-30
4.4.2.3.3 C-169 $\text{Zn}_2\text{TiO}_4\text{:K}_2\text{SiO}_3$ (Plasma)/OI	4-36
4.4.2.4 Analyses and Conclusions	4-36
4.4.3 CREF Test No. 7	4-42
4.4.3.1 Purpose/Description	4-42
4.4.3.2 Sequence	4-42
4.4.3.3 Results	4-42
4.4.3.4 Conclusions	4-47
4.4.4 CREF Test No. 8	4-52
4.4.4.1 Purpose/Description	4-52
4.4.4.2 Sequence	4-52
4.4.4.3 Test Results	4-53
4.4.4.4 Analyses	4-53
4.4.5 IRIF Test I-55 (Ref. 4.6)	4-62
4.4.5.1 Purpose/Description	4-62
4.4.5.2 Test Results	4-62
4.4.5.3 Conclusions	4-64
4.4.6 CREF Test No. 9 (Ref. 4.6)	4-71
4.4.6.1 Purpose/Description	4-71
4.4.6.2 Results	4-71
4.4.6.3 Conclusions	4-87

TABLE OF CONTENTS (cont.)

	<u>Page</u>
4.4.7 Summary	4-87
4.4.8 Conclusions	4-89
4.5 ENVIRONMENTAL TEST REPORTS - PART II	4-91
4.5.1 CREF Test No. 10	4-91
4.5.1.1 Purpose/Description	4-91
4.5.1.2 Test Results	4-91
4.5.1.3 Conclusions	4-95
4.5.2 CREF Test No. 13	4-105
4.5.2.1 Purpose/Description	4-105
4.5.2.2 Sequence	4-105
4.5.2.3 Results	4-107
4.5.3 IRIF Test No. I-67	4-115
4.5.3.1 Purpose/Description	4-115
4.5.3.2 Sequence	4-115
4.5.3.3 Test Results	4-115
4.5.4 IRIF Test I-68	4-127
4.5.4.1 Purpose/Description	4-127
4.5.4.2 Sequence	4-130
4.5.4.3 Test Results	4-130
4.5.4.4 Analyses	4-130
4.5.5 IRIF Test No. I-69	4-138
4.5.5.1 Purpose/Description	4-138
4.5.5.2 Sequence	4-139
4.5.5.3 Test Results	4-139
4.5.5.4 Conclusions	4-141
4.5.6 CREF Test No. 15	4-154

TABLE OF CONTENTS (cont.)

	<u>Page</u>
4.5.6.1 Purpose/Description	4-154
4.5.6.2 Sequence	4-155
4.5.6.3 Test Results	4-155
4.5.6.4 Conclusions	4-165
4.5.7 IRIF Test I-70	4-165
4.5.7.1 Purpose/Description	4-165
4.5.7.2 Sequence	4-165
4.5.7.3 Test Results	4-167
4.5.7.4 Conclusions	4-168
4.5.8 IRIF Test No. I-71	4-173
4.5.8.1 Purpose/Descriptions	4-173
4.5.8.2 Sequence	4-175
4.5.8.3 Test Results	4-175
4.5.8.4 Analyses	4-185
4.5.9 CREF Test No. 16	4-188
4.5.9.1 Purpose/Description	4-188
4.5.9.2 Sequence	4-188
4.5.9.3 Test Results	4-138
4.5.9.4 Analyses and Conclusions	4-195
4.5.10 Summary and Conclusions	4-196
4.6 ENVIRONMENTAL TEST REPORTS - PART II	4-197
4.6.1 IRIF Test I-72 (Ref. 4.10)	4-198
4.6.1.1 Purpose/Description	4-198
4.6.1.2 Sequence	4-198
4.6.1.3 Test Results	4-198
4.6.1.4 Conclusions	4-211
4.7 STOICHIOMETRIC PIGMENT CHARACTERIZATION STUDIES	4-213

TABLE OF CONTENTS (cont.)

	<u>Page</u>
4.7.1 Introduction	4-213
4.7.2 Process Chemistry	4-214
4.7.2.1 Background	4-215
4.7.2.2 Chemistry	4-215
4.7.2.3 Oxalate Molecular Weight Determinations	4-216
4.7.2.3.1 Zinc Oxalate	4-216
4.7.2.3.2 "TiOX" Molecular Weight	4-217
4.7.3 "TiOX" Energetics	4-222
4.7.4 Conclusions	4-224
4.7.5 Reflectance Spectra Analyses	4-224
4.7.5.1 Materials Descriptions: The Reflectance Spectra of Pigments Prepared at Various Zn/Ti Ratios	4-224
4.7.5.2 Optical Analyses: Zn/Ti Ratios 0.5:1- 2.5:1.0	4-225
4.7.5.3 Optical Analyses: Zn/Ti Ratios 1.8:1.0 - 2.05:1.0	4-234
4.7.6 Summary	4-240
4.8 REFERENCES	4-241
5.0 BINDER DEVELOPMENT	5-1
5.1 INTRODUCTION	5-1
5.2 OWENS-ILLINOIS 650 "GLASS RESIN" IMPROVEMENT STUDY	5-1
5.2.1 Internal Plasticizing of OI-650 Glass Resin by Copolymerization	5-2
5.2.2 Modification of OI-650 Resin by Partial End-Blocking with Trimethylchlorosilane	5-4

TABLE OF CONTENTS (cont.)

	<u>Page</u>
5.5 REFERENCES	5.9
6.0 ELECTRON PARAMAGNETIC RESONANCE INVESTIGATIONS	6.1
6.1 BACKGROUND	6.1
6.1.1 Experimental Equipment and Procedures	6-2
6.1.2 Experimental Results	6-5
6.1.2.1 ZnO	6-5
6.1.2.2 Anatase Titanium Dioxide Converted to Rutile	6-5
6.1.2.4 B-454, $\text{Zn}_2\text{TiO}_4(\text{B-229})\text{:Li}_2\text{SiF}_6$	6-14
6.1.2.5 Zn_2TiO_4 with Excess TiO_2	6-14
6.2 DISCUSSION OF RESULTS	6-14
6.2.1 ZnO	6-14
6.2.2 TiO_2	6-18
6.2.3 Metastable Species	6-18
6.2.4 ZnO in Untreated Zn_2TiO_4 (B-2.)	6-19
6.2.5 Zn_2TiO_4 (B-229)	6-19
6.2.6 Li_2SiF_6 Treated Zn_2TiO_4 (B-454)	6-20
6.2.7 Zn_2TiO_4 with Excess TiO_2	6-20
6.2.8 Zinc Orthotitanate in OI-650 "Glass Resin"	6-20
6.3 PRELIMINARY MODEL FOR DAMAGE IN Zn_2TiO_4	6-22
6.4 CONCLUSIONS	6-23
6.5 REFERENCES	6-24
7.0 GENERAL COATINGS INVESTIGATIONS	7-1
7.1 INTRODUCTORY REMARKS	7-1
7.2 FORMULATION AND EVALUATION OF A-429M	7-1
7.2.1 Evaluation	7-2
7.2.2 Irradiation Tests	7-2

TABLE OF CONTENTS (cont.)

	<u>Page</u>
7.2.2.1 Sample Description	7-2
7.2.2.2 Test Results	7-3
7.2.3 Conclusions	7-3
7.3 STRIPPABLE PRE-LAUNCH PROTECTION COATINGS EVALUATIONS	7-3
7.3.1 Introductory Remarks	7-3
7.3.2 Objectives	7-6
7.3.3 Coatings Evaluations	7-7
7.3.3.1 Strippability Investigations	7-7
7.3.3.2 Ultraviolet Irradiation Tests	7-12
7.3.4 Conclusions	7-16
7.4 SALT SPRAY EFFECTS ON S-13G	7-16
7.5 REFERENCES	7-19
8.0 PROGRAM SUMMARY - CONCLUSIONS AND RECOMMENDATIONS	8-1
9.0 GLOSSARY	9-1
APPENDICES	

LIST OF TABLES

<u>Table No.</u>		<u>Page</u>
2-1	REQUIREMENTS FOR PHYSICAL PROPERTIES OF PAINT COMPONENTS	2-4
3-1	COPRECIPITATION PROCESS OF Zn_2TiO_4 PRODUCTION	3-9
3-2	EFFECT OF INITIAL Zn/ Ti MOL RATIO ON COPRECIPITATION	3-11
3-3	EFFECTS OF OXALIC ACID CONCENTRATION AND REACTION TIMES ON COPRECIPITATION	3-13
3-4	SUMMARY OF COPRECIPITATED BATCHES	3-15
3-5	SUMMARY OF X-RAY DIFFRACTION STUDIES OF Zn_2TiO_4	3-22
3-6	SUMMARY OF SEM ANALYSES OF PIGMENTS PREPARED FROM COPRECIPITATED OXALATE PRECURSORS (COP)	3-33
3-7	WEIGHT LOSSES FOR ZINC OXALATE, "TiOX" AND COPRECIPITATED OXALATES AS A FUNCTION OF TEMPERATURE	3-35
3-8	APPEARANCE AND PHASES PRESENT FOR ZINC OXALATE, "TiOX" AND MIXED OXALATES AS A FUNCTION OF TEMPERATURE	3-37
3-9	HEAT TREATMENT STUDIES OF "TiOX"	3-42
3-10	SUMMARY OF CALCINATION STUDIES COMPARING COP AND MOX MATERIALS	3-51
3-11	SUMMARY OF ZnO_x PRECIPITATION STUDIES	3-68
3-12	SUMMARY OF ZINC ORTHOTITANATE SYNTHESIS USING DIFFERENT ZINC OXALATE SOURCES	3-76
3-13	SUMMARY OF REACTION SYNTHESIS STUDIES	3-78
3-14	EFFECT OF STOICHIOMETRY ON PROPERTIES OF $ZnO \cdot TiO_2$ MATERIALS	3-80
3-15	SUMMARY OF STOICHIOMETRY STUDIES	3-94
3-16	COMPOSITIONS FOR $ZnO-ZrO_2$ STUDIES	3-97

LIST OF TABLES (Cont'd)

<u>Table No.</u>		<u>Page</u>
3-17	SPECTRAL REFLECTANCE VALUES BEFORE AND AFTER ULTRAVIOLET IRRADIATION OF NEW PIGMENT MATERIALS	3-99
3-18	SOLAR ABSORPTANCE VALUES OF NEW PIGMENTS BEFORE AND AFTER 1200 ESH	3-100
4-1	RESULTS OF CREF 5, COMBINED RADIATION TEST OF (SS) ZINC ORTHOTITANATE PAINTS AND OWENS - ILLINOIS GLASS RESIN	4-17
4-2	RESULTS OF CREF-6 COMBINED RADIATION TEST OF ZINC ORTHOTITANATE PAINTS	4-35
4-3	COMBINED IRRADIATION EFFECTS IN $Zn_2TiO_4:K_2SiF_6/$ PS-7	4-41
4-4	COMBINED IRRADIATION EFFECTS IN $Zn_2TiO_4:K_2SiO_3$ (Plasma)/OI-650	4-41
4-5a	COMBINED IRRADIATION (CREF No. 7) TEST DATA Zn_2TiO_4 PAINTS	4-43
4-5b	CREF-7 ZINC ORTHOTITANATE PAINT SAMPLES AND TREATMENTS	4-44
4-6	CREF-8 ZINC ORTHOTITANATE PAINT SAMPLES AND TREATMENTS	4-54
4-7	RADIATION-INDUCED REFLECTANCE CHANGES AT SELECTED WAVELENGTHS IN ENCAPSULATED ZINC ORTHOTITANATE PIGMENTS - CREF-8	4-61
4-8	SAMPLE DESCRIPTIONS IRIF TEST NO. I-55	4-63
4-8a	ENVIRONMENTALLY INDUCED REFLECTANCE CHANGES AT PEAK DAMAGE WAVELENGTHS IN ENCAPSULATED ZINC ORTHOTITANATE PIGMENTS - CREF-8	4-71
4-9	CREF TEST No. 9 - SOLAR ABSORPTANCE VALUES VS ULTRAVIOLET EXPOSURE (ESH)	4-72
4-10	CREF TEST NO. 10 - SOLAR ABSORPTANCE VALUES OF COP Zn_2TiO_4 PIGMENT VS ULTRAVIOLET EXPOSURE (ESH)	4-91b
4-11a	SELECTED SPECTRAL REFLECTANCE DATA: CREF #13 ZINC ORTHOTITANATE.OI-650G PAINTS	4-108

LIST OF TABLES (Cont'd)

<u>Table No.</u>		<u>Page</u>
4-12	SOLAR ABSORPTANCE VALUES, IRIF TEST I-67	4-116
4-13	SELECTED REFLECTANCE DATA FROM IRIF TEST I-67	4-116
4-14	IRIF TEST I-68 TEST RESULTS	4-131
4-15	TEKTRONIX PIGMENTS	4-139
4-16	IRIF I-69 ULTRAVIOLET IRRADIATION TEST RESULTS	4-140
4-17	CREF-15 IRRADIATION TEST RESULTS	4-156
4-18	SELECTED IRRADIATION TEST RESULTS: CREF TEST NO. 15	4-157
4-19	IRIF TEST I-70 ULTRAVIOLET RADIATION TEST RESULTS	4-166
4-20	SELECTED IRIF-I-70 DATA	4-168
4-21	IRIF TEST I-71 ULTRAVIOLET RADIATION TEST RESULTS	4-174
4-22	SELECTED IRIF-I-71 TEST DATA	4-176
4-22A	COMPARISON OF MOX-A WITH OTHER PIGMENTS	4-176
4-22B	INTERCOMPARISON OF MOX-A PIGMENTS	4-176
4-23	IRRADIATION TEST RESULTS:CREF-16	4-186
4-24	DATA COMPARISON: CREF TEST NO. 16 VS IRIF I-70	4-187
4-25	IRIF TEST I-72 ULTRAVIOLET RADIATION TEST RESULTS	4-199
4-26	SELECTED IRIF-I-72 DATA	4-212
4-26A	COMPARISON OF MOX-B POWDERS AND PAINTS	4-212
4-26B	POWDER/PAINT RATIOS	4-212
4-26C	TEMPERATURE AND TIME EFFECTS IN PAINTS	4-212
4-27	MASS LOSS DATA STATIC CALCINATION DATA	4-217
4-28	TGA DATA	4-219

LIST OF TABLES (Cont'd)

<u>Table No.</u>		<u>Page</u>
4-29	MOX PIGMENT STOICHIOMETRY SERIES RESULTS	4-232
4-30	SELECTED PROPERTIES OF STOICHIOMETRY SERIES PIGMENTS	4-235
5-1	LIST OF SOLVENTS	5-6
6-1	PARAMAGNETIC CENTERS IN ZnO	6-17
6-1b	COMPARISON OF EPR CENTERS IN ZINC ORTHOTITANATE PIGMENT VS OWENS-ILLINOIS PAINT	6-21
6-2	LIKELY DONORS AND ACCEPTORS IN Zn_2TiO_4 PHOTOLYSIS	6-22
7-1	FORMULATION OF A-429M THERMAL-CONTROL PAINT	7-1
7-2	A-429M COATINGS - EFFECTS OF CURE SCHEDULE	7-2
7-3	LIST OF STRIPPABLE COATINGS	7-8
7-4	EVALUATION OF STRIPPABLE COATINGS/FILMS	7-9
7-5	EVALUATION OF STRIPPABLE COATINGS/FILMS AFTER 139 HOURS IN ATLAS WEATHEROMETER	7-11
7-6	EFFECTS OF POTTER ON "PEELASTIC" STRIPPABLE COATING ULTRAVIOLET STABILITY OF S-13G AND Z-93	7-13
7-7	ULTRAVIOLET-INDUCED CHANGES IN SPECTRAL REFLECTANCE OF "PROTECTED" PAINT FILMS	7-15
7-8	RESULTS OF SIMULATED SALT SPRAY EXPOSURE: EFFECTS ON S-13G UV DEGRADATION	7-17

LIST OF FIGURES

<u>Figure No.</u>		<u>Page</u>
a	THE FOUR CLASSES OF THERMAL CONTROL SURFACES	1-4
1b	REPRESENTATIVE SPECTRA (ABSORPTANCE VS WAVELENGTH) FOR FOUR CLASSES OF THERMAL CONTROL SURFACES	1-4
3.1	FLOW DIAGRAM FOR B-229 SYNTHESIS OF ZINC ORTHOTITANATE PIGMENT	3-2
3.2	FLOW DIAGRAM OF COPRECIPITATION (COP) PROCESS FOR SYNTHESIS OF Zn_2TiO_4 PIGMENT	3-8
3.3	TYPICAL FLOW DIAGRAM FOR Zn_2TiO_4 SYNTHESIS FROM A PRECIPITATED BATCH	3-17
3.4	X-RAY POWDER PATTERNS OF PRECIPITATED MATERIALS	3-20
3.5	X-RAY POWDER PATTERNS OF FIRED ZINC ORTHOTITANATE MATERIALS (Zn_2TiO_4)	3-21
3.6	MICROSTRUCTURE OF ZINC OXALATE	3-24
3.7	MICROSTRUCTURE OF TITANIUM PHASE PRECIPITATE	3-25
3.8	MICROSTRUCTURE OF COPRECIPITATED ZINC- TITANIUM COMPOUND MIXTURE (LH-51)	3-27
3.9	MICROSTRUCTURE OF 700°C FIRED MATERIAL (LH-52(6))	3-28
3.10	MICROSTRUCTURE OF 900°C FIRED MATERIAL (LH-52(9))	3-29
3.11	MICROSTRUCTURE OF 1050°C FIRED MATERIAL (LH-101(6-10.5))	3-30
3.12	MICROSTRUCTURE OF 1200°C FIRED MATERIAL (LH-102(6-12))	3-31
3.13	MICROSTRUCTURE OF 1400°C FIRED MATERIAL (LH-52(6-14))	3-32
3.14	WEIGHT LOSS VS TEMPERATURE FOR ZINC OXALATE TITANIUM OXALATE AND MIXED OXALATES	3-36
3.15	ZINC OXALATE DECOMPOSITION PRODUCT AT 300°C AND 400°C	3-39

LIST OF FIGURES (Cont'd)

<u>Figure No.</u>		<u>Page</u>
3.16	ZINC OXALATE DECOMPOSITION PRODUCTS AT 500° AND 700°C	3-40
3.17	TGA THERMOGRAM OF "TiOX"	3-43
3.18	SEM VIEWS OF "TiOX" AS PRECIPITATED AND HEAT TREATED AT 150°C	3-45
3.19	SEM VIEWS OF "TiOX" HEAT TREATED AT 230°C AND 340°C	3-46
3.20	SEM VIEWS OF "TiOX" HEAT TREATED AT 500° AND 700°C	3-47
3.21	COPRECIPITATED OXALATES DECOMPOSITION PRODUCTS AT 500° AND 700°C	3-49
3.22	SEM VIEWS OF COP MATERIALS LH-103 and LH-103H	3-53
3.23	SEM VIEWS OF MOX MATERIAL AND INDIVIDUAL OXALATES	3-54
3.24	SEM VIEWS OF COP MATERIALS CALCINED AT 600°C FOR 2 HOURS	3-55
3.25	SEM VIEWS OF COMPACTED COP AND MOX MATERIALS CALCINED AT 600°C FOR 2 HOURS	3-57
3.26	SEM VIEWS OF COP MATERIALS CALCINED AT 1050°C FOR 2 HOURS	3-58
3.27	SEM VIEWS OF COMPACTED COP AND MOX MATERIALS CALCINED AT 1050°C FOR 2 HOURS	3-59
3.28	SEM VIEWS OF COP AND MOX MATERIALS CALCINED AT 600°C/2 HR.	3-61
3.29	SEM VIEWS OF COP AND MOX MATERIALS CALCINED AT 1050°C/2 HR.	3-62
3.30	REFLECTANCE SPECTRA OF LH-105(6-12) BALL MILLED VS PLAIN	3-64
3.31	REFLECTANCE SPECTRA OF MOX-A(6-12) BALL MILLED VS PLAIN	3-65
3.32	SEM VIEWS OF ZINC OXALATE PRECIPITATES CALCINED AT 600°C/2 HR.	3-71

LIST OF FIGURES (Cont'd)

<u>Figure No.</u>		<u>Page</u>
3.33	SEM VIEWS OF ZINC OXALATE PRECIPITATES CALCINED AT 600°C/2 HR.	3-72
3.34	SEM VIEWS OF ZINC OXALATE PRECIPITATES CALCINED AT 600°C.	3-73
3.35	SEM VIEWS OF ZINC OXALATE PRECIPITATES CALCINED AT 600°C.	3-74
3.36	% WEIGHT LOSS VS STOICHIOMETRY OF PRECALCINED PIGMENTS	3-84
3.37	SEM VIEWS OF MOX STOICHIOMETRY SERIES SAMPLES CALCINED AT 600°C/2 HR.	3-85
3.38	SEM VIEWS OF MOX STOICHIOMETRY SERIES SAMPLES CALCINED AT 600°C/2 HR.	3-86
3.39	SEM VIEWS OF MOX STOICHIOMETRY SERIES SAMPLES CALCINED AT 900°C/8 HR.	3-88
3.40	SEM VIEWS OF MOX STOICHIOMETRY SERIES SAMPLES CALCINED AT 900°C/8 HR.	3-89
3.41	SEM VIEWS OF MOX STOICHIOMETRY SERIES SAMPLES CALCINED AT 1200°C/2 HR.	3-90
3.42	SEM VIEWS OF MOX STOICHIOMETRY SERIES SAMPLES CALCINED AT 1200°C/2 HR.	3-91
4.1	REPRESENTATIVE Zn_2TiO_4 REFLECTANCE SPECTRA	4-4
4.2	THE COMBINED RADIATION ENVIRONMENT TEST FACILITY	4-8
4.3	COLSE-UP OF THE CREF	4-9
4.4	TOP VIEW OF THE IRIF'S UV-IRRADIATION CHAMBER SHOWING SAMPLES, SAMPLE TABLE, AND MANIPULATOR ARMS	4-10
4.5	SPECTRAL RADIANCE OF AH-6 UV RADIATION SOURCE	4-11
4.6	SPECTRAL RADIANCE OF HANOVIA 5000 WATT MERCURY-XENON LAMP	4-12

LIST OF FIGURES (Cont'd)

<u>Figure No.</u>		<u>Page</u>
4.7	REFLECTANCE SPECTRA OF PLASMA ANNEALED, K_2SiO_3 -ENCAPSULATED Zn_2TiO_4 /OI-650 - PROTONS ONLY	4-18
4.8	REFLECTANCE SPECTRA OF PLASMA ANNEALED, K_2SiO_3 -ENCAPSULATED Zn_2TiO_4 /OI-650 - ULTRAVIOLET ONLY	4-19
4.9	REFLECTANCE SPECTRA OF PLASMA ANNEALED, K_2SiO_3 -ENCAPSULATED Zn_2TiO_4 /OI-650 - PROTONS AND ULTRAVIOLET	4-20
4.10	REFLECTANCE SPECTRA OF K_2SiF_6 -ENCAPSULATED Zn_2TiO_4 /PS-7 - PROTONS ONLY	4-22
4.11	REFLECTANCE SPECTRA OF K_2SiF_6 -ENCAPSULATED Zn_2TiO_4 /PS-7 - PROTONS AND ULTRAVIOLET	4-23
4.12	REFLECTANCE SPECTRA OF K_2SiF_6 -ENCAPSULATED Zn_2TiO_4 /PS-7 - ULTRAVIOLET ONLY	4-24
4.13	REFLECTANCE SPECTRA OF $K_4SiW_{12}O_{40}$ -ENCAPSULATED Zn_2TiO_4 /PS-7 - PROTONS ONLY	4-25
4.14	REFLECTANCE SPECTRA OF $K_4SiW_{12}O_{40}$ -ENCAPSULATED Zn_2TiO_4 /PS-7 - PROTONS AND ULTRAVIOLET	4-26
4.15	REFLECTANCE SPECTRA OF $K_4SiW_{12}O_{40}$ -ENCAPSULATED Zn_2TiO_4 /PS-7 - ULTRAVIOLET ONLY	4-27
4.16	REFLECTANCE SPECTRA OF OWENS-ILLINOIS 650 GLASS RESIN UNPIGMENTED FILM - PROTONS AND ULTRAVIOLET	4-29
4.17	REFLECTANCE SPECTRA OF PLASMA ANNEALED, K_2SiF_6 -ENCAPSULATED Zn_2TiO_4 /PS-7	4-31
4.18	REFLECTANCE SPECTRA OF PLASMA ANNEALED, K_2SiF_6 -ENCAPSULATED Zn_2TiO_4 /OI-650	4-32
4.19	REFLECTANCE SPECTRA OF PLASMA ANNEALED, K_2SiF_6 -ENCAPSULATED Zn_2TiO_4 /OI-650	4-33
4.20	REFLECTANCE SPECTRA OF PLASMA ANNEALED, K_2SiF_6 -ENCAPSULATED Zn_2TiO_4 /OI-650G	4-34
4.21	REFLECTANCE SPECTRA OF K_2SiO_3 -ENCAPSULATED Zn_2TiO_4 /OI-650	4-37

LIST OF FIGURES (Cont'd)

<u>Figure No.</u>		<u>Page</u>
4.22	REFLECTANCE SPECTRA OF K_2SiO_3 -ENCAPSULATED Zn_2TiO_4 /OI-650	4-38
4.23	REFLECTANCE SPECTRA OF K_2SiF_6 -ENCAPSULATED Zn_2TiO_4 WITH AND WITHOUT PLASMA ANNEALING	4-39
4.24	REFLECTANCE SPECTRA OF $Zn_2TiO_4:K_2SiF_6$ (SRI 12-31.3)/PS-7	4-45
4.25	REFLECTANCE SPECTRA OF $Zn_2TiO_4:K_2SiF_6$ (SRI 12-31.3)/G	4-46
4.26	REFLECTANCE SPECTRA OF $Zn_2TiO_4:K_2SiF_6$ (Recalcined-1100°C)/OI	4-48
4.27	SPECTRAL REFLECTANCE OF $Zn_2TiO_4:K_2SiO_3/Li_2SiO_3$	4-49
4.28	SPECTRAL REFLECTANCE OF $Zn_2TiO_4:K_2SiO_3$ (SRI 17-35)/G	4-50
4.29	SPECTRAL REFLECTANCE OF $Zn_2TiO_4:Li_2SiF_6$ (Baked at 100C)/OI-650G	4-51
4.30	SPECTRAL REFLECTANCE OF $Zn_2TiO_4:(PO_4/SiO_3/PO_4)$ /OI	4-55
4.31	SPECTRAL REFLECTANCE OF $Zn_2TiO_4:(PO_4/SiO_3/PO_4)$ (Heat Treated)/OI	4-56
4.32	SPECTRAL REFLECTANCE OF $Zn_2TiO_4:K_2SiF_6$ /OI	4-57
4.33	SPECTRAL REFLECTANCE OF $Zn_2TiO_4:K_2SiF_6$ (Heat Treated)/OI	4-58
4.34	SPECTRAL REFLECTANCE OF $Zn_2TiO_4:K_2SiF_6$ /OI	4-59
4.35	SPECTRAL REFLECTANCE OF $Zn_2TiO_4:K_2SiF_6$ (Heat Treated)/OI	4-60
4.36	SPECTRAL REFLECTANCE OF Zn_2TiO_4 (Untreated B-229 METHOD)	4-65
4.37	SPECTRAL REFLECTANCE OF $Zn_2TiO_4:(PO_4/SiO_3/PO_4)$ (Heat Treated)	4-66
4.38	SPECTRAL REFLECTANCE OF $Zn_2TiO_4:K_2SiF_6$ (Heat Treated)	4-67

LIST OF FIGURES (Cont'd)

<u>Figure No.</u>		<u>Page</u>
4.39	SPECTRAL REFLECTANCE OF $\text{Zn}_2\text{TiO}_4:\text{Li}_2\text{SiF}_6$ (Heat Treated)	4-68
4.40	SPECTRAL REFLECTANCE OF OI-650 (STANDARD); AIR DRIED	4-69
4.41	SPECTRAL REFLECTANCE OF OI-650G (BATCH C-400); AIR DRIED	4-70
4.42	REFLECTANCE SPECTRA OF A429M	4-73
4.43	REFLECTANCE SPECTRA OF Zn_2TiO_4 (POWDER)	4-74
4.44	REFLECTANCE SPECTRA OF $\text{Zn}_2\text{TiO}_4/\text{PS-7}$	4-75
4.45	REFLECTANCE SPECTRA OF $\text{Zn}_2\text{TiO}_4/\text{OI}$	4-76
4.46	REFLECTANCE SPECTRA OF $\text{Zn}_2\text{TiO}_4:\text{K}_2\text{SiF}_6$ (POWDER)	4-77
4.47	REFLECTANCE SPECTRA OF $\text{Zn}_2\text{TiO}_4:\text{K}_2\text{SiF}_6/\text{OI}$	4-78
4.48	REFLECTANCE SPECTRA OF $\text{Zn}_2\text{TiO}_4:\text{K}_2\text{SiF}_6/\text{OI}$	4-79
4.49	REFLECTANCE SPECTRA OF $\text{Zn}_2\text{TiO}_4:(\text{PO}_4^{=}/\text{SiO}_3^{=}/\text{PO}_4^{=})$ (POWDER)	4-80
4.50	REFLECTANCE SPECTRA OF $\text{Zn}_2\text{TiO}_4:(\text{PO}_4^{=}/\text{SiO}_3^{=}/\text{PO}_4^{=})/\text{OI}$	4-81
4.51	REFLECTANCE SPECTRA OF LH-14, Zn_2TiO_4 (900°C/8 hr) (POWDER)	4-82
4.52	REFLECTANCE SPECTRA OF LH-12(1200°C/1 hr) (POWDER)	4-83
4.53	REFLECTANCE SPECTRA OF LH-12, Zn_2TiO_4 (900°C/8 hr) (POWDER)	4-84
4.54	REFLECTANCE SPECTRA OF LH-12 Zn_2TiO_4 (6-14)	4-92
4.55	REFLECTANCE SPECTRA OF LH-16 Zn_2TiO_4 (9)	4-93
4.56	REFLECTANCE SPECTRA OF LH-16 Zn_2TiO_4 (5-14)	4-94
4.57	REFLECTANCE SPECTRA OF LH-20 Zn_2TiO_4 (9)	4-96
4.58	REFLECTANCE SPECTRA OF LH-20 Zn_2TiO_4 (9-14)	4-97
4.59	REFLECTANCE SPECTRA OF LH-20 Zn_2TiO_4 (6-12)	4-98

LIST OF FIGURES (Cont'd)

<u>Figure No.</u>		<u>Page</u>
4.60	REFLECTANCE SPECTRA OF LH-22 Zn_2TiO_4 (9)	4-99
4.61	REFLECTANCE SPECTRA OF LH-22 Zn_2TiO_4 (6-12)	4-100
4.62	REFLECTANCE SPECTRA OF LH-22 Zn_2TiO_4 (9-14)	4-101
4.63	REFLECTANCE SPECTRA OF LH-26 Zn_2TiO_4 (6-11)	4-102
4.64	REFLECTANCE SPECTRA OF LH-27 Zn_2TiO_4 (6-12)	4-103
4.65a	REFLECTANCE SPECTRA OF LH-27 Zn_2TiO_4 (9-14)	4-104
4.65b	REFLECTANCE SPECTRA OF LH-30 (6-12-A-10)	4-109
4.66	REFLECTANCE SPECTRA OF LH-30 (6-14-A-10)	4-110
4.67	REFLECTANCE SPECTRA OF LH-31 (6-12-A-10)	4-111
4.68	REFLECTANCE SPECTRA OF LH-31 (6-14-A-10)	4-112
4.69	REFLECTANCE SPECTRA OF LH-51 (6-12)	4-113
4.70a	REFLECTANCE SPECTRA OF LH-51 (6-14)	4-114
4.70b	REFLECTANCE SPECTRA OF LH-52 (6-9) (POWDER)	4-115
4.71	REFLECTANCE SPECTRA OF LH-52 (6-9)/OI	4-118
4.72	REFLECTANCE SPECTRA OF LH-52 (6-14)/OI	4-119
4.73	REFLECTANCE SPECTRA OF LH-52 (6-14-A-10)/OI	4-120
4.74	REFLECTANCE SPECTRA OF LH-53 (6-12)/OI	4-121
4.75	REFLECTANCE SPECTRA OF LH-53 (6-12-A-10)/OI	4-122
4.76	REFLECTANCE SPECTRA OF LH-53 (6-13)/OI	4-123
4.77	REFLECTANCE SPECTRA OF LH-53 (6-13-A-10)/OI	4-124
4.78	REFLECTANCE SPECTRA OF LH-22 (9)/OI	4-125
4.79	REFLECTANCE SPECTRA OF D-260(SS) Zn_2TiO_4 (POWDER)	4-126
4.80	EFFECT OF CALCINATION TEMPERATURE ON Zn_2TiO_4 STABILITY: UNTREATED VS ACETIC ACID WASHED PIGMENTS	4-128

LIST OF FIGURES (Cont'd)

<u>Figure No.</u>		<u>Page</u>
4.81	EFFECT OF CALCINATION TEMPERATURE ON Zn_2TiO_4 REFLECTANCE CHANGE AT 900nm	4-128
4.82	EFFECT OF FREE ZnO ON STABILITY OF Zn_2TiO_4 / OI-650 PAINTS	4-129
4.83	FREE ZnO CONTENT OF Zn_2TiO_4 PIGMENT VS CALCINATION TEMPERATURE	4-129
4.84	REFLECTANCE SPECTRA OF TEKTRONIX Zn_2TiO_4 (900°C/9 HR)	4-132
4.85	REFLECTANCE SPECTRA OF TEKTRONIX Zn_2TiO_4 (1200°C/1 HR)	4-133
4.86a	REFLECTANCE SPECTRA OF TEKTRONIX Zn_2TiO_4 (1250°C/24 HR)	4-134
4.86b	REFLECTANCE SPECTRA OF TEKTRONIX Zn_2TiO_4 (1250°C/24 HR)	4-135
4.87	REFLECTANCE SPECTRA OF TEKTRONIX Zn_2SiO_4	4-136
4.88	REFLECTANCE SPECTRA OF TEKTRONIX $\text{Zn}_2\text{SiO}_4:\text{Mn}$	4-137
4.89	REFLECTANCE SPECTRA OF ZINC ORTHOTITANATE POWDER (T-2)	4-142
4.90	REFLECTANCE SPECTRA OF ZINC ORTHOTITANATE PAINT (T-2/OI)	4-143
4.91	REFLECTANCE SPECTRA OF ZINC ORTHOTITANATE PAINT (T-2/G)	4-144
4.92	REFLECTANCE SPECTRA OF ZINC ORTHOTITANATE POWDER (T-2: K_2SiO_3)	4-145
4.93	REFLECTANCE SPECTRA OF ZINC ORTHOTITANATE PAINT (T-2 K_2SiO_3 /G)	4-146
4.94	REFLECTANCE SPECTRA OF ZINC ORTHOTITANATE PAINT (T-2:A-10/OI)	4-147
4.95	REFLECTANCE SPECTRA OF ZINC ORTHOTITANATE PAINT (T-3/OI)	4-148
4.96	REFLECTANCE SPECTRA OF ZINC ORTHOTITANATE POWDER (T-3: K_2SiO_3 /OI)	4-149

LIST OF FIGURES (Cont'd)

<u>Figure No.</u>		<u>Page</u>
4.97	REFLECTANCE SPECTRA OF ZINC ORTHOTITANATE POWDER (T-3: A-10)	4-150
4.98	REFLECTANCE SPECTRA OF ZINC ORTHOTITANATE PAINT (T-3: A-10)/OI)	4-151
4.99	REFLECTANCE SPECTRA OF ZINC ORTHOTITANATE POWDER (T-4)	4-152
4.100	REFLECTANCE SPECTRA OF ZINC ORTHOTITANATE PAINT (LH-53(6-12)/G)	4-153
4.101	REFLECTANCE SPECTRA OF LH-102(6-12)/G	4-158
4.102	REFLECTANCE SPECTRA OF LH-102(6-12-10)/G	4-159
4.103	REFLECTANCE SPECTRA OF LH-102(6-12-A)/G	4-160
4.104	REFLECTANCE SPECTRA OF LH-102(6-12-A-10)/G	4-161
4.105	REFLECTANCE SPECTRA OF LH-102(6-12):Li ₂ SiO ₃ /G	4-162
4.106	REFLECTANCE SPECTRA OF LH-102(6-12-A):Li ₂ SiO ₃ /G	4-163
4.107	REFLECTANCE SPECTRA OF LH-102(6-12-A-10):Li ₂ SiO ₃ /G	4-164
4.108	REFLECTANCE SPECTRA OF LH-105(6-12)/G	4-169
4.109	REFLECTANCE SPECTRA OF LH-106(6-12-A-10)/G	4-170
4.110	REFLECTANCE SPECTRA OF LH-106(6-12-A-10):Li ₂ SiO ₃ /G	4-171
4.111	REFLECTANCE SPECTRA OF LH-106(6-12-A-10):K ₂ SiO ₃ /G	4-172
4.112	REFLECTANCE SPECTRA OF MOX-A(6-9/5) (Powder)	4-177
4.113	REFLECTANCE SPECTRA OF MOX-A(6-10.5/2) (Powder)	4-178
4.114	REFLECTANCE SPECTRA OF MOX-A(6-10.5/8) (Powder)	4-179
4.115	REFLECTANCE SPECTRA OF MOX-A(6-12/0.5) (Powder)	4-180
4.116	REFLECTANCE SPECTRA OF MOX-A(6-12/2) (Powder)	4-181
4.117	REFLECTANCE SPECTRA OF LH-103(6-10.5/2) (Powder)	4-182
4.118	REFLECTANCE SPECTRA OF MOX(6-10.5/2) (Powder)	4-183

LIST OF FIGURES (Cont'd)

<u>Figure No.</u>		<u>Page</u>
4.119	REFLECTANCE SPECTRA OF Si_3N_4 (Powder)	4-184
4.120	REFLECTANCE SPECTRA OF LH-106(6-12): $\text{Li}_2\text{SiO}_3/\text{G}$	4-189
4.121	REFLECTANCE SPECTRA OF LH-106(6-12): $\text{K}_2\text{SiO}_3/\text{G}$	4-190
4.122	REFLECTANCE SPECTRA OF LH-106(6-12): $\text{K}_2\text{SiF}_6/\text{G}$	4-191
4.123	REFLECTANCE SPECTRA OF LH-106(6-12-A-10)/G	4-192
4.124	REFLECTANCE SPECTRA OF LH-106(6-12-A-10): $\text{Li}_2\text{SiO}_3/\text{G}$	4-193
4.125	REFLECTANCE SPECTRA OF LH-106(6-12-A-10): $\text{K}_2\text{SiO}_3/\text{G}$	4-194
4.126	REFLECTANCE SPECTRA OF MOX-B(6-9/4)/G	4-200
4.127	REFLECTANCE SPECTRA OF MOX-B(6-9/16)/G	4-201
4.128	REFLECTANCE SPECTRA OF MOX-B(6-9/16) (Powder)	4-202
4.129	REFLECTANCE SPECTRA OF MOX-B(6-10.5/1)/G	4-203
4.130	REFLECTANCE SPECTRA OF MOX-B(6-10.5/4)/G	4-204
4.131	REFLECTANCE SPECTRA OF MOX-B(6-10.5/8)/G	4-205
4.132	REFLECTANCE SPECTRA OF MOX(6-10.5/2) (Powder)	4-206
4.133	REFLECTANCE SPECTRA OF MOX-B(6-10.5/8) (Powder)	4-207
4.134	REFLECTANCE SPECTRA OF MOX-B(6-12/0.5)/G	4-208
4.135	REFLECTANCE SPECTRA OF MOX-B(6-12/2)/G	4-209
4.136	REFLECTANCE SPECTRA OF MOX-B(6-12/2) (Powder)	4-210
4.137	COMPARISON OF REFLECTANCE SPECTRA OF ZnO , $\alpha\text{-TiO}_2$, r-TiO_2 AND Zn_2TiO_4	4-214
4.138	TGA THERMOGRAM OF "TiOX"	4-218
4.139	"TiOX" CONVERSION VS RECIPROCAL TEMPERATURE	4-220
4.140	REFLECTANCE SPECTRA OF 900°C, MOX PIGMENTS WITH VARIOUS Zn/Ti MOLE RATIOS	4-226
4.141	REFLECTANCE SPECTRA OF 1200°C MOX PIGMENTS WITH VARIOUS Zn/Ti MOLE RATIOS	4-227

LIST OF FIGURES (Cont'd)

Figure No.		Page
4.142	REFLECTANCE SPECTRA OF (6-9) Zn_2TiO_4 PIGMENTS PREPARED AT VARIOUS Zn/Ti RATIOS	4-228
4.143	REFLECTANCE SPECTRA OF (6-12) Zn_2TiO_4 PIGMENTS PREPARED AT VARIOUS Zn/Ti RATIOS	4-229
4.144	REFLECTANCE SPECTRA OF Zn_2TiO_4 PIGMENTS PREPARED AT VARIOUS Zn/Ti RATIOS FROM SOLID STATE PRECURSORS	4-230
4.145	RELATIVE ABSORPTION COEFFICIENT AT $\lambda = 350nm$ VS Zn/Ti RATIO IN Zn_2TiO_4 PIGMENTS	4-238
4.146	UV SPECTRAL STABILITY VS Zn/Ti RATIO	4-239
6.2	EPR SPECTRA OF ZnO AT 77°K: EFFECT OF ULTRAVIOLET IRRADIATION AT 77°K	6-6
6.3	EPR OF ZnO AT 77°K: EFFECT OF WARMING UV-CREATED CENTER TO ROOM TEMPERATURE	6-7
6.4	EPR SPECTRAL OF ZnO AT 77°K: EFFECT OF O_2 (ONE TORR) ON ULTRAVIOLET-CREATED CENTER	6-8
6.5	EPR AT $\sim 77^\circ K$ OF F.F. (ANATASE) TiO_2 AT $\sim 10^{-2}$ TORR.	6-8
6.6	EPR AT $\sim 77^\circ K$ OF F.F. (ANATASE) TiO_2 HEATED AT 500°C FOR SIX HOURS AT 10^{-6} - 10^{-7} TORR.	6-9
6.7	EPR AT $\sim 77^\circ K$ OF LW ANATASE HEATED AT 500°C FOR FOUR HOURS at 10^{-6} TORR.	6-9
6.8	EPR AT $\sim 77^\circ K$ OF SAMPLE B-229, Zn_2TiO_4 PIGMENT, HEATED AT 500°C FOR FOUR HOURS AT 10^{-7}	6-11
6.9	EPR SPECTRA OF ZnO EXCESS-PRODUCED Zn_2TiO_4 : INVESTIGATION OF METASTABLE CENTERS (a) AFTER IRRADIATION (b) AFTER RE-WARMING TO $\sim 20^\circ C$ AND RE-COOLING TO 77°K	6-12
6.10	EPR SPECTRA OF Zn_2TiO_4 WITH EXCESS ZnO	6-13
6.11	EPR AT 77°K OF $Zn_2TiO_4 \cdot 2SiF_6$	6-15
6.12	EPR SPECTRUM OF Zn_2TiO_4 WITH EXCESS TiO_2	6-16
7.1	SPECTRAL REFLECTANCE OF IITRI'S A-429M: $ZnO:SiO_3/OI-650G$	7-4

LIST OF FIGURES (Cont'd)

<u>Figure No.</u>		<u>Page</u>
7.2	SPECTRAL REFLECTANCE OF IITRI'S A-429M: ZnO:SiO ₃ /OI-650G	7-5
7.3	UV DEGRADATION OF STANDARD AND SALT SPRAY TREATED S-13G	7-18

1.0 INTRODUCTION

Early in the history of Space Technology, space vehicle designers recognized the importance of thermal control. The performance or function of temperature-sensitive components, if permitted to transgress their individual operating temperature limits, might seriously jeopardize a vehicle's mission. Approaches to effective temperature control involve primarily both materials selection, and systems considerations. In the materials approach the absorption of solar energy is determined, as is the thermal emission, by the radiative properties of the surface of materials selected. The latter approaches, in general, accomplish temperature control by optimum location of components with respect to one another and to the solar vector. Overall thermal control is achieved by regulation of absorbed solar energy and of thermal energy radiated to space.

In this report we will present the R&D accomplishments of a program initiated in early 1971 to develop stable thermal control coatings for large space vehicles. To place it in context let us first describe the relationship and utility of this work to the field of spacecraft thermal control. Among the first documents to treat the overall problem of spacecraft thermal control were those authored by Gaumer and McKellar (ref. 1) and by Heller (ref. 2). Many papers and reports (e.g. ref's 3-8) which succeeded these first two indicate the role of the properties α_s (solar absorptance) and ϵ (thermal emittance).

Indeed, it is of interest that the importance of these properties in controlling local spacecraft surface temperatures has been demonstrated in various arguments from the simple to the most elegant and elaborate (e.g., ref. 3) with the same conclusion:

The properties α_s and ϵ are the primary materials factors in spacecraft temperature control. A simple development of the relationship between their ratio (α_s/ϵ) and temperature proceeds from an analysis of the energy balance on a flat plate oriented normal to the solar vector in the space environment (where convection is totally absent). Thus, if $\alpha_s E_s$ is the rate of solar energy absorption per unit area and $2\epsilon\sigma T^4$ is the rate of thermal emission per unit area (the plate absorbs on one side but emits from both sides), then, assuming equilibrium (i.e., $mc_p \cdot dT/d\theta = 0$),

$$T = \left(\frac{\alpha_s}{\epsilon} \right)^{\frac{1}{4}} \cdot \left(\frac{E_s}{2\sigma} \right)^{\frac{1}{4}} \quad (1)$$

Apart from small cyclic variations the term $(E_s/2\sigma)$ is a constant at the earth's distance from the sun, i.e. at 1 A.U. E_s is the solar flux (at 1 A.U.) and σ is the Stefan-Boltzmann constant. The importance of α_s and ϵ can be understood from some elementary considerations of spacecraft heat transfer. In eq. 2 we set out the basic heat balance for a spacecraft:

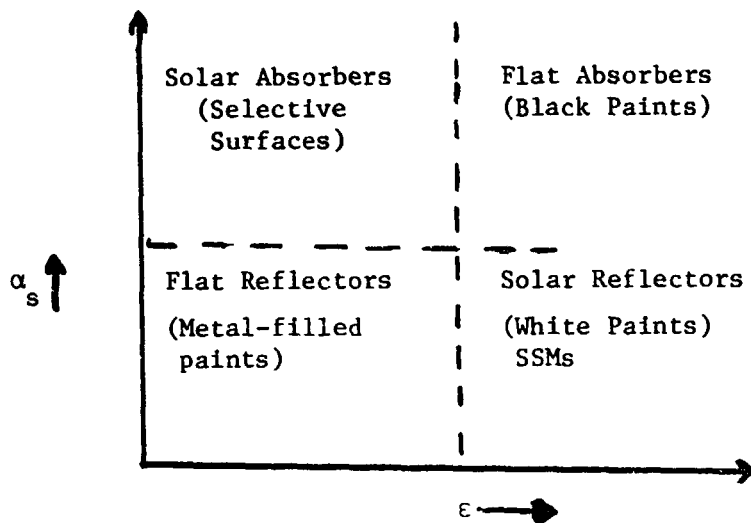
$$Q_s + Q_A + Q_I + Q_E = A\epsilon\sigma T^4 + mc_p dT/d\theta, \quad (2)$$

where Q is energy absorbed and the subscripts S, A, I and E refer, respectively, to solar, earth albedo, internal spacecraft power, and to earth shine (thermal emission). These terms are general and do not indicate the relative contribution of each to the total heat balance. However, since there is only one dissipation term, $A\epsilon\sigma T^4$, and since the functions of most spacecraft involve substantial auxiliary power requirements, the absorptance of radiant energy (in this case primarily solar) must be minimized. The prime purpose of a low α_s/ϵ surface is to decrease the dependence on a temperature-sensitive energy dissipation mechanism.

Traditionally, materials have been classified according to their respective α_s/ϵ ratios, and four general classes have been identified (refs. 1,4). Figure 1 illustrates these classes, shows their relationship to one another and gives some examples of typical materials within each. The figure, unfortunately, does not portray the considerably greater emphasis in research and development focussed on low α_s/ϵ systems or their generally greater overall utility in practical applications.

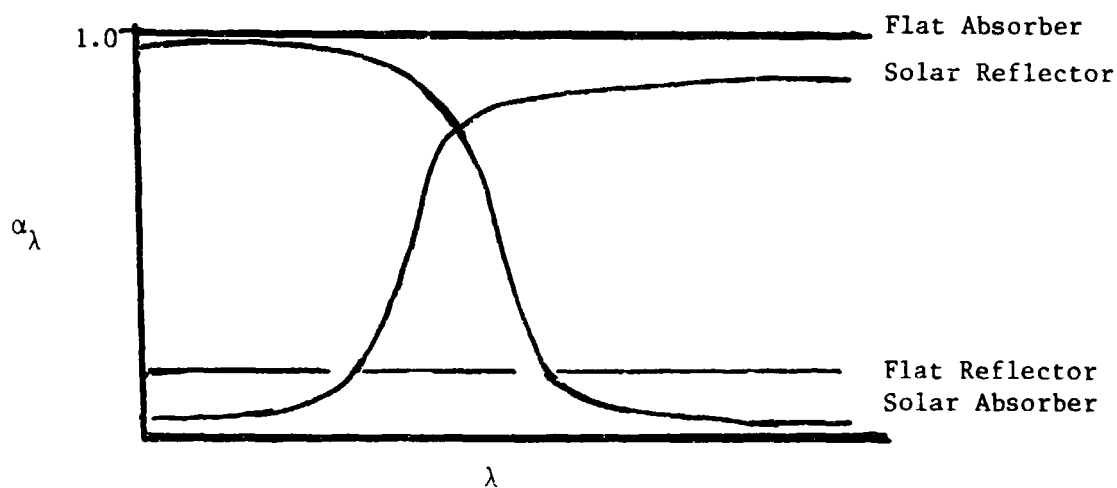
Having briefly established a perspective regarding relationships between classes of thermal control (TC) surfaces, we can now discuss the one all-important requirement of all TC surfaces, viz., optical stability. The usefulness of a material or a system of materials in any particular spacecraft application cannot be determined solely on the basis of meeting specific α_s/ϵ requirements. In the total environment to which the spacecraft will be exposed, low α_s/ϵ materials must also retain their initial optical properties during the course of the mission. They must not degrade through radiation interactions nor suffer physical changes which cause catastrophic failures (e.g., through delamination).

While there is an abundance of materials with low α_s/ϵ ratio, very few have been shown to be stable (refs. 5-8). Fewer yet are intrinsically stable and, of those that are, other considerations generally deny or limit their practical use. Fused silica, for example, is intrinsically stable to ultraviolet (UV) radiation when in sheet or slab form, making its use not only costly but very cumbersome. (In powder form (ref. 9-10) it is grossly unstable). Stability ranks in most applications as the foremost consideration in materials selection; outgassing, difficulty of application, cleanability, cost and similar considerations are of somewhat lesser consequence, with some individual exceptions.



The Four Classes of Thermal Control Surfaces

Figure 1a



Representative Spectra (Absorptance vs Wavelength) for Four Classes of Thermal Control Surfaces

Figure 1b

Designers prefer solar reflector surfaces with the lowest α_s/ϵ ratio, since such materials provide a greater tolerance in the thermal balance. But they must also be stable in order to maintain a reasonable tolerance during the mission. Experience provides two important considerations in their selection. First, stability tends to be more difficult or costly to achieve with decreasing α_s/ϵ ratio. This is because low α_s requires low intrinsic absorption, which in turn requires low levels of impurities, and very few materials are sufficiently pure or able to be made so. Furthermore, the optical effect of induced defects (color centers) increases with increasing transparency. Second, as α_s decreases, the effect of a unit change in α_s becomes larger, i.e., $\Delta\alpha_s/\alpha_s$ will be more important, the lower α_s is. We note that in general the emittance of a dielectric material is stable; from experience we know that solar absorptance, however, is subject to environmental degradation.

These aims have provided the impetus for obtaining materials with ultra-low α_s/ϵ ratio and with long-term optical stability. From a practical point of view, the ideal solar reflector material should be a spray paint because of its adaptability to "real" spacecraft surfaces. Unfortunately, ready-to-use paint systems with very low α_s/ϵ ratios and ultra-stability have not been developed, at least not with their full theoretical capability.

A spacecraft paint system is an incredibly complex mixture of materials. In succeeding pages the nature and depth of this complexity will be explored and analyzed with almost singular concentration on zinc orthotitanate pigment and the silicone paint systems incorporating them.

In introducing this report we have indicated the principal requirements to which programs such as this one are addressed, along with some brief historical, but relevant, notes. Most researchers will appreciate the fact of continually changing

requirements in such efforts and also that research is a step-by-step process in which any given step almost always depends on the results of the one which preceded it. In subsequent sections we will provide detailed technical background so that the program's objectives and the approaches will, in light of these remarks, be also better appreciated.

1.1 TECHNICAL BACKGROUND

In very general, engineering terms we will develop the technical background which begins with definitions of program requirements, indicates the theoretical approaches to the development of materials satisfying them, briefly describes IITRI's previous experience in similar programs and then outlines the program goals. The latter, again in general terms, follow logically from determinations of what we want, theoretical ideas of how to get there, where we are and a set of milestones defining how we get there from here.

1.1.1 Low α_s/ϵ Requirements

The immediate engineering/applications objective of this program is the attainment of surface coatings with low α_s/ϵ ratio stable in the space environment. The term "stable" refers, ideally, to a zero time rate of change of solar absorptance and infrared emittance, and in this sense connotes zero "degradation". The concept of stability will be treated in great detail in later discussions.

A low α_s/ϵ surface is one which predominantly reflects solar energy and which absorbs (emits) thermal energy strongly. For an exact definition and clear understanding of the term "solar absorptance", α_s , it is defined as follows:

$$\alpha_s = \frac{\int_0^\infty \alpha_\lambda \cdot E_{s,\lambda} \, d\lambda}{\int_0^\infty E_s \cdot d\lambda} \quad (3)$$

where

α_λ = Spectral absorption coefficient at wavelength λ

$E_{s,\lambda}$ = Spectral solar energy flux (watts/cm²-μ) in a wavelength region $d\lambda$ about the wavelength λ .

Emittance, ϵ , is defined as the fraction of thermal energy emitted by a real surface compared to that emitted by a black-body at the same temperature and under the same conditions. It is defined similarly to eq. 3:

$$\epsilon = \frac{\int_0^\infty \epsilon_\lambda \cdot E_{b,\lambda} \cdot d\lambda}{\int_0^\infty E_{b,\lambda} \cdot d\lambda} \quad (4)$$

In reality both α_s and ϵ are defined by the relationship:

$$\alpha_s, \epsilon = \frac{\int_0^\infty (1-R_\lambda) \cdot E_s(\lambda) \cdot d\lambda}{\int_0^\infty E_s(\lambda) \cdot d\lambda} \quad (5)$$

where

R_λ = spectral reflectance in the appropriate spectral region,

$E_s = E_{b,\lambda}$ in the solar spectrum, and

= $C_1 \lambda^{-5} [\exp(C_2/\lambda T) - 1]^{-1}$ (Planck's Law) in the thermal spectrum.

Since $E_s(\lambda)$ is not a mathematically tractable function, α_s is calculated in practice from the formula:

$$\alpha_s = \sum_{n=1}^{50} (1-\bar{R}_\lambda) \cdot 0.02 \quad (6)$$

Thus, the solar spectrum is divided into fifty (50) equal energy increments (of 0.02 solar constants each). The average reflectance in each wavelength interval containing 0.02 solar constant is

subtracted from unity and the product with 0.02 is tabulated. The substitution of $(1-\bar{R}_\lambda)$ requires of course, that the material be opaque at all these same appropriate wavelengths. Appendix 1 is an example of the procedure for reducing raw spectral reflectance data to α_s .

1.1.2 Basic Approaches

A low α_s/ϵ surface can be realized in several fundamentally different ways, only two of which are practical. The simplest approach employs the principle of scattering in a non-absorbing dielectric medium to achieve high solar reflectance. In another approach, second surface mirrors (SSMs), low α_s/ϵ is obtained by overcoating a solar reflective substrate (a metal) with a transparent dielectric. Nearly all efforts to develop low α_s/ϵ systems have taken one or the other of these two approaches. Both, of course, possess unique advantages and disadvantages. The most common SSMs are fused silica and teflon (FEP), on which a thin film of either Ag or Al has been deposited and over which a corrosion protective layer may sometimes be applied. The resulting "laminate" is then applied to a vehicle substrate using an appropriate adhesive (ref. 11).

In a sense the program efforts we describe were directed at the development of a second-generation paint system, the achievement of a major improvement in solar reflectance as well as solar reflectance stability. Although to date we have not developed zinc orthotitanate paints to a "NASA Specification" status, the potential for achieving α_s values below 0.1 and ϵ values above 0.92 in such systems and stabilities of $\Delta\alpha_s = 0.05$ in 10 years at low earth altitudes has been demonstrated.

1.2 SUMMARY OF PREVIOUS PROGRAM RESULTS

IITRI has had a number of programs (refs. 12, 13) leading to the development of stable low α_s/ϵ paint systems. In one of the earliest of these programs (ref. 12) the basic S-13 formula was developed consisting of New Jersey Zinc Co. SP-500 zinc oxide

in General-Electric Co. LTV602 methyl silicone elastomer. In 1965 the in-situ vacuum effect was discovered (ref. 14), and S-13 and many other paint systems were shown to be unstable (ref. 15). The discovery that reflectance changes induced by UV in vacuo were in most cases bleached by exposure to O_2 (as happened in simulation facilities prior to 1965) drastically revolutionized the evaluation procedures employed from that time hence (ref. 14).

IITRI developed the IRIF (In-Situ Reflectance/Irradiation Facility), in which the spectral reflectance of specimens can be measured in the same high vacuum before and after UV irradiation without interrupting that vacuum; oxygen bleaching effects were thus eliminated. In this same program S-13G was stabilized by encapsulating the SP-500 ZnO pigment in potassium silicate (Sylvania Electric Co. No. PS-7). The process was developed on an engineering basis under NASA-JPL sponsorship (ref. 16). The paint system was re-designated S-13G; in the meantime G.E. Co. also re-named their product LTV602 as RTV602. Thus the composition of S-13G became $ZnO:K_2SiO_3/RTV602$. (This notation will be explained in detail in a later section). S-13G became a "work-horse" paint system; it has been used extensively on NASA and USAF satellites and also on European Satellites.

In 1971 IITRI initiated extensive efforts under a NASA program (ref. 17) to develop an ultra-low α_s/ϵ , ultra-stable paint system. R&D previous to this new program (ref. 13) indicated that zinc orthotitanate, Zn_2TiO_4 , had excellent potential. It was recognized at the same time that, even though RTV602 was the most stable (to UV) of the commercial silicones, it would not be compatible, optically; its relatively high index of refraction (≈ 1.6) tends to lower solar reflectance. Accordingly, we initiated a search for commercial vehicles with high UV stability, high pigment binding power and low index of refraction. A product marketed by Owens-Illinois of Toledo, Ohio,

known as OI-650 "Glass Resin", was found to meet most of these requirements. This product, in fact, is similar to the stable silicone resins synthesized at IITRI (ref. 18).

IITRI's experience with several previous programs consequently provided extensive technological background, a number of materials candidates which exhibited excellent application potential, and equally importantly, the facilities, procedures and methods for conducting and evaluating space simulation tests of these materials. These then are the accomplishments of previous programs which have directly supported our zinc orthotitanate development efforts. The first phase of this work - the previous program - concentrated primarily on the development of Zn_2TiO_4 pigment via solid state reaction of DuPont's FF anatase titania with New Jersey Zinc Co's SP-500 zinc oxide. The "solid state" studies have been fully documented in ref. 19. In this report we deal with the continued R&D efforts beyond the solid state studies. We will, however, not summarize here the accomplishments of the "solid state" studies (ref. 19). Since many of them interface directly and intimately with the present program, they will be discussed frequently with respect to the oxalate method for producing zinc orthotitanate precursors.

1.3 PROGRAM GOALS

The ultimate goal of the program is to produce a specification defining the processes and conditions for the preparation of zinc orthotitanate pigment, the paint binder, and of the paint itself. This ultimate goal implies the development of definitive processes with self-consistent production controls and with sufficiently reproducible products, completion of short and long term space simulation studies, development of applicable paint engineering data, measurement of outgassing/contamination properties and all others which affect the selection of the coating or the manner of its use.

To be somewhat more specific our program goals are predicated upon the achievement and demonstration of the following objectives:

Basic low α_s and high ϵ properties of the pigment.

Stable α_s of the pigment; viz., $\Delta\alpha_s < 0.02$ in 10^5 ESH.

Effectiveness of protective encapsulant for pigment (if necessary).

Intrinsic optical stability of paint binder.

Physical compatibility of pigment and binder.

Photolytic compatibility of pigment and binder.

Long term UV stability of Zn_2TiO_4 paint systems.

Selection of baseline paint systems.

Long term UV testing of baseline paint systems.

Selection of specification paint system.

Full engineering characterization of specification paint system.

Publication of properties, performance and characteristics of specification paint system.

Delivery of specification paint system in gallon quantities to demonstrate large scale output capabilities of pigment, binder and paint production processes.

The above objectives also reflect the chronological milestones of a logical development plan.

1.4 BIBLIOGRAPHY

1.4.1 Cited References

1. R.E. Gaumer and L.A. McKellar, "Thermal Radiative Control Surfaces for Spacecraft," Technical Report, Lockheed Missiles and Space Division, Report, LMSD-704014, Mar. 1961.
2. G. Heller, "Thermal Problems of Satellites", in Materials in The Space Environment, Proceedings of the 5th Sagamore Ordnance Materials Research Conference, W. Steurer (ed.), Sagamore Conference Center, Laqueppend, N.Y., Sept. 16-19, 1958.
3. W.G. Camack and D.K. Edwards, "Effect of Surface Thermal-Radiation Characteristics on The Temperature Control Problem in Satellites," pp. 5-54 in First Symposium on Surface Effects on Spacecraft Materials, F.J. Clauss (ed.), Wiley & Sons, New York, N.Y., 1960.
4. W.C. Snoddy, "Pegasus Thermal Experimental Results", pp. 27-28, in Research Achievements Rev., Vol. II. NASA-MSFC, NASA, 1966.
5. M. Lillywhite, P. Pizzolato, K. Karki et. al., "Improved Radiation Stable Thermal Control Coatings", Technical Report AFML-TR-70-94, Part I, April 1970.
6. G.R. Cunningham, J.R. Grammer, and F.J. Smith, "Emissivity Coatings for Low-Temperature Space Radiators" NASA Contract Report No. CR-1420, Sept. 1969.
7. T.R. Scollon and R.E. Killen, "Long Life High Reliability Thermal Control Systems Study", Final Report on Contract NAS8-26252, General Electric Co., Report No. 72SD4243, Aug. 1972.
8. D.M.J. Compton, T.E. Firlie, and J.T. Neu, "Mechanisms of Degradation of Polymeric Thermal Control Coatings", Technical Report AFML-TR-68-334, Part I., Jan. 1969.
9. K. Kubo, "Radiation Induced Optical Absorptions in Crystalline Quartz and Fused Silica", J. Phys. Soc. (Japan), 16, (1), Jan. 1961; M. Levy and J.H.O. Varley, "Radiation Induced Color Centers in Fused Quartz", Proc. Phys. Soc., B68, pp. 223-33, 1955; W.L. Smith and A.J. Cohen, "Color Centers in X-Irradiated Soda-Silica Glasses", J. Am. Ceram. Soc. 47, (11), pp. 564-70, Nov. 1964.

Cited References (Cont'd)

10. G.A. Zerlaut and Y. Harada, "Stable White Coatings", JPL Contract No. 950111, IITRI Report No. C207-25 (Summary Report), Aug. 27, 1963; and H.E. Pollard, "The Development of Thermal Control Surfaces for SNAP-10A Flight Test Spacecraft (U)", Lockheed Missiles and Space Co., Report No. SSD-TDR-64-193, Dec. 1964.
11. Personal Communications with W.S. Slomp, NASA-Jangle Research Center. (re: Extensive Development Activities in Metallized Plastic Films for Solar Reflectors and in non-outgassing Adhesives).
12. G.A. Zerlaut, J.E. Gilligan and Y. Harada, "Stable White Coatings", JPL Contract No. 950746, IITRI Report No. C6027-16 (Interim Technical Progress Report), June 30, 1965.
13. NASA Contract No. NAS8-26791, Jan. 4, 1971 to Feb. 15, 1976.
14. H.F. MacMillan, A.F. Sklensky, and L.A. McKellar, "Apparatus for Spectral Bidirectional Reflectance Measurements During Ultraviolet Irradiation in Vacuum", in AIAA Progress in Astronautics and Aeronautics Series, G. Heller, (Ed.) Vol. 18, Academic Press, New York, N.Y., 1966.
15. G.A. Zerlaut and J.E. Gilligan, "Study of In-Situ Degradation of Thermal Control Surfaces", NASA Contract No. NAS8-21074, IITRI Report No. U6061-17 (Interim Summary Report), Mar. 7, 1969; and IITRI Report No. U6061-29 (Final Report), Feb. 20, 1970.
16. F.O. Rogers and G.A. Zerlaut, "Development of S-13G-Type Coatings as Engineering Materials", IITRI Report No. U6053-11 (Final Report), Jet Propulsion Laboratory Contract No. 951746, Mar. 5, 1969.
17. NASA Contract No. NAS8-5379, 20 May, 1963 to 8 Oct. 1971.
18. G.A. Zerlaut and Y. Harada, "Stable White Coatings", JPL Contract No. 950111, IITRI Report No. C207-25 (Summary Report), Aug. 27, 1963.
19. NASA Contract No. NAS8-26791, Jan. 4, 1971 to Feb. 15, 1976.

1.4.2 Uncited Bibliography

J.E. Richmond, (ed.) Measurement of Thermal Radiation Properties of Solids, NASA SP-31, National Aeronautics and Space Administration, Washington, D.C., 587pp., 1963.

S. Katzoff, (ed.), Symposium on Thermal Radiation of Solids, NASA SP-55, National Aeronautics and Space Administration, Washington, D.C., 620 pp., 1965.

Space Simulation Conference, American Society for Testing and Materials, Philadelphia, Pennsylvania, 219pp., 1967.

G.B. Heller, (ed.), Thermophysics of Spacecraft and Planetary Bodies, Radiation Properties of Solids and The Electromagnetic Radiation Environment in Space, Academic Press Inc., New York, New York, 975 pp., 1967.

Proceedings of the Institute of Environmental Sciences 14th Annual Technical Meeting "New Horizons", Institute of Environmental Sciences, Mt. Prospect, Illinois, 567pp., 1968.

Proceedings, The Environments and Man, Institute of Environmental Sciences, Mt. Prospect, Illinois, 648pp., 1966.

Thermodynamics and Thermophysics of Space Flight, Proceedings, Lockheed Missiles and Space Co., Palo Alto, California, 276 pp., March 23-25, 1970.

Annual Technical Meeting Proceedings, Institute of Environmental Sciences, Mt. Propsect, Illinois, 492pp., 1971.

Space Simulation, NASA SP-298, National Aeronautics and Space Administration, Washington, D.C. 1071pp., 1972.

Space Simulation, NASA SP-336, National Aeronautics and Space Administration, Washington, D.C., 953pp., 1973.

J.W. Lucas, (ed.), Fundamentals of Spacecraft Thermal Design, The Massachusetts Institute of Technology, Cambridge, Massachusetts, 603pp., 1972.

J.C. Richmond, (ed.), Space Simulation, National Bureau of Standards Special Publication 336, Washington. D.C., 984pp., October 1970.

J.B. Rittenhouse, and J.B. Singletary, Space Materials Handbook, NASA SP-3051, National Aeronautics and Space Administration, Washington, D.C., 735pp., 1969.

R.G. Breckenridge, B.R. Russel, and E.E. Hahn, (ed.), Photoconductivity Conference, John Wiley and Sons, Inc., New York, N.Y., 653pp., 1956

H.M. Crosswhite, and H.W. Moos, (ed.), Optical Properties of Ions in Crystals, John Wiley and Sons, Inc., New York, 352 pp., 1967.

L.H. Little, Infrared Spectra of Absorbed Species, Academic Press Inc., New York, New York, 428 pp., 1966.

H.C. van de Hulst, Light Scattering by Small Particles, John Wiley and Sons, Inc., New York, New York, 470pp., 1957.

D. McIntyre, and F. Gormick, (ed.), Light Scattering from Dilute Polymer Solutions, Gordon Breach Science Publishers, New York, N.Y., 318 pp., 1964.

R.C. Meissner, (ed.), Seventh National Symposium on Vacuum Technology Transactions, Pergamon Press, New York, 427pp., 1961.

C. Giori, T. Yamauchi and F. Jarke, "Investigation of Space Radiation Effects in Polymeric Film Forming Materials", Report No. IITRI C6318-8, Contract No. NAS1-13292, October 1975.

M.E. Siebert, "Inorganic Surface Coatings for Space Applications", Lockheed Missiles and Space Co., Technical Report No. 3-77-61-12, August 1961.

L.J. Leger, and R.W. Bricker, "Apollo Experience Report-Window Contamination" NASA TN-D-6721, March 1972.

J.S. Choate, and V.L. Mongold, "Analysis of Products Evolved from Selected Thermal Control Coating Materials During Ultraviolet Radiation in Vacuum", AIAA Paper No. 69-640, AIAA 4th Thermophysics Conference, San Francisco, California, June 16-18, 1969.

E.G. Cravalho and E.L. Coburn, "The Effect of Thin Surface Films on Radiative Properties of Metal Surfaces", AIAA Paper No. 69-623, AIAA 4th Thermophysics Conference, San Francisco, California, June 16-18, 1969.

C.P. Boebel and M.A. Turner, "Thermal Control Coatings - An Analytical Treatment," Technical Report AFML-TR-70-8, March 1970.

B.W. Kennedy, "Outgassing Contamination of Dielectric Materials Used in the ATM Program", NASA Technical Memorandum NASA-X-53669, November 7, 1967.

M. Lillywhite, and Cassandra, Environmental Awareness, Institute of Environmental Sciences, Second Annual Session, Martin Marietta, Denver Division, April 27, 1971.

J.E. Gilligan and G.A. Zerlaut, "Investigation on the Influence of the Near Solar Space Environment on Low α/ϵ Thermal Control Surfaces," Report No. IITRI U6013-17 (Final Report), February 1966.

J.E. Gilligan and J. Brzuskiwicz, "Development of Space Stable, Low Solar Absorptance, Pigmented Thermal Control Coatings," Report No. IITRI C6166-12 (Final Report), NASA Report CR 66917, November 19, 1969. See also J.E. Gilligan and J. Brzuskiwicz, "A Theoretical and Experimental Study of Light Scattering in Thermal Control Materials," presented at AIAA 5th Thermophysics Conference, Los Angeles, California, June 29, 1970. AIAA Paper No. 70-831.

J.E. Gilligan, "The Induced Optical Properties of Zinc Oxide," presented to AIAA 5th Aerospace Sciences Meeting, New York, New York, January 1967, AIAA Paper No. 67-214. See also J.E. Gilligan, "The Optical Properties Inducible in Zinc Oxide," Progress in Astronautics and Aeronautics: Thermophysics of Spacecraft and Planetary Bodies, Vol. 20, Edited by G.B. Heller, Academic Press, New York, 1967.

J.E. Gilligan and G.A. Zerlaut, "The Role of Gaseous Adsorption in Thermal Coatings Degradation," presented to AIAA/ASTM/IES 4th Space Simulation Conference, Los Angeles, Calif., Sept. 8-10, 1969, AIAA Paper No. 69-1025.

J.E. Gilligan and G.A. Zerlaut, "Combined Space Radiation Environmental Effects in Zinc Oxide and Other White Pigments," presented to 6th AIAA Thermophysics Conference, Tullahoma, Tennessee, April 26-29, 1971.

G.A. Zerlaut, J.E. Gilligan and N.A. Ashford, "Space Radiation Environmental Effects in Reactively Encapsulated Zinc Orthotitanates and Their Paints," AIAA Paper No. 71-449, presented to AIAA 6th Thermophysics Conference, Tullahoma, Tennessee, April 26-28, 1971.

2.0 TECHNICAL DISCUSSIONS

2.1 LOW α_s/ϵ SURFACES

2.1.1 General Qualities

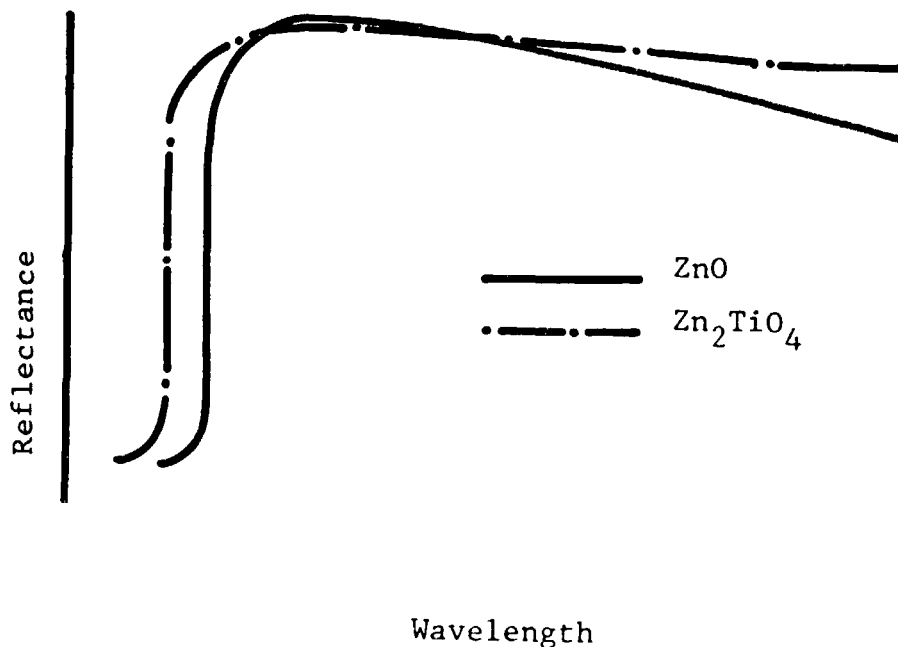
Although no particular intrinsic value resides in the classification of low α_s/ϵ systems, for comparison and for the sake of discussion they may be grouped in three categories:

A: $\alpha_s/\epsilon > 0.25$; B: $0.1 < \alpha_s/\epsilon < 0.25$; and C: $\alpha_s/\epsilon < 0.1$

Category A materials are, for the most part, environmentally unstable but are commercially available or can be obtained by appropriate blending of commercial materials. Category B materials are specially developed materials such as IITRI's S-13G and Z-93, which are covered by NASA Specifications (refs.2.1-2). Category C materials presently available are second surface mirrors (SSMs), transparent dielectric films the rear sides of which are coated with a vapor deposited metal (e.g., Ag, Al) (refs.2.3-4); they are usually difficult to apply and are limited to substrate surfaces which are relatively contourless or have only one radius of curvature. The lack of a paint system in category C provides the justification and incentive for developing zinc orthotitanate paint systems; comparatively, a paint in this category should not only be significantly less expensive but unrestricted in application as far as substrate contours are concerned. There are, however, other important differences between paints and SSM's, e.g., thickness dependence, specularity, outgassing characteristics and adherence to substrates. For paint coatings α_s tends to decrease with thickness and for SSM's to increase. Paints are usually highly diffuse, while the SSM's tend to retain much of the specularity, in the solar regime, of the reflective metal. The outgassing characteristics of paints usually reflect those of the binder; in SSM's especially the glass types, outgassing is nil, except for the adhesives used to mount them.

2.1.2 Optical Requirements

Optical requirements of Category C materials have already been stated in terms of the α_s/ϵ ratio. For α_s/ϵ to be less than 0.1 with $\epsilon \approx 0.92$, α_s must therefore not exceed 0.09. Measurements of some early experimental zinc orthotitanate systems have shown values of 0.085/0.94 (≈ 0.09). In the near earth extra-terrestrial solar intensity spectrum approximately 94% of the sun's energy lies between 325nm (0.325 μ) and 2600nm (2.6 μ). Accordingly for a paint system to have an $\alpha_s < 0.10$ it must have a diffuse spectral reflectance averaging greater than 90% over this spectral range. (As will be seen, many zinc orthotitanate specimens exhibit spectral reflectance values exceeding 95% over a major portion of this range). In Figure 2.1 is a comparison of the spectra of ZnO and Zn₂TiO₄ in the 300-2600nm region. Note that both have very high visible reflectance values, but that Zn₂TiO₄ excels in two important ways: it has a UV cut-off at a shorter wavelength, and, because we can adjust its particle size, it has greater infrared reflectance.



Most dielectrics are strong absorbers (and thus emitters). In stating the optical requirements for the paint systems, we must also indicate how they translate to required properties of the paint components. Physically, we are dealing with a two component system: a pigment dispersed homogeneously in a binder. For maximum solar reflectance the pigment should have a particle size distribution which possesses maximum light scattering effectiveness in the solar spectrum. The pigment must be intrinsically transparent - as non-absorbing (i.e., uncolored) - in the solar spectrum as possible. The solar transparency requirement is equally, if not more, important in the case of the binder; additionally, the binder should have a low value of the refractive index.

2.1.3 Physical Requirements

Separating the paint system again into its two major components we can outline their respective physical requirements. Table 2.1 lists some of their more desirable properties.

The context in which each of these properties is important can vary greatly depending upon the criteria of performance. Many of the so-called "requirements" listed are not peculiar to each category; thus, particle size is an important consideration from a physical point of view, because of dispersion requirements, as well as from an optical point of view, because of light scattering characteristics.

2.1.4 Application Requirements

In its broadest sense, the term application covers a multiplicity of practical requirements ranging from thoroughness of substrate preparation, to curing conditions, and to cost. It is not possible to quantify all of these considerations, much less use them directly in the formulation of paint systems. Ease of application, another general requirement, implies achievement of an effective coating without the necessity for complicated or unusual procedures. Ideally, a paint system could be applied as a single, air-curing coat to any substrate without the necessity for any prior surface preparation or primer.

Table 2-1

Requirements for Physical Properties of Paint Components

Pigment

High melting point*
Optimum particle size (distribution)
High index of refraction
Crushable/grindable
Stable in highly divided form
Insolubility
Binder-wettable

Binder

Film-forming capability
Pigmentable
Adherence (with primers, if necessary)
High melting/decomposition temperature*
High softening temperature*
Forms impervious, flexible films*

*not necessary but desirable and useful

Since every experimental coating must be applied to test coupons for optical measurements, ultraviolet irradiation or similar tests, a substantial amount of experience is thus generated in so doing. In almost every instance substrate preparation is the most important preliminary requirement. When primers are required, their application will be critical.

Without exception the paints developed in this program have been formulated for spray application, rather than for brush or other methods. The wide range of individual tastes and practices in paint application make it mandatory that the viscosity of paint formulations be readily modifiable by addition of appropriate thinners to achieve preferred consistencies.

REF
ORIG.

Whether or not a TC material will indeed be used in spacecraft applications depends strongly upon many practical considerations. Generally, it must be compatible with and adhere to a variety of substrates, be applied with reasonable ease and be cost-effective. Adherence is frequently very difficult to achieve, and primers or adhesion promoters are required in addition to careful substrate surface preparation procedures.

Cost may be the ultimate criterion of practicality, since many aspects of practicality are, at least theoretically, reducible to cost - either in terms of direct application costs or indirectly in terms of reduced mission performance. Although it would seem that the practicality of a TC material could be expressed quantitatively, on a unit area basis as, for example, $\$/\alpha_s$ or $\$/(\Delta\alpha_s/ESH)$, such indices fail to account for the myriad of other important practical and technical requirements, some of which may be highly mission-specific.

2.2 ENVIRONMENTAL STABILITY

Since the earliest days of R&D of spacecraft thermal control materials, comparatively little effort has been devoted to understanding the fundamental mechanisms of optical degradation in the space environment (refs. 2.5-7). More than any other single aspect of spacecraft thermal control (TC), environmental stability ranks as the most important - by far. Regardless of what other properties a candidate TC material might have, no responsible designer would employ any TC material without having at least a rough estimate of that material's space environmental stability, i.e., of its time rate of change of α_s and ϵ with space exposure.

The total exposure to active degradative influences depends heavily upon orbital parameters. The actual exposure of spacecraft surfaces to solar electromagnetic and particulate radiation fluxes in general depends upon their orientation, orbital parameters and time. All space vehicles will encounter solar electromagnetic radiation, but not necessarily particulate radiations

(e.g., alpha particles, protons, and electrons, as in the Van Allen belts and auroral regions). Unless otherwise indicated the term environment in the remainder of this report refers to the low-orbit, near-earth environment. The charged particle radiation studies reported in a subsequent section imply much higher orbits or interplanetary environments, and consequently should be viewed as extensions to the basic low earth orbit information gained in the environmental tests.

As we use it here the term "environmental stability" holds the more restricted, though conventional, meaning of stability to in-vacuo solar UV radiation. The latter is nominally defined as the energy in the extraterrestrial solar spectrum (at the earth's distance from the sun, 1 A.U., below 400nm (0.4μ)). Most of the space radiation tests were conducted using simulated solar electromagnetic radiation. Stability to particulate radiation, nevertheless, has been estimated for several of the more advanced pigment systems. By convention, environmental stability is measured in terms of the $\Delta\alpha_s$ resulting from an exposure to a specified amount of UV radiation (expressed in units of ESH, equivalent sun-hours). More precisely, ESH refers to the total amount of equivalent solar UV radiation.

Environmental tests serve several purposes including that of predicting the performance of a material in space applications. Unfortunately, lab and flight test data do not always agree (refs. 2.8-9); inevitably, flight data show more degradation than would be expected from lab predictions. The explanations depend on individual circumstances, but usually involve prelaunch and/or in-flight contamination or inadequate simulation of the radiation environment. The results of several Skylab experiments (refs. 2.10-12) offer dramatic evidence of in-flight contamination.

In any event, space environmental stability depends very importantly on the surface conditions of the thermal control surfaces at launch. IITRI has consistently and strongly recommended the protection of thermal control surfaces prior to launch.

An IITRI study (ref. 2.13) showed the effects of an oceanside environment (NASA-KSFC) on unprotected S-13G surfaces. These and other studies make it patently clear that prelaunch protection of thermal control surfaces is absolutely essential. Unless this is accomplished, the intrinsic stability of any affected material may be seriously compromised and the validity of any predictions of in-flight performance, such as those made from the model given in Appendix II may also be lost. Nevertheless, properly interpreted laboratory test data remain a highly valid tool for such predictions; however, because of unpredictable circumstances, they can only reflect ideal performances.

The prediction of environmental stability traditionally had been accomplished without consideration of the effects of contamination or space charge accumulation (SCA). We will, for the sake of completeness, discuss these two phenomena briefly because they have recently become the subject of intense discussion and of moderate R&D efforts (ref's 2.14-18). Appendix III provides more detail on contamination parameters; and Appendix IV, some brief remarks on electrical conductivity and its role in Space Charge Accumulation (SCA). Contamination long ago (ref. 2.19) was pointed out as a critically important factor affecting spacecraft performance.

The term "contamination" usually refers to the outgassing products of materials and to their subsequent condensation on surfaces, and most importantly to the possible changes in the optical properties of the latter. Of equal importance, however, is the concept of contaminability - the facility with which a surface attracts and/or retains a condensed substance. Con-

taminability is quite probably affected by surface charge distribution and overall "passivity" of surface absorbates (which may not necessarily be easily outgassed).

Space charge accumulation (SCA) results from the accumulation of and interaction with energetic charged particles, e.g., those of the solar wind, the van Allen Belts, and polar Aurorae. The differing dielectric properties of the various surface materials of a spacecraft compound the problem of dissipating charges. SCA can be, under certain circumstances, very destructive to surface materials (refs. 2.20-21). As charges accumulate, including those due to secondary electron emission, the local potential may exceed the dielectric strength of the material. Electrical discharges may occur, especially at localized flaws or surface defects, resulting in severe local mechanical failures.

We have addressed the overall contamination problem in developing zinc orthotitanate paint systems, primarily in terms of reducing binder outgassing. While we are aware of the SCA problem, we have not undertaken any efforts to reduce the susceptibility of zinc orthotitanate paint system to SCA effects. Contamination poses a risk in any spacecraft application; SCA effects may or may not. Consequently, we urge that potential users of zinc orthotitanate paint systems (of any TC material, for that matter) consider the potential of SCA toward mission degradation for their particular mission(s).

2.3 SUMMARY REMARKS

Environmental stability connotes the ability of a TC material to remain unaltered in its optical properties after exposure to active degradative agencies whose magnitude(s) may, and frequently do, vary with time and orbital parameters. Although solar UV radiation is a predominant degradative agency especially in the near-earth environment, additional, but not necessarily linearly additive, optical degradation occurs as a result of concurrent exposure to massive energetic radiation. In the discussions of environmental test results we will

analyze the reflectance changes spectrally, associating changes in certain-spectral regions with a specific material defect and with their causes. This approach allows an explanation of so-called synergistic effects. Furthermore, it contrasts, but is by no means incompatible, with the more engineering-oriented understanding of $\Delta\alpha_s$ vs ESH. We will make these relationships more clear in a succeeding section where the spectra of irradiated materials are analyzed in detail. The important points to observe here are 1.) that environmental degradation implies that each active environment produces one or more characteristic spectral reflectance changes, 2.) that the magnitude of each induced change is proportional to the appropriate magnitudes (including time) of the agency producing it, and 3.) that the total change, measured in terms of $\Delta\alpha_s$, is the summation of all of these spectral changes relative to the solar intensity spectrum. Environmental stability, at least from a materials standpoint, thus results from minimizing the spectral response of a material to a degradative agency, especially in the spectral regions of greatest solar intensity. This in turn is accomplished by adjusting paint compositions in accordance with the optical, physical and applications requirements which the paint system must also meet.

2.4 BIBLIOGRAPHY

2.1 CITED REFERENCES

1. "Paint, S-13G, Temperature Control, Specification For", NASA-Marshall Space Flight Center, Specification No. 10M01835, Rev. C., Mar. 26, 1969; and
"Paint, S-13G, Temperature Control, Application of, Specification For", NASA-Marshall Space Flight Center Specification No. 10M01836. Rev. I.
2. "Paint Z-93, Temperature Control, Specification For", NASA-Marshall Space Flight Center, Specification No. 10M01837; and
"Paint, Z-93, Temperature Control, Application of, Specification For", NASA-Marshall Space Flight Center Specification No. 10M01838.
3. W.S. Slomp, Personal Communications (re: NASA-Langley Research Center Development Activities in Metallized Teflon for low α_s/ϵ spacecraft applications).
4. Optical Solar Reflector "OSR", basically, a silver coated quartz second surface mirror, available commercially from Optical Coatings Laboratory, Inc., Santa Rosa, Calif.
5. H. Levin, V.R. Honnold, and C. C. Berggren, "Study of Color Center Formation in White Powder Compounds", Hughes Aircraft Co., NASA Contractor Report No. CR-73337, July, 1969.
6. G.A. Zerlaut and J.E. Gilligan, "Study of In-Situ Degradation of Thermal Control Surfaces", NASA Contract No. NAS8-21074, IITRI Report No. U6061-17 (Interim Summary Report), March 7, 1969, and IITRI Report No. U6061-29 (Final Summary Report), Feb 20, 1970.
7. W.T. Peria, "Optical Absorption and Photoconductivity in Magnesium Oxide Crystals", Phys. Rev. 112, (2), p. 423, Oct. 1958.
8. N.J. Stevens and G.R. Smolak, "Report on The Flight Performance of the Z-93 White Paint Used in the SERT-II Thermal Control System," AIAA Paper No. 71-455, Presented to AIAA 6th Thermophysics Conference, Tullahoma, Tenn., Apr. 26-28, 1971.

Cited References (Cont'd)

9. J.J. Triolo, "General Aspects of Space Simulation Validity and Comparison Between Laboratory and In-Flight Degradation", Presented to International Symposium on Simulation and Space, Toulouse, France, Sept. 10-14, 1973.
10. W.L. Lehn and C.J. Hurley, "Skylab DO24 Thermal Control Coatings and Polymeric Films Experiment," AIAA Paper No. 74-1228, Presented to AIAA/AGU Conference on Scientific Experiments of Skylab, Huntsville, Ala., Oct. 30-Nov. 1, 1974; Also issued as U.S. Air Force Materials Lab Report No. AFML-TR-75-77, March 1975.
11. W.L. Lehn and C.J. Hurley, "Results of the Polymeric Films Skylab DO24 Experiment," AIAA Paper No. 75-689, Presented to AIAA 10th Thermophysics Conference, Denver, Colo., May 27-29, 1975; also issued as U.S. Air Force Materials Laboratory Report No. AFML - TR - 75-165, Aug. 1975.
12. J.A. Muscari, Skylab T027 Contamination Experiment, Martin-Marietta Corp., "Optical Scattering and Contamination Experiment", NASA Contract No. NAS8-21495.
13. J.E. Gilligan and H.M. King, "The Vacuum-Ultraviolet Degradation of Salt-Spray-Contaminated Thermal Control Coatings", Presented to Seventh Conference on Space Simulation, Los Angeles, Calif. Nov. 12-14, 1973, and published in NASA SP-336, 1973; also IITRI Report No. C6258-5 (Final Report), 27 Nov. 1972.
14. Proceedings of 8th Space Simulation Conference, Nov. 3-5, 1975, Silver Spring, Md.
15. Proceedings of 7th Space Simulation Conference, Los Angeles, Calif. Nov. 12-14, 1973, NASA SP-336, 1973
16. "Fundamentals of Spacecraft Thermal Design," Vol. 29 Progress in Astronautics and Aeronautics, Ed. by J.W. Lucas, MIT Press, Cambridge, Mass., June, 1972.
17. A. Rosen, "Large Discharges and Arcs on Spacecraft", AIAA J. Astronautics and Aeronautics, pp. 36-44, June 1975; see also A. Rosen, "Spacecraft Charging: Environment-Induced Anomalies", AIAA Paper No. 75-91, presented to AIAA 13th Aerospace Sciences Meeting, Pasadena, Calif., Jan. 20-22, 1975.

Cited References (Cont'd)

18. G.T. Inouye, "Spacecraft Charging Model", AIAA Paper No. 75-225, Presented to AIAA 13th Aerospace Sciences Meeting, Pasadena, Calif., Jan. 20-22, 1975.
19. V. L. Mangold, "The Origin of Deposits Formed on the Surface of Thermal Control Materials by the Action of Extreme Ultraviolet Radiation", U.S. Air Force Flight Dynamics Laboratory Report No. AFFDL-TR-68-155, February, 1969.
20. L.B. Fogdall et. al, "Combined Environmental Effects on Polymers," Presented to 8th Space Simulation Conference, Nov. 3-5, 1975, Silver Spring, Md.
21. L.B. Fogdall and S.S. Cannaday, "Effects of High Energy Simulated Space Radiation on Polymeric Second-Surface Mirrors," Boeing Aerospace Final Report (under NASA Contract No. NAS1-13530) No. CR-132725, Oct. 1975.

3.0 PIGMENT STUDIES

A great deal of research has been performed to obtain pigment materials stable to the ultraviolet-vacuum environment. Much of the early screening of inorganic powders was conducted at IITRI and has been documented in several reports (Refs. 3.1-3). From this work, zinc oxide and subsequently zinc orthotitanate (Zn_2TiO_4) were determined to be the most stable pigments.

The purpose of the pigment technology studies was to develop methods for producing zinc orthotitanate (Zn_2TiO_4) thermal control pigments of high reflectivity (low α_s) and stability. These production methods were to be amenable to scale-up so that moderately large quantities of pigment powder, e.g., ten pound batches, could be produced. Coprecipitation, reaction sintering, and heat treatment studies were conducted.

In addition, a limited amount of investigative effort was devoted to pigments other than Zn_2TiO_4 . The details of the various studies are presented in the following sections.

3.1 ZINC ORTHOTITANATE STUDIES

3.1.1 Background

Studies conducted at IITRI have demonstrated that zinc orthotitanate has excellent potential as a pigment for solar reflector coatings (Ref. 3.3). A flow diagram for the previous synthesis method for Zn_2TiO_4 used at IITRI is shown in Figure 3.1. The process is one of reacting zinc oxide with titanium dioxide. A series of grinding and mixing operations are carried out at low temperature to assure good particle-to-particle contact, and hence, reactivity, of the two oxides. Formation of the Zn_2TiO_4 pigment is accomplished by firing at 925°C for 18 hours, additional grinding, followed by reactive encapsulation and/or induction plasma calcining (Ref. 3.4) to obtain a stable product. A total of 4 hours of wet grinding and 1/2 hour of dry grinding is conducted prior to firing and

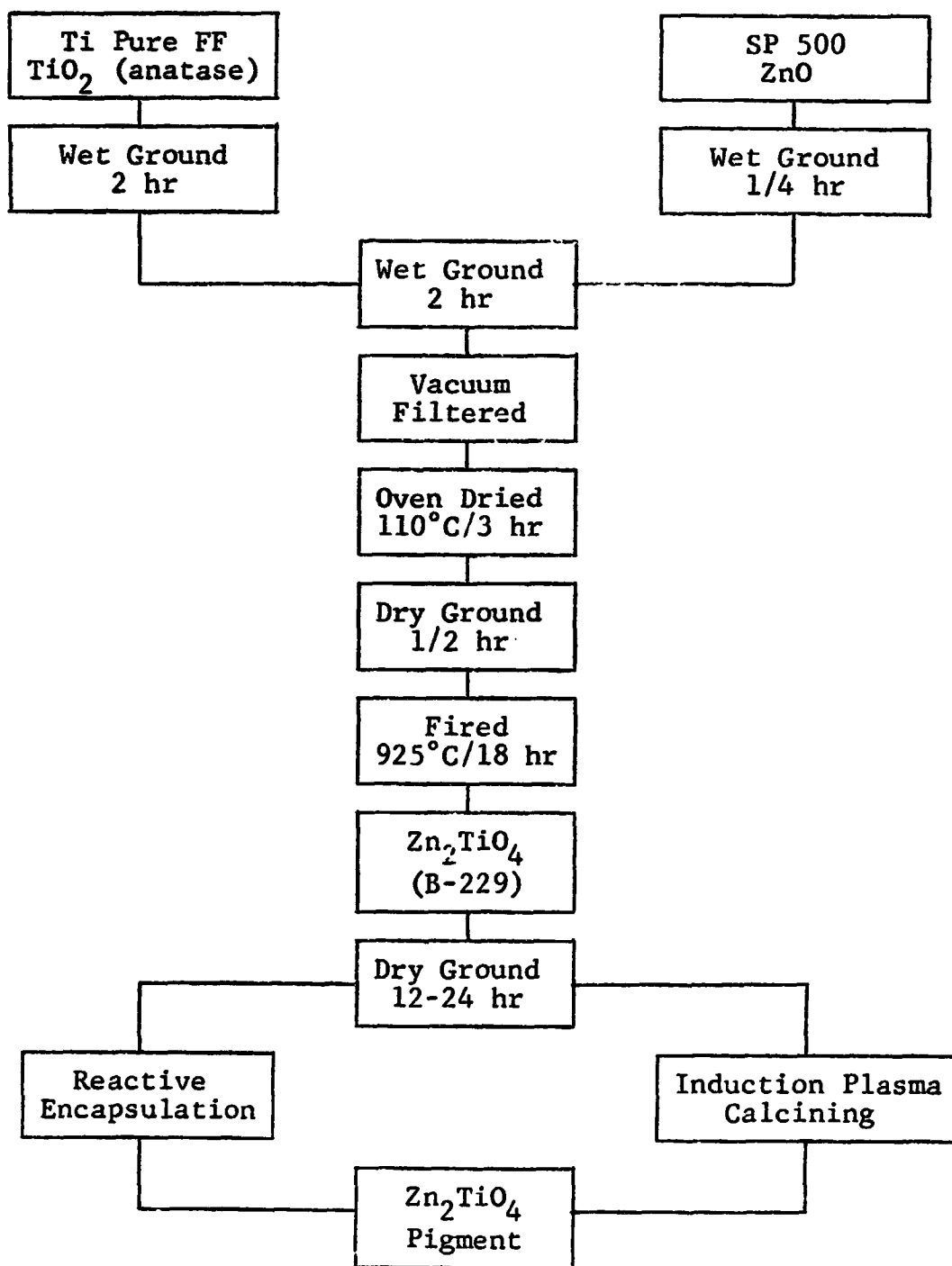


Figure 3.1 FLOW DIAGRAM FOR B-229 SYNTHESIS OF ZINC ORTHOTITANATE PIGMENT (Ref 3.4).

this is followed by an additional 12-24 hours of grinding for comminution of the Zn_2TiO_4 product.

Spectrographic analysis of a series of zinc orthotitanates prepared by this method revealed the following major impurities (Ref. 3.5):

<u>SAMPLE</u>	<u>GRIND TIME</u>	<u>Si</u>	<u>Al</u>
A-0	24 hrs	0.5	0.3
B-0	24 hrs	1.2	0.7
D-0	12 hrs	0.1	0.25

The rather large amounts of Al and Si may be attributed to contamination from the porcelain grinding balls and would appear to be a function of grind time. Such impurities in a material can be a source of optical degradation in an ultraviolet-vacuum environment. Minimization of grinding times would reduce contaminants and minimize introduction of crystallographic defects. This should be beneficial in obtaining improved stability and was one of the aims of the study.

Stabilization of zinc orthotitanate subsequent to its synthesis at 925°C to prevent optical degradation is accomplished by the following methods: reactive encapsulation and/or very high heat treatment by induction plasma calcining. The latter process involves a rather sophisticated apparatus, and the yield is somewhat low.

In the current study, attempts were made to obtain stable Zn_2TiO_4 by either elimination or simplification of the various steps shown in Figure 3.1. The means by which this was to be accomplished was: 1) the use of salt precursors to obtain enhanced reaction; 2) the use of coprecipitation to achieve intimate mixing of these precursors; and 3) the use of rapid heat treatment methods to minimize particle size growth.

The production techniques which have been investigated are:

1. Coprecipitation - Obtaining an intimate zinc salt-titanium salt mixture by coprecipitation and firing of this product at relatively low temperatures (600°-1000°C) to produce Zn_2TiO_4 .
2. Reaction Sintering - Reaction of a physical mixture of a zinc compound with a titanium compound by rapid firing (less than 2 hours) at 900° - 1400°C.
3. Heat Treatment of Powders - Accelerated heat treating of powders by flash heating (heating and cooling ramp times of less than 15 minutes each with soak times at temperature of about 2 hours).

3.1.2 Methods of Evaluation

In the studies of preparing zinc orthotitanate, evaluation methods primarily used were gravimetric, x-ray, and scanning electron microscopy (SEM). Weight change data due to chemical reaction, decomposition, or calcination, were used to monitor completeness or the extent of any of these processes by comparison with theoretical behavior. X-ray analysis was used routinely for phase identification. The size and shape of powder particles could be determined readily with the use of the SEM.

3.1.2.1 Gravimetric Analysis

Weight measurements were made on precipitated materials after they had been dried at 90°C/4 hours, and calcined powders were weighed after cooling to ambient temperature. Amounts up to 200 grams were weighed to 0.0001 grams, and larger amounts were weighed to a tenth of a gram. These accuracies were also maintained in the preparation of reactants, both in solid or solution forms.

3.1.2.2 X-Ray Analysis

Debye-Scherrer powder patterns were employed to identify different phases in a particular sample by comparison with standard National Bureau of Standards data. Line intensity was also used as an estimate for quantitative analysis. Nelson-Riley plots were employed to determine lattice constants. Detailed description of these techniques can be found in the literature (Ref. 3.6).

Certain limitations existed in material identification by X-ray methods. Phases were not detected if they were amorphous or non-crystalline, were in small quantity (generally 4 to 5% or less of the total sample), were extremely fine in size (<100 angstroms), or were poorly crystallized. Examples are discussed in the text of this report.

3.1.2.3 SEM Analysis

Examination of powder particles by SEM was carried on at Marshall Space Flight Center (NASA) by Mr. D.W. Gates, Project Monitor, using a JEOL JSM U-3 instrument. Sample preparation consisted of the following steps: 1) disperse powder in USP ethyl alcohol; 2) transfer powder-alcohol to a brass stub sample holder using a capillary tube; and 3) air dry. Three samples were placed on a stub as depicted below, thus permitting rapid examination and comparison without removal of the stub from the SEM.



Using this method of depositing very thin sample layers, it was determined that a conductive coating to prevent charge build-up was not necessary. Dispersion of particles was excellent, permitting examination of discrete grains.

3.1.2.4 Optical Analysis

The reflectance spectra of Zn_2TiO_4 pigments were also used to characterize these materials in terms of α_s and $\Delta\alpha_s$, i.e., stability to ultraviolet irradiation in vacuum. Additionally, reflectance characteristics in the near ultraviolet from 0.325 to 0.5 microns revealed compositional information. The location of the absorption edge as well as the "knee" reflectance were used to determine the existence (or lack thereof) of free TiO_2 and ZnO . These analyses will be treated separately subsequently.

3.2 SYNTHESIS BY COPRECIPITATION/CALCINATION (COP)

The purpose of the coprecipitation method is to obtain an intimate mixture of zinc and titanium compounds. This excellent mixing along with the highly reactive nature of the oxides derived upon decomposition of these compounds, permits conversion to Zn_2TiO_4 under moderate conditions of $600^\circ\text{C}/2$ hrs. Other investigators (Refs. 3.7 and 3.8) have shown that higher temperatures and/or longer times are necessary using less reactive zinc and titanium precursors.

The coprecipitation method involves the simultaneous addition of a mixed solution of zinc and titanium chlorides to a solution of oxalic acid. The resulting solution is then heated to and held at a specified temperature, during which time it is continuously stirred while the precipitate is formed.

The zinc and titanium sources were Reagent Grade ZnCl_2 and Purified TiCl_4 , and the oxalic acid was Reagent Grade. Zinc chloride and oxalic acid solutions were prepared by conventional dissolving of the crystals in distilled water at 40°C . The TiCl_4 solution was prepared by dropwise addition of the TiCl_4 into distilled water which was cooled in an ice bath in order to prevent formation of hydrolyzed titanium.

Precipitation of mixed oxalates was conducted by addition of a mixed chloride solution (having varying Zn to Ti ratio) to oxalic acid at 40°C. This was followed by heating of the system with stirring to 90°C where it was held from one to four hours, the hold time depending on the batch size.

Filtration was performed in a Buchner funnel system under slight vacuum. The precipitate was washed thoroughly with hot water until there was no evidence of acid in the filtrate.

Calcination and firing were performed in standard atmospheric Globar furnaces. Powders were contained in fused silica boats for firings up to 1300°C and in platinum crucibles at 1400°C.

A flow diagram for this process is shown in Figure 3.2 and is summarized in Table 3.1. The designation "TiOX" is used in this document for the reaction product of TiCl_4 with oxalic acid. As shown later in this report, this material was not completely characterized in the course of this program.

Various effects affecting the coprecipitation process were examined during the course of the program. These are discussed in the following sections.

3.2.1. Precipitation Effects

The initial step in the coprecipitation study was to optimize the technique for rapid mixing of reactants, and for obtaining reproducibility. The variables were the oxalic acid solvent (water or alcohol), starting mixture (mol ratio of Zn:Ti), addition method (dropwise or direct dump), and reaction rates and conditions (temperature and holding time). Precipitations were carried out in an all Pyrex system to preclude contamination such as iron. Gross compositions of the precipitates were evaluated using x-ray techniques.

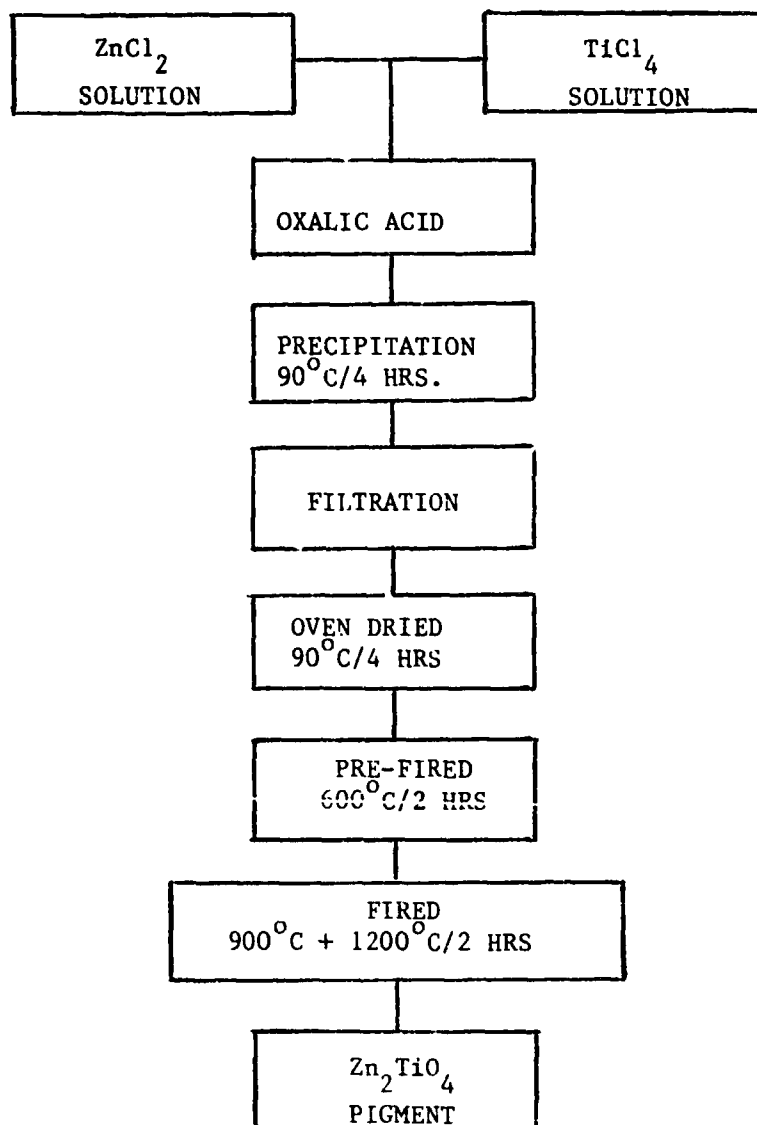
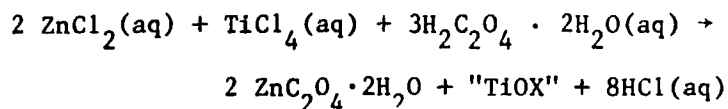


Figure 3.2 FLOW DIAGRAM OF COPRECIPITATION (COP) PROCESS FOR SYNTHESIS OF Zn_2TiO_4 PIGMENT

TABLE 3.1
COPRECIPITATION PROCESS OF Zn_2TiO_4 PRODUCTION

Coprecipitation Reaction:



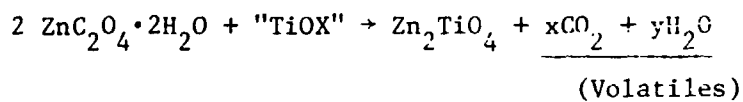
Materials Preparation:

- 1) Mix 20% $TiCl_4(aq)$ and 20% $ZnCl_2(aq)$ solutions to obtain 2:1 mol ratio of zinc to titanium (cold).
- 2) Prepare 15% oxalic acid(aq).

Coprecipitation Procedure:

- 1) Heat oxalic acid solution to $40^\circ C$, add mixed chloride solution with stirring;
- 2) Heat to $\sim 90^\circ C$ with stirring, and digest for 4 hours at $90^\circ C$ with stirring;
- 3) Cool, and filter precipitate (mixed oxalates) with generous water washings until pH = 7; and
- 4) Dry at $90^\circ C/4$ hr.

Calcination Reaction (Conversion):



Pre-Calcination:

$600^\circ C/2$ hrs (time to $600^\circ C \sim 30$ min).

Flash Calcination:

Insert directly into furnace at desired temperature and remove after required hold time; the following schedules are representative:

<u>Temp., °C</u>	<u>Time to Temp., Min.</u>	<u>Hold Time, Min.</u>	<u>Container</u>
1050	~ 7	120	fused quartz
1200*	~ 8	120	fused quartz
1400	~ 10	5	platinum

Hand-pulverize pigment (minimal) to reduce agglomerates.

Acetic Acid Treatment (Free ZnO Removal):

- 1) Treat pigment in 50% acetic acid at $80^\circ C/1$ hr with stirring;
- 2) Filter with repeated water washing until pH ≈ 7 ;
- 3) Dry at $120^\circ C/16$ hr.
- 4) Calcine at $1000^\circ C/2$ hrs (time to $1000^\circ C \approx 1$ hour).

*A $1200^\circ C$ flash calcination appears to produce Zn_2TiO_4 of optimum physical and optical properties.

Firing of these materials was conducted at 900°C for 2 hrs in fused quartz or porcelain containers, and the resulting powders were examined by x-ray diffraction to determine gross composition and crystal structure. The temperature and time conditions of calcination (900°C for 8 hr) for the early studies were selected because previous studies had established that under such conditions a stable product was obtained (Ref. 3.4); and, of course, they were established in order to compare on an uniform basis products prepared under parametric conditions.

Theoretically, the use of a 2:1 mole ratio of Zn to Ti in the mixed chloride solution should yield titanate of the desired stoichiometry, i.e., Zn_2TiO_4 . Previous experience had also shown (Ref.3.4) that in the mixed oxide reaction, an excess of ZnO in the product was very much preferred to an excess of TiO_2 , mainly because of the latter's insolubility and thus its unextractability. An initial objective of this work was thus to determine the effect of the Zn:Ti mol ratio on the composition of the final product.

The effect of using water or methyl alcohol as the solvent for oxalic acid was also examined. To simplify and speed up this step in the processing, the mixed chlorides were added rapidly to the oxalic acid solution at room temperature. The systems were then heated to 90°C in the case of water, or to 55°C in the case of alcohol to complete the precipitation. After cooling, the solid product was obtained and heat treated at 900°C for 8 hr to obtain Zn_2TiO_4 . The product was of a particle size small enough for direct use as a pigment, thus precluding the possibility of contaminant introduction in any grinding process that might be employed.

The data in Table 3.2 summarize the initial studies of co-precipitation. X-ray analyses showed that the precipitation product in the water system was two-phased, consisting of zinc oxalate and a second crystalline material which is designated as "TiO X". No standard X-ray pattern corresponding to the pattern

Table 3.2

EFFECT OF INITIAL Zn:Ti MOL RATIO ON COPRECIPITATION

Batch No.	Zn:Ti Mol Ratio in Mixed Chlorides	Precipitation			Precipitation Product	Fired Product, 900°C/8 hr
		Solvent for Oxalic Acid	Temp., °C	Time, min.		
LH-2	4:1	Water	90	5	$\text{ZnC}_2\text{O}_4 \cdot 2\text{H}_2\text{O} + \text{"TiO"}_2$	$\text{Zn}_2\text{TiO}_4 + \text{ZnO}$
LH-5	2:1	Water	90	5	$\text{ZnC}_2\text{O}_4 \cdot 2\text{H}_2\text{O} + \text{"TiO"}_2$	$\text{Zn}_2\text{TiO}_4 + \text{ZnO}$
LH-8	1.5:1	Water	90	5	$\text{ZnC}_2\text{O}_4 \cdot 2\text{H}_2\text{O} + \text{"TiO"}_2$	$\text{Zn}_2\text{TiO}_4 + \text{TiO}_2$
LH-4	4:1	Methanol	55	5	$\text{ZnC}_2\text{O}_4 \cdot 2\text{H}_2\text{O}$	$\text{Zn}_2\text{TiO}_4 + \text{ZnO}$
LH-9	3:1	Methanol	55	5	$\text{ZnC}_2\text{O}_4 \cdot 2\text{H}_2\text{O}$	$\text{Zn}_2\text{TiO}_4 + \text{ZnO}$
LH-6	2:1	Methanol	55	5	$\text{ZnC}_2\text{O}_4 \cdot 2\text{H}_2\text{O}$	TiO_2
LH-16	2:1	Water	90	60	$\text{ZnC}_2\text{O}_4 \cdot 2\text{H}_2\text{O} + \text{"TiO"}_2$	$\text{Zn}_2\text{TiO}_4 + \text{ZnO}$
LH-13	2:1	Methanol	55	60	$\text{ZnC}_2\text{O}_4 \cdot 2\text{H}_2\text{O}$	$\text{Zn}_2\text{TiO}_4 + \text{TiO}_2$

of this second phase could be found in the literature. Communication with NBS personnel revealed that this was indeed a new compound.

Analyses of fired products of water-based systems showed that using a Zn:Ti mole ratio of 2:1 or higher resulted in zinc orthotitanate plus free zinc oxide. The 2:1 ratio (Zn:Ti) using a one hour hold during precipitation, followed by a 900°C/8 hr firing, produced a Zn_2TiO_4 product with very small amounts of excess ZnO.

In the alcohol systems, there was no evidence of "TiOX" in any of the precipitates. As shown in Table 3.2, all of the methanol systems precipitates gave x-ray patterns of zinc oxalate with no evidence of any crystalline titanium phase. However, all of the precipitates when fired at 900°C for 8 hr yielded free TiO_2 or Zn_2TiO_4 . Thus the titanium phase in the precipitate is either extremely fine or is in an amorphous state. For the alcohol system, a Zn:Ti mole ratio in excess of 2.5:1 but less than 3:1 was necessary to obtain Zn_2TiO_4 with no TiO_2 and a minimum of excess ZnO.

3.2.2 Scale-Up Studies

The early work in coprecipitation of oxalates from the mixed chlorides revealed a low yield of about 59 to 71% of theoretical. The low yield may be attributed to non-optimum precipitation conditions, e.g., too low a temperature, short times, and/or insufficient amounts of reactants. In efforts to increase this yield, the amount of oxalic acid involved in the reaction was increased to a 40 mol % excess. As the data in Table 3.3 show, this resulted in an increase to about a 90% yield as seen by comparing data from batch LH-16 with those from batch LH-20. Furthermore, the fired product of LH-20 showed no X-ray evidence of ZnO, indicating a close approach to the 2Zn/Ti stoichiometry.

Table 3.3

EFFECTS OF OXALIC ACID CONCENTRATION AND REACTION TIMES ON COPRECIPITATION

Batch No.	Precipitation		Fired Product, 900°C/8 hr
	Temp, °C	Time, Min.	
LH-16*	90	60	Zn ₂ TiO ₄ + ZnO
LH-20**	90	60	Zn ₂ TiO ₄
LH-22***	90	60	Zn ₂ TiO ₄ + ZnO
LH-30***	90	120	Zn ₂ TiO ₄ + ZnO
LH-31***	90	240	Zn ₂ TiO ₄

* 0 mol % excess oxalic acid.

** 40 mol % excess oxalic acid, also used for LH-22, -30, and -31.

*** Large batch, ~200 g precipitate

Note: All precipitates showed ZnC₂O₄·2H₂O and "TiOX" as identified by X-ray analyses.

The batch amounts for LH-1 through LH-20 were 50 grams of precipitate. In experiments designed to obtain a precipitate of 200 grams, the initial results (see LH-22) showed a lowering of precipitate yield to 78%, and the fired product contained amounts of excess ZnO detectable by x-rays. In efforts to increase the yield, digestion (hold) times were increased to 2 hr (LH-30) and 4 hr (LH-31). The yield was increased to about 90% by these longer holds as seen in Table 3.4. In the fired products, LH-30 showed very faint x-ray lines for ZnO whereas LH-31 showed none.

Larger batch production of zinc orthotitanate was continued in the LH-50 series. Three 200 gram mixed oxalate precipitates (designated LH-51, LH-52 and LH-53) were prepared. The first two of these batches were digested for 4 hours at 90°C; it was established previously that under these conditions a relatively pure Zn_2TiO_4 would result on subsequent firing. The third batch, LH-53, was digested for 8 hours in an effort to increase the yield. The percent yields obtained, based on mole % of theoretical, for the three precipitates were 90.5%, 93.5%, and 93.1% for LH-51, LH-52 and for LH-53, respectively. These data show that extending the digestion time from 4 to 8 hours does not increase the yield. In this particular precipitation process, an equilibrium is apparently attained after about 4 hours. The final scale-up in this program involved precipitate batches of about 1000 grams in the LH-100 series. These along with pertinent batches of smaller size are summarized in Table 3.4.

The results of these studies show that for obtaining Zn_2TiO_4 of minimum ZnO excess reproducibly, the following parameters are of importance:

- 1.) Use of water as opposed to methyl alcohol as the solvent for oxalic acid.
- 2.) Use of a 2:1 mol ratio of zinc to titanium in the mixed chlorides.
- 3.) Use of about a 40 mol% excess oxalic acid in the reaction; and
- 4.) Precipitation at 90°C with a 4 hour hold.

Table 3.4

SUMMARY OF COPRECIPITATED BATCHES

Batch No.	Raw Materials, gms			Precipitation		Yield, gms
	ZnCl ₂	TiCl ₄	H ₂ C ₂ O ₄	Time, hrs.		
LH-20	28.0	20.0	62.7	1		50
LH-22	112.0	80.0	250.8	1		170
LH-30	112.0	80.0	250.8	2		197
LH-31	112.0	80.0	250.8	4		202
LH-51	112.0	80.0	250.8	4		200
LH-52	112.0	80.0	250.8	4		206
LH-53	112.0	80.0	250.8	8		205
LH-101	560.0	400.0	1254.0	4		965
LH-102	560.0	400.0	1254.0	4		970
LH-103	560.0	400.0	1254.0	4		990
LH-104	560.0	400.0	1254.0	4		1010
LH-105	672.0	480.0	1505.0	4		1175
LH-107	672.0	480.0	1505.0	4		1157
LH-108	672.0	480.0	1505.0	4		1180
LH-109	672.0	480.0	1505.0	4		1167
LH-110	672.0	480.0	1505.0	4		1153

3.2.3 Sample Designation

Synthesis of zinc orthotitanates by coprecipitation and calcination involves a series of standardized operations. In order to render sample designations as descriptive as possible, a coding system was used during the course of the program. For example, in the designation LH-30(6-12-A-10), "LH-30" refers to the batch precipitate, "6" refers to an initial firing of 600°C/2 hrs, "12" refers to a subsequent firing at 1200°C/2 hrs, "A" refers to the acetic acid leach, and "10" refers to the final firing at 1000°C/2 hrs. All samples were designated in this manner in order to present a codified history and identification of the particular material. Shown in Figure 3.3 is a typical flow diagram for materials obtained from a particular precipitation batch.

3.2.4 Heat Treatment Studies

Studies were conducted to determine the effect of heat treatment temperature of Zn_2TiO_4 on its physical and optical properties. The temperatures of interest were varied from 900°C to 1400°C. The precipitates were fired in fused quartz crucibles because of the excellent thermal shock resistance of quartz. These were then inserted directly into a furnace and soaked for 2 hr at temperature (or 5 minutes at 1400°C), and then removed to room temperature conditions for rapid cooling. This rapid heat treatment method has been termed flash calcination.

Initial experiments with the coprecipitate i.e., the mixture of zinc oxalate and "TiOX", resulted in a rather violent disturbance of the powder due to the extremely rapid evolution of decomposition gases. Therefore, in subsequent studies materials were pre-calcined at 600°C for 2 hrs, a treatment which removes all volatiles without disruption of the precipitate. Powders subjected to temperatures up to 1200°C were essentially free flowing; the slight caking is easily broken up. However, a 1400°C treatment caused apparent agglomeration as observed microscopically in the coarseness of the particles. This was confirmed in scanning electron microscopy (SEM) studies, which clearly showed "necking" (fusing together of particles) or the

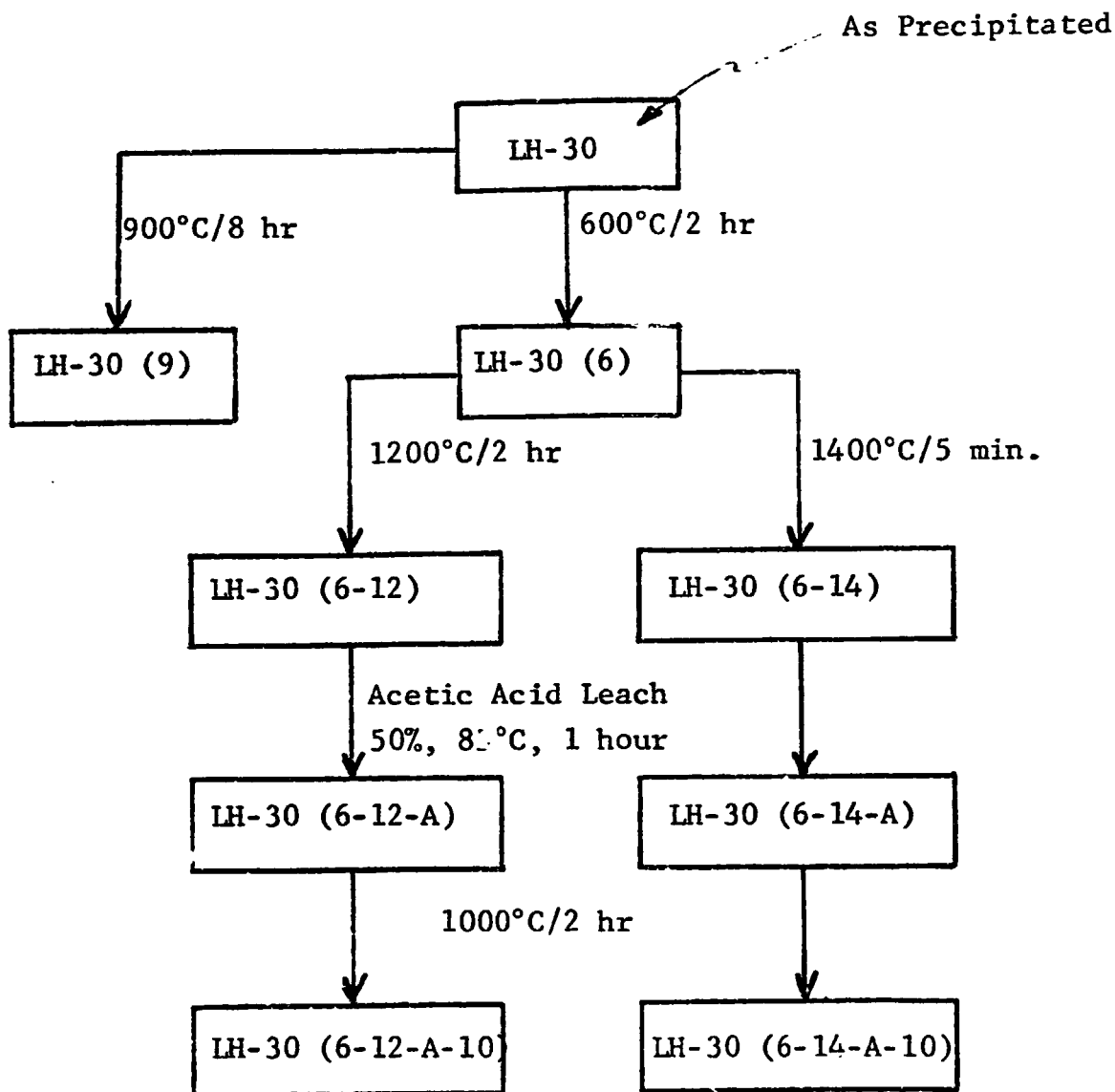


Figure 3-3. TYPICAL FLOW DIAGRAM FOR Zn_2TiO_4 SYNTHESIS FROM A PRECIPITATED BATCH

onset of sintering by diffusion. The results of SEM analyses appear in a later section.

In some of the materials calcined at 900°C, zinc metatitanate (ZnTiO_3) was observed. Firing of these materials to a temperature of 1200°C resulted in the changes described below:

Batch No.	Phases Present After Heat Treatment at:	
	900°C/8 hr	1200°C/1 hr
LH-10	ZOT* + ZMT* + TiO_2	ZOT + TiO_2
LH-11	ZOT + ZMT + TiO_2	ZOT + TiO_2
LH-12	ZOT + ZMT + ZnO	ZOT

*ZOT = zinc orthotitanate, ZMT = zinc metatitanate

Zinc metatitanate was not observed in any of the 1200°C calcined samples. This can be explained by examination of the ZnO- TiO_2 phase diagram proposed by Dulin and Rase (Ref. 3.7) in which dissociation at 945°C of ZnTiO_3 to Zn_2TiO_4 plus TiO_2 is indicated. Significantly, in LH-12, ZMT and ZnO were present in the 900°C material. A heat treatment of 1200°C resulted in a material which revealed only ZOT lines, indicating reaction between the excess ZMT and ZnO to form ZOT. The observed incompleteness of reaction of 900°C was the exception rather than the rule. However, evidence of ZMT was observed in some of the 600°C (pre-calcined) materials, indicating that the reaction to form the orthotitanate may be stepwise, i.e., metatitanate is an intermediate product at some relatively low (<900°C) temperatures.

3.2.5 Acid-Leach Studies

The coprecipitation process was designed to yield a product with excess ZnO. The removal of free ZnO can lower α_s by about 0.02 due to elimination of the "knee" in the 0.325 - 0.375 micron region.

A series of Zn_2TiO_4 powders were treated with acetic acid to remove ZnO. The reaction of acetic acid with zinc oxide leads to soluble zinc acetate; Zn_2TiO_4 is inert to the acid.

Samples LH-30(6-12) and LH-31(6-12) were thoroughly stirred in acetic acid at 80°C for one hour. After filtering and washing, the materials were fired at 1000°C/2 hrs to drive off any residual acetates.

Gravimetric analysis showed a weight loss (presumably ZnO) of 7.9% for LH-30(6-12-A-10) and 3.7% for LH-31(6-12-A-10). The removal of ZnO from the LH-30 material was verified by X-ray analyses in that no phases other than Zn_2TiO_4 could be detected. In addition, reflectance data revealed either an increase at the "knee" (350nm) or its complete removal (see section 4.7). Sample LH-31(6-12) had shown no X-ray evidence of ZnO prior to the acid leach. Apparently the 3.7% ZnO content as determined in the acid leach experiment was too small an amount to be detected by X-rays.

Samples from batches LH-51 and LH-52 were also subjected to acid washing. Weight losses for LH-51(6-12-A-10) and LH-52(6-14-A-10) were 2.2 and 2.3%, respectively, showing that these materials contained a very small amount of ZnO. In general, losses of 2 to 3% were observed for all Zn_2TiO_4 subjected to this processing. An important requirement of the acid washing process is the post-calcination at 1000°C to remove any degradable residues, as space simulation tests show (see sections 4.4 and 4.5).

3.2.6 X-Ray Analyses

All materials obtained at the various stages in processing (see Figure 3.3 for typical materials) were examined routinely by X-ray analysis. Representative powder patterns are presented for as-precipitated materials in Figure 3.4 and for heat treated materials in Figure 3.5. The "TiOX" product formed by the reaction between TiCl_4 and $\text{H}_2\text{C}_2\text{O}_4 \cdot 2\text{H}_2\text{O}$ exhibited a characteristic X-ray pattern (Fig. 3.4a.) which cannot be identified as any indexed material. This pattern was common to all of the various "TiOX" powders examined, thus showing that this compound is reproducible and unique. Also shown in Figure 3.4 are the patterns

a) Single phase - "TiOX"



b) Single phase - Zinc Oxalate - $\text{ZnC}_2\text{O}_4 \cdot 2\text{H}_2\text{O}$



c) Coprecipitated mixture - Zinc and "TiOX"



Figure 3.4. X-ray Powder Patterns of Precipitated Materials

a) Zinc Orthotitanate, Batch - LH-51(6)



b) Zinc Orthotitanate, Batch - LH-30(9)



c) Zinc Orthotitanate, Batch - LH-30(6-12-A-10)



Figure 3.5. X-ray Powder Patterns of Fired Zinc Orthotitanate Materials (Zn_2TiO_4)

for zinc oxalate and a coprecipitated mixture. The former corresponds nicely to well documented data for $\text{ZnC}_2\text{O}_4 \cdot 2\text{H}_2\text{O}$, and the latter comprises a mixture of the two patterns.

Representative X-ray powder patterns of fired materials presented in Figure 3.5 show that, in the 600°C material, LH-30(6), the Zn_2TiO_4 lines are not sharply defined, indicating poor crystallinity. On the other hand, the patterns of the 900°C material, (LH-30(9)), show good crystallinity as evidenced by line sharpness and the emergence of back reflection lines. The pattern of the acid washed sample contains no lines for ZnO, indicating the effectiveness of the acetic acid removal of ZnO.

Another aspect of X-ray analyses has been to determine any relationship between crystallographic size and processing history and/or stability to ultraviolet irradiation in vacuum. The results of these studies are shown in Table 3.5; the lattice constants (a_0) of pigments calcined at 1100°, 1200° and 1300°C were similar, while the 1400°C material revealed a cell size more closely approaching the reported value of 8.456Å (Ref.3.8) for fused Zn_2TiO_4 . Thus, there was no clear trend, at least in the 1100° to 1300°C temperature range, toward the ideal crystal size with increasing temperature.

Table 3.5
SUMMARY OF X-RAY DIFFRACTION STUDIES OF Zn_2TiO_4

Material	Calcination Temp., °C	Lattice Constant, Å	ZnO	$\Delta\alpha_s$ 2054 ESH **
LH-53(6-11)	1100	8.4668	Yes	.051
LH-53(6-11-A-10) *	1100	8.4639	No	.071
LH-53(6-12)	1200	8.4673	Yes	.064
LH-53(6-12-A-10) *	1200	8.4641	No	.075
LH-53(6-13)	1300	8.4668	Yes	.109
LH-53(6-13-A-10)	1300	8.4638	No	.051
LH-53(6-14)	1400	8.4643	Yes	.129
LH-53(6-14-A-10) *	1400	8.4628	1%	.055

*Acid washed, followed by heating at 1000°C/2 hrs.

**Space simulation test IRIF-I-67

A difference in lattice constants did appear to exist between as-calcined pigments and those of the acid washed materials. The latter materials clearly exhibit smaller constants than the non-acid washed samples. Since acid washing removed the ZnO from the Zn_2TiO_4 , this decrease in a_0 may indicate a limited solubility of ZnO in the Zn_2TiO_4 . In other words, removal of the ZnO permits a closer approach of the Zn_2TiO_4 crystal size to the ideal. However, it is also possible that the apparent contraction in crystal size may have been due to an annealing effect of the added heat treatment of $1000^\circ\text{C}/2$ hrs. Examination of the lattice constant versus Δa_s data failed to reveal any correlation.

The X-ray diffraction scans also indicated the effectiveness of acid treatment; ZnO was detected in the as-calcined and not in the acid-treated samples. No trace of TiO_2 was observed in any of these samples by X-ray.

3.2.7 SEM Analyses

The various materials generated in the Zn_2TiO_4 studies, from precipitates to high fired powders, were examined by scanning electron microscopy (SEM). These studies provided a valuable analytical tool in examining morphology of materials and, importantly, in determining the reproducibility in this morphology from batch to batch. In general, the coprecipitated batches and Zn_2TiO_4 derived from them at various temperatures showed good reproducibility. Therefore, the photomicrographs which are discussed in the following paragraphs may be considered typical for any batch.

Shown in Figures 3.6 and 3.7 are SEM photomicrographs of individually precipitated zinc oxalate and titanium compounds. The $\text{ZnC}_2\text{O}_4 \cdot 2\text{H}_2\text{O}$ particles (Figure 3.6) are fairly regular in shape and appear to be of the order of 2 to 10μ in size. The titanium phase precipitate ("TiOX") has a smaller particle size range, about 0.5 to 4μ (Figure 3.7). The particles are somewhat irregular and are not as sharply defined as those for the zinc oxalate.

10 μ



Mag. 3,000X

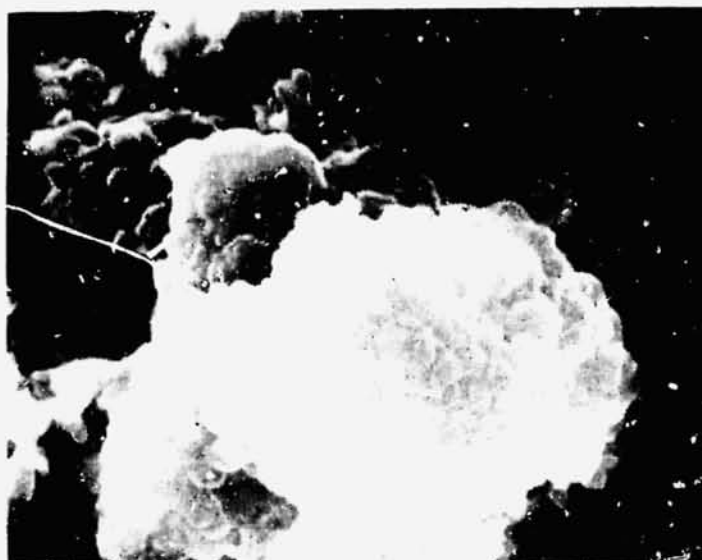
1 μ



Mag. 10,000X

Figure 3.6 MICROSTRUCTURE OF ZINC OXALATE

10 μ



Mag. 3000X

1 μ



Mag. 10,000X

Figure 3.7 MICROSTRUCTURE OF TITANIUM PHASE PRECIPITATE

The coprecipitated material (i.e., the mixture of Zn and Ti ppts) shown in Figure 3.8 appears to be a mixture of the two phases described above. In addition, "agglomerates" and "needles" can be observed.

X-ray analyses of material fired at 600°C generally reveal the presence of Zn_2TiO_4 and ZnO . It is likely that some form of titanium compound also exists but it may be either amorphous or too fine, to be detected by X-rays. Figure 3.9 shows that this material consists of extremely fine (submicron) particles in addition to larger ones of about 1 to 5 microns. At this low calcination temperature, the material is quite heterogeneous as might be expected of a partially decomposed-reacted mixture.

After a 900°C firing for 8 hours, Zn_2TiO_4 with no other X-ray detectable phase is obtained. As Figure 3.10 shows, this powder has fairly well-ordered particles in a size range from about 0.8 to 5 μ . The shape of the particles are angular as opposed to rounded. The high fired materials have been identified by X-ray as Zn_2TiO_4 , with perhaps 2 to 4% excess ZnO , which acid leaching experiments have also shown. A 1050°C firing produces a material (Figure 3.11) which no longer has the fine, submicron particles exhibited by the 900°C Zn_2TiO_4 material (Figure 3.10). The average particle size for the 1200°C material (Figure 3.12) is even greater. For the 1400°C powder (Figure 3.13), the particle size appears to be in the range of 2 to 6 μ with evidence of "necking" between particles. The spherical nature of the particles suggests an approach to a minimum surface energy state.

This review has presented the morphologies of the various powders produced via the coprecipitation process as a function of heat treatment temperature. These observations are summarized in Table 3.6.

10 μ



Mag. 3,000X

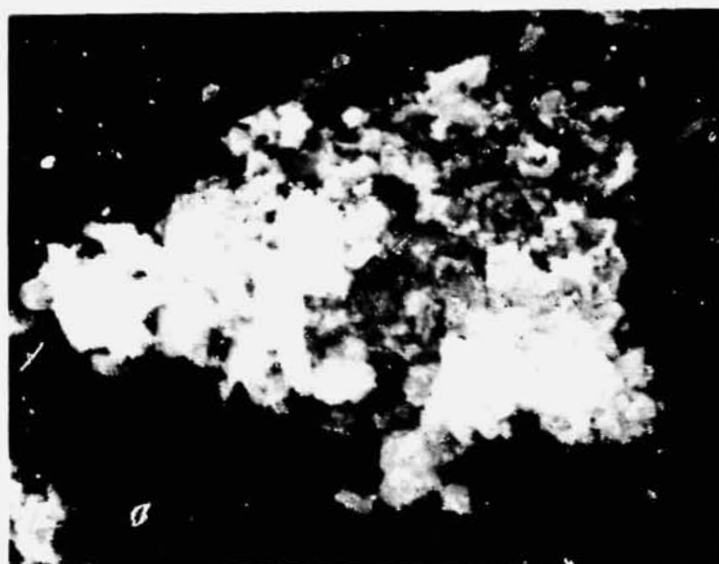
1 μ



Mag. 10,000X

Figure . . 8 MICROSTRUCTURE OF COPRECIPITATED
ZINC-TITANIUM COMPOUND MIXTURE
(LH-51)

10 μ



Mag. 3,000X

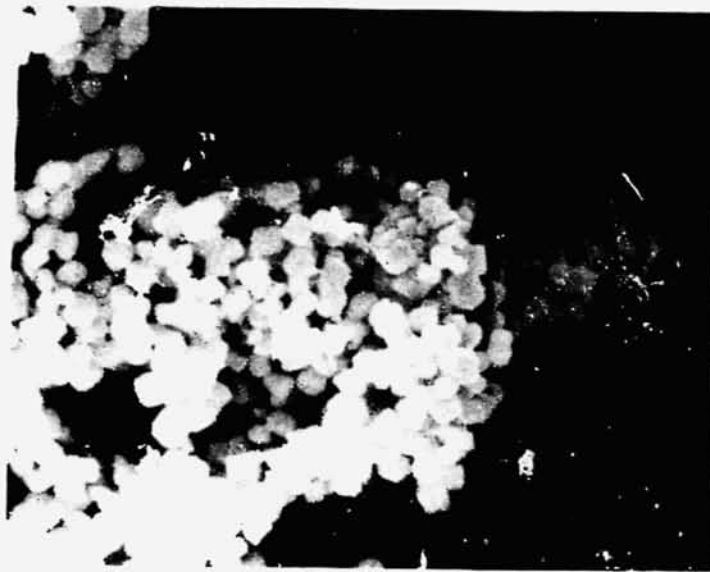
1 μ



Mag. 10,000X

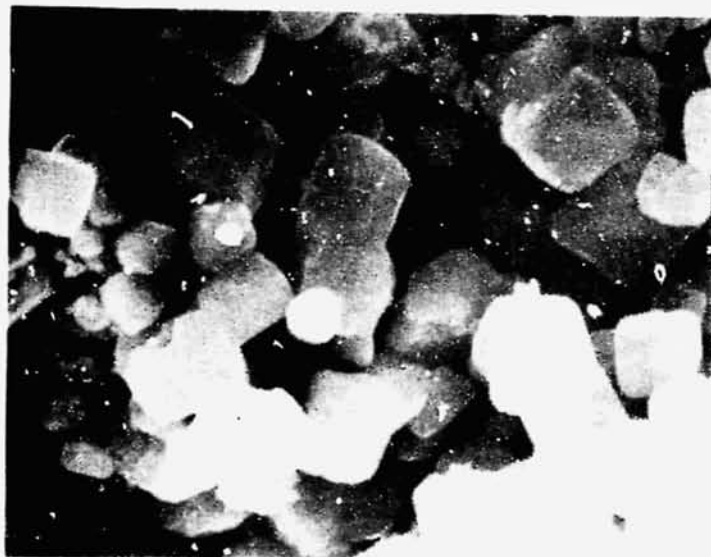
Figure 3.9 MICROSTRUCTURE OF 700°C FIRED MATERIAL (LH-52(6))

10 μ



Mag. 3,000X

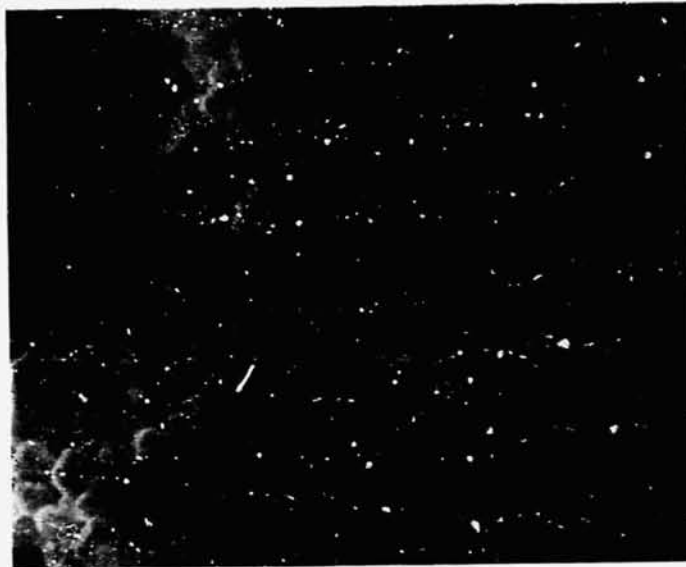
1 μ



Mag. 10,000X

Figure 3.10 MICROSTRUCTURE OF 900°C
FIRED MATERIAL (LH-52(9))

10 μ



Mag. 3,000X

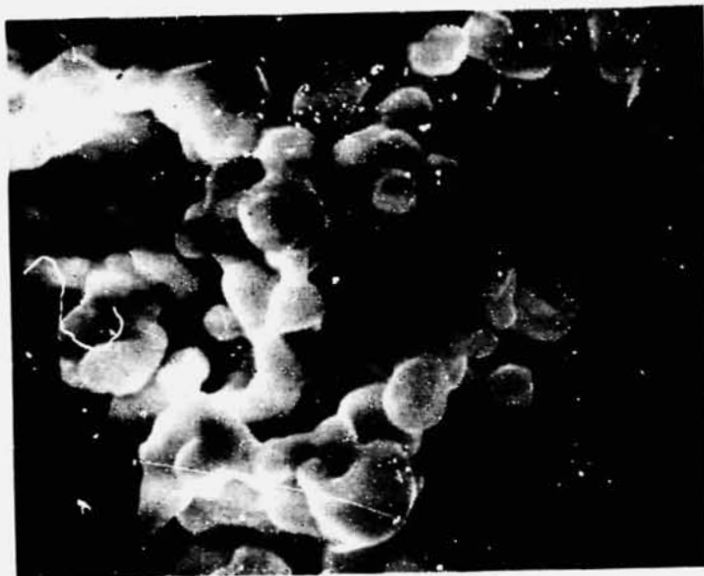
1 μ



Mag. 10,000X

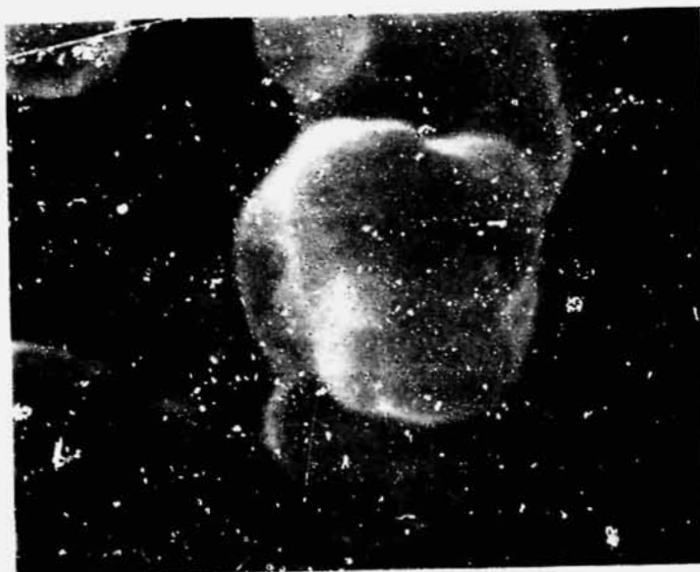
Figure 3.11. MICROSTRUCTURE OF 1050°C FIRED
MATERIAL (LH-101(6-10.5))

10 μ



Mag. 3,000X

1 μ



Mag. 10,000X

Figure 3.12. MICROSTRUCTURE OF 1200°C FIRED
MATERIAL (LH-102(6-12))

10 μ



Mag. 3,000X

1 μ



Mag. 10,000X

Figure 3.13. MICROSTRUCTURE OF 1400°C
FIRED MATERIAL (LH-52 (6-14))

Table 3.6

SUMMARY OF SEM ANALYSES OF PIGMENTS PREPARED
FROM COPRECIPITATED OXALATE PRECURSORS (COP)

<u>COP Materials</u>	<u>Particle Size*</u>	<u>Comments</u>
As Precipitated	SM-5 μ	Needle-like, as well as equiaxed shapes.
600°C/2 hrs	SM-5 μ	Agglomeration, caking effect.
600°C/2 hrs + 900°C/8 hrs	SM-5 μ	Rounding of particles, less agglomeration than 600°C material.
600°C/2 hrs + 1050°C/2 hrs	1-5 μ	Some necking between particles. No evidence of submicron material.
600°C/2 hrs + 1200°C/2 hrs	2-5 μ	Moderate necking, rounded particles, no sharp edge effects.
600°C/2 hrs + 1400°C/5 min.	2-5 μ	Strong necking. Further rounding of particles.

*SM = submicron

3.2.8 COP Materials for Other Laboratories

Approximately four pounds of Zn_2TiO_4 were produced by the COP method and forwarded to Stanford Research Institute (SRI) for their study: 1200 grams of LH-111(6-12) to Mr. Eldon Farley, for plasma annealing studies, and 600 grams, to Dr. Kenneth Sancier for surface treatment experiments.

The precipitate was prepared in four batches of approximately 1200 gms. each. These batches were designated as LH-107, LH-108, LH-109, and LH-110.

Precalcination (600°C) was conducted on the combined batches of LH-107 + LH-109, and on those of LH-108 + LH-110. The final 1200°C calcination was performed in one large batch to produce about 2000 grams of Zn_2TiO_4 pigment. This was designated as LH-111(6-12), i.e., the material furnished to SRI.

3.3 DECOMPOSITION STUDIES

Coprecipitation by reacting two chloride solutions with oxalic acid can produce a single compound such as in the case of $\text{BaTiO}(\text{C}_2\text{O}_4)_2 \cdot 4\text{H}_2\text{O}$ (Ref. 3.9). Our material is, as described earlier, a mixture of zinc oxalate and "TiOX". In efforts to define more clearly the precipitation and thermal conversion processes, studies were conducted with the individual zinc and titanium precipitates as well as with the coprecipitated material.

Experimentally, powder samples of zinc oxalate, "TiOX", or the mixture were heated at temperatures from 120° to 700°C for two hours each. Each sample was heat treated using direct insertion into, and removal from, the furnace at temperature, in order to minimize the effects of heat-up and cool-down. The results of the gravimetric analyses are tabulated in Table 3.7 and graphically illustrated in Figure 3.14. The appearance of the powders after heat treatment along with the results of X-ray powder pattern analyses are presented in Table 3.8. These results are discussed in the following sections.

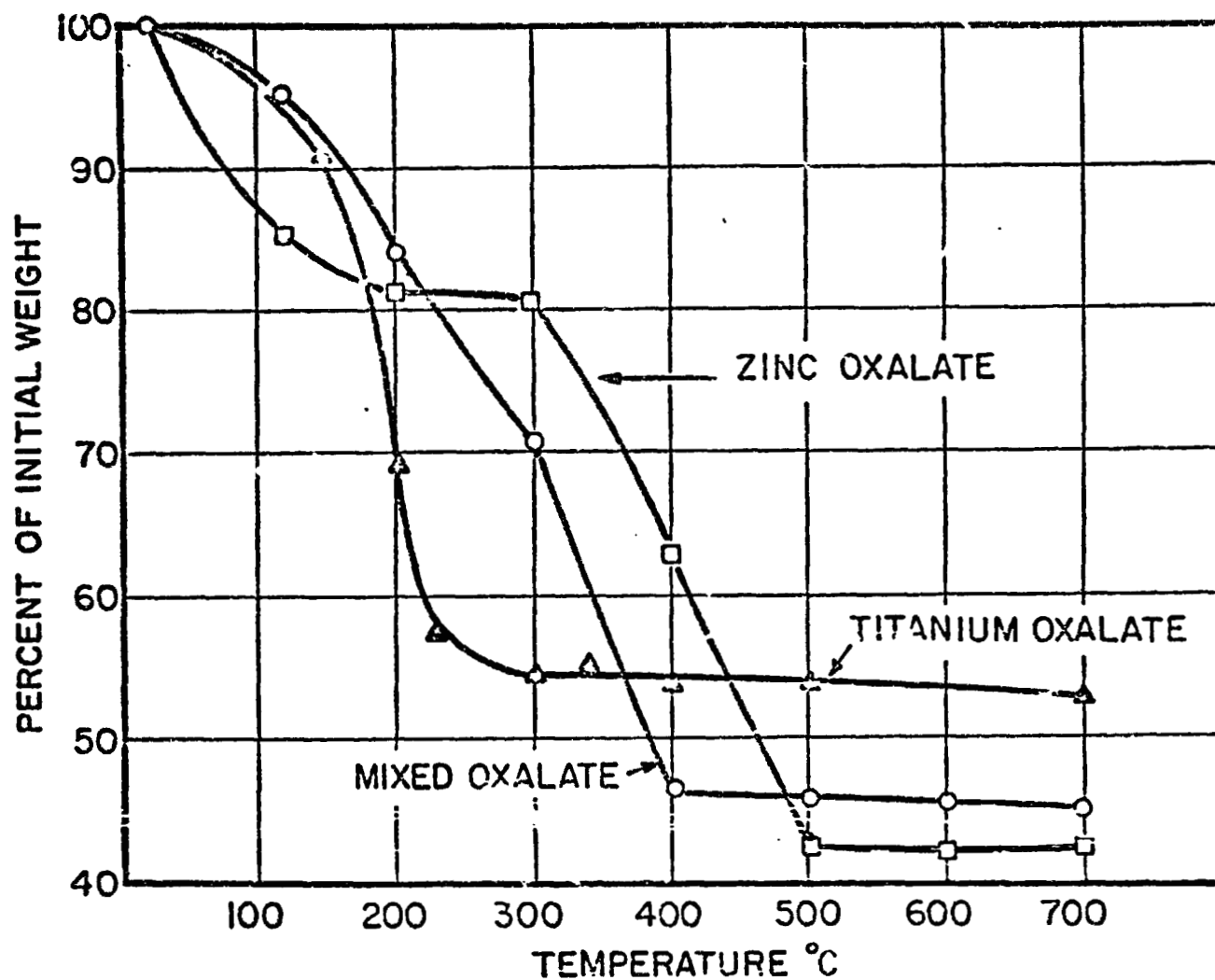
3.3.1 Zinc Oxalate

The zinc compound precipitate was clearly identified as $\text{ZnC}_2\text{O}_4 \cdot 2\text{H}_2\text{O}$ by X-ray analyses (See Figure 3.4). The thermal decomposition of zinc oxalate to zinc oxide was determined by gravimetric analysis to be 57.2 - 57.4% weight loss. The calculated loss based on formula weights is 57.04%. The slight excess in actual loss may be attributed to adsorbed water.

Table 3.7

WEIGHT LOSSES FOR ZINC OXALATE, "TiOX" AND
COPRECIPITATED OXALATES AS A FUNCTION OF TEMPERATURE

<u>Temperature, °C</u>	<u>% Wt. Loss</u>		
	<u>Zinc Oxalate</u>	<u>"TiOX"</u>	<u>Coprecipitated Oxalates</u>
120	14.5		4.8
150		8.1	
200	18.4	30.7	15.8
230		42.2	
300	19.0	45.7	28.0
340		44.5	
400	36.7	46.0	53.4
500	57.2	45.5	53.5
600	57.3		
700	57.4	46.4	54.0



WEIGHT LOSS VS TEMPERATURE FOR ZINC OXALATE,
TITANIUM OXALATE AND MIXED OXALATES

Figure 3-14

Table 3.8

APPEARANCE AND PHASES PRESENT FOR ZINC OXALATE, "TiOX"
AND MIXED OXALATES AS A FUNCTION OF TEMPERATURE

A P P E A R A N C E *			P H A S E S P R E S E N T **		
Temp., °C	Zinc Oxalate	"TiOX"	Coprec. Oxalates	Zinc Oxalate	"TiOX" Coprecipitated Oxalates
120	White		White		"TiOX"
200	White	Light Yellow	White	ZnOx	"TiOX" ZnOx + "TiOX" + "X"
300	White	Light Yellow	Light Yellow	ZnOx + "X"	"X"
400	Gray, Lumpy	Light Yellow	Yellow	ZnOx + "X"	ZnO
500	Light Gray, Lumpy	Light Yellow	Yellow	ZnO	ZnO + TiO ₂
600	Tan	White	White	ZnO	Zn ₂ TiO ₄ + ZnO
700	Yellow	White	White	ZnO	Zn ₂ TiO ₄ + ZnO

* All powders free flowing unless otherwise indicated.

** ZnOx - Zinc oxalate, "X" - apparently an intermediate phase in the decomposition of zinc oxalate.

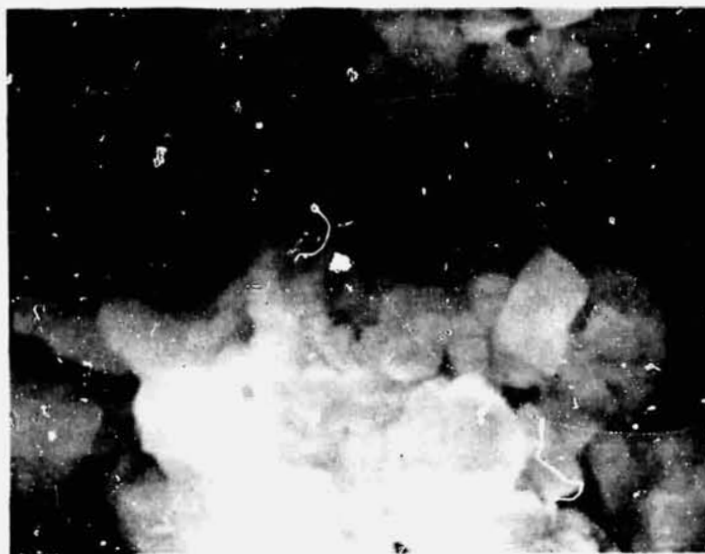
***A ' samples calcined for two hours.

Weight loss as a function of temperature (Figure 3.14) shows a slower rate of decomposition for zinc oxalate as compared to "TiOX". The weight loss up to 300°C is probably loss of water of hydration. Calculations based on molecular weights show the water content to be 19.0%, a value to which the experimental determinations (Figure 3.14 and Table 3.7) correspond well. Beyond 300°C, a rapid weight loss is observed, and decomposition is complete by 500°C.

X-ray analyses (Table 3.8) revealed the existence of an intermediate phase in the decomposition of zinc oxalate. The principal lines for this phase, termed the "X" phase are 3.70, 2.36 and 4.10Å. "X" was also found in the lower temperature coprecipitated oxalate samples (200° and 300°C). The intermediate decomposition products of zinc oxalate were rather curious in appearance. After the 400°C and 500°C calcinations, the material was gray and lumpy. Weight loss data show that this is the range where rapid decomposition occurs. The converted zinc oxalate samples which had been calcined at 400°C to 700°C all displayed some coloration; however, the 600°C and 700°C materials were much less agglomerated than the lower temperature materials. The gray to yellow coloration is probably due to small amounts of residual carbon produced during decomposition. The carbon is, of course, oxidized at higher temperatures. A similar effect has been observed by other investigators with thorium oxalate (Ref. 3.10).

SEM examination of the products at 400°C and higher (or those undergoing or having undergone decomposition) revealed an extremely fine particle morphology. This can be seen by comparing the 300°C and 400°C materials in Figure 3.15. This fine particle size persists also in the 500°C and 700°C products, as shown in Figure 3.16.

10 μ

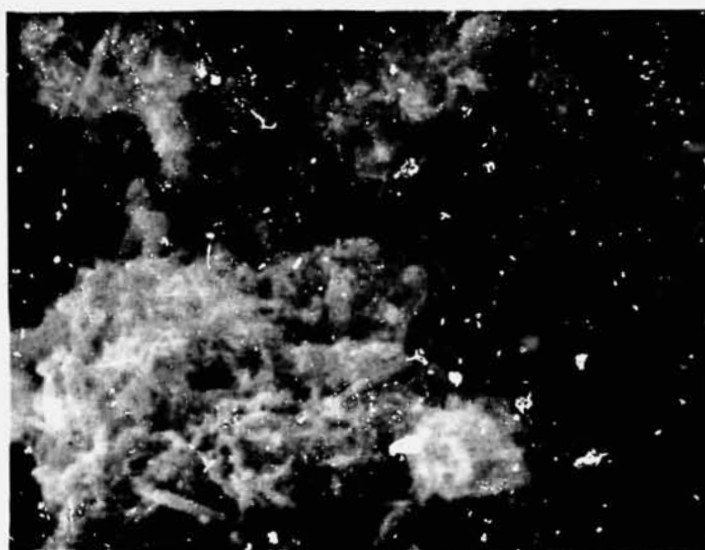


#0293

a)

300°C

3000X



#0292

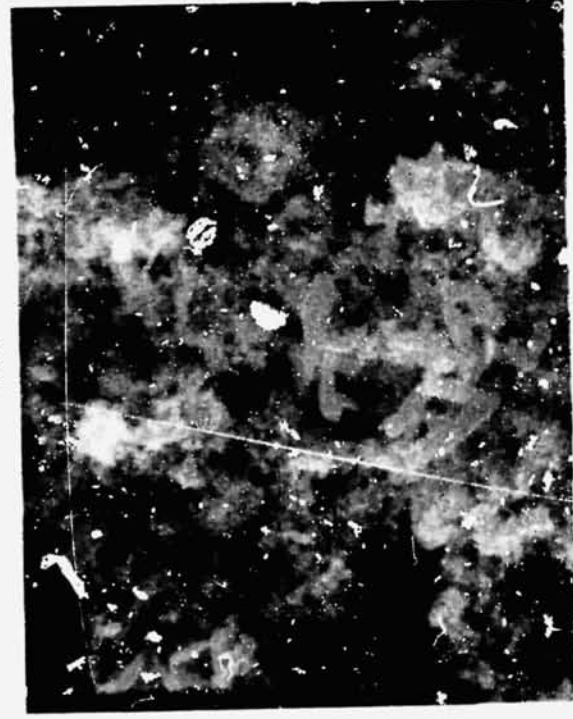
b)

400°C

3000X

Figure 3.15. ZINC OXALATE DECOMPOSITION
PRODUCT AT 300° and 400°C

10 μ



#0290

a)

500°C

3000X



#0289

b)

700°C

3000X

Figure 3.16. ZINC OXALATE DECOMPOSITION
PRODUCTS AT 500° AND 700°C

C-2

3.3.2 "TiOX"

The reaction of TiCl_4 with $\text{H}_2\text{C}_2\text{O}_4 \cdot 2\text{H}_2\text{O}$ in an aqueous medium yields a finely divided white precipitate which is designated "TiOX". X-ray analyses of this material revealed a well defined powder pattern (Figure 3.4). This material displayed a weight loss on conversion to TiO_2 at 600°C of 45 to 46% which was reproducible from batch to batch. Thus, the molecular weight of "TiOX" appears to be in the range of 145-148, averaging about 147. The anticipated product in the reaction of TiCl_4 with $\text{H}_2\text{C}_2\text{O}_4$ would be $\text{Ti}(\text{C}_2\text{O}_4)_2$ or a hydrate of it. However, the molecular weight of such a compound would be 223.9 or higher; thus "TiOX" is not a simple oxalate. Chemical analyses of "TiOX" samples have revealed carbon contents of 9.4 to 9.8% and a hydrogen content of about 2.5%. The closest chemical formula fit would be $\text{Ti}(\text{OH})_2 (\text{CO}_3)$ which has a molecular weight of 142. The balance between 142 and 147 can be due to water of hydration.

The decomposition of "TiOX" appears to occur more rapidly than that of zinc oxalate (Figure 3.14). These data are based on a 2 hour hold at a particular temperature. A summary of heat treatment studies of "TiOX" subject to selected temperatures for varying times appears in Table 3.9. The particular temperatures were chosen on the basis of apparent changes in volatilization and/or decomposition behavior suggested by preliminary thermograv-analyses (Figure 3.17).

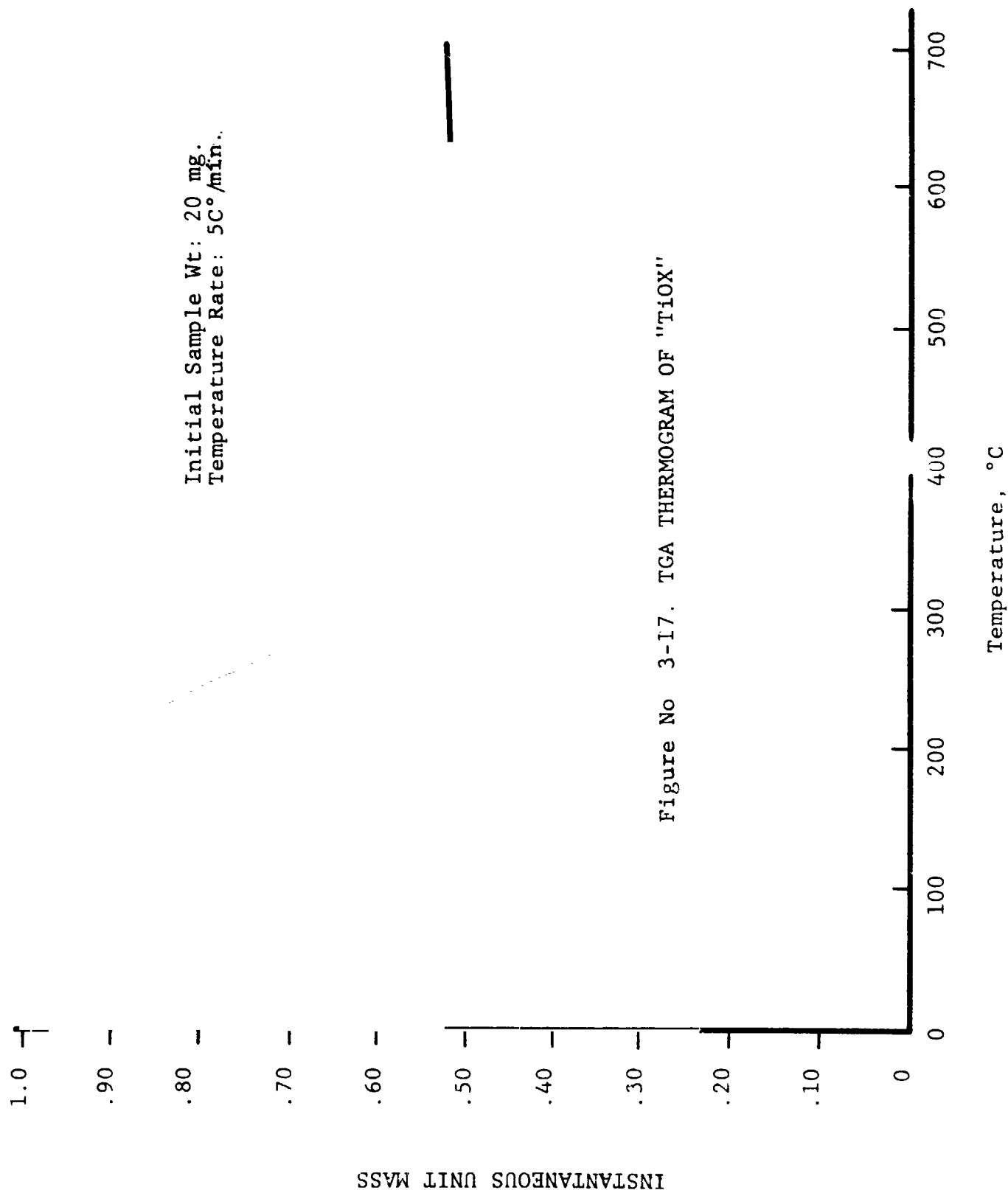
The data (Table 3.9) show that after 48 hours at 150°C a weight loss of about 8.5% is obtained. The 4 hour weight loss of 8.1% suggests that equilibrium is essentially reached in a much shorter time than 48 hours. Since the X-ray powder pattern of these two products is identical to that of unheated "TiOX", this initial weight loss can be attributed in part to physically bound water, since an anhydrous material would exhibit a different crystal structure from its hydrated form. The $230^\circ\text{C}/5$ min. product displayed an X-ray pattern identifiable as "TiOX". The additional weight loss, i.e., 17.4% at 230°C vs. 8.5% at 150°C , may be due to

Table 3.9

HEAT TREATMENT STUDIES OF "TiOX"

<u>Temp., C°</u>	<u>Time</u>	<u>Wt. Loss, %</u>	<u>Phase Present (X-ray)</u>
150	1 hr	6.96	"TiOX"
	4 hrs	8.07	"TiOX"
	48 hrs	8.46	"TiOX"
230	5 min.	17.44	TiO ₂ *
	1 hr	39.93	
	2 hrs	42.24	
	4 hrs	44.34	
340	5 min.	43.73	TiO ₂
	1 hr	44.43	
	2 hrs	44.46	
	4 hrs	44.89	
500	1 hr	45.56	TiO ₂
	4 hrs	45.52	
700	1 hr	46.66	TiO ₂
	4 hrs	46.37	

*TiO₂ patterns in all cases are anatase. Progressively greater crystallinity and/or particle size was indicated with increasing temperature as reflected in sharper lines.



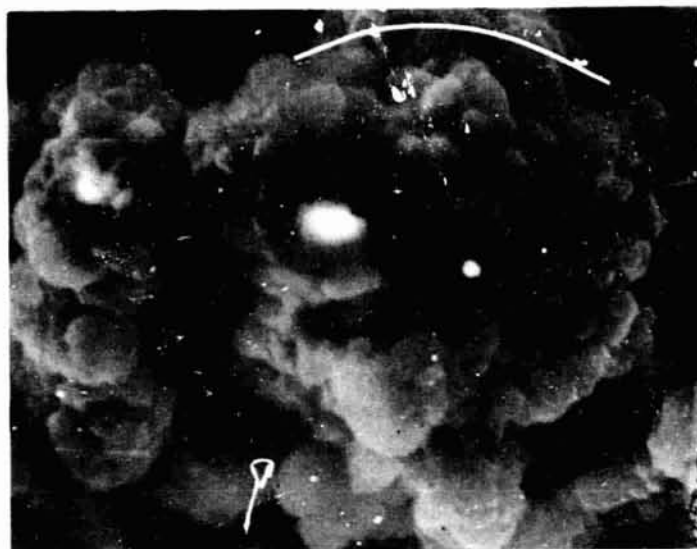
additional water loss, to partial decomposition, or to both. The absence of titania X-ray lines does not rule out the latter, since the amount of TiO_2 may be insufficient or the TiO_2 may be too fine in particle size to yield a pattern. At longer times increasingly greater weight losses occur. An X-ray study of the $230^\circ\text{C}/2$ hr product showed it to be the anatase form of TiO_2 , and the broadness of the lines suggested a very fine particle size and poor crystallinity. The data for 340°C show that weight losses at this temperature are similar to those of the $230^\circ\text{C}/4$ hr., indicating no additional decomposition losses. At 500°C and 700°C , however, slight increases in weight loss were observed. This may be attributed to a complete oxidation of any residual carbon from the decomposition process, since such oxidation begins at about 400°C to 500°C .

Macroscopic examination of the various decomposition products (Table 3.8) revealed a slight yellowing for the lower temperature (300°C - 500°C) materials while the 600°C and 700°C titanias are white. As in the case of zinc oxalate, this may be due to burning off of residual carbon. Unlike zinc oxalate materials, those derived from "TiOX" are all free flowing. Microstructural examination of these materials revealed no significant changes in morphology as the material decomposed to TiO_2 (Figure 3.18-20). Although the higher temperature (500° and 700°C) titanias did show a greater uniformity in particle shape, they along with the lower temperature products were relatively heterogeneous in particle size as well as shape.

3.3.3 Coprecipitated Material

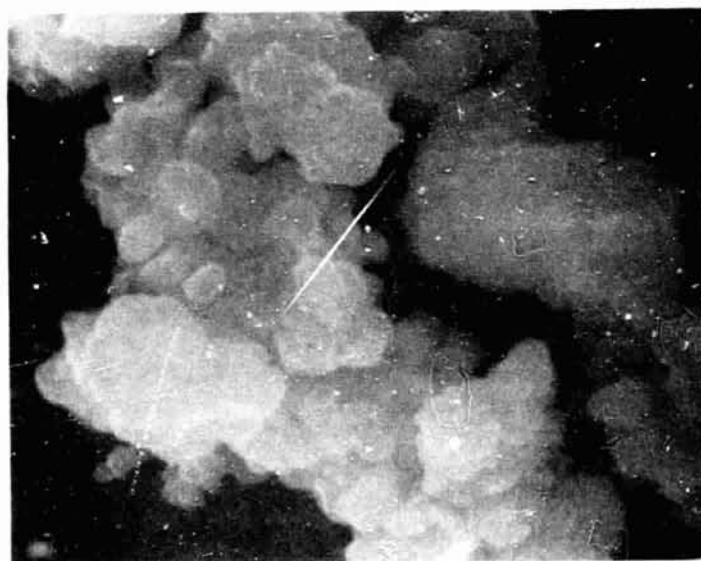
As pointed out in an earlier discussion, the coprecipitated material is a mixture of zinc oxalate and "TiOX" as confirmed in X-ray powder patterns (Figure 3.4). Weight loss on conversion to the oxides was of the order of 54 to 55%. The weight loss curve for the coprecipitate (Figure 3.14) lies between the curves for the individual components, reflecting their different rates of decomposition. Essentially complete decomposition has occurred at

10 μ



As-Precipitated

3,000X

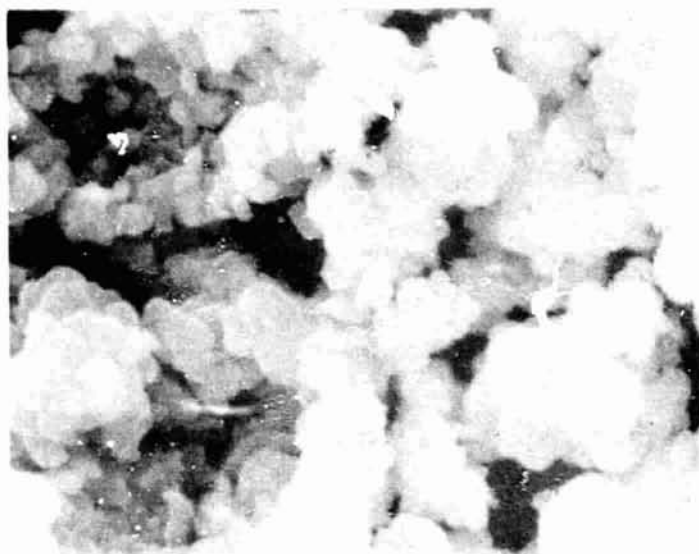


Heat Treat at 150°C/48 hrs.

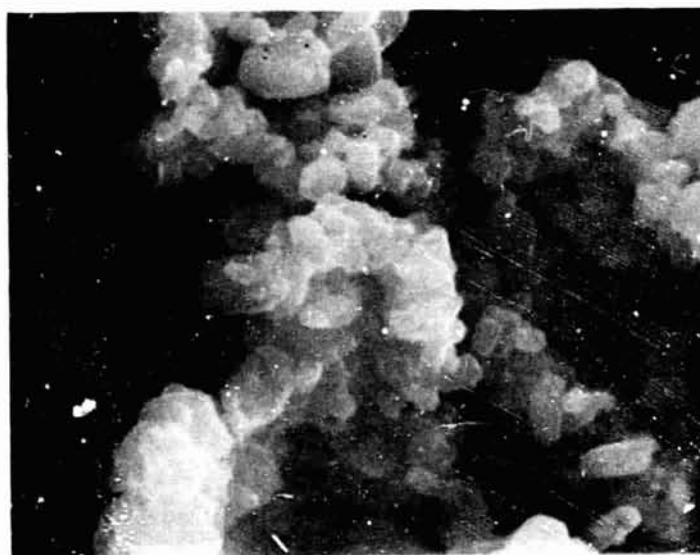
3,000X

Figure 3.18 SEM VIEWS OF "TiO₂" AS
PRECIPITATED AND HEAT TREATED
AT 150°C

10 μ



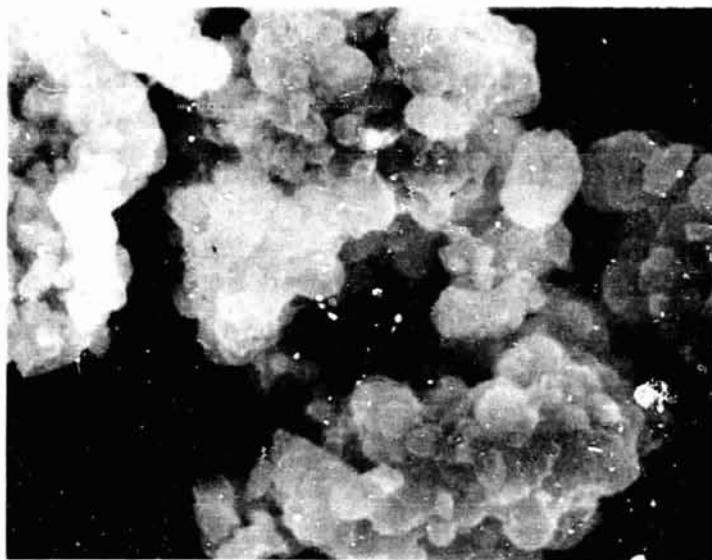
Heat Treated at 230°C/2 hrs. 3,000X



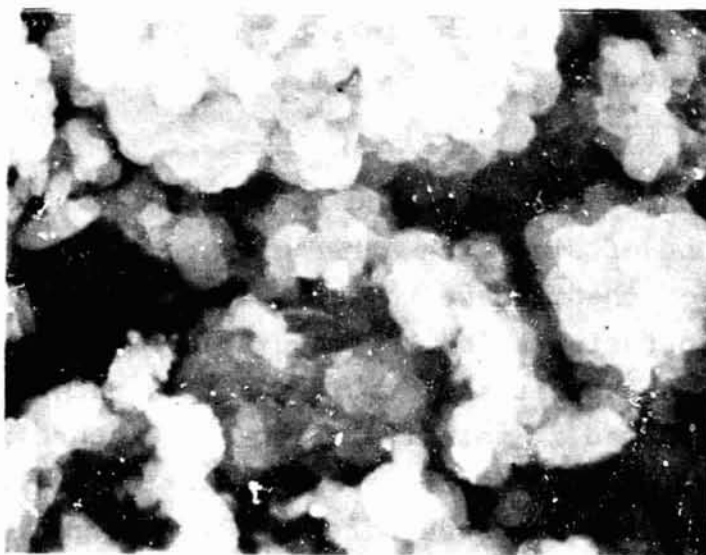
Heat Treated at 340°C/2 hrs. 3,000X

Figure 3.19 SEM VIEWS OF "TiOX" HEAT TREATED
AT 230°C AND 340°C

10 μ



Heat Treated at 500°C/1 hr. 3,000X



Heat Treated at 700°C/1 hr. 3,000X

Figure 3.20 SEM VIEWS OF "TiOX" HEAT TREATED
AT 500° AND 700°C

Analyses of the various products by X-ray techniques show that at 500°C, a mixture of ZnO and TiO₂ is present. A 600°C/ 2 hr heat treatment yields Zn₂TiO₄ plus ZnO in approximately equal amounts (judging from the X-ray line intensities). A significant result is the formation of Zn₂TiO₄ under relatively moderate conditions, testifying to the highly reactive nature of the ZnO with TiO₂ and/or their intermediate compounds formed in this process.

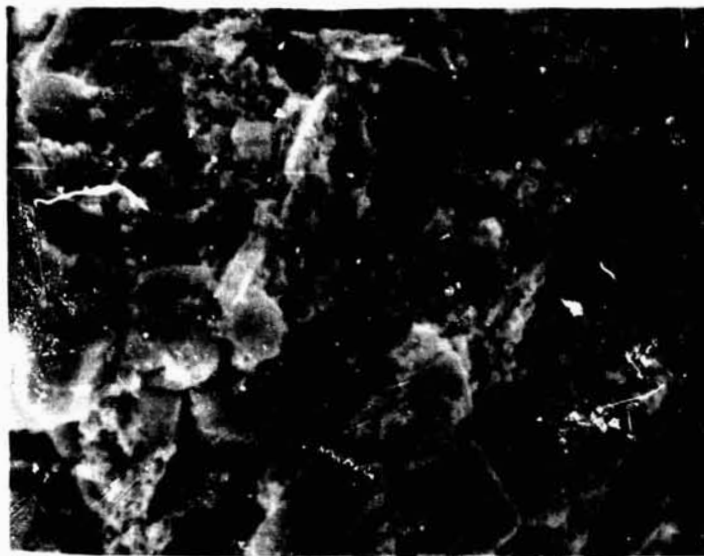
The mixed oxalate samples calcined at the various temperatures are quite fine in particle size and do not display the aggregation shown by zinc oxalate samples. Samples calcined at 600°C and 700°C are white, although the lower temperature samples show some coloration, similar to the "TiOX" materials.

In SEM examinations, these materials appear more heterogeneous (Fig. 3.21) than might be expected from the appearance of the individual oxalate products. There also exist some comparatively large particles. This may be due to interrupted or enhanced grain growth due to the intimacy of the two phases in the coprecipitated material.

3.4 SYNTHESIS BY REACTION SINTERING

The reaction synthesis method consists of a physical blending of a compound of zinc with a titanium compound, followed by heat treatment of the mixture to form zinc orthotitanate. As is the case with coprecipitation, decomposable salt precursors are used, in order to exploit the highly reactive nature of nascent oxide surfaces formed at relatively low temperatures. This method offers potential advantages in closer control of starting weights of materials and hence, of stoichiometry; the use of salts such as carbonates, nitrates, etc.; and the ability to use individually precipitated oxalate materials. The control of particle size of each of the components offers the potential of obtaining optimum particle size in the fired Zn₂TiO₄ product.

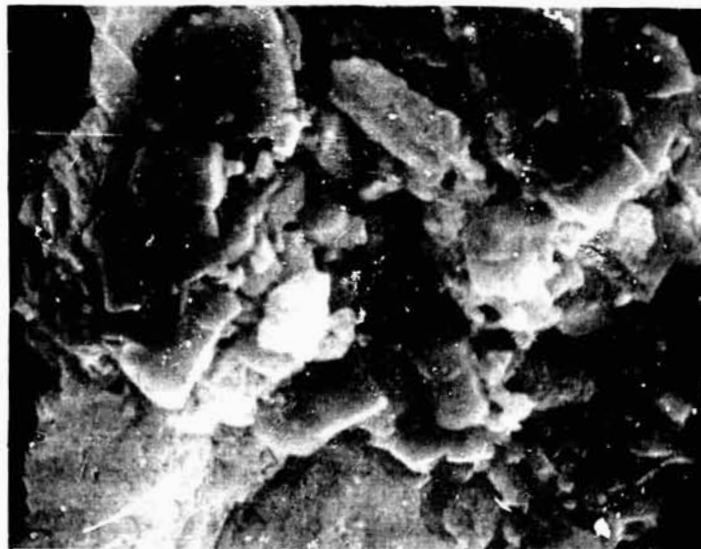
10 μ



#0240

500°C

3000X



#0241

700°C

3000X

Figure 3.21 COPRECIPITATED OXALATES DECOMPOSITION PRODUCTS
AT 500° AND 700°C.

The reaction synthesis studies were concerned mainly with the use of oxalates as starting materials. Limited experiments were conducted with other precursors. The various studies are discussed in the following sections.

3.4.1 Comparison of Mixed Oxalate (MOX) Processing

The objective of these studies was to determine whether the particle size of the precursor oxalates and the Zn_2TiO_4 product obtained from their calcination, could be controlled. The parameters investigated were calcination temperature and times of pretreatment of the coprecipitated (COP) material and of the mixed oxalate (MOX) material. The various powders were processed as follows:

1.) Control - oxalate mixture as coprecipitated, filtered and dried (designated LH-103). 2.) Homogenized - LH-103 ground-mixed using porcelain mortar and pestle to improve mix uniformity and to reduce agglomeration (designated LH-103H). 3.) Compacted - LH-103H compacted into one inch diameter discs under 5000 psi to reduce agglomeration and enhance particle-to-particle intimacy (designated LH-103C). 4.) Mixed oxalates - porcelain ball-milling of a mixture (to yield a 2.05 ZnO :1.00 TiO_2 /mol ratio) of individually precipitated zinc oxalate and "TiOX" (designated MOX). Samples of these four sets of materials were calcined at 600°C for 10 minutes, 1 hour, and 2 hours, by the flash calcine process, i.e., direct insertion into the furnace at temperature followed by removal after the prescribed time period. In addition, samples of each set were flash calcined at 1050°C for complete conversion to zinc orthotitanate.

The results of these studies are shown in Table 3.10. The weight losses for the different series calcined for 2 hours at 600°C were quite similar, i.e., 53.6%(LH-103), 53.6%(LH-103H), 53.7%(LH-103C), and 53.8%(MOX). Since the MOX series samples were also carefully weighed to yield a 2.05 ZnO :1.00 TiO_2 mixture, these weight loss data suggest a close approach to this ratio for the coprecipitated materials.

Table 3.10

SUMMARY OF CALCINATION STUDIES COMPARING COP AND MOX MATERIALS

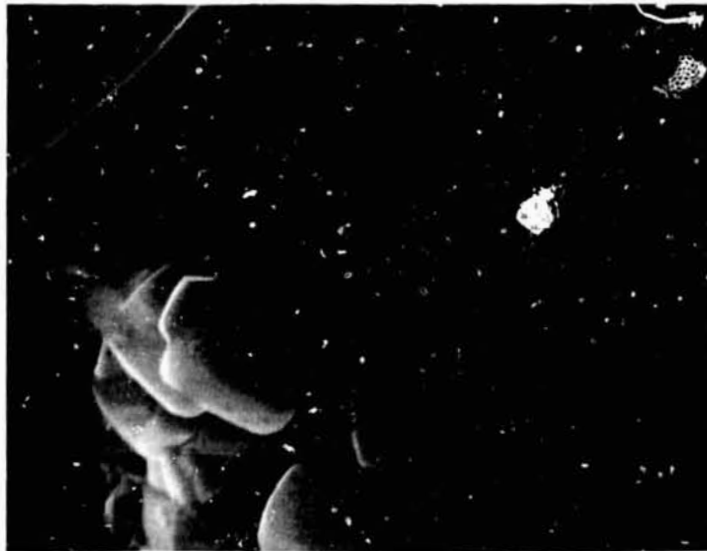
Sample	Calcination		Wt. Loss, %	Phases Present
	Temp., °C	Time, min.		
LH-103(6/.17)	600	10	53.46	ZnO + TiO ₂
LH-103(6/1)	600	60	53.36	ZnO + TiO ₂
LH-103(6/2)	600	120	53.59	ZnO + TiO ₂
LH-103(6-10.5)	1050	120	-	Zn ₂ TiO ₄
LH-103H(6/.17)	600	10	53.25	ZnO + TiO ₂
LH-103H(6/1)	600	60	53.47	ZnO + TiO ₂
LH-103H(6/2)	600	120	53.59	ZnO + TiO ₂
LH-103H(6-10.5)	1050	120	-	Zn ₂ TiO ₄
LH-103C(6/.17)	600	10	53.33	ZnO + TiO ₂
LH-103C(6/1)	600	60	53.61	ZnO + TiO ₂
LH-103C(6/2)	600	120	53.65	ZnO + TiO ₂ + Zn ₂ TiO ₄ (faint)
LH-103C(6-10.5)	1050	120	-	Zn ₂ TiO ₄
MOX(6/.17)	600	10	53.52	ZnO + TiO ₂
MOX(6/1)	600	60	53.77	ZnO + TiO ₂ + Zn ₂ TiO ₄ (moderate)
MOX(6/2)	600	120	53.80	ZnO + TiO ₂ + Zn ₂ TiO ₄ (moderate)
MOX(6-10.5)	1050	120	-	Zn ₂ TiO ₄

The products were examined using X-ray powder pattern techniques to determine compositions. For the mixtures fired at 600°C, the results show the presence of zinc orthotitanate only in the compacted sample fired for 2 hours (LH-103(6/2)). The higher reactivity shown for this sample was probably due to the greater intimacy between particles resulting from compaction. Previous studies conducted at 600° to 800°C with the coprecipitated powder had shown the formation of Zn_2TiO_4 at these temperatures when the heatup time to 600°C was about 1 hour. This suggests that for a flash calcination, the reaction threshold for COP materials is somewhere between 600°C and 700°C. The X-ray studies revealed that all of the materials fired at 1050°C had converted fully to Zn_2TiO_4 . There is no evidence of any free ZnO , TiO_2 or ZnTiO_3 to the level detectable by X-ray. Interestingly, the mixed oxalate samples, in which particle intimacy might be assumed to be poorer than in a coprecipitated material, show greater reactivity at 600°C as seen by the results for MOX(6/1) and MOX(6/2). The reason for this greater reactivity may be due to a finer particle size for the MOX as compared to the COP materials.

The various precursors and calcined products were examined using the SEM. The homogenization procedure, i.e., mortar and pestle grinding, did not appear to change the morphology substantially as seen from the SEM views of LH-103 and LH-103H in Figure 3.22. On the other hand, the MOX material exhibited a finer particle size as seen in Figure 3.23. Also shown in this Figure are the individual oxalates which appear somewhat coarser than after mixing (MOX). This suggests that the ball milling does cause attrition, possibly in the breakup of agglomerates.

Examination of calcined materials shows that the particle size differences between COP and MOX precursor materials are reflected in the 600°C decomposition products. The microstructure of LH-103(6/2) and LH-103H(6/2) (Figure 3.24) were similar as was the case for their precursors (Figure 3.22). The appearance of

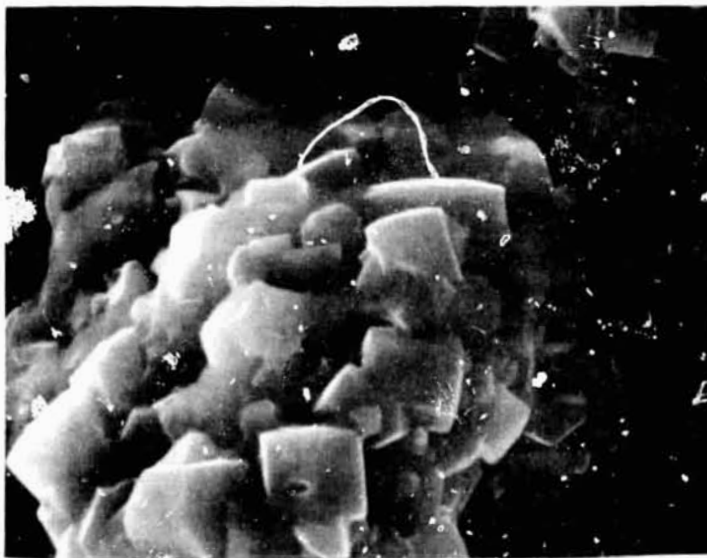
10 μ



317

3000 X

LH-103



318

3000 X

LH-103H

Figure 3.22. SEM VIEWS OF COP MATERIALS LH-103 and LH-103H

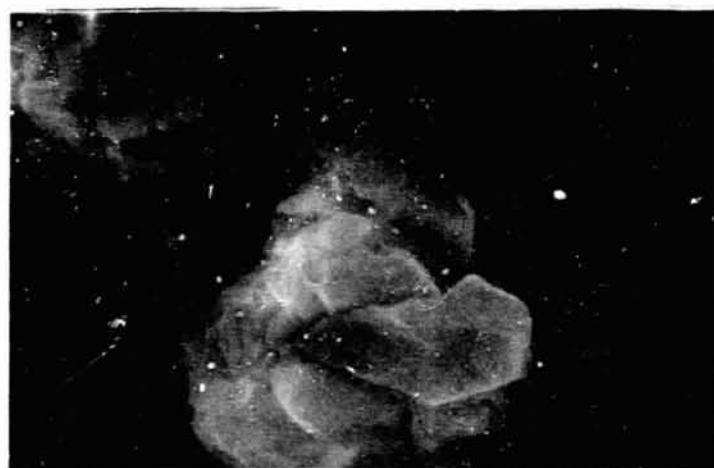
10 μ



MOX

320

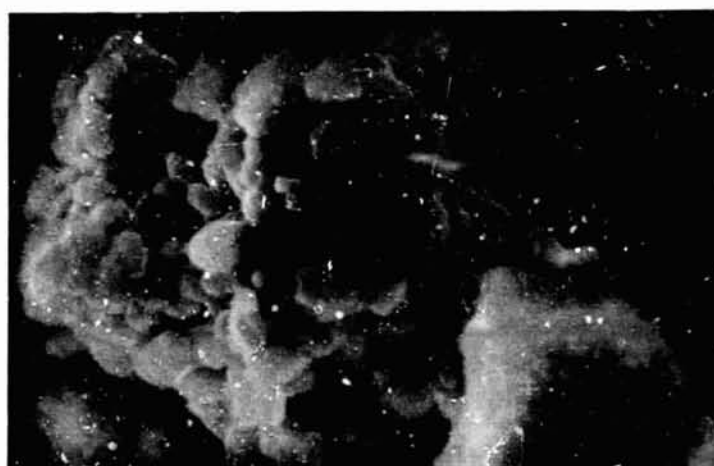
3000 X



Titanium oxalate

215

3000 X



Zinc oxalate

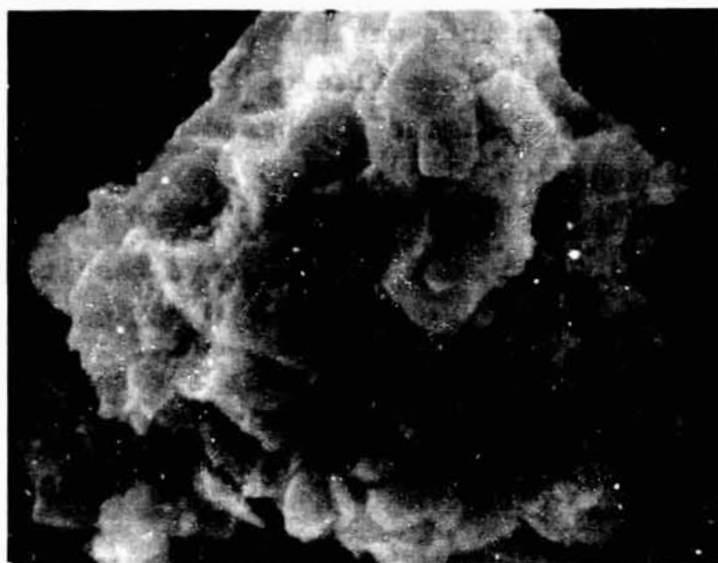
217

3000 X

Figure 3.23. SEM VIEWS OF MOX MATERIAL AND INDIVIDUAL OXALATES

REPRODUCIBILITY OF THE
ORIGINAL PAGE IS POOR

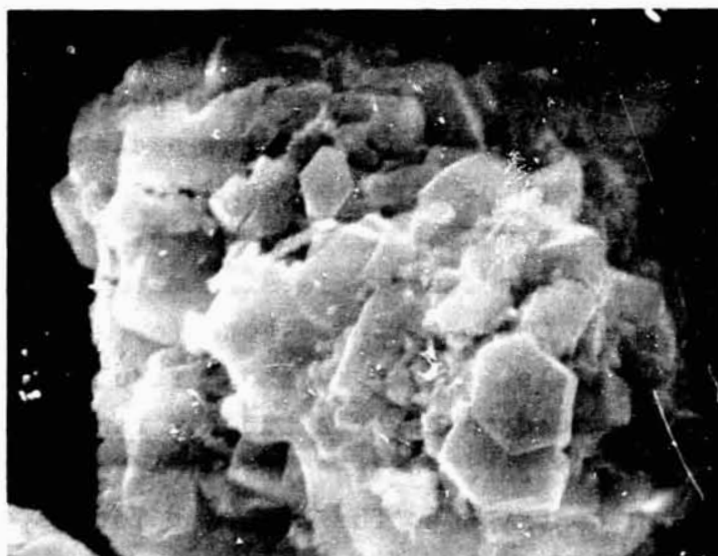
10 μ



310

3000 X

LH-103 (6/2)



312

3000 X

LH-103H (6/2)

Figure 3.24. SEM VIEWS OF COP MATERIALS CALCINED AT 600°C FOR 2 HOURS

REPRODUCTION OF
ORIGINAL PHOTOGRAPH

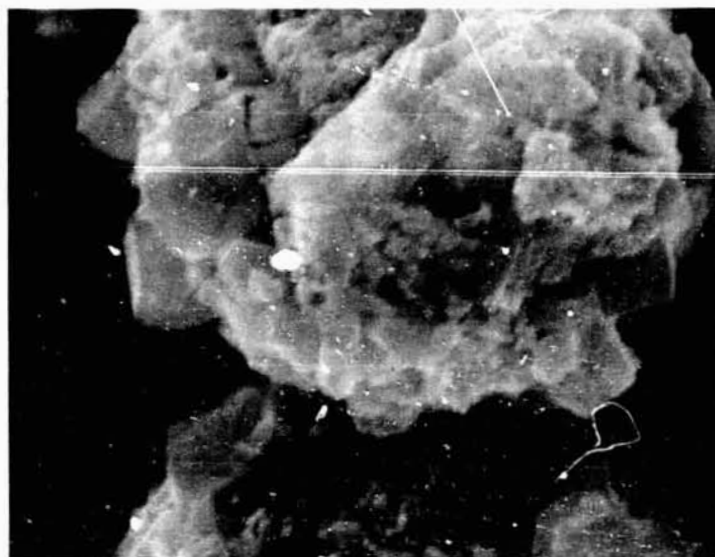
LH-103C(6/2) was similar to that for the other LH-103-based materials. The major departure was the microstructure of MOX(6/2) shown in Figure 3.25; the particle size of this material was significantly smaller than that of the COP-based materials. These particle size relationships also carried over to the Zn_2TiO_4 powders produced at 1050°C as seen in Figure 3.26 and 3.27. The greater reactivity observed at 600°C for MOX may have resulted from the fine particle size/high surface area of the MOX material.

These studies show that MOX materials are as reactive as COP materials and also that a potential exists for achieving a pigment of finer particle size. This leads to the MOX studies discussed in the following sections.

3.4.2 Particle Size ("MOX" Process)

The mixed oxalate studies were conducted to determine if the particle size of the precursor oxalates and the Zn_2TiO_4 obtained from their calcination could be controlled. This investigation was prompted by the observation that COP materials had a tendency toward agglomeration, which might be avoided through mixing of the individually precipitated zinc and titanium oxalates. In these investigations, three sets of experiments were conducted leading to 3 batches designated: MOX, MOX-A and MOX-B. In the preceding section we noted that a finer particle size material was obtained with MOX as compared to COP materials, both for the precursors and the calcined materials. Based on these results, the "MOX" process studies were expanded to cover a broader range of calcination conditions. Larger batches (645 grams) of MOX-A and (276 grams) MOX-B were used - in contrast to the 23 grams for MOX. The MOX-A materials had a ZnO/TiO_2 ratio of 1.5:1, whereas the MOX-B and MOX had a ratio of 2.05:1. The lower ratio for MOX-A resulted from a miscalculation of yield for the mixture.

10 μ



313

3000 X

LH-103C (6/2)



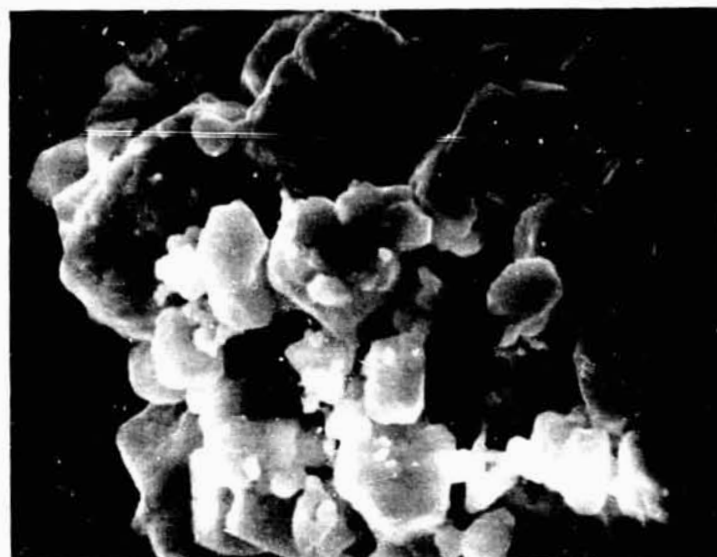
322

3000 X

MOX (6/2)

Figure 3.25. SEM VIEWS OF COMPACTED COP AND MOX MATERIALS
CALCINED AT 600°C FOR 2 HOURS

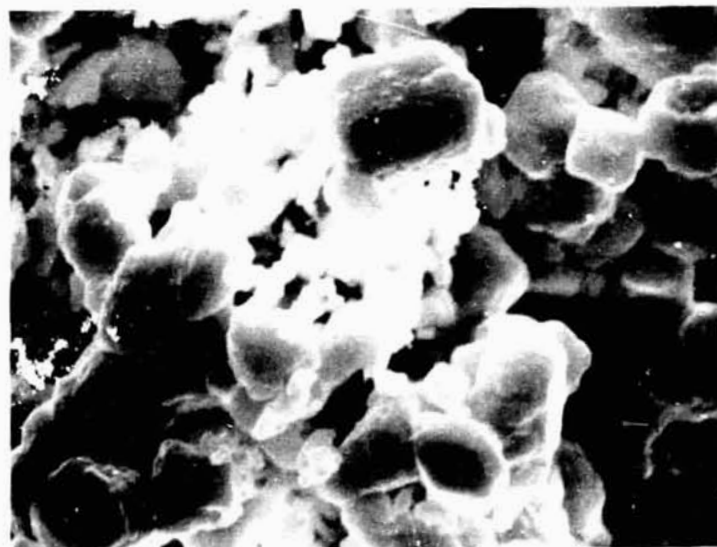
10 μ



366

3000 X

LH-103 (6-10.5)



368

3000 X

LH-103H (6-10.5)

Figure 3.26. SEM VIEWS OF COP MATERIALS CALCINED AT 1050°C FOR 2 HOURS

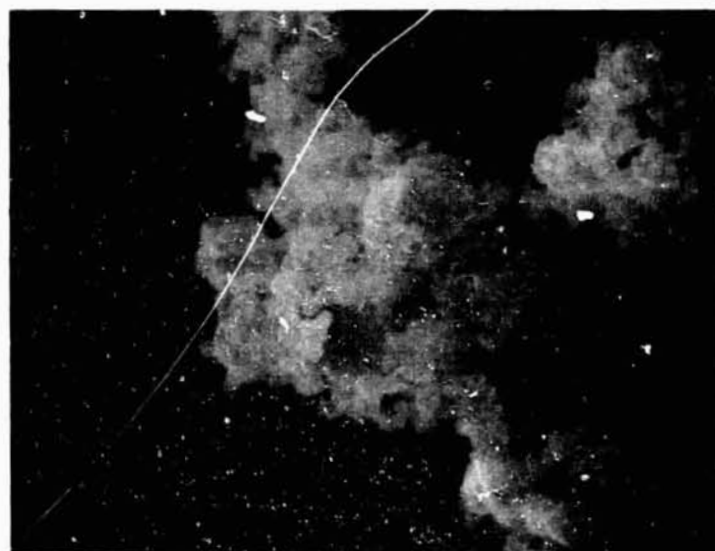
10 μ



367

3000 X

LH-103C (6-10.5)



419

3000 X

MOX (6-10.5)

Figure 3.27. SEM VIEWS OF COMPACTED COP AND MOX MATERIALS CALCINED AT 1050°C FOR 2 HOURS

The heat treatments used for MOX-A and MOX-B were as follows:

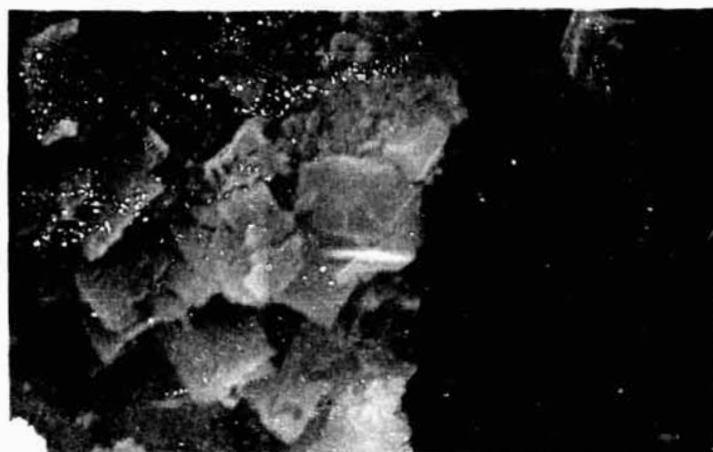
MOX-A:	900°C	-	4, 8, and 16 hours
	1050°C	-	1, 2, 4, and 8 hours
	1200°C	-	0.5, 1, and 2 hours
MOX-B:	900°C	-	4 and 16 hours
	1050°C	-	1, 4, and 8 hours
	1200°C	-	0.5 and 2 hours

All samples were first pre-calcined at 600°C to remove volatiles, prior to the final flash calcinations listed above.

X-ray analyses of MOX-A materials using both powder and diffraction pattern techniques show the presence of Zn_2TiO_4 in all samples. There is no evidence of any other phase such as ZnTiO_3 , ZnO , or TiO_2 . This observation is very significant; the 1.5 $\text{ZnO}/1.0 \text{ TiO}_2$ ratio used should have resulted in a pigment with a substantial amount of free TiO_2 . Analyses of MOX-B samples yielded the same results.

All samples were examined using SEM techniques. MOX-A and MOX-B materials exhibited a particle size similar to that for COP materials (Figures 3.28 and 3.29). In contrast, the earlier MOX material calcined at 1050°C had a significantly smaller average particle size. In general the individually precipitated oxalates and the pigments obtained from these precursors possess a smaller average particle size than do those prepared in the COP method. This difference in average particle size may have resulted from the ball-milling employed to blend the individually precipitated oxalates. COP materials are not ball-milled. As pointed out earlier, the batch sizes of MOX-A and MOX-B pigments were much larger than the original MOX batch. In the mixing process the ball charge was about 30% for MOX and 15% for MOX-A and MOX-B. In addition, the ball-to-powder charge ratio was about 1:1 for MOX whereas it was about 1:4 for the larger batch MOX-A and MOX-B. Thus, the smaller MOX particle size could have resulted from a more rigorous grinding.

10 μ



COP
(LH-103)

No. 314

3000X



MOX-A

No. 473

3000X



MOX-B

No. 486

3000X

Figure 3.28. SEM VIEWS OF COP AND MOX MATERIALS
CALCINED AT 600°C/2hr.

10 μ



COP
(LH-103)

No. 366

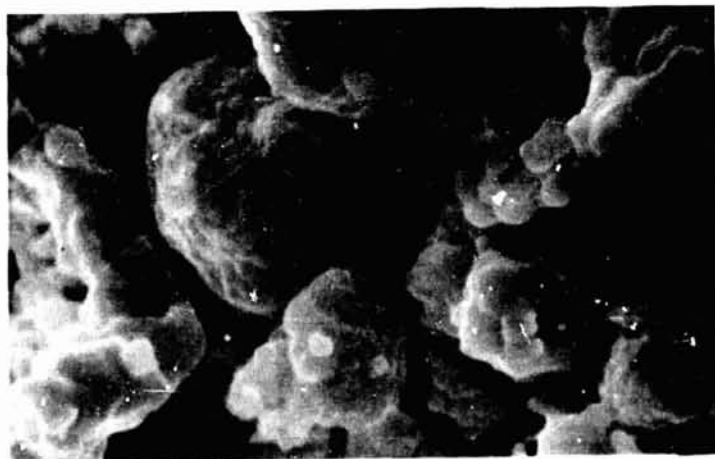
3000X



MOX-A

No. 468

3000X



MOX-B

No. 490

3000X

Figure 3.29. SEM VIEWS OF COP AND MOX MATERIALS
CALCINED AT 1050°C/2hr.

3.4.3 Effect of Ball Milling

To evaluate the effect of ball-milling oxalate precursors (i.e., prior to calcination) on the particle size and optical properties of pigments, samples of a COP precursor material and of a "MOX" material were subjected to a controlled ball milling experiment. The ball milling was accomplished using a ball-to-charge ratio of 1:1 and a ball milling time of 16 hrs. After ball-milling, the samples (LH-105BM and MOX-A BM) and the control (i.e., non-ball milled) materials were pre-calcined at 600°C/2 hr and then calcined at 1200°C/2 hr.

The ball-milled, uncalcined powders are somewhat finer than the non-ball-milled powders and have fewer agglomerates. For the pigments prepared at 600°C the same relationship exists. For the 1200°C calcined materials, the differences are more subtle. In the ball milled samples, LH-105BM(6-12) and MOX-A BM(6-12), the larger particles were about the same size as those in the non-ball milled samples, i.e., about 3-5 μ . However, there was definite evidence of finer particles and of less necking for the BM samples, as compared to the non-ball milled.

These pigments were sprayed onto IRIF coupons as powders. Diffuse reflectance spectra were recorded in the spectral range 325-2600nm. Figure 3.30 and 3.31 show these spectra in the 325-500nm range; the spectra of the powders in the 500-2600nm region was essentially flat. The pertinent data are as follows:

<u>Pigment</u>	<u>Reflectance Values</u>			<u>Coating Wt. gms.</u>
	<u>R₃₅₀</u>	<u>R₄₅₀</u>	<u>R_{i-r}</u>	
LH-105(6-12)	62.3	81.8	85.5	.0454
LH-105(6-12) BM	62.7	84.9	89.0	.0813
MOX-A(6-12)	62.3	81.5	86.0	.0710
MOX-A(6-12) BM	66.5	84.9	88.5	.0836

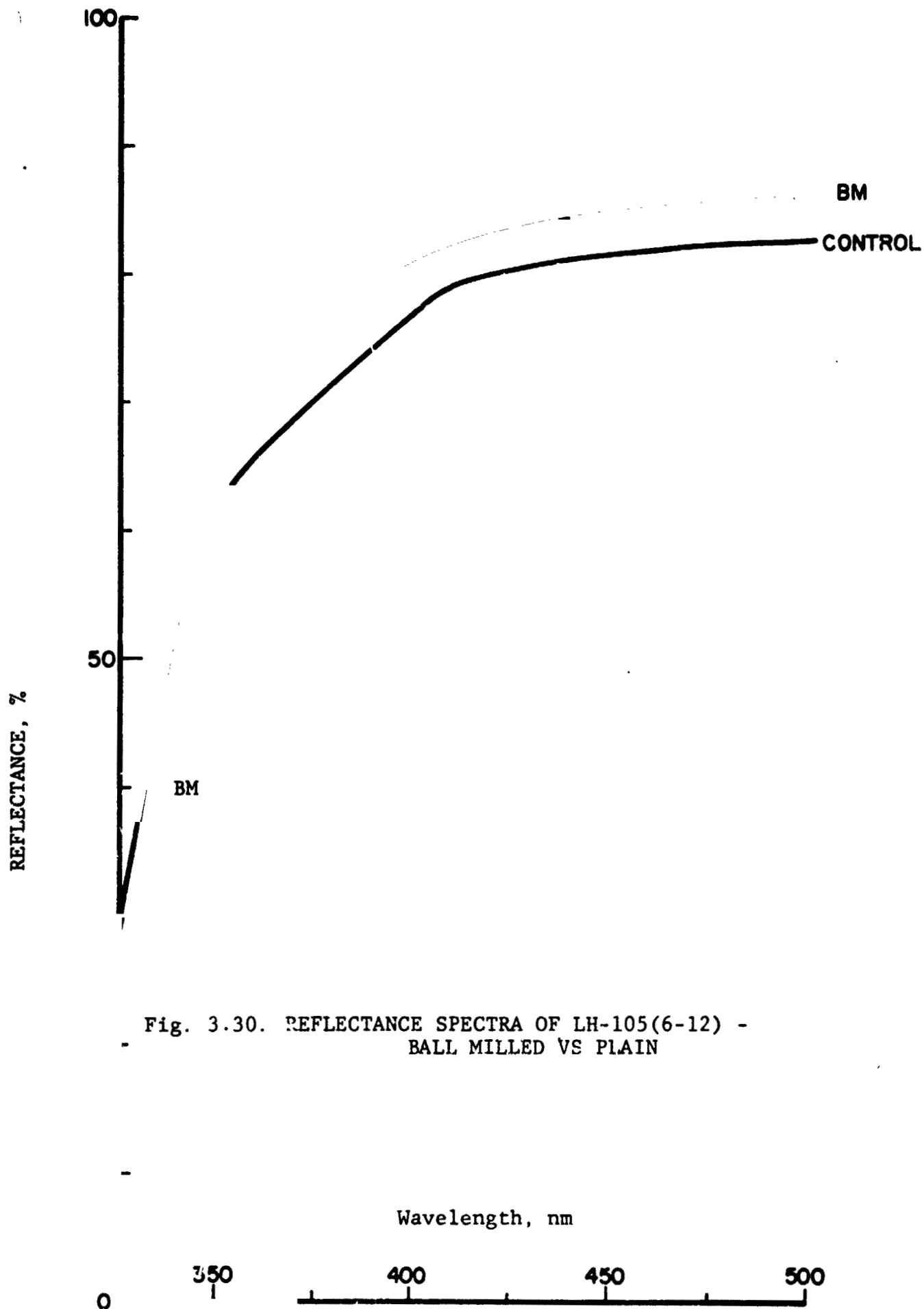
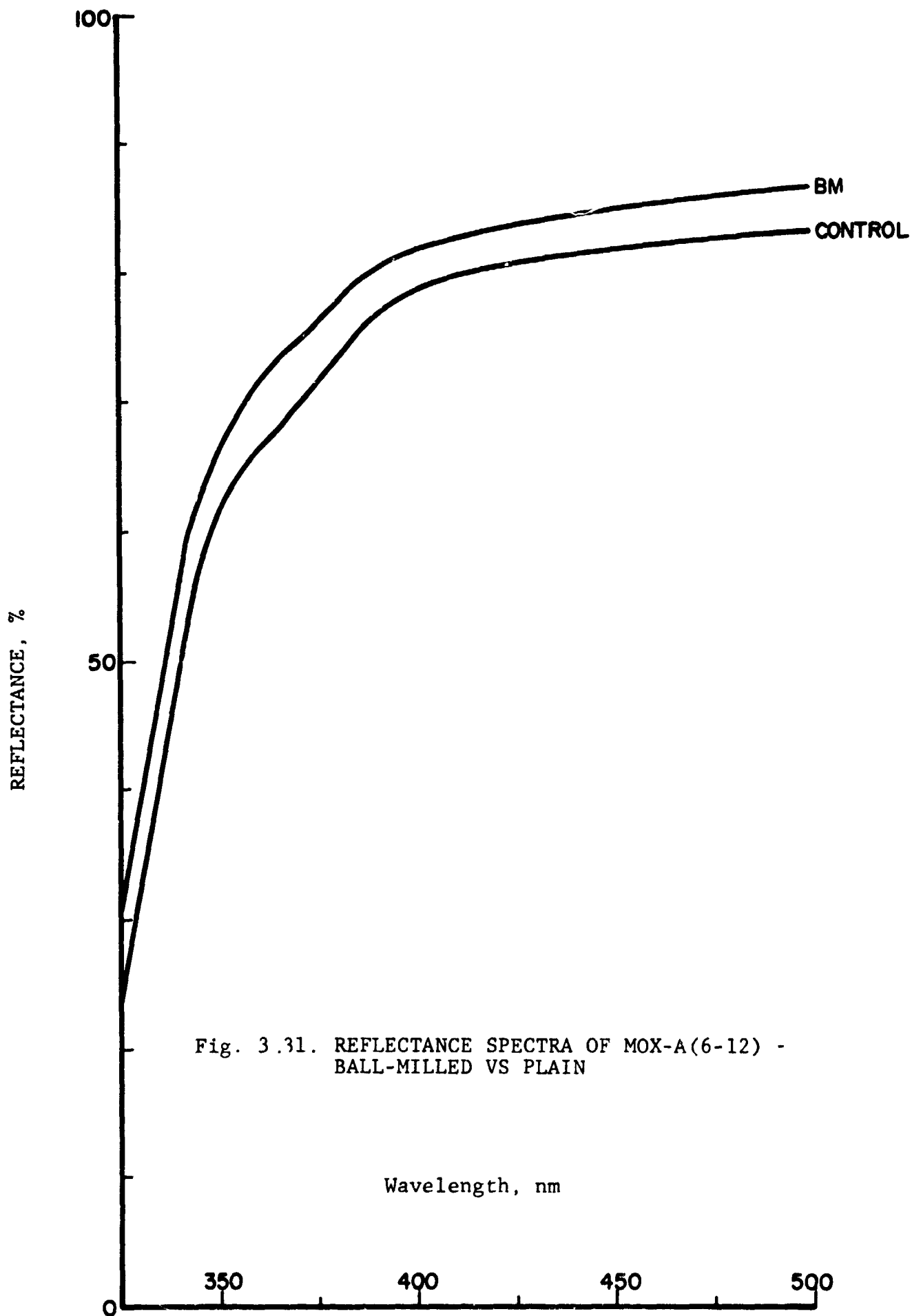


Fig. 3.30. REFLECTANCE SPECTRA OF LH-105(6-12) -
BALL MILLED VS PLAIN



The reflectance levels in both the COP and MOX pigments were higher for the ball milled than for the non-ball milled, as shown in Figures 3.30 and 3.31. The obvious differences in the coating weights of the samples points to the possibility of higher reflectance due to greater thickness. The increase in reflectance, however, was similar for the two materials, and the much higher coating weight difference between LH-105(6-12) and LH-105(6-12) BM did not result in a gross increase in any of the R values. Therefore, ball milling apparently does effect a real increase in reflectance.

Ball milling parameters such as ball charge and ball to powder ratio may be quite critical to the blending/grinding process. Particle size reduction can be obtained by fairly rigorous milling conditions. However, optimum conditions for comminution have not been established in terms of their attained effects on reflectance spectra and especially on reflectance stability to ultraviolet radiation.

3.4.4 Zinc Oxalate Studies

Studies were conducted to establish a procedure for the production of a finer particle size zinc oxalate. In early studies a one hour hold at 90°C had been set as a "standard" precipitation condition for both zinc oxalate (ZnOx) and "TiOX". Precipitation of the latter requires such a condition for complete reaction. The mixed oxalate ("MOX" process) studies had revealed the following:

- 1.) The reaction between ZnCl_2 and $\text{H}_2\text{C}_2\text{O}_4$ in aqueous solution at 90°C results in a precipitate of theoretical composition $(\text{Zn}_2\text{C}_2\text{O}_4 \cdot 2\text{H}_2\text{O})$ and yield.
- 2.) The ZnOx precipitate obtained under these "standard" conditions is considerably coarser in particle size than the "TiOX".

- 3.) In calcinations of "MOX" materials, with all other conditions the same, the particle size of the fired product, Zn_2TiO_4 , is directly related to the particle size of the precursor.

A finer particle size ZnOx is desirable for two reasons: first, to obtain precursors of finer particle size and thus, also, of the fired product, and second, to obtain improved mixing of ZnOx with "TiOX". A closer match of the particle sizes of the ZrOx and "TiOX" should improve mixing characteristics, enhance their reactivity, and increase the uniformity in the reacted binary oxide.

Experimental work was directed toward establishing the conditions necessary for obtaining ZnOx of a fine particle size. It was theorized that the fairly coarse size of ZnOx from a $90^\circ\text{C}/1$ hr precipitation could result from nucleation and growth afforded by the relatively high temperature-long time conditions. Accordingly, precipitations were carried out under lower temperatures and abbreviated times as shown in Table 3.11. Some of these reactions were also carried out in alcohol (rather than aqueous) media. Early work in coprecipitation had shown that an extremely fine particle morphology could be achieved in an alcohol system.

3.4.4.1 Preparation Methods

The ZnCl_2 solutions were prepared by dissolving 50 grams of reagent grade ZnCl_2 in 100 ml of H_2O or in 150 ml of CH_3OH . The reactions were observed to be exothermic. Oxalic acid solutions were prepared by dissolving 50 grams $\text{H}_2\text{C}_2\text{O}_4 \cdot 2\text{H}_2\text{O}$ in 350 ml H_2O or in 350 ml of CH_3OH . These dissolutions are endothermic. For experiments in ethanol and isopropanol media the amounts used were 25 grams ZnCl_2 in 100 ml of alcohol and 25 grams $\text{H}_2\text{C}_2\text{O}_4 \cdot 2\text{H}_2\text{O}$ in 200 ml of alcohol.

The ZnCl_2 solution was reacted with the oxalic acid solution, with the latter being 10% in excess of the amount theoretically required for complete reaction. Precipitations in a water medium were observed to occur rapidly, resulting in rapid opacification of the liquid. On cessation of stirring, settling of the ZnOx occurred within about 10 minutes, leaving a clear supernatant liquid.

Table 3.11
SUMMARY OF ZnOx PRECIPITATION STUDIES

Sample *	Precipitation Conditions			Precipitate	
	Temp., °C	Medium	Yield, %	Particle Size, (μ)	Wt. Loss, % 600°C/2 hr
ZnOx/10/60	10	H ₂ O	100		56.97
ZnOx/RT**	Room	H ₂ O	100	0.5-2	57.07
ZnOx/RT/60	Room	H ₂ O	100	0.5-2	57.07
ZnOx/40/5	40	H ₂ O	100	0.5-3	57.06
ZnOx/40/60	40	H ₂ O	100	0.5-3	57.03
Zn /90/60	90	H ₂ O	100	1-4	57.00
ZnOx/RT/M-60	Room	CH ₃ OH	14	0.2-1	57.07
ZnOx/55/M-5***	55	H ₂ O-CH ₃ OH	56	0.5-2	57.27
ZnOx/55/M-60	55	H ₂ O-CH ₃ OH	54	0.5-2	57.55
ZnOx/RT/E-60	Room	C ₂ H ₅ OH	21		56.23
ZnOx/RT/I-60	Room	C ₃ H ₇ OH	27		56.84
		(2-propanol)			

* Sample notation: ZnOx/Temperature (°C)/time of stirring in minutes at temperature.
 ** ZnCl₂ solution added to H₂C₂O₄ solution with no stirring. All other samples stirred for times shown.
 *** H₂C₂O₄ in CH₃OH (M), in C₂H₅OH (E) and in CH₃CHOHCH₃ (I).

Alcohol precipitations exhibit somewhat different characteristics. In a methanol system, ZnOx appears to form as very fine particles. This is evidenced in a translucent (as opposed to opaque) appearance of the supernatant, and also by longer times for settling of the solids. In the cases of ethanol and iso-propanol, a gel-like precipitate formed rapidly upon addition of the reactants. The gelatinous nature of the precipitate caused it to remain in a suspended state in the ethanol or isopropanol with little settling. The ZnOx was recovered by vacuum filtration using a Buchner funnel system. All precipitates formed in aqueous media filtered readily. Of those materials formed in alcohol media, particularly in methanol, all required re-filtrations of the filtrate to completely recover the solids. This, of course, evidences the colloidal nature of these precipitates. All materials were washed thoroughly in water or alcohol (the wash medium was the same composition as the precipitation medium), until a neutral pH was achieved in the filtrate. The final step was air-drying in an oven at 80°C for 16 hours.

3.4.4.2 Characterization of ZnOx

In characterizing the various ZnOx precipitates, data were obtained on phase identification (X-ray), precipitation yield, particle morphology (SEM), and weight loss on thermal decomposition to ZnO. Analyses by X-ray techniques of precipitates obtained in water and in methanol media showed them to be $\text{ZnC}_2\text{O}_4 \cdot 2\text{H}_2\text{O}$.

The theoretical yield in the $\text{ZnCl}_2 + \text{H}_2\text{C}_2\text{O}_4$ reaction is calculated from a simple molecular weight relationship, i.e., 1 mole of ZnCl_2 or 136.28 grams will produce 1 mole of $\text{ZnC}_2\text{O}_4 \cdot 2\text{H}_2\text{O}$ or 189.42 grams. As shown in Table 3.11, a 100% yield was obtained in all of the aqueous media precipitations, including the 10°C experiment (ZnOx/10/60).

Alcoholic media result in low yields (Table 3.11). Experiments were conducted to determine if $\text{ZnC}_2\text{O}_4 \cdot 2\text{H}_2\text{O}$ might exhibit a limited solubility in alcohol. This was done by stirring $\text{ZnC}_2\text{O}_4 \cdot 2\text{H}_2\text{O}$ into various alcohols for one hour and weighing the dry powder before and after this treatment. The results show no detectable solubility of ZnOx in methanol, ethanol, or isopropanol, thus ruling this out as a possible reason for the low yields.

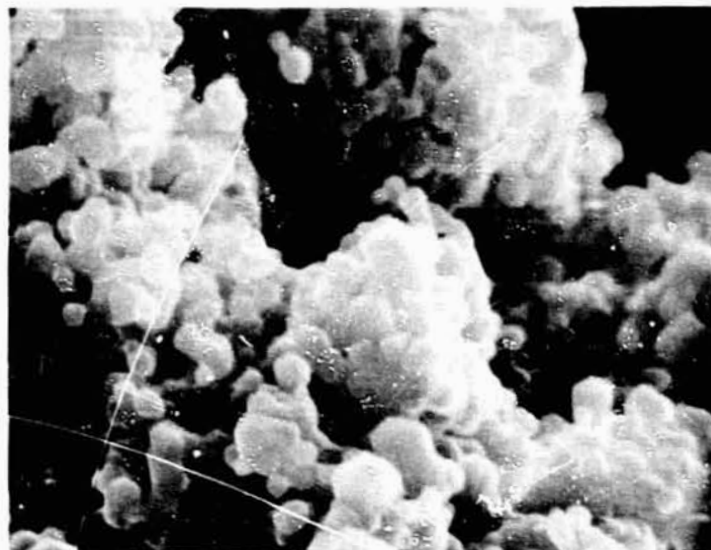
SEM photomicrographs show that precipitations conducted in water at moderate (room to 40°C) temperatures yield particles which are finer than those obtained at "standard", conditions i.e., $\text{ZnOx}/90/60$. The finest precipitate was that obtained in a methanol medium at room temperature ($\text{ZnOx}/\text{RT}/\text{M}-50$).

3.4.4.3 Calcination Studies

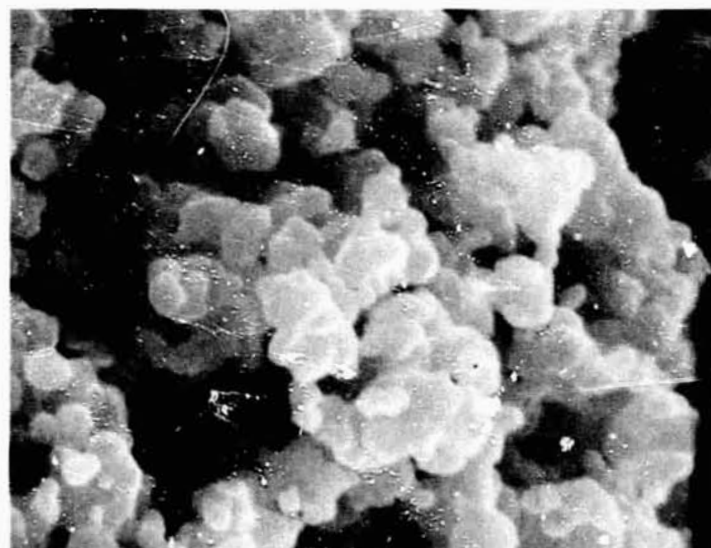
Percentage weight losses on thermal decomposition of the oxalate precursor to ZnO by calcination of $600^\circ\text{C}/2$ hrs are also listed in Table 3.11. The theoretical weight loss for this reaction is 57.04%. As the data show, the experimental values for the water precipitated materials are very close to the theoretical value. The alcohol precipitated materials exhibit calcination weight losses which are not as close, possibly due to an absorbed water effect.

Photomicrographs of zinc oxide obtained by thermal composition ($600^\circ\text{C}/2$ hrs) of zinc oxalate are presented in Figures 3.32 through 3.35. Among the precipitates, the methanol precipitate ($\text{ZnOx}/\text{RT}/\text{M}-60$) was clearly of finer particle size, and the "standard" precipitate ($\text{ZnOx}/90/60$) considerably coarser, than the other zinc oxalates. Among the calcined products, this size relationship does not hold for the methanol material, but the calcined "standard" material is significantly coarser. The materials are all composed of submicron particles with the largest size being about one micron.

1 μ



a) No. 641 ZnOx/RT(6/2) 10KX

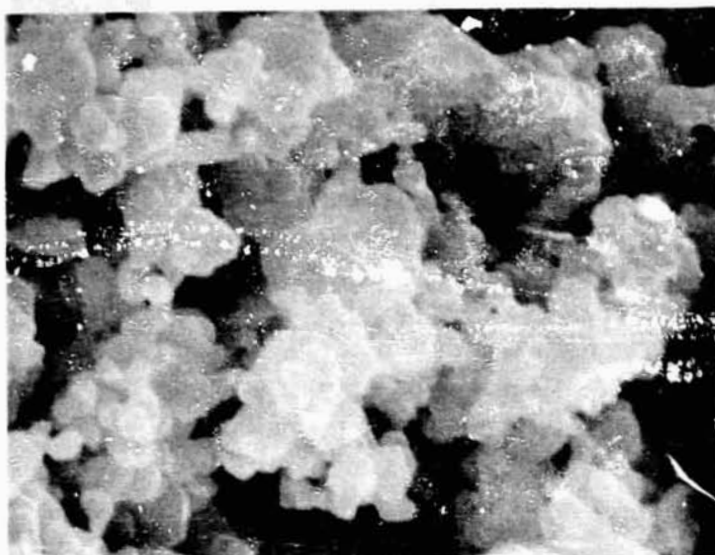


b) No. 644 ZnOx/RT/60(6/2) 10KX

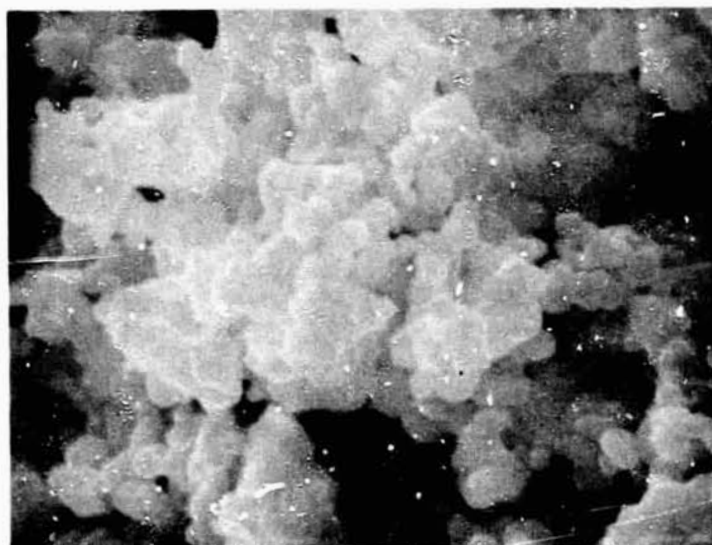
Figure 3.32 SEM Views of Zinc Oxalate Precipitates
Calcined at 600°C/2 hr.

REPRODUCIBILITY OF THE
ORIGINAL PAGE IS POOR

1 μ



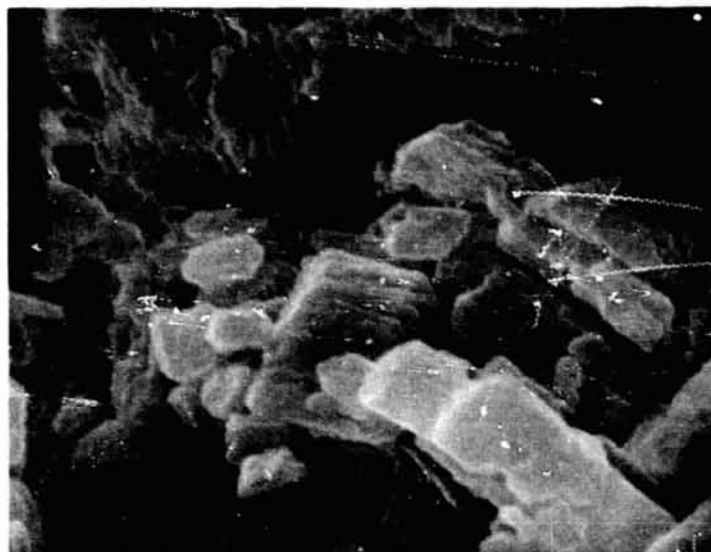
a) No. 638 ZnOx/40/5(6/2) 10KX



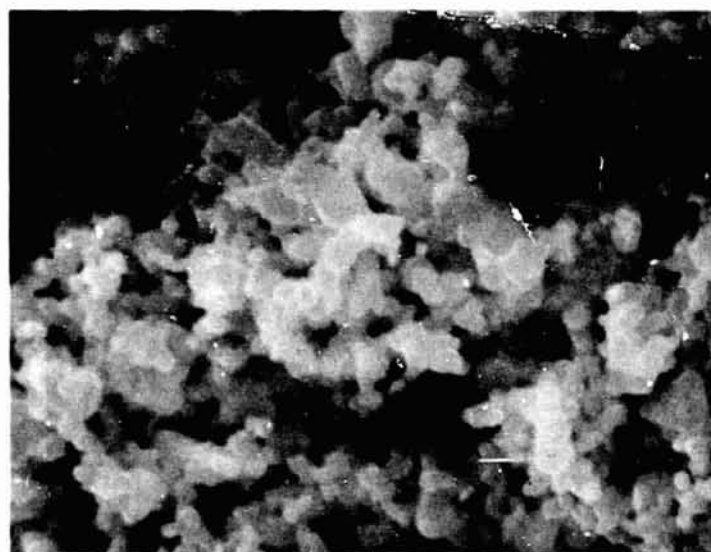
b) No. 645 ZnOx/40/60(6/2) 10KX

Figure 3.33 SEM Views of Zinc Oxalate Precipitates
Calcined at 600°C/2 hr.

1 μ



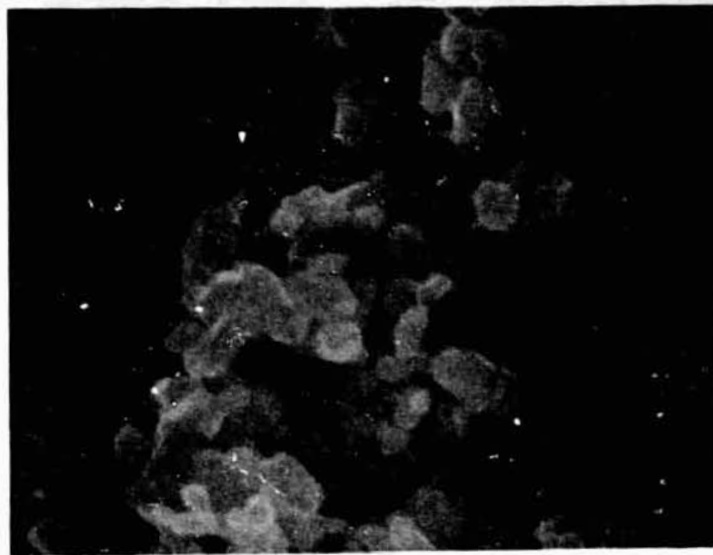
a) No. 643 ZnOx/90/60(6/2) 10KX



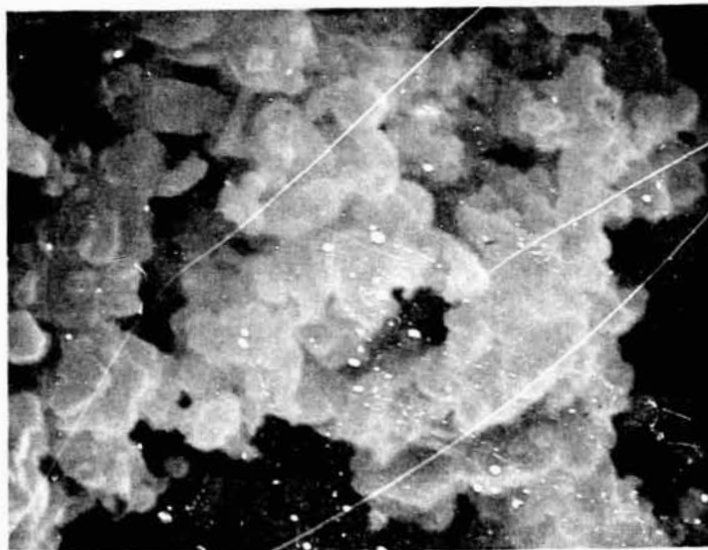
b) No. 642 ZnOx/RT/M-60(6/2) 10KX

Figure 3.34. SEM Views of Zinc Oxalate Precipitates
Calcined at 600°C.

1μ



a) No. 640 ZnOx/55/M-5(6/2) 10KX



b) No. 639 ZnOx/55/M-60(6/2) 10KX

Figure 3.35. SEM Views of Zinc Oxalate Precipitates
Calcined at 600°C

3.4.4.4 Zn₂TiO₄ Synthesis

Zinc orthotitanate materials were synthesized by reacting the different zinc oxalate sources with the standard "TiOX" powder. Since the above described ZnOx powders were shown to be of finer particle size than the "standard" ZnOx precipitated at 20°C/hr, a finer particle size zinc orthotitanate was expected.

A summary of the experiments is presented in Table 3.12. As an additional effort to obtain finer particle size materials, some of the "MOX" compositions were pre-calcined at 400°C for 10 minutes and for two hours, and at 600°C for 10 minutes, in contrast to the standard pre-calcine conditions of 600°C for 2 hours. In the decomposition studies (see Section 3.3) it had been shown that decomposition of ZnOx-"TiOX" was essentially complete after 2 hours at 400°C. Therefore, a finer particle size material might be obtained under more moderate (than 600°C/2hr) pre-calcine conditions.

Gravimetric analyses show that after an initial calcination at 400°C/10 min., decomposition is incomplete as indicated by the wt loss of 22.27%. An additional weight loss of 31.25% occurred on subsequent calcination at 900°C for complete decomposition. The other materials calcined at 400°C for a longer time (2 hrs) underwent essentially complete decomposition. Their subsequent weight losses of 1.14% and 1.17% upon calcining at 900°C were, however, significantly greater than the values of 0.20% or less for the other samples.

Particle size effects are discussed briefly below, according to the three source groups: ZnOx/RT/60, ZnOx/10/60, and ZnOx/Alcohols. A complete analysis of particle size vs precipitation parameters is given in IITRI Report C6233-52.

TABLE 3.12

SUMMARY OF ZINC ORTHOTITANATE SYNTHESIS USING DIFFERENT ZINC OXALATE SOURCES*

Designation	ZnOx Source	Calcination	
		Temperature/Time	Wt. Loss, %**
MOX/RT/60(45)	ZnOx/RT/60	400°C/10 min.	22.27
MOX/RT/60(459)		400°C/10 min. + 900°C/2 hr	31.25
MOX/RT/60(4L)	ZnOx/RT/60	400°C/2 hr	52.89
MOX/RT/60(4L9)		400°C/2 hr + 900°C/2 hr	1.14
MOX/RT/60(65)	ZnOx/RT/60	600°C/10 min.	53.67
MOX/RT/60(659)		600°C/10 min. + 900°C/2 hr	0.17
MOX/RT/60(6L)	ZnOx/RT/60	600°C/2 hr	53.75
MOX/RT/60(6L9)		600°C/2 hr + 900°C/2 hr	0.11
MOX/10/60(4)	ZnOx/10/60	400°C/2 hr	53.02
MOX/10/60(4-9)		400°C/1 hr + 900°C/2 hr	1.17
MOX/10/60(6)	ZnOx/10/60	600°C/2 hr	54.02
MOX/10/60(6-9)		600°C/2 hr + 900°C/2 hr	0.12
MOX/I-60(6)	ZnOx/RT/I-60	600°C/2 hr	54.05
MOX/I-60(6-9)		600°C/2 hr + 900°C/2 hr	0.19
MOX/I-60B(6)	ZnOx.RT/I-60B	600°C/2 hr	54.12
MOX/I-60B(6-9)		600°C/2 hr + 900°C/2 hr	0.21
MOX/E-60(6)	ZnOx/RT/E-60	600°C/2 hr	54.39
MOX/E-60(6-9)		600°C/2 hr + 900°C/2 hr	0.20

*All compositions 2.0/1.0 Zn:Ti ratio.

**Wt. loss is measured on basis of sample weight before and after each individual calcination.

ZnOx/RT/60 - A 400°C precalcine temperature produces a coarser product than does 600°C. This is probably due to incomplete decomposition at 400°C. Among the 900°C products, the materials which had been precalcined at 600°C/2hrs appeared somewhat coarser than the others. This indicates that the use of more moderate precalcine conditions, i.e., shorter times or lower temperature, can provide a finer particle size pigment. All of the materials were agglomerated to varying extents. This may be alleviated by breaking up of such clusters after the precalcine treatment by ball milling, hand dispersion, or some other technique.

ZnOx/10/60 - The difference in particle size as a function of precalcine temperature also appears with these materials. The 900°C materials were relatively coarse, the particle sizes being larger than those for the previous group. Thus, the use of a low temperature (10°C) precipitated zinc oxalate does not appear to offer any advantages.

ZnOx/Alcohols - The 900/2 Zn₂TiO₄ pigments with alcohol-precipitated zinc oxalate as one of its precursors have finer particle sizes than those with a water-based ZnOx precursor. Again, agglomeration is fairly extensive, indicating the possible need for comminution of the precursor mixture.

3.4.5 Use of Precursors Other Than Oxalates

The precursor materials which received most extensive study were the oxalates prepared in our laboratories, since these materials could be obtained in an extremely fine particle state and in a high purity condition. A limited amount of work was devoted to examination of other precursor materials. Listed in Table 3.13 are a series of mixtures which were reacted at 1400°C in the rapid heat treatment method previously described. These mixtures were prepared by dry ball-milling with porcelain balls for 16 hr.

The fired products exhibit varying states of agglomeration or sintering, ranging from a relatively soft (as in MOX-27) to extremely hard - "clinkers" - (as in MOX-25). From the limited experiments conducted, it is difficult to determine the cause for these differences. X-ray examination of the products showed Zn₂TiO₄ in all cases; however, very small amounts of unidentified phases are evident in the various samples.

Table 3.13

SUMMARY OF REACTION SYNTHESIS STUDIES

<u>Batch No.</u>	<u>Mixture*</u>	<u>Appearance (after firing)</u>
MOX-24	$\text{ZnCO}_3 + \text{TiO}_2$	Yellowish, hard particles
MOX-25	$\text{ZnCO}_3 + \text{"TiOX"}$	Light yellow, very hard agglomerates
MOX-26	$\text{ZnC}_2\text{O}_4 \cdot 2\text{H}_2\text{O} + \text{TiO}_2$	Light yellow, hard particles
MOX-27	$\text{ZnC}_2\text{O}_4 \cdot 2\text{H}_2\text{O} + \text{"TiOX"}$	White powder, soft particles

*All mixtures prepared with a Zn:Ti mol ratio of 2.05 1.

Note: Samples reacted at 1400°C/5 min.

From this study, oxalates should remain the choice for obtaining a pigment with the desired physical and optical properties. Because the full range of zinc and/or titanium precursors and their combinations have not been considered, nor calcination conditions fully explored, this area of study may require additional work to determine its full potential.

3.5 STOICHIOMETRY STUDIES

As discussed in Section 3.3.2, MOX-A has a 1.5:1 Zn/Ti ratio; it lacks 0.5 mole of Zn to be Zn_2TiO_4 , but reveals no x-ray evidence of any phases other than Zn_2TiO_4 . In order to investigate this anomaly, studies were conducted in which the Zn/Ti ratio was varied: first over the wide range of 0.5:1.0 to 2.5:1.0, and, later, over the narrow range of 1.90:1.0 to 2.05:1.0. These studies are detailed in the following discussions. An extensive discussion of the optical properties of these stoichiometry series pigments is presented in Section 4.7.

3.5.1 Zn/Ti Ratio of 0.5/1 to 2.5/1

The effects of widely different stoichiometries upon the optical properties of $\text{ZnOx}/\text{"TiOx"}$ mixtures fired at elevated temperatures were investigated. The compositions studied were as follows:

<u>Designation</u>	<u>Mol Ratio, Zn/Ti</u>	<u>Theoretical Composition Assuming Zn_2TiO_4 Formation</u>
MOX-C	0.5:/1	$\text{Zn}_2\text{TiO}_4 + 3 \text{TiO}_2$
MOX-D	1.0:1	$\text{Zn}_2\text{TiO}_4 + 1 \text{TiO}_2$
MOX-E	1.5:1	$\text{Zn}_2\text{TiO}_4 + 0.33 \text{TiO}_2$
MOX-F	2.0:1	Zn_2TiO_4
MOX-G	2.5:1	$\text{Zn}_2\text{TiO}_4 + 0.5 \text{ZnO}$

The individually precipitated oxalates were processed by ball-milling, then mixed according to the proportions indicated. Samples were precalcined at 600°C for two hours, and half of each sample composition was subsequently flash calcined at 900°C for eight hours, and the other half at 1200°C for two hours. A summary of the evaluation studies is presented in Table 3.14.

Table 3.14

EFFECT OF STOICHIOMETRY ON PROPERTIES OF $\text{ZnO} \cdot \text{TiO}_2$ MATERIALS

Sample	Zn/Ti Ratio	X-Ray Analysis				Wt. Loss, %
		Zn_2TiO_4	ZnTiO_3	ZnO	TiO_2	
MOX-C(6) ¹⁾	0.5	MAJ-1	MAJ-2			
MOX-D(6)	1.0	MAJ-1	MIN-1			
MOX-E(6)	1.5	MAJ-1	MIN-2			
MOX-F(6)	2.0	MAJ-1 *	MIN-2	MAJ-2		
MOX-G(6)	2.5	MAJ-1	MIN-2	MAJ-2		
MOX-C(6-9) ²⁾	0.5	MAJ-1		MIN-2	MIN-1	0.91
MOX-D(6-9)	1.0	MAJ-1 *	MIN-1		MIN-2	0.69
MOX-E(6-9)	1.5	MAJ-1 *				0.20
MOX-F(6-9)	2.0	MAJ-1 *				0.23
MOX-G(6-9)	2.5	MAJ-1		MIN-1		0.42
MOX-C(6-12) ³⁾	0.5	MAJ-1			MIN-1	1.05
MOX-D(6-12)	1.0	MAJ-1			MIN-1	0.64
MOX-E(6-12)	1.5	MAJ-1 *				0.24
MOX-F(6-12)	2.0	MAJ-1 *				0.25
MOX-G(6-12)	2.5	MAJ-1		MIN-1		0.33
Code: MAJ-1 Major Phase 1			* Evidence of $\text{Zn}_2\text{Ti}_3\text{O}_8$ (zinc sesqui-titanate) phase.			
MAJ-2 Major Phase 2						
MIN-1 Minor Phase 1						
MIN-2 Minor Phase 2						

Notes: 1) Calcined at 600°C/2 hr.
 2) Calcined at 600°C/2 hr and at 900°C/8 hr.
 3) Calcined at 600°C/2 hr and at 1200°C/hr.

3.5.1.1 X-Ray Analysis

X-ray diffraction techniques were used to determine the chemical composition of the various samples. As shown in Table 3.14 Zn_2TiO_4 is found to be the major phase in all samples calcined at 600°C and higher, while at 600°C zinc metatitanate (ZnTiO_3) is present (in lesser amounts) as a second phase. These findings indicate that the reaction favors the formation of the orthotitanate in spite of a zinc deficiency (as in MOX-C, MOX-D, and MOX-E). It has been reported (Ref. 3.8) that formation of the hexagonal metacitrate is favored when the TiO_2 is of the rutile crystalline modification or at least easily converted to rutile. Our work with "TiOX" has shown that anatase is formed from this precursor at about 300°C, and that it persists up to temperatures of at least 700°C. Therefore, the lack of X-ray indicated presence of the rutile modification may account for the suppression of zinc metatitanate (ZnTiO_3) formation in favor of Zn_2TiO_4 .

A third compound reported in the ZnO-TiO_2 system (ref. 3.8) is zinc sesquitanate, $\text{Zn}_2\text{Ti}_3\text{O}_8$. This compound is a simple cubic phase having a lattice constant somewhat smaller than that of the face centered cubic Zn_2TiO_4 (8.359Å vs 8.456Å). The fact that both phases are cubic and that the lattice constants are only slightly different result in almost identical d-spacing lines in the powder patterns. However, a simple cubic crystal ($\text{Zn}_2\text{Ti}_3\text{O}_8$) will exhibit a greater number of X-ray lines than a face-centered cubic material as in the case of (Zn_2TiO_4). Such extra lines have been observed in the patterns of MOX-F(6), MOX-D(9) MOX-E(9), MOX-F(9), MOX-E(12), and MOX-F(12), indicating the probable existence of the $\text{Zn}_2\text{Ti}_3\text{O}_8$ phase in these materials. This is a qualitative and not a quantitative observation.

The occurrence of $\text{Zn}_2\text{Ti}_3\text{O}_8$ in MOX-F(6), MOX-D(9), and MOX-E(9) would appear reasonable in that MOX-F(6) is not completely reacted, and MOX-D(9) and MOX-E(9) are zinc deficient compositions. MOX-F(9) and MOX-F(12), however, have Zn/Ti ratios of 2:1 so that the X-ray indication of $\text{Zn}_2\text{Ti}_3\text{O}_8$ along with a negative indication of ZnO (except in MOX-F(6)) is somewhat puzzling. In addition Dulin and Rase (ref. 3.7) reported that $\text{Zn}_2\text{Ti}_3\text{O}_8$ is transformed to $\text{Zn}_2\text{TiO}_4 + \text{TiO}_2$ at 1000°C, and thus the existence of $\text{Zn}_2\text{Ti}_3\text{O}_8$ in MOX-E(12) appears anomalous. The more detailed studies which were performed subsequently suggest that this is the actual behavior and that the formation of TiO_2 in moderately Zn-deficient materials should not be expected. The 900°C results, discussed below add further evidence to this finding. A third phase, ZnO, was detected in two of the 600°C materials, MOX-F(6) and MOX-G(6), probably because at 600°C/2hrs the reaction is not complete. The lack of any detectable TiO_2 , however, may be due to its presence as extremely fine crystallites which would not be within the sensitivity range of the X-rays.

At 900°C, Zn_2TiO_4 is the major phase in all samples - but with evidence of some $\text{Zn}_2\text{Ti}_3\text{O}_8$. The metatitanate, ZnTiO_3 , was observed only in MOX-D(9), suggesting that its conversion to the orthotitanate had occurred in the other samples. A very important observation is that MOX-E(9) does not contain any TiO_2 phase. Relative to Zn_2TiO_4 , the 1.5 to 1 ratio of Zn to Ti for MOX-E would suggest an excess of TiO_2 , but none was detected. The same observation was made in the case of MOX-A, which is of a similar composition. As discussed later, this absence of TiO_2 is confirmed in the optical properties analyses.

At 1200°C, MOX-C(12) and MOX-D(12) show excess TiO_2 as would be expected from their zinc deficient compositions. As was the case at 900°C, the MOX-E and MOX-F samples show only Zn_2TiO_4 - no TiO_2 . The zinc excess in the MOX-G composition shows up clearly as ZnO in the x-ray analysis.

3.5.1.2 Gravimetric Analysis

Upon thermal conversion, all samples calcined at 600°C underwent weight losses of 45 to 48%, corresponding to calculated theoretical decomposition losses. Weight changes were also determined for material calcined at 900° and 1200°C, and these data appear in Table 3.13 and are graphically presented in Figure 3.36. The data show the highest weight loss, about 1% for the MOX-C(12) material. A minimum can be observed for MOX-E and MOX-F materials, and a slight increase for the excess zinc MOX-G samples. There does not appear to be a strong difference between losses at the two temperatures. The observed minimum suggests that materials at or near the stoichiometry of Zn_2TiO_4 exhibit the smallest weight losses. The MOX-E and MOX-F samples also show a strong predominance of Zn_2TiO_4 . The higher weight losses occur in those materials in which TiO_2 or ZnO was detected. Thus, weight loss appears related to completeness of reaction.

Note that the weight losses were quite small, indicating very limited volatility for either the excess TiO_2 or ZnO . The facts that the TiO_2 shows up as a very minor phase (in X-ray patterns) in MOX-C(12) and in MOX-D(12), and not at all in MOX-E(12) in which a 0.33 mol excess of TiO_2 should exist make it clear that various $ZnO.TiO_2$ or titanate complexes are favored over the formation of TiO_2 in mixtures which are moderately Ti-rich relative to Zr_2TiO_4 .

3.5.1.3 SEM Analysis

Examination of SEM photomicrographs of the materials calcined at the three temperature levels have reveal the following:

At 600°C:

1. All samples heterogeneous; agglomerates and discrete particles with a range in particle size and shape.
2. Trend toward finer particles and less agglomeration with increasing Zn/Ti ratio. (See Figures 3.37 and 3.38).

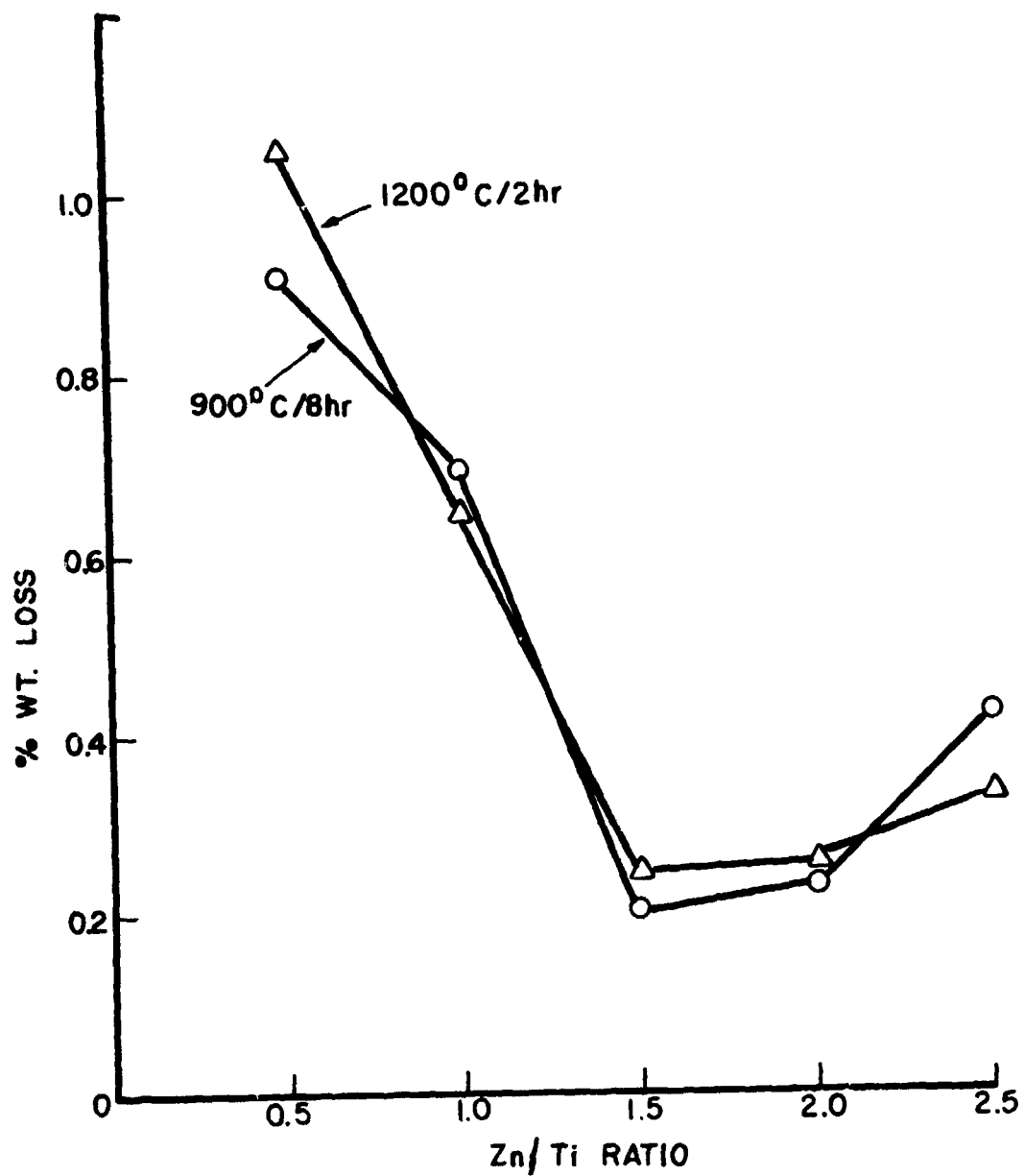
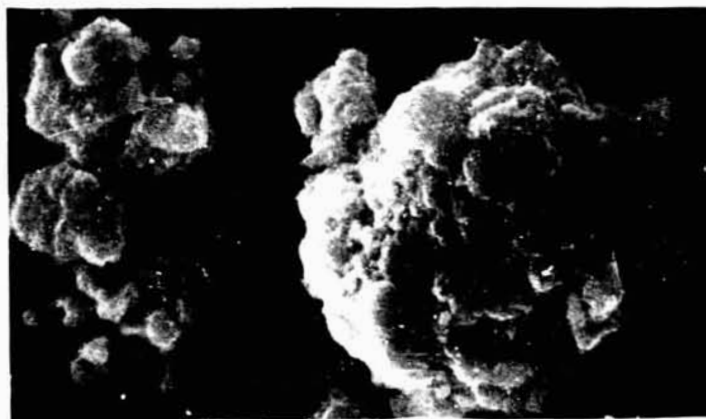


Fig.3.36 % WEIGHT LOSS VS STOICHIOMETRY OF PRECALCINED PIGMENTS

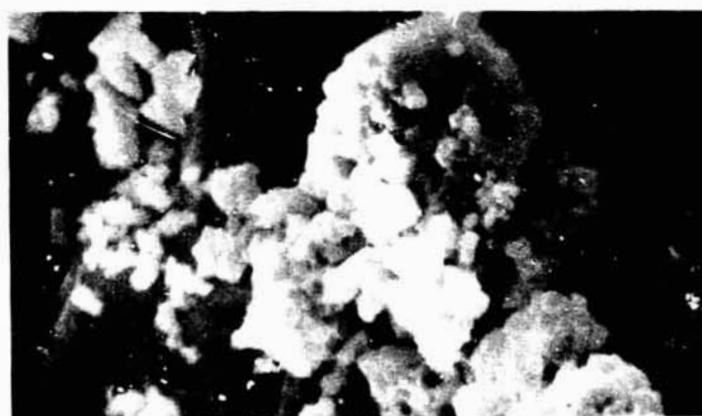
10 μ



a) 581 MOX-C (6):0.5Zn/1Ti 3000X



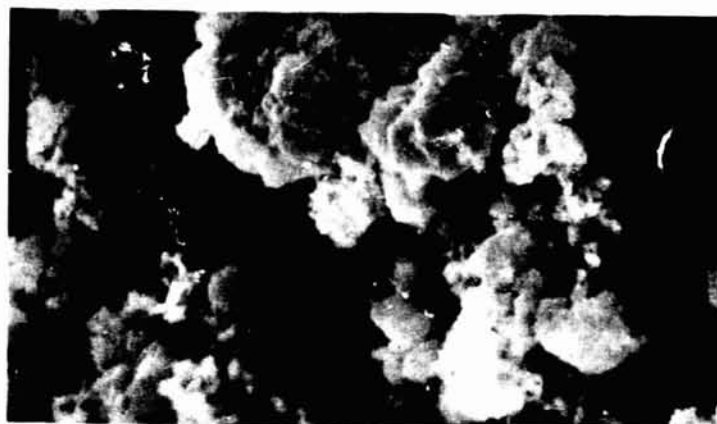
b) 588 MOX-D (6):1.2Zn/1Ti 3000X



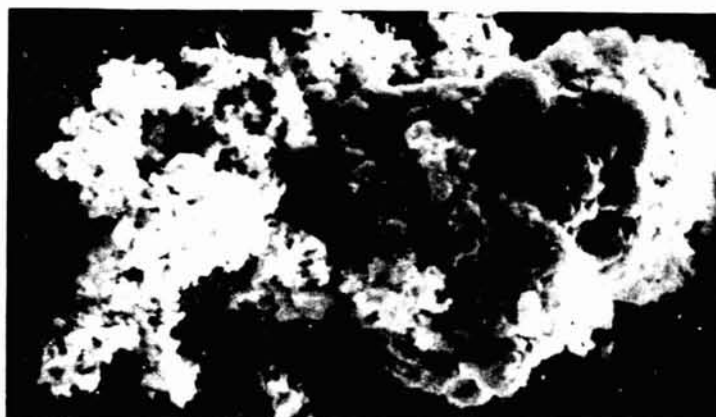
c) 577 MOX-E (6):1.5Zn/1Ti 3000X

Figure 3.37. SEM Views of MOX Stoichiometry Series Samples
Calcined at 600°C/2 Hrs.

10 μ



a) 575 MOX-F(6):2Zn/1Ti 3000X



b) 584 MOX-G(6):2.5Zn/1Ti 3000X

Figure 3.38. SEM Views of MOX Stoichiometry Series Samples
Calcined at 600°C/2 Hrs.

At 900°C:

1. Similar trend in particle size and state of agglomeration. MOX-G(9) appears to have particularly fine particles.
2. All samples contain submicron particles. Largest particles, about 2μ . (See Figures 3.39 and 3.40).

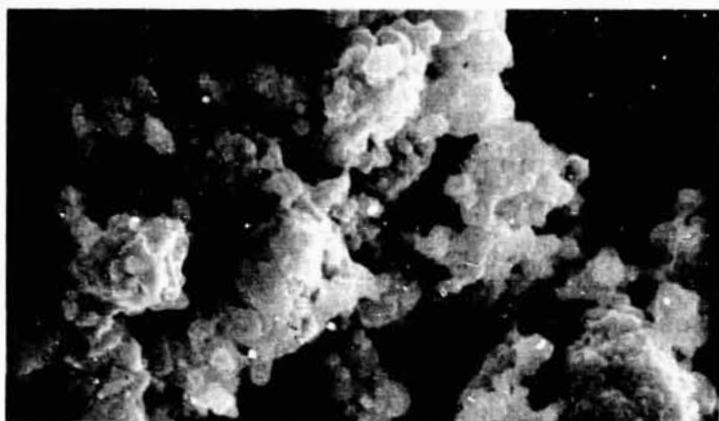
At 1200°C

1. All samples show necking and sintering of particles.
2. Particle size is significantly greater than for the 900°C samples. MOX-C(12) and MOX-D(12) contain some submicron particles. MOX-E(12), MOX-F(12), and MOX-G(12), about $1-5\mu$.
3. MOX-C(12) and MOX-D(12) particles exhibit sharper edges, whereas the others have rounded edges. The necking appears weaker for MOX-C(12) and MOX-D(12) compared to the others. (See Figures 3.41 and 3.42).

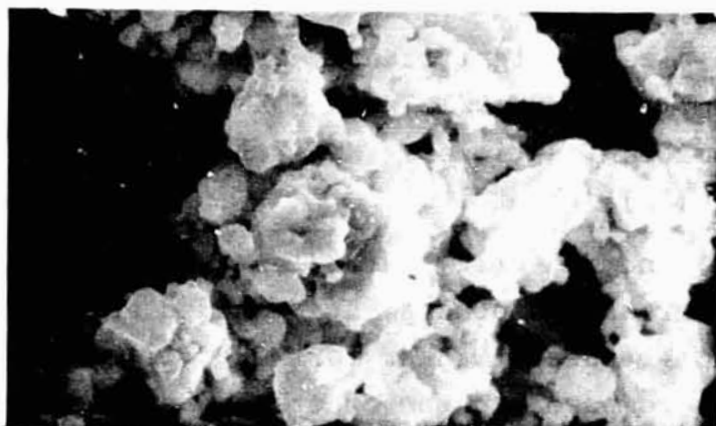
3.5.1.4 Summary

The most significant result of these experiments was the conclusion from X-ray data that relatively pure, single phase Zn_2TiO_4 is produced over a wide stoichiometry range of Zn/Ti mole ratio, viz., from 1.5:1.0 to 2.0:1.0. This is difficult to understand for the 1.5:1 ratio since a definite excess of TiO_2 (0.33 mols) should exist. However, the optical spectral also contain no evidence of free TiO_2 in MOX-E material. This is consistent with and confirms identical observations made in the case of MOX-A materials. Reflectance spectra suggest a pure Zn_2TiO_4 for MOX-E(12) and a somewhat less pure material for MOX-E(9). Detailed analyses of optical data appear in section

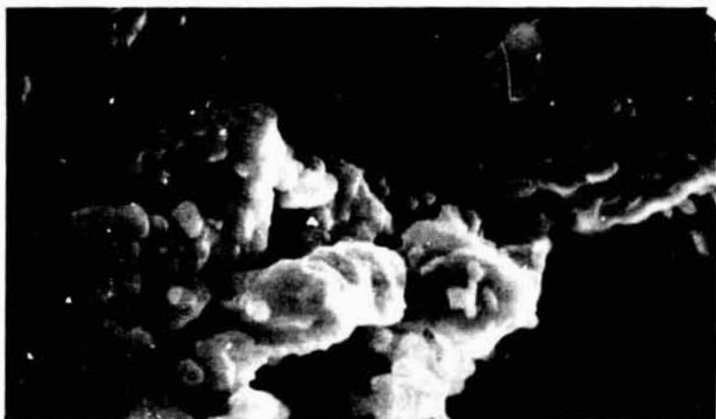
10 μ



a) 587 MOX-C(9) Zn/Ti = 0.5:1.0 3000X



b) 586 MOX-D(9) Zn/Ti = 1.0:1.0 3000X

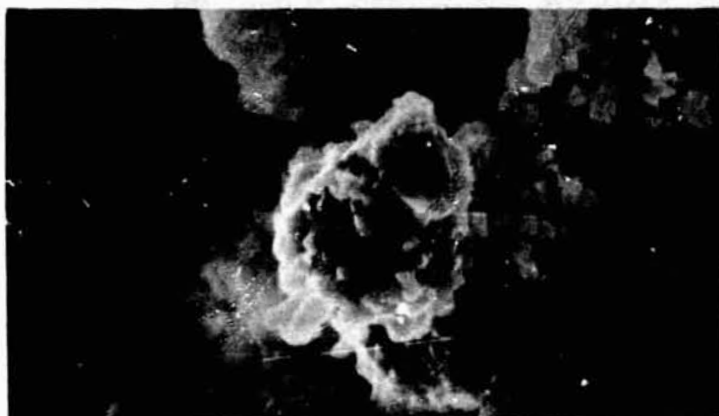


c) 582 MOX-E(9) Zn/Ti = 1.5:1.0 3000X

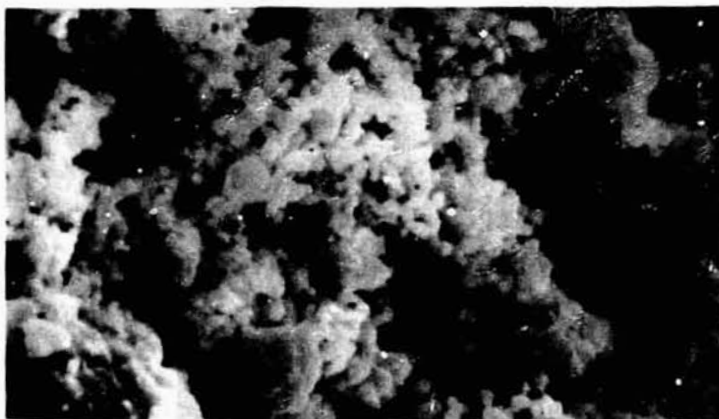
Figure 3.39. SEM Views of MOX Stoichiometry Series Samples
Calcined at 900°C/8 Hrs.

REPRODUCED
ORIGINALLY

10 μ



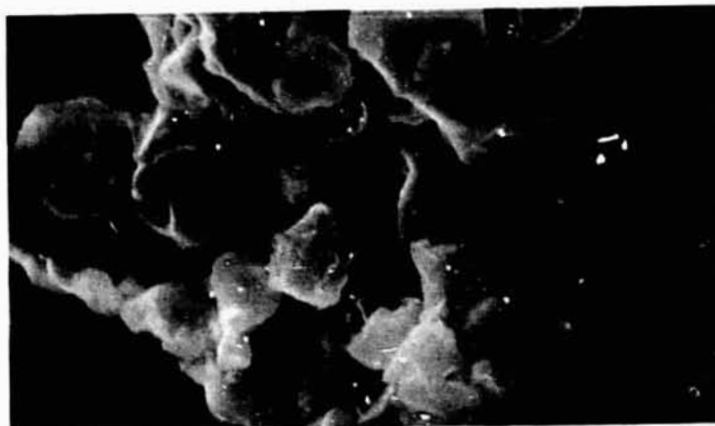
a) 579 MOX-F(9) Zn/Ti = 2.0:1.0 3000X



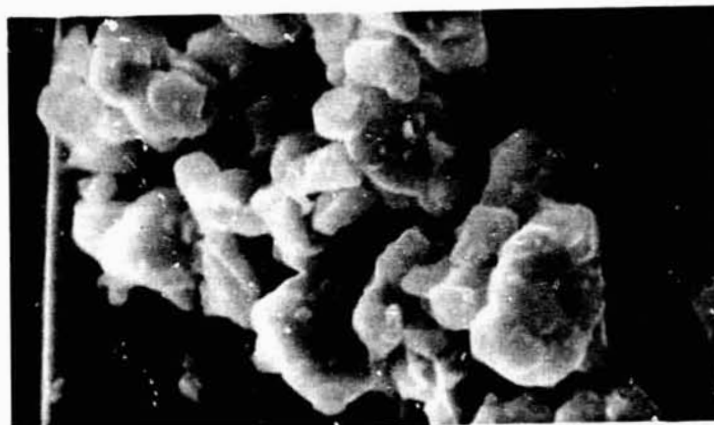
b) 578 MOX-G(9) Zn/Ti = 2.5:1.0 3000X

Figure 3.40. SEM Views of MOX Stoichiometry Series Samples
Calcined at 900°C/ 8 Hrs.

10 μ



a) 580 MOX-C(12) Zn/Ti = 0.5:1.0 3000X



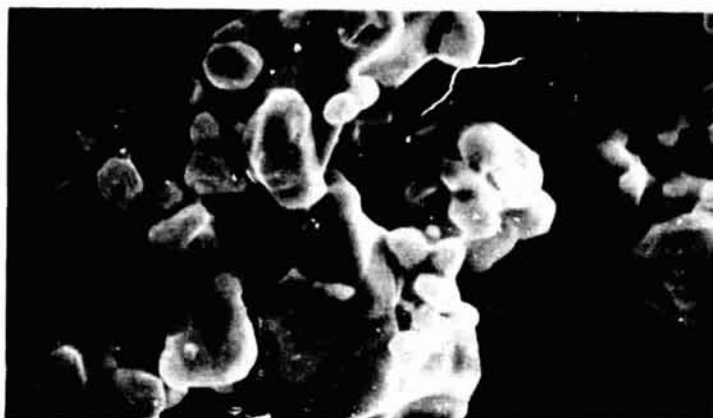
b) 576 MOX-D(12) Zn/Ti - 1.0:1.0 3000X



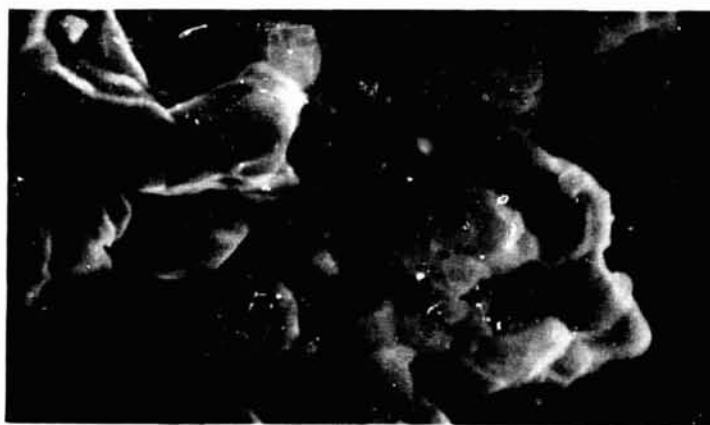
c) 583 MOX-E(12) Zn/Ti = 1.5:1.0 3000X

Figure 3.41. SEM Views of MOX Stoichiometry Series Samples
Calcined at 1200°C/2 Hrs.

10 μ



a) 585 MOX-F(12) Zn/Ti = 2.0:1.0 3000X



b) 574 MOX-G(12) Zn/Ti = 2.5:1.0 3000X

Figure 3.42. SEM Views of MOX Stoichiometry Series Samples
Calcined at 1200°C/2 Hrs.

4.7. Gravimetric data also show that the weight loss encountered at 900°C (i.e., 0.20%) is much too small to indicate a loss of material such as TiO_2 . Furthermore, the vapor pressure of TiO_2 at these temperatures is far too low for any volatilization to occur, which might otherwise explain this absence.

The stoichiometric compositions of the pigments are very unlikely to differ significantly from those experimentally designed; thus, a composition in which the Zn/Ti mole ratio in the "oxalate" precursor mixture is 1.5:1.0, for example, should maintain through calcination. First of all, from the weight loss data we can argue very strongly against any substantial changes in the Zn/Ti ratio upon thermal conversion of the oxalate mixture to the titanate. Furthermore, the presence of the sesqui-titanate phase in some pigments raises the distinct possibility that the absence of TiO_2 in the MOX-E material, for example, occurs because the formation of $\text{Zn}_2\text{Ti}_3\text{O}_8$ is energetically favored.

Zinc sesquitanate ($\text{Zn}_2\text{Ti}_3\text{O}_8$) has the same crystal structure as Zn_2TiO_4 , but it has a slightly smaller lattice parameter, a_0 , (8.359 Å vs 8.456 Å). Since these compounds have such similar lattices, distinguishing them by X-ray analysis is difficult, particularly in fine powders where line broadening occurs. Careful analyses of the back-reflection patterns of the MOX-E pigments, except for a positive indication of ZnO, indicate the presence of $\text{Zn}_2\text{Ti}_3\text{O}_8$. The presence of the sesquitanate and simultaneous absence of ZnO in all samples, except in MOX-F(6), further emphasizes the complex nature of the thermo-chemistry of the oxalate-titanate system.

Our previous assumption, for the oxide-oxide reaction, that an excess ZnO composition of 2.05 Zn/1.00 Ti is necessary for obtaining TiO_2 -free Zn_2TiO_4 (ref.3.3) obviously does not apply to the oxalate precursor methods. These studies show that Zn-deficient oxalate precursors with a Zn/Ti ratio of 1.5:1.0, when calcined, will produce a material exhibiting excellent reflectance, similar to that for a pure Zn_2TiO_4 . MOX-A materials, however,

demonstrate poor stability to ultraviolet irradiation in vacuum. From the results of MOX-A space simulation tests, we can reason that stoichiometries with a Zn/Ti ratio as close as possible to (but less than) 2.0:1.0 would be ideal, because they would result in pigments with no ZnO excess, no TiO_2 excess, and a minimum of less stable titanate species.

3.5.2 Zn/Ti Ratio of 1.90/1 to 2.05/1

In light of the above observations, very definitive stoichiometry studies, in which reflectance properties are correlated in terms of Zn/Ti ratios (in the production of $\text{Zn}_{1.2}\text{TiO}_4$), were carried out. A closer approach to a 2.0:1.0 ratio of Zn/Ti seems desirable in that the ZnO "knee" in the absorption edge could be eliminated, thus resulting in a lower α_s pigment.

Experiments were conducted with four Zn/Ti ratios: 1.90:1.00, 1.95:1.00; 2.00:1.00, and 2.05:1.00. Starting materials were "TiOX" precipitated under 90°C/1 hr conditions and zinc oxalate, 40°C/1 hr. Mixtures were ball milled dry for 16 hours using a 35% ball charge and a 50% total charge. Examination of materials after milling showed that some caking had occurred which could have resulted in poor mixing.

The weight loss data are shown in Table 3.15. All of the oxalate mixtures (of each stoichiometry) were calcined at 600°C/2 hr. One half of the mixture was then calcined at 900°C/2 hr and the other at 1200°C/2 hr.

3.5.2.1 X-Ray Analysis

All of the stoichiometry samples were evaluated using X-ray analyses. Zinc orthotitanate was the major phase in all of the samples. The results can be summarized as follows:

1. 600°C - Zn_2TiO_4 plus small amounts of ZnTiO_3 and ZnO in all samples. No evidence of TiO_2 .
2. 900°C - Zn_2TiO_4 with very faint evidence of ZnO in 2.00:1.00 and 2.05:1.00 Zn/Ti samples, estimated to be less than 4%. No other phases.
3. 1200°C - Same as 900°C.

Table 3.15

SUMMARY OF STOICHIOMETRY STUDIES

Zn/Ti Ratio	Calculation		Wt. Loss, % [*]		Particle Size, microns (SEM)
	Temp., °C	Time, Hrs	Actual	Theoretical	
1.90:1	-	-	-	-	1-5
	600	2	53.65	54.02	SM ^{**}
	900	2	0.31		SM-2
	1200	2	0.40		1-4
1.95:1	-	-	-	-	1-4
	600	2	53.73	54.07	SM
	900	2	0.32		SM-2
	1200	2	0.41		1-5
2.00:1	-	-	-	-	SM-4
	600	2	53.83	54.13	SM
	900	2	0.35		SM-2
	1200	2	0.43		1-5
2.05:1	-	-	-	-	SM-5
	600	2	53.86	54.18	SM
	900	2	0.35		SM-2
	1200	2	0.45		1-4

* Percent weight loss is determined as 100 times initial mass less final mass divided by initial mass. Actual values at 900°C ÷ 1200°C indicate percent weight loss in the precursor (i.e. 600°C) material. Theoretical weight loss is calculated based on molecular weights of precursors (ZnOx and "TiOX") and fired products (ZnC and TiO₂).

** SM - Submicron.

3.5.2.2 Gravimetric Analysis

The weight losses for the various samples after a 600°C/1 hr calcination were somewhat higher than the theoretical values (Table 3.15). The theoretical values are assumed on the basis of a 57.04% loss in the reaction $\text{ZnC}_2\text{O}_4 \cdot 2\text{H}_2\text{O} \xrightarrow{\Delta} \text{ZnO}$, and of a 46.73% loss in the reaction $\text{"TiOX"} \xrightarrow{\Delta} \text{TiO}_2$. The increasing trend in weight loss with higher Zn/Ti ratio, both for the theoretical and actual data, is consistent with the greater weight loss for the zinc component, 57.04% (vs. 46.73% for the titanium component).

Very small weight losses occurred following the 900°C and the 1200°C calcinations. It can also be seen that the relationship of increasing weight loss with increasing Zn/Ti ratio holds at these higher temperatures. These losses may be due either to thermal desorption of chemisorbed water and/or to completion of the decomposition process. The latter appears to be valid in view of the increasing weight loss versus the increasing Zn/Ti ratio relationship. Water adsorption differences due to stoichiometry changes are unlikely.

3.5.2.3 SEM Analysis

The particle sizes indicated by SEM photomicrographs of as-mixed materials are fairly large. This is most likely due to the zinc oxalate size of about 0.5-3 microns and also to some agglomeration which occurred during calcination. The materials after a 600°C/2 hr calcination were all extremely fine (sub-micron) in size. The diminution in size from a coarser precursor occurs when an oxalate (mixture) decomposes to an oxide with a substantial weight loss.

Calcination of the 600°C precursor at 900°C/2 hr and 1200°C/2 hr to obtain Zn_2TiO_4 resulted in coarser particles. Whereas a fairly high portion of the 900°C materials is submicron in size, the 1200°C calcination process causes a noticeable growth of the pigment particles. There appear no submicron particles in the samples calcined at 1200°C. Accordingly we believe that a temperature lower than 1200°C may be required to retain a

population of submicron particles. Since in this preliminary study, we did not use the finest particle size oxalates, this observation is not conclusive.

3.6 NEW PIGMENT MATERIALS STUDIES

The stability of ZnO and Zn_2TiO_4 pigment prompted an interest early in this program in other mixed oxides incorporating zinc oxide. The high extinction of ZnO should preclude the creation of ultraviolet-induced bulk damage in the second oxide, whether it be tied up as a compound or in solid solution. Other materials examined very early in the program include a series of glass frits, which are the glassy precursors for enamels. In other studies at IITRI, the stability of enamels to ultraviolet-vacuum had been clearly established; with this background, a preliminary look at frits as potential pigments was deemed appropriate. Details of these studies appear in the following sections.

3.6.1 ZnO-ZrO₂ System

Studies of the ZnO-ZrO₂ systems have been made by von Wartenberg (Ref. 3.11) and by Dietzel (Ref. 3.12). The former has reported a melting diagram for this system exhibiting a flat "eutectic" at 1810°C. Dietzel, who investigated the system at temperatures up to 1450°C, concluded that zinc zirconate does not exist as a congruent melting material. He found that there is no cubic structure at 1450°C, and, consequently, that ZnO does not behave as a stabilizer as does CaO, MgO, or Y₂O₃. The possibility, however, exists for solubility of ZnO in ZrO₂.

In order to determine the existence of "ZnZrO₃" and/or the extent of ZnO solubility in ZrO₂, we conducted experiments to react the oxides at 1800°C. Mixtures of ZrO₂ (Wal. Chang Reactor Grade-S) and ZnO (New Jersey Zinc SP 500) were dry-milled for 16 hours using porcelain balls. The three compositions (Table 3.16) were pressed into pellets at 10,000 psi to insure powder particle intimacy, and fired at 1800°C, one in a slightly reducing (CO) atmosphere and the other in a static air

environment. The heating times to temperature were 10 min and 45 min, and soak times at 1800°C were 30 min and 5 min respectively. The abbreviated heat treatments, both in heat-up and soak times, were employed to minimize loss of the zinc oxide through disproportionation.

TABLE 3.16
COMPOSITIONS FOR ZnO-ZrO₂ STUDIES

<u>Mol % ZnO</u>	<u>wt % ZnO</u>	<u>Vol % ZnO</u>
25	18.0	18.3
50	39.8	40.2
75	66.5	66.9

The samples fired under reducing (CO in graphite tube furnace) conditions revealed a black outerlayer and a somewhat grayish interior. The black surface probably resulted from carbon deposition during the firing. The 25 and 50 mol % ZnO samples appeared somewhat sintered whereas the 75 mol % ZnO sample was quite soft and friable. All samples exhibited delaminations, suggesting a gross loss of ZnO. X-ray analyses by powder pattern techniques revealed monoclinic ZrO₂ with no ZnO.

Samples fired under a static air environment remained white and exhibited fairly good retention of physical dimensions. The weight losses for the samples are: 25 mol % - 4.6%; 50 mol % - 3.7%; and 75 mol % - 0.3%. The low value for the 75 mol % ZnO is probably due to its being somewhat cooler (approximately 1700°C) during the heat treatment. Based on the starting weight percentages of 18.0, 39.8 and 66.5% (Table 3.16), it is apparent that ZnO was retained in all three compositions. Examination of the static air-fired materials using X-ray techniques reveals that the 25 mol % ZnO sample is monoclinic ZrO₂ with no ZnO; the 50 mol % ZnO, monoclinic ZrO₂ plus some ZnO; and the 75 mol % ZnO, monoclinic ZrO₂ plus ZnO. The lack of ZnO lines in the 25 mol % sample contrasts with the weight analysis which indicates that the remaining ZnO content is ~ 14.1 wt % in the fired

sample, an amount which should have resulted in a ZnO pattern. Some of the ZnO may have gone into solution in the ZrO_2 lattice. From the preliminary x-ray analysis, however, no lattice shift was observable.

3.6.2 Ultraviolet-Vacuum Irradiation Studies

Twelve potentially-stable white pigments, including the fired ZnO-ZrO_2 samples, were irradiated in IRIF Test I-43 at six suns intensity to a total ultraviolet exposure of 575 ESH. The pre- and post-test spectral hemispherical reflectance curves were studied to determine whether the materials have acceptably low solar absorptances and whether they are sufficiently stable. Table 3.17 lists the samples along with spectral reflectance values at selected wavelengths before and after irradiation. Solar absorptance values were not calculated since it is obvious that most of the materials are unstable and few have solar absorptance (α_s) values competitive with currently available stable systems.

The untreated commercial materials, zinc borate, zinc silicate and zinc stannate (obtained from Alfa Inorganics), exhibit high α_s values and, with the exception of zinc borate, poor stability. Of the Pemco frits, only No. P-1A44P was reasonably stable. The frit, No. P-1805P, obviously is very attractive from the standpoint of its initial α_s value, but can not be considered further because of its very poor stability. The IITRI zinc zirconate powders were prepared by a solid-solid reaction at 1800°C for 5 min. They exhibited poor α_s values and serious instability.

After being subjected to brief purification and calcination treatments, some of the more promising materials from the test previously discussed were subjected to 1200 ESH in IRIF Test I-45. Table 3.18 lists the pigments, their treatments, and the solar absorptance values.

REPRODUCIBILITY OF THE
ORIGINAL PAGE IS POOR

Table 3.17

**SPECTRAL REFLECTANCE VALUES BEFORE AND AFTER
ULTRAVIOLET IRRADIATION* OF NEW PIGMENT MATERIALS**

	Wavelength, Microns						
	0.4	0.5	0.6	0.7	1.0	2.0	2.6
<u>IITRI Zinc Zirconate Powders</u>							
25 wt% ZnO/75 wt% ZrO ₂	78.9 68.6	89.5 81.9	92.8 87.4	93.2 90.2	93.7 92.9	95.9 95.9	97.2 97.2
50 wt% ZnO/50 wt% ZrO ₂	77.1 65.0	88.0 80.2	91.3 86.9	91.9 89.3	92.0 91.5	93.2 93.2	95.1 94.5
75 wt% ZnO/25 wt% ZrO ₂	74.8 63.8	83.4 75.7	85.2 80.6	85.6 82.6	86.1 84.2	89.2 88.8	91.8 94.5
<u>Untreated Commercial Materials</u>							
Zinc	80.0*	81.0	80.8	80.2	88.2	70.5	50.7
Borate	74.0*	79.8	79.4	79.8	88.0	71.9	51.2
Zinc	84.0	82.3	79.9	78.0	74.3	69.5	62.0
Silicate	59.0	69.2	73.3	74.4	72.8	69.0	60.7
Zinc	80.5	87.0	88.8	89.2	87.2	67.3	49.8
Stannate	63.2	80.1	85.8	87.3	86.4	64.0	45.7
<u>Pemco Frits</u>							
P-1805-P	88.5 72.0	88.8 81.2	88.6 84.7	88.4 86.6	87.2 87.2	89.5 88.6	84.5 84.5
P-1P32P	79.9 65.5	89.1 80.5	88.9 84.5	88.3 86.0	86.0 85.3	81.9 81.9	77.0 77.0
P-1A43P	80.6 70.6	82.9 79.0	82.4 80.7	81.8 80.9	80.9 81.0	83.5 83.5	84.5 83.9
P-1A44P	79.0 72.0	88.0 85.3	88.3 87.0	88.0 87.6	86.0 85.7	88.2 88.2	84.9 84.3

*The spectral reflectance values before and after 575 ESH of UV irradiation are the upper and lower figures, respectively, in each set.

TABLE 3.18

SOLAR ABSORPTANCE VALUES OF
NEW PIGMENTS BEFORE AND AFTER 1200 ESH

Sample	Solar Absorptance		
	Initial	1200 ESH	Δa_s
Untreated Zinc Borate	0.203	0.236	0.033
Zinc Borate, 500°C/8 hr	0.232	0.263	0.031
Zinc Borate, 700°C/8 hr	0.287	0.336	0.049
Zinc Borate, 900°C/8 hr	0.179	0.244	0.065
Pemco Frits			
No. P-1A43P	0.233	0.295	0.062
No. P-1A44P	0.179	0.200	0.021
No. P-1A44P, 400°C/4 hr	0.133	0.180	0.047

3.6.3 Conclusions

None of the new pigments tested received further consideration during this program because of their limited stability. Zinc borate, even though its initial properties greatly improve with a 900°C calcination, suffers severe degradation. The Pemco frits likewise have, or can be treated to have, good initial properties, but they lack ultraviolet radiation stability. In general, none of the new pigments tested, if made into paint systems, would compete successfully with available ZnO or Zn₂TiO₄ paint systems.

3.7 REFERENCES

- 3.1 Zerlaut, G. A., and Harada, Y., "Stable White Coatings," Jet Propulsion Laboratory, Contract No. 95011, IIT Research Institute Report No. IITRI-C207-25 (August 27, 1963).
- 3.2 Zerlaut, G. A., Gilligan, J. E., and Harada, Y., "Development of Space-Stable Thermal Control Coatings," NASA-MSFC Contract No. NAS8-5379, IIT Research Institute Triannual Report No. IITRI-C6014-18 (December 21, 1964).
- 3.3 Zerlaut, G. A., Gilligan, J. E., and Ashford, N. A., "Investigation of Environmental Effects on Coatings for Thermal Control of Large Space Vehicles," NASA-MSFC Contract No. NAS8-5379, IITRI Final Report No. IITRI-U6002-97 (October 8, 1971).
- 3.4 Zerlaut, G. A., Gilligan, G. E., and Ashford, N. A., "Space Radiation Environmental Effects in Reactively Encapsulated Zinc Orthotitanates and Their Paints," AIAA Paper No. 71-449, AIAA 6th Thermophysics Conference, Tullahoma, Tennessee, April 26-28, 1971.
- 3.5 Farley, E. P., "Induction Plasma Calcining of Pigment Particles for Thermal Control Coatings," SRI Report No. 3, PMU-7083, NAS 8-21270 (May 8, 1970).
- 3.6 Clark, G. L., Applied X-Rays, McGraw-Hill, New York (1955).
- 3.7 Dulin, S. F., and Rase, D. E., "Phase Equilibria in the System ZnO-TiO_2 ," J. Am. Ceram. Soc. 43 (3) 125-31 (1960).
- 3.8 Bartram, S. F., and Slepety's, R. A., R. A., "Compound Formation and Crystal Structure in the System ZnO-TiO_2 ," J. Am. Ceram. Soc. 44 (10) 493-99 (1961).
- 3.9 Clabaugh, W. S., et al, "Preparation of Barium Titanyl Oxalate Tetrahydrate for Conversion to Barium Titanate of High Purity," J. Res. N.B.S. 56 (5) 289-91 (1957).
- 3.10 D'eye, R. W. M., and Sellman, P. G., "The Thermal Decomposition of Thorium Oxalate," Inorg. and Nuc. Chem. Vol. 1, 143-148 (1955).
- 3.11 Von Wartenberg, H., and Gurr, W., Z. anorg. u. allgem. Chem. 196, 374-383 (1931).
- 3.12 Dietzel, A., and Tober, H., "Über Zirkonoxyd und Zweistoffsysteme mit Zirkonoxyd," Ber. Deut. Keram. Ges. 30, 71-92 (1953).

4. ENVIRONMENTAL TESTING

4.1 INTRODUCTION

Irradiation testing with simulated space radiations provides a means of evaluating experimental materials for space applications. Irradiation testing, the largest single program effort, affords us the ability to compare and evaluate the properties and performance of candidate materials and methods of preparing them. It also allows valuable insight into the mechanism by which they interact with radiations as well as, in many instances, a clear indication of the ultimate merit of a particular material or method.

During the course of the program a large number of environmental tests were performed and a greater number of reflectance spectra taken. We believe that what we have elicited from these tests can be presented here without exhibiting all of the data obtained. We will present those data which best represent test conclusions, exemplify general observations of properties and performance of materials, or which have significant merit on their own. The bulk of the test data otherwise tend to be supportive.

Much of the discussion about the properties and performance of candidate materials deals with the spectral reflectance of the samples before irradiation, after exposure(s) to one or more radiation sources, and, frequently, after exposure to oxygen (subsequent to irradiation).

Of all the tests performed on candidate thermal control materials, the most meaningful and most important are the simulated space radiation tests and their associated diffuse spectral reflectance measurements. Largely the irradiation tests are comparative; the unpredictable aging behavior of light sources, inherent measurement errors and many other considerations make absolute determinations of radiation exposure and other test parameters difficult and costly

MIT RESEARCH INSTITUTE

beyond value. Although we attempt to operate every irradiation test such that realistic space simulation conditions prevail, it is also important to assure that the samples selected for any given test each "see" exactly the same environment. This condition validates intra-test results and makes them readily comparable. Consequently, many of our tests, especially in CREF, are designed to provide a maximum of comparative performance data, so that the effects of various pigment and binder preparation variables can be discerned. Comparison of inter-test results, however, is also entirely valid; one has only the uncertainty that exactly the same test conditions (if this indeed even be important) have been attained in all tests. The use of a control sample is called for in those instances in which direct inter-test comparison is essential. In essence, however, more confidence can be and usually is placed in the comparison of data resulting from a single test than in the comparison of data from separate tests, even with adequate control sample data.

4.2 INTERPRETATION OF SPECTRA

This report contains a considerable number of reflectance spectra. Let us explain their purpose and significance as well as what to look for in analyzing them. The task of analyzing reflectance spectra requires a considerable knowledge of coatings technology. The most significant information is derived by comparing the "before" and "after" curves of a given sample, and by noting the magnitude of induced changes and their spectral locations. Since it is neither practical nor entirely necessary to assure that each and every experimental coating is thick enough to be opaque at all wavelengths of interest, the possible differences in thickness between samples must be taken into account when comparing test results. Many of the coatings investigated are powders, i.e., thin films of pigments on test coupons and, depending upon pigment preparative conditions, the maximum attainable thickness may not produce optical opacity.

IIT RESEARCH INSTITUTE

Figure 4-1 illustrates several spectra of Zn_2TiO_4 pigments and we will discuss their meaning here in a general way. These curves, though arbitrarily drawn, are nevertheless quite typical. Our discussions and analyses of them exemplify those of actual test data, but are not intended to take the form of conclusions or summaries of results. The curves, labelled 1 thru 3, each display characteristic S-band damage in the 900 nm wavelength region. The dashed curves represent the spectra after UV irradiation. In one case (No. 1) we have also shown the oxygen bleach spectrum. The spectra of pigment No. 1 indicate a large pigment particle size because the maximum reflectance apparently occurs at a wavelength beyond 2600 nm. Pigment No. 2, from an analysis of its initial reflectance, appears to have suffered a major loss in reflectance in the 900 nm region (S-band) as a result, perhaps, of some processing condition. The third pigment apparently has a very small particle size, as determined by the steady reflectance loss with increasing wavelength. All Zn_2TiO_4 pigments have high reflectances in the near UV region because of the high index of refraction of Zn_2TiO_4 near the fundamental absorption edge. The shape of the reflectance curve in the 350-450 nm region is determined by a rapidly increasing index of refraction with decreasing wavelength and a steep increase in intrinsic absorption as the fundamental band gap energy is approached. The spectra of the first pigment reveals the possible presence of excess ZnO. Those of pigment No. 2, however, virtually prove its presence with the appearance of the characteristic free carrier absorption (in the i-r).

The exact value of λ_k , i.e., the wavelength of the "knee" of the curve, provides a further indication of whether the absorption is due to ZnO, or some other strong UV absorber; the value of R_k (at $\lambda = \lambda_k$) provides an indication of how much is present. Thus the shaded area below λ_k represents

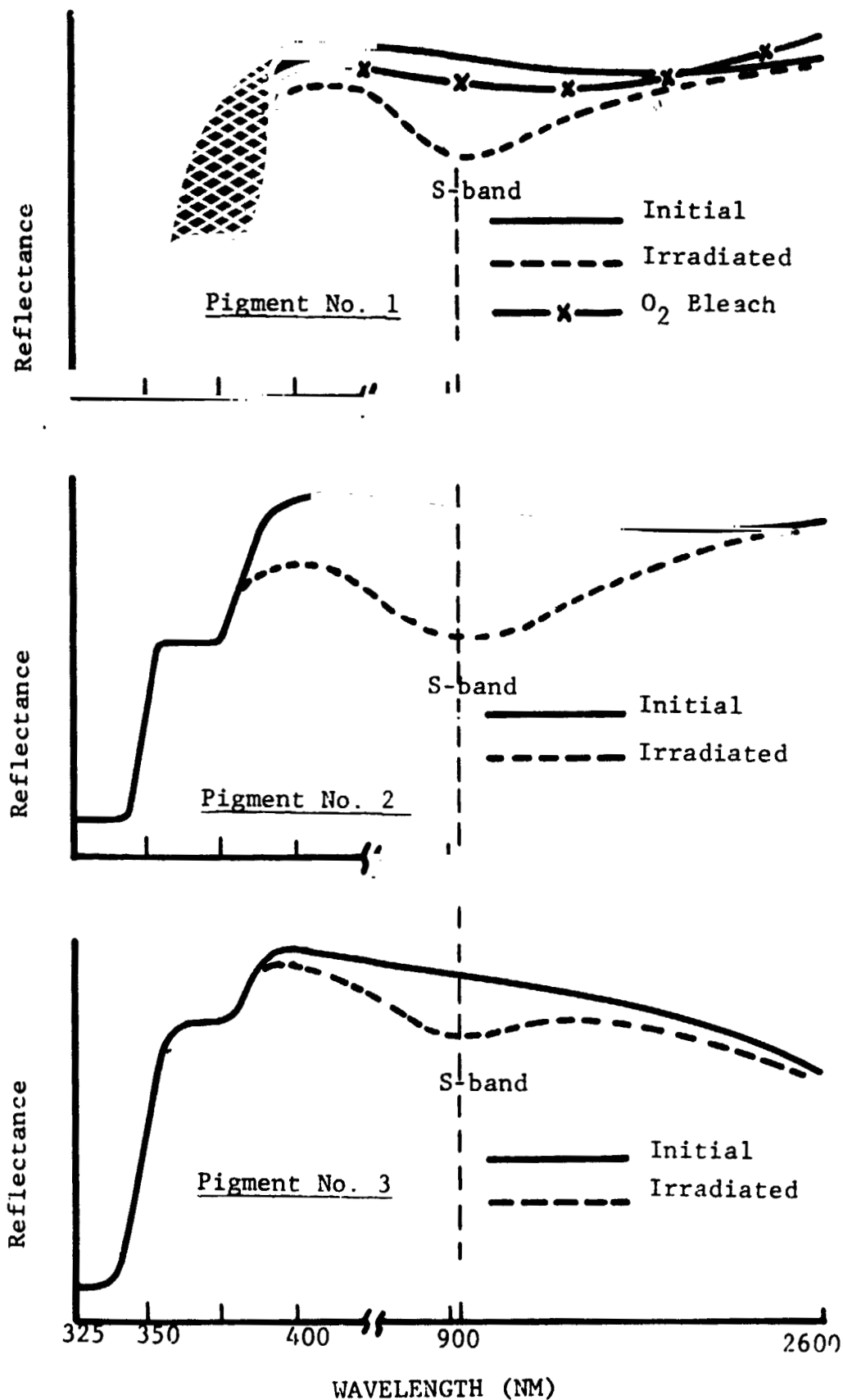


Figure No. 4.1 REPRESENTATIVE Zn_2TiO_4 REFLECTANCE SPECTRA

loss in reflectance due to such an absorber. The top (dotted) curve is the spectrum of pure Zn_2TiO_4 . The shaded area illustrates, from an engineering point of view, the importance of this region to α_s , but more importantly it underscores the tremendously valuable information available through analyses of the spectra in this region.

We observe that Zn_2TiO_4 pigment frequently degrades by induced S-band absorption, i.e., a reflectance decrease in the 900 nm region; "damage", (i.e., environment-induced reflectance decreases), also occurs at shorter wavelengths. In some cases UV-induced damage at wavelengths greater than 2000 nm results.

Zn_2TiO_4 paints also exhibit damage highly characteristic of their pigments. This is because the environment-induced damage in the OI-650 paint binders centers at wavelengths shorter than 300 nm. Consequently, the strong absorption of Zn_2TiO_4 below 350 nm will inevitably mask the damage to the binder. In severe cases binder damage does become evident as an apparent broadening of the fundamental absorption band of Zn_2TiO_4 . The spectra also make it obvious when the OI-650 binder sensitizes the pigment surface, causing greater S-band damage (at 900 nm) than occurs in the pigment alone. From the effects of O_2 bleaching on paints and pigments, we have a direct measure of pigment surface passivity. In untreated pigments, the response to O_2 , after irradiation, inversely relates to pigment surface inertness, whereas for treated pigments this response provides a measure of the effectiveness of encapsulants on chemical treatments.

Ultimately, of course, we seek to develop a pigment-binder system which totally resists environmental damage. The analyses of spectra are therefore aimed at identifying the basic causes of degradation and at eliminating them without in the process creating others. Our philosophy

IIT RESEARCH INSTITUTE

in these analyses is that the major effort should be to eliminate bulk optical damage, evidenced primarily in the visible region, because whatever surface instability remains or is created can, at least theoretically, be effectively overcome by surface chemical treatments - encapsulants.

4.3 EQUIPMENT AND FACILITIES

Irradiation with simulated space radiation, both electromagnetic and massive (particulate) is accomplished in IITRI's two space simulation systems - IRIF and CREF. The facilities, UV sources, Standard Operating Procedures, test terminology and sample notation scheme are described below.

4.3.1 Irradiation Facilities

The IRIF, an acronym for "In-Situ Reflectance/Irradiation Facility" is a multiple-sample ultraviolet-simulation facility possessing in-situ hemispherical spectral-reflectance-measurement capabilities. CREF (Combined Radiation Environment Facility) is basically an IRIF to which has been mated a solar wind simulator and several other specialized equipments. The basic measurement in both facilities is that of diffuse spectral reflectance in the 220 - to 2600 nm wavelength range. These facilities are described fully in Reference 1, but some pertinent information is provided here.

Both facilities incorporate an integrating sphere, patterned after one described by Edwards et. al., (Ref. 4.2), and modified for use with the Beckman DK spectrophotometers. The integrating spheres normally operate in vacuum. A sample transfer mechanism, during irradiation, maintains each sample in contact with a temperature-controlled sample table. The transfer under high vacuum of any sample to the integrating sphere for measurement and its subsequent return to the sample table for continued irradiation are routine operations. CREF differs from IRIF in that CREF has a multiple source

housing adaptor which permits simultaneous ultraviolet, proton, and electron irradiation. CREF also has a gas adsorbate adaptor that permits samples to be exposed to various test gases (after irradiation exposure) at pressures ranging from 10^{-6} torr to several atmospheres (accurately measurable at $p > 10^{-4}$ torr). IRIF has no provisions for adsorbate pressure measurements. Both facilities are pumped with 400 liter/sec ion pumps and are rough-pumped with cryo-sorption pumps. The solar wind simulator has auxiliary ion pumps.

A photograph of the CREF and CREF laboratory is presented in Figure 4.2 and components of this facility are shown schematically in Figure 4-3. Figure 4.4 is a top view of the sample table in both IRIF and CREF.

4.3.2 Ultraviolet Sources

Because of a number of factors, primarily economical operation, the 1000 watt A-H6 lamp (Pek, Inc.) is widely employed as an ultraviolet radiation source. Its high ratio of ultraviolet to total (radiant) energy permits accelerated ultraviolet testing at several equivalent solar factors (based on total ultraviolet only) without substantial sample heating. The intensity spectrum of a new source is shown in Figure 4.5. Accelerations of 10 equivalent solar factors are easily achieved with an A-H6 lamp (compared to a maximum of about 4 to 6 for 5-kw mercury-xenon sources and about 1.5 for 5-kw xenon sources). The A-H6 is utilized primarily with IRIF. For CREF irradiations, 5000-watt Hanovia burners, both xenon and mercury-xenon, are employed. Its radiant intensity spectrum is shown in Figure 4.6. The advantage of these burners over mercury-argon sources are the intensified emissions of ultraviolet radiation in the 200- to 230 nm wavelength region, and a closer match to the solar ultraviolet intensity spectrum. Their principle disadvantages are initial cost and comparatively short lifetimes.

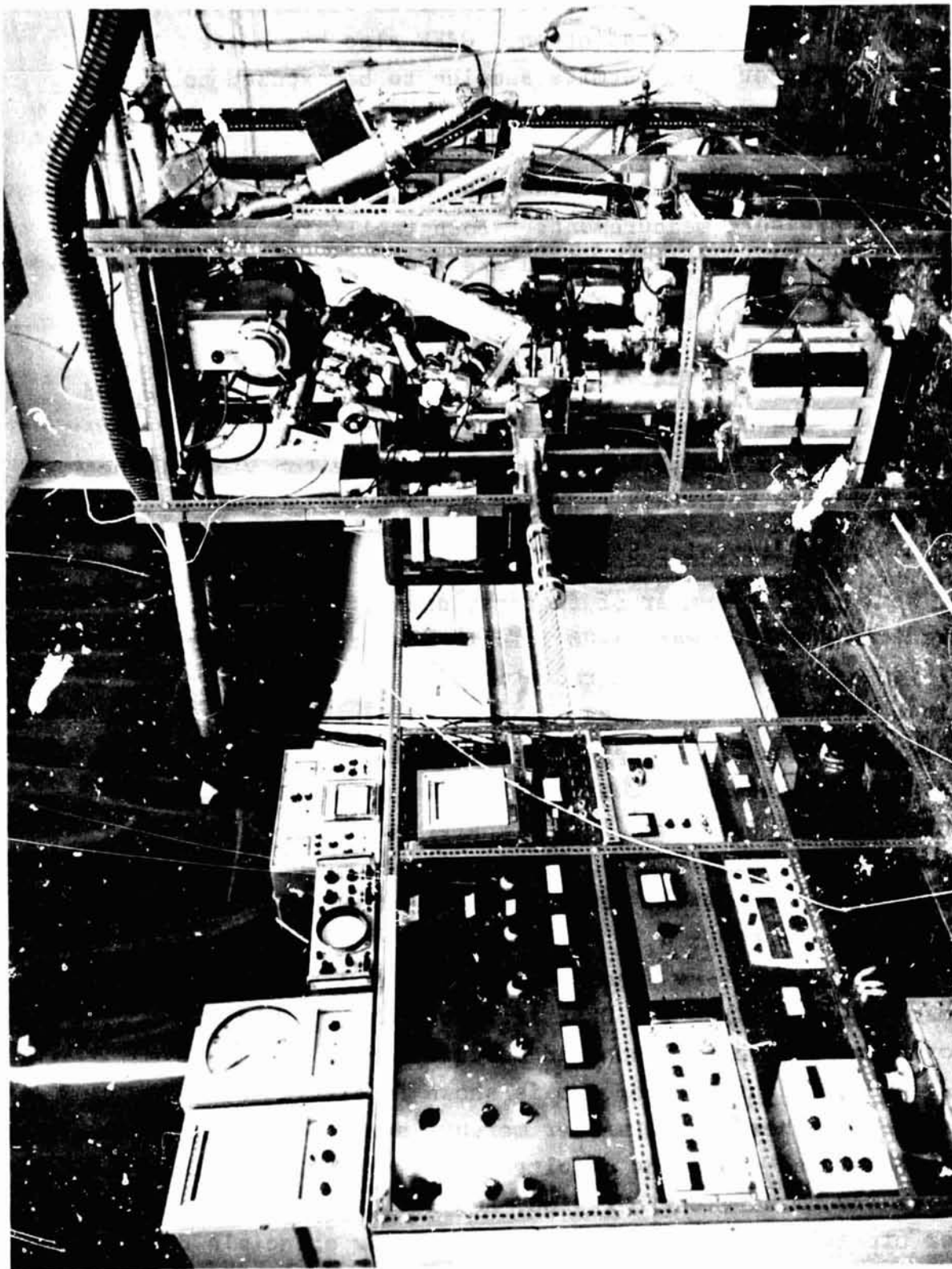


Figure 4-2 THE COMBINED RADIATION ENVIRONMENT TEST FACILITY

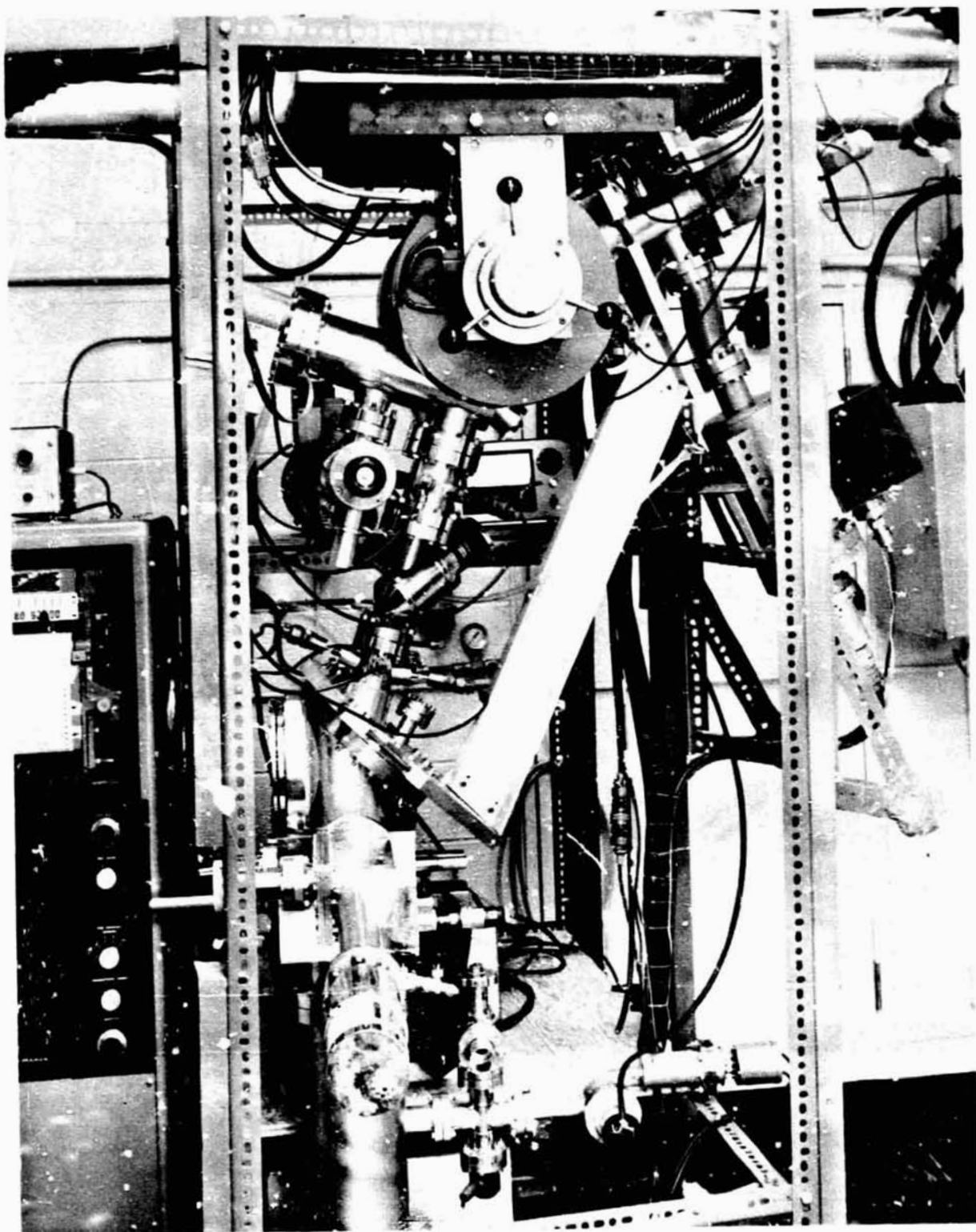


Figure 4-3 CLOSE-UP OF THE CREF

REPRODUCED FROM
ORIGINAL PAGE IS FOUR

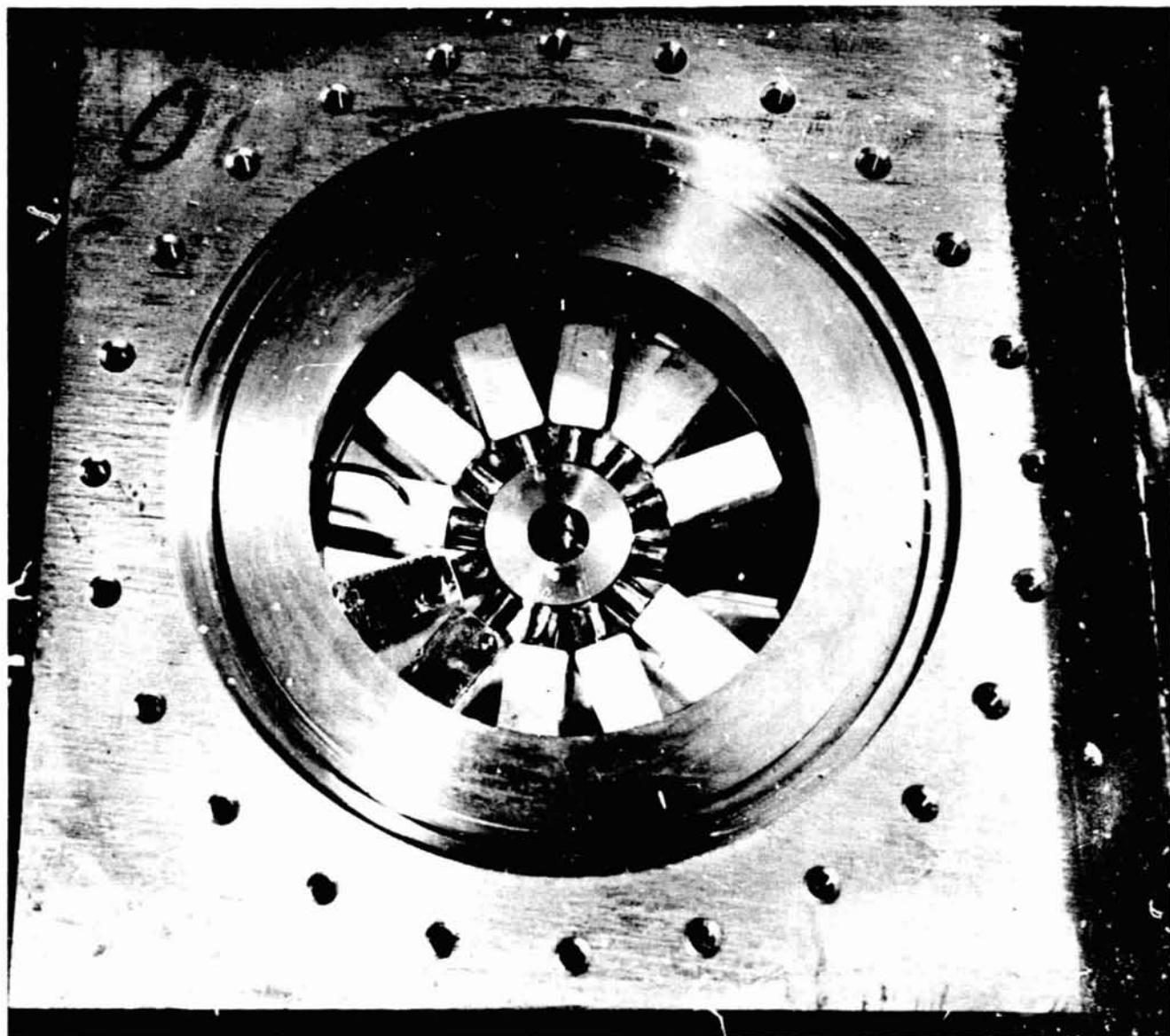


Figure 4-4

TOP VIEW OF THE IRIF'S UV-IRRADIATION CHAMBER SHOWING
SAMPLES, SAMPLE TABLE AND MANIPULATOR ARMS

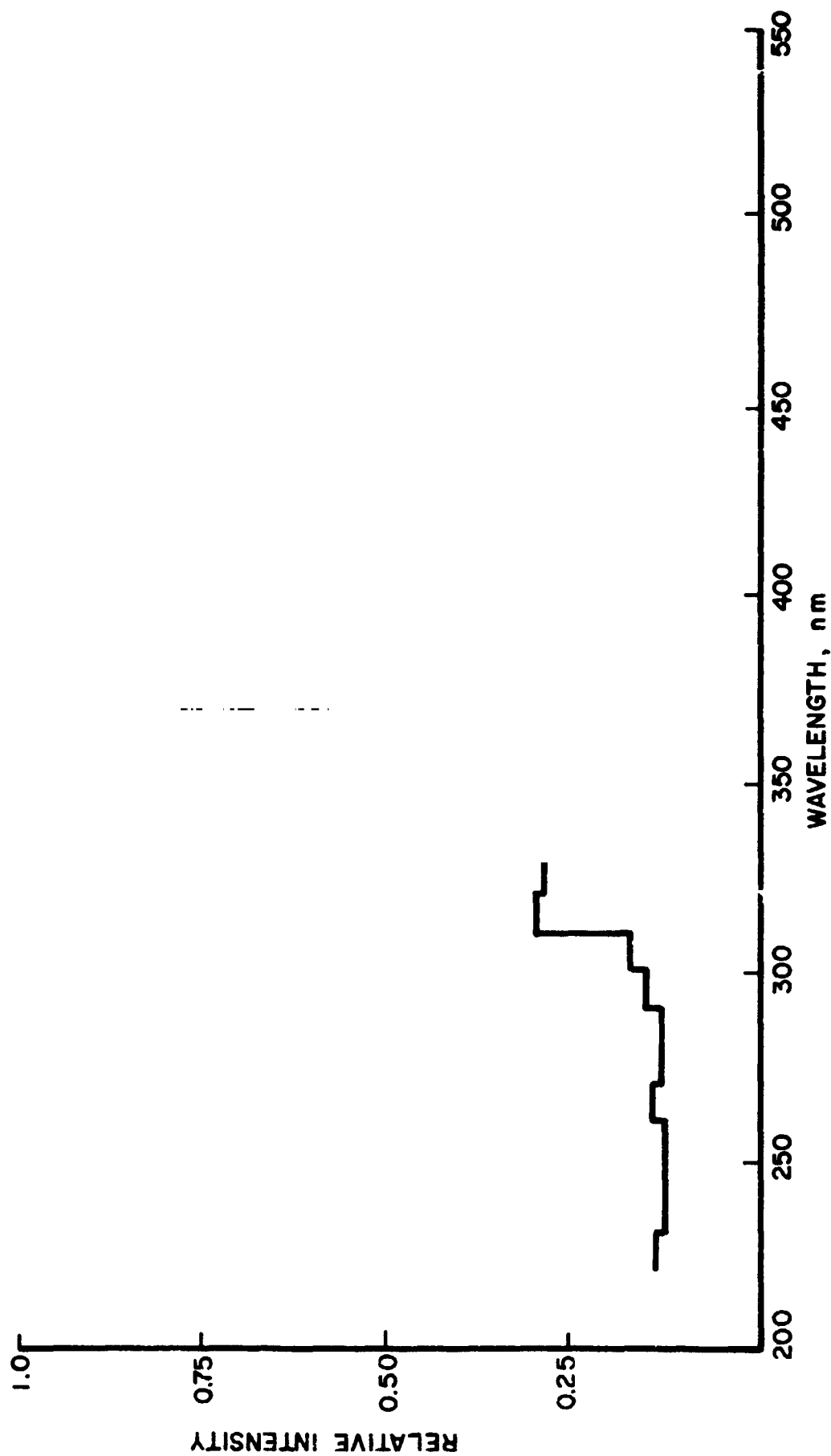


Figure 4.5 SPECTRAL RADIANCE OF AH-6 UV RADIATION SOURCE

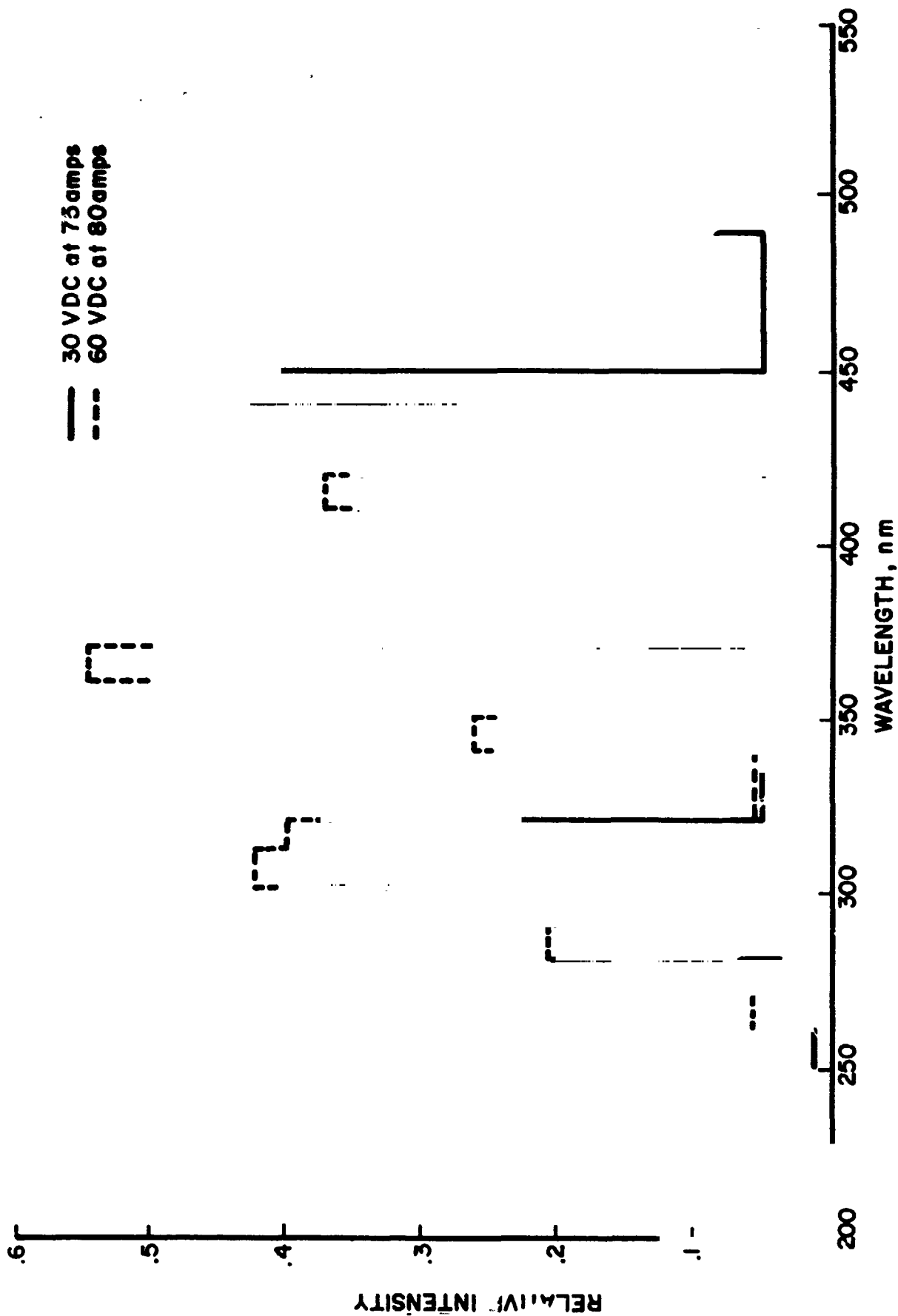


Fig. 4.6 SPECTRAL RADIANCE OF HANOVIA 5000 WATT MERCURY-XENON LAMP

4.3.3 Test Procedures

Standard Operating Procedures, in both IRIF and CREF, requires that, after pump-down, the samples be heated with warm water to remove gross volatiles (if any). Immediately prior to and during irradiation cold water is supplied to the sample cooling table. While still under high vacuum, diffuse spectral reflectance measurements are then taken of each of the test samples in the spectral range from 325 - 2600 nm. Such measurements are repeated after each prescribed test interval - after exposures of, say, 500, 1000 and 2000 ESH - and, if called for, after an oxygen bleach. In CREF operations the test intervals may be specified in terms of EWH (equivalent wind hours), particularly when the test is " p^+ only".

Unless otherwise indicated, the following conditions may be assumed in all IRIF and CREF tests. UV irradiation rates are 6 suns at the sample location in IRIF tests, and an A-H6 source is used; for CREF tests, a Hg-Xe source is normally used and is operated to provide a nominal 4 sun intensity at the sample location. Correlations of lamp intensity with distance of source to sample are used to set the desired intensity (sun) level. The output of each source is monitored and recorded. Simulated solar wind irradiations (in CREF) are conducted using analyzed 1200 eV protons. These fluxes (uncorrected) likewise are monitored and recorded. The true proton flux is read at least two times a day by shielding the samples from the UV source and then manually reading the p^+ flux of a pico-ammeter connected to a Faraday cup located near the samples. In this way the UV-induced photoelectron current is nullified. A correction for secondary electron emission from the Faraday cup, however, is not made at proton energies less than 1500 eV, since experiments here have shown that the correction is less than 10%. As with the IRIF the CREF will accommodate 12 samples, but, because of the geometry of the multiple source adaptor,

IIT RESEARCH INSTITUTE

only four samples can be irradiated with protons.

In some tests we perform an O₂ bleaching experiment. This simply means that, upon completion of the post-irradiation reflectance measurements, the system (IRIF or CREF) is backfilled with research grade oxygen and the reflectance measurements are repeated.

4.3.4 Terminology

Perhaps the most important aspect of environmental testing, aside from questions of its validity with respect to space flight conditions, is terminology. The vocabulary and the notations we employ in subsequent discussions have fairly common meanings within the field of thermophysics. Nevertheless, we believe the reader should consult the glossary (Section 9.0) regarding the definition of most of the technical terms used in this report. There are, however, some non-standard notations and some in-house terminology which deserve amplification prior to any discussions of environmental test results.

4.3.5 Sample Notation

Except where specifically and otherwise indicated, all pigments are zinc orthotitanate, and all binders are either Owens-Illinois 650 "Glass" resin, or an IITRI modification of that resin, or Sylvania Electric Co's potassium silicate, PS-7. Regardless of actual stoichiometry all zinc orthotitanate pigments are designated Zn₂TiO₄. Commercial Owens-Illinois 650 "Glass" resin is designated OI-650, or, simply OI. IITRI's modification of OI-650 is designated OI-650G or, simply, G.

A notation scheme has been developed which greatly facilitates the identification of Zn₂TiO₄ samples. The basic scheme is: Pigment (chemical and/or thermal treatment): Encapsulant/Binder. The designation, for instance Zn₂TiO₄(A-10-12):K₂SiO₃/G thus refers to an OI-650G paint incorporating a Zn₂TiO₄ pigment

IIT RESEARCH INSTITUTE

which was acid leached (A), calcined at 1000°C (10), and re-calcined at 1200°C (12), and then encapsulated in potassium silicate ($\text{:K}_2\text{SiO}_3$). The notation also indicates the sequence of treatments. For plasma calcined pigments, for example, the notation Zn_2TiO_4 (Plasma) : K_2SiO_3 and $\text{Zn}_2\text{TiO}_4\text{:K}_2\text{SiO}_3$ (Plasma) refer, respectively, to a pigment which was first plasma-calcined and then K_2SiO_3 -encapsulated and to one which was encapsulated in K_2SiO_3 and then plasma-calcined.

Although not usually used in the notation scheme, the actual source of Zn_2TiO_4 is indicated by such notations as SS, COP or MOX; when appropriate, specific batch numbers, such as LH-106, are used. SS, COP and MOX designate pigments obtained, respectively, from the solid state, oxalate coprecipitation, and mixed oxalate methods. This notation precedes the pigment designation, as in $(\text{SS})\text{Zn}_2\text{TiO}_4\text{:K}_2\text{SiF}_6/\text{PS-7}$. The text will identify the materials more closely, especially with respect to the preparation method and temperature/treatment schedules. The latter are always expressed in °C, and the notation indicates the schedule of temperature/time (in hrs). $\text{MOX}(6/1.5)$ thus denotes a Zn_2TiO_4 pigment prepared from mixed oxalate precursors by calcining at 600°C for 1.5 hrs.

4.4 ENVIRONMENTAL TEST DESCRIPTIONS - PART I

The reports on environmental tests appear in a three part series. Part I pertains to SS pigments, i.e., those prepared from oxide precursors. Parts II and III pertain to pigments prepared from oxalate precursors - COP and MOX, respectively. Tests are available in the appropriate triannual reports which are referenced.

4.4.1 CREF Test No. 5

4.4.1.1 Purpose/Description

CREF Test No. 5 (Ref. 3) was designed to compare the effectiveness of three encapsulants of Zn_2TiO_4 - potassium silico-tungstate, potassium silico-fluoride and potassium silicate.

IIT RESEARCH INSTITUTE

In each case we also wanted to determine the protection afforded against individual and combined UV and p^+ environments. OI-650 was exposed in order to determine its response in individual and combined environments.

4.4.1.2 Test Sequence

After the initial spectral reflectance measurements were made, proton, but no ultraviolet, irradiation was initiated, exposing samples No.'s 1-4 only, to a total fluence of $1.85 \times 10^{15} p^+/cm^2$. The spectral reflectance of samples No.'s 1-4 was then measured, and also of samples No.'s 5-13 to be certain that changes or "spillover" effects had not occurred in the interim. The samples were then rotated such that sample No.'s 5-8 were exposed to the proton beam; irradiation of samples No.'s 5-8 with protons and of all samples with concurrent ultraviolet radiation was then initiated. The ultraviolet exposure was 1325 ESH, and the proton exposure was $2.0 \times 10^{15} p^+/cm^2$ (to samples No.'s 5-8). Spectral reflectance measurements were then made of sample No.'s 5-12; no further measurements of sample No.'s 1-4 were performed.

4.4.1.3 Discussion

The materials tested and their pre-and post-test α_s values are given in Table 4-1.

4.4.1.3.1 Code C-070, $Zn_2TiO_4:K_2SiO_3$ (Plasma)/OI-650

This paint was prepared from a plasma-annealed pigment. The reflectance spectra are shown in Figure 4-7 and indicate that both the pigment and paint are stable to protons. Figure 4-8 shows the spectra for a paint irradiated with ultraviolet radiation, while those in Figure 4-9 show spectra for a paint irradiated with combined proton and UV radiations. The $\Delta\alpha_s$ values for samples irradiated with protons only, ultraviolet only and protons plus ultraviolet are 0.002, 0.018 and 0.013, respectively. From Figure 4-7 it is evident that protons have a negligible effect. The

IIT RESEARCH INSTITUTE

Table 4.1

RESULTS OF CREF-5, COMBINED RADIATION TEST OF
(SS) ZINC ORTHOTITANATE PAINTS AND OWENS - ILLINOIS GLASS RESIN

Sample		Solar Absorptance Values				$\Delta\alpha_s$
No.	Code ^a	Initial	p^+ only ^b	p^+ + UV ^c	UV only ^d	
1	C-070	0.194	0.196			0.002
2	OI-650	0.455	0.458			0.003
3	C-068	0.158	0.204			0.046
4	C-067	0.181	0.194			0.013
5	C-070	0.223		0.236		0.013
6	OI-650	0.423		0.431		0.008
7	C-068	0.171		0.227		0.102
8	C-067	0.184		0.229		0.045
9	C-067	0.200			0.231	0.031
10	C-068	0.179			0.204	0.025
11	C-070	0.286			0.304	0.018

^aThe code is as follows:

C-067 $Zn_2TiO_4:K_2Si_4W_{12}O_{40}(5/7)/PS-7$

C-068 $Zn_2TiO_4:K_2SiF_6/PS-7$

C-070 $Zn_2TiO_4:K_2SiO_3$ (Plasma)/OI-650

OI-650 Thin film of Owens-Illinois "Glass Resin" on an Aluminum Coupon

^b1.85 (15) p^+/cm^2 , no. UV.

^c2.00 (15) p^+/cm^2 + 1325 ESH (simultaneous)

^d1325 ESH, no p^+

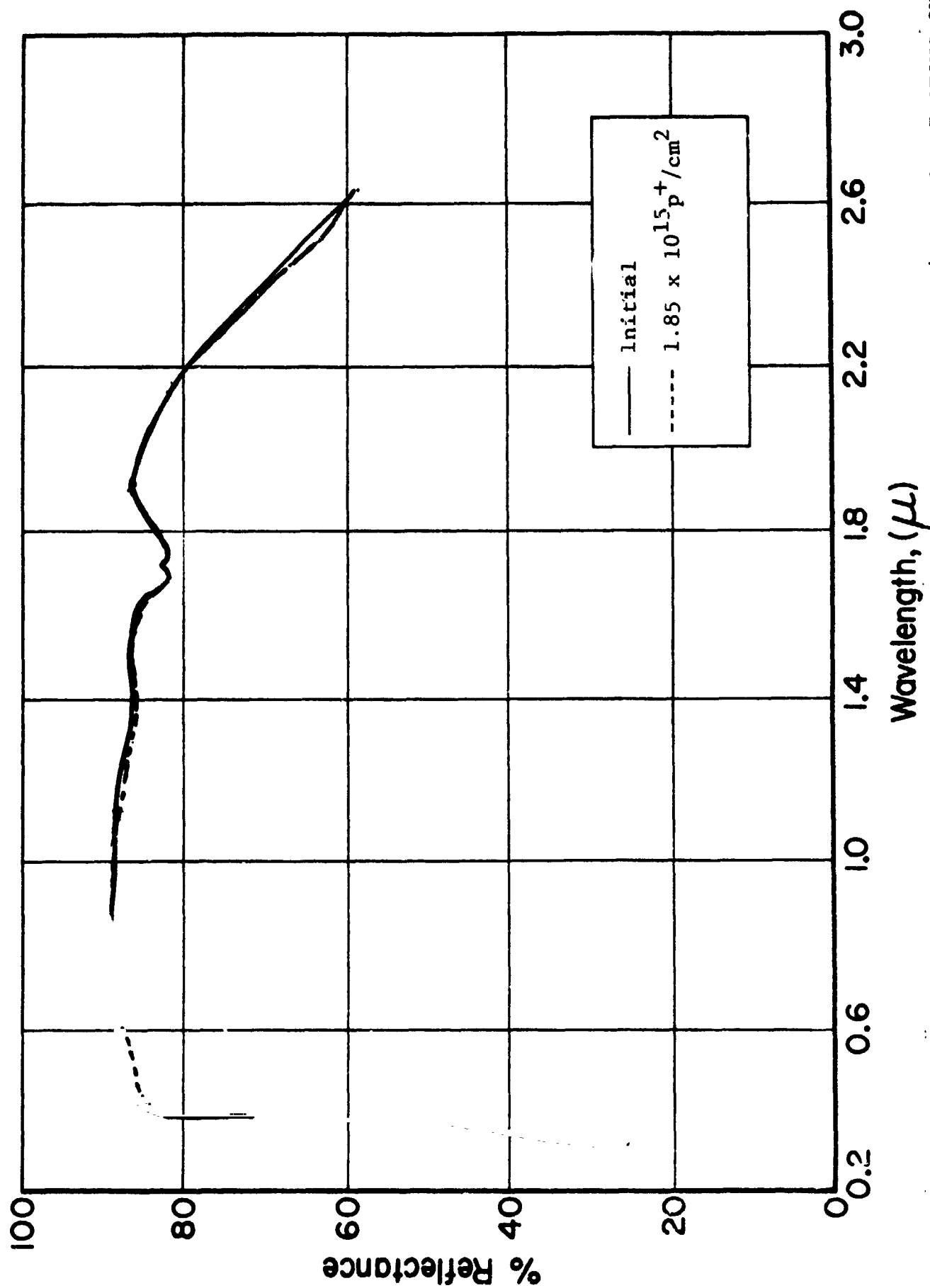


Figure 4-7 REFLECTANCE SPECTRA OF PLASMA ANNEALED, K_2SiO_3 -ENCAPSULATED $\text{Zn}_2\text{TiO}_4/\text{O-I G50}$ - PROTONS ONLY

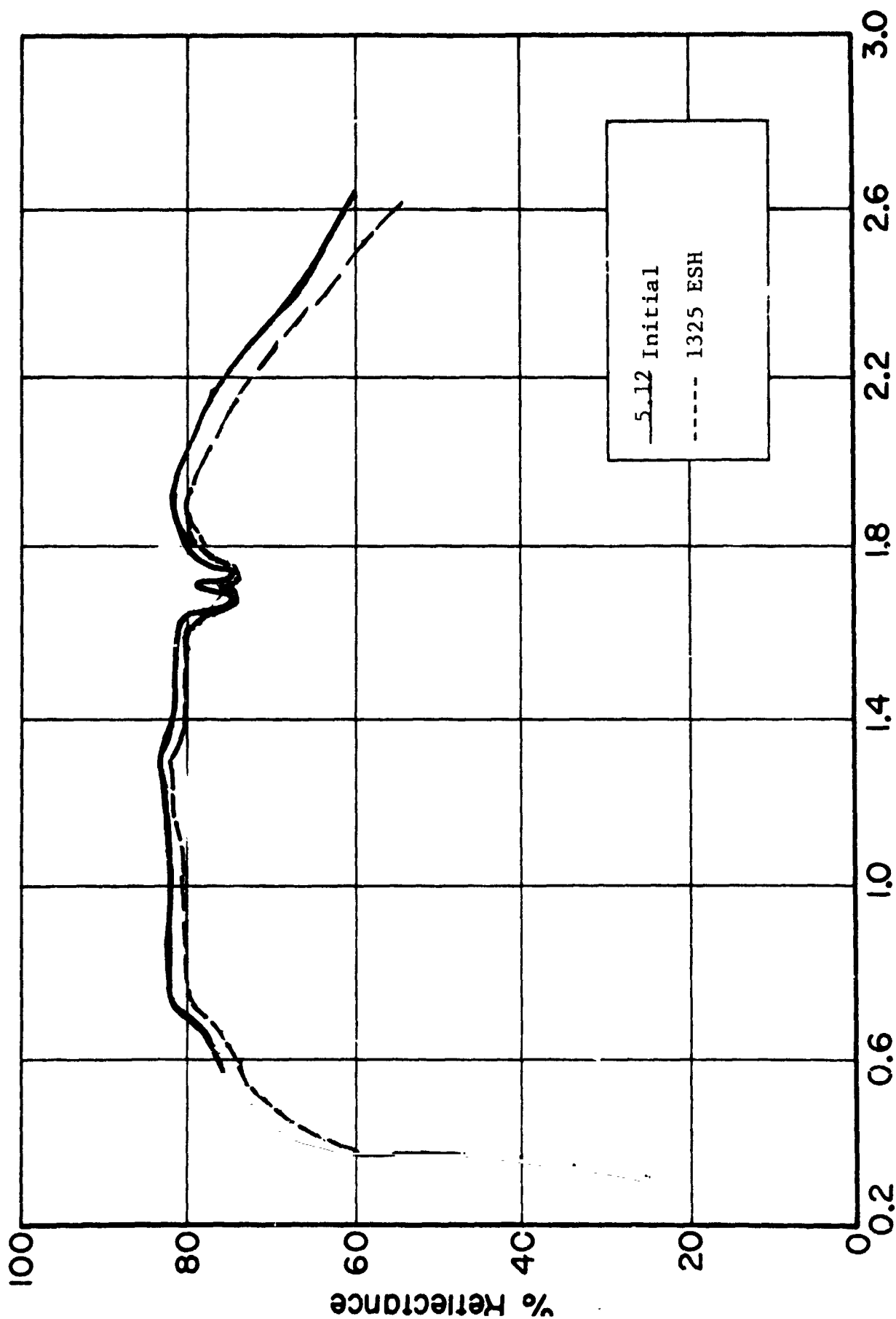
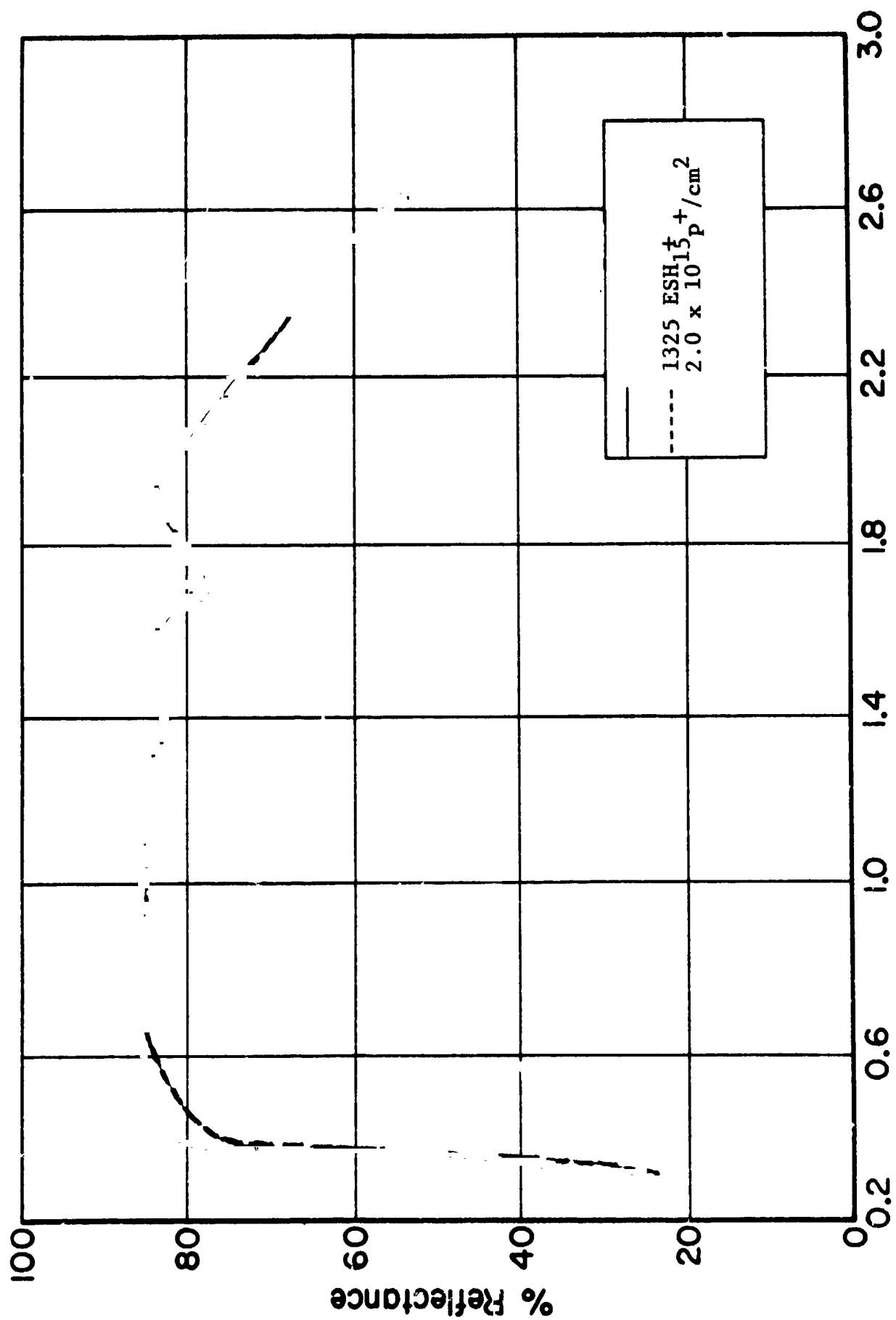


Figure 4-8 REFLECTANCE SPECTRA OF PLASMA ANNEALED, K_2SiO_3 -ENCAPSULATED $ZnTiO_4/p-i$ 650 - ULTRAVIOLET ONLY



Wavelength, (μ)

Figure 4-9. REFLECTANCE SPECTRA OF PLASMA ANNEALED, K_2SiO_3 -ENCAPSULATED $Zn_2TiO_4/0-1$ 650 - PROTONS AND ULTRAVIOLET

behavior indicated in Figures 4-8 and 4-9, however, is anomalous. The former shows considerable infrared damage, similar to ZnO degradation, as a result of an ultraviolet exposure, while, as the latter shows, a combined exposure produces slightly more overall damage, yet insignificant infrared damage. The somewhat greater degradation of the ultraviolet-irradiated paint compared to that of the same paint irradiated simultaneously with protons and ultraviolet radiation, suggests proton-induced bleaching of ultraviolet-created defects. It is possible also that this latter sample received some spillover from the proton beam during the first (proton only) part of the test. In any event, the performance of this paint system is very good - a nominal degradation of 0.015 after an exposure equivalent to that of approximately 0.25 year in space (based on full solar wind exposure and half-time solar electromagnetic exposure).

4.4.1.3.2 Code C-068, $\text{Zn}_2\text{TiO}_4:\text{K}_2\text{SiF}_6/\text{PS-7}$

Figures 4-10-12 present the spectra for samples irradiated with protons only (Figure 4-10), concurrent proton plus ultraviolet (Figure 4-11), and ultraviolet-only (Figure 4-12), with $\Delta\alpha_s$ values of 0.046, 0.056 and 0.025, respectively. The sensitivity to protons versus that to ultraviolet is apparently the converse of that of the previous paint system: proton damage exceeds ultraviolet damage. (A similarity to the $\text{Zn}_2\text{TiO}_4:\text{K}_2\text{SiO}_3$ (Plasma)/O-I 650 exists in the ZnO-like infrared damage due to ultraviolet). The overall performance of this pigment, however, compared to other encapsulated pigment materials, is not satisfactory.

4.4.1.3.3 Code C-067, $\text{Zn}_2\text{TiO}_4:\text{K}_4\text{Si}_4\text{W}_{12}\text{O}_{40}/\text{PS-7}$

The reflectance spectra are presented in Figures 4-13-15. As in the case of $\text{Zn}_2\text{TiO}_4:\text{K}_2\text{SiF}_6/\text{PS-7}$, the effect of concurrent irradiations (protons plus ultraviolet) is greater than that of the individual radiations. Proton irradiation caused the least damage (Figure 4-13), ($\Delta\alpha_s = 0.013$); in combined proton and ultraviolet radiation the $\Delta\alpha_s$ was 0.045 (Figure 4-14); and

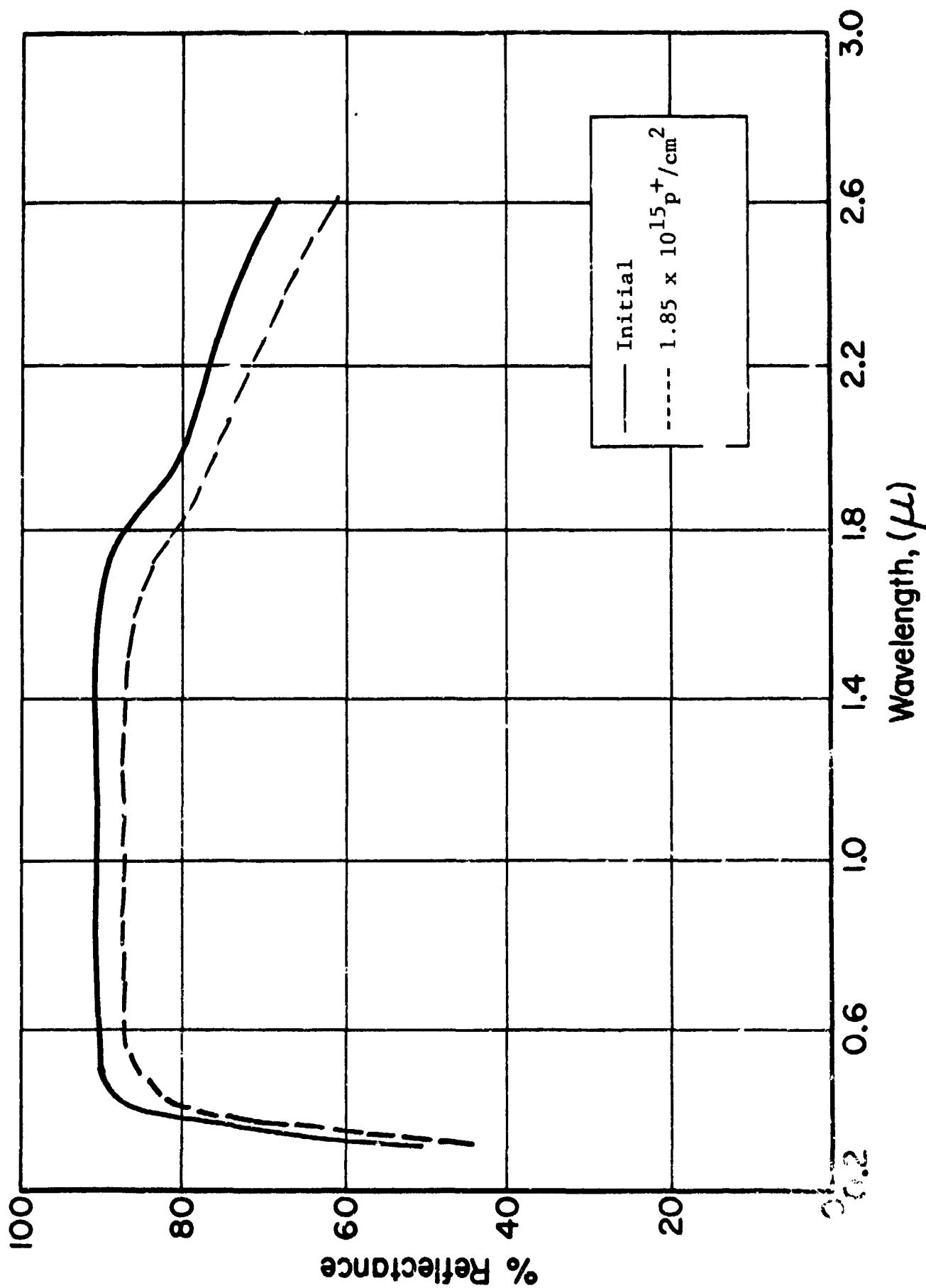


Figure 4-10 REFLECTANCE SPECTRA OF K_2SiF_6 -ENCAPSULATED $\text{Zn}_2\text{TiO}_4/\text{PS-7}$ - PROTONS ONLY

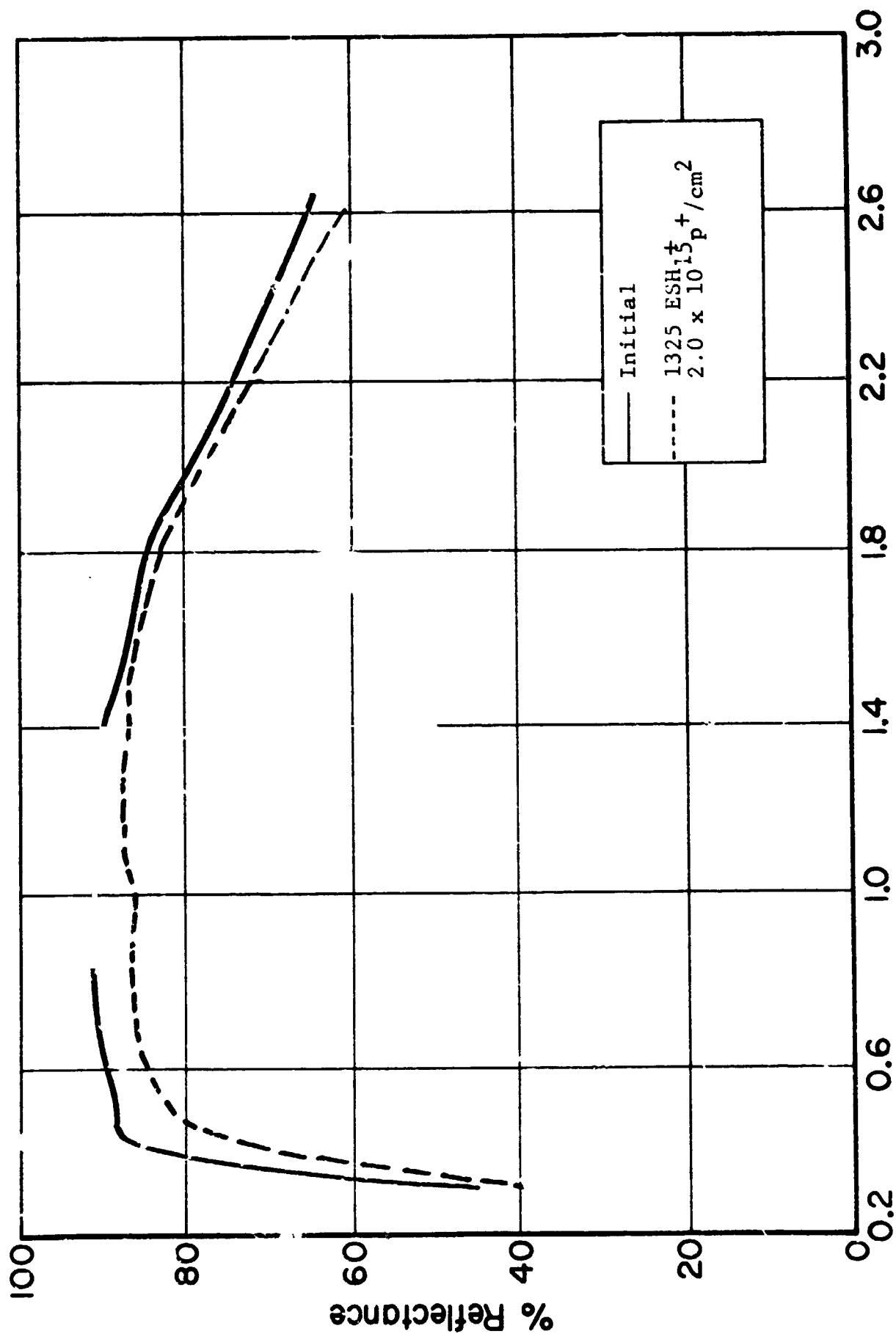


Figure 4-11 REFLECTANCE SPECTRA OF K₂SiF₆-ENCAPSULATED ZnTiO₄/PS-7 - PROTONS AND ULTRAVIOLET

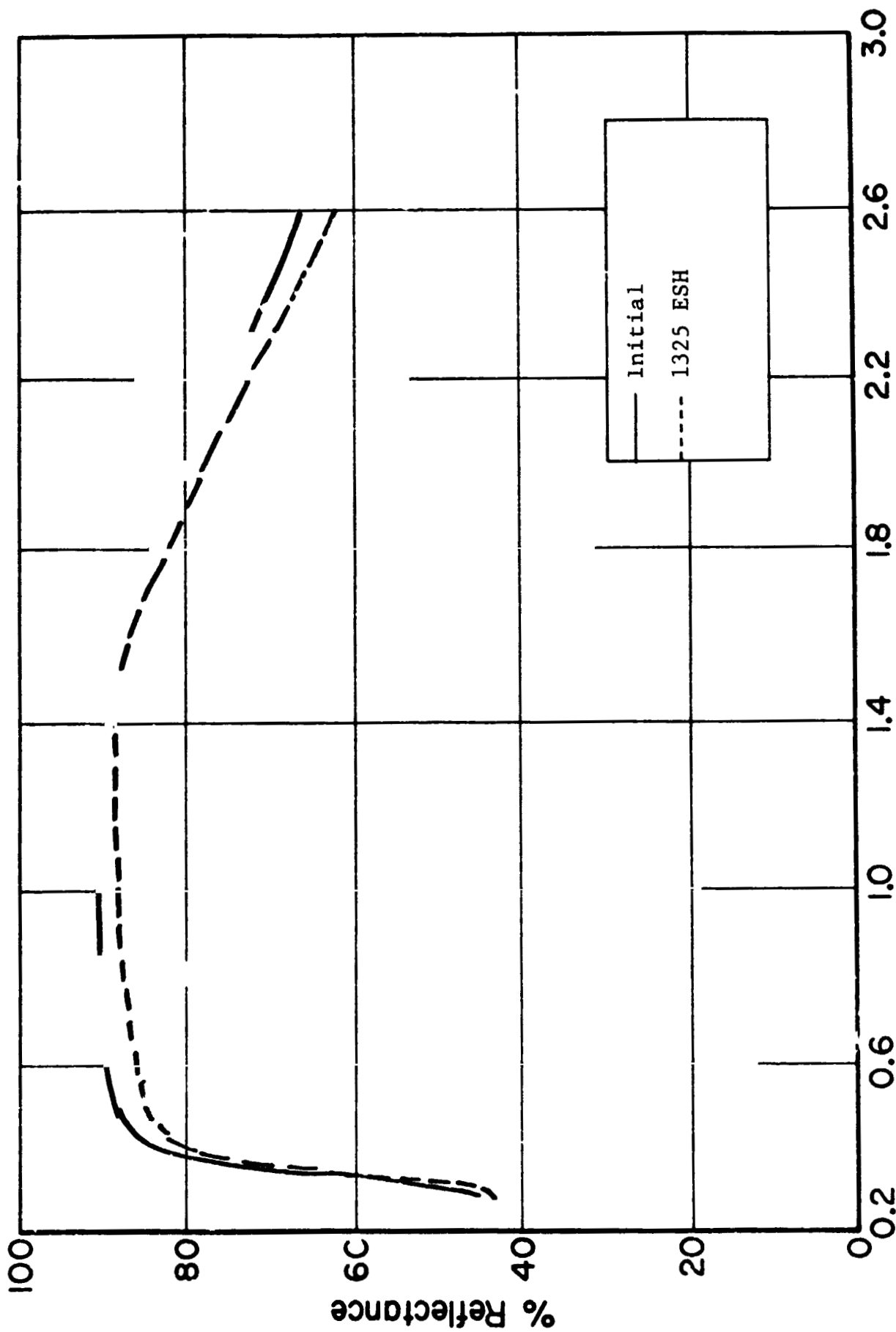


Figure 4-12 REFLECTANCE SPECTRA OF K_2SiF_6 -ENCAPSULATED $Zn_2TiO_4/PS-7$ - ULTRAVIOLET ONLY

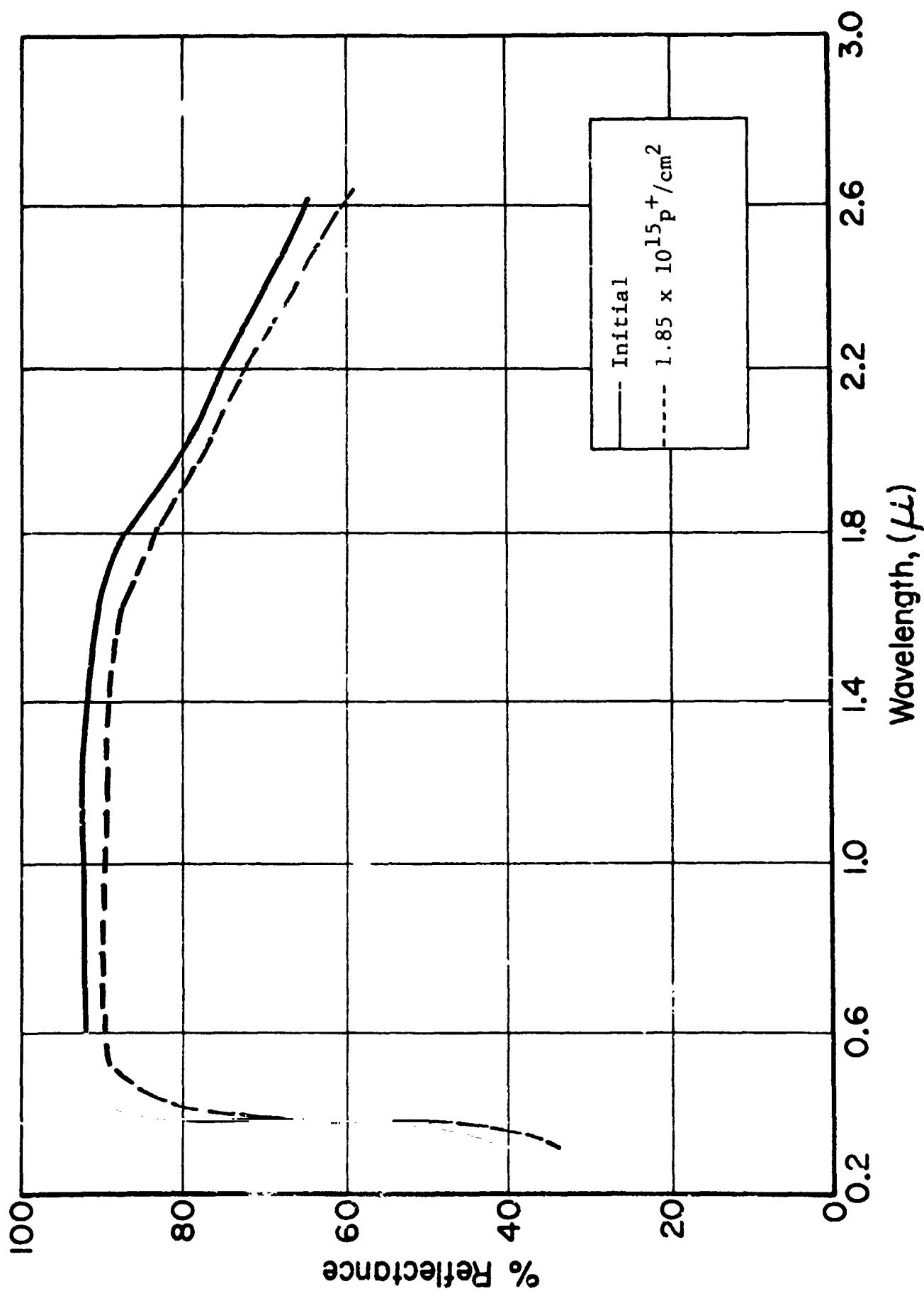


Figure 4-13 REFLECTANCE SPECTRA OF $K_4Si_4W_{12}O_{40}$ -ENCAPSULATED $Zn_2TiO_4/PS-7$ - PROTONS ONLY

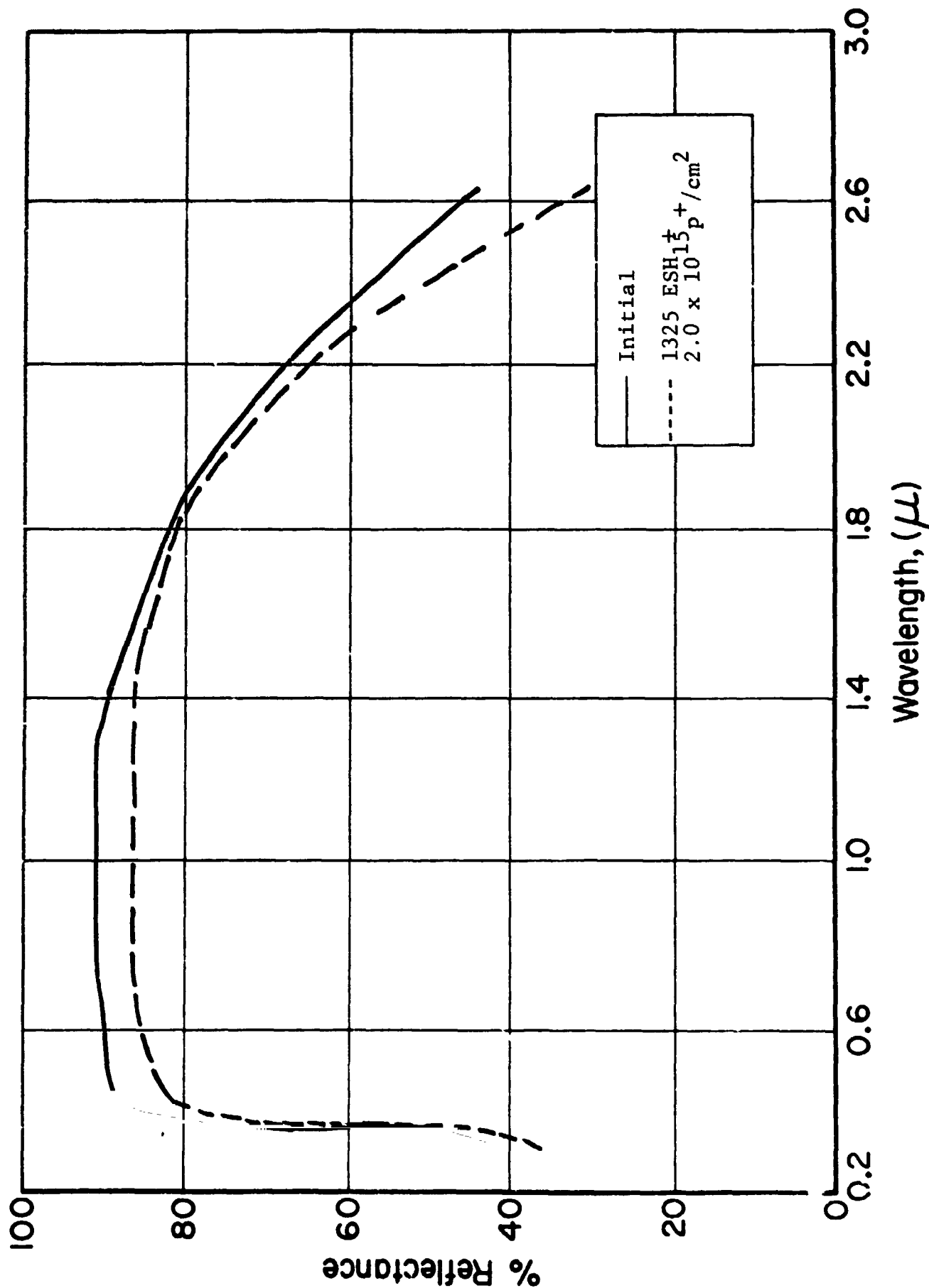


Figure 4-14 REFLECTANCE SPECTRA OF $K_4Si_4W_{12}O_{40}$ -ENCAPSULATED $Zn_2TiO_4/PS-7$ - PROTONS AND ULTRAVIOLET

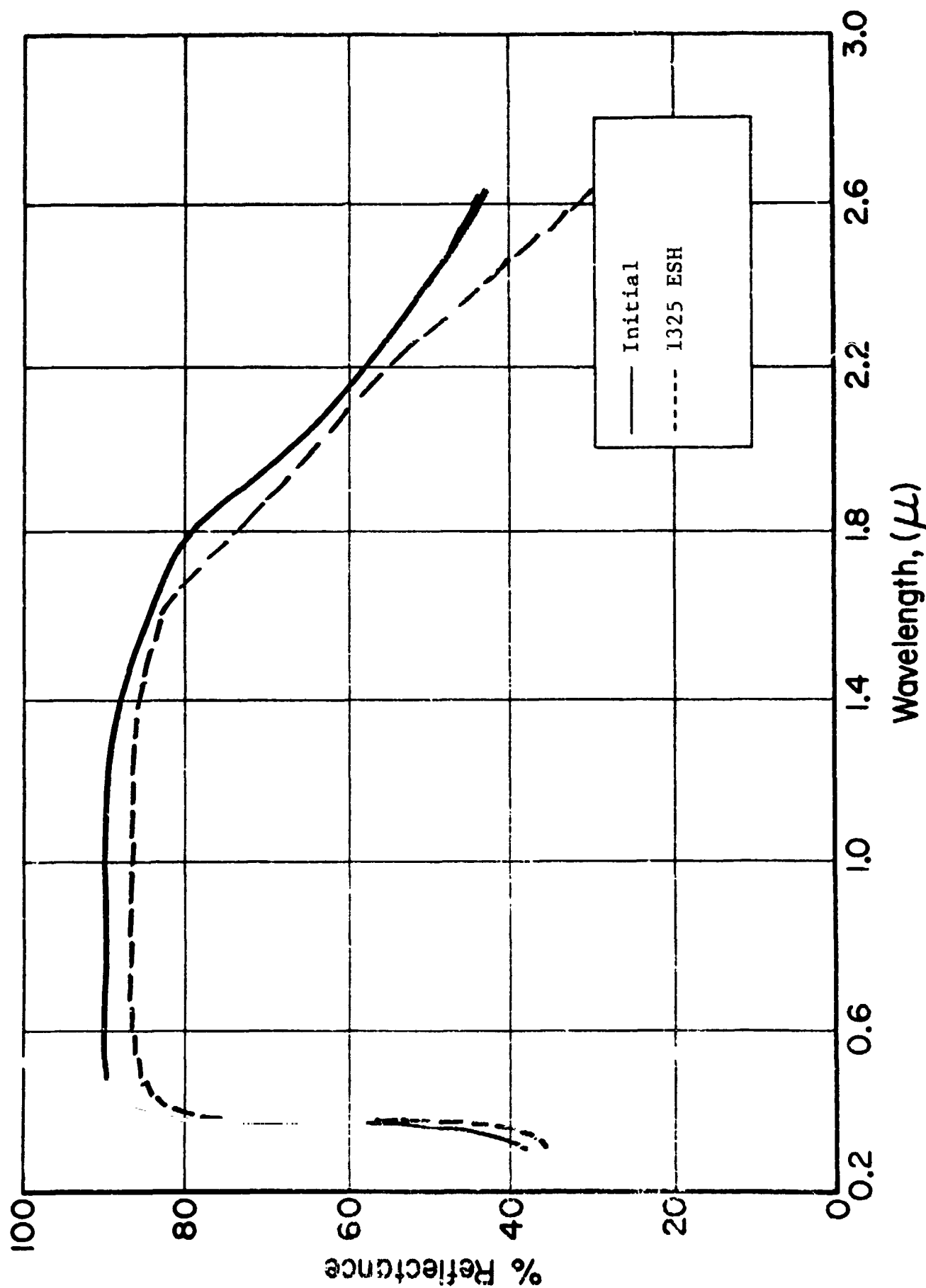


Figure 4-15 REFLECTANCE SPECTRA OF $K_4Si_4W_{12}O_{40}$ -ENCAPSULATED $Zn_2TiO_4/PS-7$ - ULTRAVIOLET ONLY

ultraviolet effects (Figure 4-15) caused a $\Delta\alpha_s$ of 0.031. The spectral damage in all cases is generally small and equally distributed over the entire spectrum, although ZnO-like infrared absorption appears more prominent after ultraviolet irradiation. The silicotungstate-encapsulated Zn_2TiO_4 pigments, nevertheless, are somewhat inferior to those encapsulated in potassium silicofluoride.

4.4.1.3.4 OI-650 "Glass" Resin

Two samples of OI-650 "Glass" Resin (O-I 650) were tested. The reflectance spectra of a sample which was exposed to protons only and of another exposed to protons and UV are shown in Figure 4-16. Although solar absorptance is hardly a valid measure of degradation in this case, the $\Delta\alpha_s$ for the proton-only sample of 0.003 (α_s : 0.455 to 0.458) underscores its excellent stability. Note that damage occurs mainly in the ultraviolet and infrared regions of the spectrum. The O-I 650 film which has been exposed to both proton and ultraviolet radiations also exhibits spectral changes which are very small and occur in the same spectral regions as for the proton-only sample. The change in α_s for the latter is from 0.423 to 0.431; ($\Delta\alpha_s = 0.008$). This behavior suggests that O-I 650 is indeed a very stable binder material and that it is probably more affected by ultraviolet radiation than by protons.

4.4.1.4 Conclusions

OI-650 "Glass" Resin is a very stable binder, both in p^+ and in UV + p^+ environments. Of the three encapsulants evaluated in this test, potassium silicate offers the greatest protection to the pigment. This may, however, result from the fact that it is plasma-calcined after encapsulation, while the other two pigments were not. It appears that the results also demonstrate classic synergistic effects in that the individual effects are not additive and, in the case of the plasma-calcined K_2SiO_3 -encapsulated pigment, the effects

ITT RESEARCH INSTITUTE

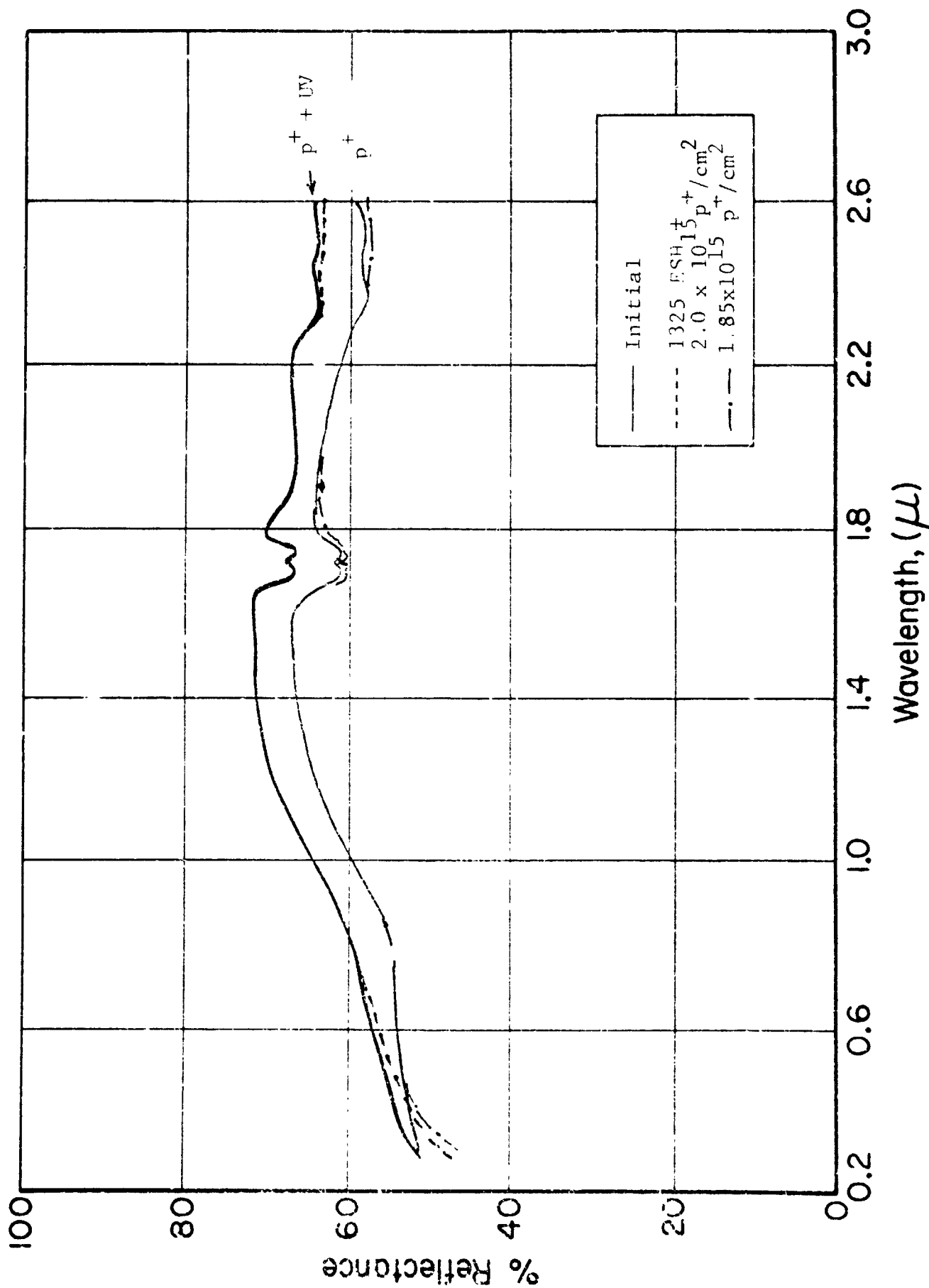


Figure 4-16 REFLECTANCE SPECTRA OF OWENS-ILLINOIS 650 GLASS RESIN UNPIGMENTED FILM - PROTONS AND ULTRAVIOLET

of proton irradiation are partly bleached by absorption of UV radiation.

4.4.2 CREF-6

4.4.2.1 Purpose/Description

The intent of test CREF-6 (Ref. 4,3) was to examine the response of the pigment $\text{Zn}_2\text{TiO}_4:\text{K}_2\text{SiO}_3$ (Plasma) in several different binders exposed to a combined (UV + p^+) environment.

4.4.2.2 Test Sequence

A simple sequence of combined radiations was employed in this test. The proton and ultraviolet radiations were simultaneous. The samples were not rotated, so that samples No.'s 2 and 3 were exposed to proton and ultraviolet radiations while the others were exposed only to ultraviolet radiation. Sample locations 1 and 4 were left blank. Spectral reflectance measurements were made after a combined exposure of $2.4 \times 10^{15} \text{ p}^+/\text{cm}^2$ and 1240 ESH, and at the end of the test after a cumulative, combined exposure of $9.6 \times 10^{15} \text{ p}^+/\text{cm}^2$ and 2250 ESH.

4.4.2.3 Discussion

The solar absorptance values for CREF Test No. 6 are given in Table 4-2.

4.4.2.3.1 Code SRI-2, $\text{Zn}_2\text{TiO}_4:\text{K}_2\text{SiF}_6$ (Plasma)/PS-7

The reflectance spectra of SRI-2 are presented in Figure 4-17. The sample was exposed to UV radiation only. The α_s value degraded 0.030 in the first part of the test, and an additional 0.005 in the second, displaying, like the others, a classically decreasing damage rate with increasing exposure.

4.4.2.3.2 Coat SRI-1,3 $\text{Zn}_2\text{TiO}_4:\text{K}_2\text{SiF}_6$ (Plasma)/OI

For this particular test three OI-650 paints were prepared; two using standard OI-650; the third using OI-650G. One sample was exposed to proton and ultraviolet radiations (Figure 4-18), and the other two (Figures 4-19 and 4-20) including

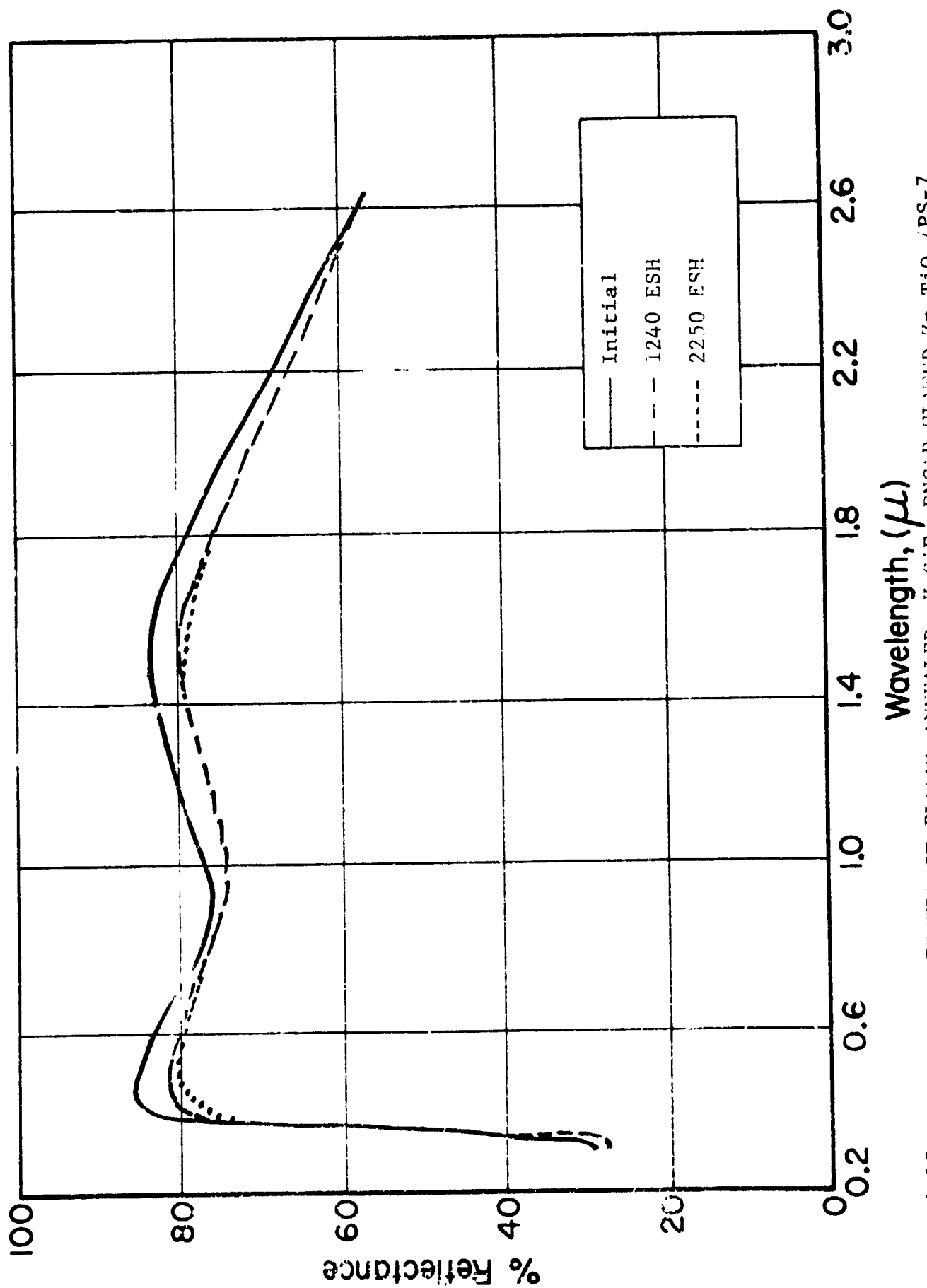


Figure 4.17 REFLECTANCE SPECTRA OF PLASMA ANNEALED, K_2SiF_6 -ENCAPSULATED $\text{Zn}_2\text{TiO}_4/\text{PS-7}$

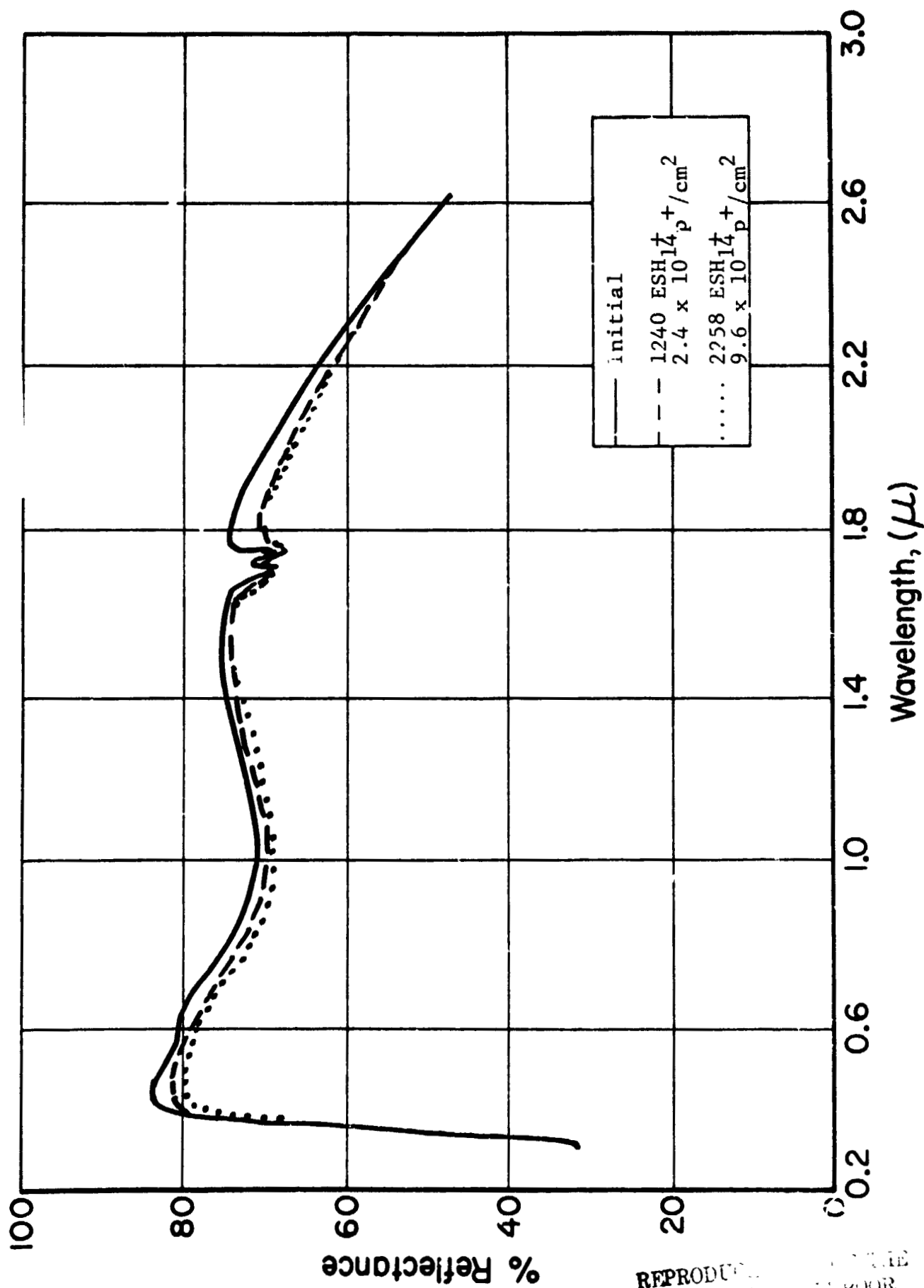


Figure 4.18 REFLECTANCE SPECTRA OF PLASMA ANNEALED, K₂SiF₆-ENCAPSULATED Zn₂TiO₄, OI-650

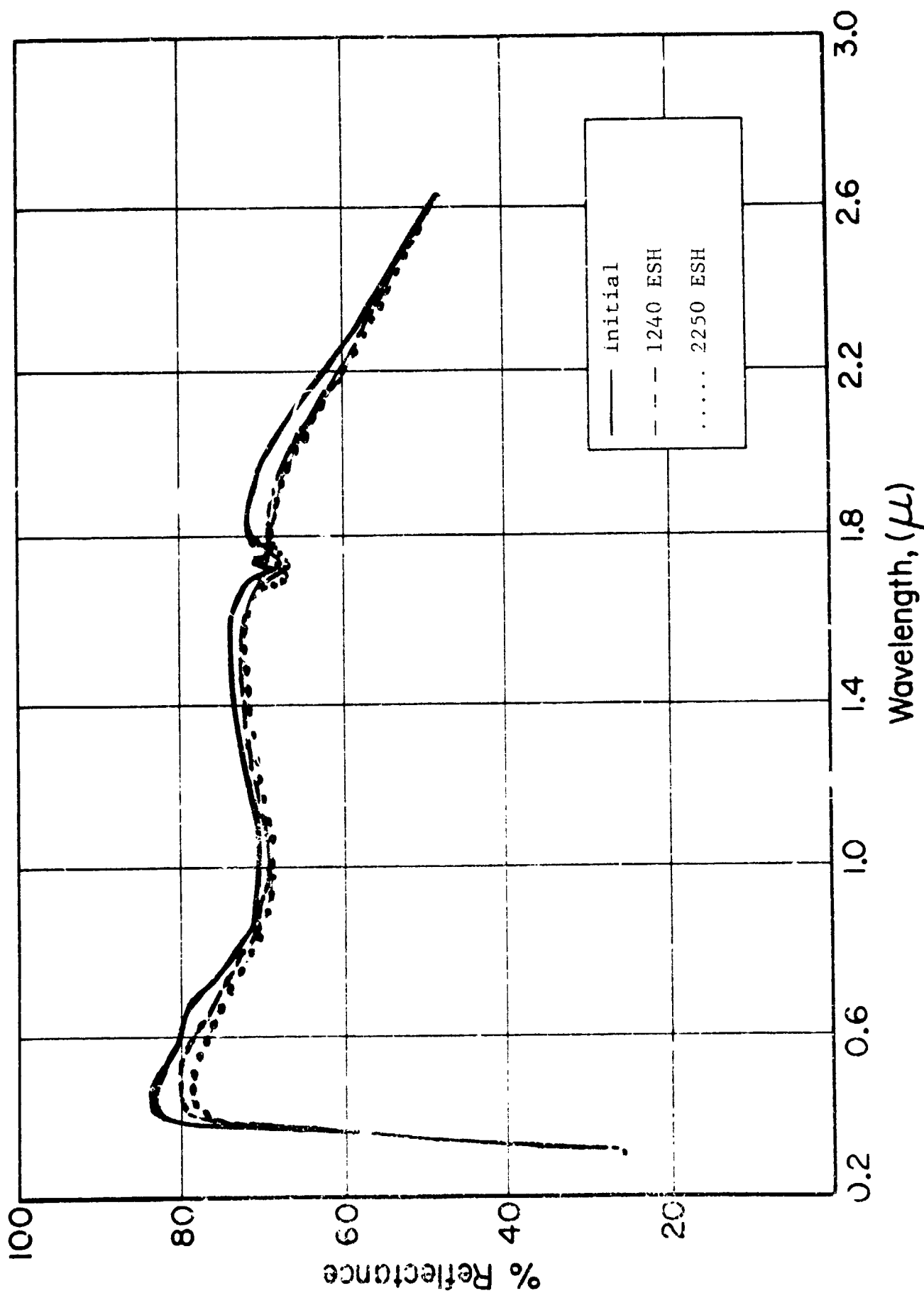


Figure 4.19 REFLECTANCE SPECTRA OF PLASMA ANNEALED, K_2SiF_6 -ENCAPSULATED Zn_2TiO_4 / OI-650

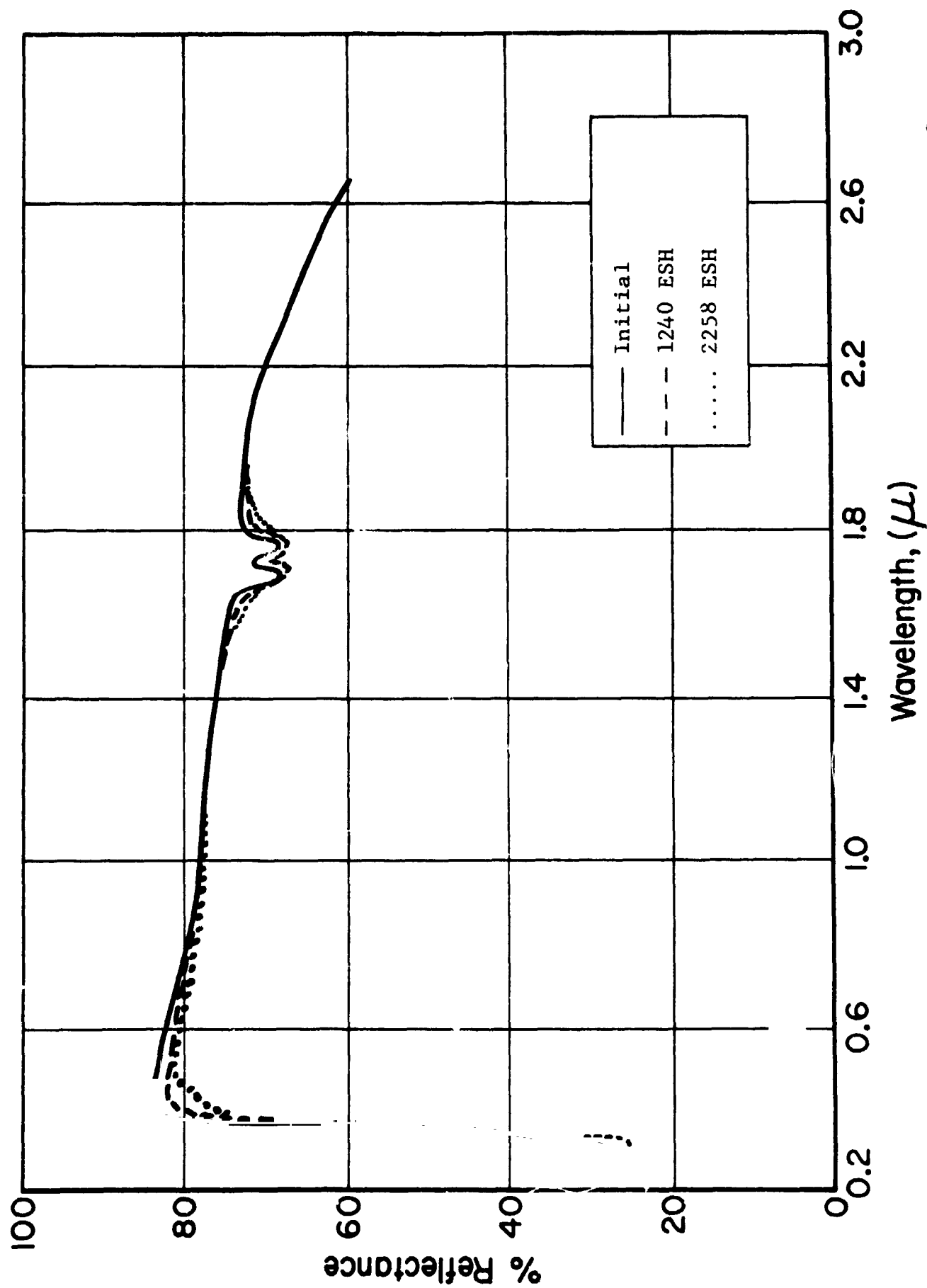


Figure 4.20 REFLECTANCE SPECTRA OF PLASMA ANNEALED, K_2SiF_6 -ENCAPSULATED $Zn_2TiO_4/O-I$ 650 G

Table 4-2

RESULTS OF CREF-6 COMBINED RADIATION TEST OF
ZINC ORTHOTITANATE PAINTS

No.	Code ^a	Initial	$(UV + p^+)_{1}^b$	$(UV + p^+)_{2}^c$	UV_1	UV_2	$\Delta\alpha_s$
2	SRI-1	0.284	0.301	0.303			.019
3	C-169	0.290	0.303	0.315			.025
6	SRI-2	0.251			0.281	0.286	.035
9	SRI-1	0.286			0.305	0.311	.025
11	C-169	0.243			0.252	0.260	.017
12	SRI-3	0.267			0.272	0.280	.013

^acode explanations:SRI-1 = $Zn_2TiO_4:K_2SiF_6$ (Plasma)/OISRI-2 = $Zn_2TiO_4:K_2SiF_6$ (Plasma)/PS-7SRI-3 = $Zn_2TiO_4:K_2SiF_6$ (Plasma)/GC-169 = $Zn_2TiO_4:K_2SiO_3$ (Plasma)/OI (same as C-070 in CREF-5)^b $(p^+ + UV)_1 = 24 (15) p^+ / cm^2$ and 1240 ESH^c $(p^+ + UV)_2 = 2.4 (15) p^+ / cm^2$ and 2250 ESH

the OI-650G paint were exposed to ultraviolet radiation only. The α_s value for the paint (with the standard binder) exposed to the combined environment degraded 0.017 in the first part of the test and an additional 0.001 in the second. The α_s value for the "standard" paint exposed to ultraviolet radiation degraded only 0.019 in the first part of the test and an additional 0.006 in the second. The stability of the paint with the modified binder is considerably better; α_s increased only 0.005 in the first part, an additional 0.003 in the second. All these changes are within experimental error, and hence not necessarily indicative of a trend. In any event the stability of this paint system is exceptionally good.

4.4.2.3.3 C-169 $\text{Zn}_2\text{TiO}_4\text{:K}_2\text{SiO}_3$ (Plasma)/OI

This paint was prepared as IITRI Batch No. C-169 and is identical, except in date of preparation, with IITRI Batch No. C-070, evaluated in CREF 5. The reflectance spectra for the two samples one irradiated with UV radiation only and the other with protons and UV radiation, are given in Figures 4-21 and 4-22. The α_s value of the sample whose spectra are shown in Figure 4-21 degraded 0.009 in the first part, and 0.008 in the second. In the case of the combined radiation sample (Figure 4-22), α_s degraded 0.013 in the first part and an additional 0.012 in the second. Within experimental error, these are consistent results.

4.4.2.4 Analyses and Conclusions

The stability of $(\text{SS})\text{Zn}_2\text{TiO}_4$ pigments which have been plasma-annealed compared to that of pigments not so treated has long been apparent. Plasma annealing, however, in certain cases evidently causes some permanent damage very similar to that it is intended to prevent. Although not considered very likely, the possibility exists that this damage was introduced in the grinding process after plasma annealing. In Figure 4-23 we compare the initial (unirradiated) spectral

IIT RESEARCH INSTITUTE

C-3

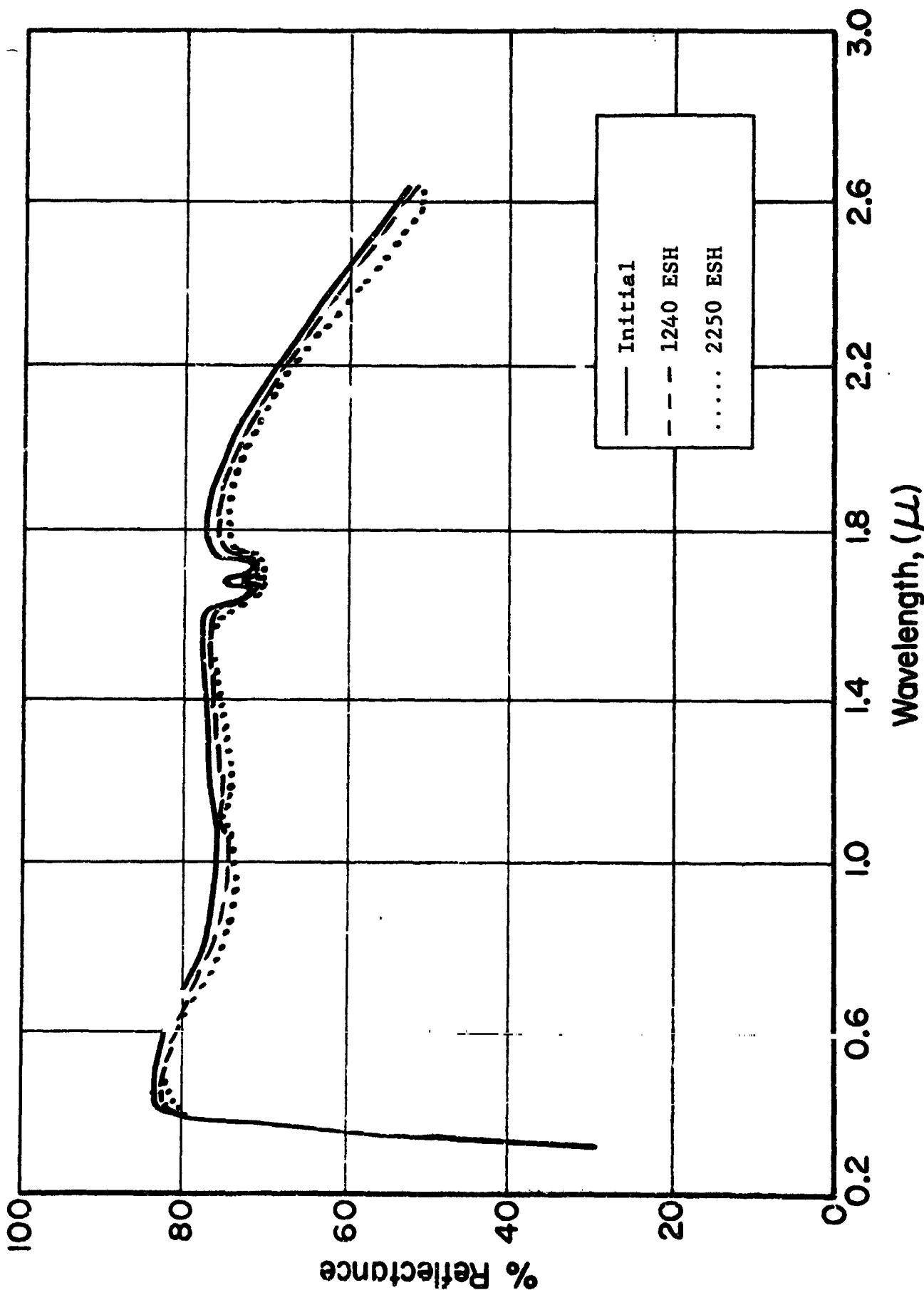


Figure 4.21 REFLECTANCE SPECTRA OF K_2SiO_3 -ENCAPSULATED $Zn_2TiO_4/O-1\ 650$

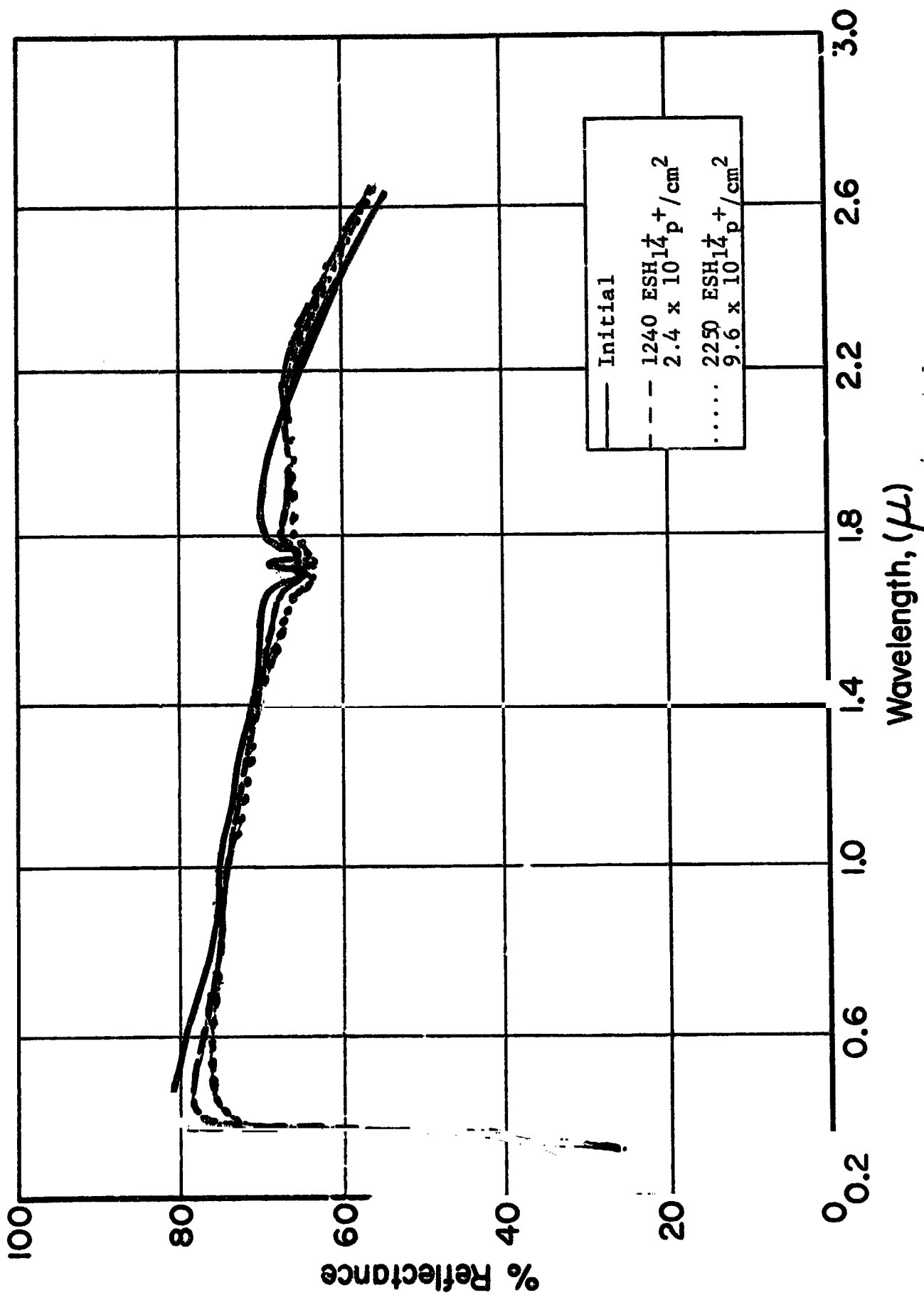


Figure 4.22 REFLECTANCE SPECTRA OF K_2SiO_3 -ENCAPSULATED $Zn_2TiO_4/O-I$ 650

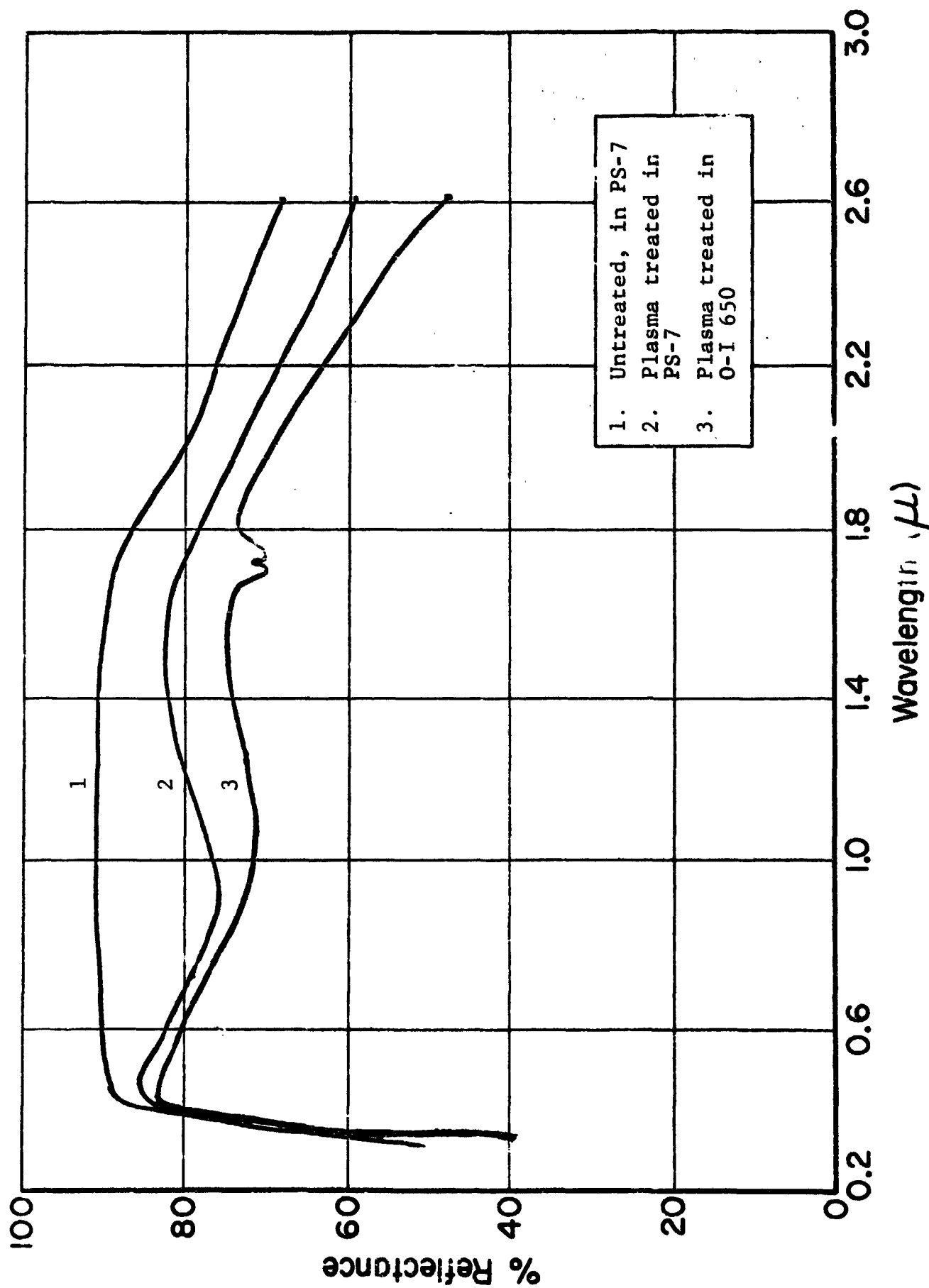


Figure 4.23 REFLECTANCE SPECTRA OF K_2SiF_6 -ENCAPSULATED Zn_2TiO_4 WITH AND WITHOUT PLASMA ANNEALING

reflectance of $\text{Zn}_2\text{TiO}_4:\text{K}_2\text{SiF}_6$, with and without plasma annealing. The effect of the treatment is evident in the large induced absorption in the visible and S-band regions (the annealed pigment appeared "gray"). Stability of the plasma annealed pigment, however, was only slightly improved. In this case, the $\Delta\alpha_s$ attributable to plasma annealing alone is about 0.1. Table 4-3 summarizes the appropriate data from CREF-5 and CREF-6 for silicate paints of the pigment $\text{Zn}_2\text{TiO}_4:\text{K}_2\text{SiF}_6$.

The performance of $\text{Zn}_2\text{TiO}_4:\text{K}_2\text{SiO}_3$ pigments is considerably better than that of any of the other encapsulated pigments. Table 4-4 compares the results obtained in CREF-5 with those in CREF-6 for the paints $\text{Zn}_2\text{TiO}_4:\text{K}_2\text{SiO}_3$ (Plasma)/OI.

In both tables for comparable exposures, the results of Part 2 of the CREF-5 should be compared with those of Part 1 of CREF-6. The comparison is good - within experimental error. The stability of the $\text{Zn}_2\text{TiO}_4:\text{K}_2\text{SiO}_3$ paint system is very good. The largest part of the damage sustained by the paint after combined UV + p^+ exposure is in the pigment, and most of that is caused by UV radiation.

The data from CREF-5 and CREF-6 along with the results of many preceding tests make it very evident that, while plasma annealing does ordinarily improve pigment stability, it also in some cases has caused significant, and unacceptable, permanent increases in optical absorption - in one instance, greater than the $\Delta\alpha_s$ caused environmentally in a pigment not plasma annealed. Some pigments, therefore, are benefitted more from the plasma heat treatment than others. In theory, however, the plasma heating conditions can be optimized to produce stable pigments without otherwise affecting their optical properties. An analysis of all the available data suggest that, to be successful, the plasma annealing process must affect the pigment surface - and only the pigment surfaces; otherwise, excessive internal high temperatures cause significant, permanent optical damage. The nature of the

Table 4-3

COMBINED IRRADIATION EFFECTS IN $\text{Zn}_2\text{TiO}_4:\text{K}_2\text{SiF}_6/\text{PS-7}$

<u>Exposure</u>	<u>Initial</u>	α_s Values	
		<u>Part I</u>	<u>Part 2</u>
<u>C-068 (CREF-5)</u> <u>(Not plasma annealed)</u>			
Protons Only	0.158	0.204	--
Protons + ultraviolet	0.171	---	0.227
Ultraviolet only	0.179	--	0.204
<u>SRI-2 (CREF-6)</u> <u>(Plasma annealed)</u>			
Ultraviolet only	0.251	0.281	0.286

Table 4-4

COMBINED IRRADIATION EFFECTS IN $\text{Zn}_2\text{TiO}_4:\text{K}_2\text{SiO}_3$ (Plasma)/OI-650

<u>Exposure</u>	<u>Initial</u>	<u>$\Delta\alpha_s^*$</u>	<u>Part 1</u>	<u>$\Delta\alpha_s$</u>	<u>Part 2</u>
<u>C-070 (CREF-5)</u>					
Protons only	0.194	(0.002)	0.196		
Protons + ultraviolet	0.223			0.013	0.236
Ultraviolet only	0.286			0.018	0.304
<u>C-169 (CREF-6)</u>					
Protons + ultraviolet	0.290	(0.013)	0.303	(0.025)	0.315
Ultraviolet only	0.243	(0.009)	0.252	(0.017)	0.260

* $\Delta\alpha_s$ values determined with respect to initial value.

encapsulant consequently takes on a more important role than previously ascribed to it. Overall optical stability would thus relate to its interaction with the pigment and how this is affected by the plasma treatment. The facts that plasma heat treatment damages some encapsulated pigments more than it benefits them and that some encapsulants are nearly as effective as an ideal plasma heat treatment suggest that the "stable" surface treatment may be attainable chemically as well as by plasma annealing.

4.4.3 CREF Test No. 7

4.4.3.1 Purpose/Description

This test is a long duration, combined environment irradiation to determine the effectiveness of three Zn_2TiO_4 encapsulants - K_2SiF_6 , K_2SiO_3 and Li_2SiF_6 . The test (Ref. 4.4) was also designed to show whether the effectiveness of the encapsulant could be improved by plasma-calcination, and also to indicate the compatibility and performance of these pigments in both silicone and silicate vehicles.

4.4.3.2 Sequence

Samples No.'s 1-4 were irradiated with combined UV + p^+ radiations; sample No.'s 5-12 were irradiated with UV radiation only. Reflectance measurements were made initially, and after exposures of 1000 ESH and 1800 ESW 1700 ESH and 3750 ESW 2850 ESH and 7700 ESW, 3850 ESH and 10,500 ESW, and finally after an O_2 bleach.

4.4.3.3 Results

Table 4-5 displays the solar absorptance values of the test materials. Selected spectra are presented in Figures No. 4.24-29. No efforts were made to optimize either the particle size of the pigments or the thickness of the paint specimens: their α_s values were, therefore, expectedly variant. The spectra of $\text{Zn}_2\text{TiO}_4:\text{K}_2\text{SiF}_6$ (plasma)/PS-7 (Figure 4-24) when compared with those of the same pigment in OI-650G (Figure 4-25)

IIIT RESEARCH INSTITUTE

Table 4-5a
COMBINED IRRADIATION (CREF NO. 7) TEST DATA - Zn_2TiO_4 PAINTS

Sample No.	Batch No.	Encapsulant/Treatment	Vehicle	Solex Absorptances							$\Delta\alpha$ ***
				Initial	1000 ESH* 1800 EWH	1700 ESH 3750 EWH	2850 ESH 7700 EWH	3850 ESH 10,500 EWH	O ₂ Bleach		
1	C-262	K ₂ SiF ₆ SRI 12-31.3	PS-7	0.221	0.227	0.238	0.259	0.251		0.030	
2	C-261	K ₂ SiF ₆ SRI 12-31.3	OI-650G	0.269	0.278	0.286	0.309	0.308		0.039	
3	C-267	K ₂ SiF ₆ Recalcined-1100°C	OI-650	0.207	0.225	0.229	0.251	0.265	0.259 $\Delta\alpha = +0.006$	0.059	
4	C-245	K ₂ SiO ₃	Li ₂ SiO ₃	0.118	0.144	0.178	0.217	0.198		0.08	
5	C-268A	K ₂ SiO ₃ SRI 17-35	OI-650G	0.227	0.277	0.250	0.278	0.291	0.263 $\Delta\alpha = +0.023$	0.065	
6	C-240	Li ₂ SiF ₆	OI-650	0.193	0.209	0.217	0.224	0.229		0.036	
7	C-262	K ₂ SiF ₆ SRI 12-31.3	PS-7	0.268	0.279	0.281	0.283	0.284		0.016	
8	C-261	K ₂ SiF ₆ SRI 12-31.3	OI-650G	0.269	0.280	0.283	0.291	0.293		0.024	
9	C-267	K ₂ SiF ₆ Recalcined-1100°C	OI-650	0.199	0.224	0.228	0.239	0.241	0.224 $\Delta\alpha = +0.017$	0.042	
10	C-245**	K ₂ SiO ₃	Li ₂ SiO ₃								
11	C-244	Li ₂ SiF ₆ (Baked at 100°C)	OI-650G	0.181	0.202	0.209	0.226	0.250	0.214	0.035	
12	C-244	Li ₂ SiF ₆ (Air Dried)	OI-650G	0.167	0.192	0.213	0.221	0.220	0.190	0.027	

*Only Sample No.'s 1, 2, 3 and 4 received both ultraviolet and proton radiations.

**Lost early in test.

***Final $\Delta\alpha$ data after 3850 ESH (and 3850 ESH + 10,500 EWH).

Table 4-5b
CREF ZINC ORTHOTITANATE PAINT* SAMPLES AND TREATMENTS

Sample (Position) Number	Treatment/Vehicle	Paint Batch No.	Figure Number	Solar Absorptance Values			
				Initial	400 ESH**	1000 ESH	O ₂ Bleach
1	:(PO ₄ /SiO ₃ /PO ₄)/OI-650	C-384	5	.134	.218	.225	.179
2	:(PO ₄ /SiO ₃ /PO ₄)(heat treated)/OI-650	C-379	7	.214	.342	.399	.332
3	:K ₂ SiF ₆ (re-heat treated)/OI-650	C-378	9	.245	.299	.346	.310
4	:K ₂ SiF ₆ /OI-650	C-383	11	.171	.216	.228	.197
5	:K ₂ SiF ₆ (re-heat treated)/OI-650	C-317	13 (AFML Flt. Exp.)	.152	.189	.194	--
6	:(PO ₄ /SiO ₃ /PO ₄)/OI-650	C-384	6	.154	.170	.191	.157
7	:(PO ₄ /SiO ₃ /PO ₄)(heat treated)/OI-650	C-379	8	.242	.357	.393	.325
8	:K ₂ SiF ₆ (re-heat treated)/OI-650	C-378	10	.244	.324	.332	.284
9	:K ₂ SiF ₆ /OI-650	C-383	12	.143	.203	.225	.184
10	:Li ₂ SiF ₆ /OI-650	C-382	14	.143	.162	.202	--
11	:Li ₂ SiF ₆ (heat treated)/OI-650	C-377	15	.175	.240	.256	--
12	Heat treated SP500 ZnO	--	4	.169	.178	.198	--

*All the raw zinc orthotitanate was from IITRI Batch No. C-316, except Sample No. 5 which came from IITRI Batch No. B-492.

**Samples 1-4 also received $5.5 \times 10^{14} \text{ p}^+(1.2 \text{ keV})/\text{cm}^2$.

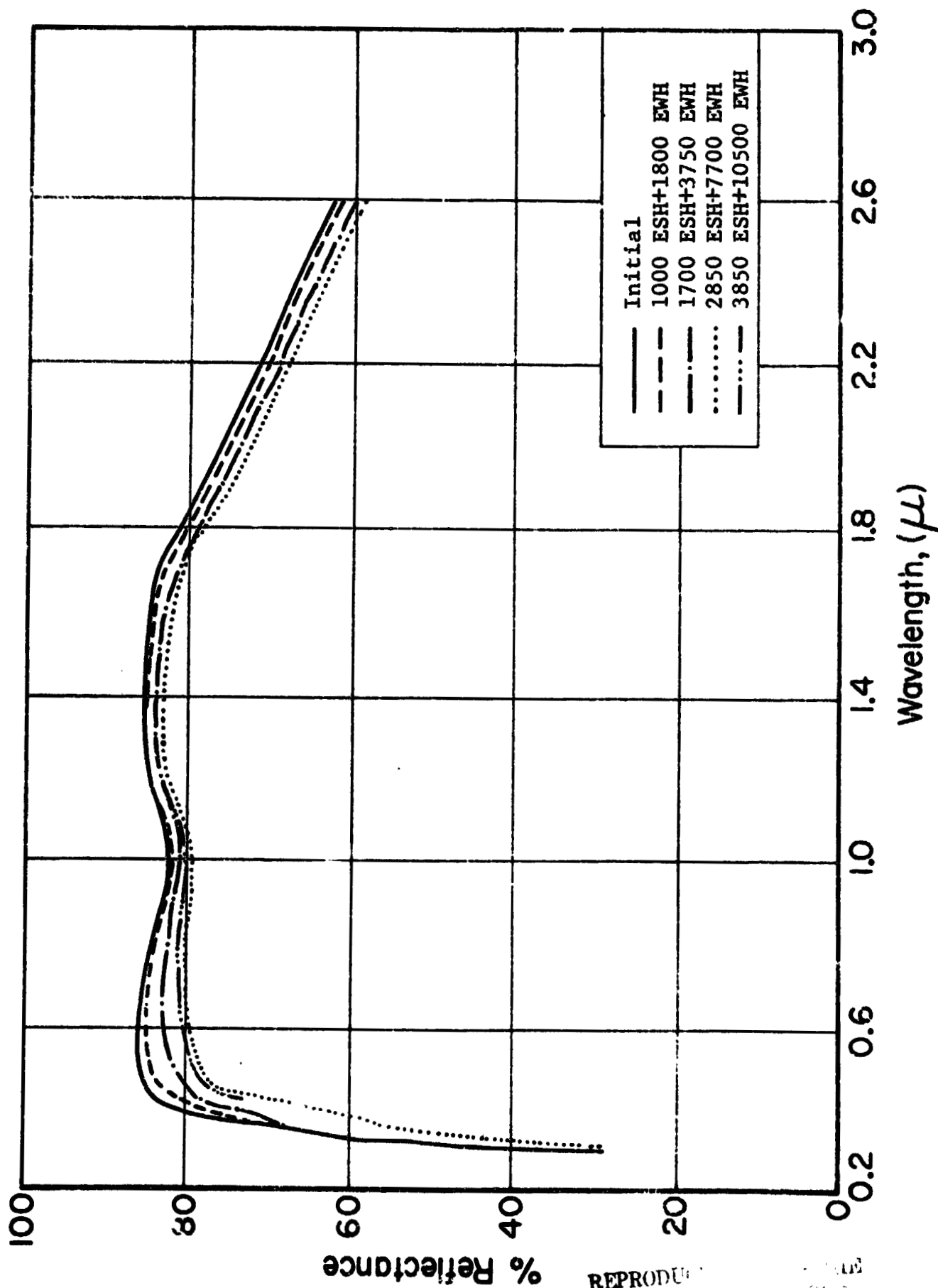


Figure 4.24 REFLECTANCE SPECTRA OF $\text{Zn}_2\text{TiO}_4:\text{K}_2\text{SiF}_6$ (SRI 12-31.3)/PS-7

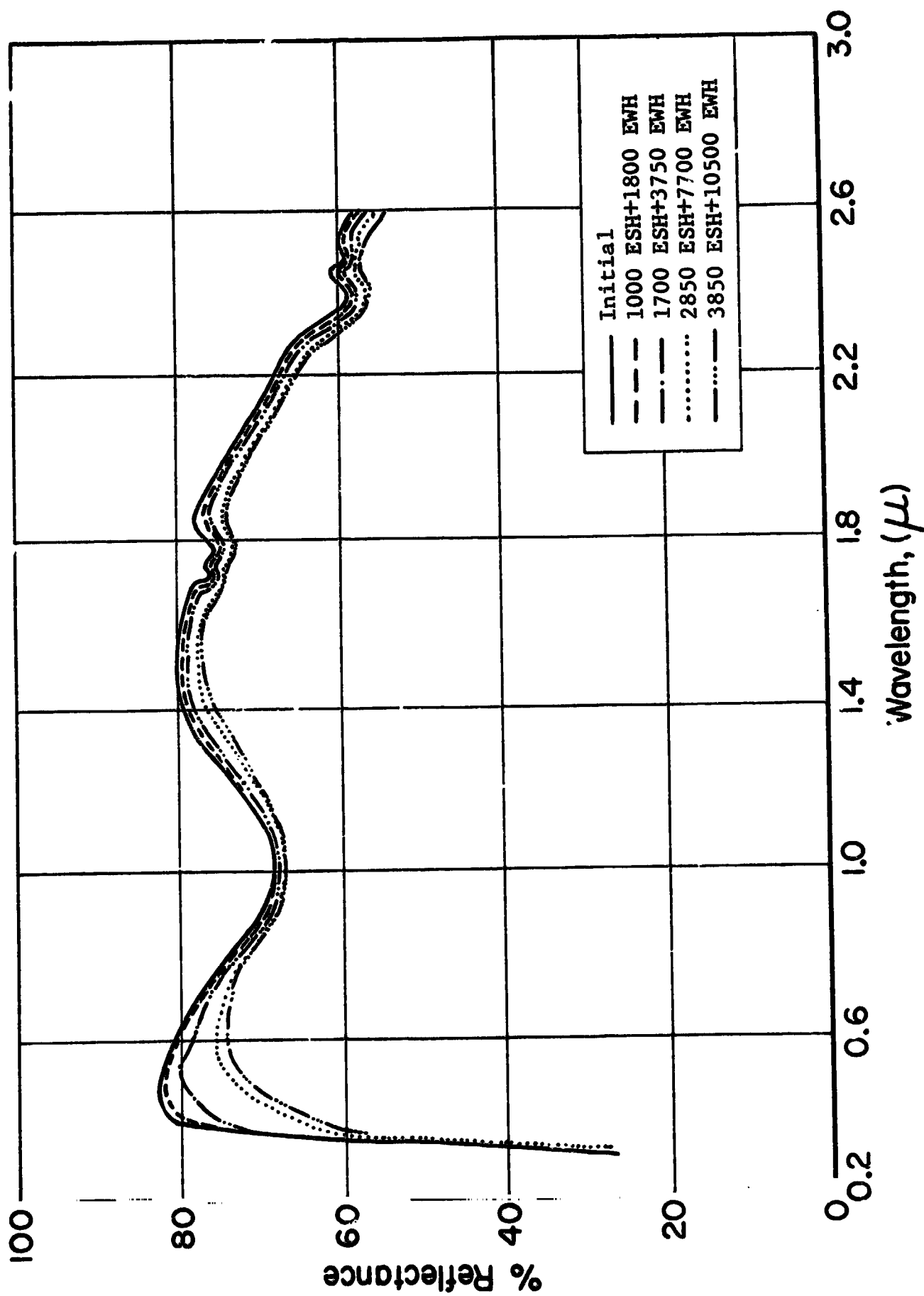


Figure 4.25 REFLECTANCE SPECTRA OF $Zn_2TiO_4:K_2SiF_6$ (SRI 12-31.3)/G

show that OI-650 paints are equally as stable as, if not more so than, PS-7 paints. Note, however, the loss of reflectance at 900 nm as a result of an interaction between the pigment and the OI650 binder. The reflectance spectra of Figure 4-26 shows $\text{Zn}_2\text{TiO}_4:\text{K}_2\text{SiF}_6/\text{OI}$, the pigment of which has been recalcined (by IITRI) at $1100^\circ\text{C}/1\text{hr}$. The treatment in this case was helpful but not as effective as plasma annealing. This particular material, however, exhibits almost no instability in the infrared region. The O_2 bleach spectra indicate that encapsulation surface coverage was not complete. As expected the performance of these UV + p^+ samples when compared with that of their UV-irradiated counterparts show that radiation produces a greater overall effect.

The paint, $\text{Zn}_2\text{TiO}_4:\text{K}_2\text{SiO}_3/\text{L}_2\text{SiO}_3$ (Figure 2-27) shows some promise. The lack of any response to the O_2 bleach indicates that the silicating process - either the potassium silicate encapsulant or the lithium silicate binder, or both - is effective in preventing characteristic S-band damage. It has surprisingly low solar absorptance, but it also degraded badly.

Figure 4-28 shows the spectral reflectance of an $\text{Zn}_2\text{TiO}_4:\text{K}_2\text{SiO}_3(\text{plasma})/\text{G}$. Its S-band bleached slightly but the fact that infrared damage recovered almost completely suggests that the encapsulant coverage was not complete.

In Figure 4-29 are the spectra of the paint $\text{Zn}_2\text{TiO}_4:\text{Li}_2\text{SiF}_6/\text{G}$; its stability is excellent, and encapsulant coverage appears to be adequate.

4.4.3.4 Conclusions

Degradation induced by irradiation of these paints occurs primarily within the pigment (rather than on its surface) and in the vehicle. OI-650 is basically more stable than PS-7 (potassium silicate). It is evident that in the more stable paint systems the degradation rate essentially vanishes after

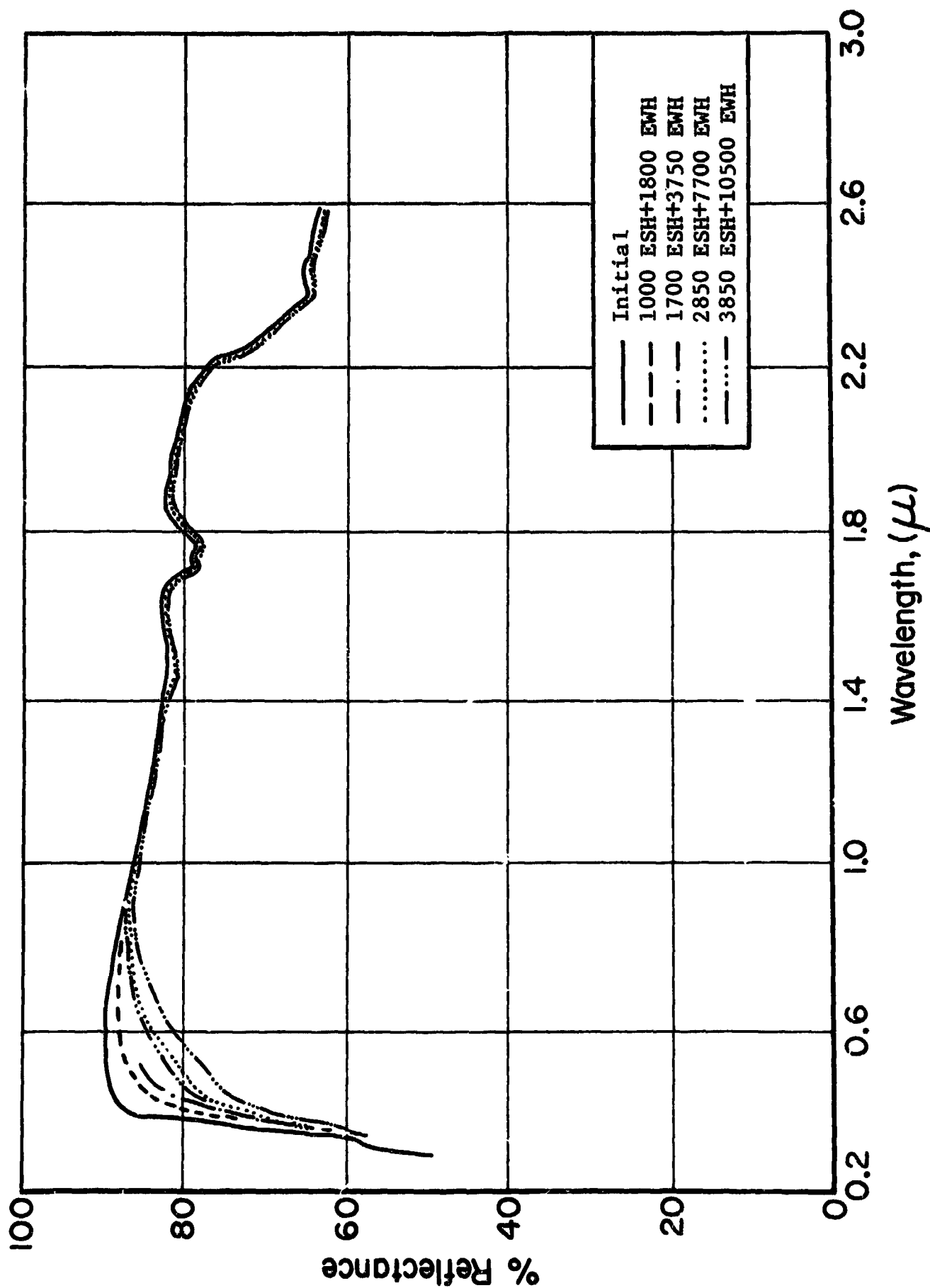


Figure 4.26 REFLECTANCE SPECTRA OF $\text{Zn}_2\text{TiO}_4:\text{K}_2\text{SiF}_6$ (Recalcined-1100°C)/OI

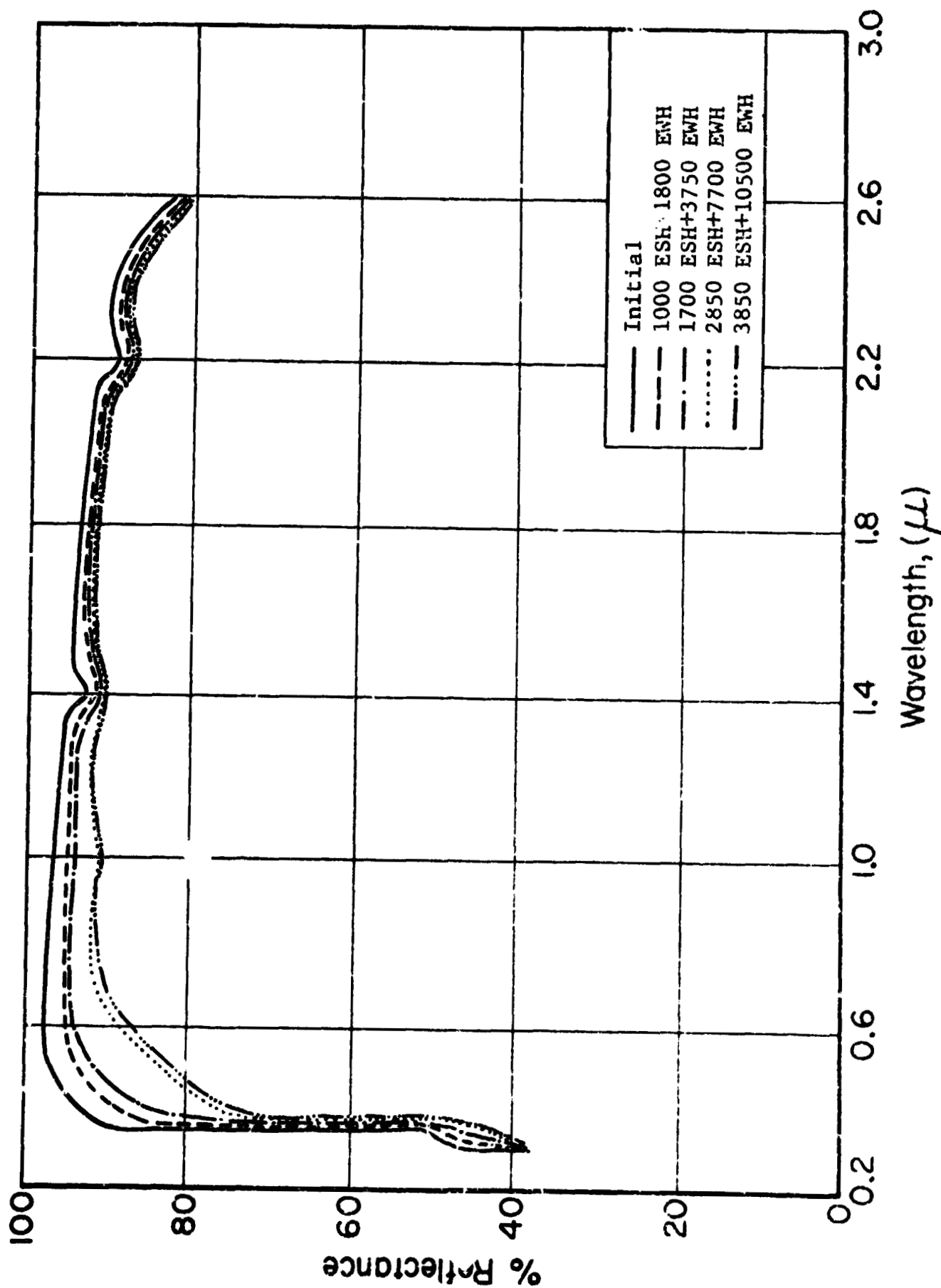


Figure 4.27 SPECTRAL REFLECTANCE OF $Zn_2TiO_4:K_2SiO_3/Li_2SiO_3$

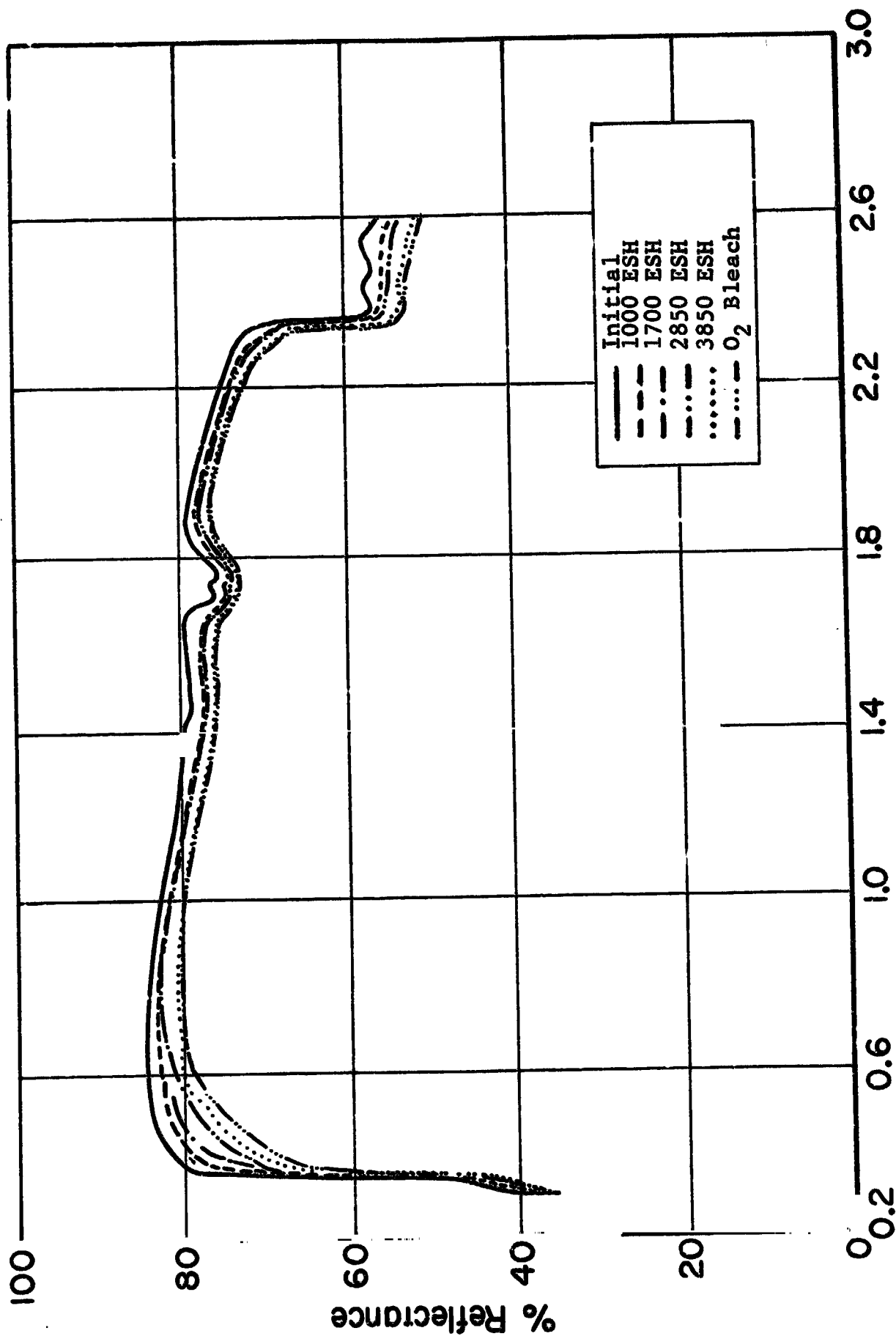


Figure 4.28 SPECTRAL REFLECTANCE OF $\text{Zn}_7\text{TiO}_4:\text{K}_2\text{SiO}_3$ (SRI 17-35)/G

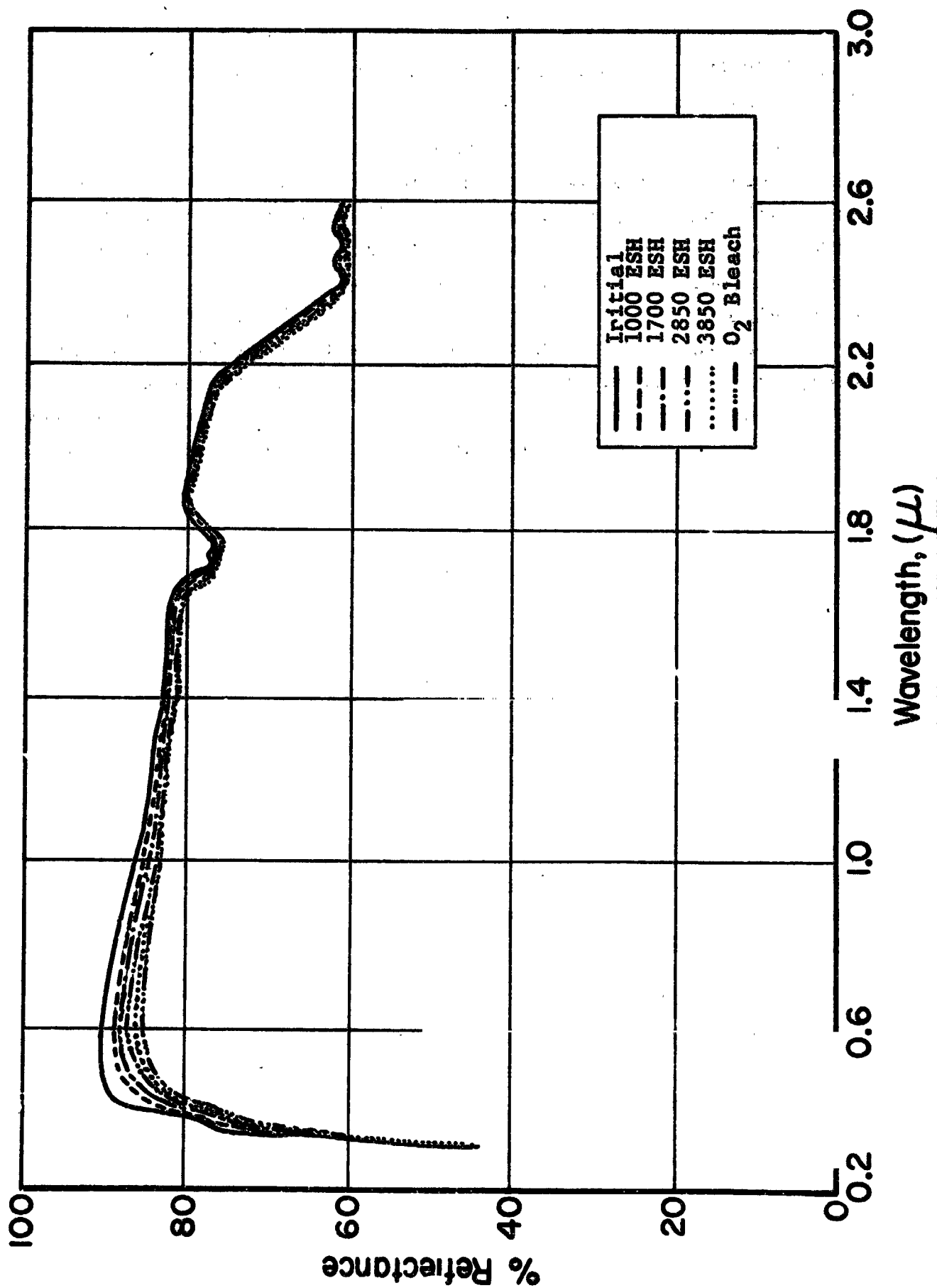


Figure 4.29 SPECTRAL REFLECTANCE OF $\text{Zn}_2\text{TiO}_4:\text{Li}_2\text{SiF}_6$ (Baked at 100°C)/OI-650G

about 3000 ESH; in some cases, no further degradation occurs after an exposure of 2000 ESH.

Encapsulants for zinc orthotitanate pigments are effective only in preventing S-band growth. OI-650 predisposes an otherwise stable pigment, if unencapsulated, to severe optical degradation in the visible and near infrared regions of the spectrum. The mechanism by which an encapsulant affords protection to the pigment is not completely understood. The data, however, support our earlier hypothesis that S-band damage is due to the desorption of hydroxyl groups (as H_2O). Thus, depending on its chemical nature, the encapsulant reacts with, and eventually ties up, the active surface groups, which are in this case principally OH^- groups.

4.4.4 CREF Test No. 8

4.4.4.1 Purpose/Description

This CREF test (ref. 4.5) was conducted to provide relative performance information for three encapsulants of Zn_2TiO_4 pigments - K_2SiF_6 , Li_2SiF_6 and K_2SiO_3 . In the latter case the pigment is washed with NaH_2PO_4 (sodium hydrogen phosphate) to neutralize the pigment surface, potassium silicate-treated and then re-washed (re-neutralized) with NaH_2PO_4 . Determining the effects of heat treatment ($1200^\circ C/5$ min) on encapsulated pigments in terms of α_s and $\Delta\alpha_s$ (stability) was also an objective. All of the materials tested are OI-650 paints incorporating the subject pigments, except sample No. 12, an SP-500 ZnO powder which was included for reference.

4.4.4.2 Sequence

Spectral reflectance measurements were made prior to irradiation, after 400 ESH and $5.5 \times 10^{14} p^+/cm^2$, and, with no further proton irradiation, after an additional 300 ESH, and finally after an O_2 bleach.

4.4.4.3 Test Results

The effects of ultraviolet exposures of nominally 400 ESH (plus $5.5 \times 10^{14} \text{ p}^+/\text{cm}^2$ in the case of samples 1-4), and of an additional 630 ESH can be seen in the reflectance spectra in Figures 20.4-15. The corresponding solar absorptance values are provided in Table 4.6.

4.4.4.4 Analyses

A comparison of the spectra of sample numbers 1 and 2 (Figures 4.30, 31) and of those of sample numbers 4 and 3 (Figures 4.32, 33) reveals that the heat treatment ($1200^\circ\text{C}/5 \text{ min}$), especially in the case of the phosphate-silicate-phosphate surface treatment, not only reduces the initial reflectance of the paint prepared from the treated pigment but predisposes it to considerable S-band damage. Similarly, the heat treatment affects the Li_2SiF_6 -encapsulated pigments (Figures 4.34, 35) in terms of initial properties, but its effect on stability is considerably more complicated.

In Table 4.7 we have compiled the spectral reflectance changes induced by exposure to a nominal 1000 ESH at several wavelengths including the nominal center of the S-band. From degradation (damage) data and the spectral response to oxygen (recovery), some important deductions can be made regarding the effects and effectiveness of encapsulation and of the pigment heat-treatment. Heat treatment in every case increases the S-band damage, but, except in the case of the $(\text{PO}_4/\text{SiO}_3/\text{PO}_4)$ encapsulant, it reduces bulk damage. Comparison of the spectra of paints prepared from heat treated pigments with those of the paints prepared from the respective precursor pigments indicates substantial reflectance losses as a result of particle aggregation.

The relatively greater effects of combined environments were as expected. The spectra of identical samples, one irradiated with UV + p^+ , and one with UV only, suggest that the protons

Table 4-6

CREF-8 ZINC ORTHOTITANATE PAINT* SAMPLES AND TREATMENTS

Sample Number	Encapsulant (Treatment)**	Paint Batch No.	Initial	400 ESH** 5.5(14) p/cm ²	1030 ESH 4.4(14) p/cm ²	O ₂ Bleach
1	: (PO ₄ /SiO ₃ /PC ₄)	C-384	.134	.218	.225	.179
2	: (PO ₄ /SiO ₃ /PO ₄) (heat treated)	C-379	.214	.342	.399	.332
3	: K ₂ SiF ₆ (heat treated)	C-378	.245	.299	.346	.310
4	: K ₂ SiF ₆	C-383	.171	.216	.228	.197
<hr/>						
				400 ESH	1000 ESH	
5	: K ₂ SiF ₆ (heat treated)	C-377	.152	.189	.194	--
6	: (PO ₄ /SiO ₃ /PO ₄)	C-384	.154	.170	.191	.157
7	: (PO ₄ /SiO ₃ /PO ₄) (heat treated)	C-379	.242	.357	.393	.325
8	: K ₂ SiF ₆ (heat treated)	C-378	.244	.324	.332	.284
9	: K ₂ SiF ₆	C-383	.143	.203	.225	.184
10	: Li ₂ SiF ₆	C-382	.143	.162	.202	--
11	: Li ₂ SiF ₆ (heat treated)	C-377	.175	.240	.256	--
12	Heat treated SP500 ZnO powder	--	.169	.178	.198	--

*All Zn₂TiO₄ is from Batch No. C-316, except in Sample No. 5 which came from IITRI Batch No. B-492.

**All samples, except #12, are OI-650 paints.

***Only samples 1-4 received 5.5×10^{14} p (1.2 keV)/cm².

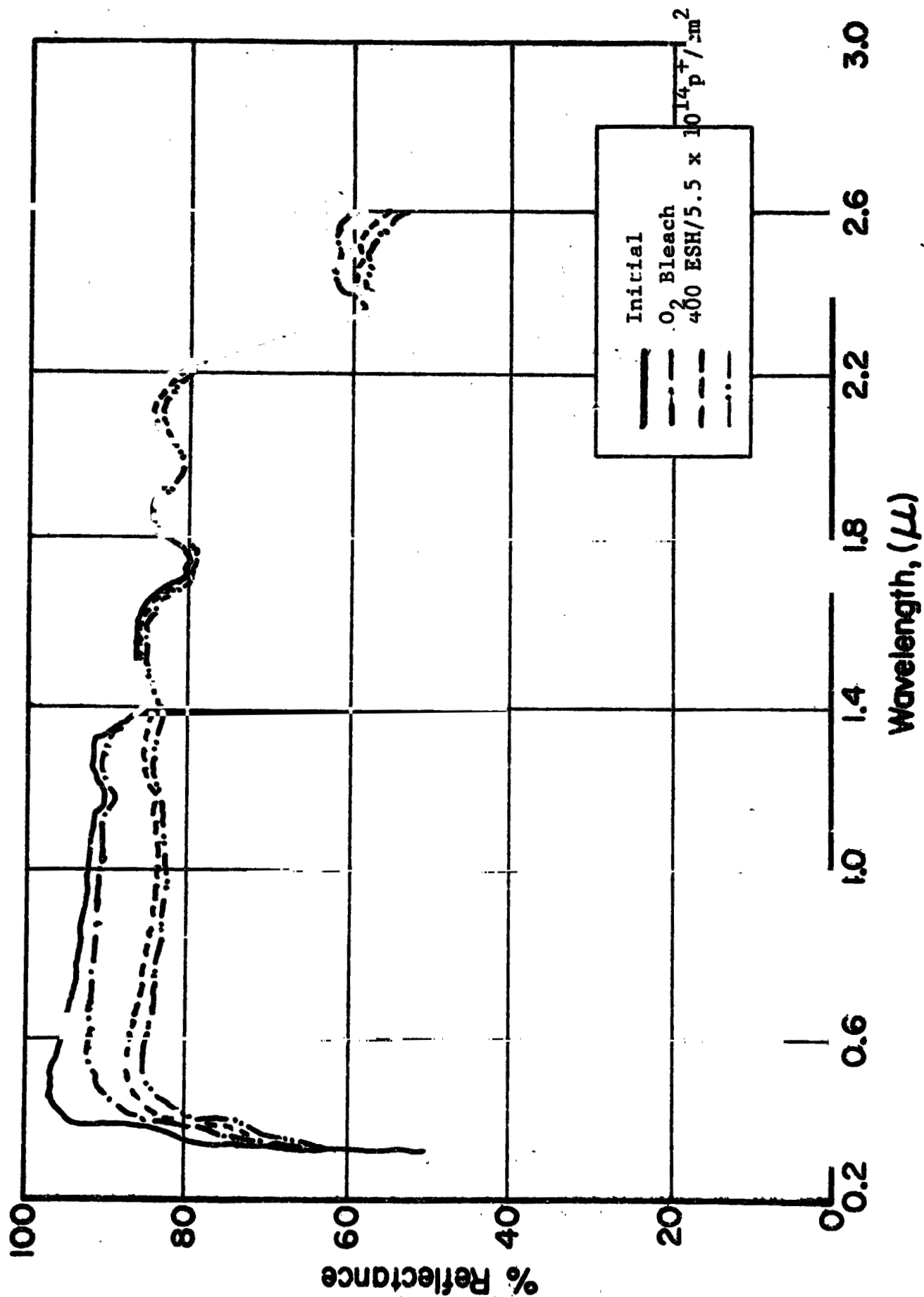


Figure 4.30 SPECTRAL REFLECTANCE OF $Zn_2TiO_4: (PO_4/SiO_3/PO_4)/OI$

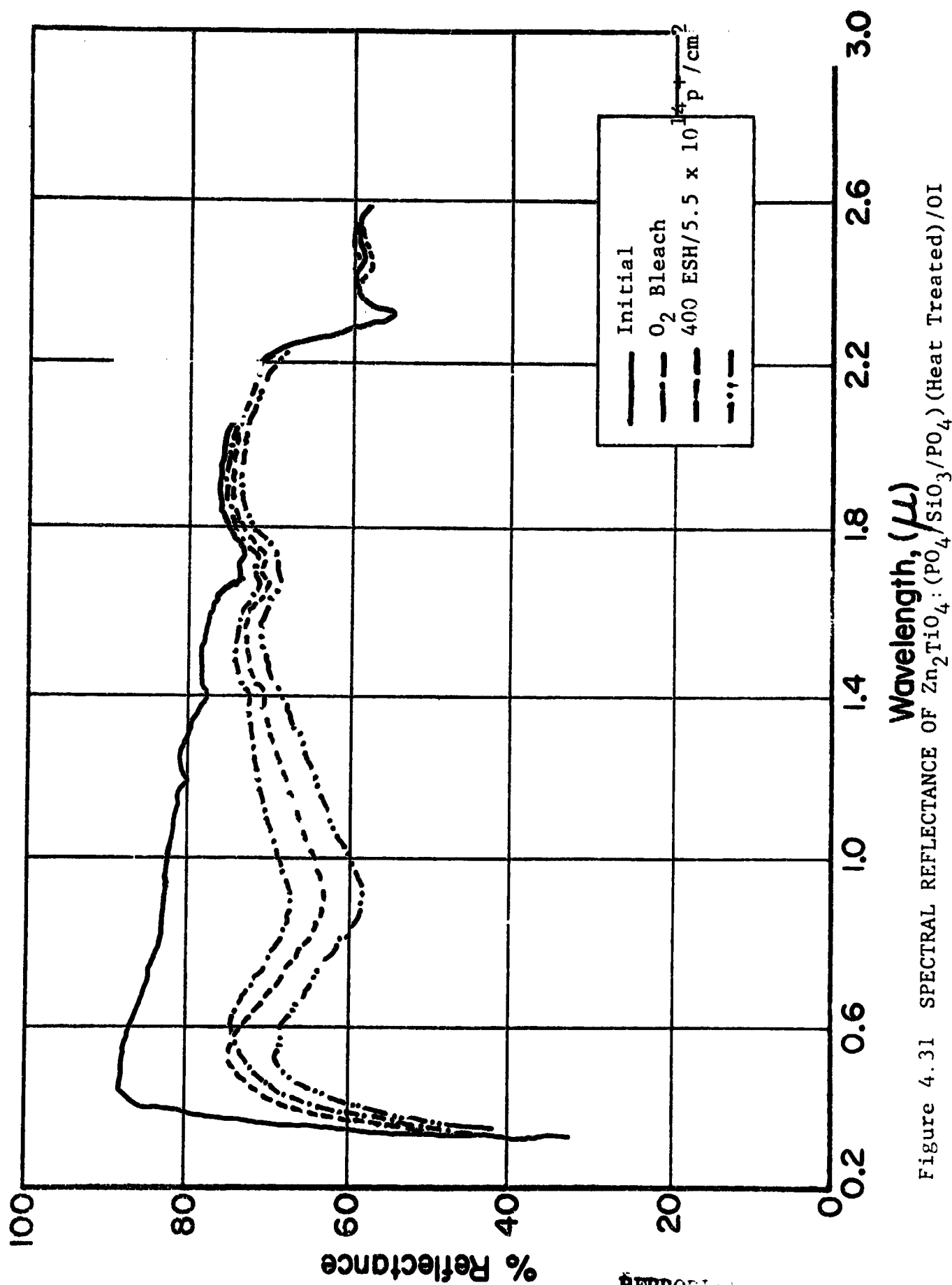


Figure 4.31 SPECTRAL REFLECTANCE OF $\text{Zn}_2\text{TiO}_4:(\text{PO}_4/\text{SiO}_3/\text{PO}_4)$ (Heat Treated)/OI

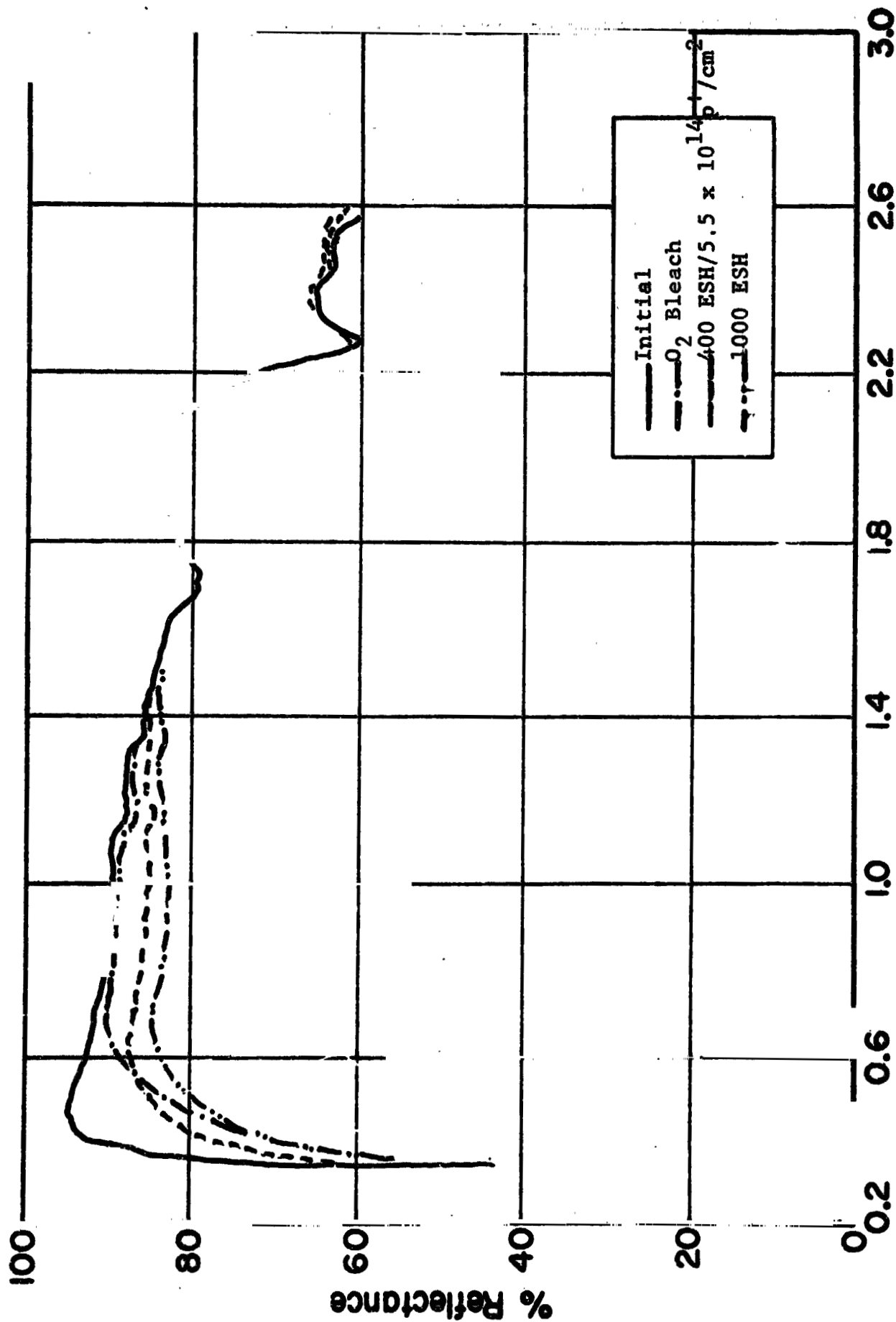


Figure 4.32 SPECTRAL REFLECTANCE OF $\text{Zn}_2\text{TiO}_4:\text{K}_2\text{SiF}_6/\text{OI}$

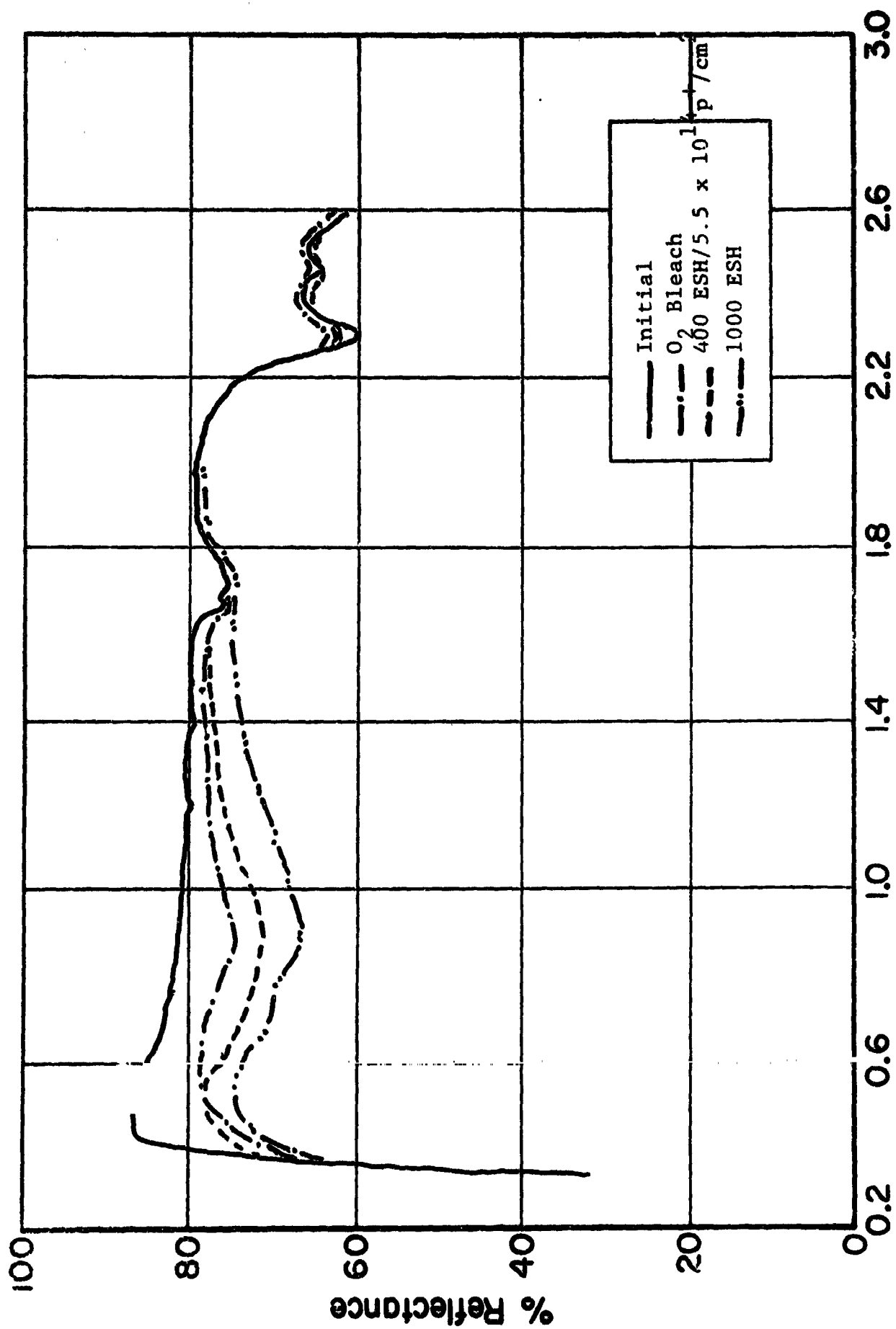


Figure 4.33 SPECTRAL REFLECTANCE OF $Zn_2TiO_4:K_2SiF_6$ (Heat Treated)/OI

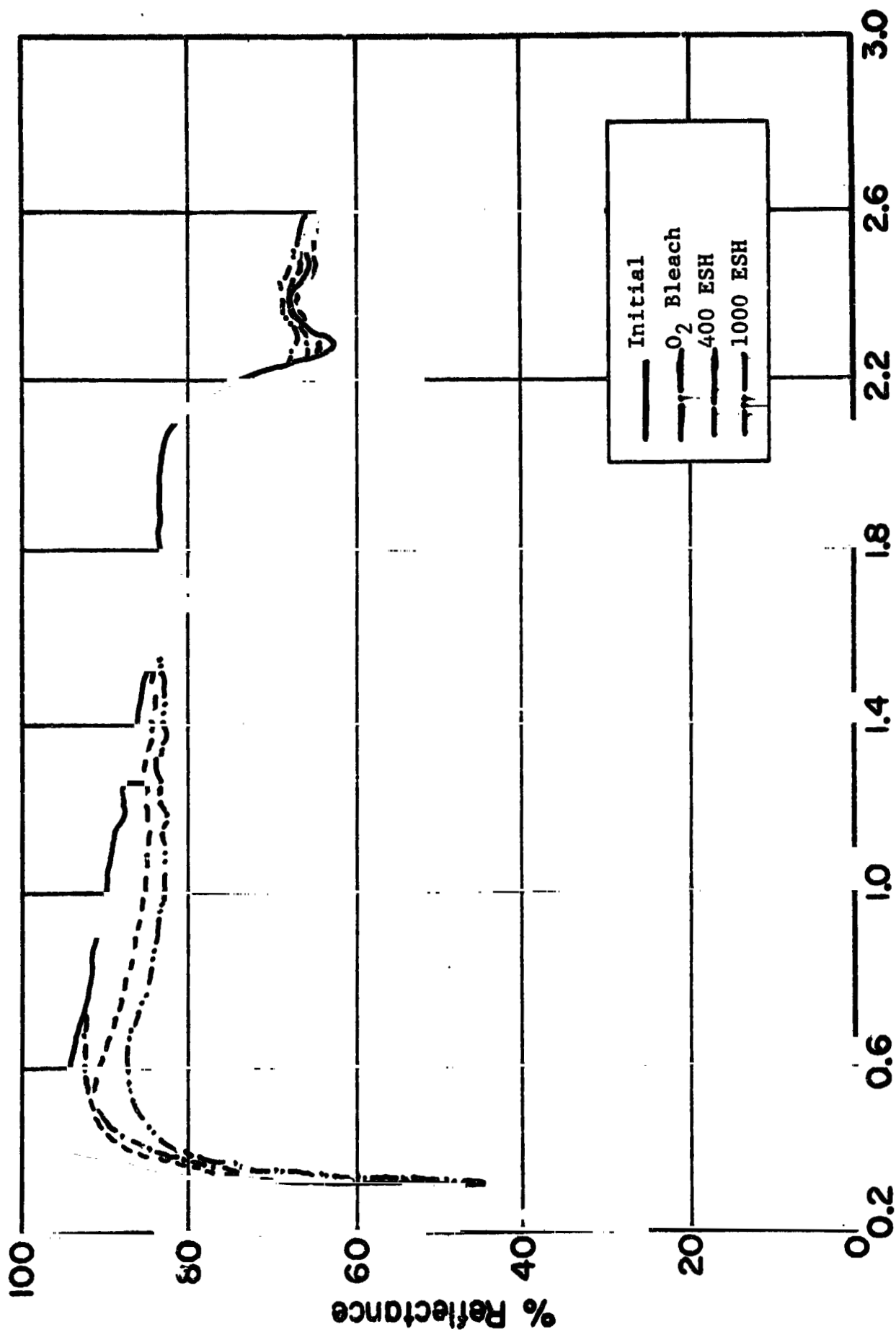


Figure 4.34 SPECTRAL REFLECTANCE OF $\text{Zn}_2\text{TiO}_4:\text{K}_2\text{SiF}_6/\text{OI}$

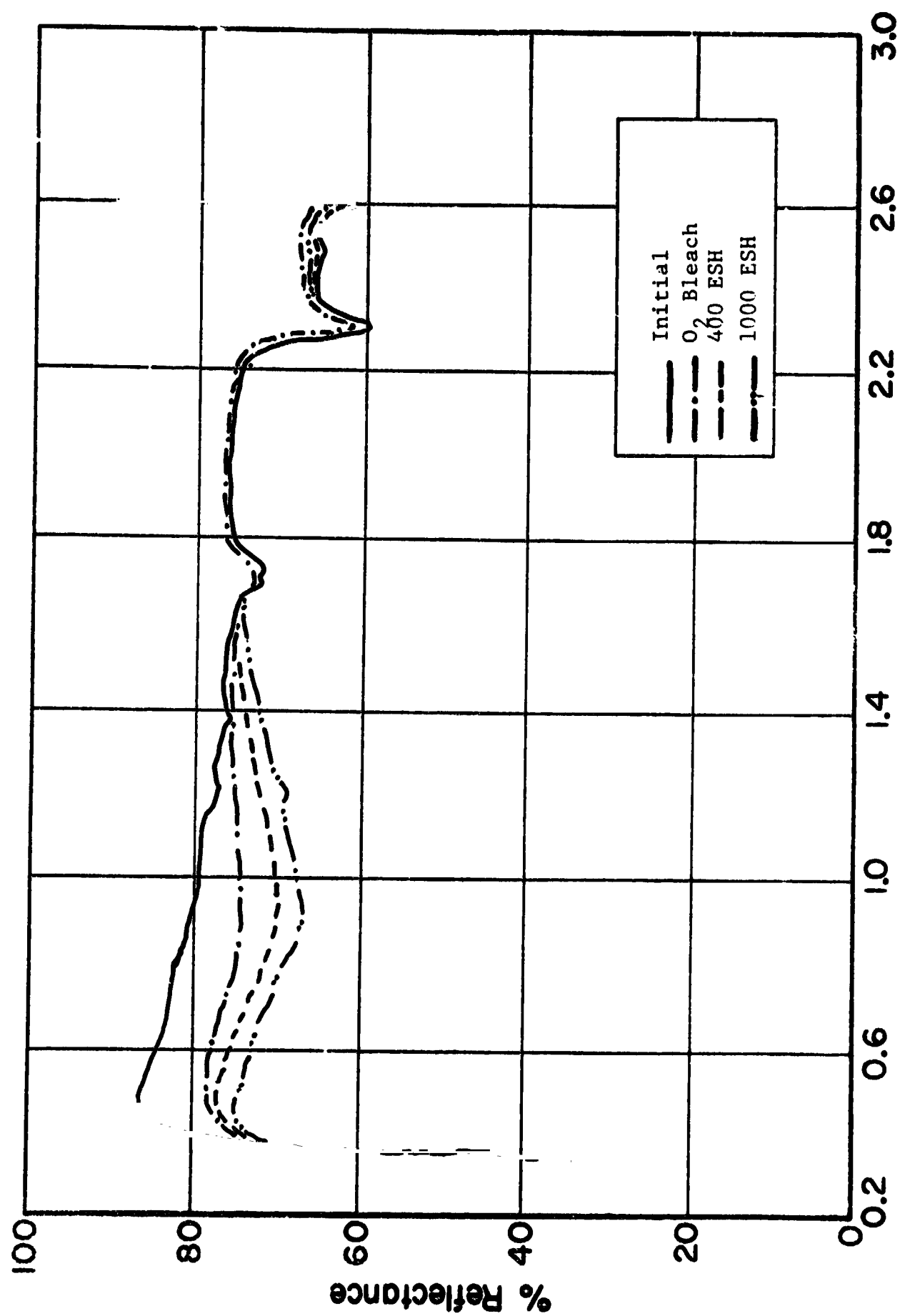


Figure 4.35 SPECTRAL REFLECTANCE OF $\text{Zn}_2\text{TiO}_4:\text{K}_2\text{SiF}_6$ (Heat Treated)/OI

Table 4-7

RADIATION INDUCED REFLECTANCE CHANGES AT SELECTED WAVELENGTHS IN
ENCAPSULATED ZINC ORTHOTITANATE PIGMENTS - CREP-8

Treatment	Sample Number	ΔR (at wavelengths) - p^+ + UV ¹				ΔR (at central wavelengths) UV only ²			
		360nm	410nm	S-Band (900nm) Damage	0 2 Recovery	360nm	410nm	S-Band (900nm) Damage	0 2 Recovery
:PO ₄ /SiO ₃ /PO ₄	1	.13	.15	.11	.09	.02	.04	.05	.05
:PO ₄ /SiO ₃ /PO ₄ -HT*	2	.13	.21	.25	.11	.08**	.15	.24	.09
:K ₂ SiF ₆ -HT	3	.12**	.15	.15	.09	.11	.12	.13	.08
:K ₂ SiF ₆	4	.20	.19**	.07	.06	.16	.15	.08	.06
:K ₂ SiF ₆ -HT	5**	.02**	.04	.01*	---				
:Li ₂ SiF ₆						.12	.12	.07	---
:Li ₂ SiF ₆ -HT						.02	.07	.13	---

*HT = pigment heat treated at 1200° C/5 min.

**Received some p^+ from spillover effect.

1.) Total Exposure: 400 ESH + $5.5 \times 10^{14} p^+/cm^2$ (Samples 1-4 only) + additional 630 ESH.

2.) Total Exposure: 400 ESH + additional 630 ESH.

create substantial bulk damage but have little, if any effect on surface (S-band) damage, as evidenced by the ΔR_λ values at the S-band in comparable samples (e.g., No. 4 vs No. 9).

Finally, it must be noted that these paints sustained relatively severe degradation. From the development pattern of the induced absorption the causes would appear to be intrinsic defects. Surface contamination, however, cannot be ruled out, since heat treating tends to reduce bulk damage in K_2SiF_6 -encapsulated pigments, to increase it in $PO_4/SiO_3/PO_4$ encapsulated pigments, and in all pigments to promote S-band development. From this behavior we can infer that different surface treatments, including contamination, can and do cause large and very different damage effects. In any event, an unusually large amount of spectral degradation has occurred in the paint samples, and is very likely due to intrinsic defects. Although anomalous in magnitude, the degradation spectra are characteristic, thus ruling out contamination in the test system as an explanation. Contamination of the samples during their preparation, however, remains a distinct possibility.

4.4.5 IRIF Test I-55 (Ref. 4.6)

4.4.5.1 Purpose/Description

The successful development of a Zn_2TiO_4 /OI-650 paint-system depends in part upon the elimination of interactions between its components, which lead to instabilities (mainly in the S-band). This test was conducted to determine properties and performance data of individual components and to compare components prepared in different ways. These components, which were irradiated as paints in CREF Test No. 8 (ref. 4.6), are listed in Table 4.8.

4.4.5.2 Test Results

The reflectance spectra of the basic and the treated pigments are presented in Figures 4.36-39 which are spectra of (SS) B-229 type Zn_2TiO_4 powders. Figures 4.40,41 are typical OI-650

Table 4-8

SAMPLE DESCRIPTIONS
IRIF TEST No. I-55

Sample (Position) Number	Sample Description
1	Zn_2TiO_4 , untreated, (COP method) - $900^\circ\text{C}/8 \text{ hr}$
2	OI-650 glass resin, standard, air dried
3	OI 650G (Batch C-400), air dried
4	OI-650G (Lot 34-2), air dried
5	Zn_2TiO_4 , untreated, Batch C-316 (B-229 method)
6	$\text{Zn}_2\text{TiO}_4:(\text{PO}_4/\text{SiO}_3/\text{PO}_4)^*$ - heat treated $1200^\circ\text{C}/5 \text{ min.}$
7	$\text{Zn}_2\text{TiO}_4:\text{Li}_2\text{SiF}_6^*$ - heat treated $1200^\circ\text{C}/5 \text{ min.}$
8	OI-650G, cured $150^\circ\text{C}/1 \text{ hr}$
9	OI-650G, cured overnight at 80°C
10	OI-650, cured overnight at 80°C
11	$\text{Zn}_2\text{TiO}_4:\text{K}_2\text{SiF}_6^*$ - heat treated $1200^\circ\text{C}/5 \text{ min.}$
12	Blank

* Zn_2TiO_4 , from batch C-316.

and OI-650G spectra, respectively. Generally, all of the B-229 type Zn_2TiO_4 pigments appear to be quite stable, sustaining only a fraction of the damage occurring in their OI-650 paints.

For the basic (unencapsulated and un-heat treated) Zn_2TiO_4 pigment, there appears (from Fig. 4.36) to be only a slight development of bulk damage and a perceptible decrease in S-band reflectance. The phosphate/silicate/phosphate pigment (heat-treated at $1200^\circ\text{C}/5$ min) whose spectra are shown in Figure 4.37, indicates definite developments of bulk damage and the S-band. Very much like those of the basic powder, the spectra of the pigment $\text{Zn}_2\text{TiO}_4 \cdot \text{K}_2\text{SiF}_6$ ($1200^\circ\text{C}/5$ min) in Fig. 4.38 exhibit no induced UV absorption but still a definite bulk damage as well as S-band development. The lithium silicofluoride encapsulated pigment (also heat-treated at $1200^\circ\text{C}/5$ min) in Figure 4.39 displays similar stability.

The spectra in Figures 4.40 and 4.41 are the reflectance spectra of thin films of standard and modified Owens-Illinois 650 "Class Resin", respectively, applied to aluminum IRIF coupons. Thus, the important feature to notice is the very low UV-induced absorption, (as indicated by a loss in UV reflectance). All of these films are exceptionally transparent and stable, especially those that have been heat cured.

4.4.5.3 Conclusions

The magnitude of optical damage in OI-650G is very small, and at least as inherently stable as the standard product; and this stability is increased by heat curing.

The performance of the zinc orthotitanate pigments in this test demonstrates that they all are basically stable. Their performance in CREF Test No. 8, where they were tested in the form of silicone paints, however, emphatically points up a deleterious interaction between the pigment and the vehicle. The nature of this interaction appears to have an effect on the pigments' bulk

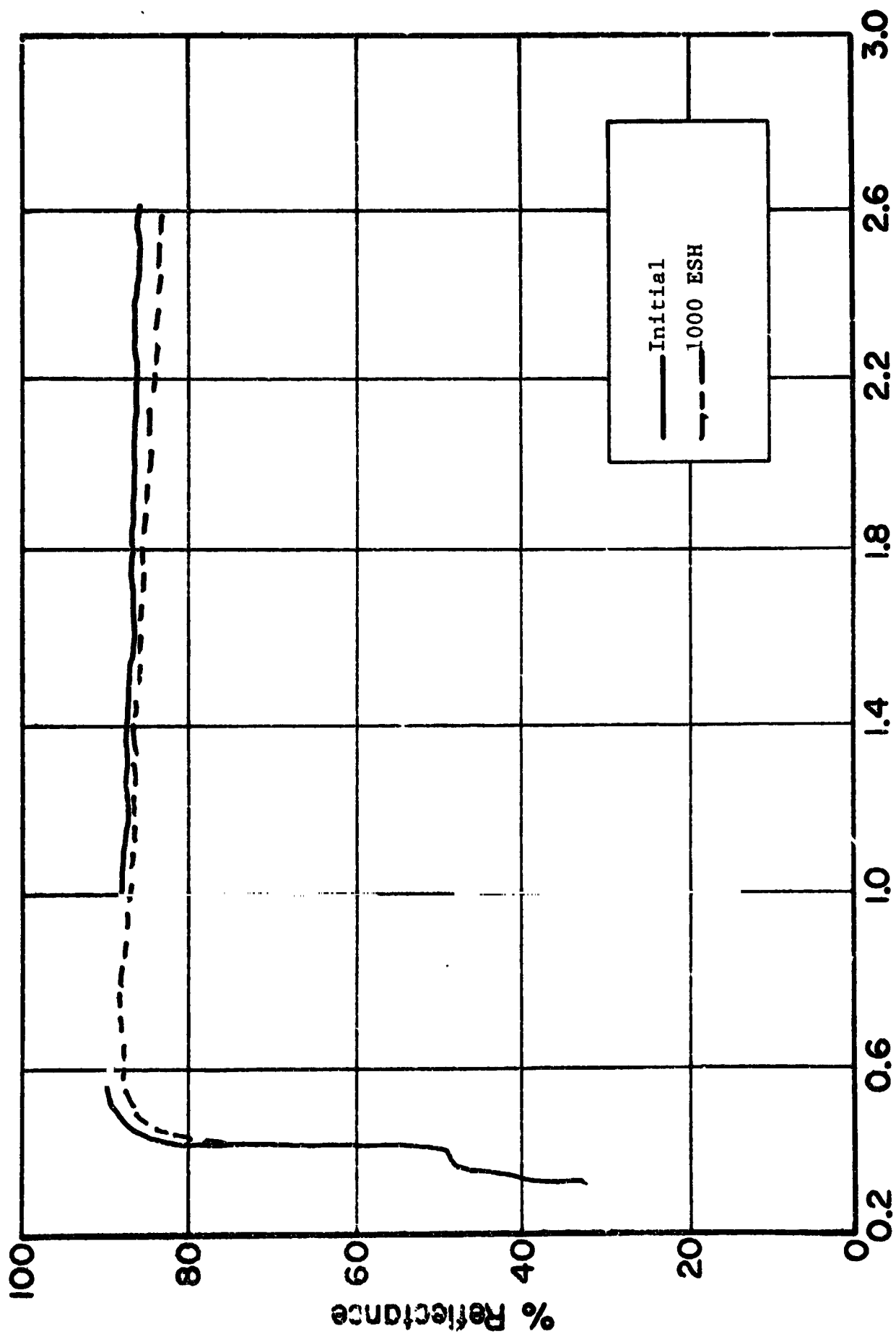


Figure 4.36 SPECTRAL REFLECTANCE OF Zn_2TiO_4 (Untreated B-229 METHOD)

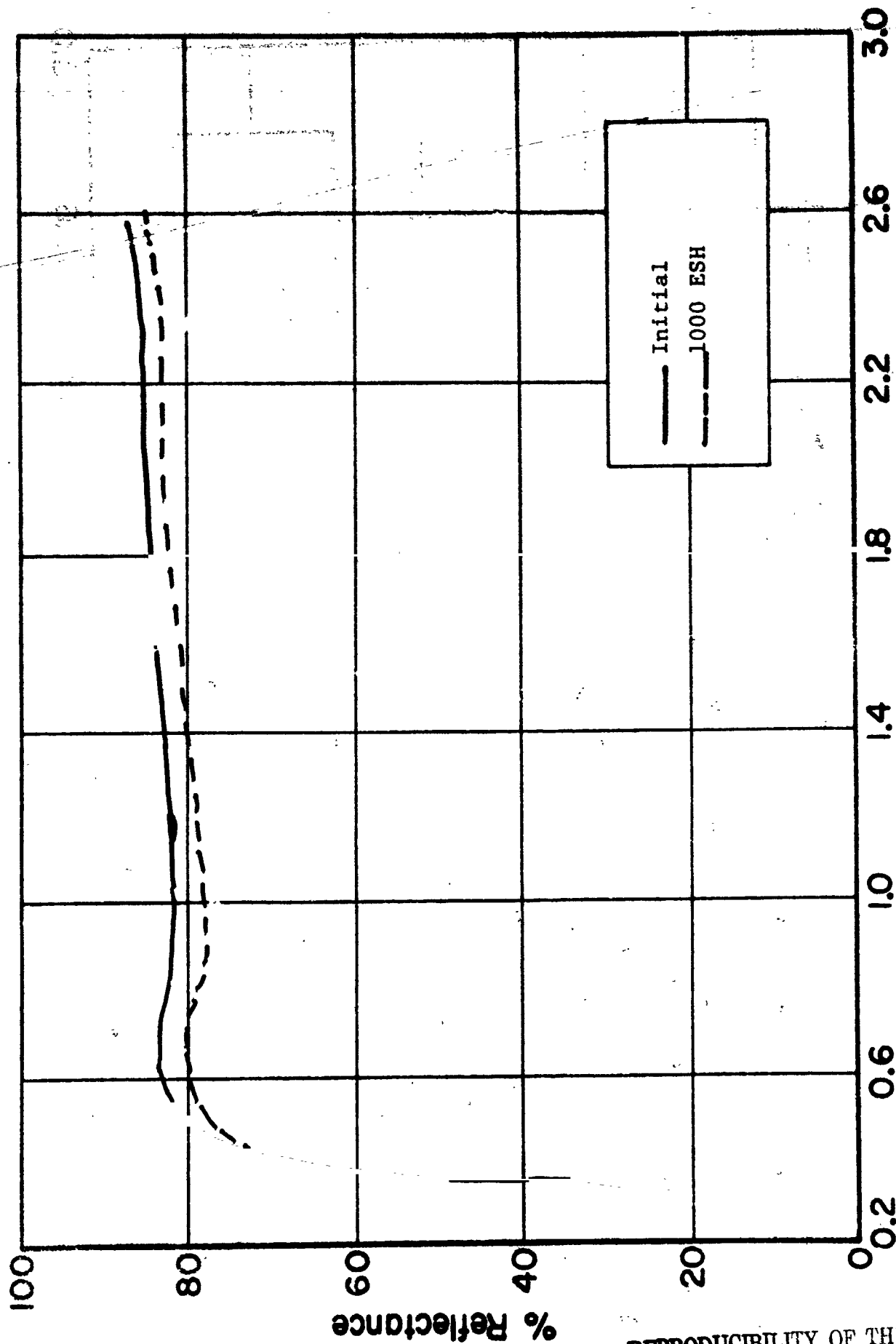


Figure 4.37 SPECTRAL REFLECTANCE OF $\text{Zn}_2\text{TiO}_4:(\text{PO}_4/\text{SiO}_3/\text{PO}_4)$ (Heat Treated)

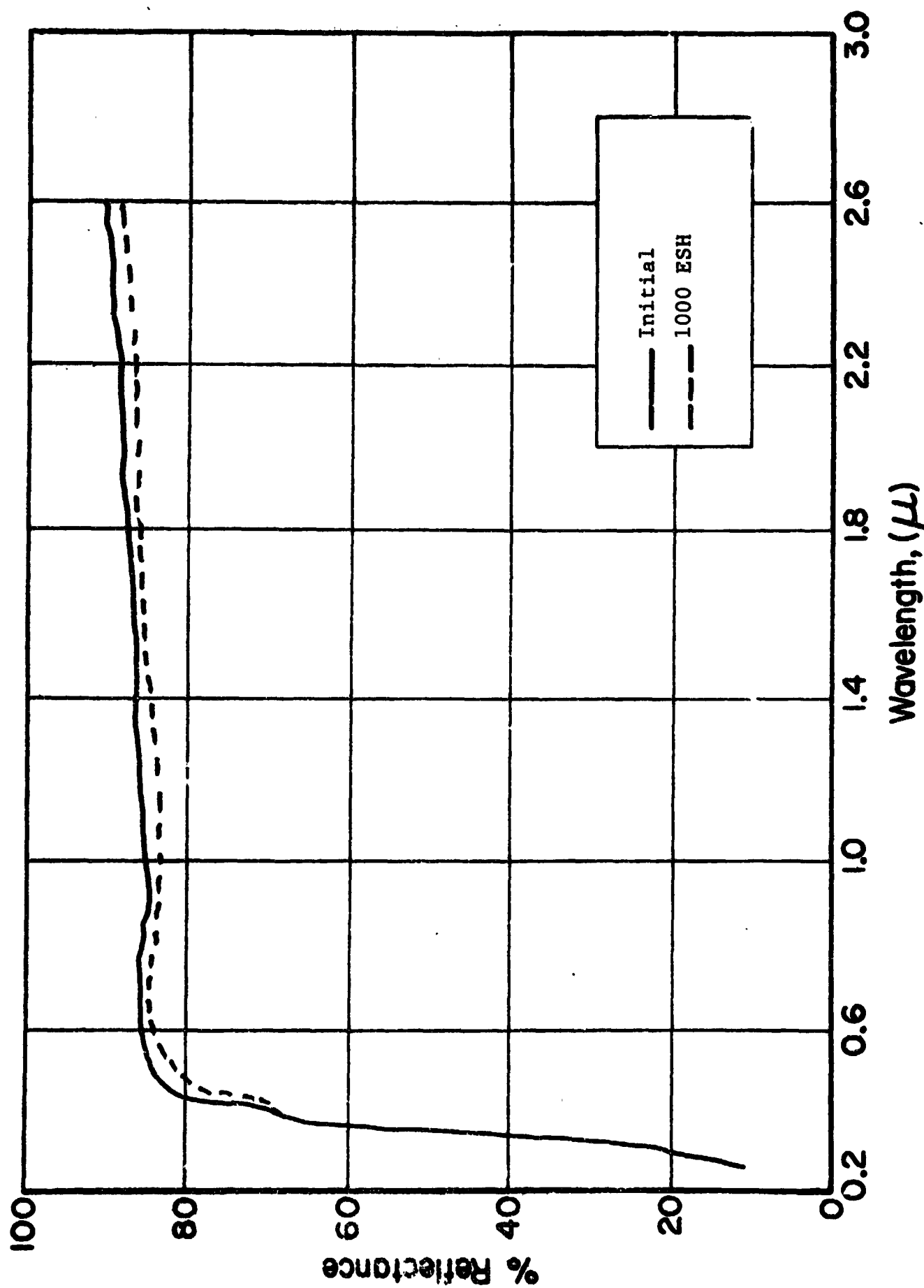


Figure 4.38 SPECTRAL REFLECTANCE OF $\text{Zn}_2\text{TiO}_4:\text{K}_2\text{SiF}_6$ (Heat Treated)

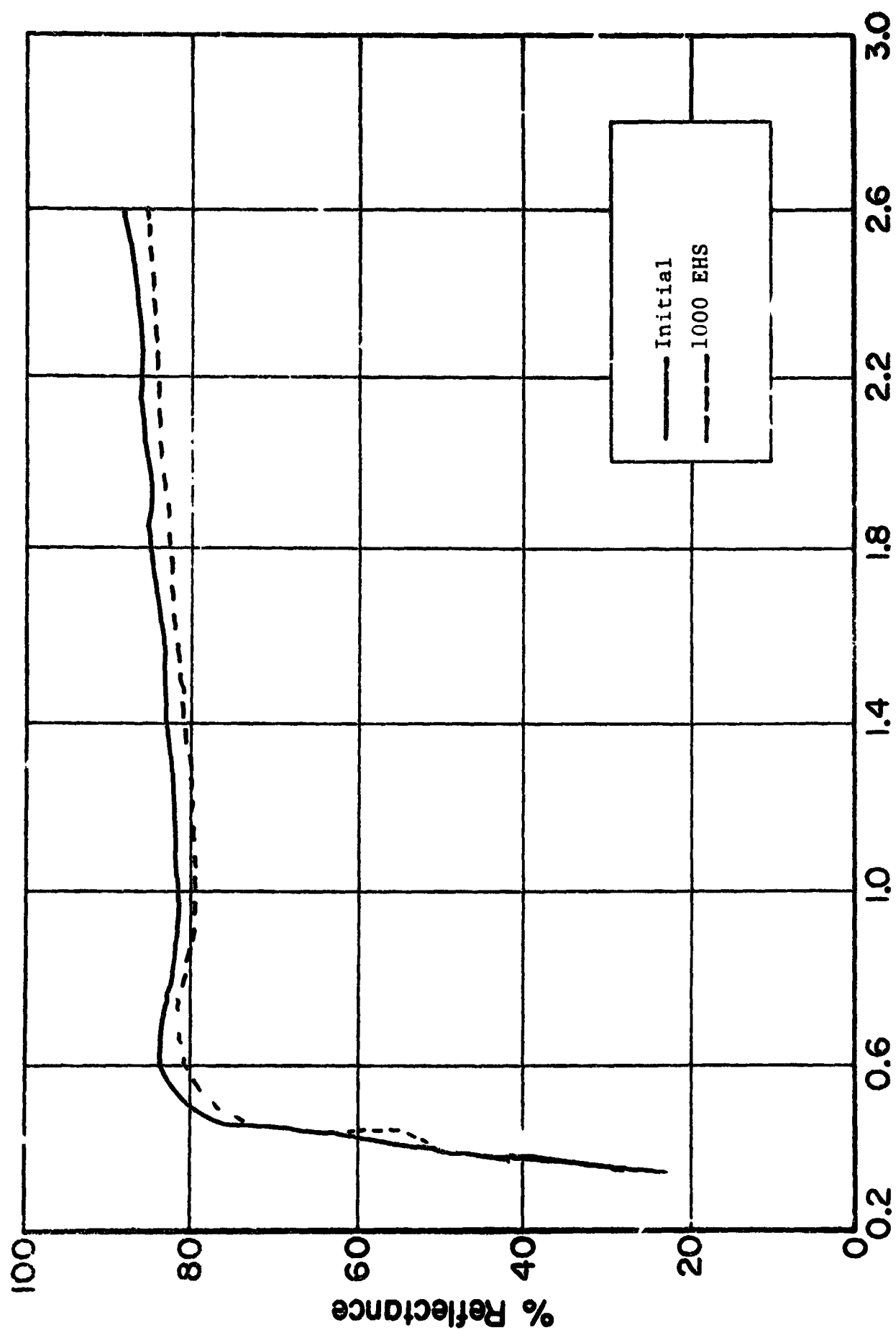


Figure 4.39 SPECTRAL REFLECTANCE OF $\text{Zn}_2\text{TiO}_4:\text{Li}_2\text{SiF}_6$ (Heat Treated)

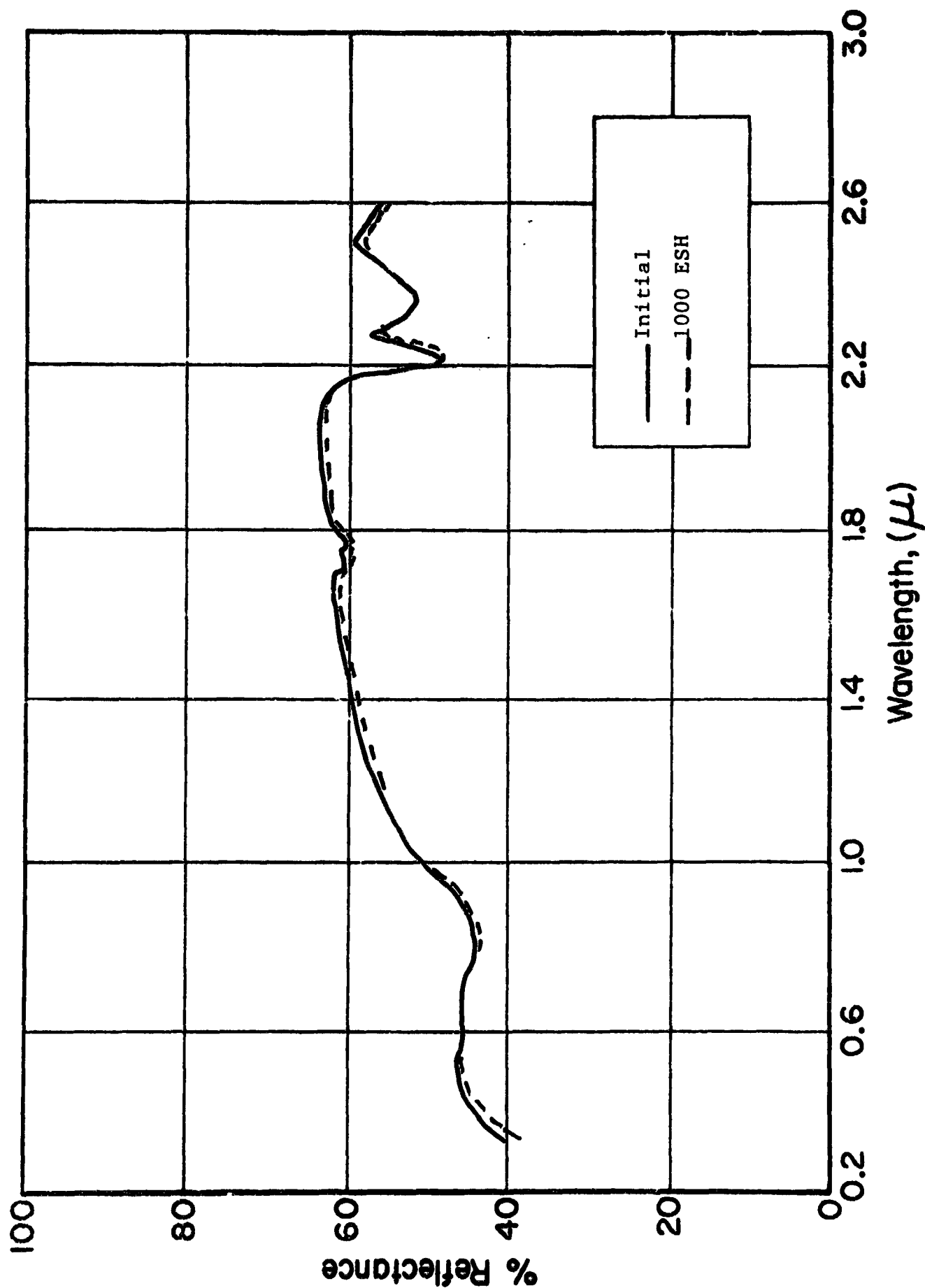


Figure 4.40 SPECTRAL REFLECTANCE OF OI-650 (STANDARD), AIR DRIED

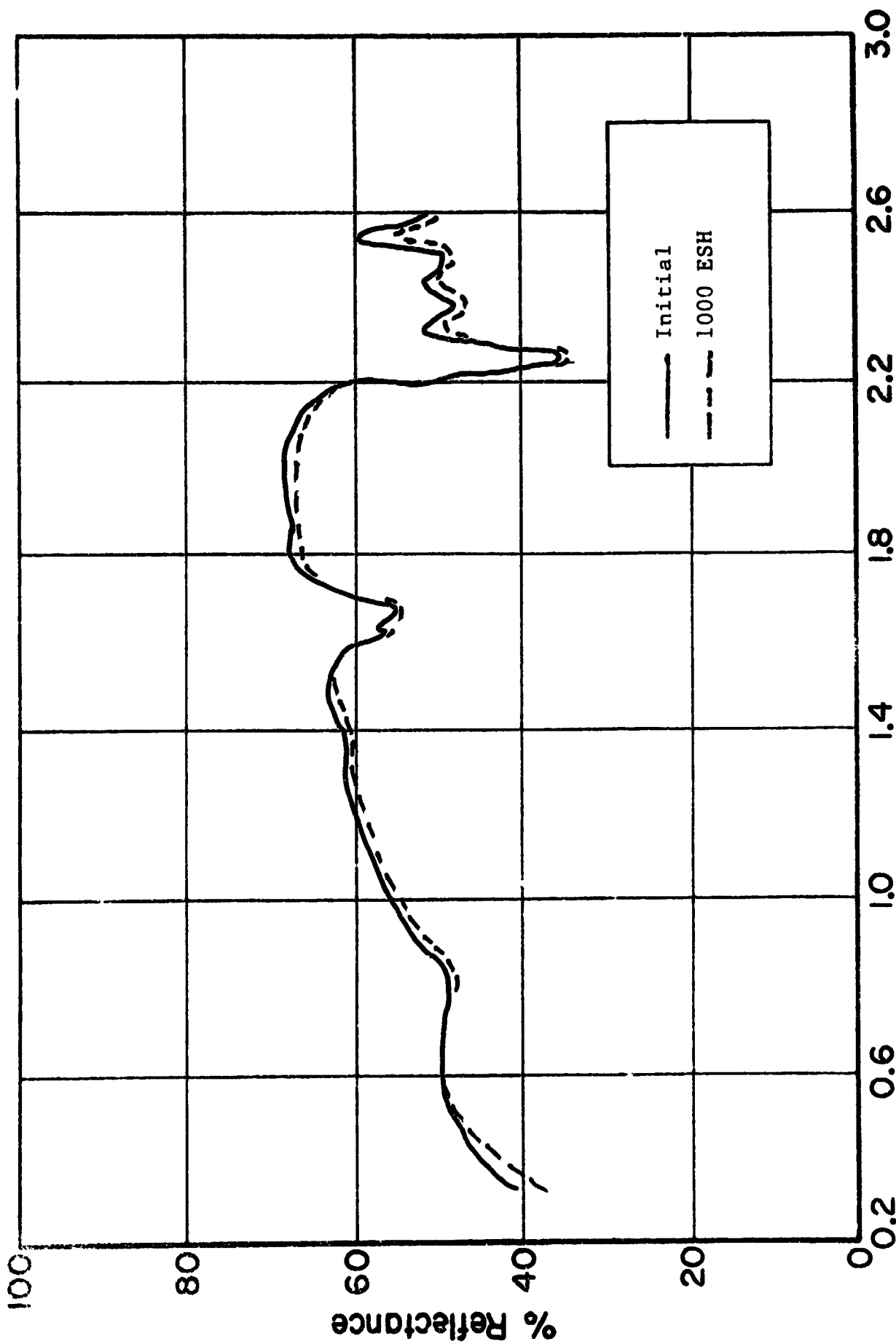


Figure 4.41 SPECTRAL REFLECTANCE OF OI-650G (BATCH C-400); AIR DRIED

Table 4-8a
ENVIRONMENTALLY INDUCED REFLECTANCE CHANGES AT PEAK DAMAGE WAVELENGTHS
IN ENCAPSULATED ZINC ORTHOTITANATE PIGMENTS - CREP-8

Treatment	Sample Number	ΔR (at central wavelengths)-p ⁺ + UV ^T					ΔR (at central wavelengths)-UV Only ^T				
		360 nm T ₁ *	410 nm T ₂ *	900 nm S*	Recovery O ₂ ΔR	% Z	360 nm T ₁	410 nm T ₂	900 nm S	Recovery O ₂ ΔR	% Z
:PO ₄ /SiO ₂ /PO ₄	1	.13	.15	.11	.09	82	.02	.04	.05	.05	100
:PO ₄ /SiO ₂ /PO ₄ - Heat Treated ⁴	2	.13	.21	.25	.11	44	.08**	.15	.24	.09	37
:K ₂ SiF ₆ -Heat Treated ⁶	3	.12**	.15	.15	.09	60	.11	.12	.13	.08	61
:K ₂ SiF ₆ -Heat Treated ⁶	4	.20*	.19**	.07	.06	86	.16	.15	.07	.06	86
:K ₂ SiF ₆ -Heat Treated ⁶	5***	.02***	.04	.01*	---	--	---	---	---	---	---
:Li ₂ SiF ₆											
:Li ₂ SiF ₆ - Heat Treated											
	10						.12	.12	.07	---	--
	11						.02	.07	.13	---	--

^T Total Exposure: 1032 ESH; 5.5×10^{14} p⁺/cm² (Samples 1-4 only)

*T₁ designates band centered at 360 nm; T₂, 410 nm; and S, bleachable "belly" absorption band.

**Actual peak not discernible.

***Received some p⁺ from spillover effect.

properties as well as on its surface properties. The fact that bulk damage occurs in irradiated pigment powders and not in clear resin films establishes the fact that the resin-pigment interaction affects the pigment and not the resin.

The K_2SiF_6 and Li_2SiF_6 encapsulants both protect and pigment better than does the $PO_4/SiO_3/PO_4$ treatment.

4.4.6 CREF Test No. 9 (Ref. 4.6)

4.4.6.1 Purpose/Description

In this test, the performance of zinc orthotitanate pigment, prepared in a scrupulously iron-free process, both untreated and with K_2SiF_6 and K_2SiO_3 encapsulants, is of paramount interest. An analysis of the results of CREF Test No. 8 (Ref. 4.5) and of the processes involved in preparing the pigments used in that test leads us to suspect that a significant amount of iron contamination may have been introduced into the pigments. Accordingly, one purpose of this test is to determine whether iron (or any other metal) contaminant may be responsible for the anomalous degradation of Zn_2TiO_4 pigments observed in CREF Test No. 8. Another important objective is to extend our knowledge of the properties and performance of encapsulated pigments in longer duration tests.

4.4.6.2 Results

The Zn_2TiO_4 pigments, in this test have been prepared in accordance with the standard high temperature solid-solid reaction but without any metallic contact. They do not contain iron in quantities measurable by colorimetric analytical methods. The samples are listed in Table 4.9 and their reflectance spectra are presented in Figures 4.42-53. Note the consistently low values of α_s . Figure 4.42 illustrates the excellent stability of A-429M, the designation for the paint system $ZnO:K_2SiO_3$ (which is S-13G pigment)/OI-650G. Figures 4-43 through 4.53 pertain to iron-free zinc orthotitanate. In Figure 4.43 are the spectra for the basic (iron-free) pigment (untreated and

Table 4-9

CREF TEST No. 9 - SOLAR ABSORPTANCE VALUES VS ULTRAVIOLET EXPOSURE (ESH)

<u>Pigment</u>	<u>Treatment/Remarks</u>	<u>Binder</u>	<u>Initial</u>	<u>575</u>	<u>2010</u>	<u>3035</u>	<u>4070</u>	<u>O₂ Bleach</u>
SP500 ZnO	PS7	G*	0.175	0.178	0.184	0.189	0.195	0.195
Zn ₂ TiO ₄ **	---	---	0.114	0.139	0.144	0.148	0.174	0.152
Zn ₂ TiO ₄	---	PS7	0.164	0.177	0.166	0.176	0.195	0.187
Zn ₂ TiO ₄	---	OI	0.171	0.196	0.197	0.205	0.207	0.295
Zn ₂ TiO ₄	K ₂ SiF ₆	---	0.158	0.173	0.186	0.199	0.198	0.190
Zn ₂ TiO ₄	K ₂ SiF ₆	OI	0.216	0.255	0.297	0.307	0.310	0.262
Zn ₂ TiO ₄	K ₂ SiF ₆	G	0.253	0.279	0.283	0.287	0.297	0.285
Zn ₂ TiO ₄	PO ₄ /SiO ₃ /PO ₄	---	0.150	0.155	0.169	0.184	0.190	0.188
Zn ₂ TiO ₄	PO ₄ /SiO ₄ /PO ₄	OI	0.147	0.175	0.194	0.203	0.215	0.165
Zn ₂ TiO ₄	LH-14(9/B)	---	0.142	0.216	0.213	0.265	.270	0.171
Zn ₂ TiO ₄	LH-12(12/1)	---	0.278	---	---	---	---	---
Zn ₂ TiO ₄	LH-12(9/8)	---	0.174	0.207	0.245	---	---	---

*Silicated ZnO pigment (S-13G pigment) and OI-650G resin, paint is designated A-429M

**With the exception of those designated LH-12 or LH-14, all of the Zn₂TiO₄ pigments used in this test were prepared from the basic iron-free pigment as IITRI-Batch C-405.

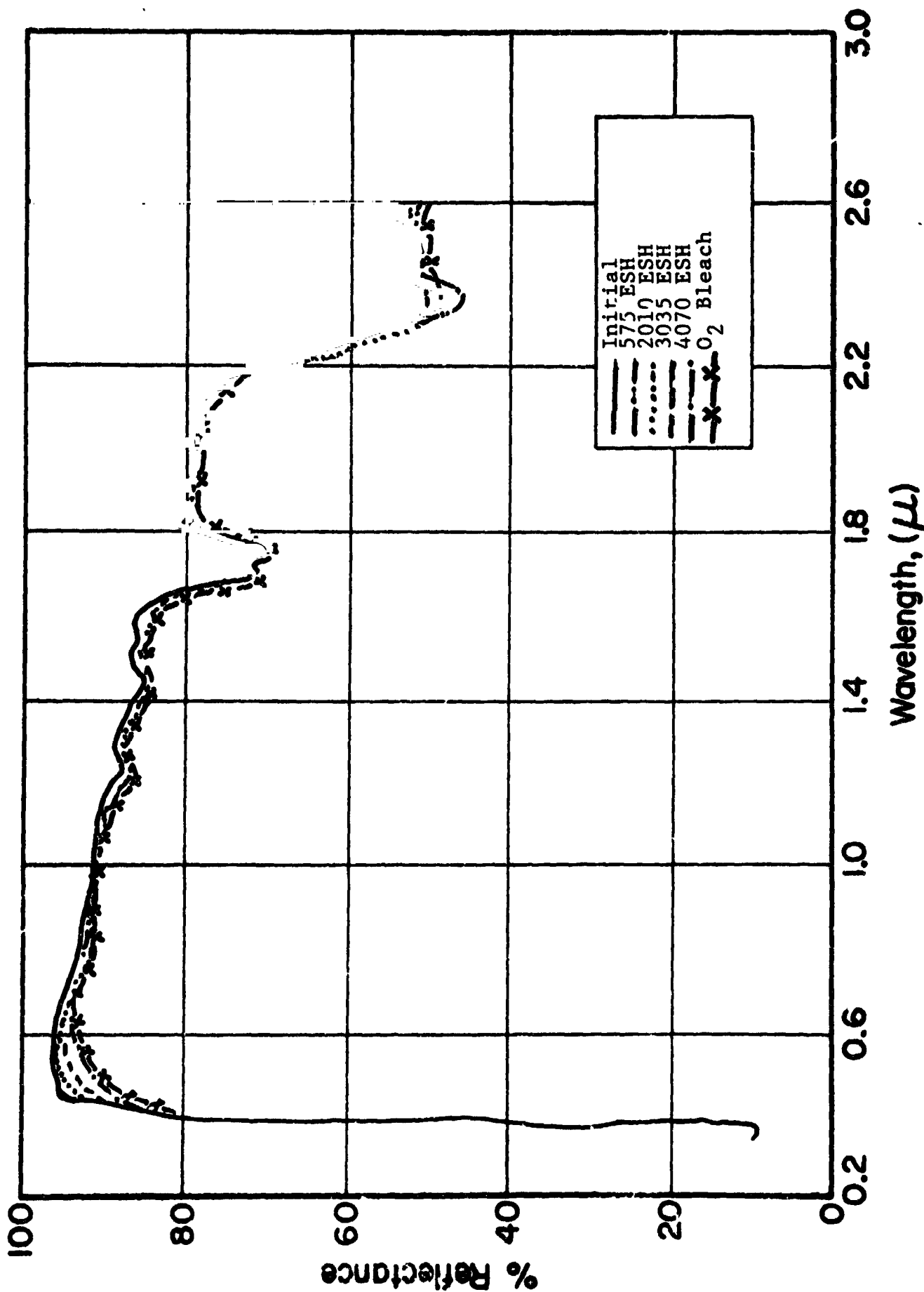


Figure 4.42 REFLECTANCE SPECTRA OF A429M

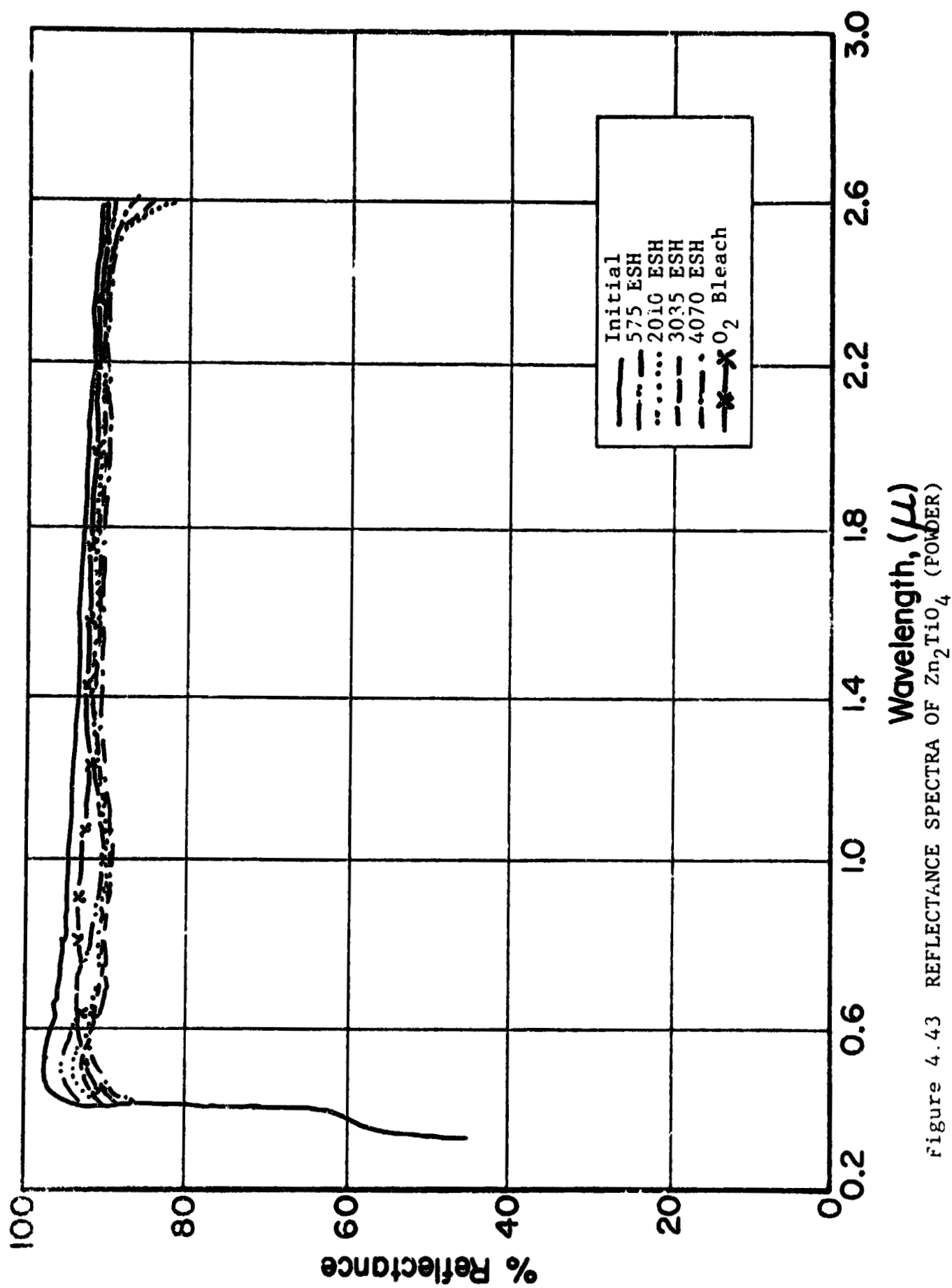


Figure 4.43 REFLECTANCE SPECTRA OF Zn_2TiO_4 (POWDER)

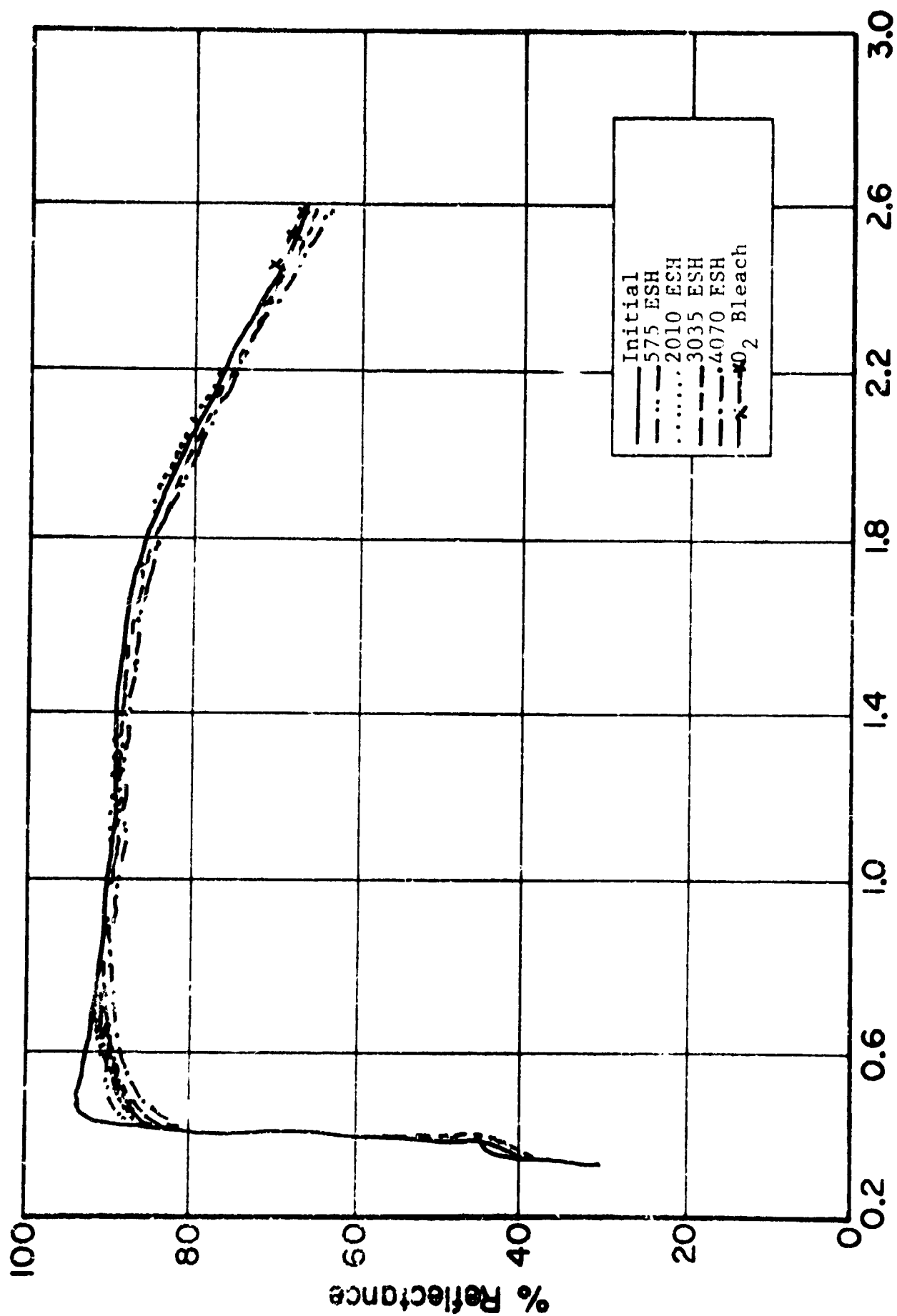


Figure 4.44 REFLECTANCE SPECTRA OF Zn₂TiO₄/PS-7

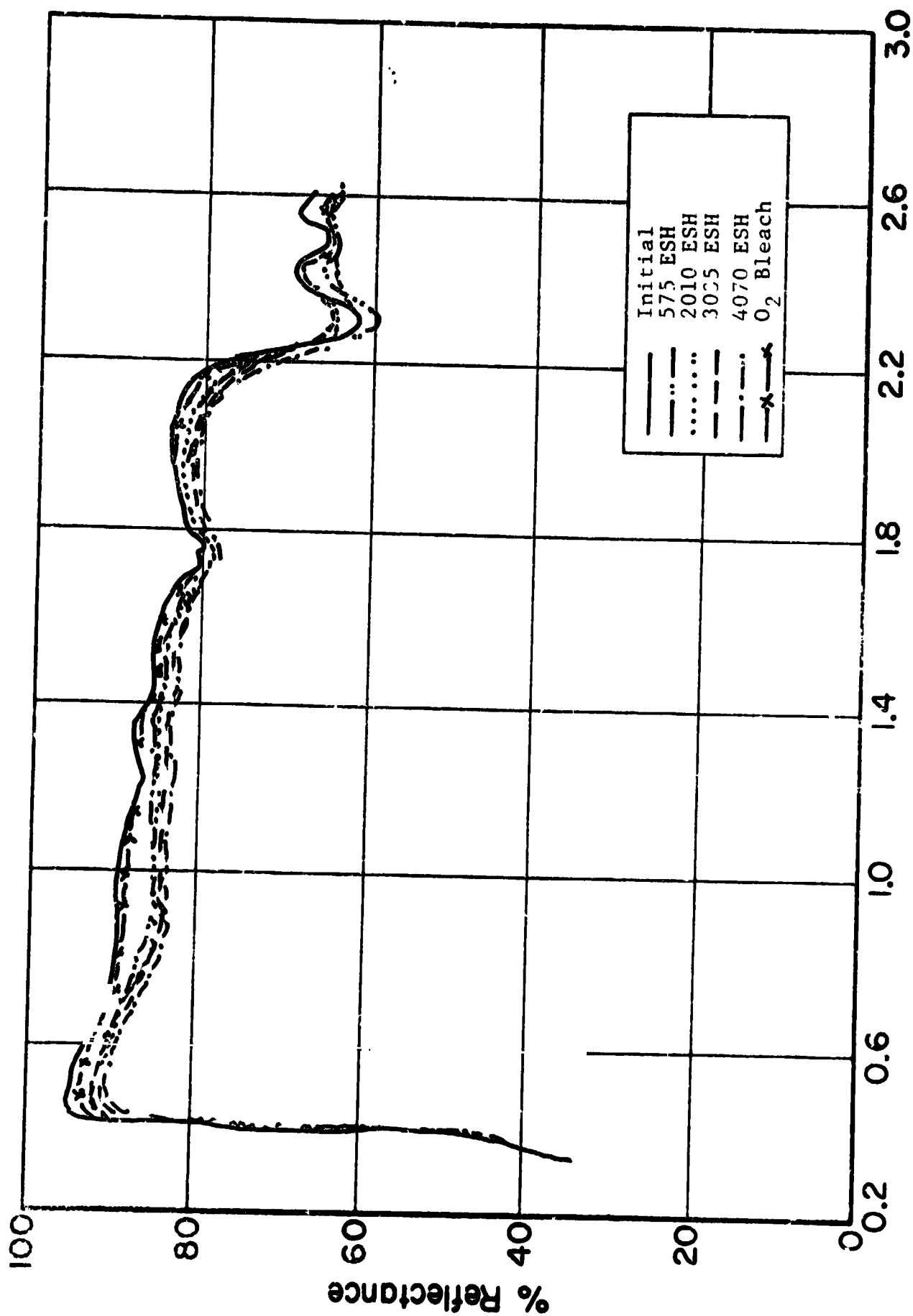
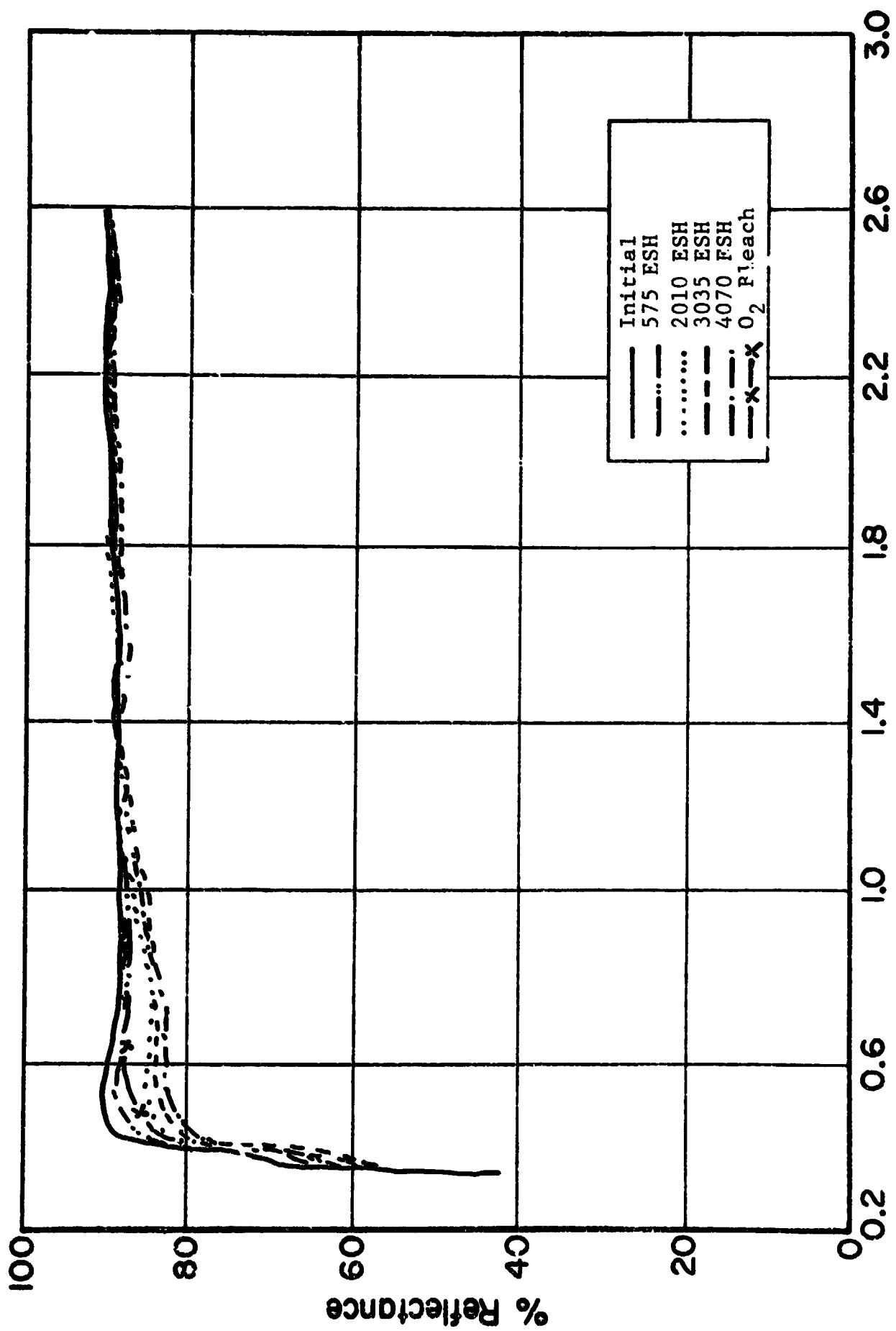


Figure 4.45 REFLECTANCE SPECTRA OF Zn_2TiO_4/OI



Wavelength, (μ)

Figure 4.46 REFLECTANCE SPECTRA OF $\text{Zn}_2\text{TiO}_4:\text{K}_2\text{SiF}_6$ (POWDER)

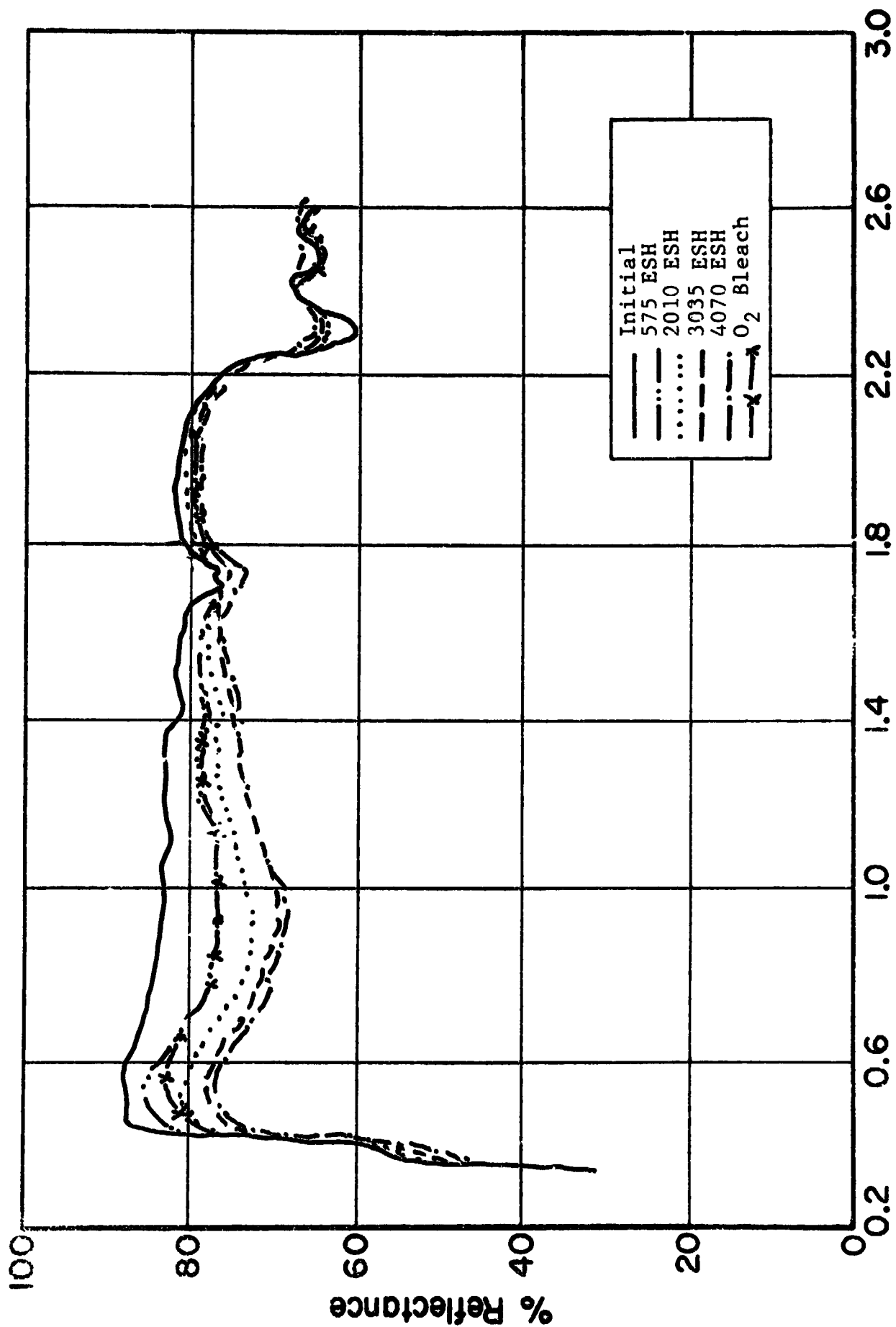


Figure 4.47 REFLECTANCE SPECTRA OF $\text{Zn}_2\text{TiO}_4:\text{K}_2\text{SiF}_6/\text{OI}$

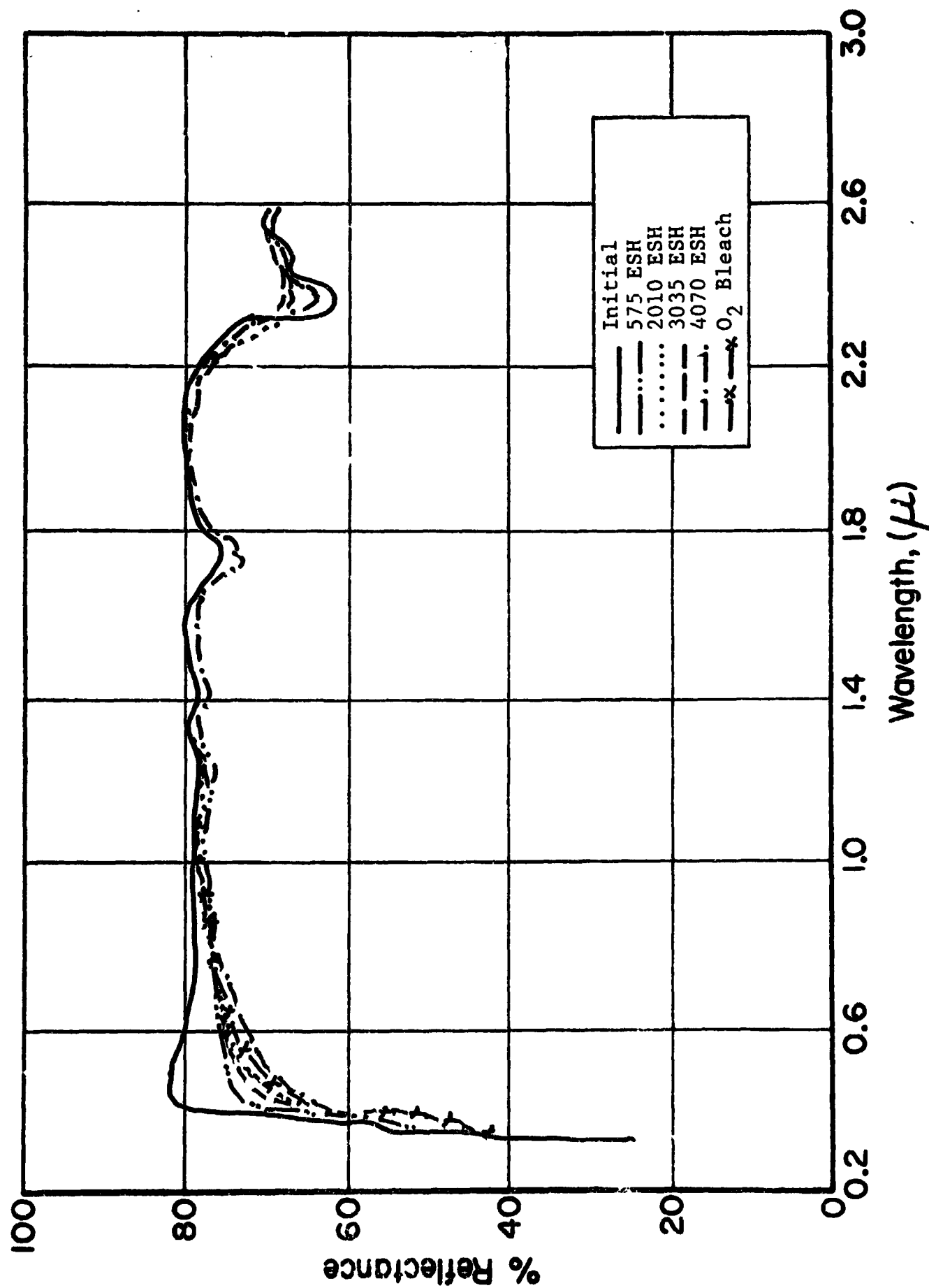


Figure 4.48 REFLECTANCE SPECTRA OF ZnO·TiO₂:K₂SiF₆/OT

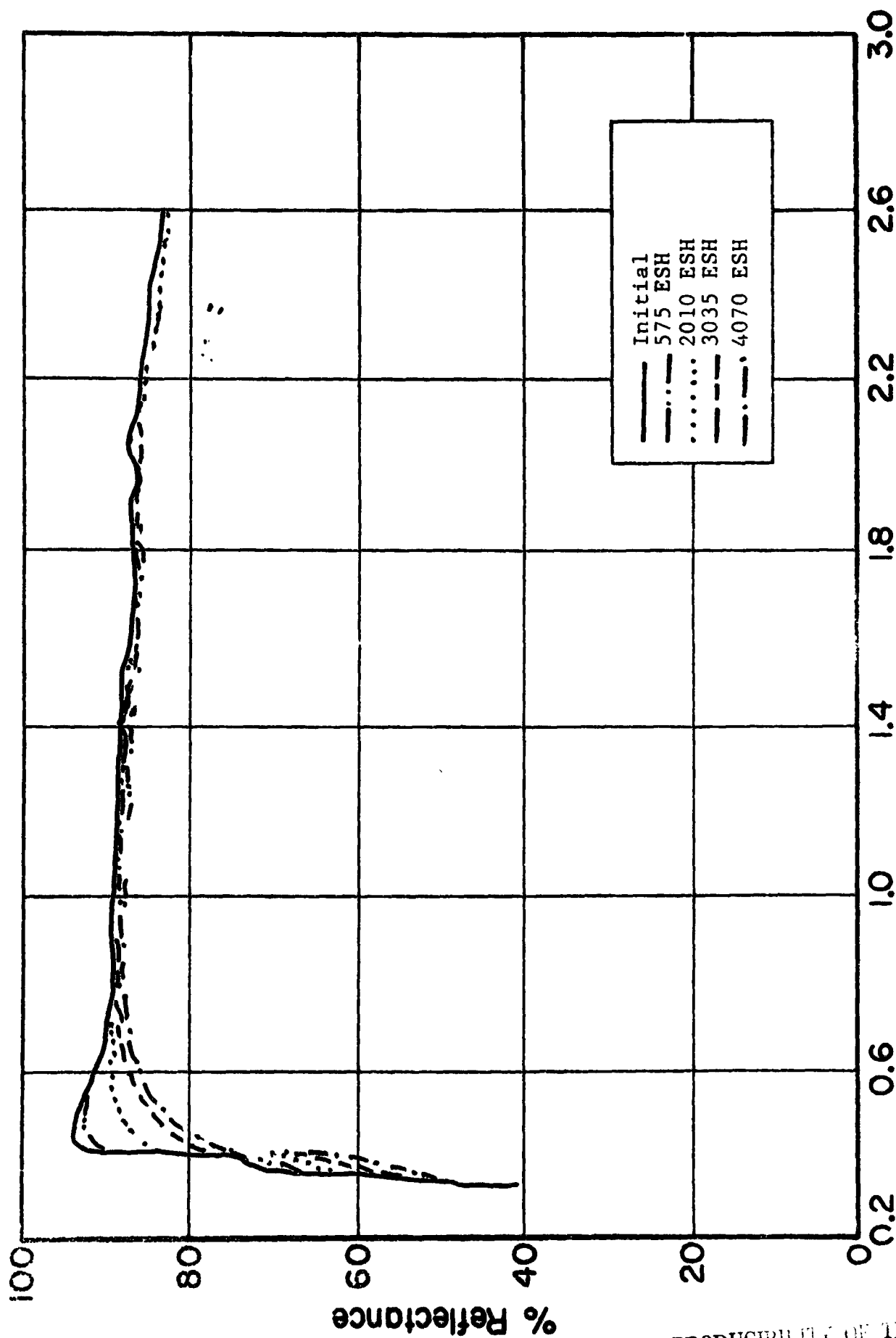


Figure 4.49 REFLECTANCE SPECTRA OF $\text{Zn}_2\text{TiO}_4:(\text{PO}_4^{=}/\text{SiO}_3^{=}/\text{PO}_4^{=})$ POWDER

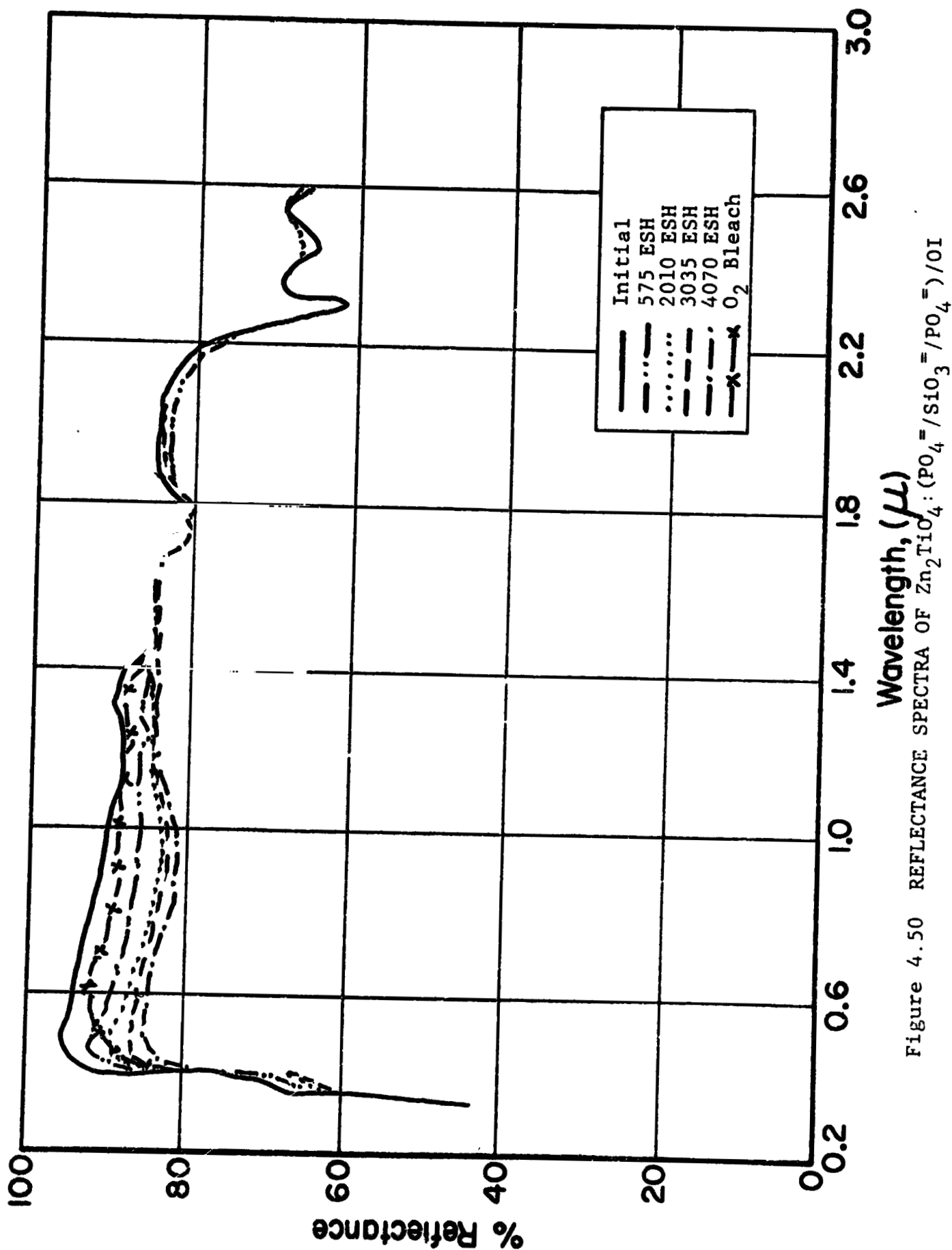


Figure 4.50 REFLECTANCE SPECTRA OF $\text{Zn}_2\text{TiO}_4:(\text{PO}_4^{=}/\text{SiO}_3^{=}/\text{PO}_4^{=})/\text{OI}$

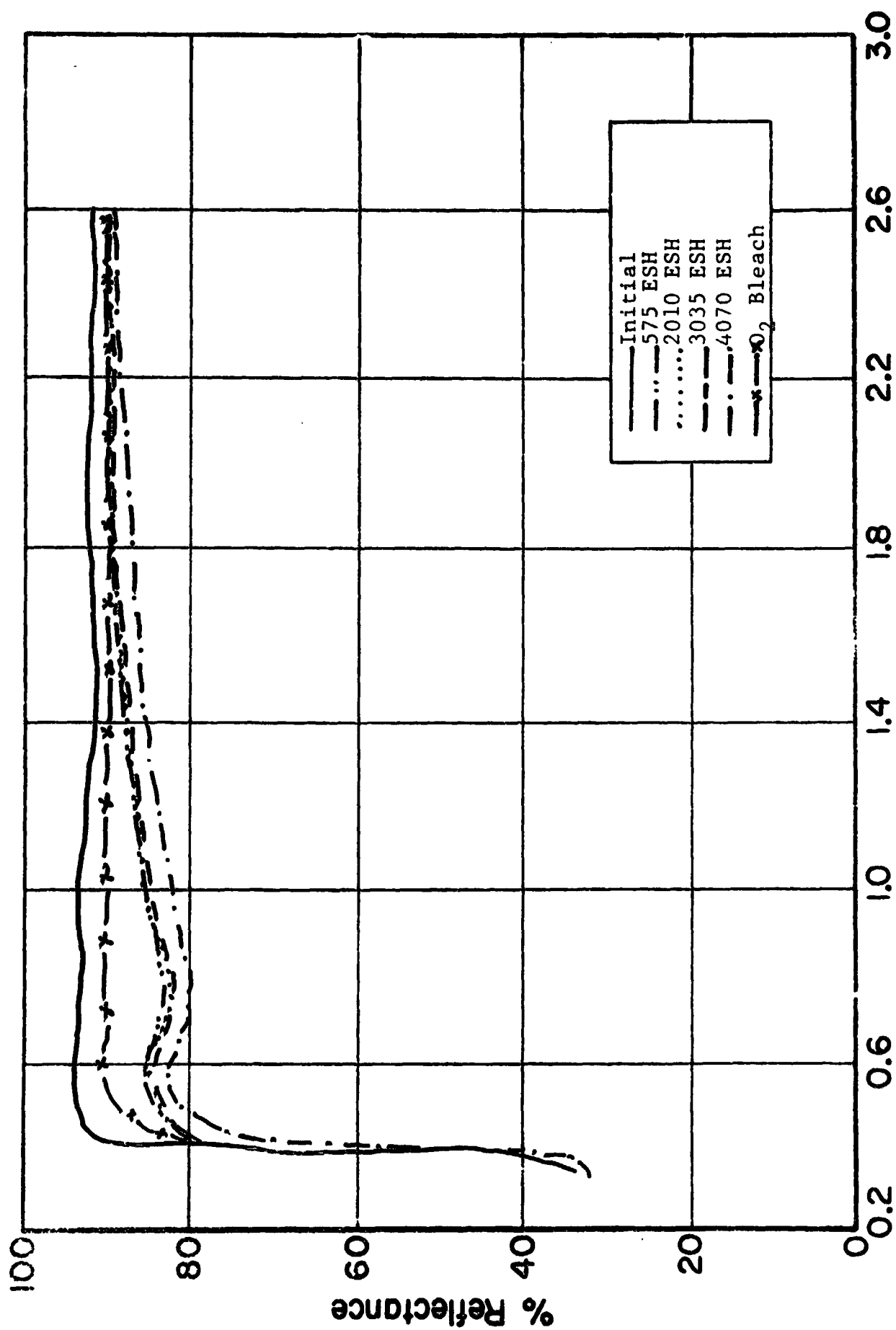


Figure 4.51 REFLECTANCE SPECTRA OF LH-14, Zn₂TiO₄ (900°C/8 hr) (POWDER)

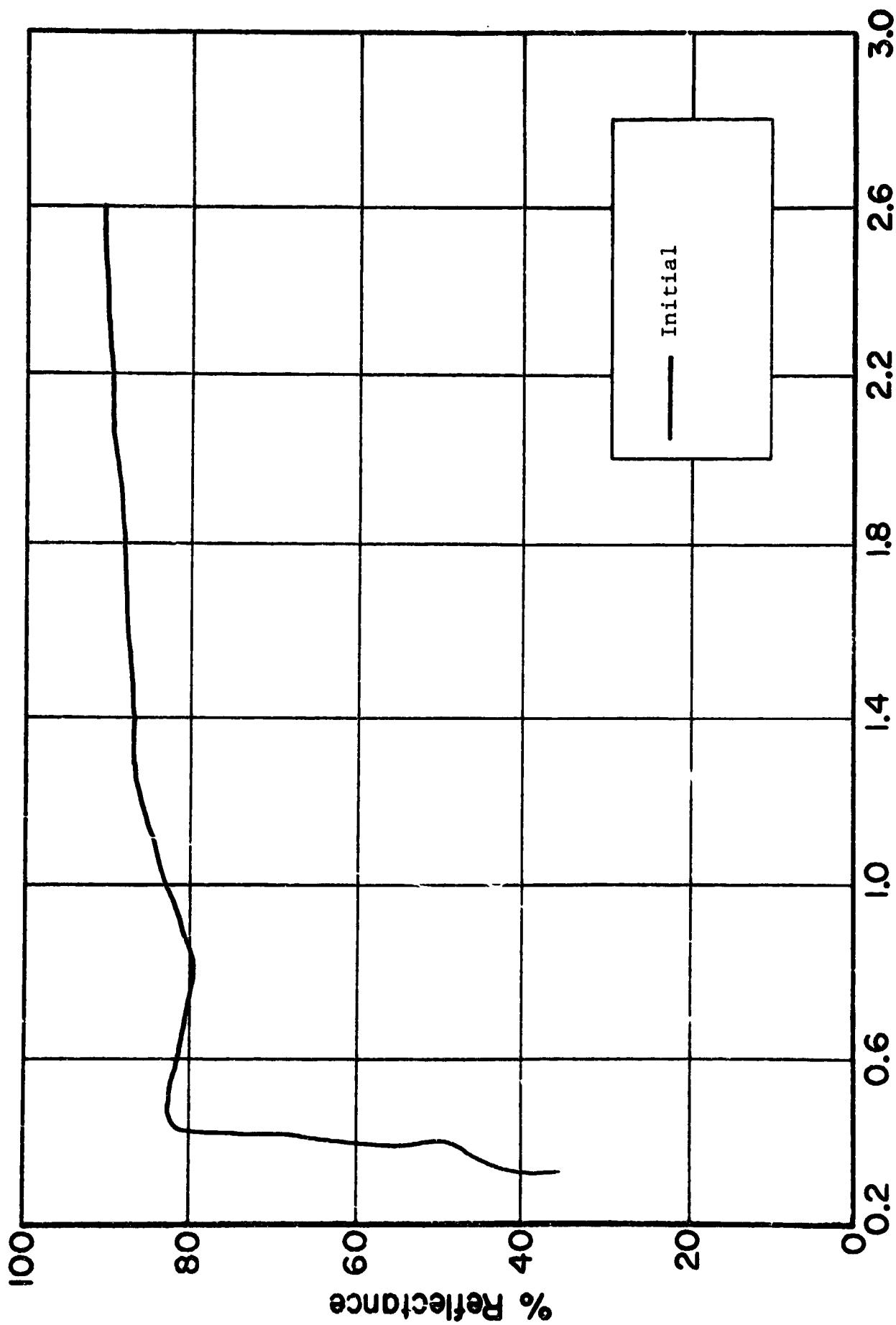


Figure 4.52 REFLECTANCE SPECTRA OF LH-12 (1200°C/1 hr) (POWDER)

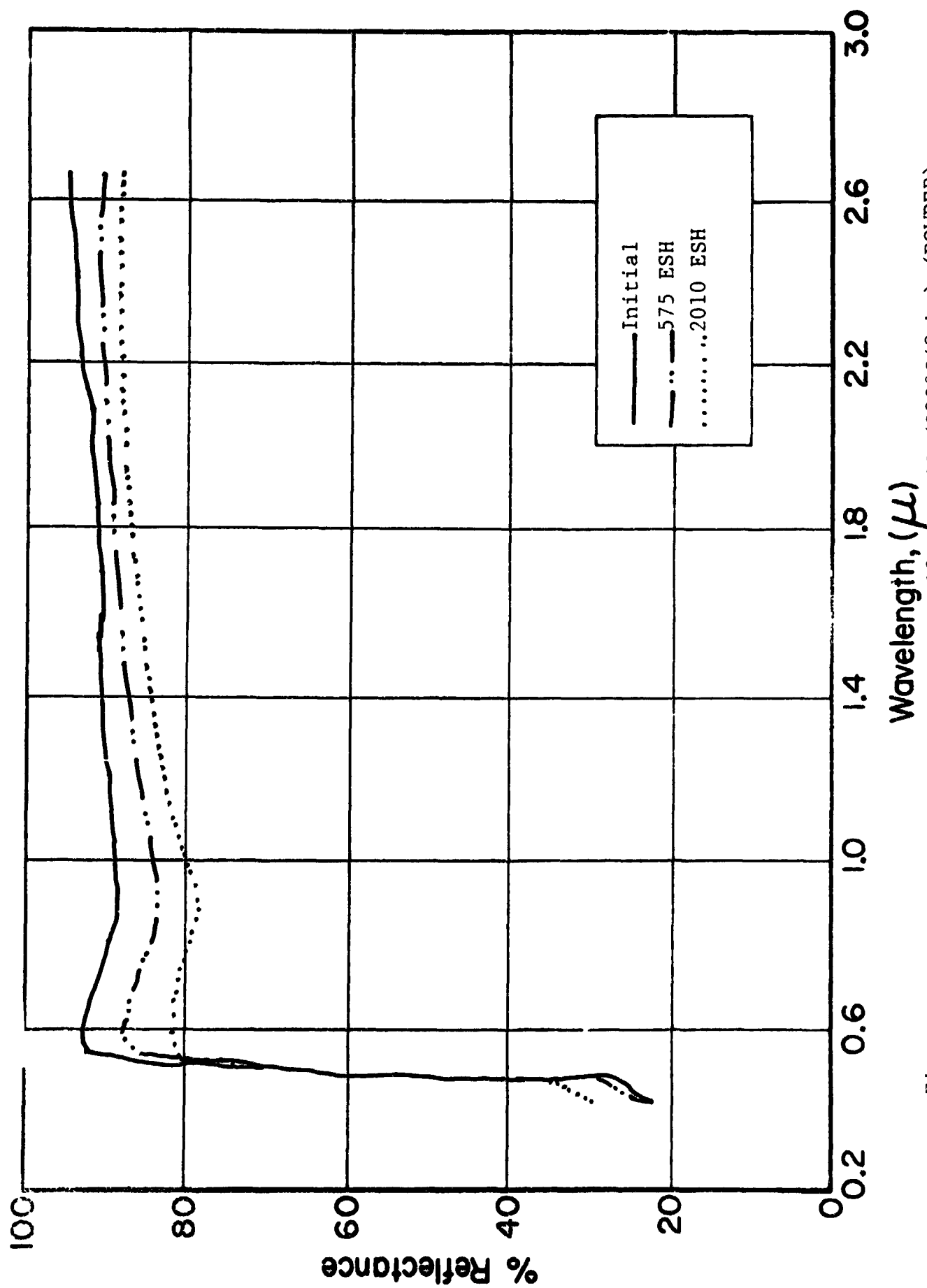


Figure 4.53 REFLECTANCE SPECTRA OF LH-12, Zn_2TiO_4 (900°C/8 hr) (POWDER)

unencapsulated) prepared and irradiated as a powder. The UV radiation-induced degradation appears to saturate after approximately 500 ESH, and the damage in the S-band region is not prominent. A potassium silicate paint of this pigment is somewhat more stable, particularly in the S-band, as shown in Figure 4.44. Note also (in Figure 4.43) that the i-r damage is also reduced compared to that in the powder. Reflectance spectra of the same pigment in OI-650 (Fig. 4.45), quite obviously show that the untreated pigment sustains considerable S-band damage.

In Figures 4.46-48 we present the reflectance spectra of $\text{Zn}_2\text{TiO}_4:\text{K}_2\text{SiF}_6$; in Figure 4.46 are the spectra of the powder; in Figures 4.47 and 4.48, the spectra of the OI-650 and OI-650G paints, respectively. The pigment exhibits good stability, with optical damage appearing to saturate at about 2000 ESH. The K_2SiF_6 encapsulation also affords some protection against S-band damage, and the encapsulated pigment is obviously more stable than the unencapsulated pigment (Fig. 4.43); yet the two pigments have, except for the S-band, very similar degradation characteristics.

The $\text{Zn}_2\text{TiO}_4:\text{K}_2\text{SiF}_6$ prepared using OI-650G exhibits a stability comparable to that of its pigment, while the OI-650 paint is severely degraded, especially in the S-band region. In this case, the OI-modification mitigates the interaction between pigment and vehicle. The interaction, however, is either between the binder and the encapsulant or is promoted by the encapsulant, because the unencapsulated pigment in OI-650 (Fig. 4.45) does not show extensive S-band development as does the paint with encapsulated pigment.

To a lesser extent than is evident above, the degradation in $\text{Zn}_2\text{TiO}_4:(\text{PO}_4^{=}/\text{SiO}_3^{=}/\text{PO}_4)$ is also, as Figure 4.49 shows, increased by the presence of the OI-650 vehicle (Fig. 4.50).

The reflectance spectra of three pigment powders which have been prepared by the COP (coprecipitation) method are shown in Figures 4.51-53. Their performance, however, is poor. Even though they are experimental pigments from the first coprecipitation attempts, their spectra (eg. Fig. 4.52) give encouragement, since they indicate an excess of ZnO, which can be removed by acid leaching.

4.4.6.3 Conclusions

The performance of the A-429M paint system is especially encouraging; the initial solar absorptance of this coating system, when all formulation parameters are optimized, may approach 0.160 in practice. The $\Delta\alpha_s$ of 0.02 in 4000⁺, ESH, moreover, is typical of this system. Since the $\Delta\alpha_s$ is unchanged upon O₂ bleaching, the silicate encapsulation is effective, and it is probable that the OI-650G binder materially aids this effectiveness.

A direct comparison of equivalent paints in this test and in CREF Test No. 8, while not conclusive, strongly implicates a foreign material in the CREF-8 samples. Although we suspect iron, the contaminant may be any metal which the pigment precursors contact in the pigment preparation process. This is further borne out by the fact that the stability of the basic Zn₂TiO₄ pigment in this test is very good, and it improves considerably when placed in PS-7 ($\Delta\alpha_s$ = 0.031 in 4070 ESH) or in OI-650 ($\Delta\alpha_s$ = 0.036). We associate the increased damage in OI-650 paints with the higher hydroxyl content of the OI-650 (as opposed to OI-650G). The silicate pigment has approximately the same stability as the untreated pigment, but here also its apparently increased interaction with OI-650G causes a pronounced increase in degradation. In all cases the interaction causes increased S-band absorption, which is made obvious by the oxygen bleach spectra.

The three (3) zinc orthotitanate pigments produced by the COP method are entirely experimental. Yet, from a comparison of the performance of zinc orthotitanate pigments prepared by firing the heretofore standard solid-solid (B-229) oxide precursors with those prepared from COP precursors, it is seen that these pigments exhibit different optical spectra and respond differently to the irradiation tests, especially in the near ultraviolet region.

4.4.7 Summary

The stability of Zn_2TiO_4 pigments which have been plasma-annealed compared to that of pigments not so treated has long been apparent (ref. 4.7). Plasma annealing, however, in certain cases evidently causes some permanent damage very similar to that it is intended to prevent. Although not considered very likely, the possibility exists that this damage was introduced in the grinding process after plasma annealing.

The encapsulant K_2SiF_6 , either with or without plasma annealing the treated pigment evidently causes substantial S-band absorption (the annealed pigment appeared "gray" in one instance - see par. 4.4.2.4); its stability, however, is only slightly improved.

The performance of $\text{Zn}_2\text{TiO}_4:\text{K}_2\text{SiO}_3$ pigments is considerably better than that of any of the other encapsulated pigments.

While plasma annealing does ordinarily improve pigment stability, it also in some cases has caused significant, and unacceptable, permanent increases in optical absorption. The facts that plasma heat treatment-induced damage often exceeds its benefits, and that some encapsulants are nearly as effective as an ideal plasma heat treatment, suggest that a stable surface may be attainable chemically as well as by plasma annealing.

Encapsulants for zinc orthotitanate pigments are effective only in preventing S-band absorption. (Earlier research showed that optical damage at longer wavelengths was associated with excess ZnO). (Ref. 4.8). OI-650 predisposes an otherwise stable pigment, if unencapsulated, to severe optical degradation in the visible and near infrared regions of the spectrum. Without being specific regarding the mechanisms, we reason that, in the case of OI-650 paints, the encapsulant serves two purposes - first, as a barrier to photodesorption from the pigment surface, and secondly, as a barrier to interactions of free radicals (or electrons) in the silicone resin with the pigment, such as discussed in Ref. 4.7. The UV-induced appearance of the S-band in OI-650 paints incorporating otherwise stable pigments implies either that the encapsulant is not intrinsically effective (with respect to prevention of pigment vehicle interactions) or its surface coverage is incomplete. The O_2 bleach results show that both possibilities exist. Many of the pigments show higher initial absorption in the S-band region - absorption attributable to an encapsulant pigment interaction. The additional degradation due to irradiation is O_2 bleachable, suggesting that coverage may be a major problem. With respect to these considerations, we conclude that potassium silicate affords the greatest protection from the standpoint of surface coverage; moreover, it does not cause directly, nor predispose the pigment to, excessive S-band absorption. On the basis of intrinsic effectiveness K_2SiF_6 ranks highest, although it directly or indirectly affects the pigment's optical properties.

The relatively greater effects of protons are as expected. Protons create substantial bulk damage but have little, if any effect on surface (S-band) damage. In those tests in which effects due to UV + p^+ can be compared with those due to UV or p^+ alone, we find, not surprisingly, that UV + p^+ damage is more severe than UV alone, and, in turn, that UV effects outweigh p^+ effects. The non-additive nature of these effects may,

in part, be understood from the fact that UV and p^+ cooperate/ compete to create optical damage at visible and near UV wavelengths, and that UV, in addition, creates near S-band and, occasionally, free carrier damage.

4.4.8 Conclusions

Zn_2TiO_4 pigment prepared via the solid-solid (SS) high temperature reaction of ZnO and α - TiO_2 exhibits great potential for exceptional stability in space environmental applications. This stability, however, is sensitive to the Zn/Ti stoichiometry, at least as this ratio determines the excess ZnO in the pigment; metallic contamination also affects its stability. A sensitivity of surface damage and of bulk damage to either of these factors has also been evident. Also evident is the improvement in S-band stability obtained by encapsulation of SS pigments with K_2SiF_6 and $PO_4/SiO_3/PO_4$, and the further improvement when these encapsulated pigments are plasma-calcined. The stronger sensitivity of SS pigments to UV-induced S-band damage in OI-650 paints than in OI-650 paints implicates OH^- as the radical responsible for the development of surface (S-band) degradation.

These conclusions, it should be remembered, pertain to pigments which were prepared with a ZnO excess. In light of several important observations made in subsequent investigations (ref. 4.6), the validity of many of the other conclusions reached in these studies is questionable. Certainly, we know that a 2.05 Zn/Ti ratio is not ideal, even though this was, at the time of these studies strongly believed to be necessary. Nevertheless, these studies clearly show that S-band stability relates very closely to surface passivity, and subsequent studies further confirm this observation. The attainment of surface passivity - be it through optimum temperature-time pigment calcination schedules, reactive encapsulation, or plasma calcination - almost certainly depends upon initial Zn/Ti stoichiometry.

Table 4-10
 CREF TEST No. 10 - SOLAR ABSORPTANCE VALUES
 OF COP Zn_2TiO_4 PIGMENTS VS ULTRAVIOLET EXPOSURE (ESH)

Sample No.	Description	Solar Absorptance Values			Δa_s
		Initial	750 ESH	1460 ESH	
10	LH-12(6-14)	0.163	0.200	0.324	0.161
12	LH-16(6-14)	0.193	0.222	0.246	0.053
9	LH-16(9)	0.130	0.163	0.177	0.047
4	LH-20(6-12)	0.146	0.148	0.157	0.011
8	LH-20(9)	0.116	0.127	0.136	0.020
6	LH-20(9-14)	0.19	0.198	0.176	0.007
3	LH-22(6-12)	0.173	0.175	0.220	0.047
11	LH-22(9)	0.141	0.171	0.169	0.028
5	LH-22(9-14)	0.196	0.201	0.220	0.024
1	LH-26(6-12)	0.178	0.181	0.186	0.008
2	LH-27(6-12)*	0.201	0.247	0.246	0.045
7	LH-27(9-14)*	0.166	0.202	0.209	0.043

*Batch 27 was produced by the mixed oxalate (MOX) method.

4.5 ENVIRONMENTAL TEST REPORTS - PART II

The reports of irradiation studies in Part II of this section deal primarily with pigments prepared from oxalate precursors via the COP method.

4.5.1 CREF Test No. 10

4.5.1.1 Purpose/Description

This test (ref. 4.6) in general was designed to compare the effects of various firing conditions on the initial reflectance properties and ultraviolet-stability of five COP (coprecipitation) production batches and one experimental MOX (mixed oxalate) batch. (Unfortunately, most of the coatings, prepared as powders on IRIF coupons, were not sufficiently adherent to the coupons to allow confidence in more than the initial (pre-irradiation) spectral reflectance measurements).

This series of COP Zn_2TiO_4 pigments were fired under different temperature/time conditions, UV irradiated to exposure levels of approximately 750 and 1460 ESH. The samples and their solar absorptance values are listed in Table 4.10. In some of these pigments excess ZnO was detected by X-ray, as well as by the classic ZnO infrared free carrier spectra (ref. 4.9).

4.5.1.2 Test Results

Figure 4.54 shows the effects of ultraviolet irradiation on an early production pigment, LH-12(6-14). The S-band development is especially prominent, even though some substrate show-through was experienced. Figures 4.55, 56 are spectra of LH-16(9) and of LH-16(6-14), respectively; both exhibit ZnO excess. In these materials the UV radiation damage was not excessive, but the ZnO excess is clearly evident from the induced free carrier absorption, especially in LH-16(9). The LH-16(6-14) pigment sustains somewhat more S-band damage than does the LH-16(9) pigment.

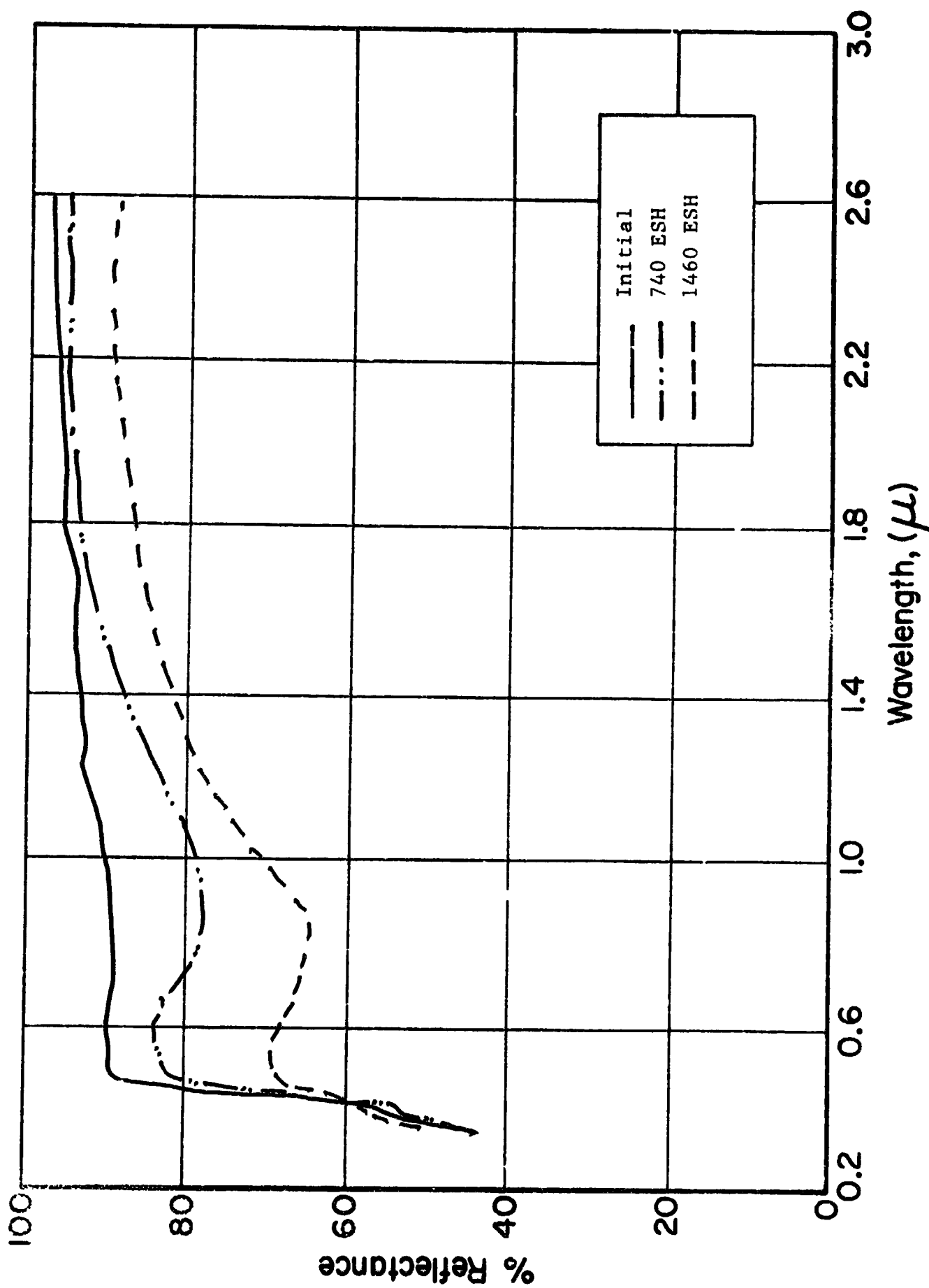


Figure 4.54 REFLECTANCE SPECTRA OF LH-12 Zn_2TiO_4 (6-14)

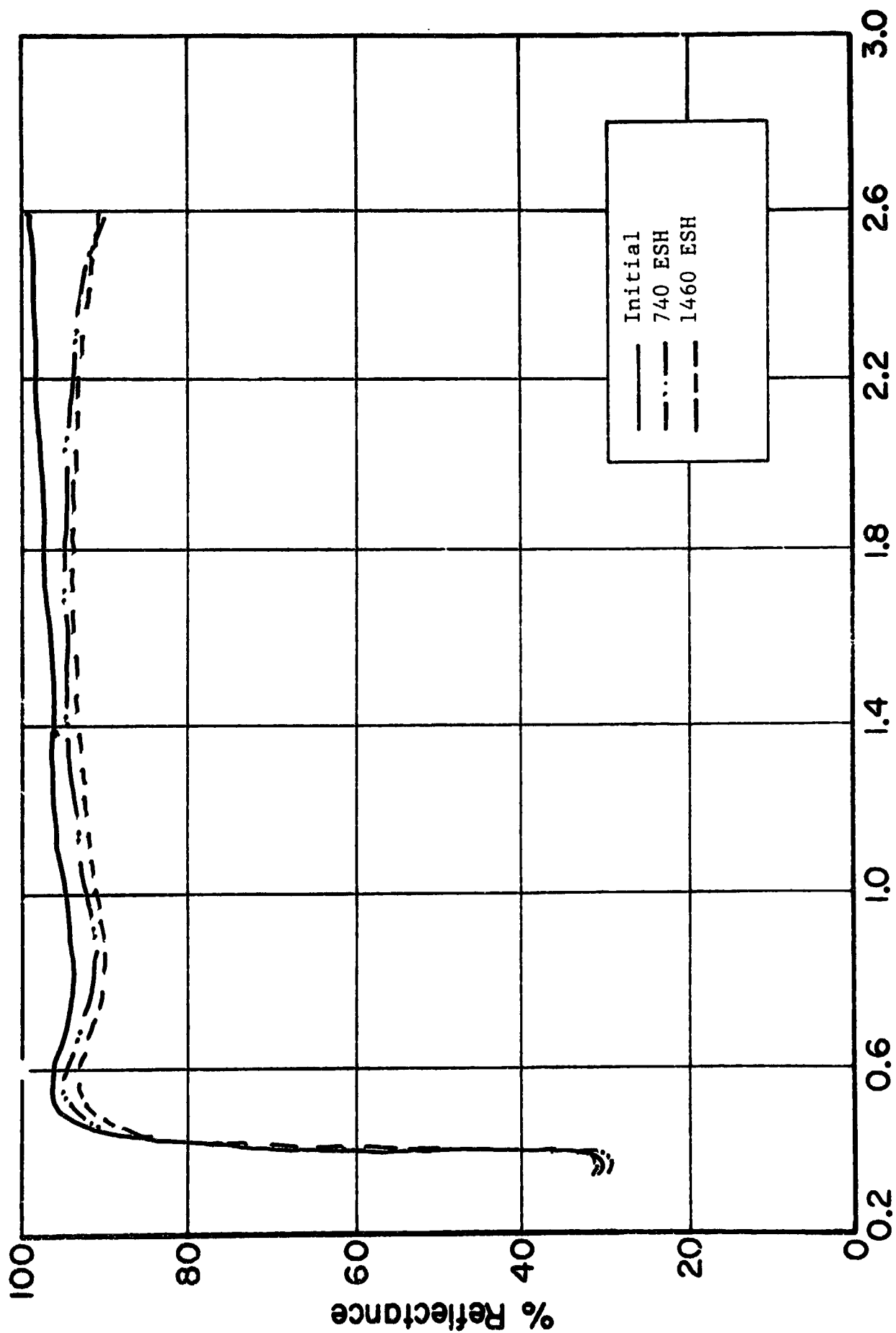
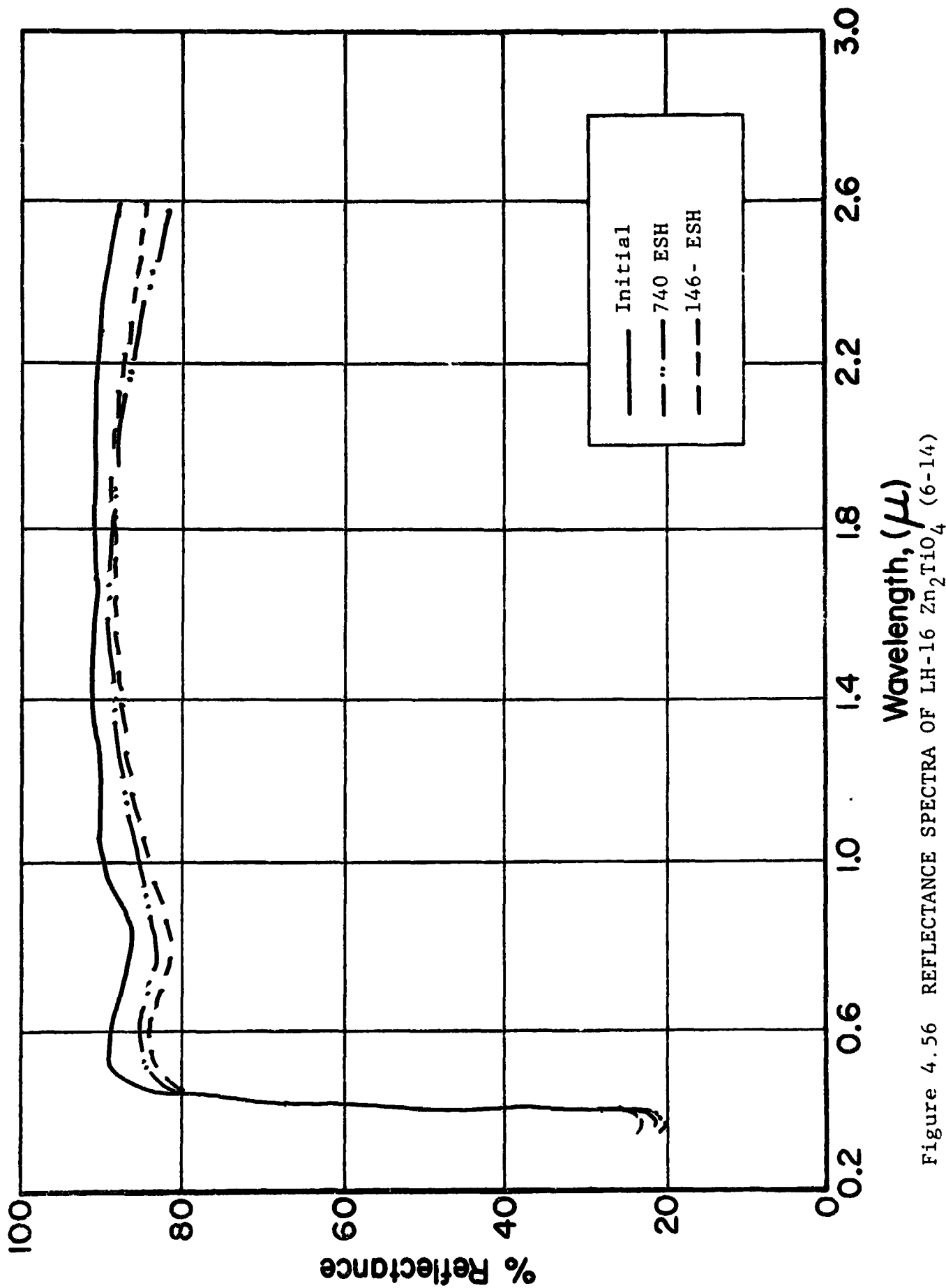


Figure 4.55 REFLECTANCE SPECTRA OF LH-16 Zr_2TiO_4 (9)



The reflectance spectra of three pigments prepared from Batch LH-20 viz., (9), (9-14), and (6-12) are presented in Figures 4.57-59. (The post-irradiation i-r spectral reflectance of the (6-12) pigment, exceeds its initial value because of a loss of adherence). In this series, the higher conversion temperatures tend to produce greater S-band damage.

The spectra of the three LH-22 pigments, viz., (9), (6-12) and (9-14), prepared from COP batch LH-22, belie a noticeable excess of ZnO. Reflectance stability of this series also appears to be sensitive to the heat treatment schedule. The (6-12) pigment (Fig. 4.61) shows poor stability (adherence was a problem also), while the (9) pigment (Fig. 4.60), even with the characteristic ZnO i-r absorption, demonstrates greater stability. The (9-14) pigment (Fig. 4.62) exhibits excellent UV radiation stability. The trend in this respect, however, is somewhat opposite to that witnessed in the LH-20 pigments, quite probably because of the ZnO excess.

Although the reflectance spectra for LH-26(6-12) in Fig. 4.63 show the presence of excess ZnO, this pigment possesses good initial properties and considerable stability.

In Figures 4.64-65 are the reflectance spectra for two pigments from COP batch LH-27. The lack of adherence of the (6-12) sample obscured the UV-induced i-r absorption, if any. In any case the (9-14) treatment evidently produces a pigment superior to that of the (6-12) treatment.

4.5.1.3 Conclusions

The surface passivity of many of the tested pigments is evident from the fact that they do not adhere well to their test coupons nor do they exhibit much cohesion. Adhesion losses were experienced in all of the (6-12) pigments, with varying effect. Test results for this reason are difficult to analyze;

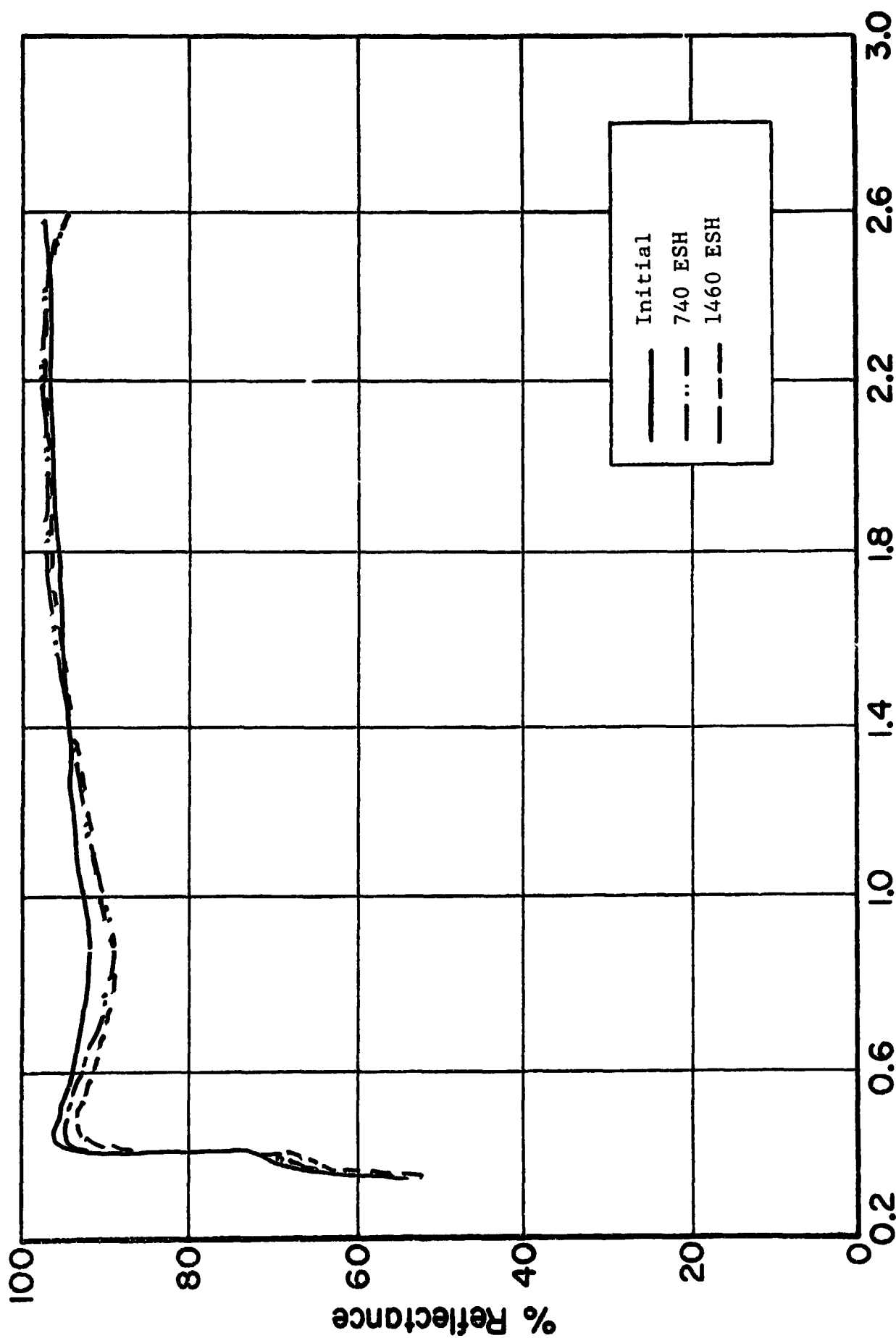


Figure 4.57 REFLECTANCE SPECTRA OF LH-20 Zn_2TiO_4 (9)

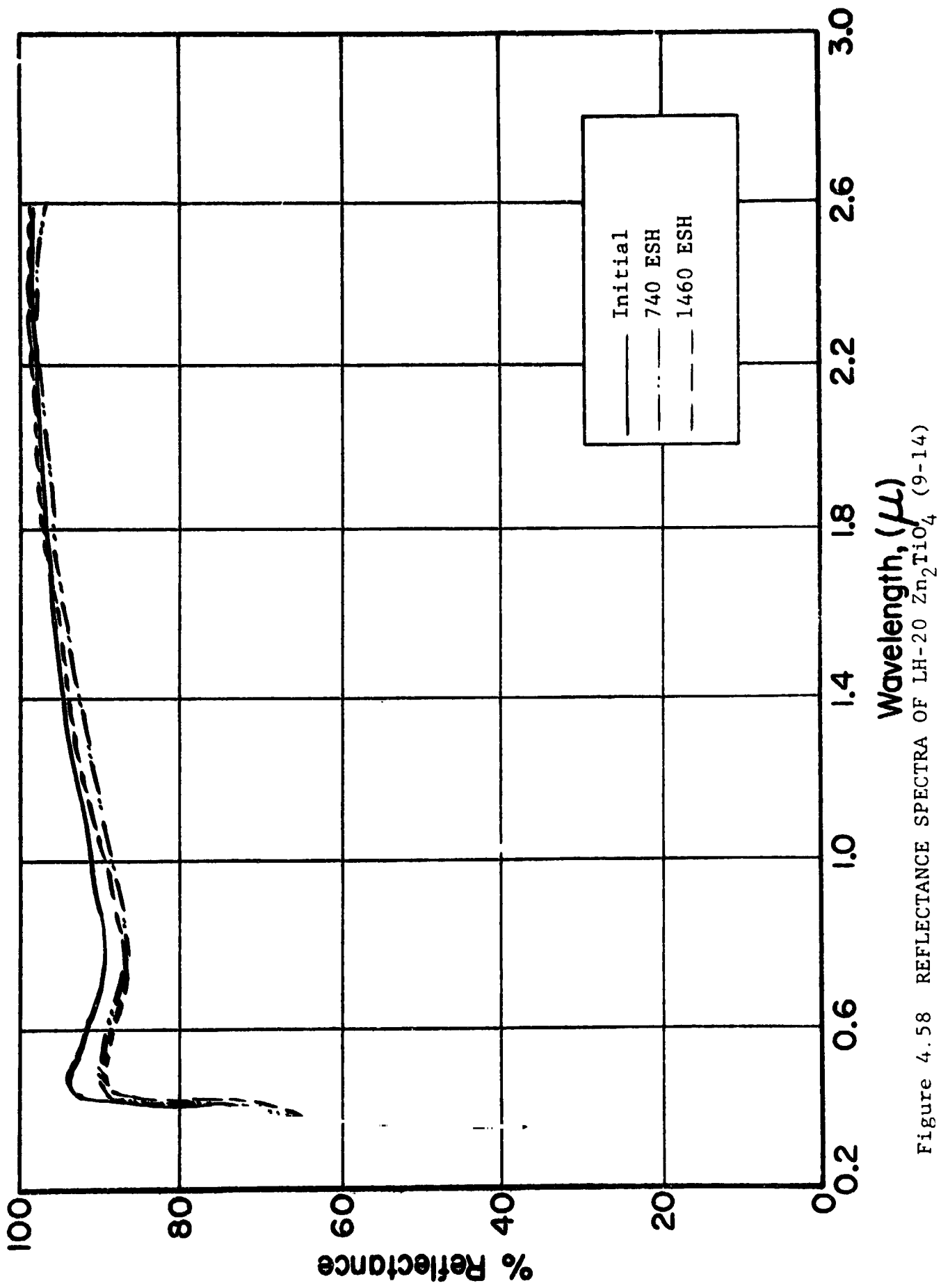


Figure 4.58 REFLECTANCE SPECTRA OF LH-20 Zn_2TiO_4 (9-14)

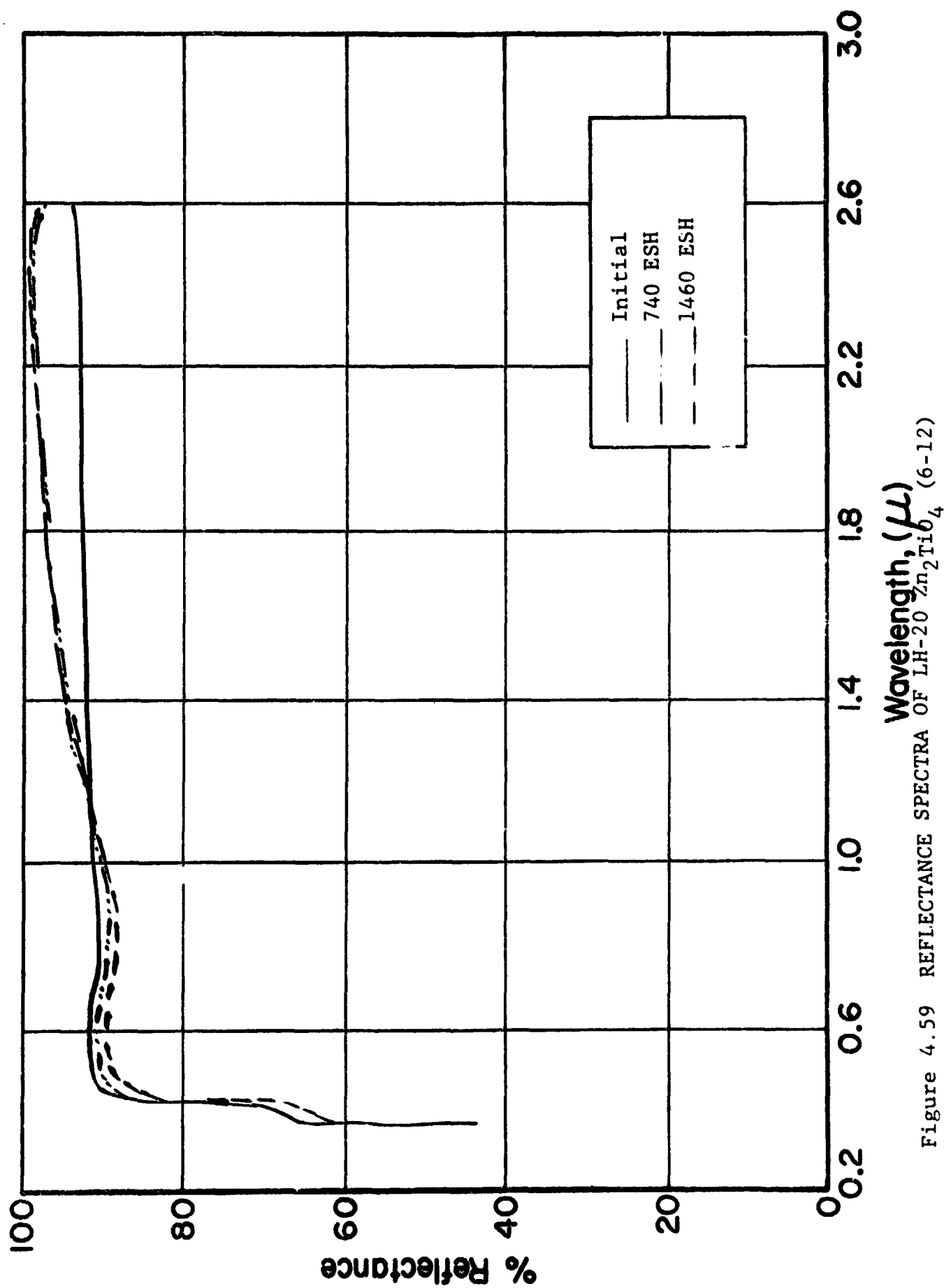


Figure 4.59 REFLECTANCE SPECTRA OF LH-20 Zn_2Ti_6 (6-12)

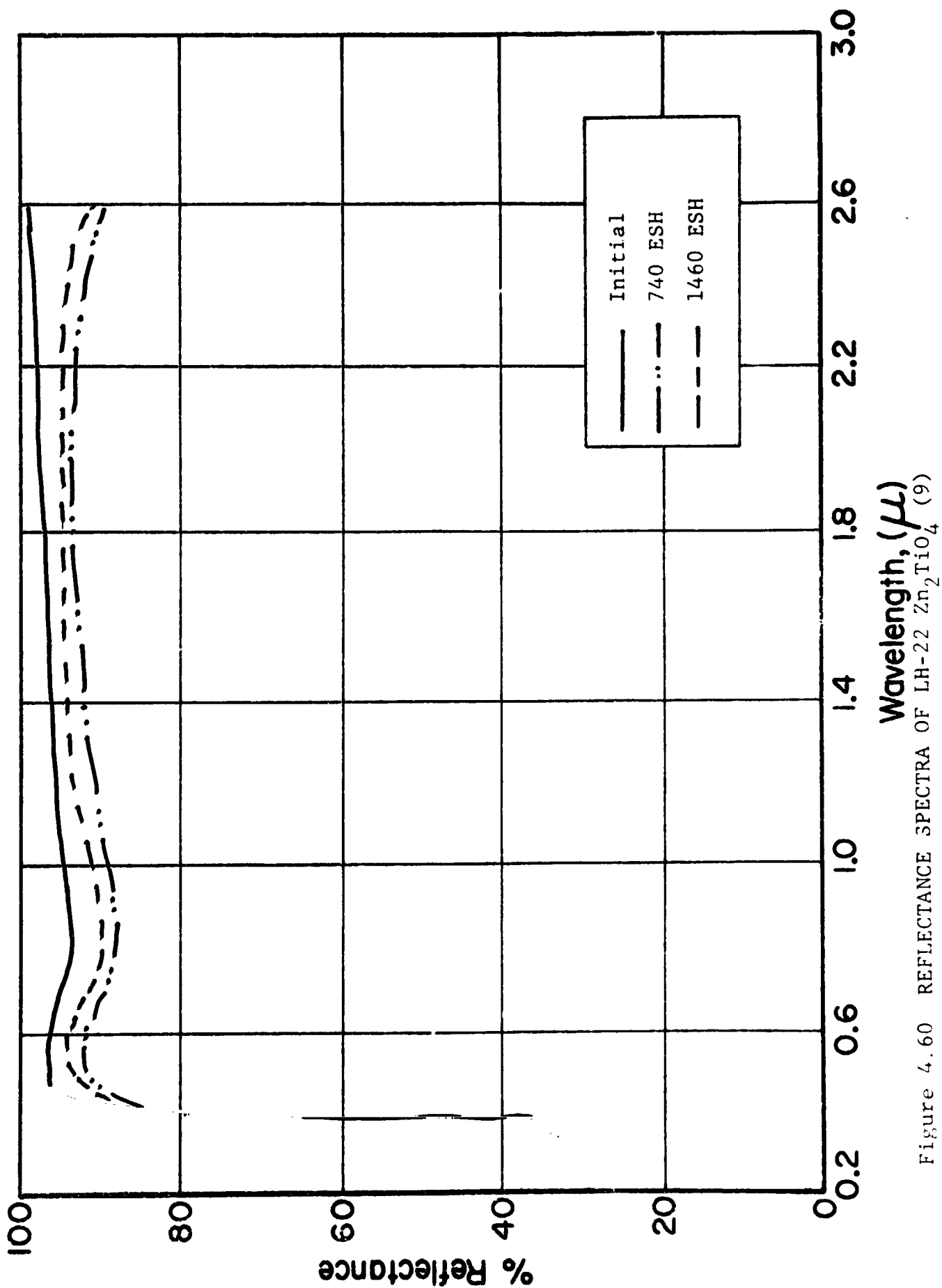


Figure 4.60 REFLECTANCE SPECTRA OF LH-22 Zn_2TiO_4 (9)

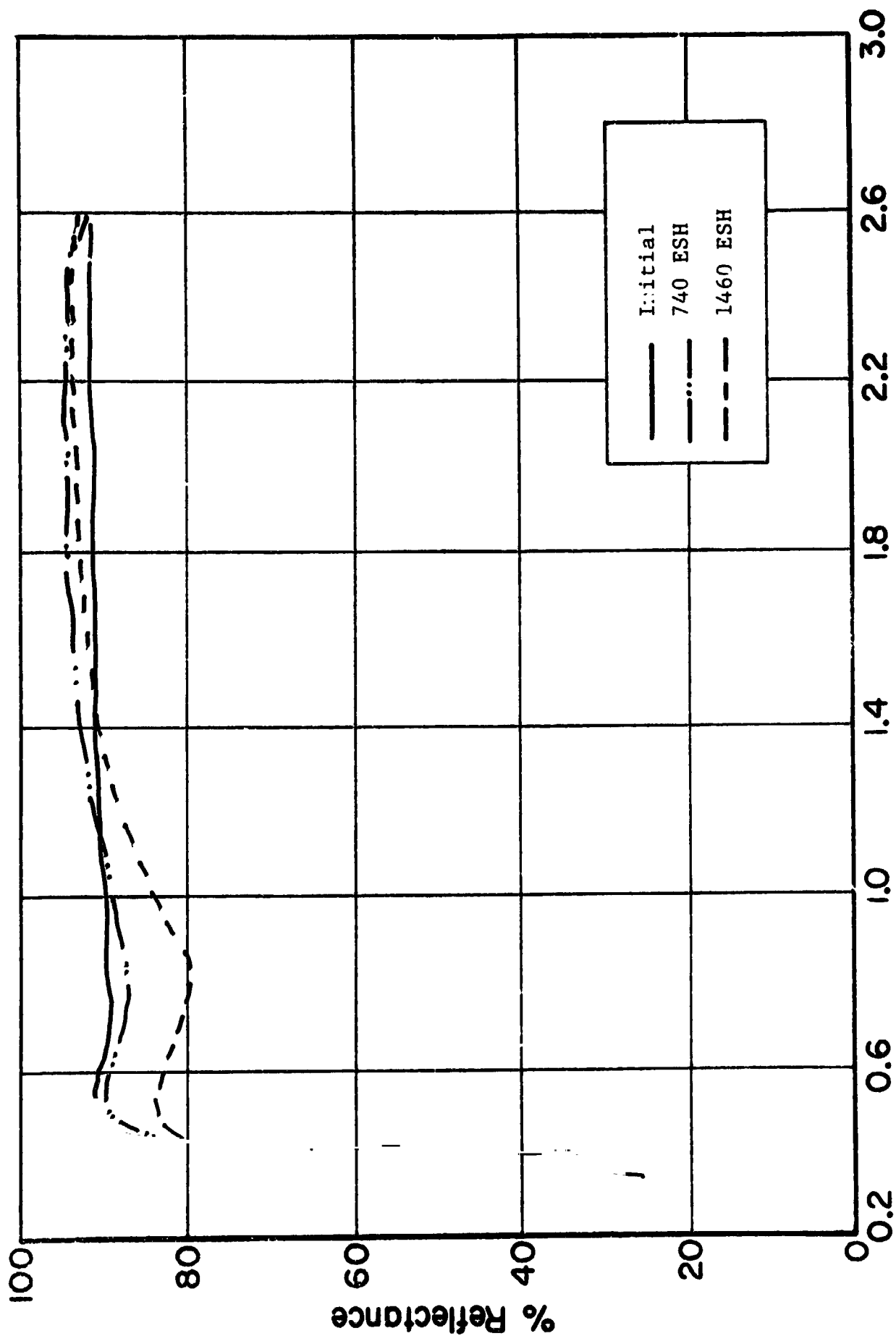


Figure 4.61 REFLECTANCE SPECTRA OF LH-22 Zn_2TiO_4 (6-12)

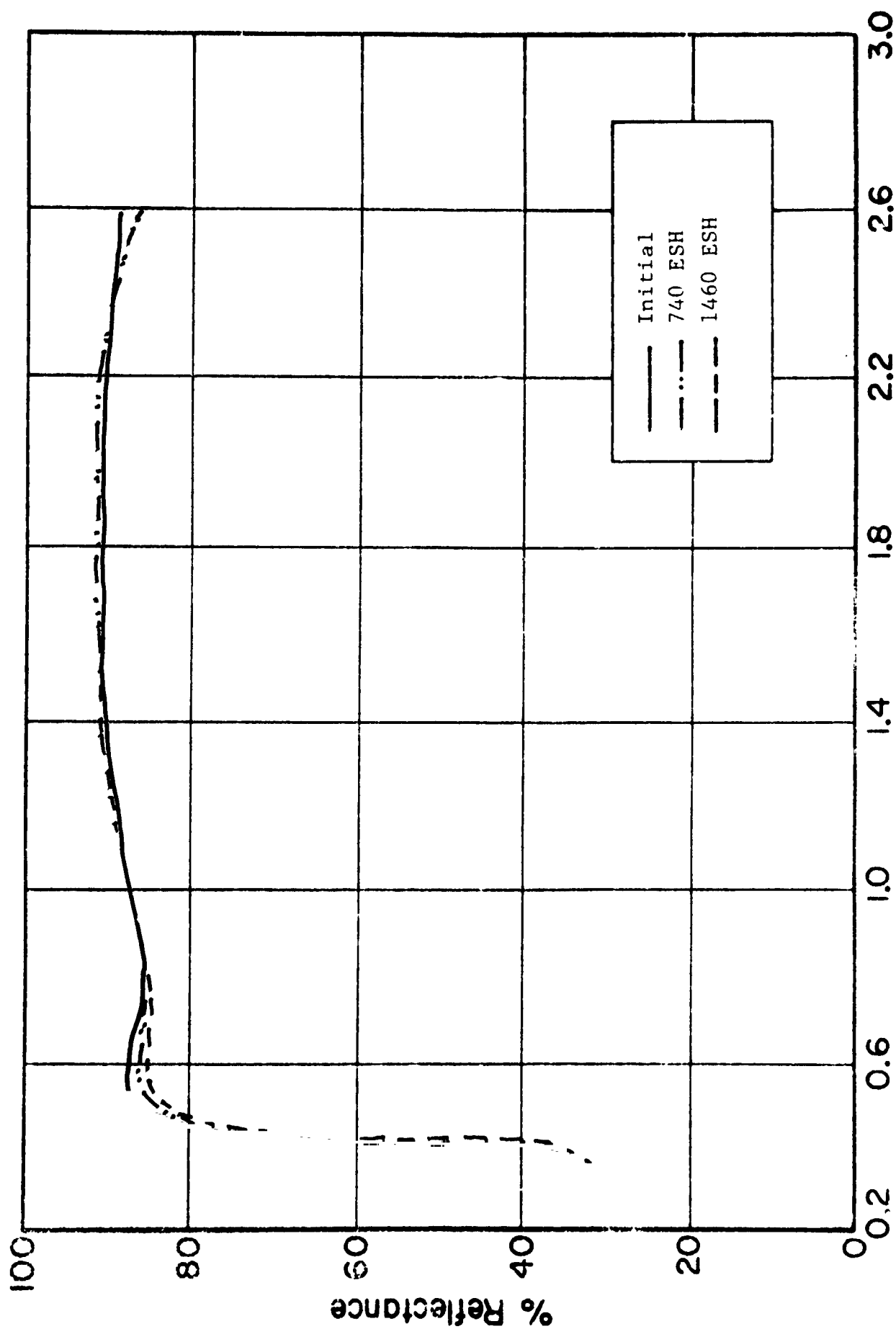


FIGURE 4.62 REFLECTANCE SPECTRA OF LH-22 Zn_2TiO_4 (9-14)

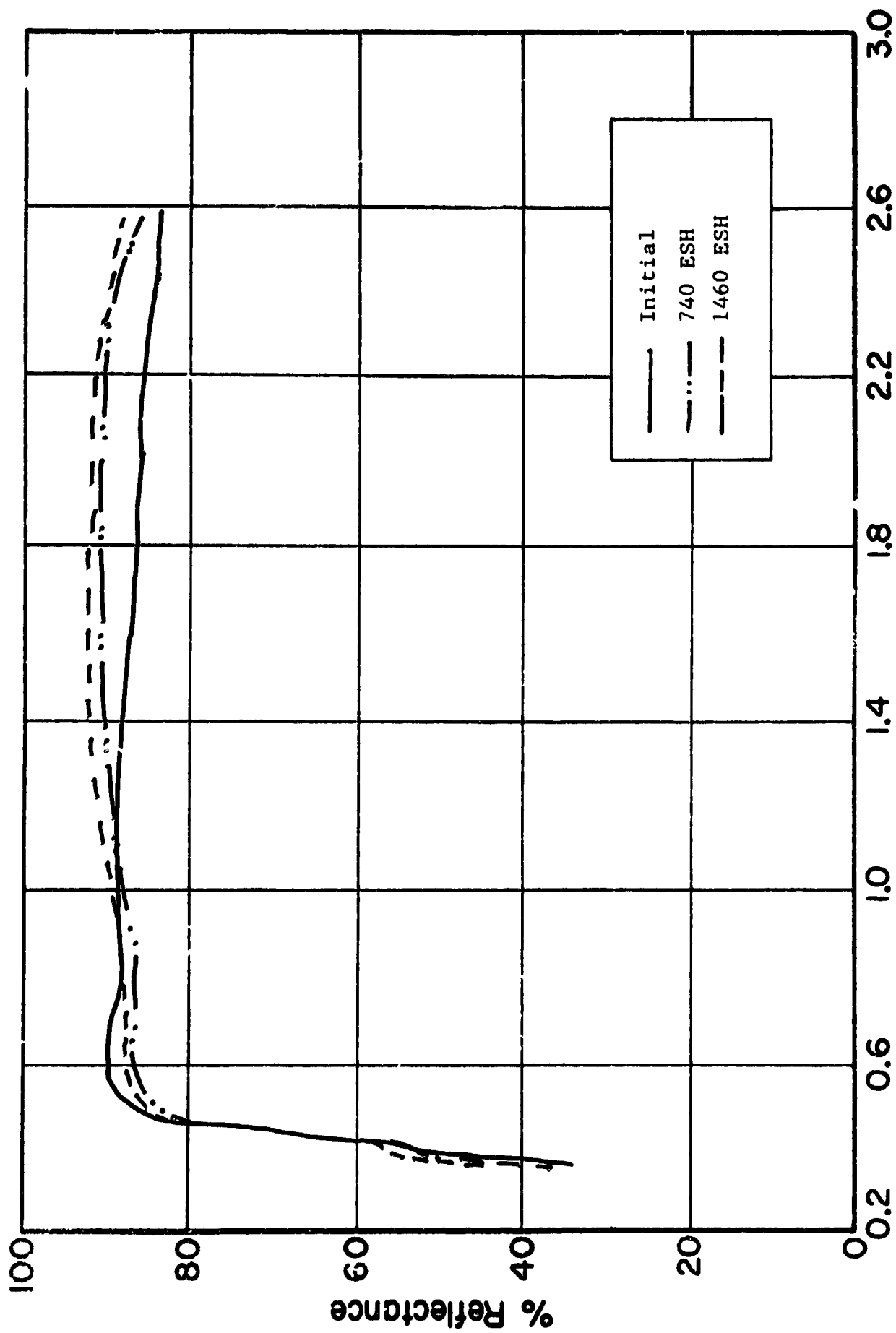
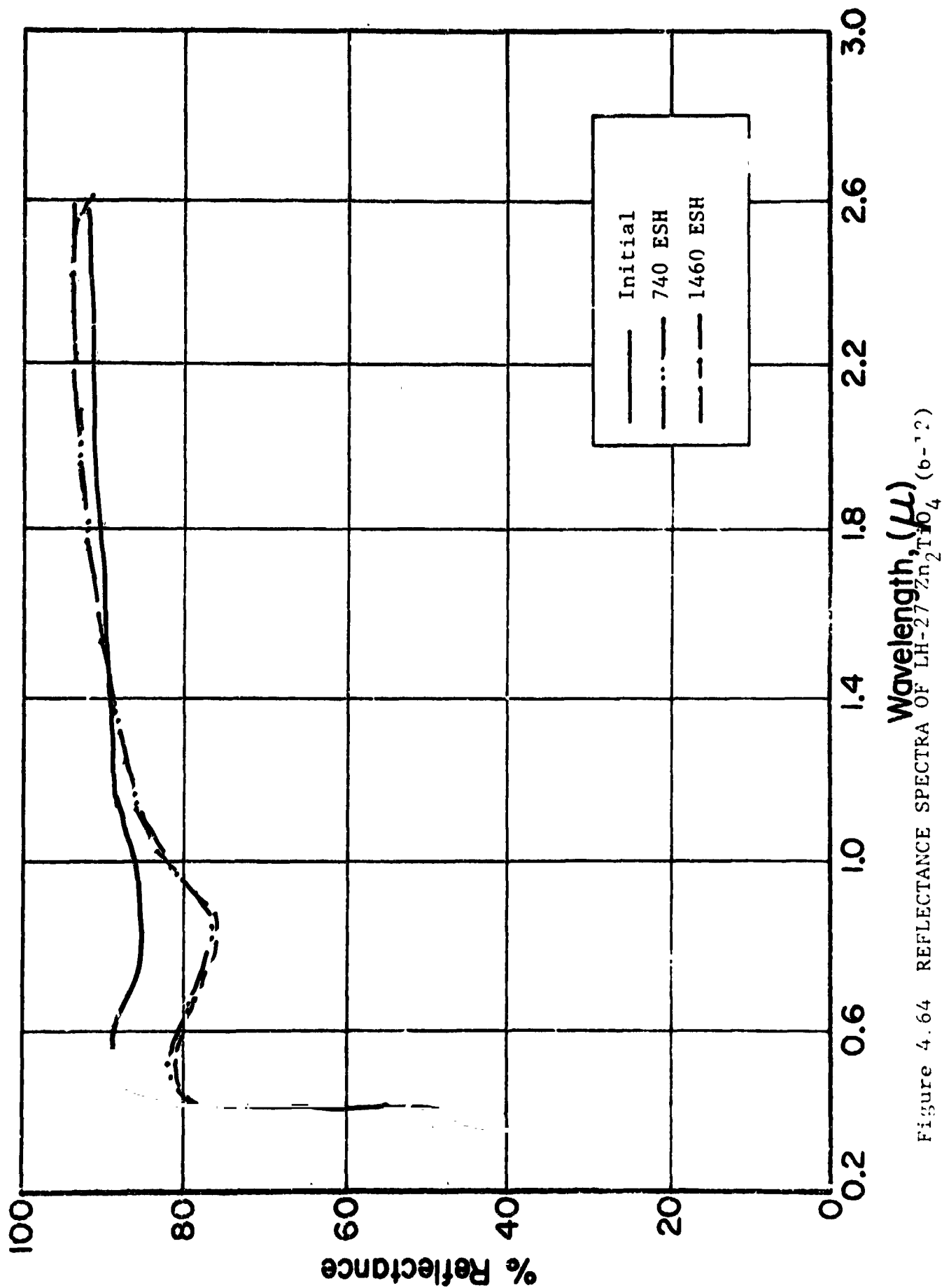


Figure 4.63 REFLECTANCE SPECTRA OF LH-26 Zn_2TiO_4 (6-11)



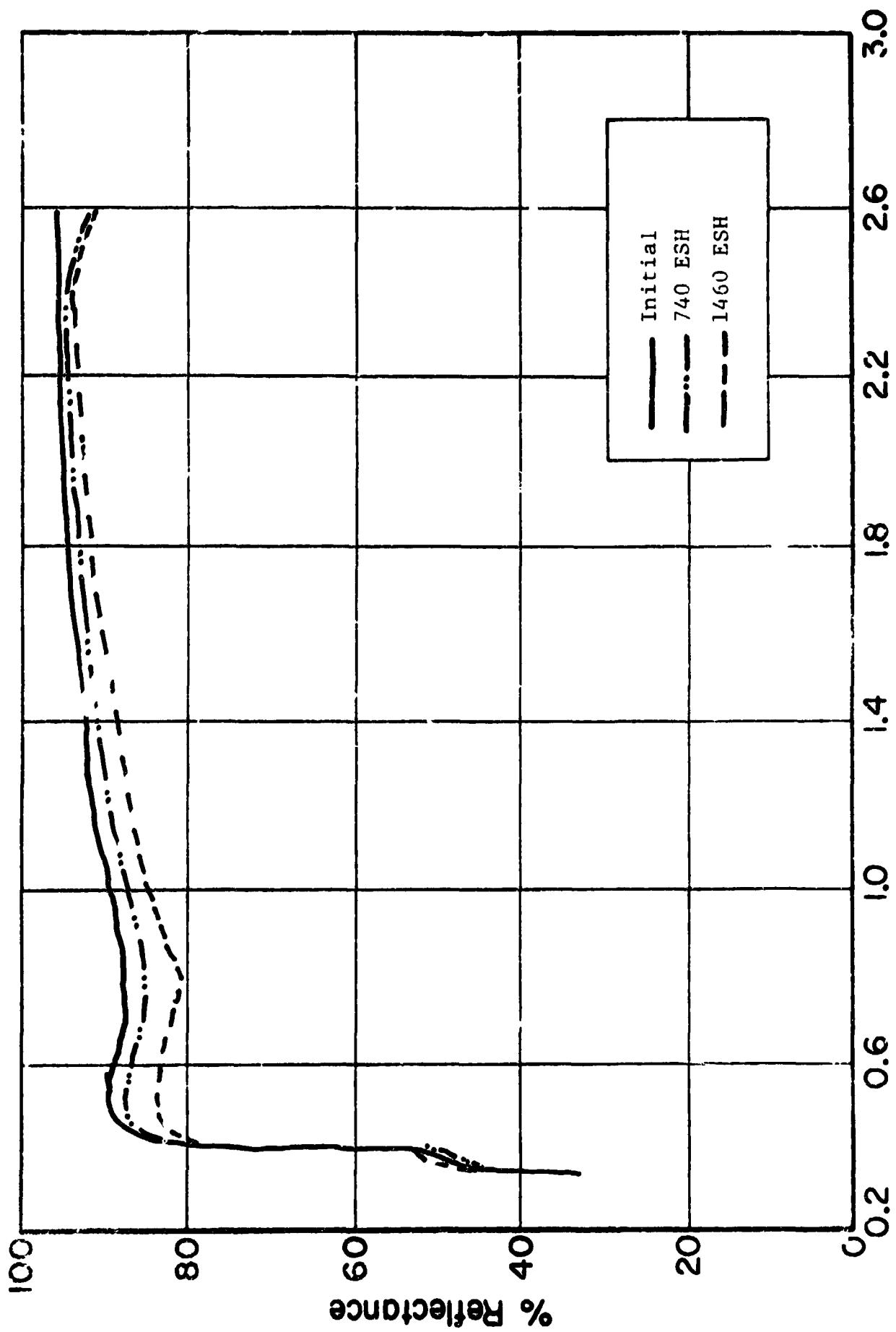


Figure 4 65 REFLECTANCE SPECTRA OF LH-27 Zn_2TiO_4 (9-14)

the variable film thicknesses compound this difficulty. But the results do bear out the basic properties and performance of Zn_2TiO_4 pigments, justifying the investigation of the COP process as a method for producing them. The appearance of UV-induced free carrier absorption signifies a ZnO excess, which probably relates to the sample preparative conditions, since these pigments were not subjected to a specific ZnO removal treatment.

4.5.2 CREF Test No. 13

4.5.2.1 Purpose/Description

The overall stability of a Zn_2TiO_4 /OI-650G paint system depends not only on the inherent stability characteristics of its components but upon interactions between them, and therefore, in the case of Zn_2TiO_4 , on the surface properties of the pigments. The tests performed must allow for discerning whether induced optical damage resides in the interior of a pigment, in the vehicle, or as is frequently the case with Zn_2TiO_4 , on the pigment surface. The ability to so distinguish proceeds from tests of individual components and of paints and from analyses of reflectance degradation spectra of all of these. It must further allow for determining the pigment surface modification treatments most effective in mitigating these interactions. This test (ref. 4.9) involves four preparative variables - pigment calcination schedule, acid leaching of pigment to remove ZnO, precipitation hold time, and thermal treatment of the silicone paint. Table 4.11 lists the materials tested (all OI-650 paints) and their appropriate α_s values.

4.5.2.2 Sequence

CREF-13 was operated as an UV-only radiation test. Spectral reflectance measurements (in-vacuo) were recorded prior to irradiation, after exposures of 435 ESH, 1100 ESH and of 2100 ESH, and in O_2 after final in-situ measurements.

Table 4-11

CREF #13 SOLAR ABSORPTANCE VALUES
ZINC ORTHOTITANATE/OI-650G PAINTS

<u>Pigment Description</u>	<u>Solar Absorptance</u>			
	<u>Initial</u>	<u>Exposure, ESH</u>		
		<u>435</u>	<u>1100</u>	<u>2100</u>
				<u>O₂ Bleach</u>
LH-51(6-12,	.278	.314	.331	.344
				.301
LH-51(6-12)-B*	.278	.317	.326	.348
				.301
LH-51(6-14)	1.49	.181	.204	.218
				.165
LH-51(6-14)-B	.157	.204	.219	.229
				.194
LH-30(6-12-A-10)	.259	.312	.335	.336
				.282
LH-30(6-12-A-10-B	.270	.294	.301	.304
				.283
LH-30(6-14-A-10)	.234	.265	.277	.279
				.256
LH-30(6-14-A-10)-B	.212	.238	.246	.256
				.226
LH-31(6-12-A-10)	.252	.295	.311	.318
				.279
LH-31(6-12-A-10)-B	.227	.277	.293	.311
				.255
LH-31(6-14-A-10)	.184	.241	.266	.282
				.216
LH-31(6-14-A-10)-B	.189	.235	.256	.270
				.211

*"B": samples were baked at 250°F for 16 hrs.

4.5.2.3 Results

In Table 4.11a we present for better insight the spectral degradation at several selected wavelengths: 365nm, 450nm, 865nm, and 1900nm. The 365nm wavelength was selected because it is very close to, but on the short wavelength side of, the fundamental absorption edge, λ_g , of ZnO, but on the long wavelength side of that of Zn_2TiO_4 . The 450nm wavelength is in a region of high reflectance for Zn_2TiO_4 . The 865nm wavelength lies within the S-band. The 1900nm wavelength lies sufficiently far into the i-r region that induced free carrier absorption in the pigment, if present, will be observable and will not be masked by the natural absorption of the binder. Representative spectra are given in Figs. 4.65-70.

For reference, the original COP batches LH-30, LH-31, and LH-51 were co-precipitated from oxalic acid solutions at $\sim 90^\circ\text{C}$ with hold times of 1 hr for LH-30, and of 4 hrs for LH-31 and LH-51.

Pigment calcination temperature apparently does not have a strong influence on UV radiation stability although 1200°C temperatures tend to produce pigments more stable than that of 900°C . All of the paints sustained UV damage, roughly half of which is pigment surface-related. The permanent damage, occurring mainly in the visible and near UV regions of the spectrum, may be subject to reduction by better control of initial (oxalate) stoichiometry. The acetic acid wash (followed by a re-calcination at 1000°C) has a beneficial effect on initial reflectance, without significantly affecting photo-stability.

The unusual degradation which occurred in LH-31 and LH-51 pigmented paints contrasts with the relatively good stability of the paints made from the LH-30 series pigments. This difference in behavior between LH-30 pigments and the others points to a possibly significant difference in the Zn/Ti ratio

Table 4-11a

SELECTED SPECTRAL REFLECTANCE DATE: CREF #13

ZINC ORTHOTITANATE/OI-650G PAINTS

Sample (IH No.)	Reflectance Loss (Maximum/Permanent)*					R365/R450	**Δ _{as} max
Pigment (in OI-650G)	365 nm	450 nm	865 nm	1900 nm			
LH-51 (6-12)	6.5/4.0	8.0/4.0	8.5/2.0	3.0/1.0		65.5/79.5	0.066
LH-51 (6-12)-B	6.5/2.5	6.5/2.0	14.0/2.0	3.0/1.5		65.0/78.0	0.061
LH-51 (6-14)	5.5/2.0	8.5/2.0	9.0/6.5	3.5/1.5		64.5/94.0	0.069
LH-51 (6-14)-B	5.0/2.0	7.5/5.0	10.0/3.5	4.0/3.0		66.0/92.0	0.072
LH-30 (6-12-A-10)	11.0/5.0	9.0/4.0	9.5/2.0	6.0/1.0		77.5/81.5	0.077
LH-30 (6-12-A-10)-B	5.0/3.0	5.5/3.0	3.0/1.0	2.0/6.5		76.0/80.0	0.034
LH-30 (6-14-A-10)	5.0/3.0	6.0/3.0	2.0/1.5	2.5/2.0		81.0/85.5	0.045
LH-30 (6-14-A-10)-B	6.0/2.5	6.0/2.0	5.0/1.0	1.5/0.5		83.5/88.5	0.044
LH-30 (6-12-A-10)	8.5/5.0	8.5/4.5	8.0/1.5	3.5/2.0		80.5/83.5	0.066
LH-31 (6-12-A-10)-B	10.0/3.5	9.5/3.5	10.0/3.5	7.5/3.0		84.0/86.0	0.084
LH-31 (6-14-A-10)	11.0/5.5	10.0/5.0	14.0/4.0	5.5/2.0		86.5/91.0	0.098
LH-31 (6-14-A-10)-B	8.0/3.5	8.5/3.5	11.5/2.5	5.0/1.5		85.0/90.0	0.081

*Spectral Reflectance in % units (ΔR after 2106 ESH/ΔR after O₂ Bleach)

**Absolute Spectral Reflectance at 365 nm and at 450 nm shows effect of ZnO

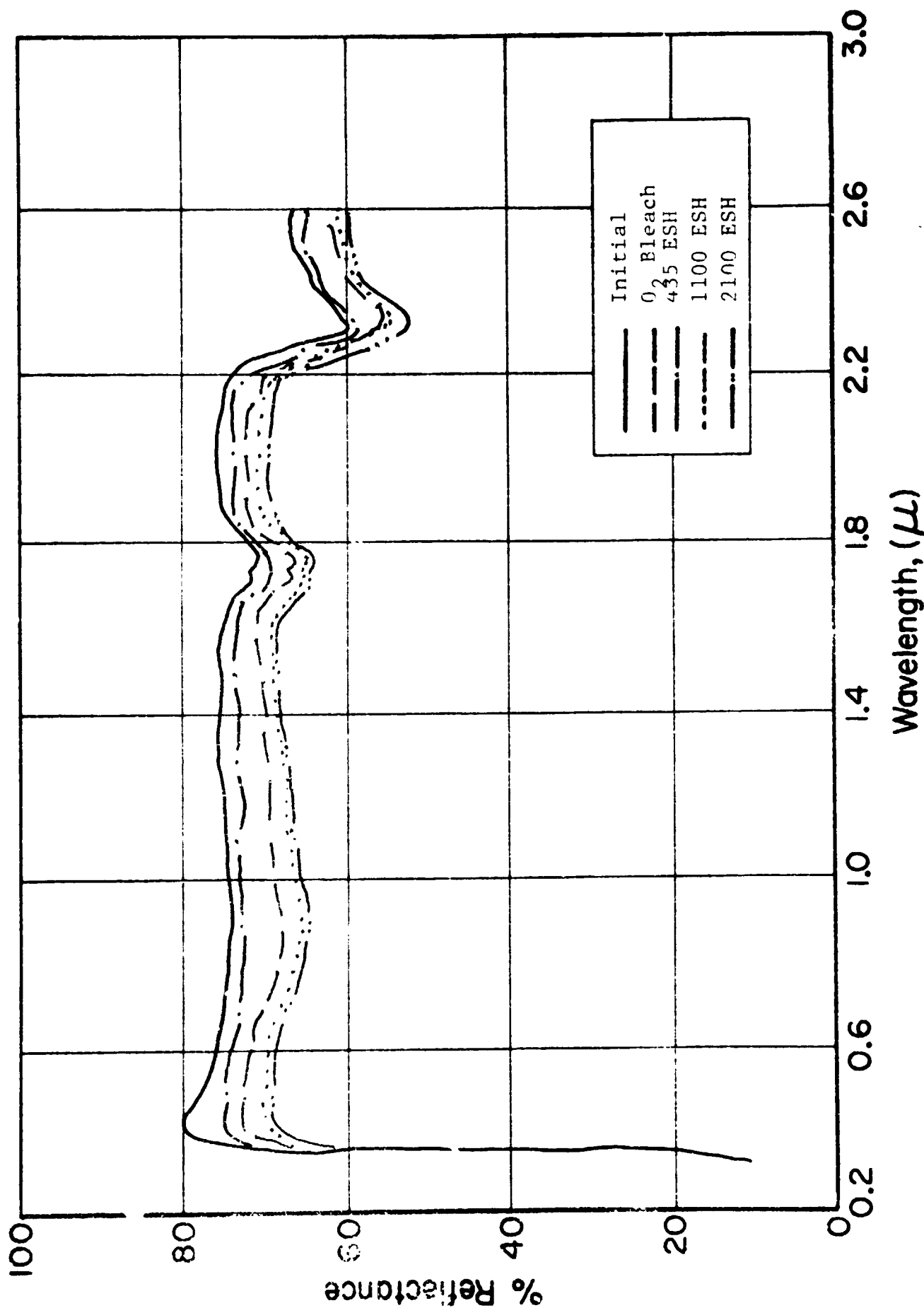


Figure 4.65b REFLECTANCE SPECTRA OF LH-30(6-12-A-10)

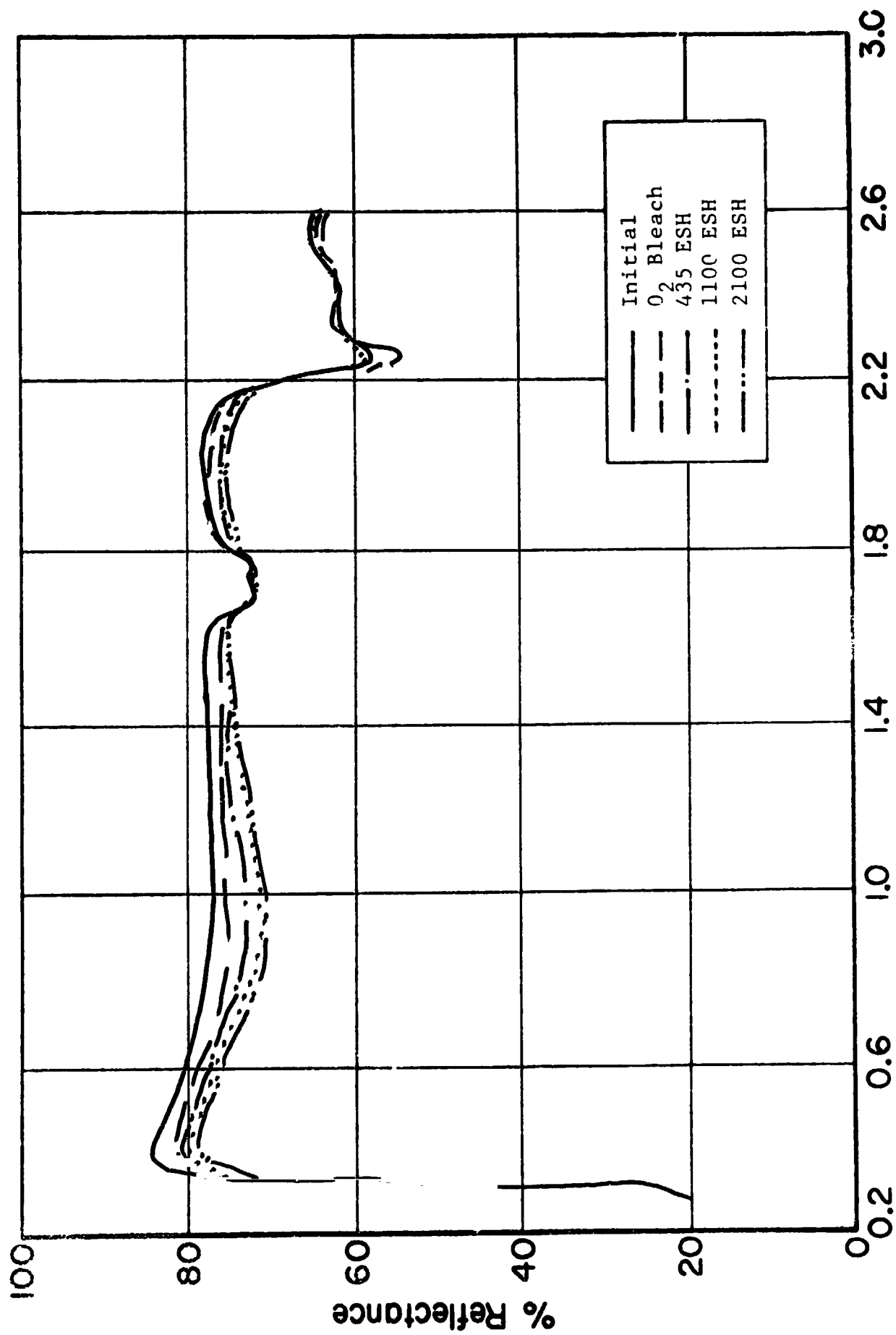


Figure 4.66 REFLECTANCE SPECTRA OF LH-30(6-14-A10)

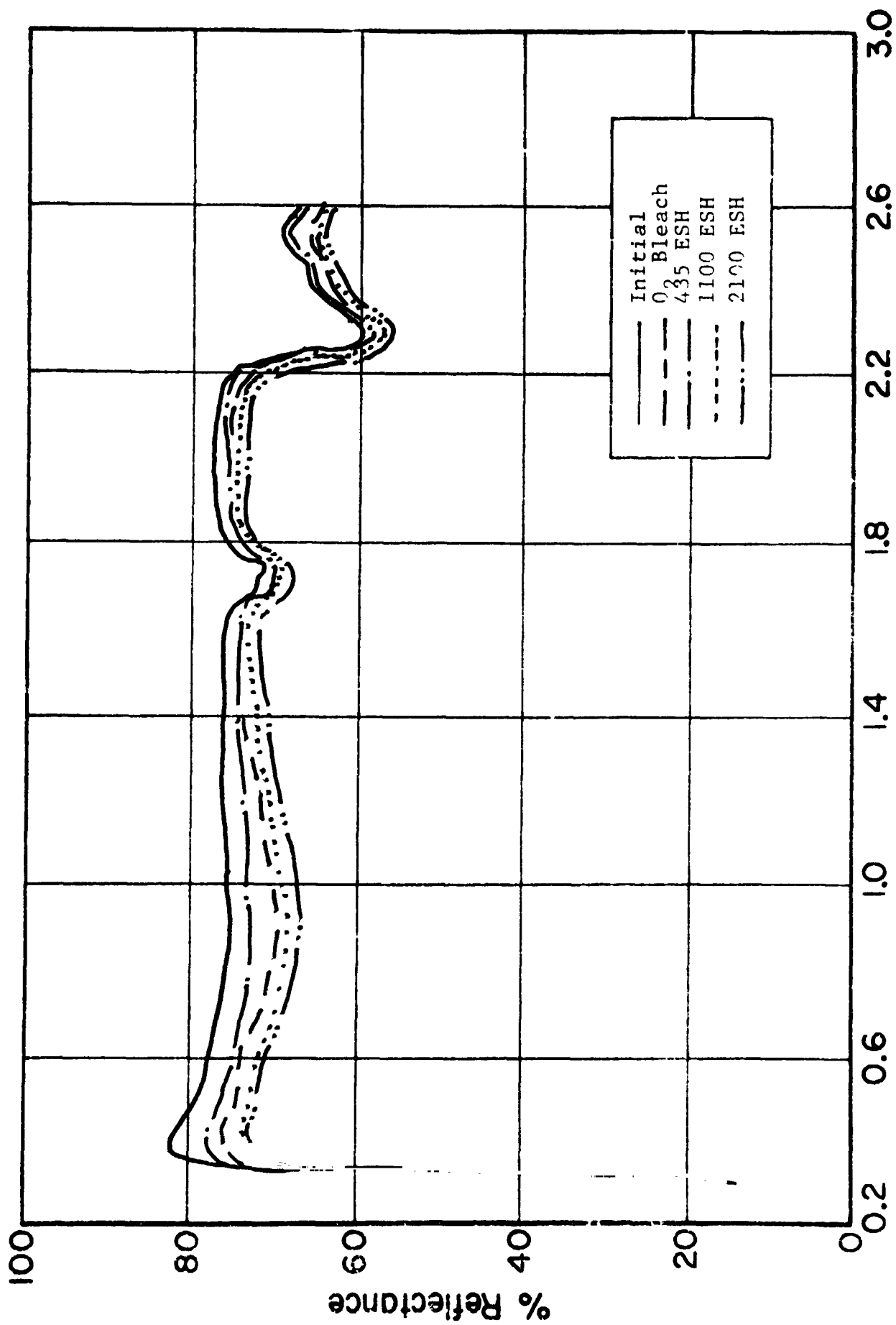


Figure 4.67 REFLECTANCE SPECTRA OF LH-3I(6-12A-10)

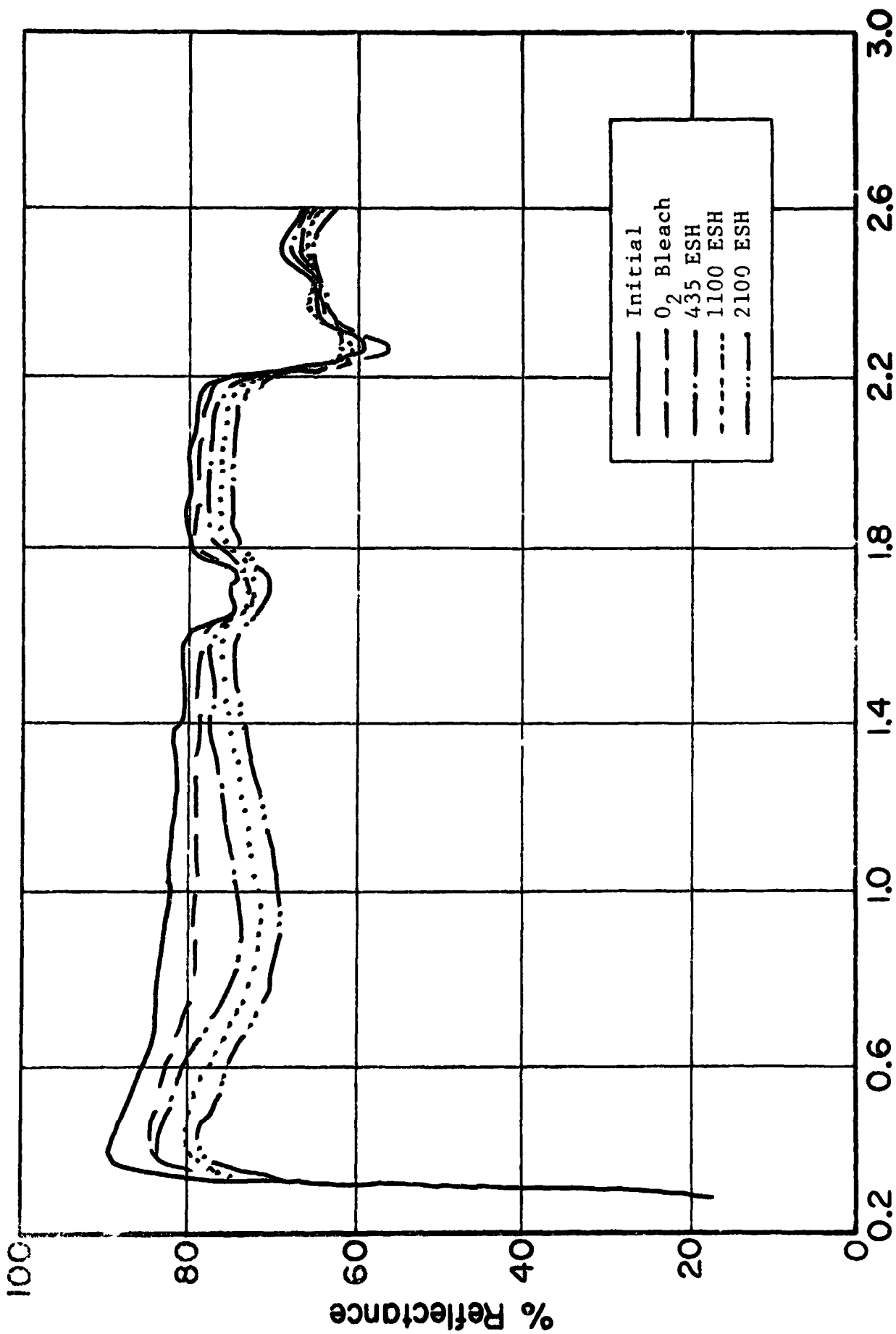


Figure 4.68 REFLECTANCE SPECTRA OF LH-31 (6-14-A-10)

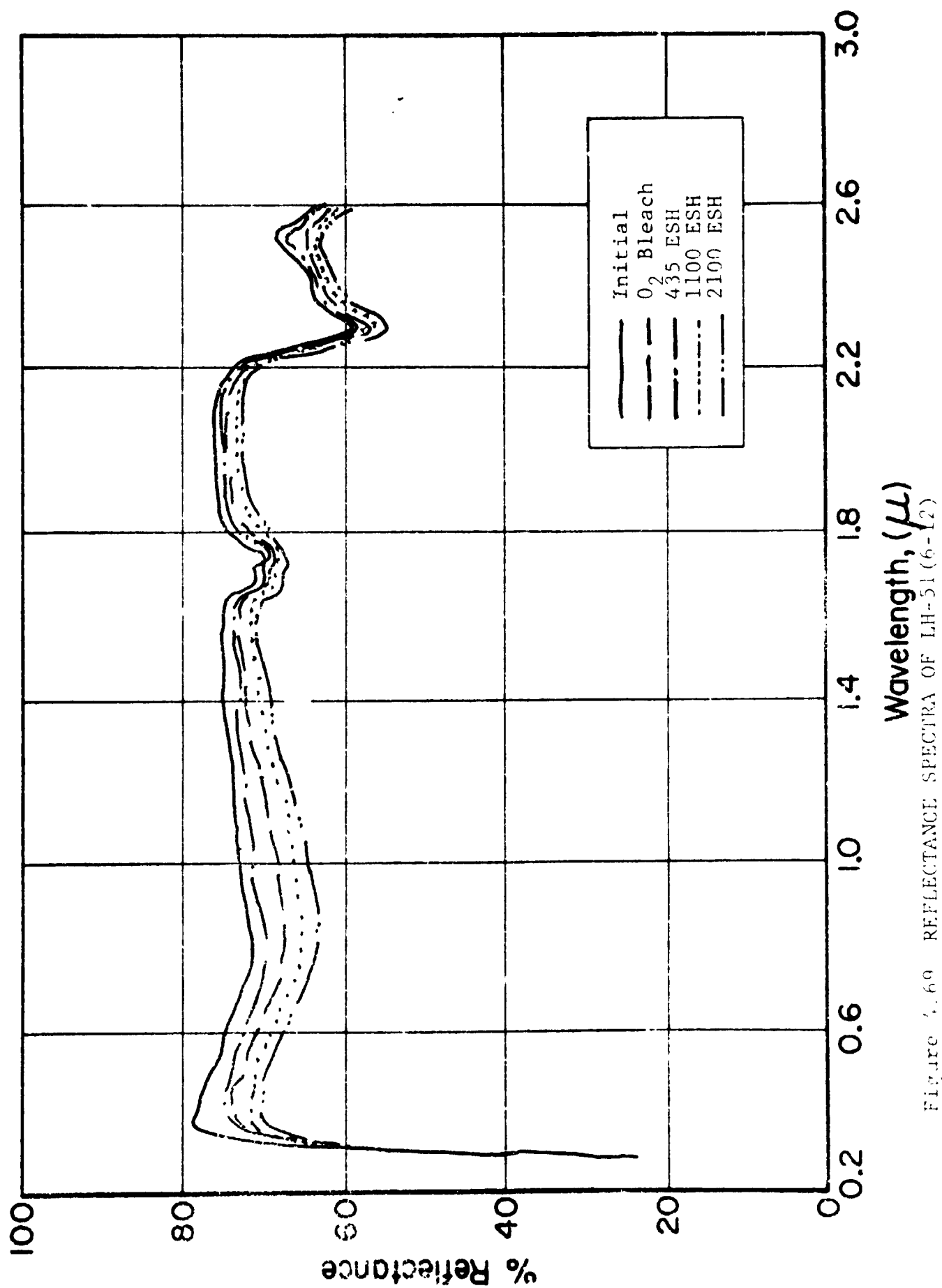


Figure 4.69 REFLECTANCE SPECTRA OF LH-51 (6-12)

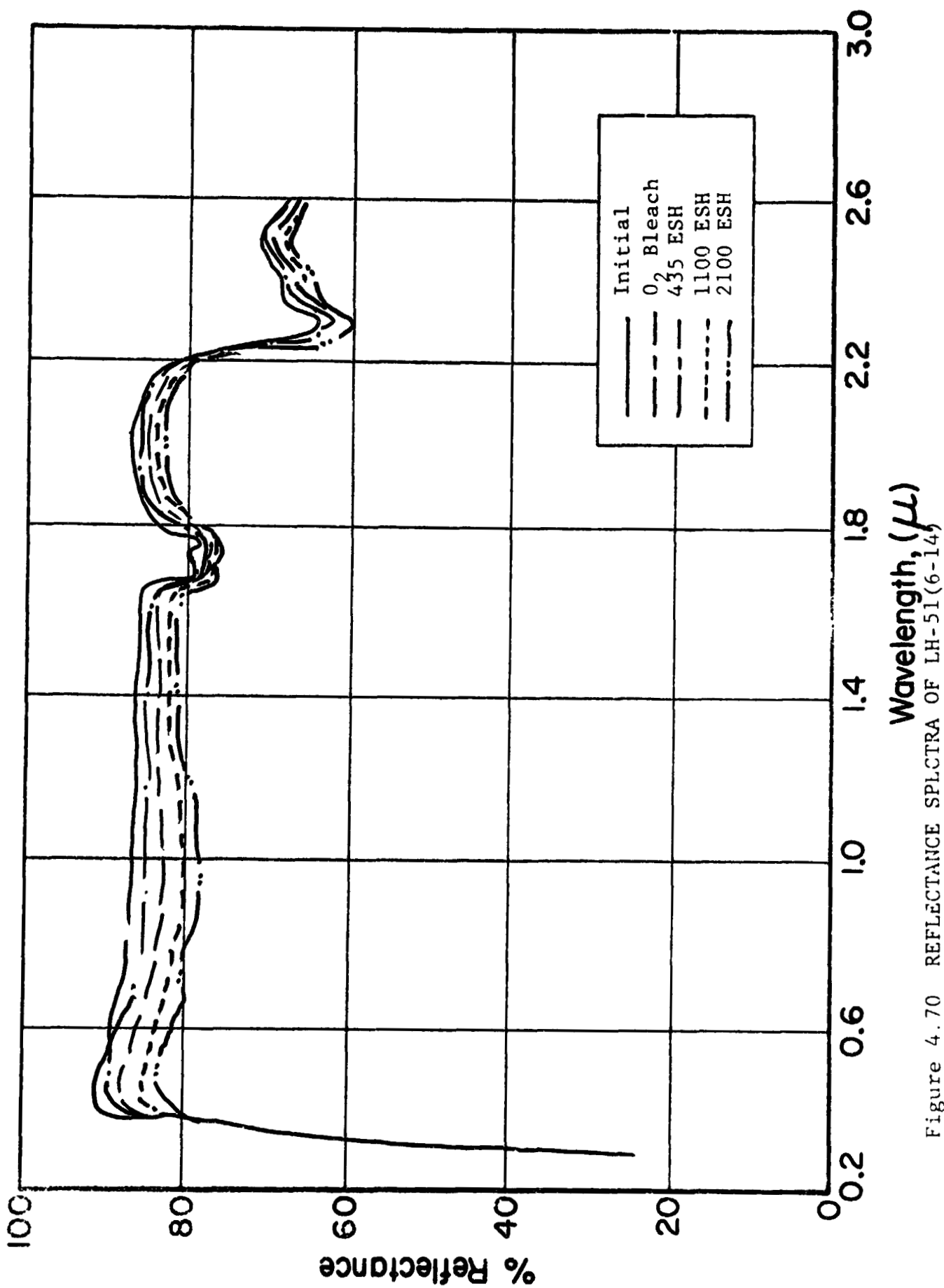


Figure 4.70 REFLECTANCE SPECTRA OF LH-51(6-14)

of the co-precipitate as a result of different hold times. The shorter hold time favors a higher Zn/Ti ratio. This possibility apparently is reduced in its effect by the A-10 treatment.

Baking the paints overnight at 250°F tends to have little effect on $\Delta\alpha_s$; pigments calcined at 1200°C seem to be slightly more stable when baked than those made from 1400°C pigments.

4.5.3 IRIF Test No. I-67

4.5.3.1 Purpose/Description

The purpose of the IRIF-I-67 space simulation test (ref. 4.9) was to determine the effects of calcination temperature and of acid removal of ZnO from Zn_2TiO_4 pigments on the stability of Zn_2TiO_4 /OI-650 paints when subjected to UV irradiation.

4.5.3.2 Sequence

In-situ reflectance measurements (in-vacuo) were made initially, after 540 ESH and after 2050 ESH; after the final in-situ measurements, oxygen was admitted to the system, and spectral reflectance measurements repeated.

4.5.3.3 Test Results

Table 4.12 summarizes the α_s values for this test, while Table 4.13 presents some selected reflectance data. Representative spectra are presented in Figs. 4.70-79. These spectra have been analyzed to determine the trends of several parameters and these have been summarized in Figs. 4.80-83. From these latter figures (graphs) we may deduce correlations of stability (i.e., $\Delta\alpha_s$) with calcination temperature, T_c , of (bleachable) S-band damage with T_c , of stability with ZnO content, and of free ZnO content with T_c .

The data in Figure 4.80 suggest an increased susceptibility of unwashed samples to degradation as a function of calcination temperature. For the A-10 (acid-washed and re-calcined) samples, this trend is reversed.

Table 4-12

SOLAR ABSORPTANCE VALUES, IRIF TEST I-67

Pigment Material*	Solar Absorptance Values			
	Initial	840 ESH	2050 ESH	O ₂ Bleach
LH-52(6-9) (pwdr)	.156	.168	.173	.163
LH-52(6-9)	.287	.332	.370	.311
LH-52(6-14)	.250	.330	.370	.298
LH-52(6-14-A-10)	.309	.338	.364	.327
LH-53(6-11)	.220	.254	.271	.234
LH-53(6-11-A-10)	.286	.329	.351	.307
LH-53(6-12)	.262	.311	.325	.281
LH-53(6-12-A-10)	.259	.299	.330	.280
LH-53(6-13)	.249	.315	.354	.290
LH-53(6-13-A-10)	.304	.328	.352	.323
LH-22(9)	.24	.26	.28	.25
D-260** (pwdr)	.14	.16	.17	.16

*Unless designated "pwdr" (powder) all samples are COP Zn₂TiO₄/OI-650 Paints.

**Zn₂TiO₄, Powder coating; material obtained from Tektronix, Inc., - Solid State Reaction.

Table 4-13

SELECTED REFLECTIVE DATA FROM IRIF TEST I-67

Pigment	$\Delta\alpha_s^*$		$\Delta R(\%)$ 900nm	R_{450}/R_{350}^{**}
	Total	Permanent		
LH-53(6-11)	0.051	0.014	9.5	1.47
LH-53(6-11-A-10)	0.065	0.021	11.5	1.09
LH-53(6-12)	0.063	0.019	12.0	1.70
LH-53(6-12-A-10)	0.071	0.021	12.5	1.13
LH-53(6-13)	0.105	0.041	18.0	1.62
LH-53(6-13-A-10)	0.048	0.019	8.0	1.33
LH-52(6-14)	0.120	0.048	21.5	1.85
LH-52(6-14-A-10)	0.055	0.018	9.0	1.73

*Total $\Delta\alpha_s$ refers to the in-vacuo loss; permanent $\Delta\alpha_s$, to loss measured after O₂ admission (and subsequent bleaching).

**Ratio of initial spectral reflectance of 450nm to that at 350nm.

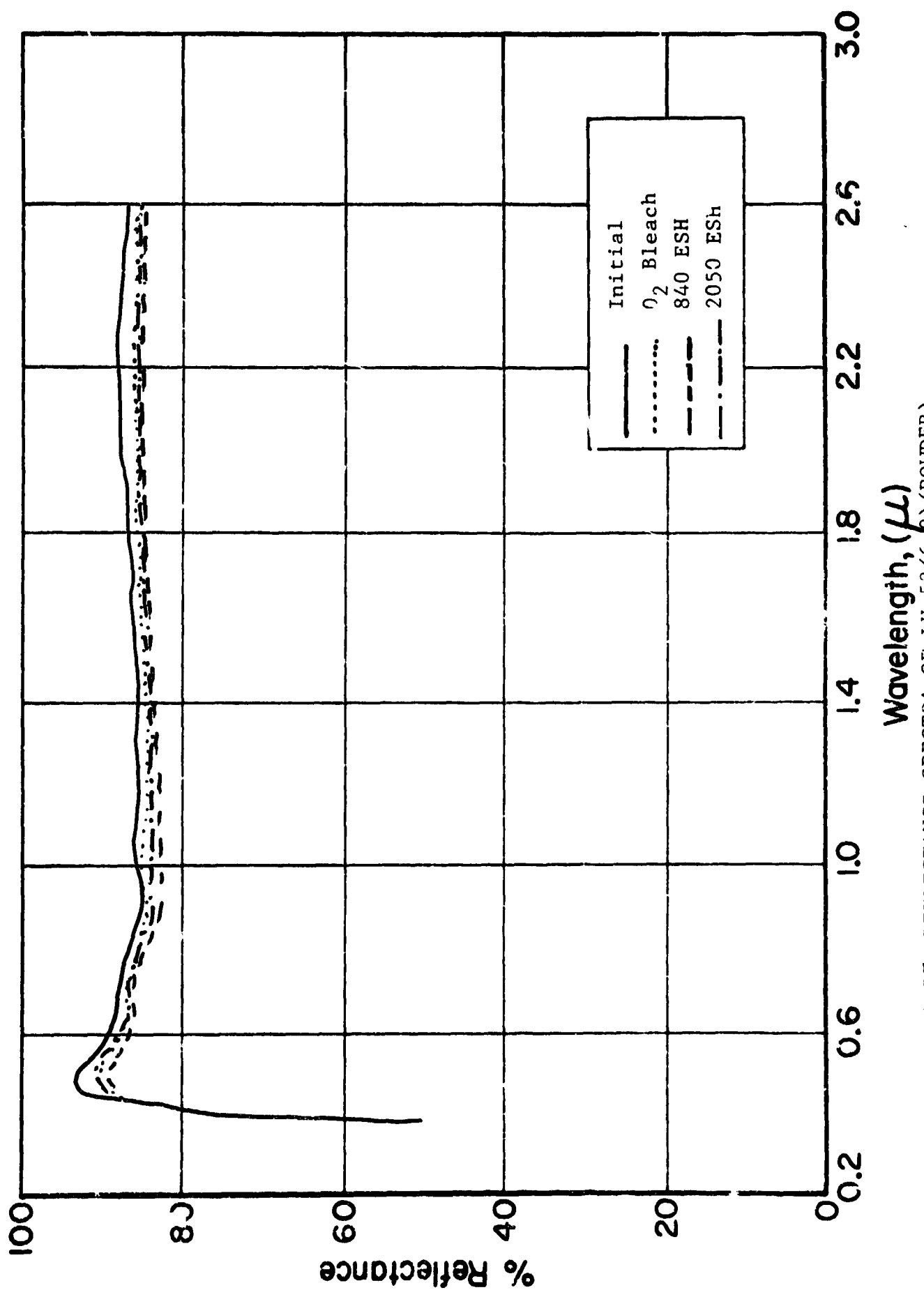


Figure 4.70b REFLECTANCE SPECTRA OF LH-52 (6-9) (POWDER)

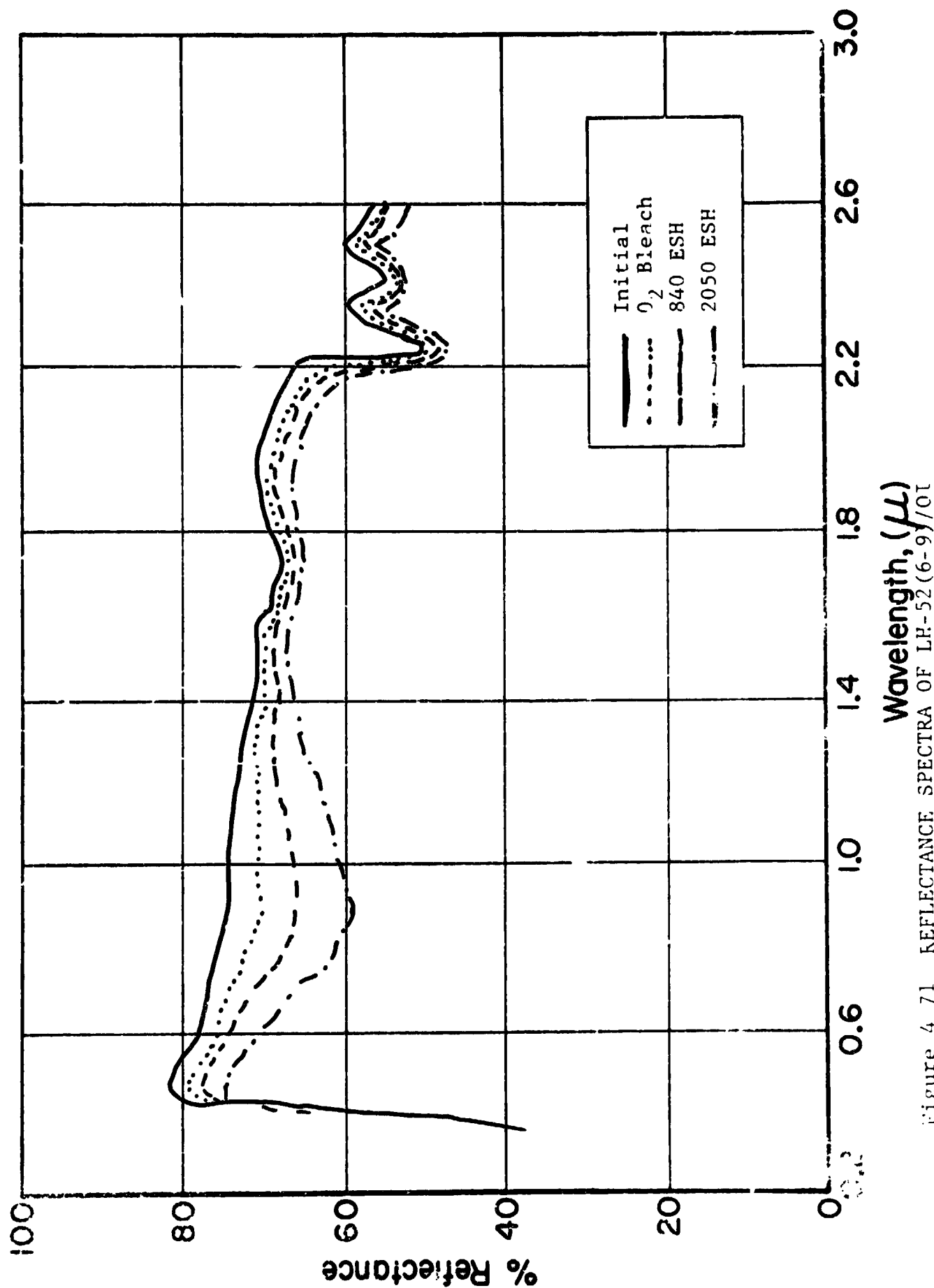


Figure 4 71 REFLECTANCE SPECTRA OF LH-52 (6-9/01)

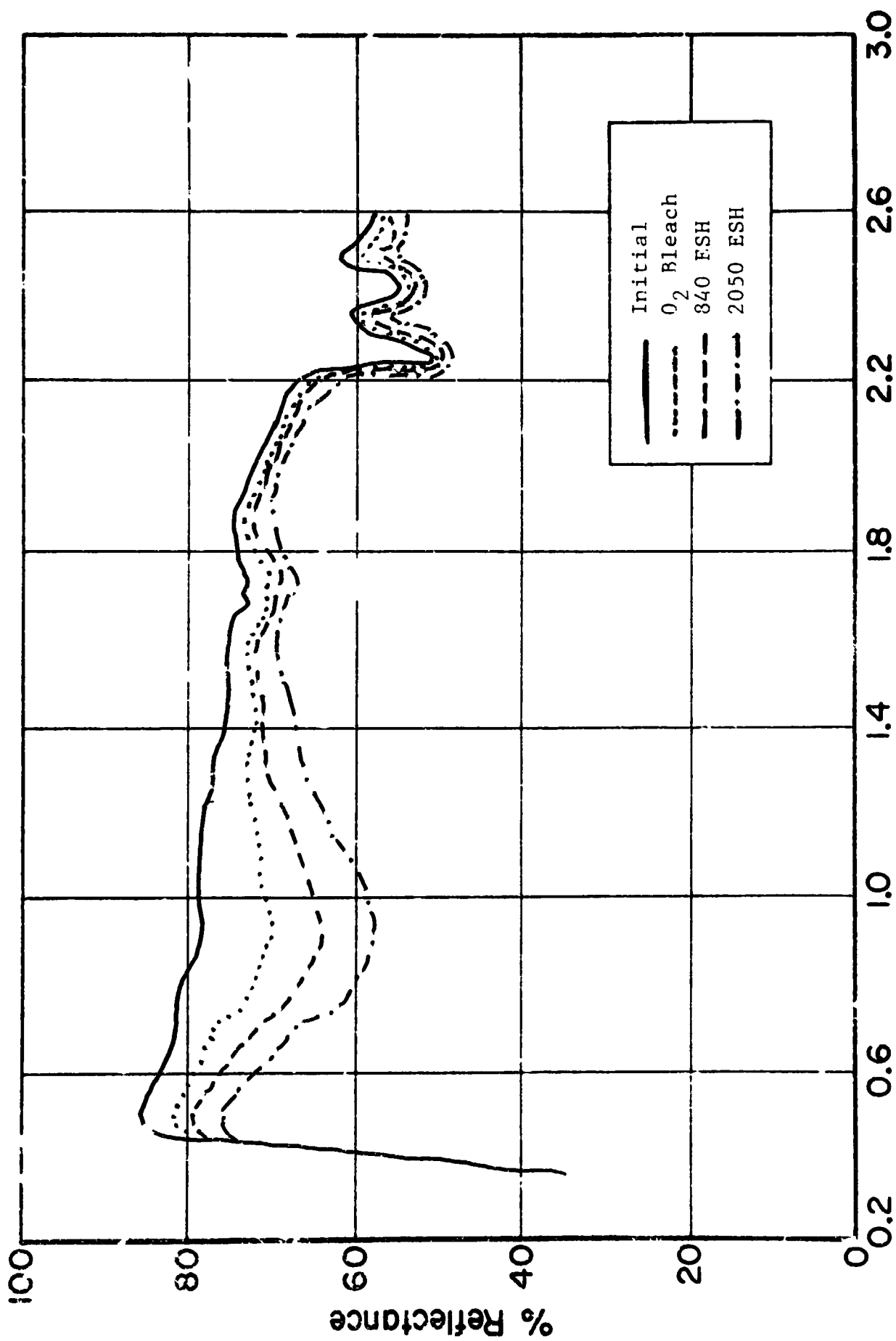


Figure No. 4.72 REFLECTANCE SPECTRA OF LH-52(6-14)/OI

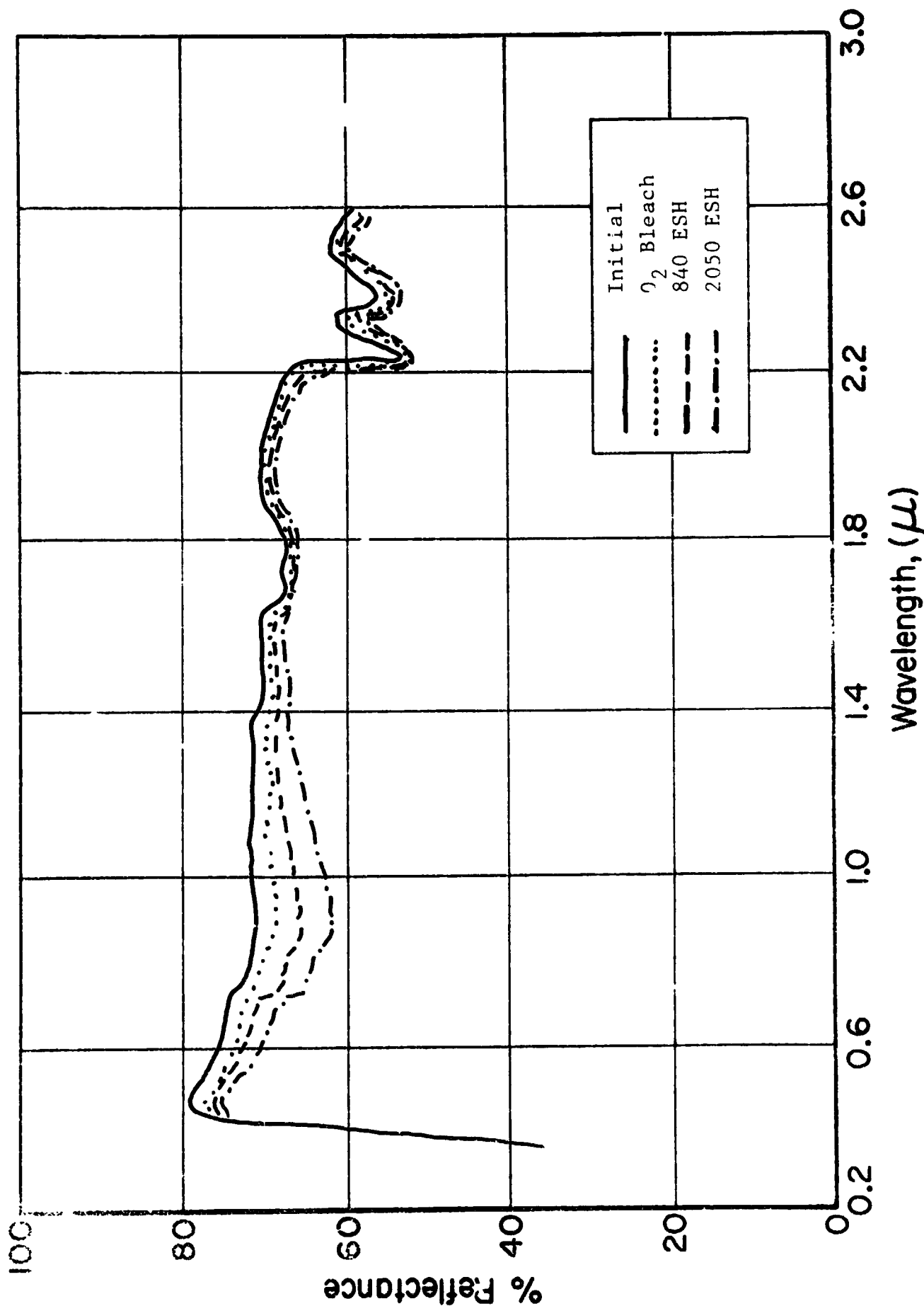


Figure 4.73 REFLECTANCE SPECTRA OF LH-52 (6-14-A-10) / OI

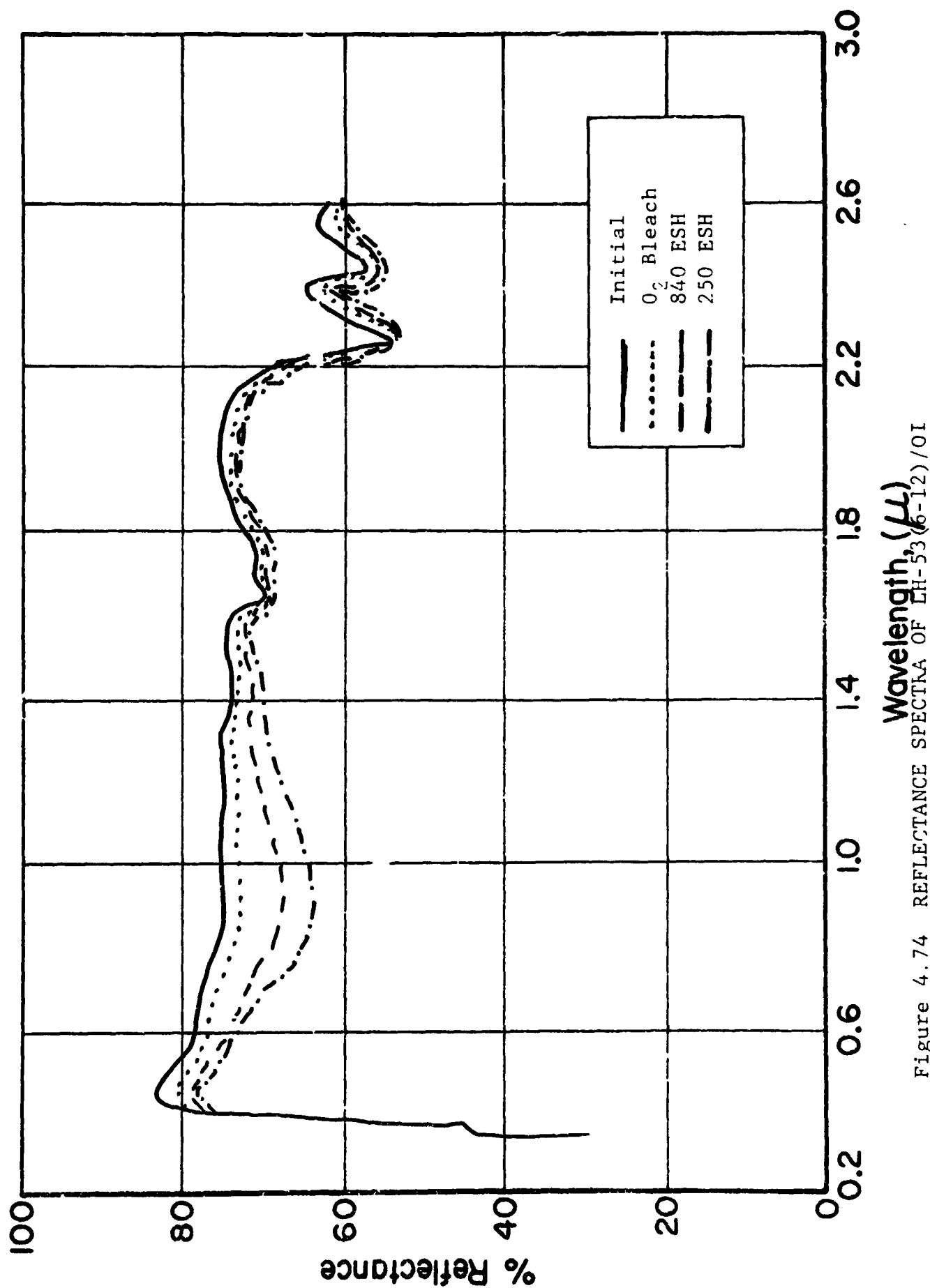


Figure 4.74 REFLECTANCE SPECTRA OF LH-53(6-12)/OI

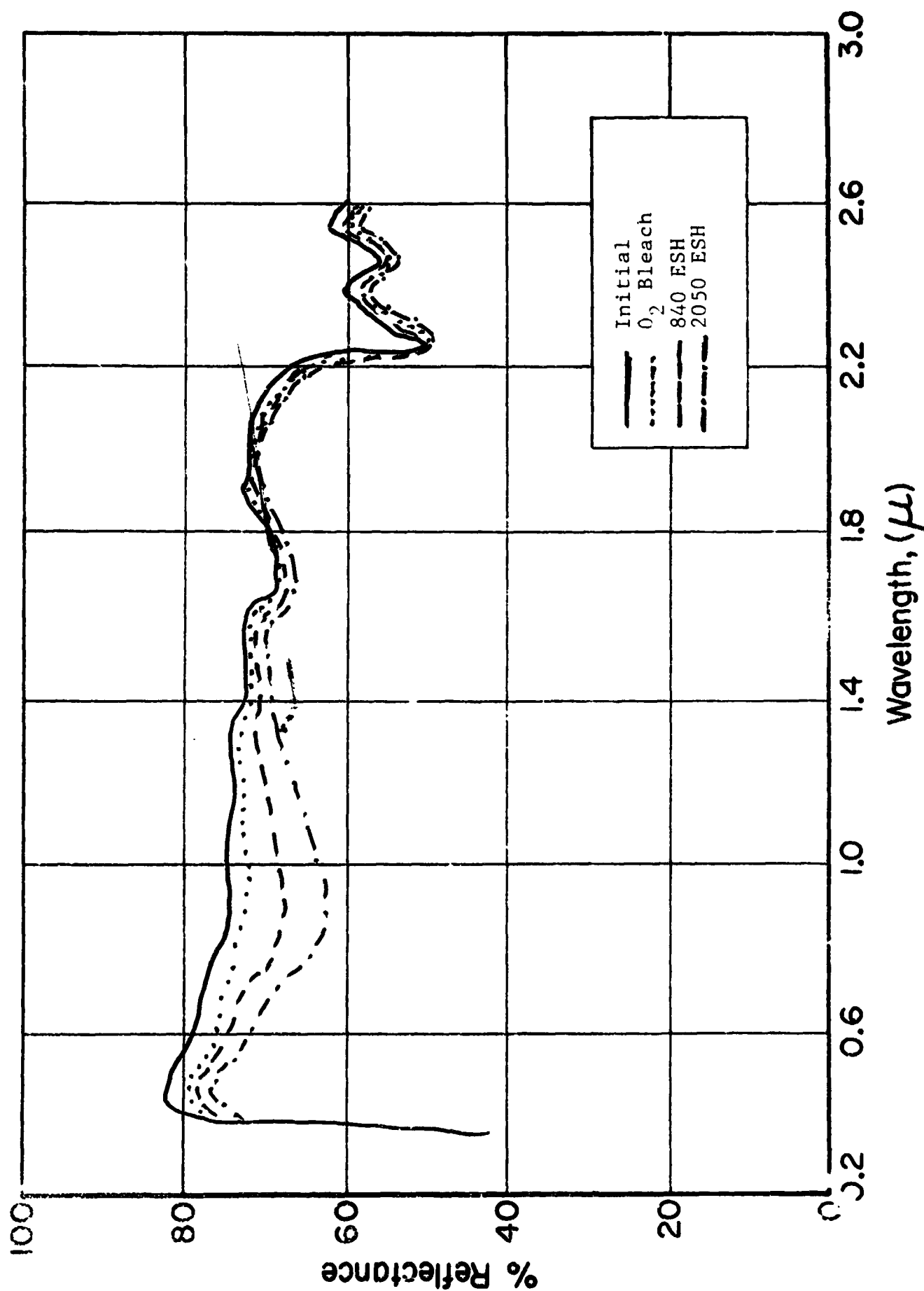


Figure 4.75 REFLECTANCE SPECTRA OF LP-53 (6-12-A-10)/OI

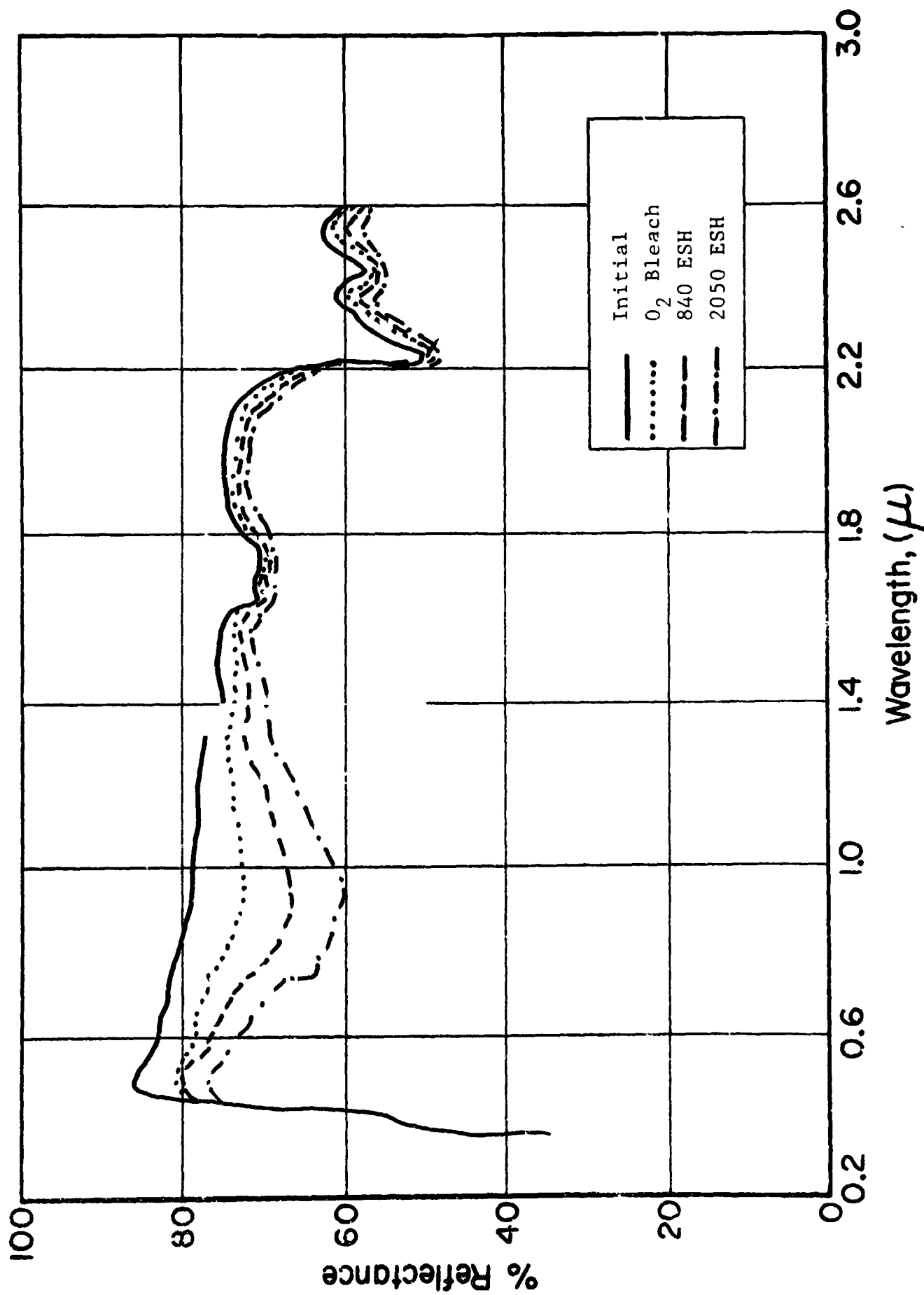


Figure 4.76 REFLECTANCE SPECTRA OF LH-53(6-13)/OI

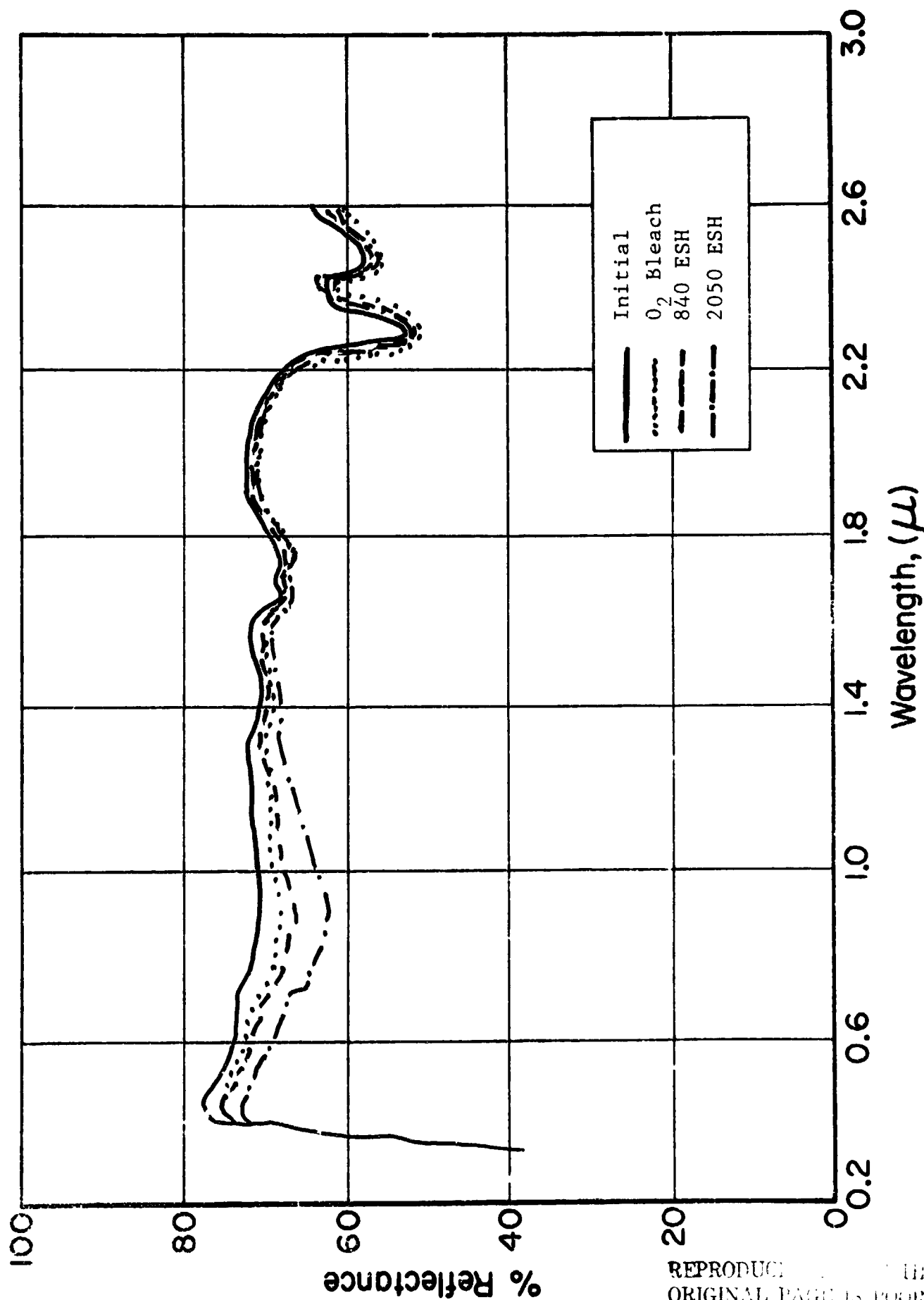
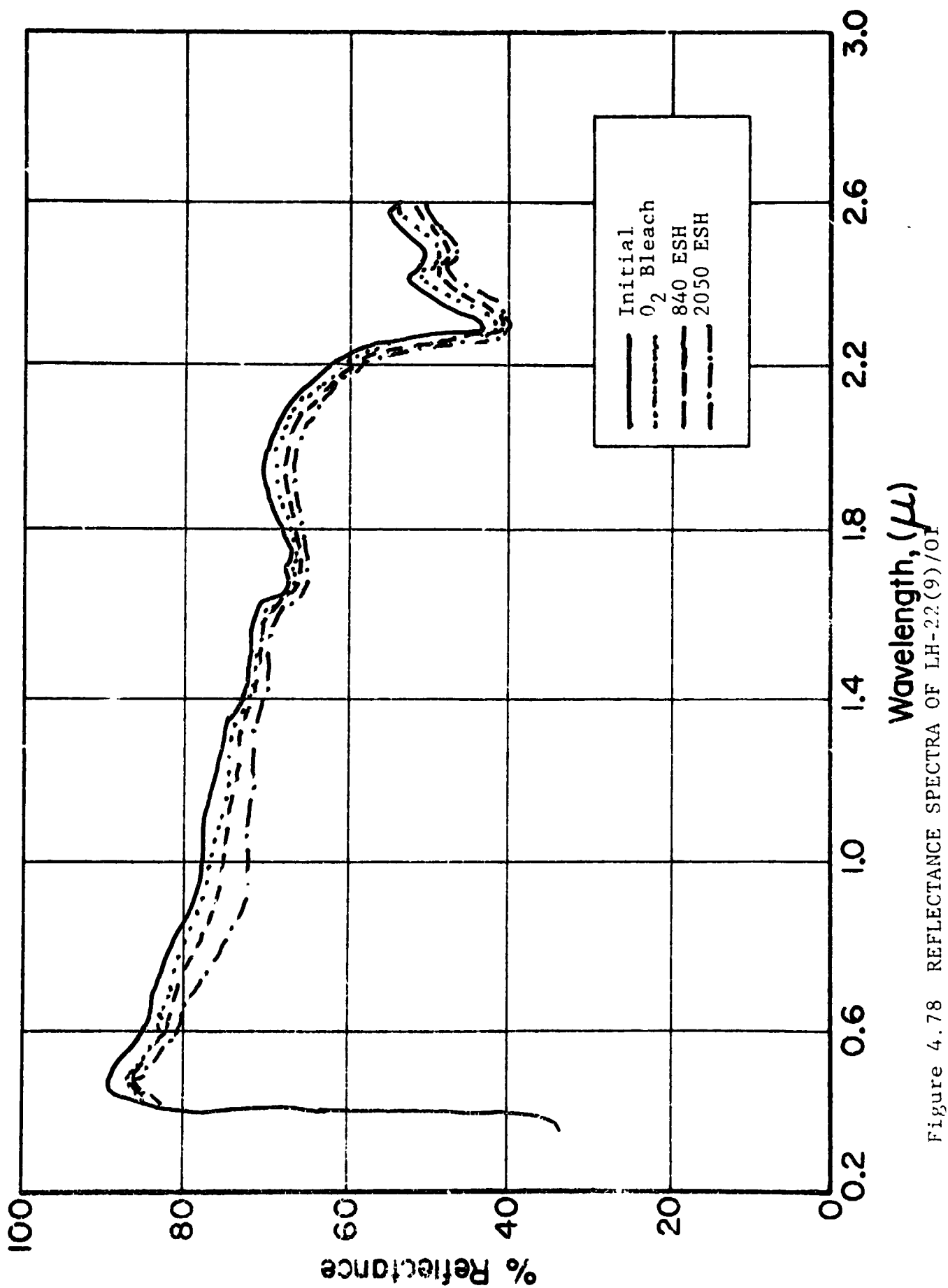


Figure 4.77 REFLECTANCE SPECTRA OF LH-53(6-13-A-10)/OI

REPRODUCED FROM THE
ORIGINAL PAGE IS POOR



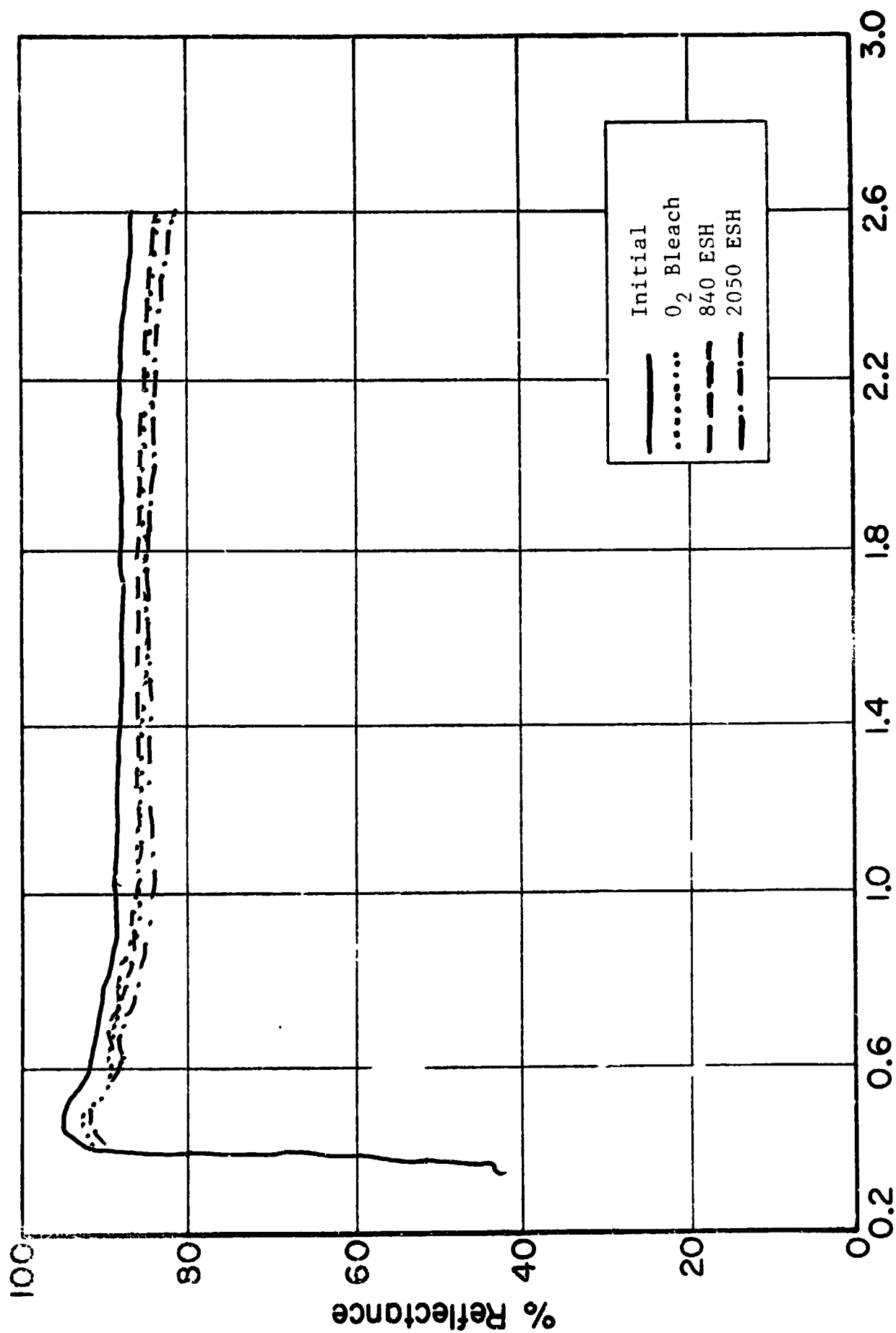


Figure 4.79 REFLECTANCE SPECTRA OF D-260(SS)Zn₂TiO₄ (POWDER)

Quite obviously, as Fig. 4.80 shows, acid leaching removes ZnO from the calcined pigments but with less efficiency at increasing temperatures. The O₂ bleach spectra indicate substantial UV-induced S-band development, which might be minimized by an appropriate encapsulant. As Fig. 4.81 shows, the same general trends are apparent in S-band damage.

Figure 4.82 shows the relationship between the total $\Delta\alpha_s$ of a paint and the ratio of R_{450}/R_{350} , the latter ratio being directly indicative of free ZnO content. This figure also emphasizes the value of acid-washing. However, the curves for untreated pigments show a break corresponding to the upper calcination temperature ranges. The important point is that acid washing does increase stability of COP Zn₂TiO₄ pigments - up to a point!

In Figure 4.83 we show the effect of calcination temperature on the ratio R_{450}/R_{350} , whose log is directly proportional to the free ZnO content. The data here strongly confirm our earlier observations of the importance of acid washing. In addition, the beneficial effect of acid washing is seen here also to exist only in the lower temperature range, (i.e., <1200°C); the free ZnO content increases very greatly with increasing temperature.

Figures 4.80-83 emphatically display the distinct differences in the stability of pigments calcined at temperatures above 1200°C and those prepared at and below 1200°C.

4.5.4 IRIF Test I-68

4.5.4.1 Purpose/Description

IRIF Test I-68 (ref. 4.10) was conducted to investigate the properties and performance of Zn₂TiO₄ and two commercial pigments, all produced by Tektronix, Inc., Beaverton, Ore. A major concern in this test was whether (SS) Zn₂TiO₄ produced

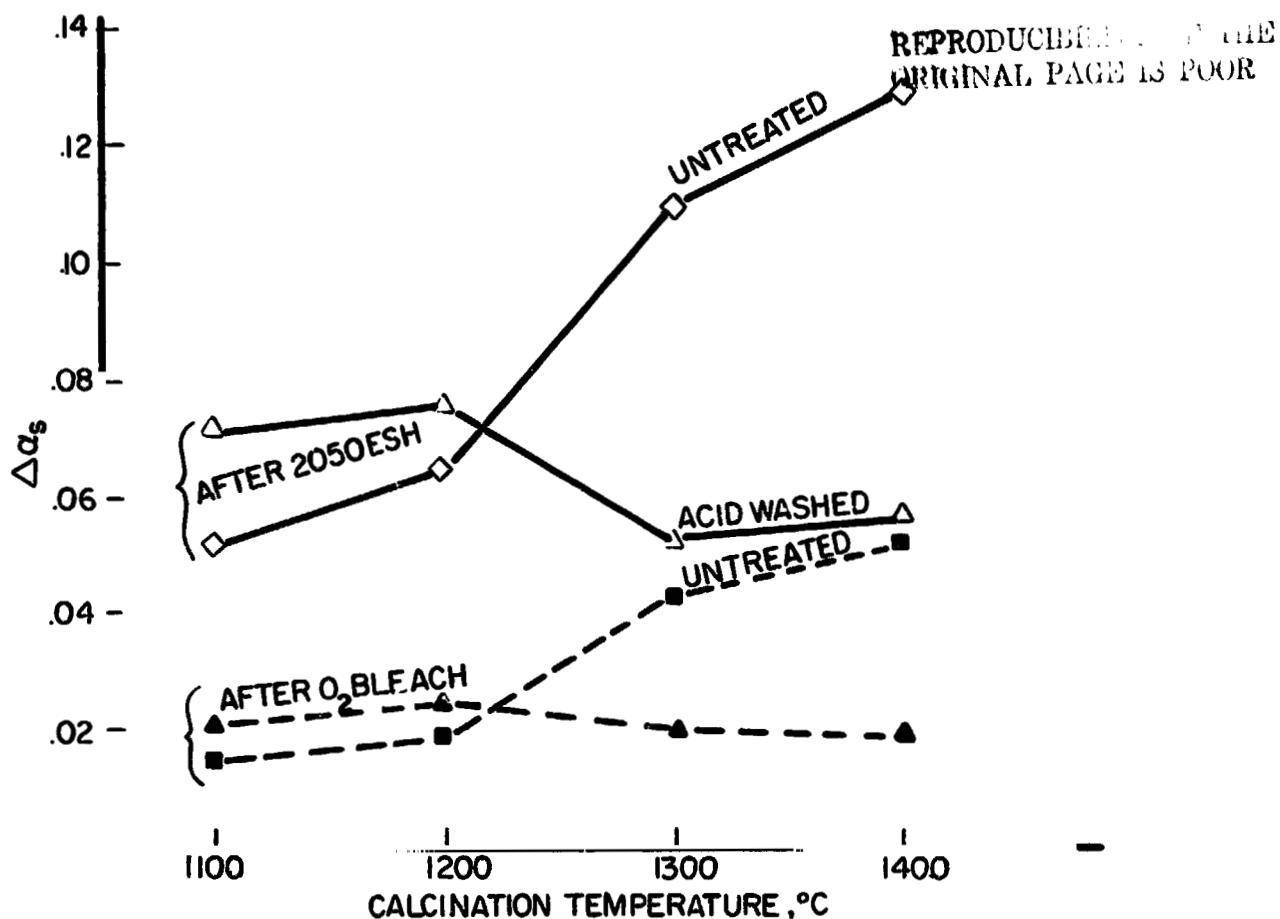


Fig. 4.80 EFFECT OF CALCINATION TEMPERATURE ON Zn_2TiO_4 STABILITY: UNTREATED VS ACETIC ACID WASHED PIGMENTS.

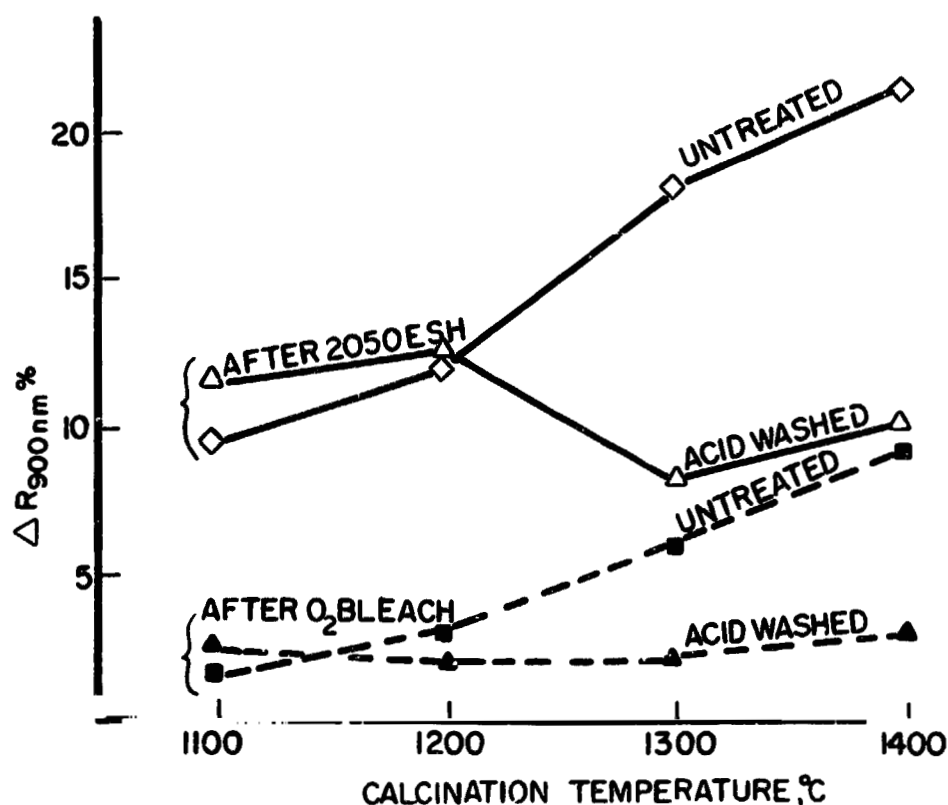


Fig. 4.87 EFFECT OF CALCINATION TEMPERATURE ON Zn_2TiO_4 : REFLECTANCE CHANGE AT 900 nm

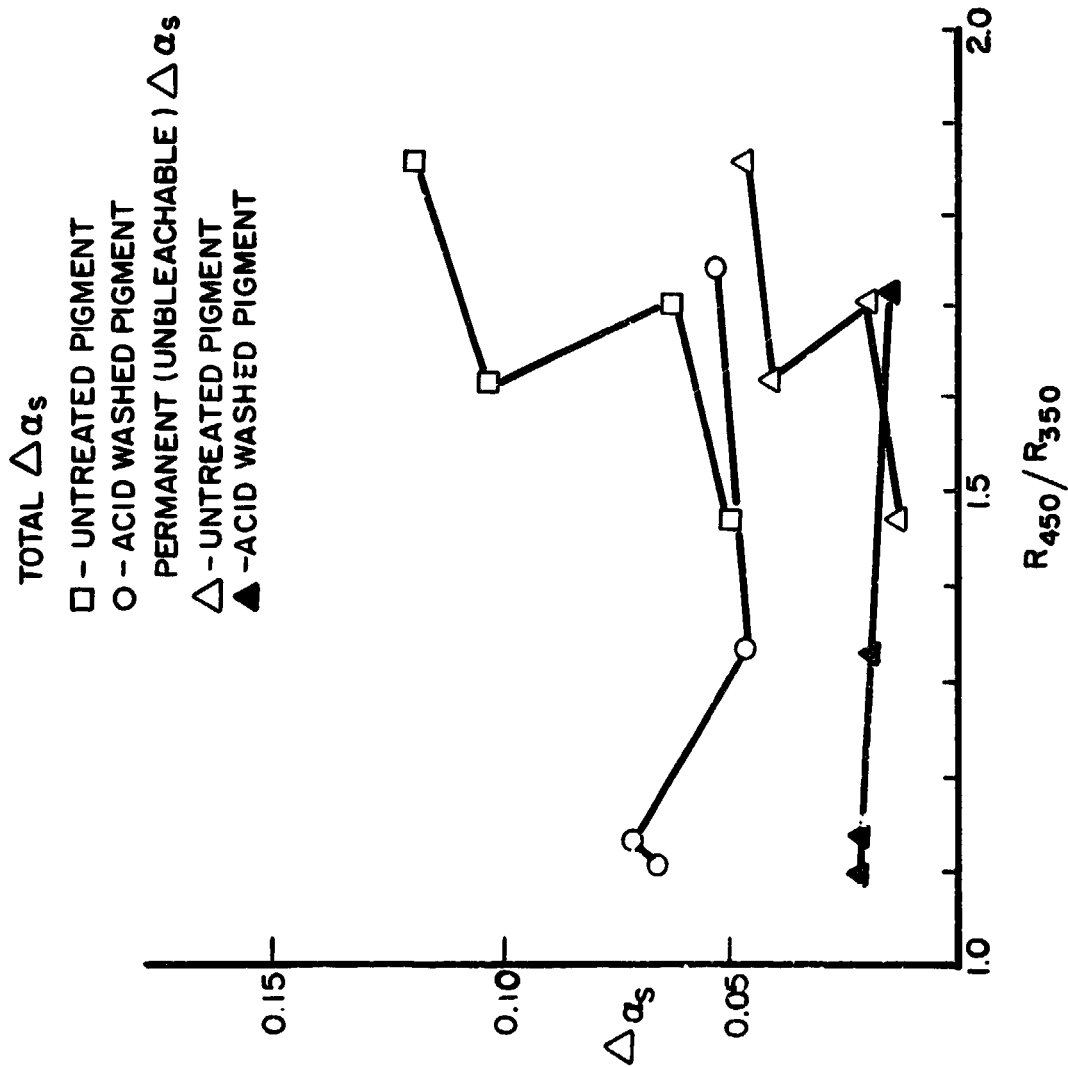


Fig. 4.82 EFFECT OF FREE ZnO ON STABILITY OF $Zn_2TiO_4/01$ 650 PAINTS

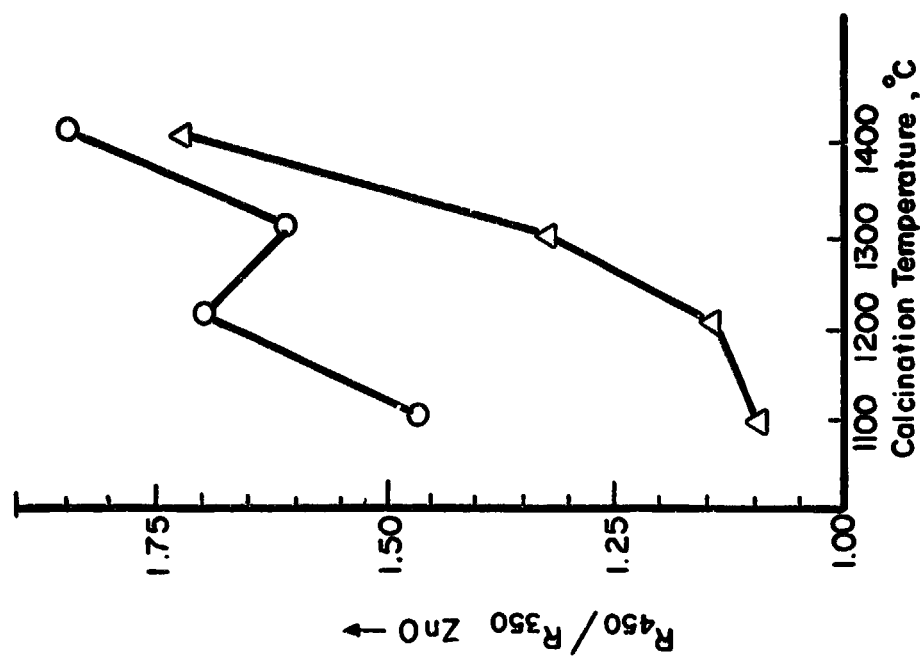


Fig. 4.83 FREE ZnO CONTENT OF Zn_2TiO_4 PIGMENT VS CALCINATION TEMPERATURE

using large scale manufacturing equipment would be stable. Two of these pigments, both zinc orthosilicates are in routine production at Tektronix. For further descriptions of these pigments, see par. 4.5.5). For reference purposes, samples of zinc oxide and of anatase titania, the precursors of Zn_2TiO_4 in the SS process, were also irradiated along with a sample of rutile titania. All samples were irradiated as powders.

4.5.4.2 Sequence

Spectral hemispherical reflectance measurements were made of each sample prior to irradiation, after UV radiation exposures of 1340 ESH and 2570 ESH; after irradiation, the IRIF was back-filled to 760 Torr with oxygen and reflectance measurements were again made of each sample.

4.5.4.3 Test Results

The sample descriptions and test results are summarized in Table 4.14. The Tektronix Zn_2TiO_4 pigments obviously are quite stable. The ZnO and TiO_2 pigments were irradiated for comparison, and, as expected, degrade moderately. (like many other surface-active pigments, they degrade severely in an organic binder). The zinc orthosilicate pigments are CRT phosphors manufactured by Tektronix, one of which is intrinsically doped with manganese to improve its luminescence properties. Both are relatively unstable.

The performance of the Zn_2TiO_4 pigments in OI-650G vehicles has already been determined and reported (Ref. 4.12). Their performance here however, especially the bleaching behavior, confirms that these pigments are inherently very stable.

4.5.4.4 Analyses

Figures 4.84-88 show the reflectance spectra of Zn_2TiO_4 and Zn_2SiO_4 (zinc orthosilicate) samples prepared by Tektronix. The spectra, (not shown) of a basic mixture of 2.05:1 ZnO/TiO_2 (designated T-1), which was spray dried at 250°C and not further

Table 4-14

IRIF TEST I-68
TEST RESULTS

Sample Description	Solar Absorptance Values				
	Initial	1340 ESH	2570 ESH	$\Delta\alpha_s$	O ₂ Bleach
Zn ₂ TiO ₄ (unfired)* (T-1)	.236	.268	.294	.058	.269
Zn ₂ TiO ₄ (900°C/8hr)* (T-2)	.150	.162	.183	.033	.176
Zn ₂ TiO ₄ (1200°C/1 hr)* (T-3)	.225	.245	.250	.025	.244
Zn ₂ TiO ₄ (1250°C/24hr)* (T-4)	.268	.282	.285	.017	.300
Zn ₂ SiO ₄ **	.229	.252	.272	.043	.247
Zn ₂ SiO ₄ :Mn**	.159	.176	.209	.050	.214
ZnO (N.J. Zinc SP-500)	.259	.258	.282	.033	.264
a-TiO ₂ (DuPont FF)	.206	.289	.356	.150	.253
r-TiO ₂ (DuPont R-900)	.286	.321	.341	.055	.310

*Tektronix, Inc. Zn₂TiO₄

**Tektronix, Inc. phosphors

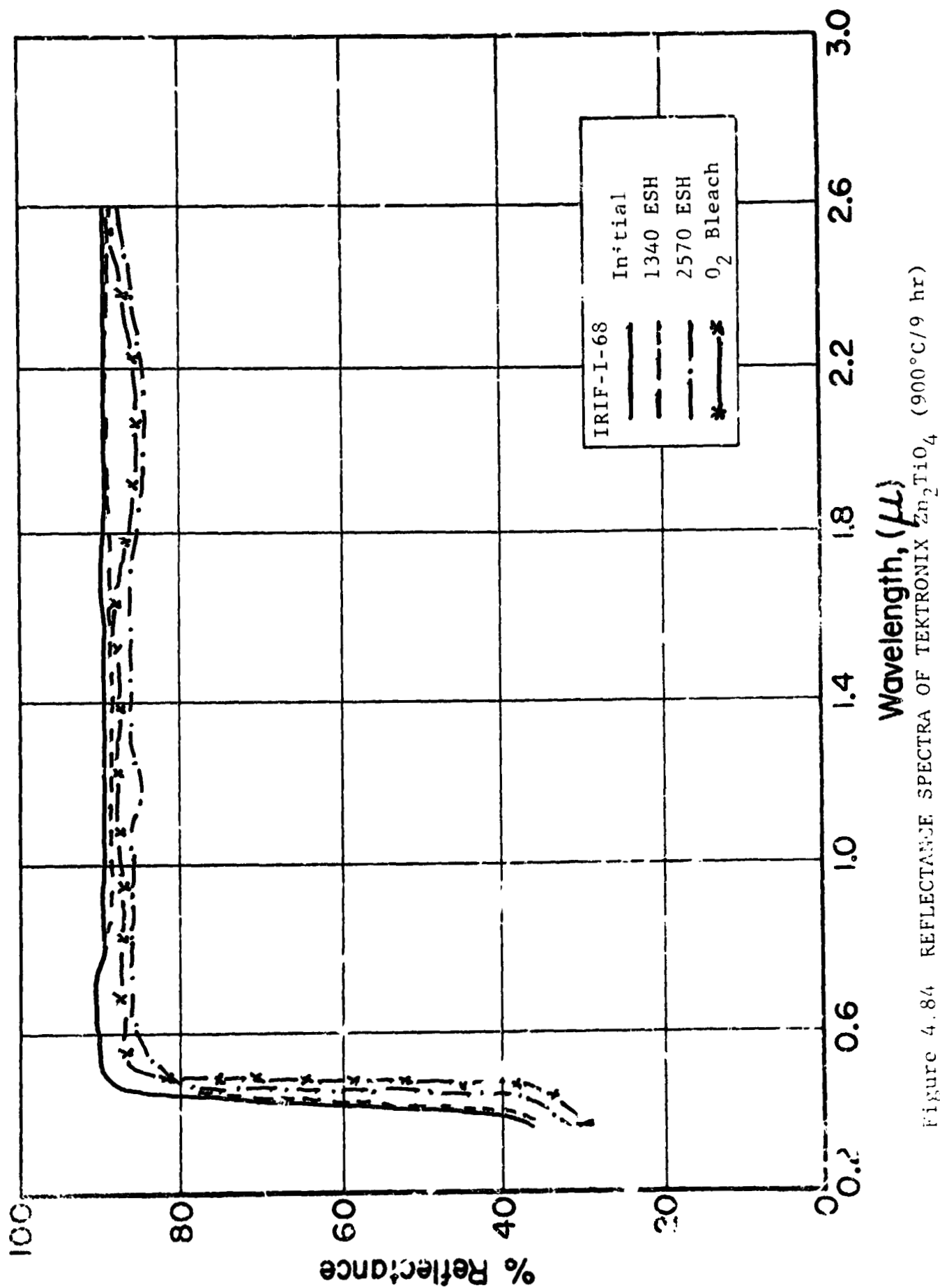


Figure 4.84 REFLECTANCE SPECTRA OF TEKTRONIX Zn_2TiO_4 ($900^\circ\text{C}/9\text{ hr}$)

24

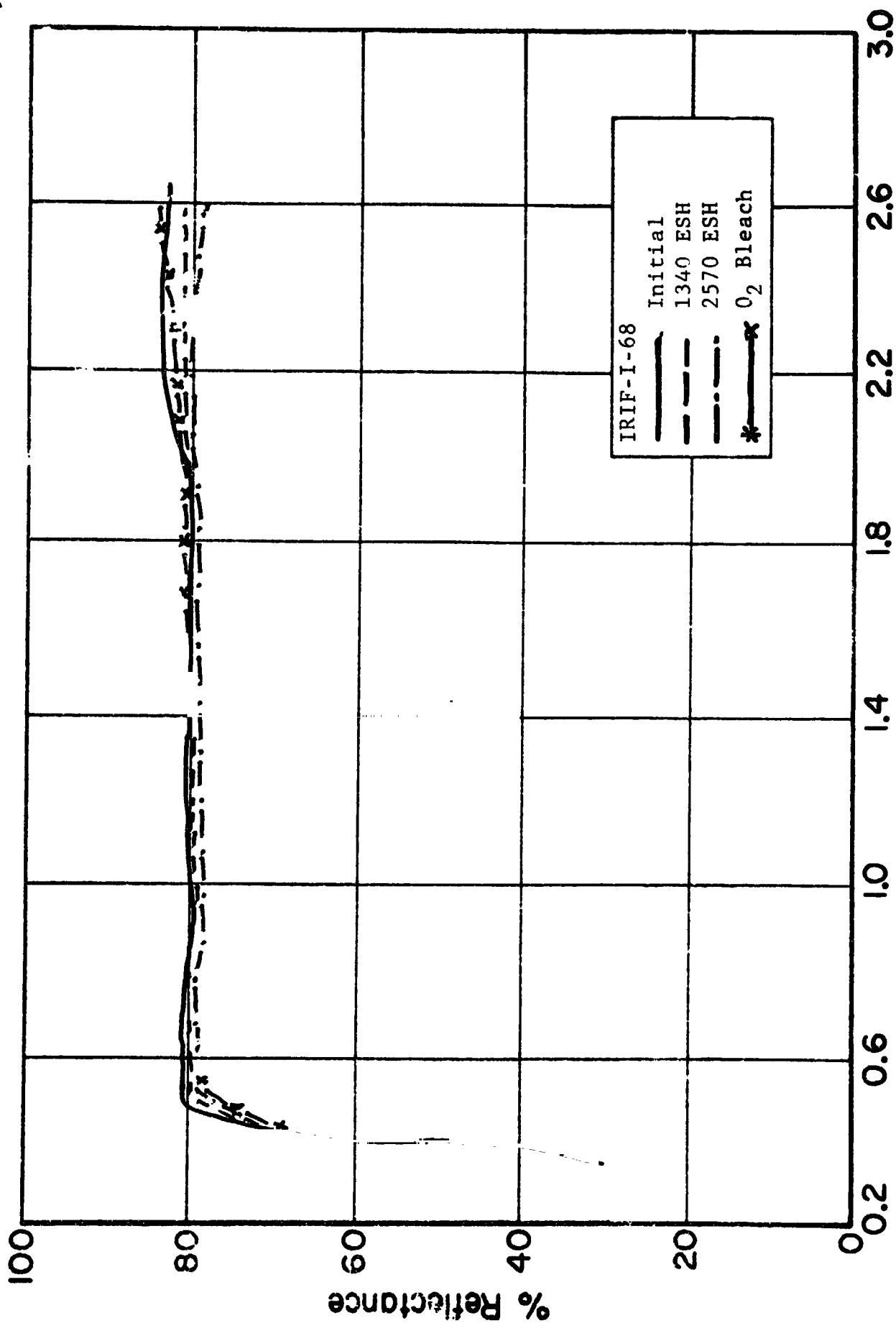


Figure 4.85 REFLECTANCE SPECTRA OF TEKTRONIX Zn_2TiO_4 (1200°C/1 hr)

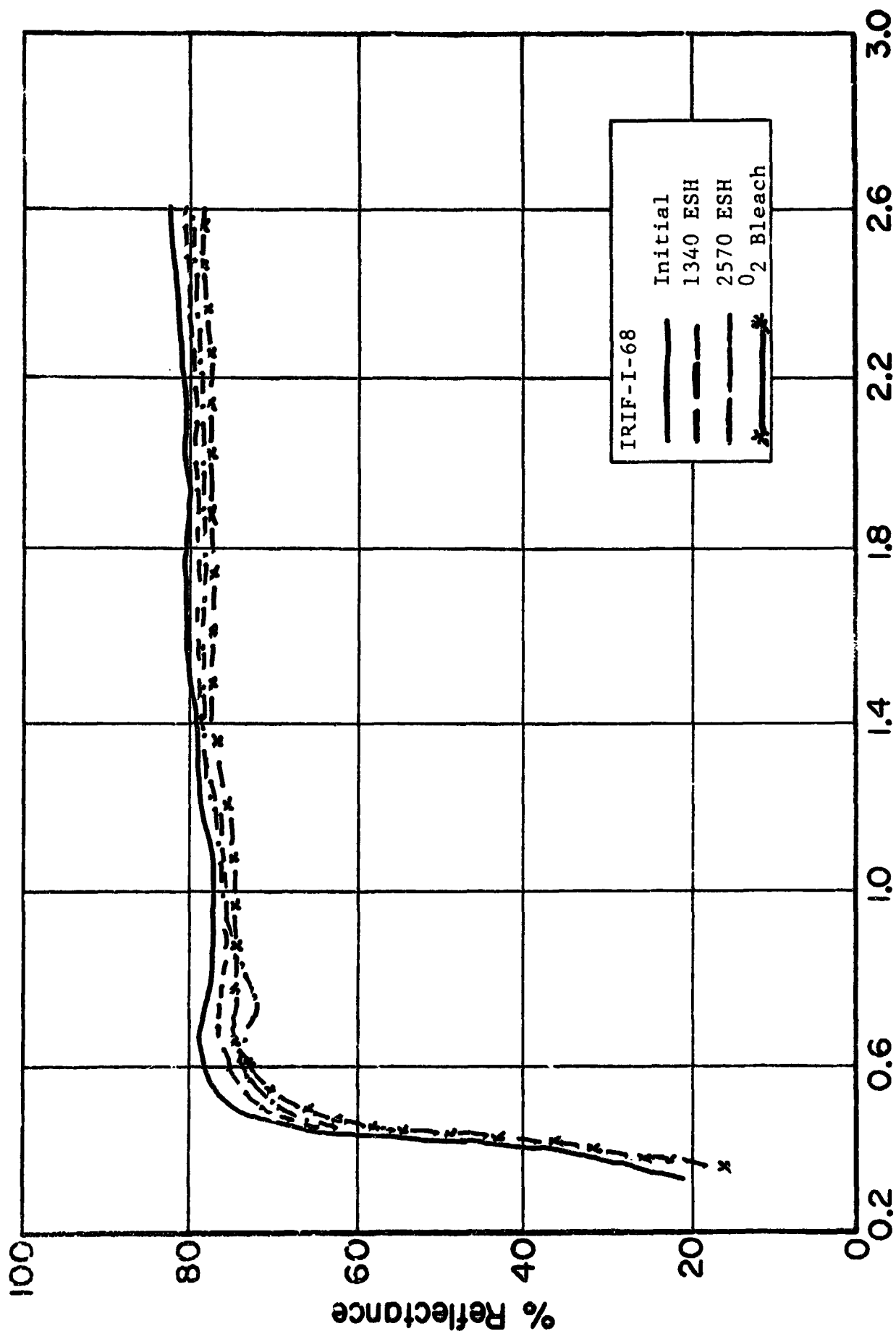


Figure 4.86 REFLECTANCE SPECTRA OF TEKTRONIX Zn_2TiO_4 (1250°C/24 hr)

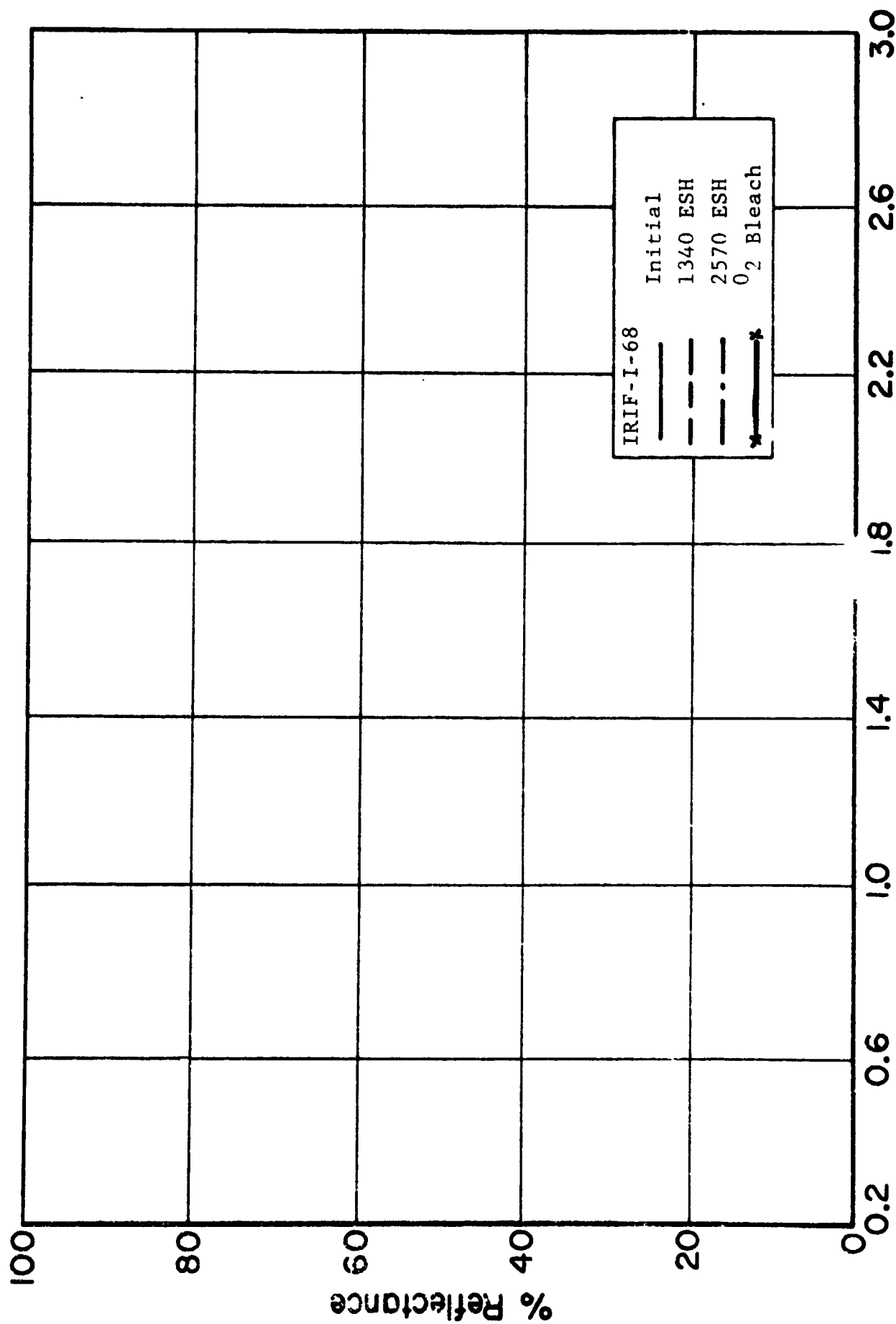


Figure 4.86b REFLECTANCE SPECTRA OF TEKTRONIX Zn_2TiO_4 (1250°C/24 hr)

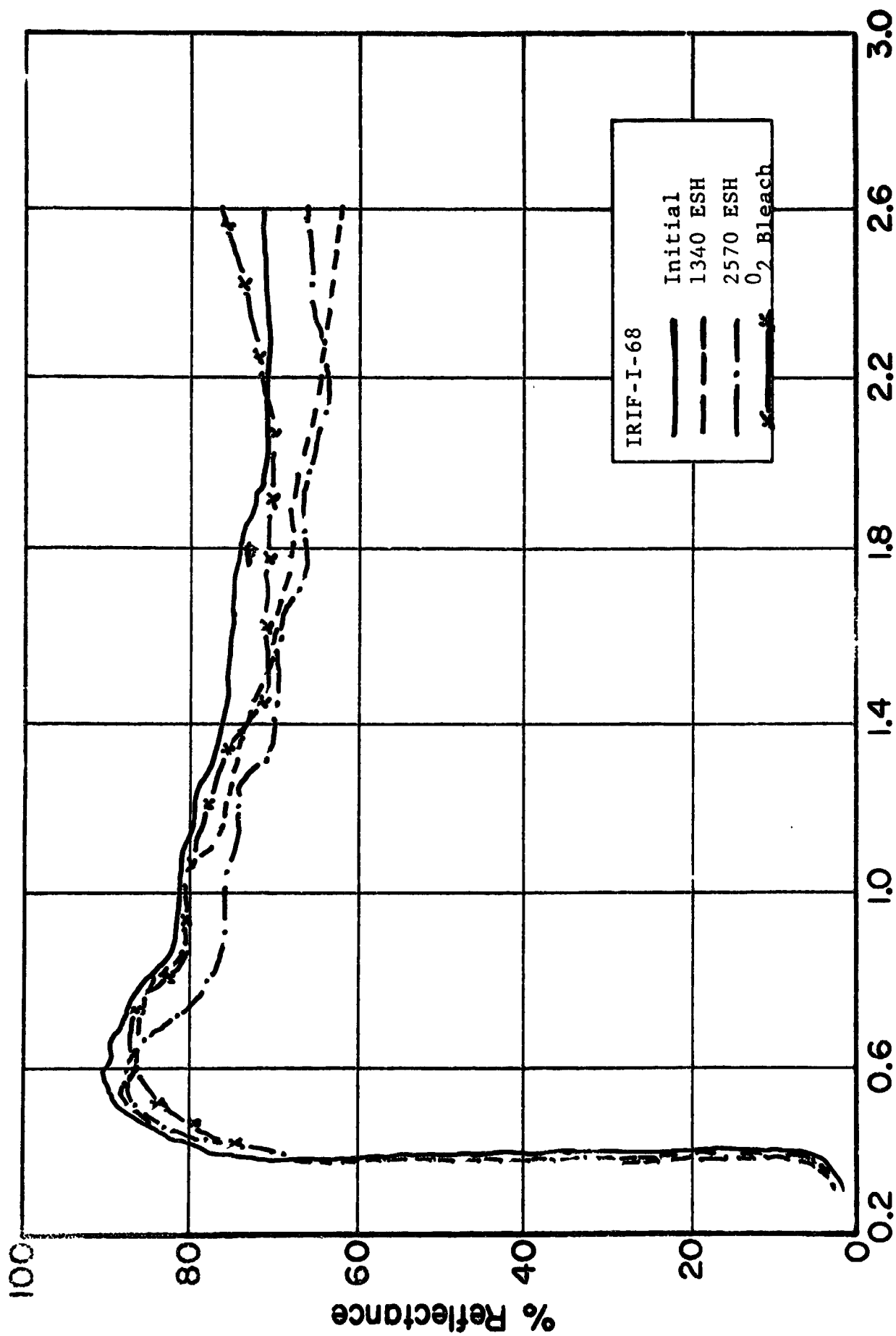


Figure 4.87 REFLECTANCE SPECTRA OF TEKTRONIX Zn_2SiO_4

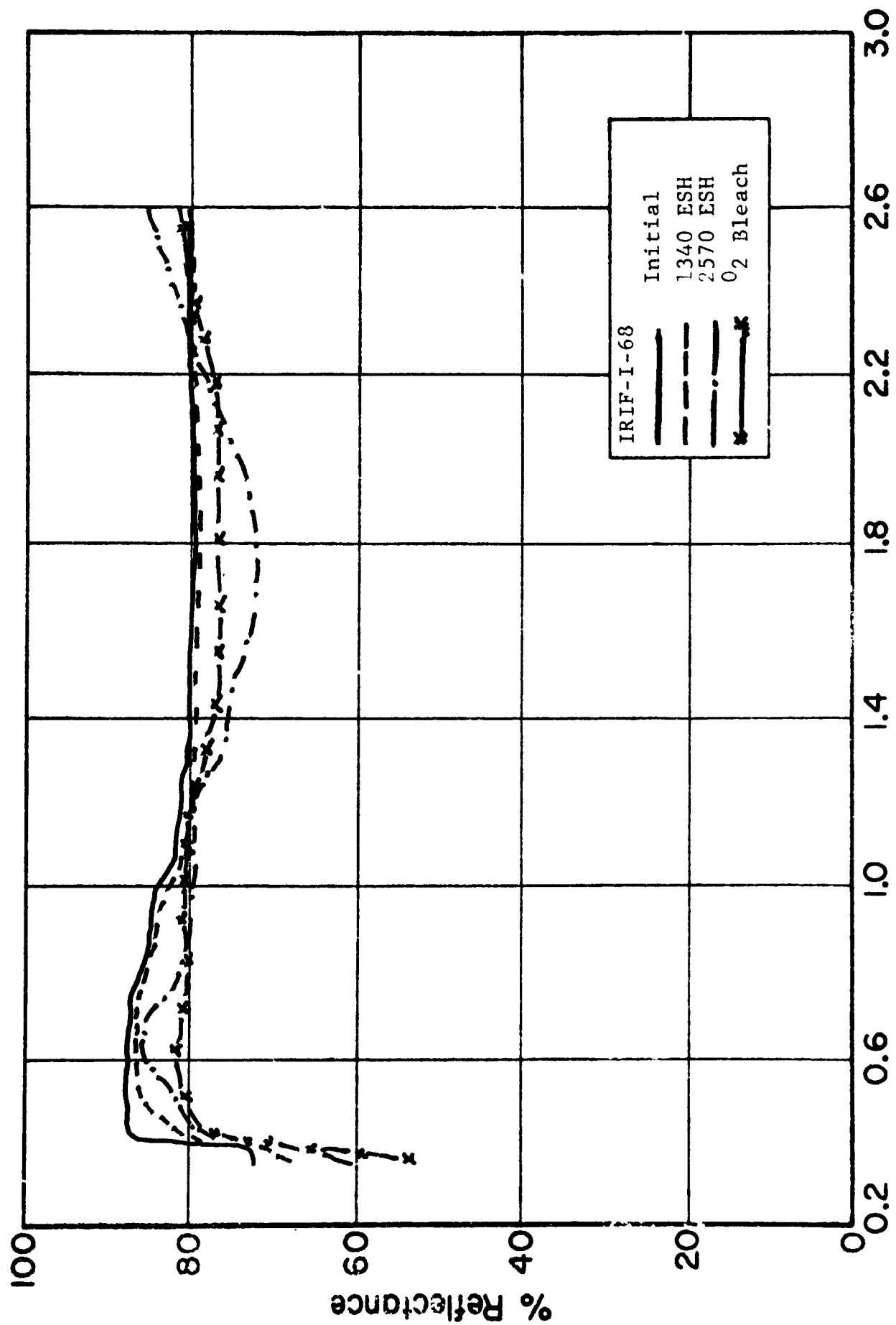


Figure 4.88 REFLECTANCE SPECTRA OF TEKTRONIX $Zn_2SiO_4:Mn$

treated thermally, show substantial instability and, not surprisingly, free ZnO. The spectra of the same material which has been fired at 900°C/9 hrs (designated T-2) appears in Fig. 4.84. Here the stability is excellent. The spectra also reveal slight bleaching, again probably because of the moderate free ZnO content. (The latter is also evident from the "knee" in the UV reflectance spectrum). Materials fired at 1200°C/1 hr (T-3) and at 1250°C/24 hrs (T-4) exhibit excellent stability as figs. 4.85 and 4.86, respectively, show. In the firing process the T-3 material remained reasonably powdery, while the T-4 material formed large and very hard "clinkers". Both, however, exhibit very little bleaching, while the T-4 material shows a substantially greater proportion of free ZnO, as indicated by the knee in the UV reflectance spectrum. This extends the observations made earlier, (see Fig. 4.83) regarding the increasing ZnO concentration with increasing calcination temperature.

The zinc orthosilicate (Zn_2SiO_4) samples, also supplied by Tektronix, are not as stable as Zn_2TiO_4 . From a comparison of the spectra in Fig's 4.87 and 4.88, it is obvious that manganese doping stabilizes Zn_2SiO_4 against the production of bleachable infrared damage but does not confer any significant degree of overall optical stability upon this material.

4.5.5 IRIF Test No. I-69

4.5.5.1 Purpose/Description

This test (ref. 4.11) involved a series of Zn_2TiO_4 pigments produced in a plant with a large manufacturing capability for specialty pigments. The purpose, consequently, was to evaluate the properties and performance of Zn_2TiO_4 pigments manufactured in a large-scale production facility.

Except for one IITRI pigment, all of the pigments tested were obtained from Tektronix, Inc., Beaverton, Ore. through the courtesy and cooperation of Dr. Ralph Mossman. IITRI furnished

the preparation instructions and approximately ten (10) pounds each of SP-500 ZnO and anatase titania (α -TiO₂), Tektronix prepared these materials by first slurring in distilled water at a 2.05/ZnTi mole ratio, drying the slurry in a large high temperature spray-dryer, and then by calcining according to specified temperature schedules. Table 4.15 describes the materials involved.

Table 4-15
Tektronix Pigments

<u>Designations</u>		<u>Descriptions</u>
<u>IITRI</u>	<u>Tektronix</u>	
T-1	J-1156-65	Spray-Dried, Unfired
T-2	J-1156-65A	Spray-Dried, Fired at 900°C/8 hr.
T-3	J-1156-65B	Spray-Dried, Fired at 1200°C/1 hr.
T-4	J-1156-65C	Spray-Dried, Fired at 1250°C/24 hr.

T-1 is a simple mixture of ZnO and α -TiO₂; the spray-drying temperature, however, was apparently sufficiently high to effect some conversion to Zn₂TiO₄. The T-1 preparation is the precursor material for the other T-series pigments.

4.5.5.2 Sequence

Spectral reflectance measurements were accomplished (in-situ) prior to UV irradiation, after 915 ESH, 2085 ESH and after 2660 ESH; a final scan was made after the system pressure was increased to 760 torr using pure O₂.

4.5.5.3 Test Results

The materials tested in IRIF I-69 are listed in Table 4.16 wherein also are the pertinent test results. The materials are grouped according to their descriptions in Table 4.15. In this particular test, with a relatively new basic pigment, a few examples of sample notation may be useful. Under T-2, we have listed, for example a) "powder", b) "OI-650", c) "K₂SiO₃ powder", and d) "(A-10)/OI-650". These descriptions refer respectively to the T-2 pigment which was irradiated a) as a powder, b) as an

Table 4-16

IRIF I-69
ULTRAVIOLET IRRADIATION TEST RESULTS

T-2 Pigments =	Solar Absorbance Values				O ₂ Bleach			
	$1R_{max}$	$2R_k$	$3\Delta R_{400}$	Initial				
Powder	89	31	0.11	.187	.182	.208	.236	
OI-650	90	38	0.14	.187	.196	.297	.300	
OI-650G	94	30	0.065	.112	.130	.140	.158	
:k ₂ SiO ₃ powder	90	43	0.10	.166	.179	.185	.196	
:k ₂ SiO ₃ /OI-650G	94	28*	0.07*		.142	.146	.224	0.187
A-10/OI-650	82	72	0.08	.233	.229	.260	.267	
T-3 Pigments =								
OI-650	75	25	0.05	.318	.316	.325	.345	.343
:k ₂ SiO ₃ /OI-650	68	23	0.04	.372	.376	.386	.398	
-A-10 powder**	84	65	0.16	.210	.218	.233	.261	
-A-10/OI-650	74	62	0.08	.319	.326	.339	.362	.365
T-4 Pigment								
-A-10 powder	83	53	0.13	.224	.230	.299	.303	.298
II TRI Pigment								
LH-53(6-12)/OI-650G	65	32	0.15	.391	.385	.428	.429	0.429

REPRODUCIBILITY OF THE
ORIGINAL PAGE IS POOR

*Value in this instance is that after 915 ESH
**Sample was marred during testing; data somewhat doubtful

Notes

1. R_{max} , highest reflectance value in region 325 - 2600nm
2. R_k , reflectance at 370nm, the "knee" in the Zn_2TiO_4 spectra.
3. ΔR_{400} , the maximum induced reflectance change at 400nm.

OI-650 paint. c) as a potassium silicate encapsulated pigment (powder); and, d) as an acetic acid washed pigment, fired at 1000°C/2hr, and then dispersed in OI-650 resin.

The spectral reflectance curves are presented in Figures 4.89-4.100. Solar absorptance values and selected spectral reflectance data are presented in Table 4.16. The column in this table designated R_{\max} gives the value of the highest reflectance of the unirradiated material in the spectral region 325 to 260nm. The next column, R_k , lists the reflectance values of the unirradiated materials at 370nm. The significance of R_k , the "knee" reflectance, is that it relates to the amount of free ZnO present in the pigment.

The initial reflectance spectrum of sample No. 6, (T-2:K₂SiO₃/OI-650G), was scaled improperly. Hence, in the analysis of the performance of this material we will rely primarily on the relationship of the "irradiated" spectra to one another. Other performance data, such as the ΔR at 900nm, were also studied, but they have not been listed because, in the case of these pigments at least, there has been no substantial S-band damage, that is, UV-induced reflectance losses of 5% or more. In fact, most materials suffered less than 2% reflectance loss in this region, where sensitivity to surface defects becomes strongly prominent.

4.5.5.4 Conclusions

The Tektronix pigments and paints demonstrate very good optical stability. In terms of induced solar absorptance change, they compare very favorably with the IITRI baseline pigment, LH-53(6-12), (Fig. 4.100). The best paint tested was T-2/G (Fig. 4.91); among the Tektronix pigments not only did this material display the best stability ($\Delta\alpha_s = 0.046$), but it possesses the lowest solar absorptance ($\alpha_s = 0.112$) again demonstrating the inherently good properties and stability of Zn₂TiO₄/G paints.

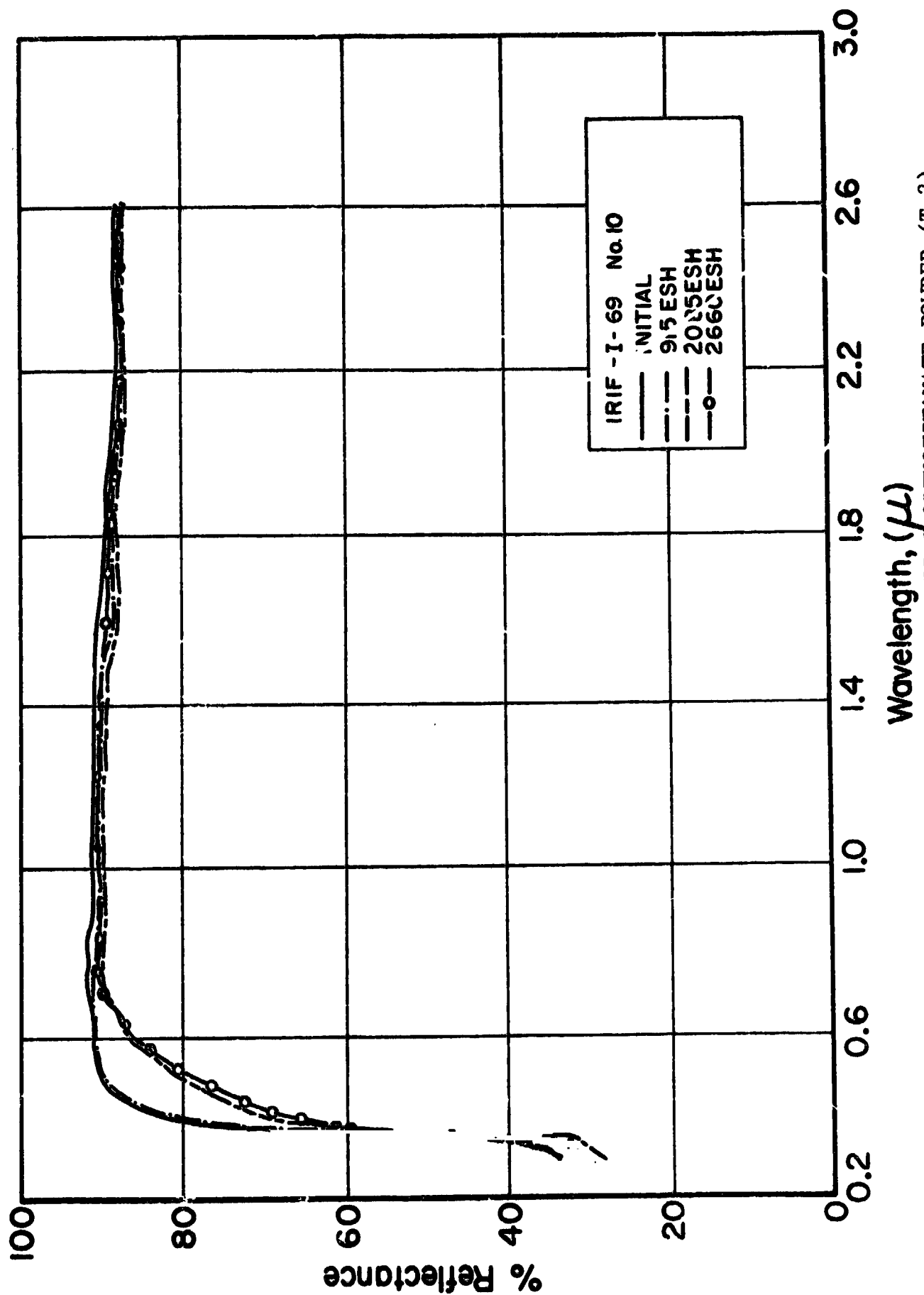


Figure 4.89 REFLECTANCE SPECTRA OF ZINC ORTHOTITANATE POWDER (T-2)

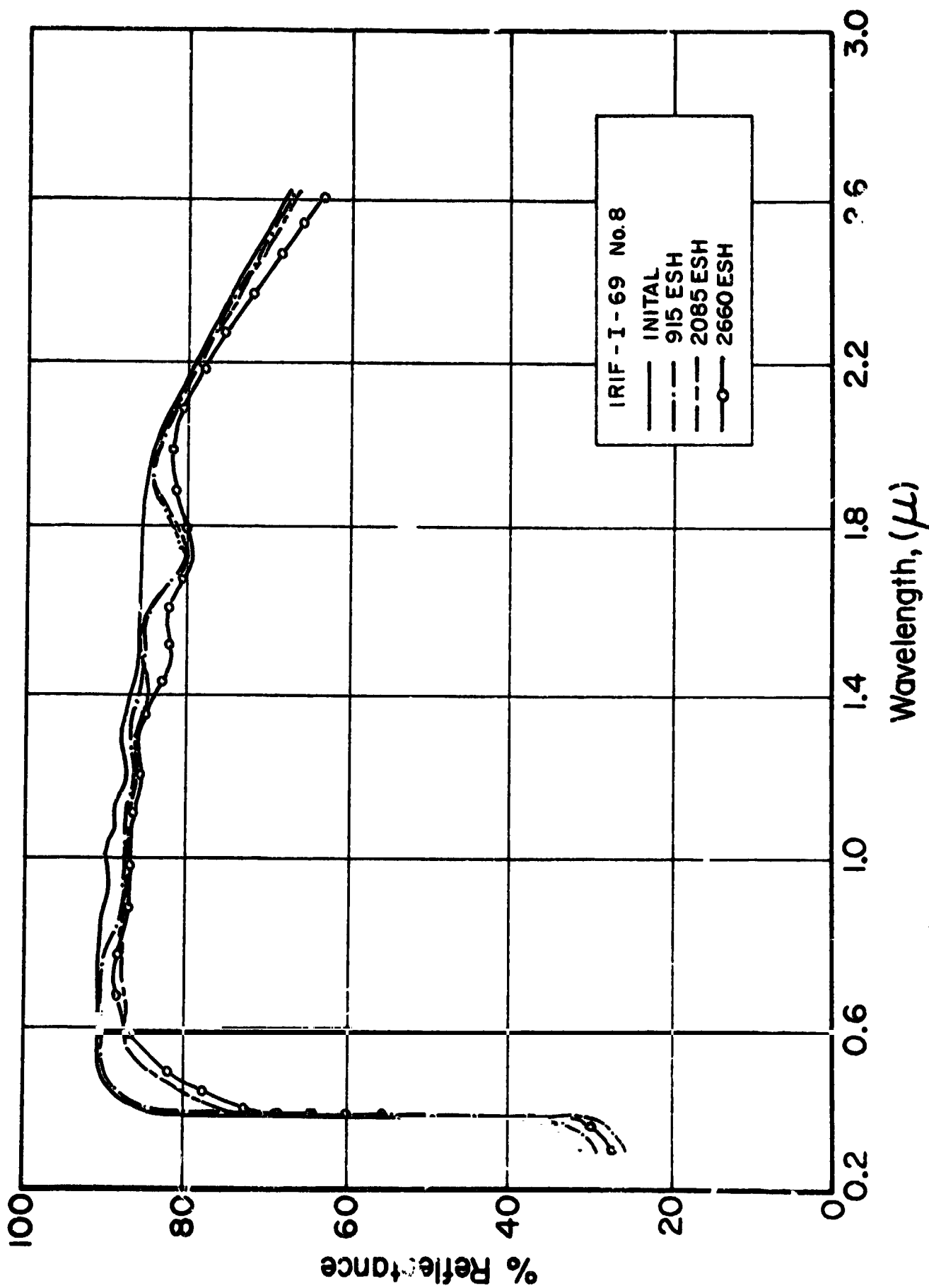


Figure 4.90 REFLECTANCE SPECTRA OF ZINC ORTHOTITANATE PAINT (T-200)

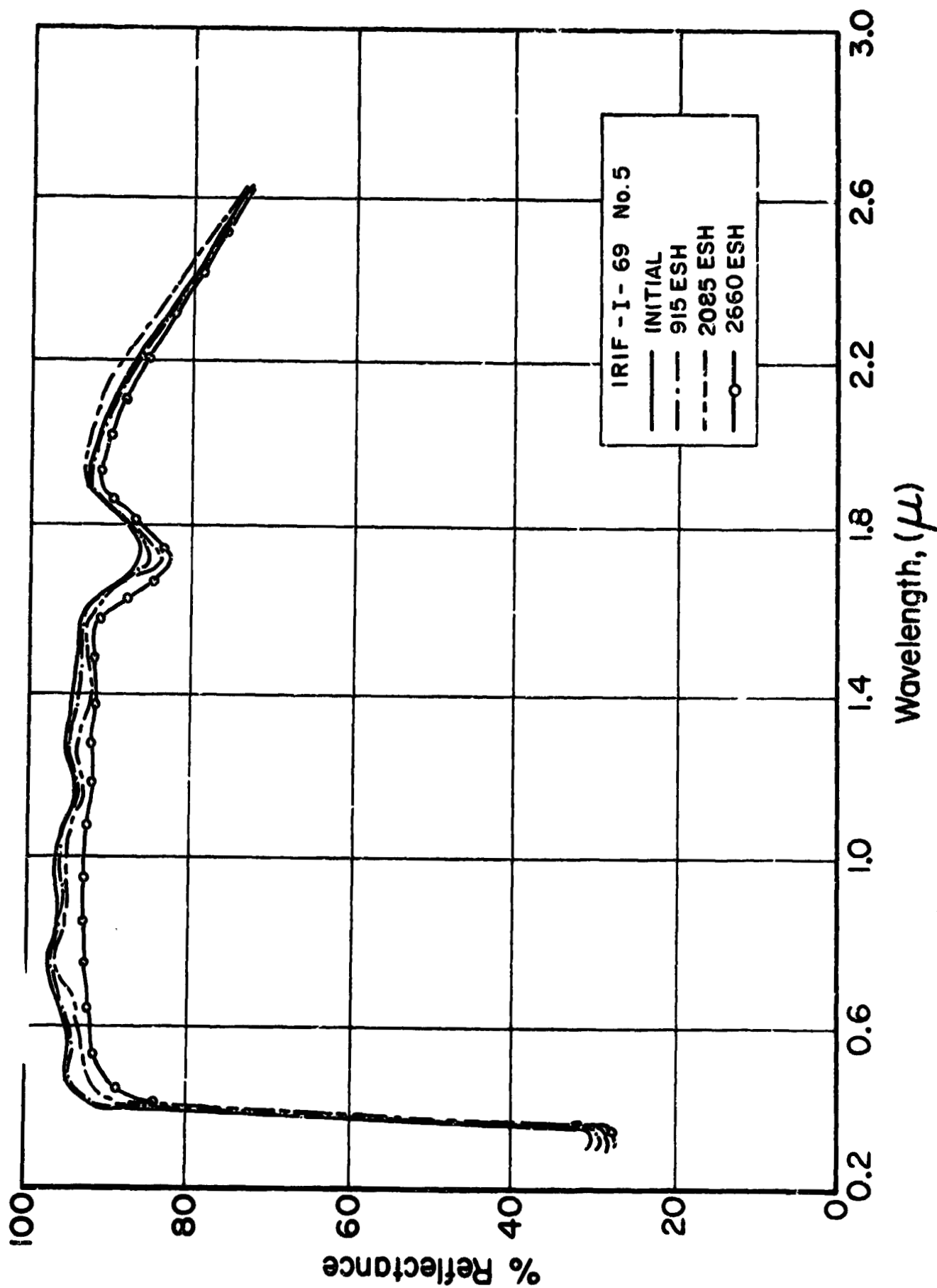


Figure 4.91 REFLECTANCE SPECTRA OF ZINC ORTHOTITANATE PAINT (T-2/6)

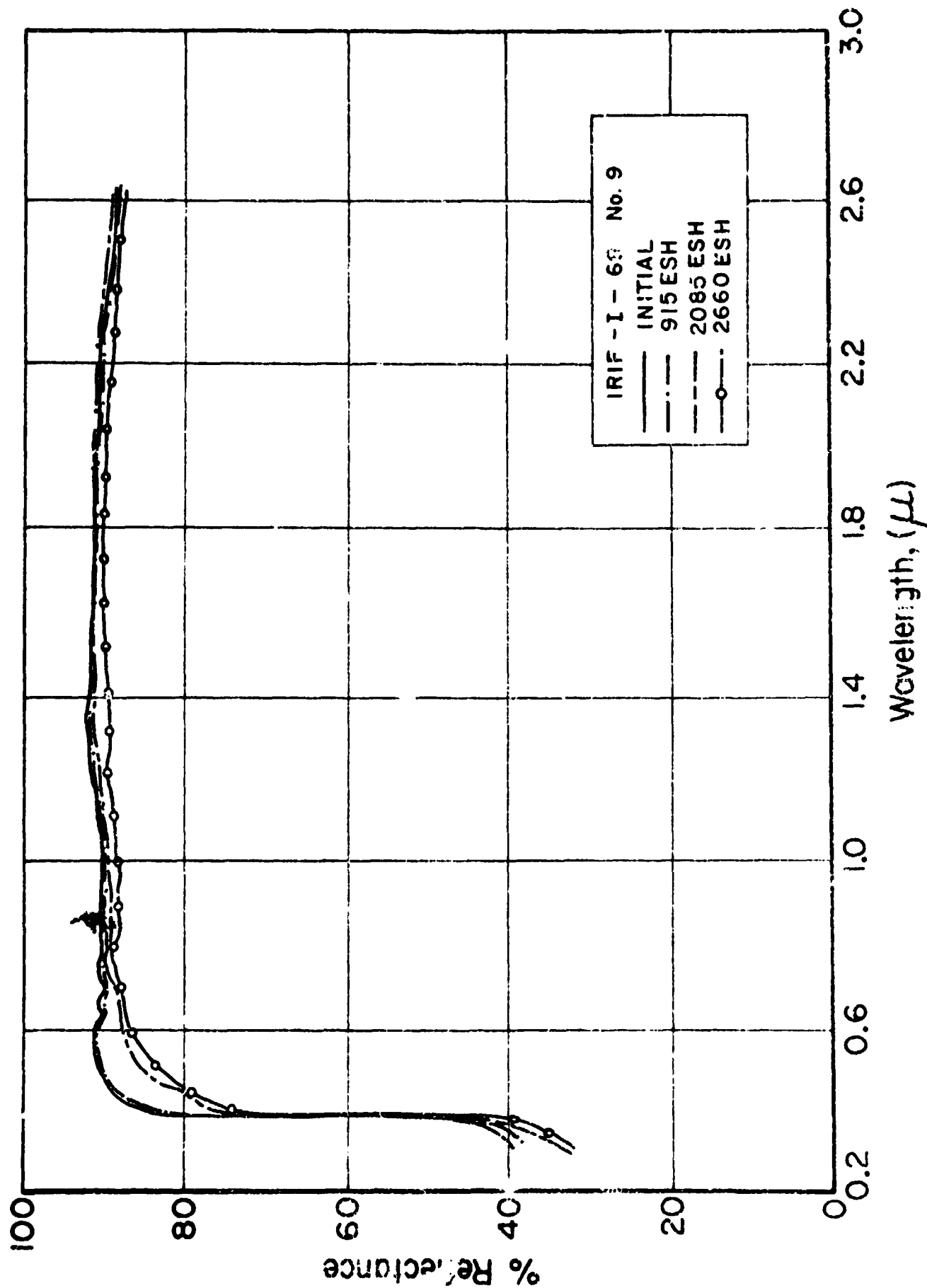
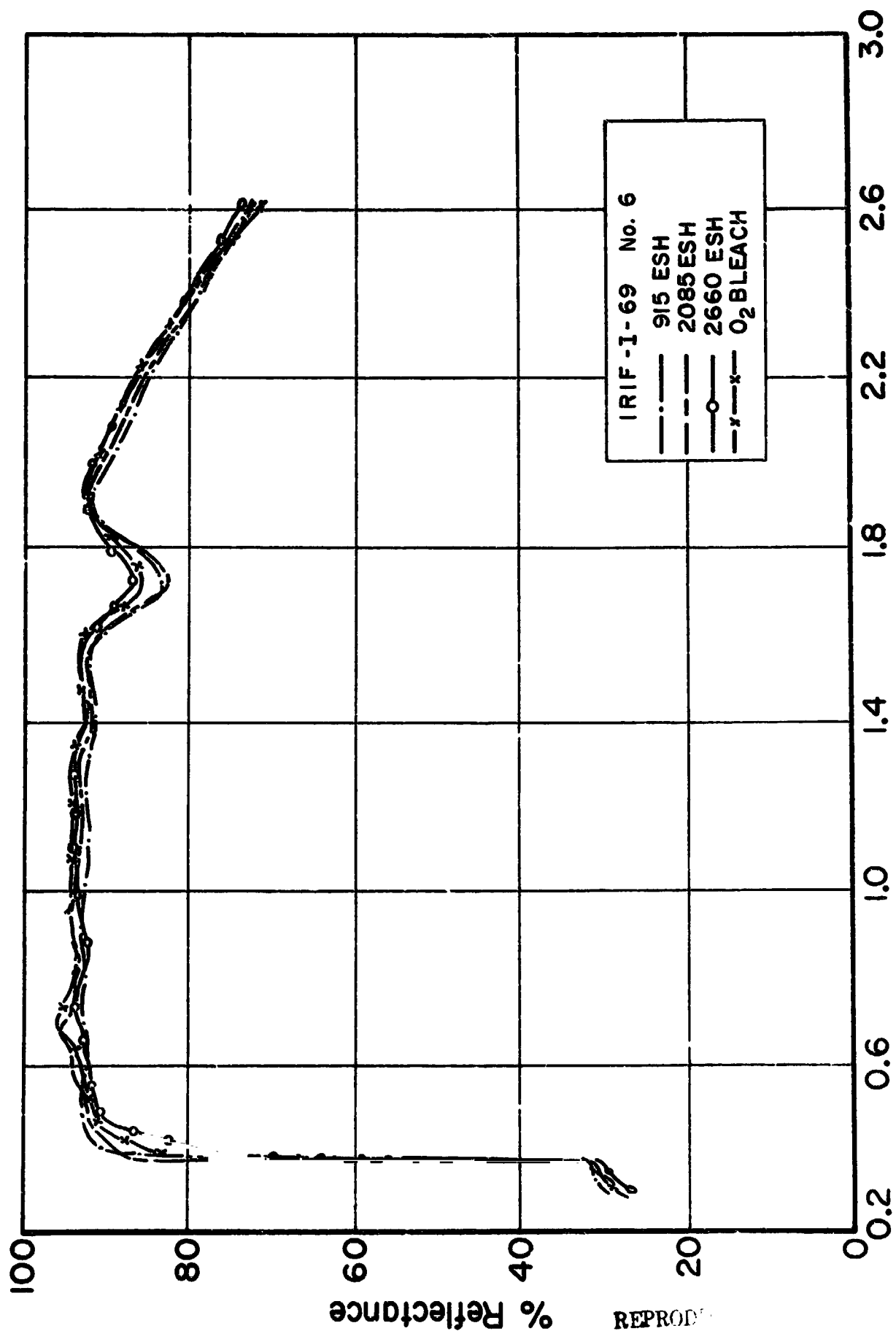


FIGURE 2. REFLECTANCE SPECTRA OF ZINC OXIDE POTASSIUM PEROXIDE (T-2-18-510)



Wavelength, (μ)

Figure 4.93 REFLECTANCE SPECTRA OF ZINC ORTHOTITANATE PAINT (T-2 K_2SiO_3/G)

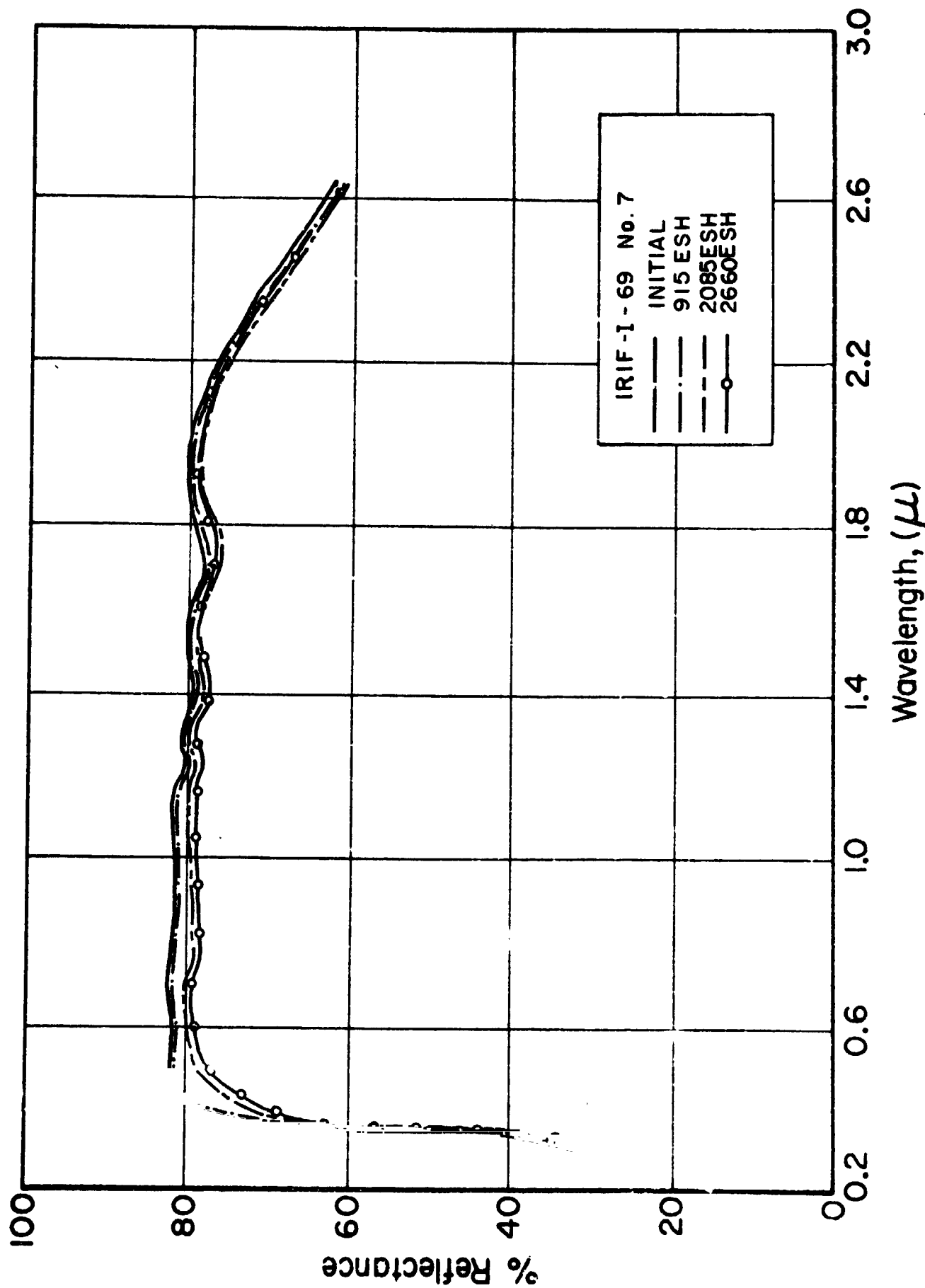


Figure 4.94 REFLECTANCE SPECTRA OF ZINC ORTHOTITANATE PAINT (T-2:A-10/OD)

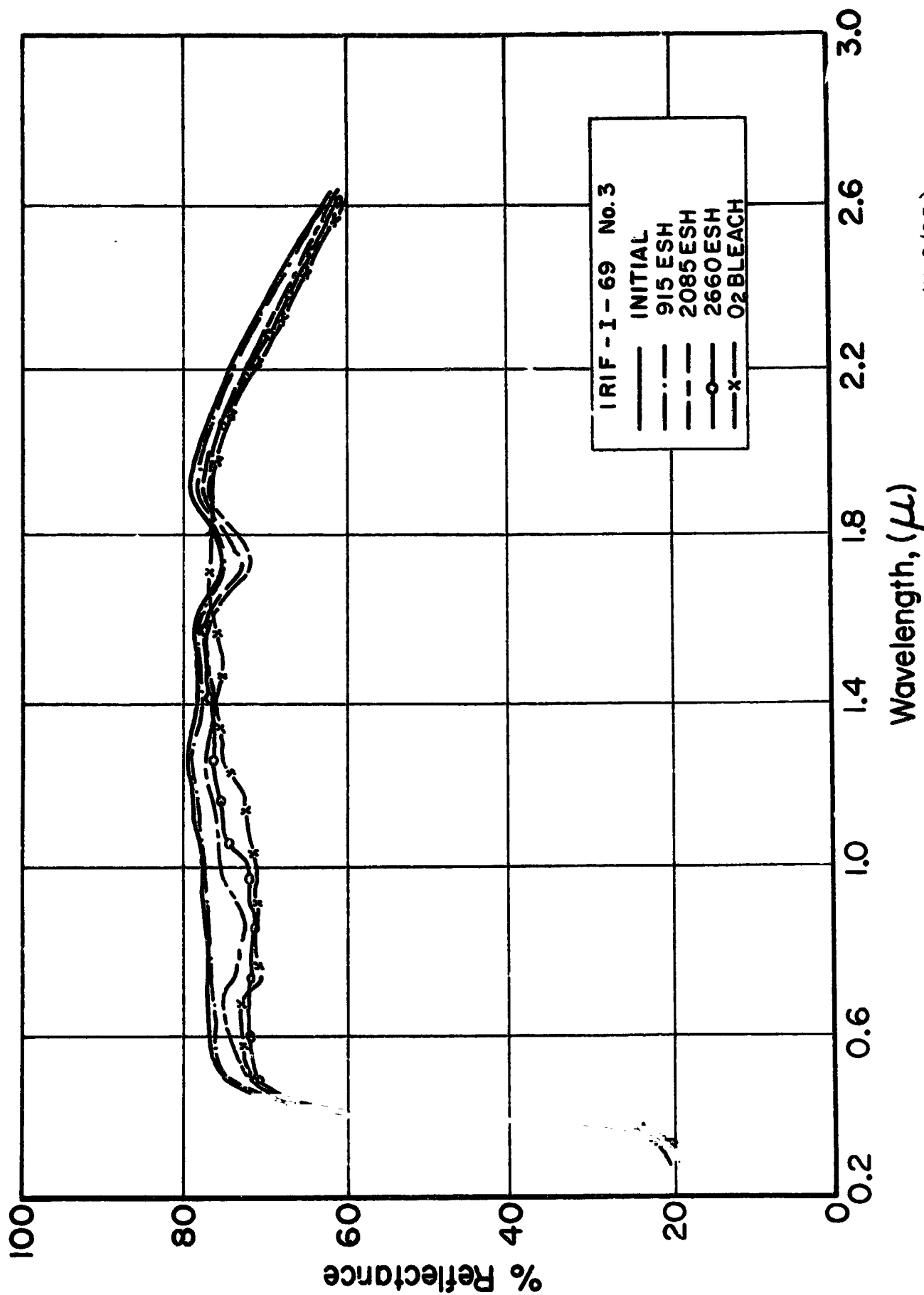


Figure 4.95 REFLECTANCE SPECTRA OF ZINC ORTHOTITANATE PAINT (T-3/OI)

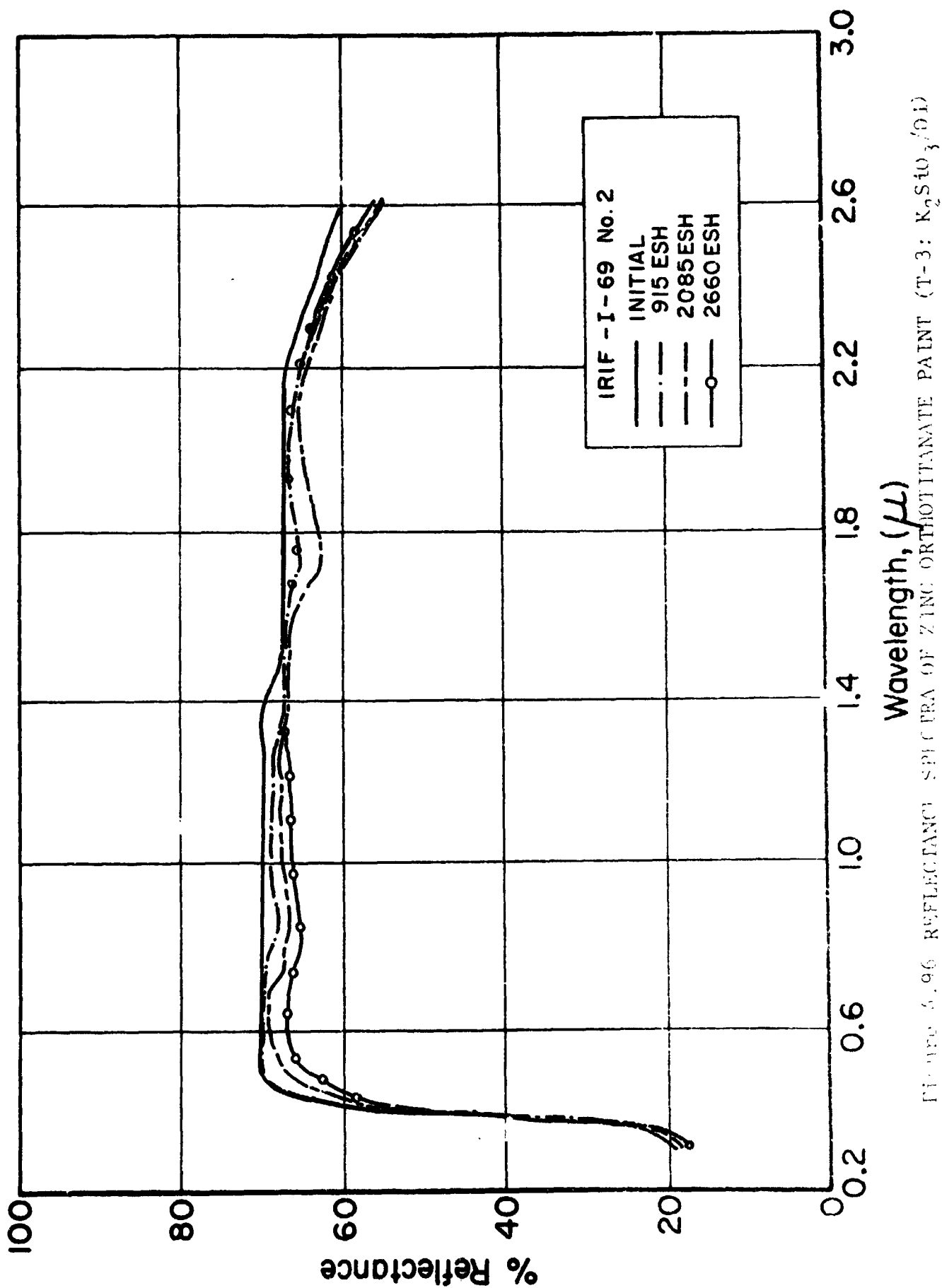


FIGURE 4.96 REFLECTANCE SPECTRA OF ZINC ORTHOTITANATE PAINT (T-3: $K_2SiO_3 \cdot 0.1$)

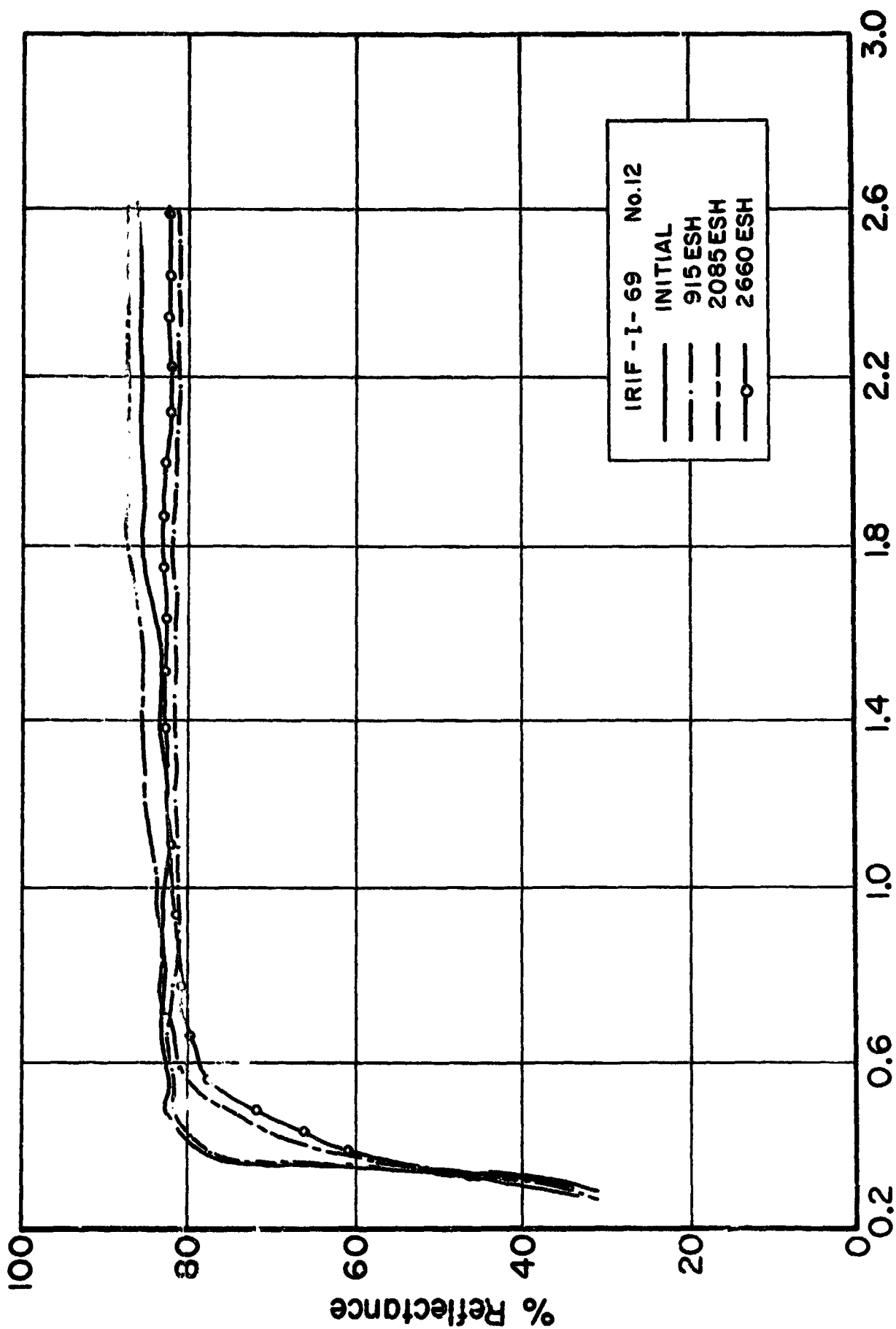
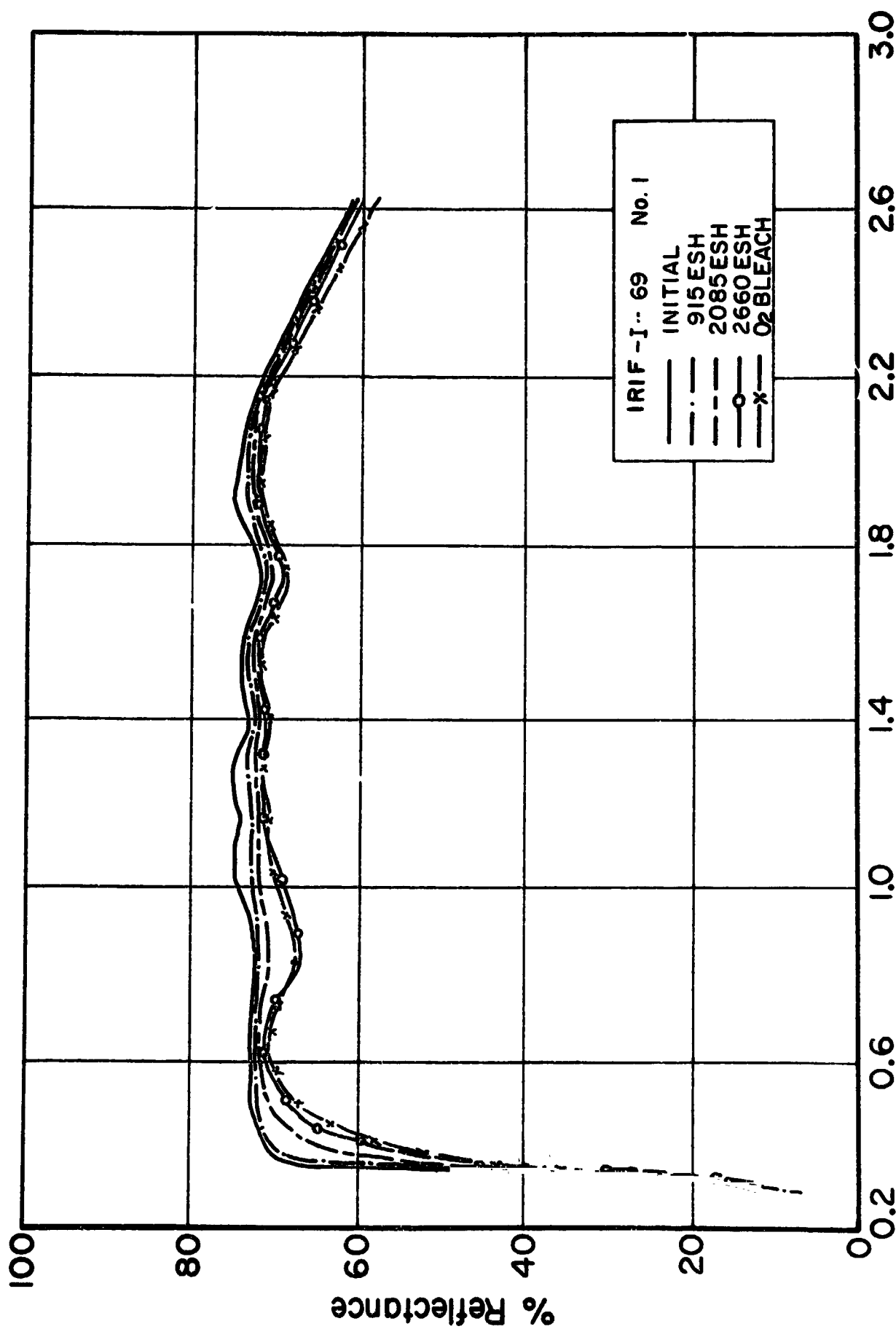


Figure 4.97 REFLECTANCE SPECTRA OF ZINC ORTHOTITANATE POWDER (T-3: A-10)



Wavelength, (μ)

Figure 4.98 REFLECTANCE SPECTRA OF ZINC ORTHOTITANATE PAINT (T-3: A-10/OI)

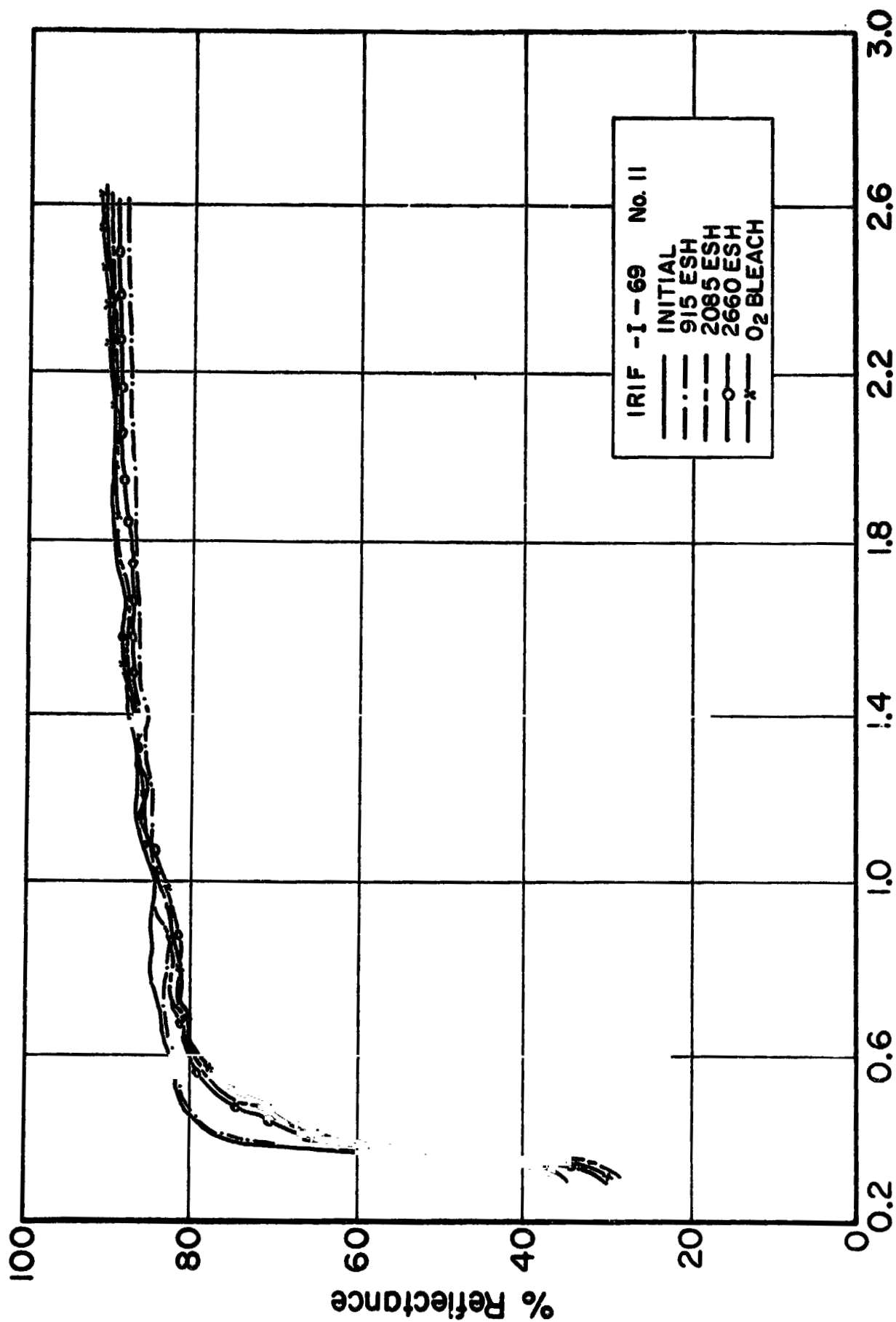


Figure 4.99 REFLECTANCE SPECTRA OF ZINC ORTHOTITANATE POWDER (T-4)

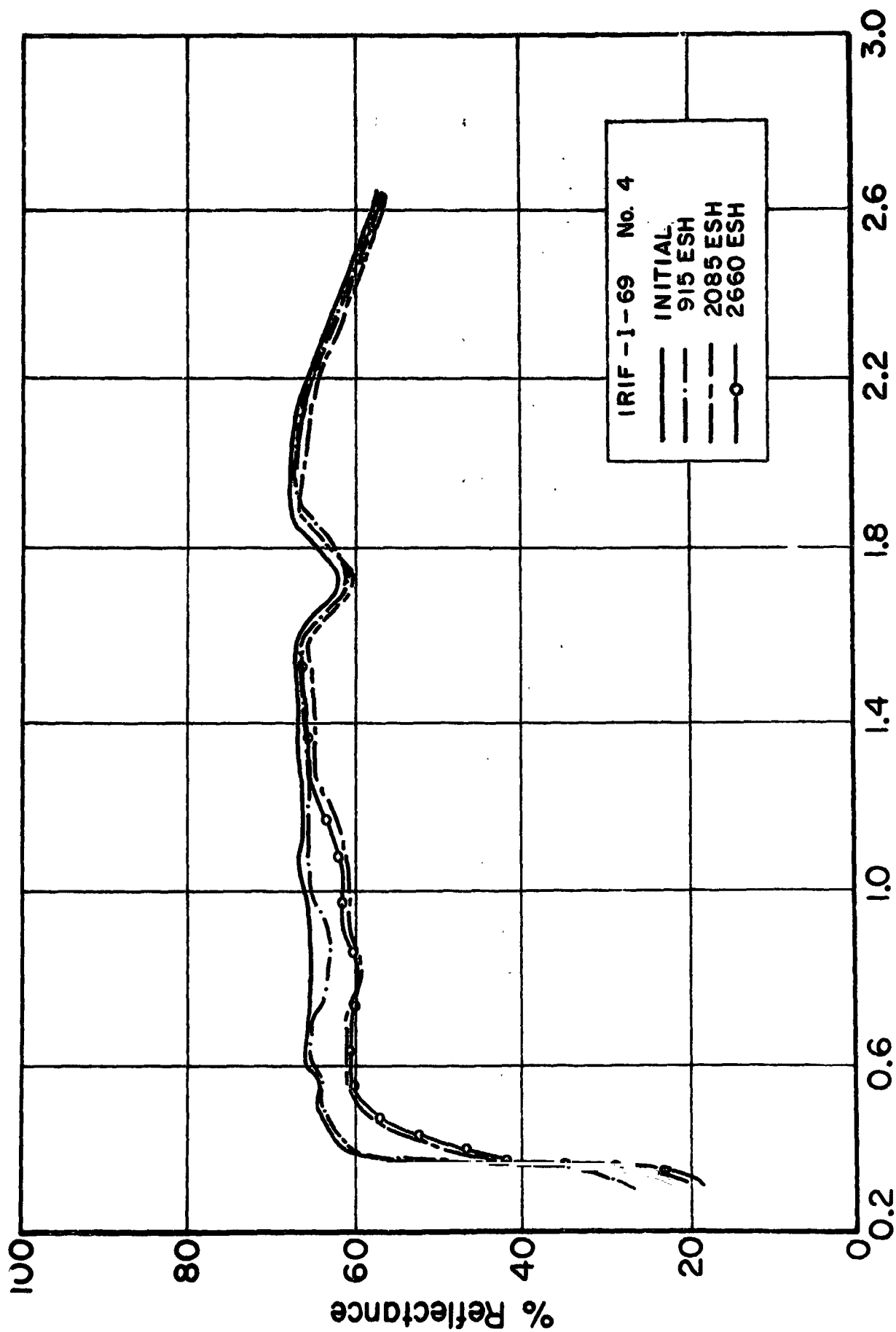


Figure 4.100 REFLECTANCE SPECTRA OF ZINC ORTHOTITANATE PAINT (LH-53(6-12)/G)

High reflectance as well as good stability is attained at 900°C, thus negating, for these pigments at least, any advantage of a 1200°C calcination. It may be that an intermediate temperature might produce an even more stable pigment, particularly since T-4 pigments (1250°C/24hr) have not displayed as good stability.

For Tektronix pigments the acid leaching and subsequent recalcination at 1000°C/2hr. in every case enhances the visible reflectance but does not substantially affect optical stability. The A-10 treatment, therefore, remains as a reasonable approach to the improvement of α_s of these paints. The effectiveness of encapsulation of these pigments with K_2SiO_3 , though this process is somewhat valuable in improving α_s , cannot be as easily determined. In general, encapsulation of Tektronix pigments tends not to affect stability. This latter observation is true mainly because these particular pigments show little, if any, tendency to surface defect formation as evidenced by a reflectance loss in the 900nm region.

The test results make it plain that the Tektronix spray-dry process is a viable one. The pigments are inherently stable and the paints made from them are also sufficiently reflective and stable that we can consider this process a logical alternative to the current processes. Understood in proper perspective, the Tektronix process would require, as would any other, extensive testing and further development. This test simply demonstrates that the method is clearly worth pursuit, if current methods are shown to be insufficient.

4.5.6 CREF Test No. 15

4.5.6.1 Purpose/Description

The beneficial effect of acetic acid leaching of Zn_2TiO_4 pigments containing a ZnO excess is well established. In CREF Test No. 15 (ref. 4.12) the acid leaching process is investigated more closely to elicit the effects of individual operations in the treatment of acid-leached pigments including post-calcination

and encapsulation. The test scheme is embodied in the sequence of thermal and chemical treatments: 6-12, 6-12-10, 6-12-A, and 6-12-A-10.

4.5.6.2 Sequence

Reflectance scans were made prior to irradiation, after exposures to 470 ESH, 1150 ESH, 1650 ESH and to 2190 ESH, and finally after a post-irradiation O_2 bleach (at 760 Torr). The samples were not subjected to proton irradiation.

4.5.6.3 Test Results

Solar absorptance values are given in Table 4.17. Table 4.18 provides relevant diagnostic data. Reflectance spectra of all the test samples are presented in Figures 4.101-107 inclusive. Most obvious are the facts that re-calcination is necessary after an acid wash, and that S-band absorption arises principally from UV-activated surface defects. The degradation is much greater in the case of the Li_2SiO_3 -encapsulated pigment. This encapsulant is obviously not effective; in fact it appears to magnify the damage, as a comparison of the S-band development in Fig's 4.103 and 4.106 shows. The O_2 bleaching in the case of the Li_2SiO_3 -encapsulated pigment leaves little doubt as to the validity of this assertion. However, the residual acid (from the leaching process) may block the encapsulant and prevent its attachment to the pigment surface; other explanations may exist and include a reaction between the residual acid and the Li_2SiO_3 . But, as an encapsulant, Li_2SiO_3 does not provide protection against the formation of the optical defects causing ΔR_{900} as is evident in comparing the performances of paints with Li_2SiO_3 -encapsulated pigments with those of paints with un-encapsulated pigments.

In Table 4.18 are some of the pertinent properties and performance indices. Using the LH-102(6-12) data as a baseline, it is evident that only the A-10 treatment produces any significant improvement, that the -10 treatment alone has essentially no effect, and that the -A treatment alone drastically increases $\Delta \alpha_s$. The effects of Li_2SiO_3 on LH-103(6-12) are to increase R_k

Table 4-17

CREF-15

IRRADIATION TEST RESULTS

Sample No.	Sample Description*	Solar Absorbance Values					$\Delta\alpha_s$	
		Exposure (ESH)						
		Initial	474	1150	1650	2190	O ₂ Bleach	
1	LH102(6-12):Li ₂ SiO ₃	.192	.204	.233	.238	.247	.218	.054
2	LH102(6-12-10):Li ₂ SiO ₃	.217	.231	.260	.264	.273	.289	.056
3	LH102(6-12-A-10):Li ₂ SiO ₃	.224	.247	.265	.262	.268	.246	.044
4	LH102(6-12)	.183	.196	.221	.234	.230	.214	.041
5	LH102(6-12-10)	.226	.230	.252	.275	.272	.248	.046
6	LH102(6-12-A)	.272	.274	.374	.388	.387	.279	.115
7	LH102(6-12-A-10)	.214	.217	.220	.230	.235	.224	.021
8	LH103(6-12):Li ₂ SiO ₃	.209	.222	.230	.252	.251	.241	.042
9	LH103(6-12)	.219	.222	.236	.246	.245	.241	.026
10	LH102(6-12-A):Li ₂ SiO ₃	.229	.250	.406	.434	.457	.258	.228

*All samples are OI-650G paints containing the pigments described.

Table 4-18
SELECTED IRRADIATION TEST RESULTS
CREF Test No. 15

No.	Sample Description*	R _k (%)	ΔR_{400}^{**}	ΔR_{900}^{**}	Initial α_s	$\Delta \alpha_s(2190 \text{ ESH})$
4	LH-102(6-12)	61	.08/.09	.054/.025	.183	.047
5	LH-102(6-12-10)	64	.06/.08	.05/.005	.226	.046
6	LH-102(6-12-A)	55.5	.08/.04	.185/.005	.272	.117
7	LH-102(6-12-A-10)	69	.045/.03	.02/.005	.214	.016
1	LH-102(6-12):Li ₂ SiO ₃	64.5	.09/.095	.065/.015	.193	.045
2	LH-102(6-12-10):Li ₂ SiO ₃	68.5	.16/.165	.05/.02	.217	.047
10	LH-102(6-12-A):Li ₂ SiO ₃	59	.19/.12	.335/.03	.229	.205
3	LH-102(6-12-A-10):Li ₂ SiO ₃	59.5	.16/.16	.035/.00	.224	.038
9	LH-103(6-12)	23	.05/.05	.04/.025	.219	.027
8	LH-103(6-12):Li ₂ SiO ₃	38	.04/.05	.025/.01	.209	.042

*All samples are OI-650G paints

**Value of ΔR is given after 2190 ESH and after a subsequent O₂ bleach.

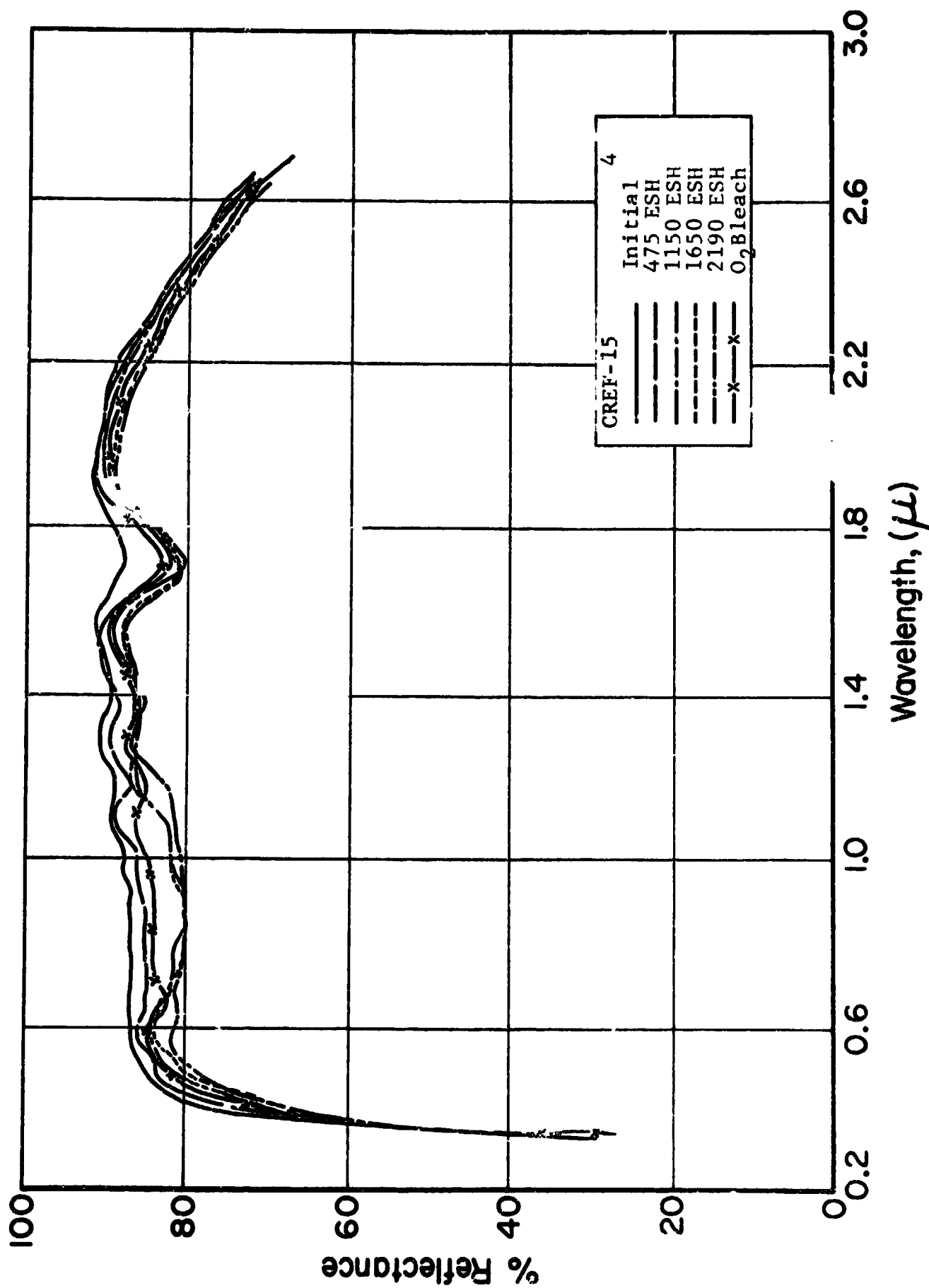


Figure 4.101 REFLECTANCE SPECTRA OF LH-102 (6-12)/G

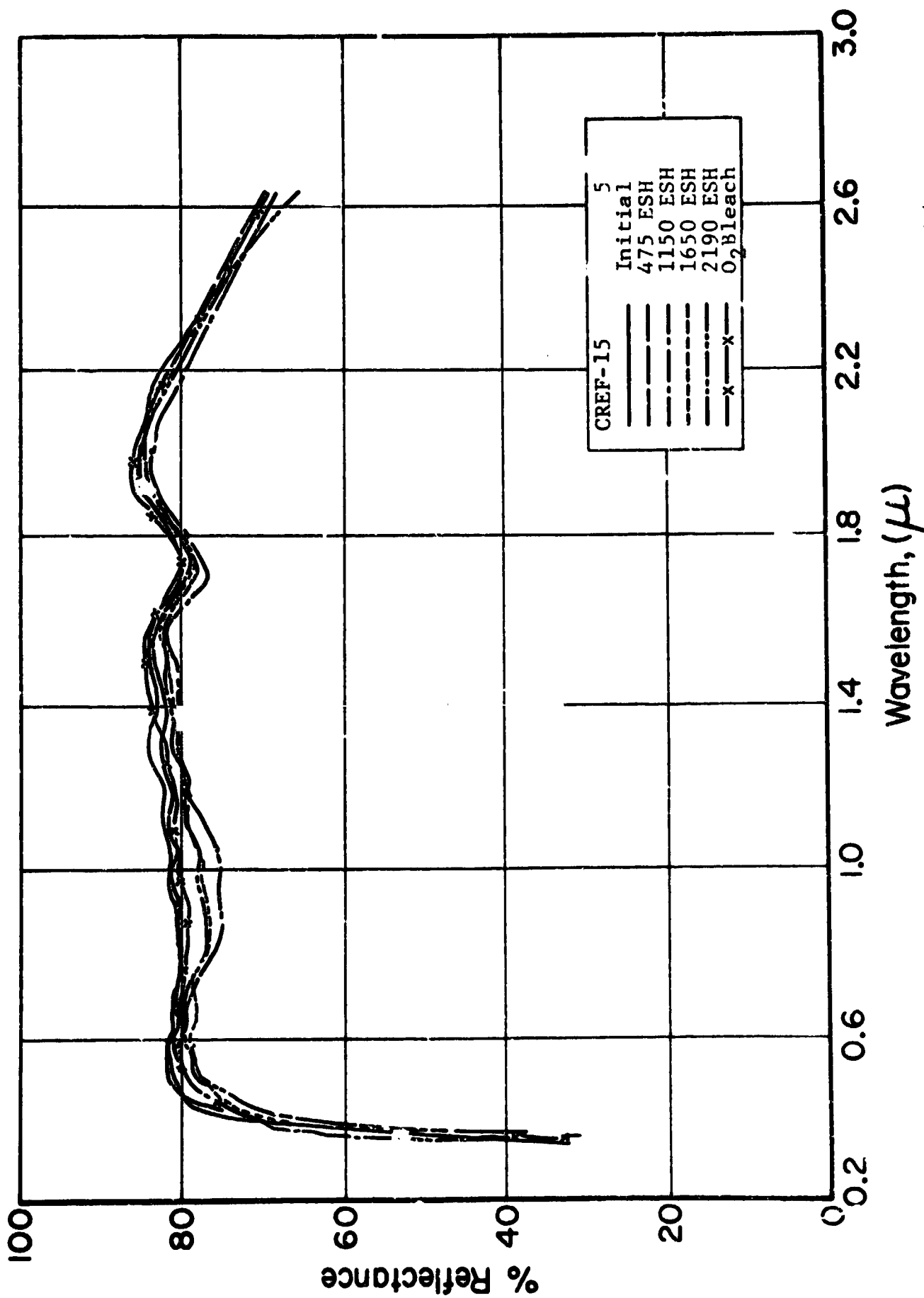


Figure 4.102 REFLECTANCE SPECTRA OF LH-102(5-12-17)/C

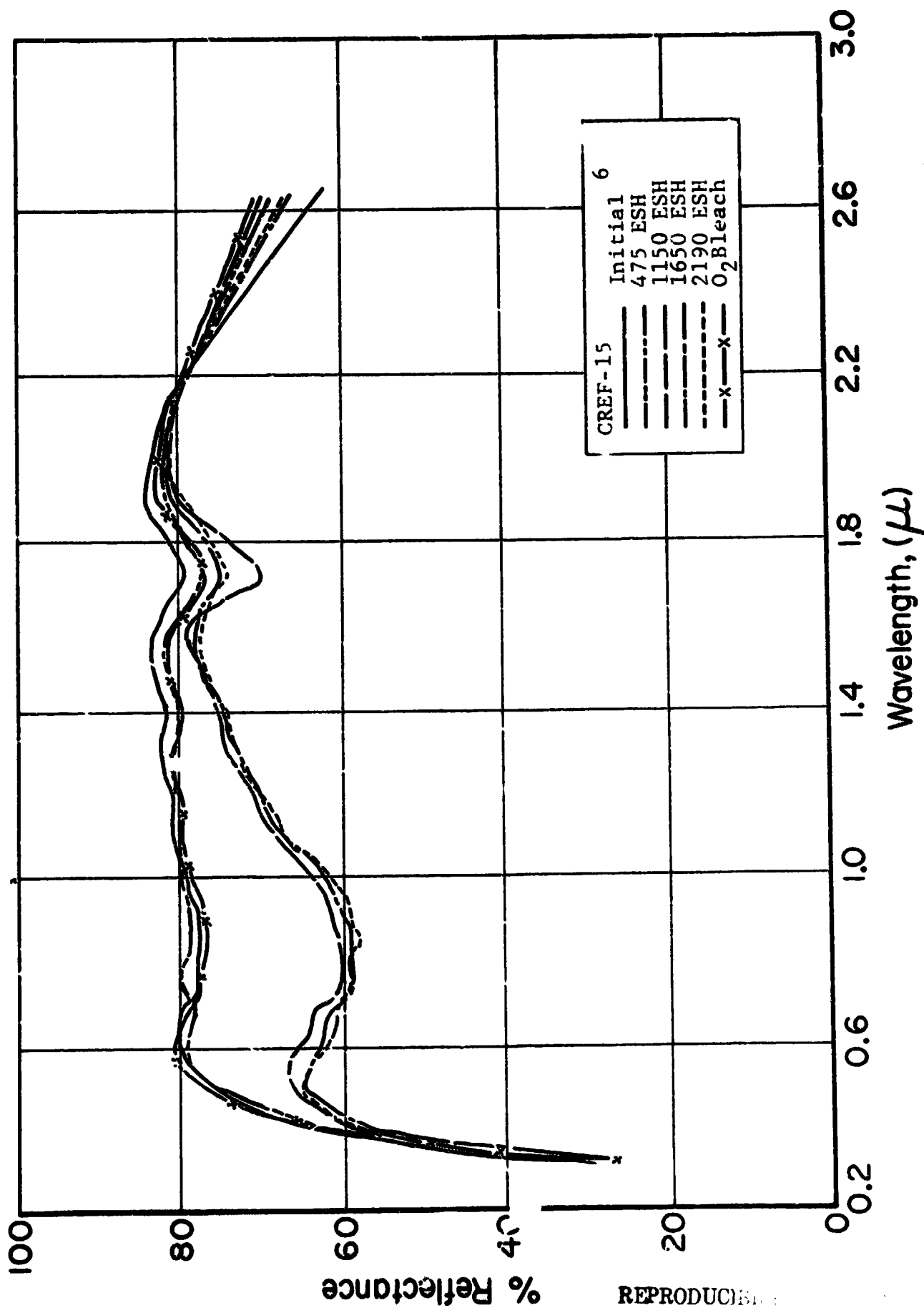


Figure 4.103 REFLECTANCE SPECTRA OF LH-102 (6-12-A)/G

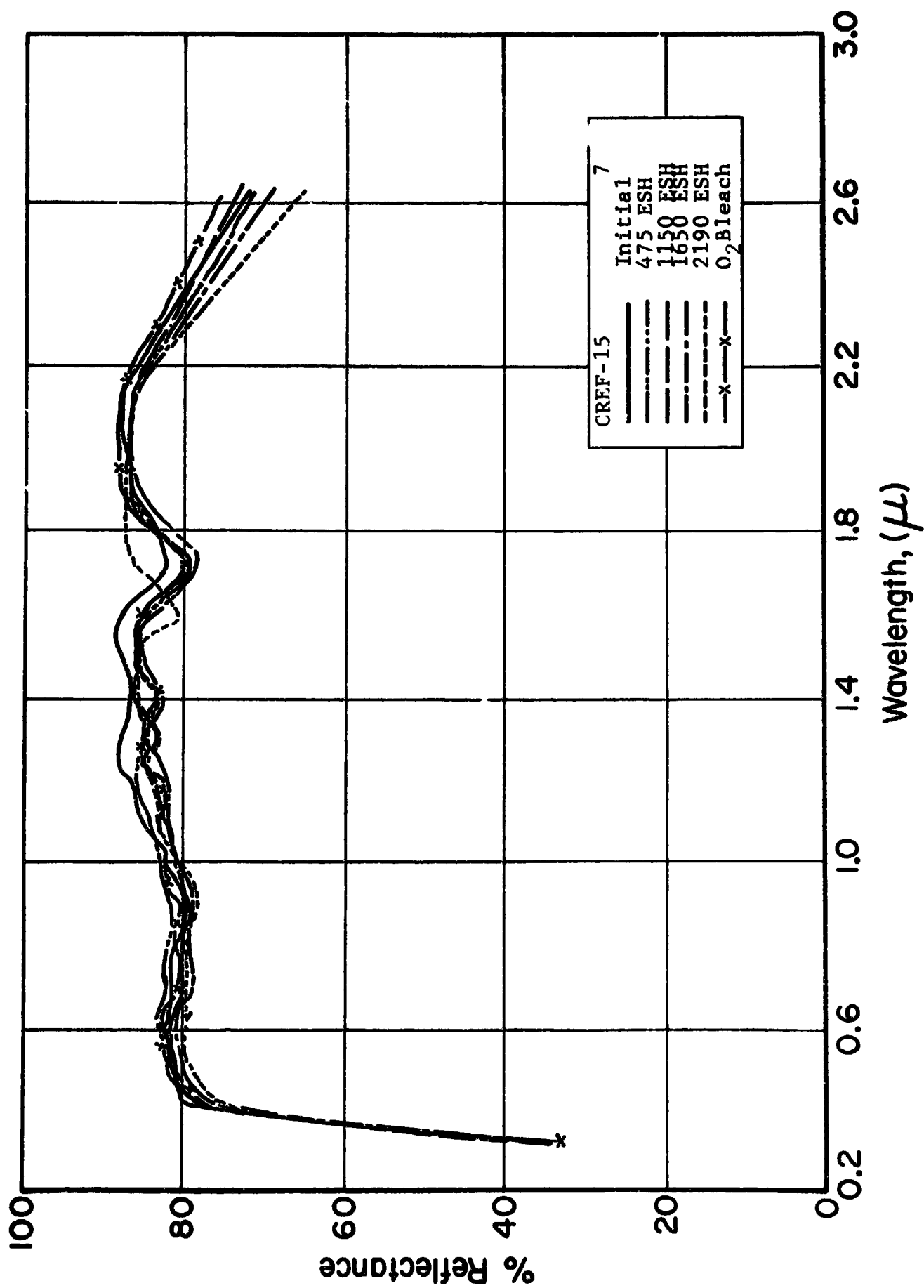


Figure 4.104 REFLECTANCE SPECTRA OF LH-102 (6-12-A-10)/G

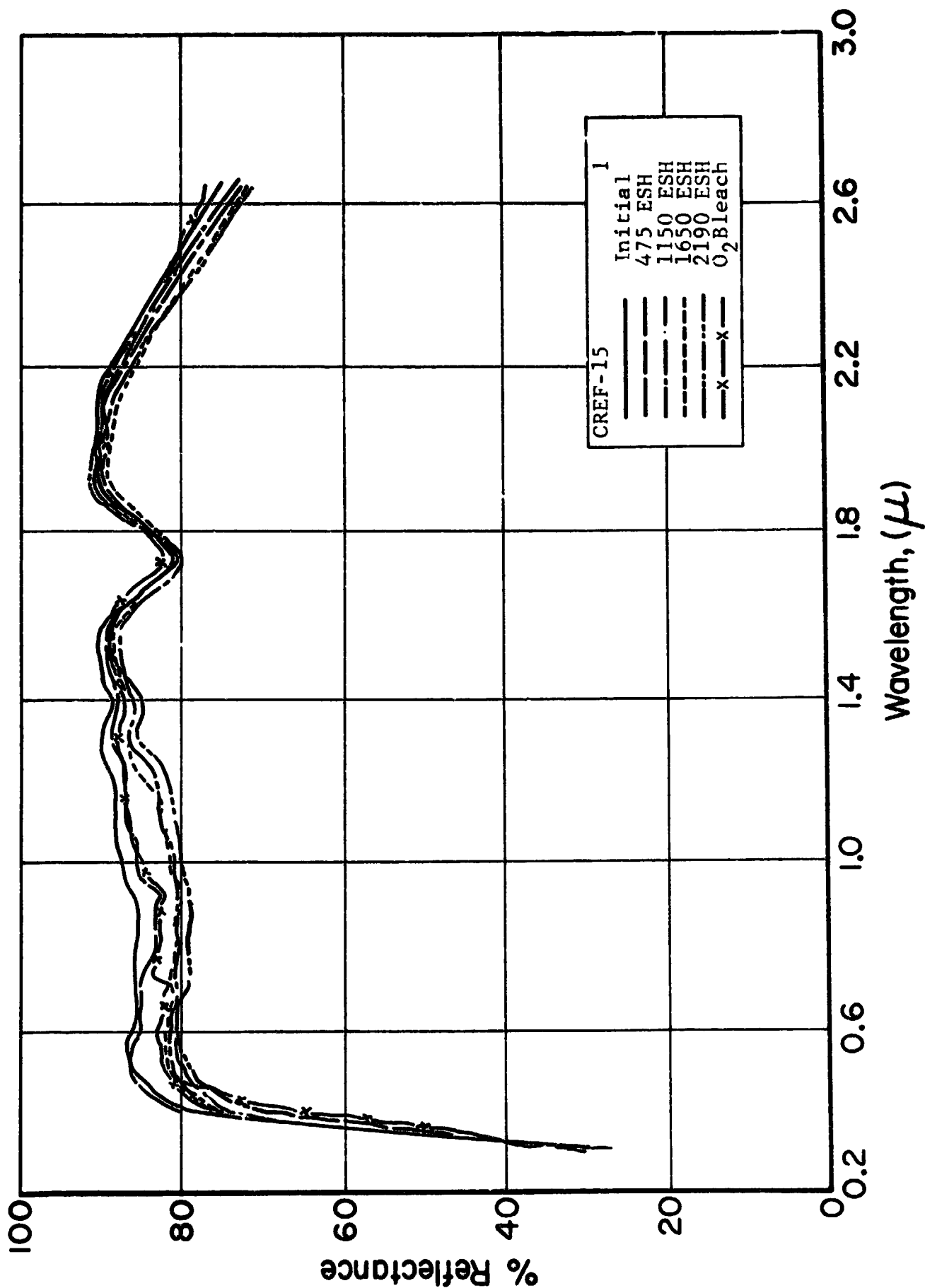


Figure 4.105 REFLECTANCE SPECTRA OF LH-102(6-12):Li₂SiO₃/C

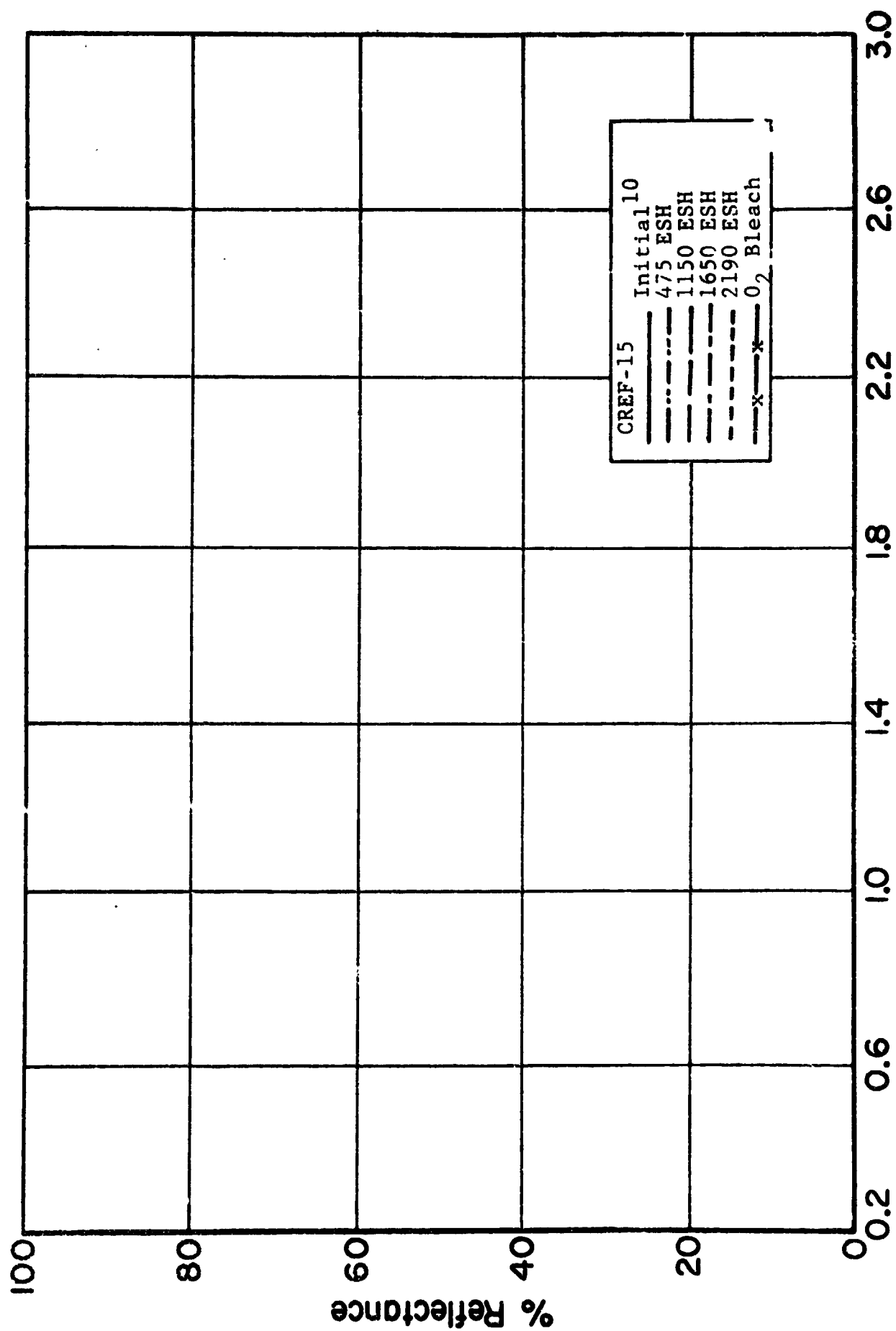


Figure 4.106 REFLECTANCE SPECTRA OF LH-102(6-12-A):L₁₂SiO₃/G

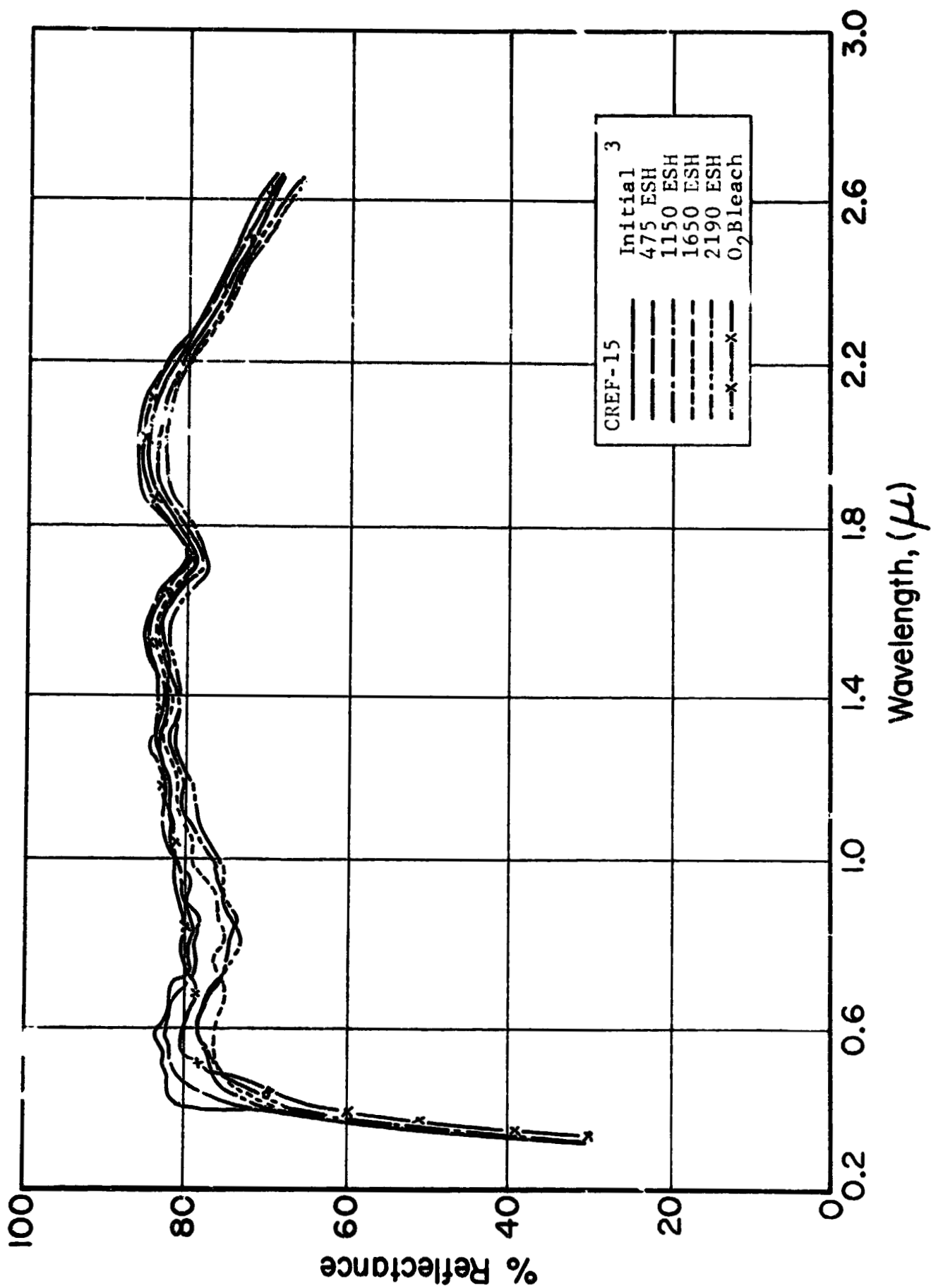


Figure 4.107 REFLECTANCE SPECTRA OF LH-102 (5-12-A-10):1.2SiO₃/C

and also $\Delta\alpha_s$. The tendency of the encapsulant to increase R_k is also noticeable in the LH-102 series of pigments. The LH-103 series paints have much lower R_k values than do those of the LH-102 series. This apparent anomaly may result from a slight difference in the initial Zn/Ti ratio.

The stability of the LH-102(6-12-A-10) paint is excellent. The other paints, with the exception of the "A" treated ones, respond nominally to a 2190 ESH exposure. In the LH-102 series, the Li_2SiO_3 -encapsulant greatly increases the degradation at 400nm. The spectra reveal also that the degradation in all cases occurs primarily in the visible region of the spectrum and is non-bleachable in O_2 .

4.5.6.4 Conclusions

The A-10 treatment is effective and helpful; the -"A" treatment alone, however, has obviously deleterious effects, while the -"10" treatment is relatively innocuous. Encapsulation of these pigments in Li_2SiO_3 in general decreases environmental stability and in some instances actually appears to accelerate the degradation of the vehicle. The value of α_s is somewhat higher in these series than in other paints prepared from COP pigments, partly because of a non-optimized particle size and partly because of the low R_k values.

4.5.7 IRIF Test I-70

4.5.7.1 Purpose/Description

IRIF Test I-70 (Ref. 4.10) was designed and conducted to discern optimum treatments for the (COP) baseline (6-12) pigment, specifically acetic acid washing, recalcination and encapsulation.

4.5.7.2 Sequence

Reflectance measurements were made (in-situ) prior to UV irradiation, after 540 ESH, 1060 ESH and after 3130 ESH; a final scan was made of certain samples after the system pressures was increased to 760 torr using pure O_2 .

Table 4-19

IRIF TEST I-70

ULTRAVIOLET RADIATION TEST RESULTS

No.	Sample Description*	Solar Absorbance Values						$\Delta\alpha_s$
		ΔR_{400}	ΔR_{900}	Initial	540	1060	3130	O ₂ Bleach
1	(6-12)	.04	.065	.152	.173	.173	.171	.161
2	(6-12-10)	.045	.06	.180	.204	.203	.214	.189
3	(6-12-A-10)**	.025	.065	.213	.220	.221	.243	.226
4	(6-12):Li ₂ SiO ₃ **	.03	.05	.203	.209	.211	.224	.216
5	(6-12-10):Li ₂ SiO ₃ **	.03	.025	.194	.204	.209	.212	.018
6	(6-12-A-10):Li ₂ SiO ₃ **	.03	.02	.180	.188	.190	.194	.014
7	(6-12):K ₂ SiO ₃ **	.025	.02	.232	.239	.242	.244	.012
8	(6-12-10):K ₂ SiO ₃	.025	.02	.187	.191	.196	.203	.016
9	(6-12-A-10):K ₂ SiO ₃ **	.025	.02	.210	.219	.220	.225	.015
10	(6-12):K ₂ SiF ₆ **	.03	.03	.192	.202	.207	.213	.206
11	(6-12-10):K ₂ SiF ₆ **	.03	.025	.215	.225	.230	.231	.016
12	(6-12-A-10):K ₂ SiF ₆	.03	.05	.206	.228	.226	.234	.210

*All samples contain Zn₂TiO₄ from batch LH106 and treated as indicated; all are OI-650G paints

**Also irradiated in CREF Test No. 16

REPRODUCIBILITY OF THE
ORIGINAL PAGE IS POOR

4.5.7.3 Test Results

The materials tested in IRIF I-70 are described in Table 4.19, wherein also are pertinent test results. All the pigments have been derived from batch LH-106 and all samples are OI-650G paints. Representative reflectance spectra are presented in Fig's 4.108-111, inclusive. Table 4.19 and the figures are organized to show progressively the effects of acetic acid washes, recalcinations and encapsulants.

In Table 4.20 we summarize some of the relevant data. A general survey of the spectra shows that most of the paints are relatively stable. The induced changes range from 0.12 for the paint with the pigment (6-12): K_2SiO_3 to 0.34 for that with the (6-12-10) treatment. The 6-12 pigments of LH-106 do not exhibit a "knee", i.e., a low value of R_k . Consequently, the resulting "knee" reflectance R_{360} values range from 72 to 76%.

Table 4.20 suggests that, in the LH-106(6-12) pigments, acid washing has no significant effects, and, most importantly, that K_2SiO_3 provides much better protection than do any of the other encapsulants. This may be seen both at 400nm and at 900nm in all three series. The spectra of most samples show oxygen bleaching, (i.e. a recovery of ΔR_{900}). The ΔR_{900} data are particularly important because they indicate the effectiveness of an encapsulant. For instance, the .07/.01 ratio for ΔR_{900} of the (6-12) pigment reflects the fact that it is unencapsulated. In the same series the K_2SiO_3 permitted a ΔR_{900} of only .01 (O_2 bleaching spectra were not taken for this sample). The values of ΔR before and after O_2 bleaching at both 400nm and 900nm provide a measure of how good an O_2 barrier the encapsulant is. Consideration of both wavelength values is necessary, because in some instances absorption bands in other spectral regions affect the ΔR_{900} value. At 400nm the oxygen effect may result from an oxygen-related defect in the resin; equally likely it may be provoked by the encapsulant or the surface defects of an unprotected pigment (Ref. 4.7).

TABLE 4-20
SELECTED IRIF-I-70 DATA

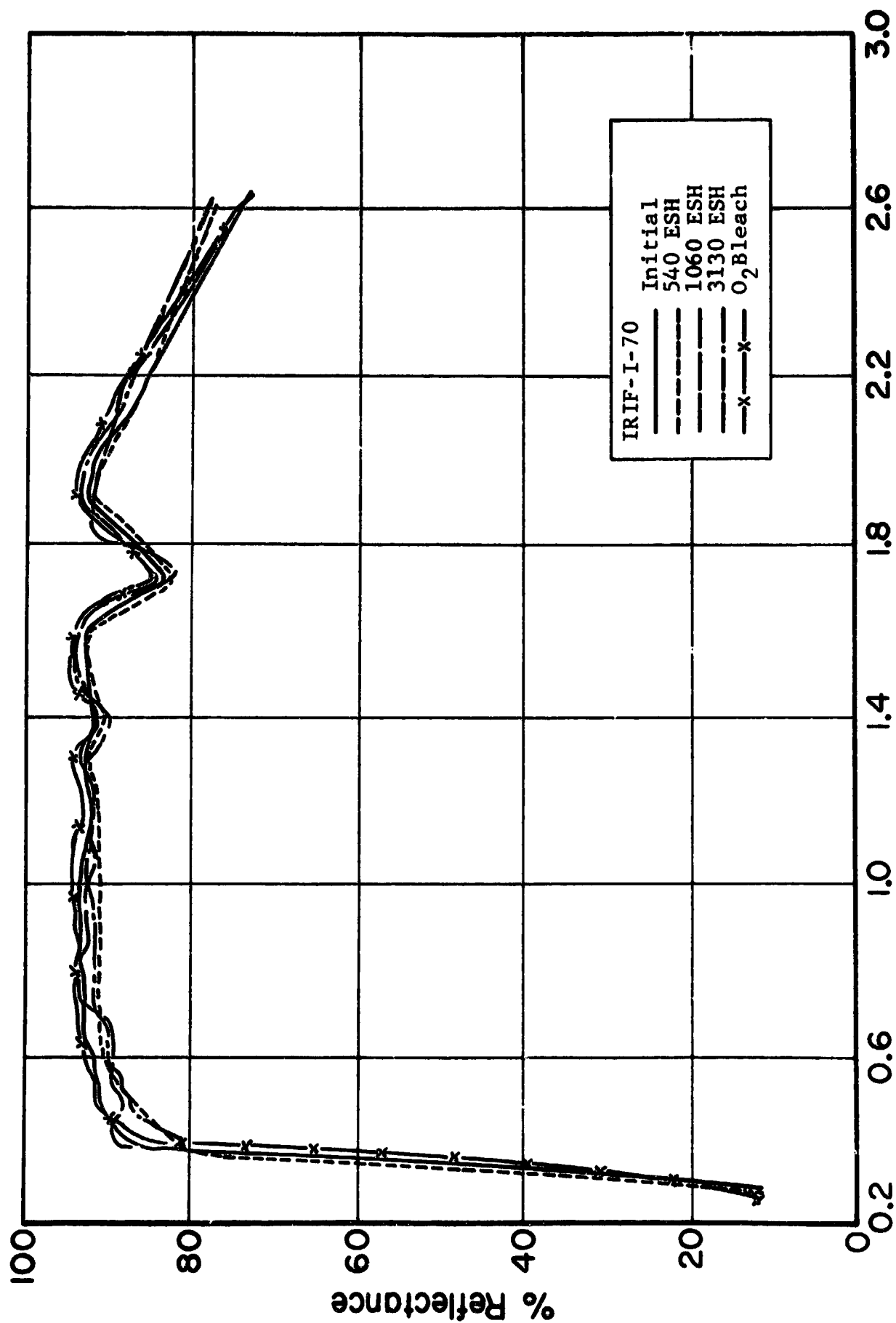
Paint Pigment		α_s	$\Delta\alpha_s$	ΔR_{400}^*	ΔR_{900}^*
Series	Treatment				
<u>6-12</u>		.152	.019	.04/.005	.07/.01
	<u>Li₂SiO₃</u>	.203	.021	.03/.005	.045/.025
	K ₂ SiO ₃	.232	.012	.025/-	.01/-
	K ₂ SiF ₆	.192	.021	.03/.005	.035/.02
<u>6-12-A-10</u>		.213	.030	.03/.01	.06/.03
	<u>Li₂SiO₃</u>	.180	.014	.03/-	.025/-
	K ₂ SiO ₃	.210	.015	.015/-	.015/-
	K ₂ SiF ₆	.206	.028	.03/.005	.055/.015
<u>6-12-10</u>		.180	.034	.045/.015	.06/.01
	<u>Li₂SiO₃</u>	.194	.018	.03/-	.03/-
	K ₂ SiF ₆	.187	.016	.025/-	.02/-
	K ₂ SiF ₆	.215	.016	.03/-	.03/0

* ΔR values are given before and after O₂ bleaching.

4.5.7.4 Conclusions

The LH-106 series is obviously an intrinsically stable pigment and results in very stable paint systems. The fact that none of the three series prepared evidences a knee may bear upon the explanation for this stability. We observe also that acid washing should not be expected to produce any significant results in a pigment which has no "knee". Further, a stoichiometry in which an excess of either ZnO, TiO₂ or other reaction product(s) is not evident may also create a different defect structure, thus changing the amount and nature of the surface defects whose optical effects an encapsulant must mitigate or prevent.

Some of the I-70 paints were irradiated in CREF-16, which will be discussed later in detail. These paints substained much greater degradation in CREF-16 than was evident in I-70. A



Wavelength, (μ)

Figure 4.108 REFLECTANCE SPECTRA OF LH-106(6-12)/G

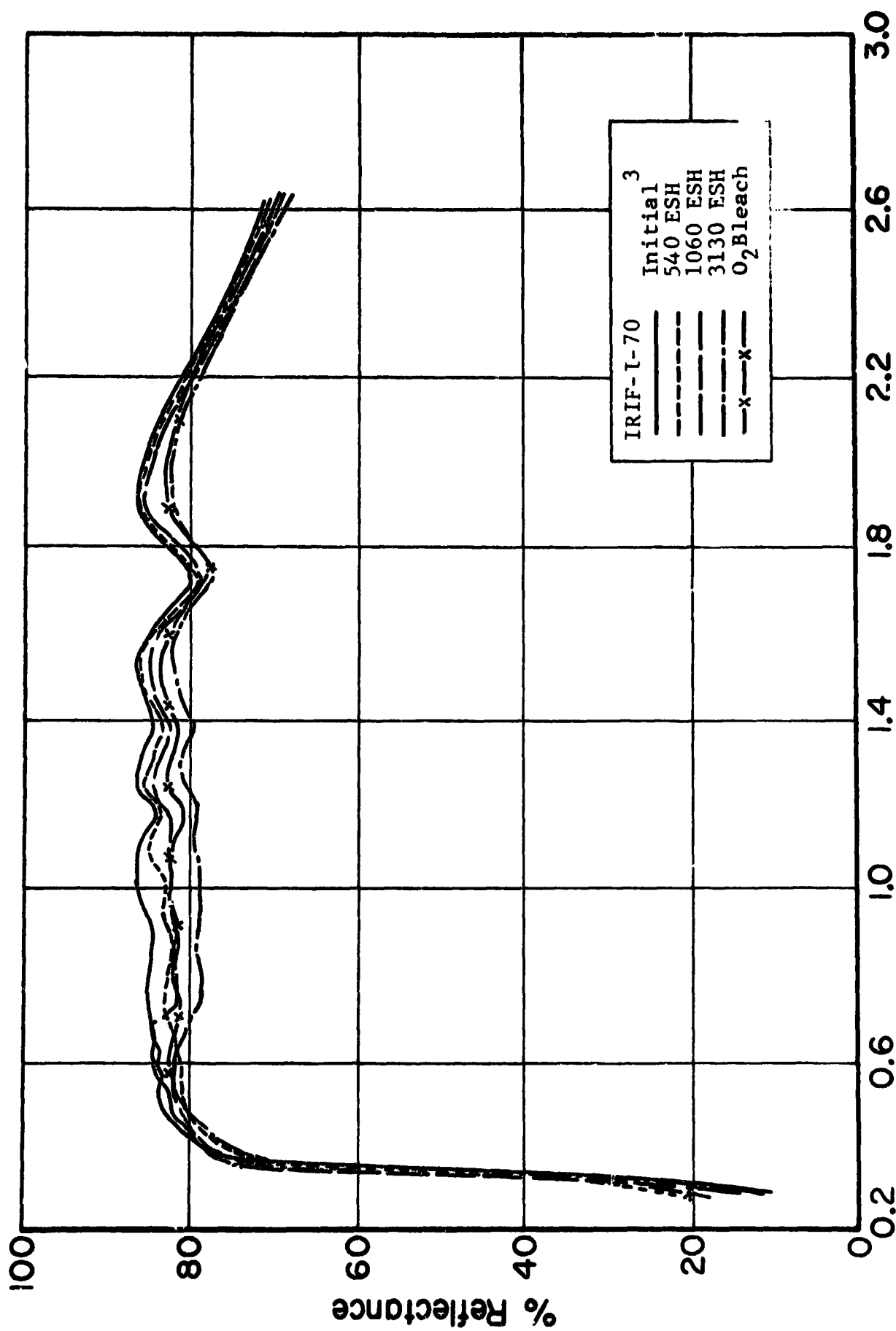


Figure 4.109 REFLECTANCE SPECTRA OF LH-106(6-12-A-10)/C

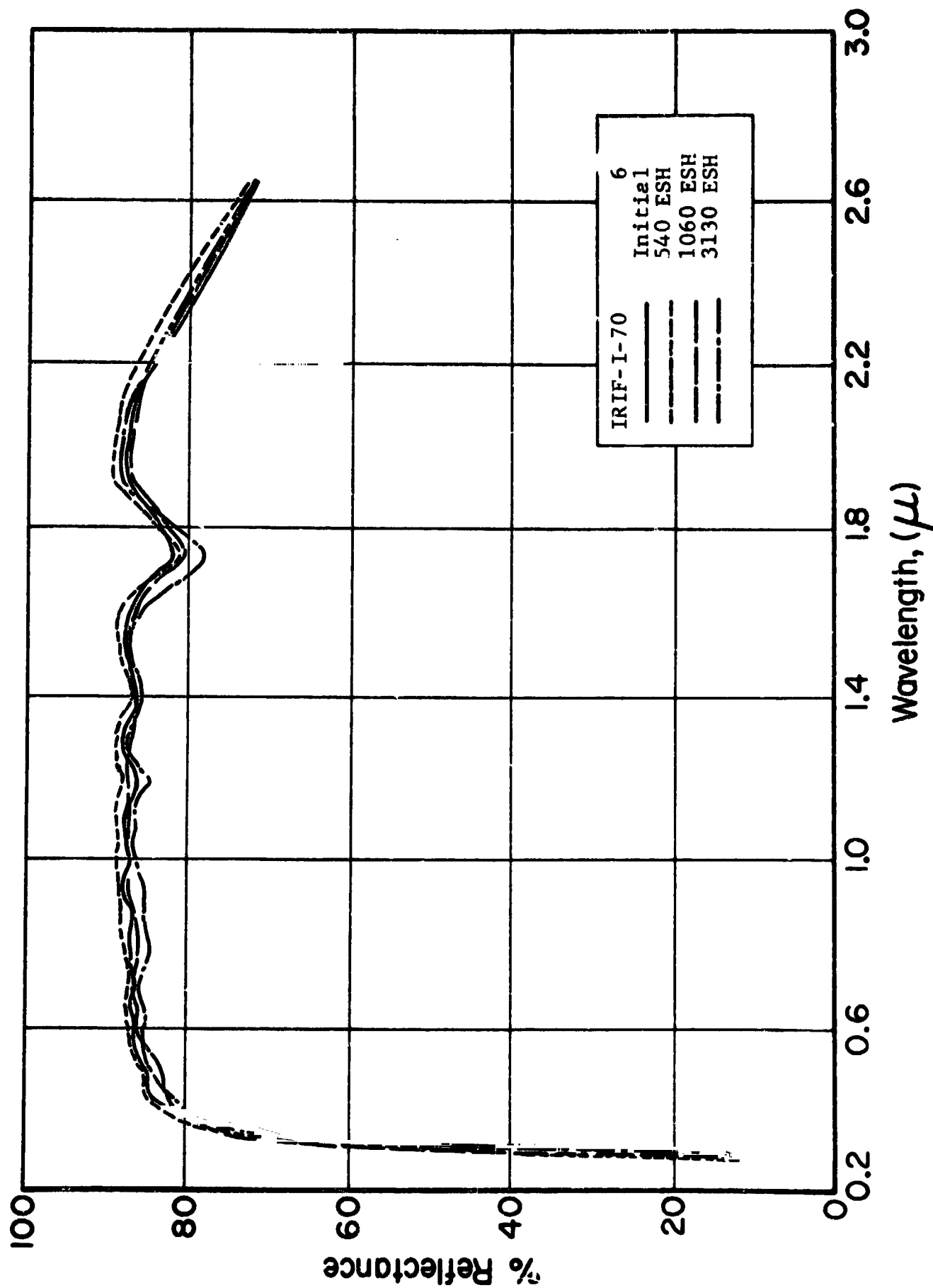


Figure 4.110 REFLECTANCE SPECTRA OF LH-106(6-12-A-10):Li₂SiO₃/C

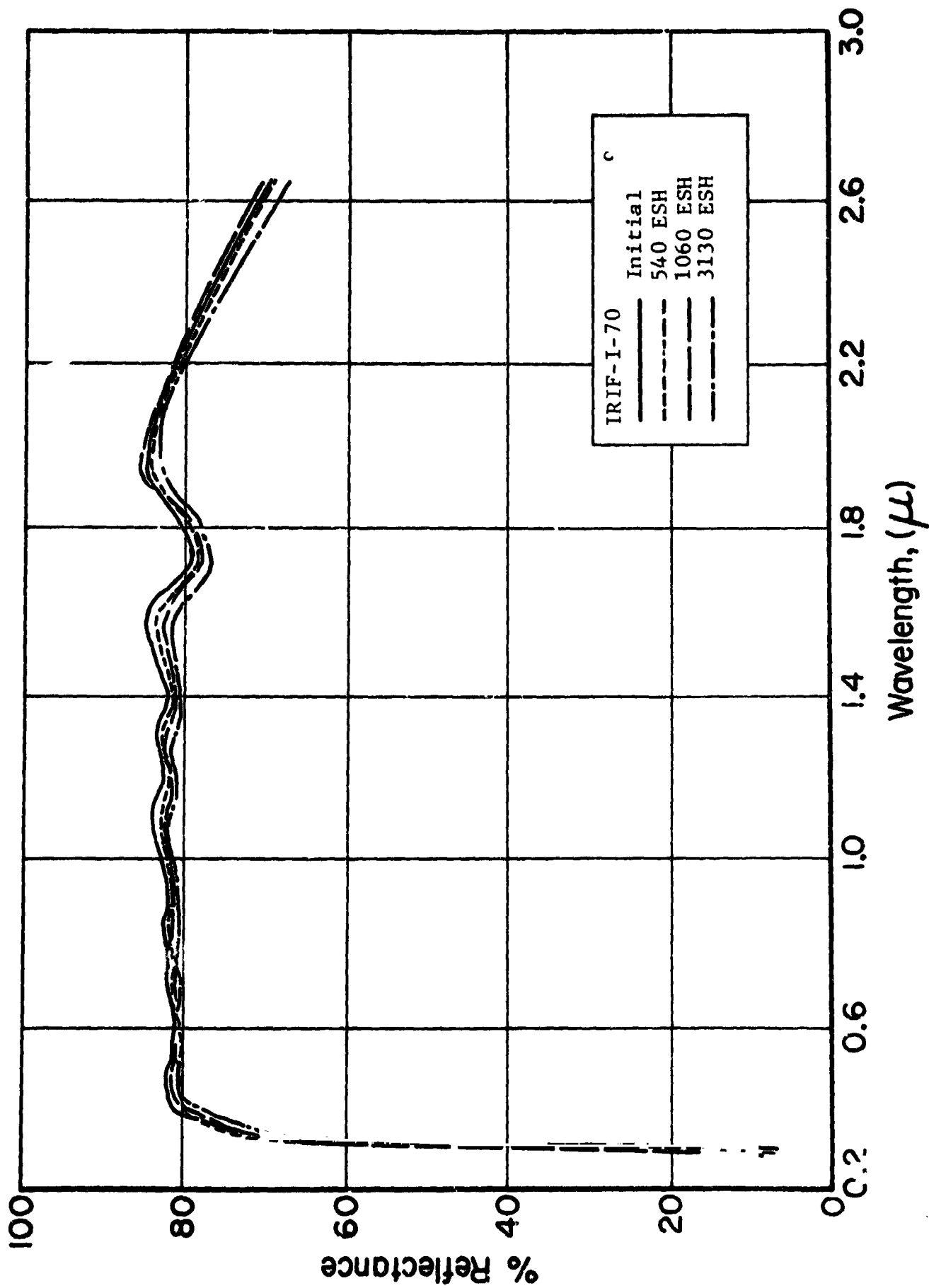


Figure 4.111 REFLECTANCE SPECTRA OF LH-106(6-12-A-10):K₂SiO₃/C

later inspection of the IRIF disclosed that a corroded heat exchanger had introduced contamination in the A-H6 water cooling system, diminishing its UV transmission and thus the effective UV intensity at the sample location. (The UV monitor not being spectrally selective, showed only a small reduction in total intensity). Nevertheless the comparative results of I-70 and the conclusions reached from them remain valid, - with two qualifications. The data should not be used for engineering purposes. Since the absorption introduced into the A-H6 cooling water very probably increases strongly with decreasing wavelength, the silicone resin would tend to look very much more stable: ΔR_{400} values for IRIF-I-70 are therefore substantially less, comparatively, than those for CREF-16.

4.5.8 IRIF Test No. I-71

4.5.8.1 Purpose/Descriptions

The samples in IRIF Test No. I-71 (Ref. 4.10), with the exception of S-13G, are all Zn_2TiO_4 powder films on IRIF coupons. The full complement of test samples is listed in Table 4.21, along with their associated solar absorptance values. The MOX-A materials (where MOX refers to "mixed oxalates" and "A", to a specific batch) differ from previous Zn_2TiO_4 pigments in two important ways. First, and most important, an error was made in the formulation of the MOX-A material resulting in a 1.49:1.0 1.49 Zn/Ti mole ratio rather than the theoretically required 2.0 value. This will be discussed in detail in a subsequent section. Second, the MOX-A pigments were prepared by mixing individually precipitated zinc and titanium "oxalates" and then converting the mixture to Zn_2TiO_4 . This differs from previous Zn_2TiO_4 pigments in that their precursors were coprecipitated and then converted. The important advantage to the MOX method is the ability to utilize optimum size precursor oxalates, thus allowing control of the pigment particle size upon conversion.

Table 4-21

IRIF TEST I-71

ULTRAVIOLET RADIATION TEST RESULTS

Sample No.	Description*	Solar Absorbance Values					$\Delta\alpha_s$ 460
		Initial	130 ESH	460 ESH	1060 ESH	O ₂ Bleach	
7	MOX-A(6-9/4)	.170	.190	.194			.024
8	MOX-A(6-9/16)	.157	.176	.173			.016
9	MOX-A(6-10.5/2)	.124	.150	.158			.034
10	MOX-A(6-10.5/4)	.143	.163	.173			.030
5	MOX-A(6-10.5/8)	.160	.190	.209			.049
6	MOX(6-10.5/2)	.132	.140	.138	.172	.158	.008
3	LH-103(6-10.5/2)	.165	.181	.198			.033
4	LH-103(C6-10.5/2)**	.160	.181	.182			.022
2	MOX-A(6-12/0.5)	.116	.167	.184			.068
11	MOX-A(6-12/2)	.114	.143	.148			.034
12	S-13G (D274)	.165	.178	.193	.216	.226	.028
1	Si ₃ N ₄	.178	.203	.241			.063

*All samples, except for S-13G, are powders

**C6 indicates precursor oxalates were compressed at 5000 psi prior to 600°C pre-calcination

REPRODUCED
ORIGINAL PAGE IS POOR

Also in the test complement is a sample of "MOX", the original mixed oxalate batch with a Zn/Ti mole ratio of 2.05:1.0. For comparison purposes two samples of a COP pigment are also included.

An experimental pigment, silicon nitride, was included because of its very high purity and good whiteness. S-13G was placed in the test as a control. The test was carried out to evaluate the MOX method samples and to compare their properties and performance with other Zn_2TiO_4 pigments.

4.5.8.2 Sequence

Reflectance measurements were made prior to irradiation, at exposures of 130 ESH, 460 ESH, and (for 2 selected samples) at 1060 ESH, and (again for the same 2 samples) after a post-irradiation O_2 bleach.

4.5.8.3 Test Results

Properties and performance data are presented in Table 4.21. Table 4.22 points up some differences between MOX-A, MOX and LH-103 pigments. The reflectance spectra of the samples appear in Figures 4.112-119 inclusive.

As Table 4.21 shows, the degradation of the MOX-A pigments exceeds reasonable limits. The test (for all but the S-13G and the MOX pigment samples) was terminated after only 460 ESH. This was done because the degradation of Zn_2TiO_4 irradiated as a pigment is always less than in OI-650G paints. The results, nonetheless, are very informative. The absence of substantial damage in the S-band of the MOX-A pigments raises a serious challenge to our long standing requirement for a 2.05:1.0 Zn/Ti mole ratio in Zn_2TiO_4 pigments. This requirement was based on two observations: one, that a Zn excess in the Zn_2TiO_4 product can be chemically extracted, while a Ti excess can not; and, second, that a Ti excess would promote S-band damage, presumably caused by photo-induction of the reaction $\text{T}_i^{+4} \xrightarrow{h\nu} \text{T}_i^{+3}$. This second observation may indeed yet be true for SS pigments.

Table 4-22

SELECTED IRIF-I-71 TEST DATA

Table 4 22A

COMPARISON OF MOX-A WITH OTHER PIGMENTS

Index	Pigment: Treatment:	MOX-A		MOX		LH-103		LH-103	
		$\frac{(6-10.5/2)}{(6-10.5/2)}$		$\frac{(6-10.5/2)}{(6-10.5/2)}$		$\frac{(6-10.5/2)}{(6-10.5/2)}$		$\frac{(6-10.5/2)}{(6-10.5/2)}$	
R_k		71		56		39		41.5	
R_{max}		98		93		90.5		91	
ΔR_{400}		.035		.02		.03		.025	
ΔR_{900}		.055		.132		.065		.04	
$\Delta \alpha_s$.034		.006		.033		.022	

Table 4 22B

INTERCOMPARISON OF MOX-A PIGMENTS

Index	MOX-A Pigment									
	$\frac{6-9/4}{6-9/16}$	$\frac{6-9/16}{6-10.5/2}$	$\frac{6-10.5/2}{6-10.5/4}$	$\frac{6-10.5/4}{6-10.5/8}$	$\frac{6-10.5/8}{6-12/0.5}$	$\frac{6-12/0.5}{6-12/2}$				
R_k	63	69.5	71	69	72	81.5	88.5			
R_{max}	91	93	98	97.5	90.5	97	97.5			
ΔR_{400}	.03	.02	.035	.02	.03	.05	.025			
ΔR_{900}	.05	.045	.055	.055	.085	.12	.055			
α_s	.170	.157	.124	.143	.160	.116	.114			
$\Delta \alpha_s$.024	.016	.034	.030	.049	.058	.032			

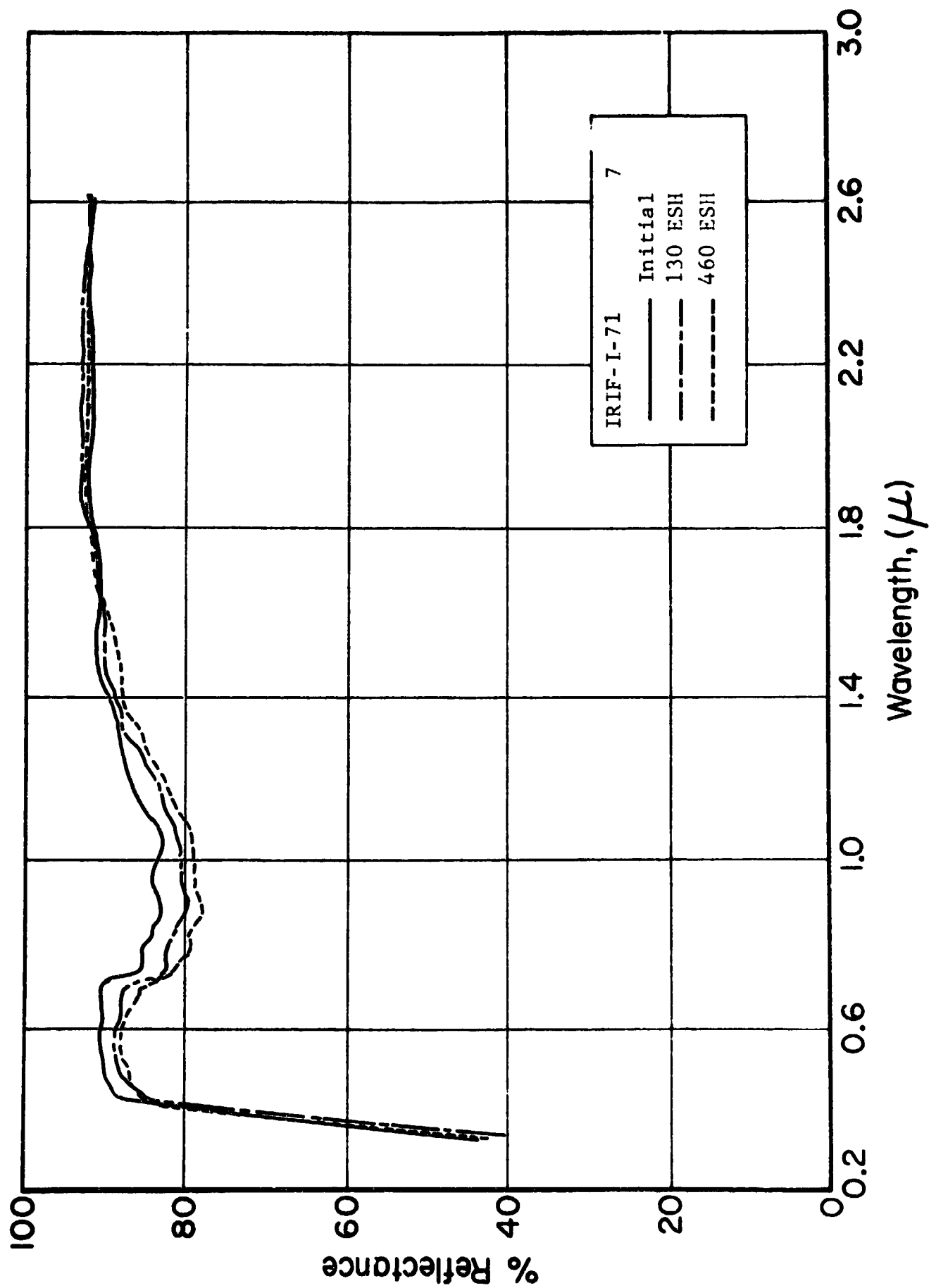
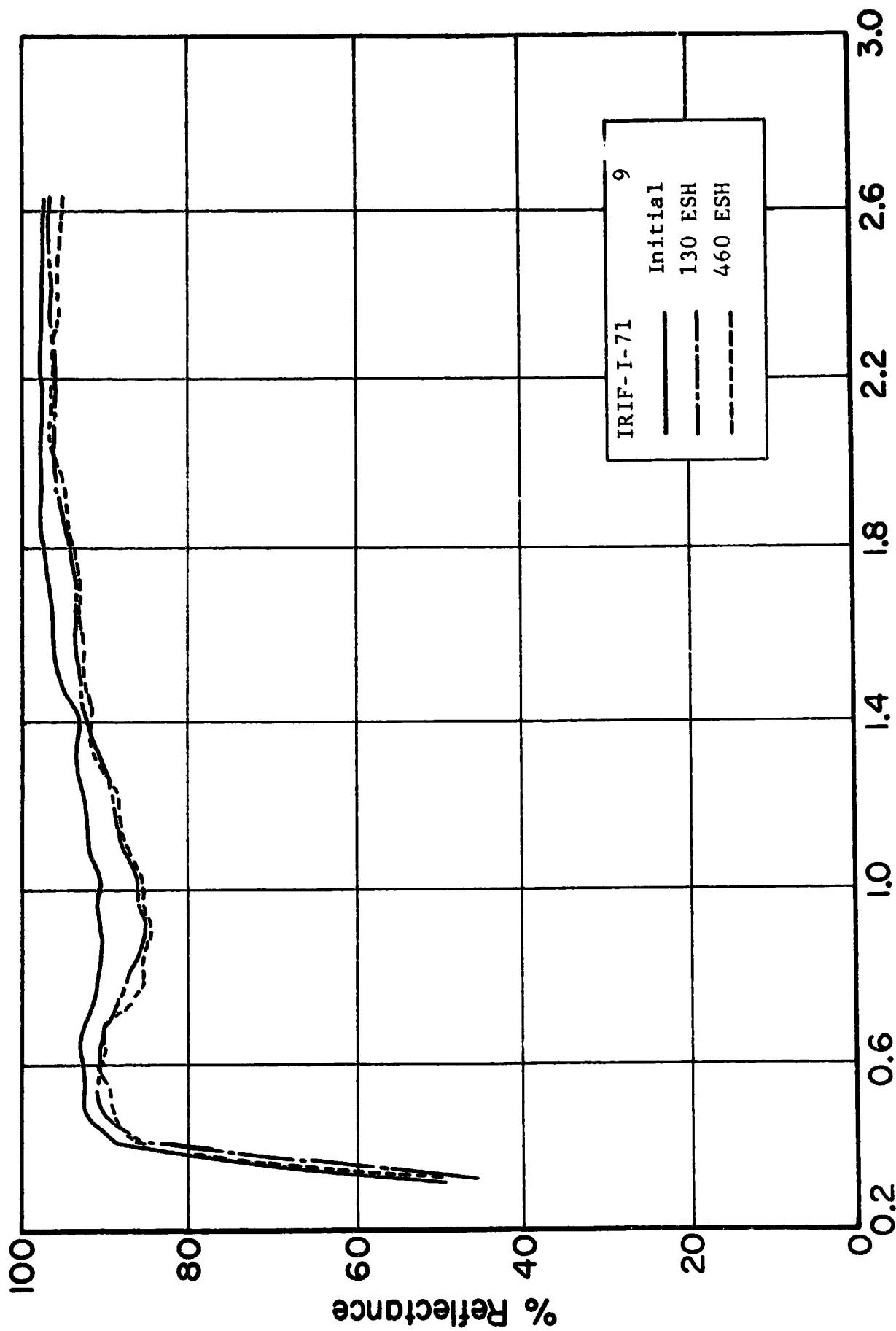


Figure 4.112 REFLECTANCE SPECTRA OF MOX-A(6-9/4) (Powder)



Wavelength, (μ)

Figure 4.113 REFLECTANCE SPECTRA OF MOX-A(6-10.5/2) (Powder)

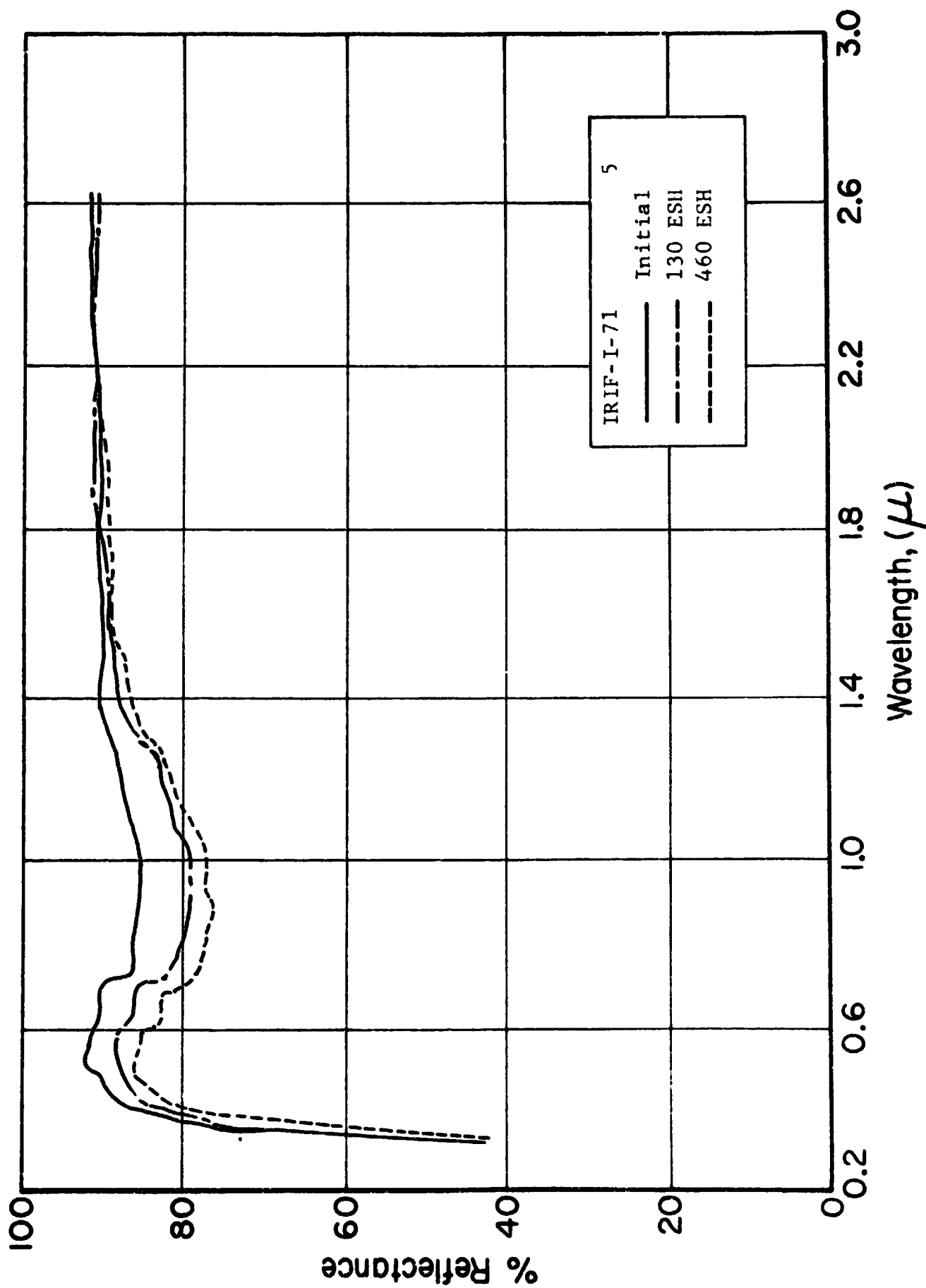


Figure 4.114 REFLECTANCE SPECTRA OF MOX-A (6-10.5/8) (Powder)

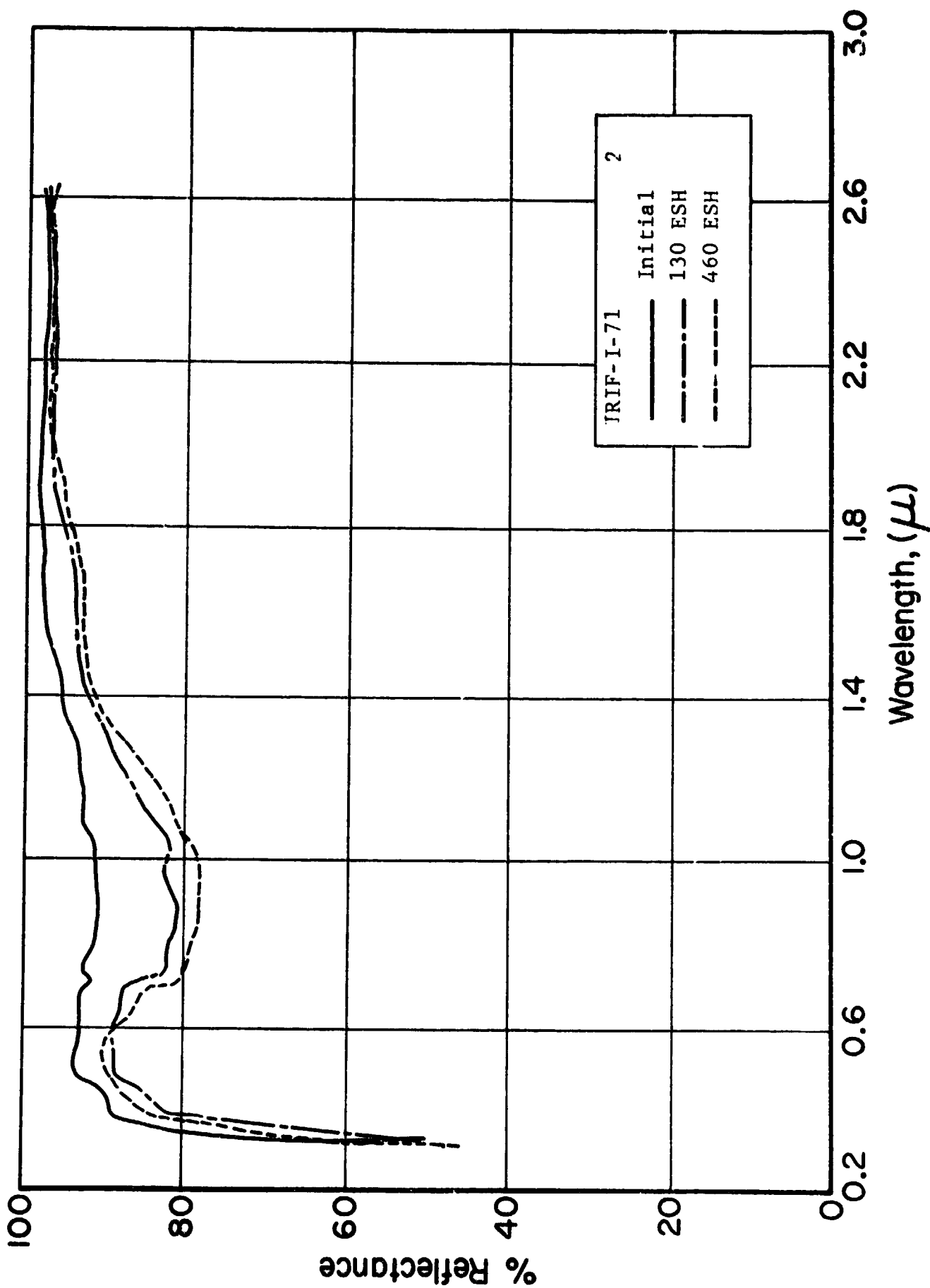


Figure 4.115 REFLECTANCE SPECTRA OF MOX-A(6-12/0.5) (Powder)

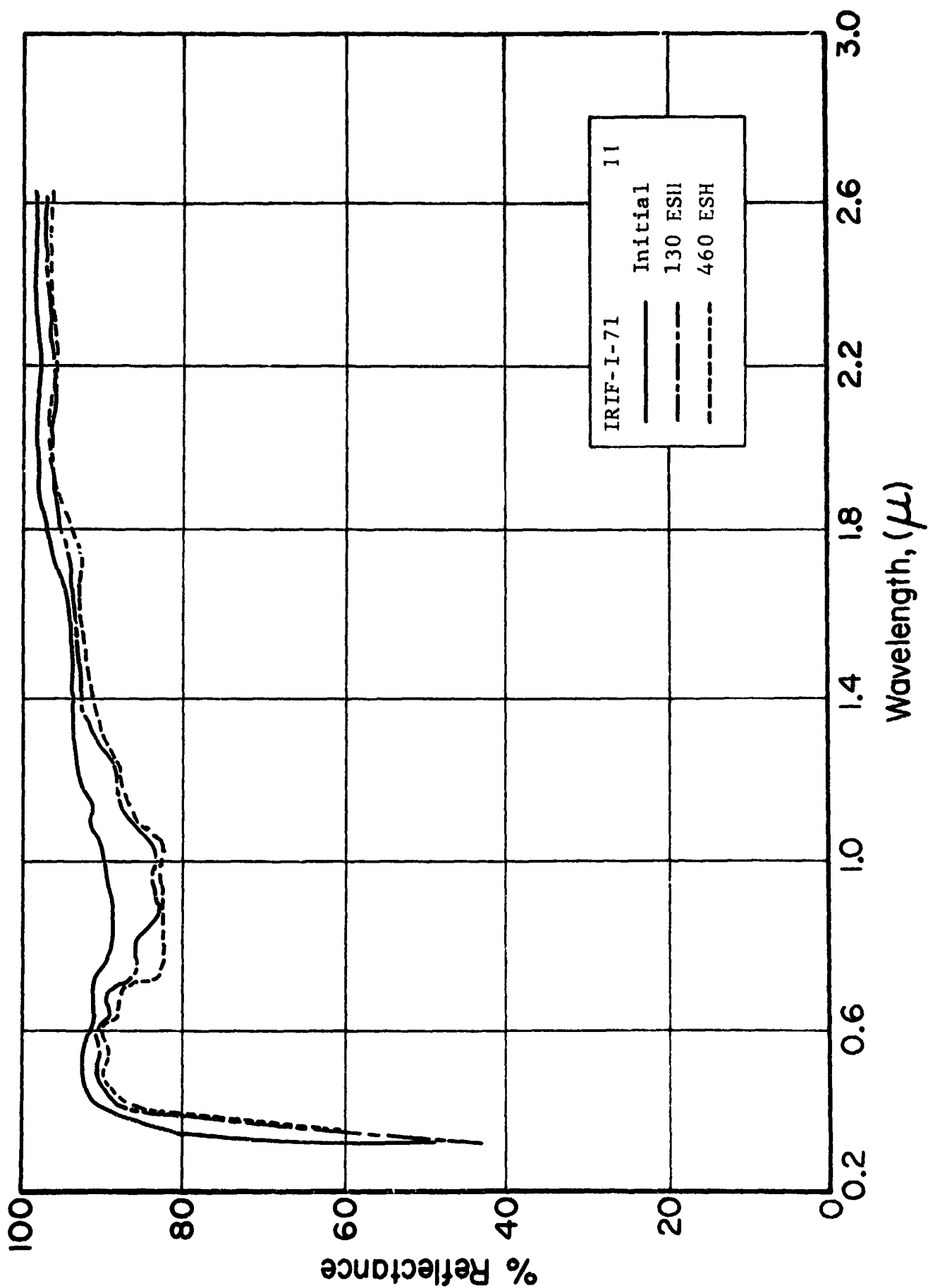


Figure 4.116 REFLECTANCE SPECTRA OF MOX-A(6-12/2) (Powder)

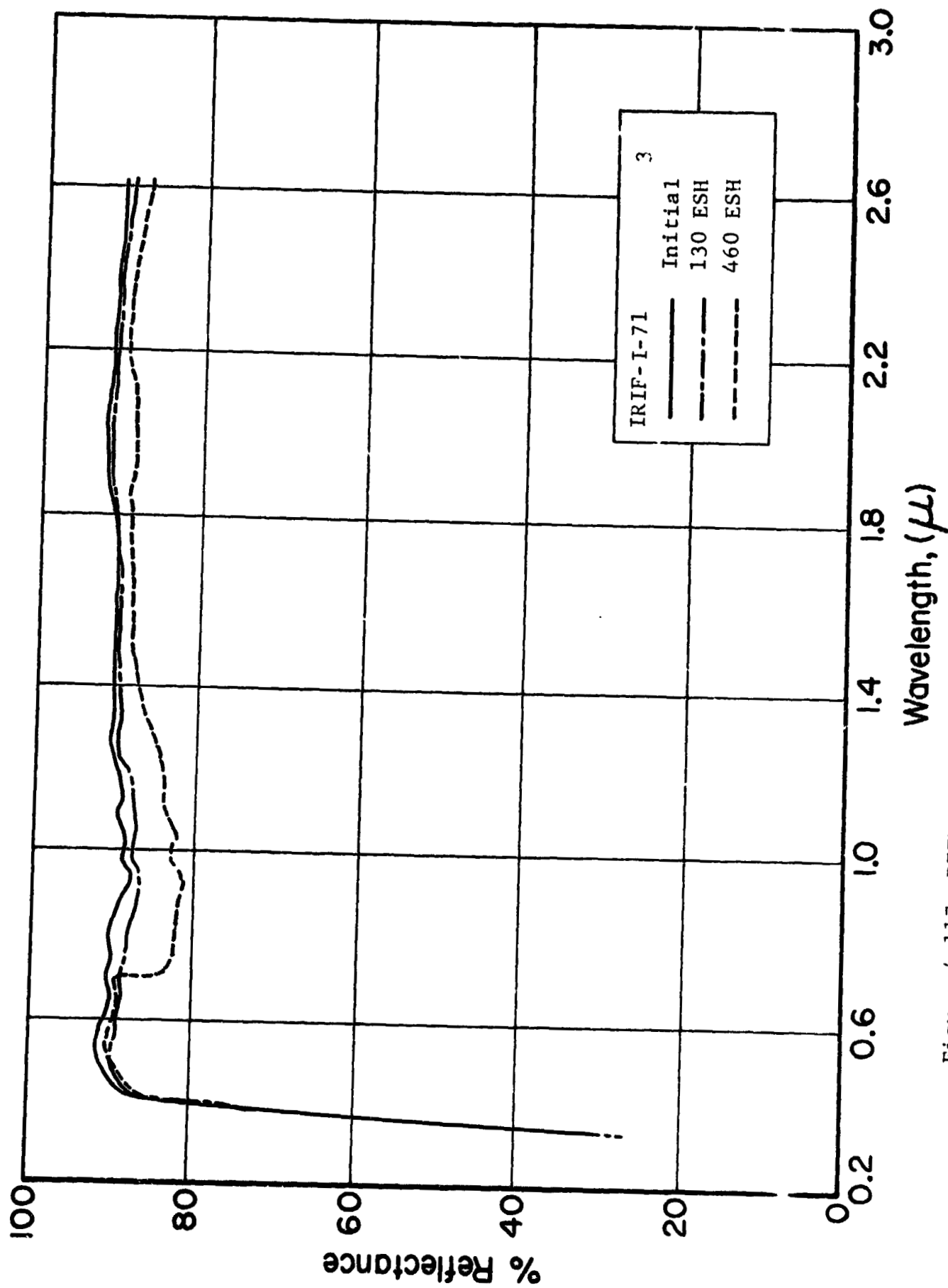


Figure 4.117 REFLECTANCE SPECTRA OF LH-103(6-10.5/2) (Powder)

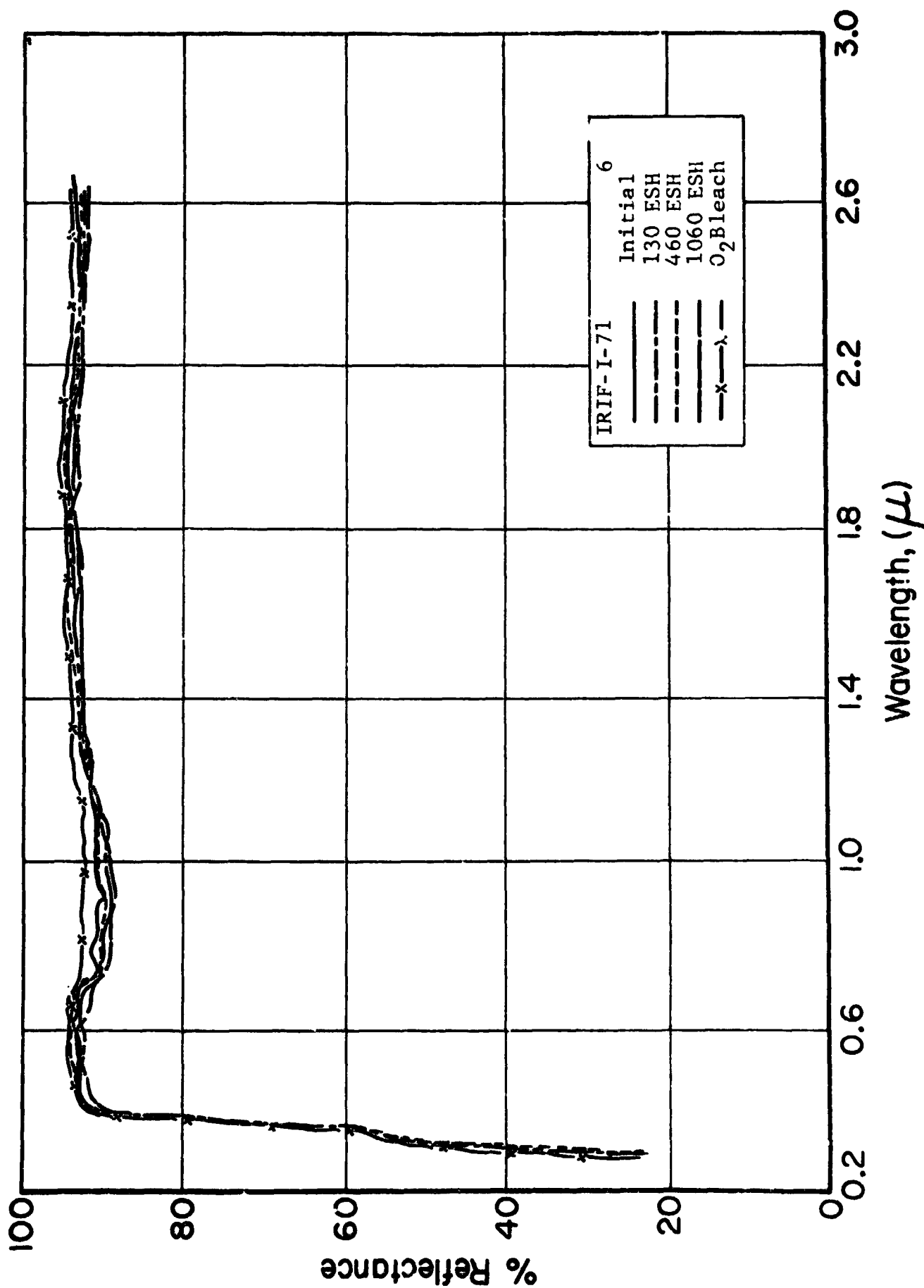


Figure 4.118 REFLECTANCE SPECTRA OF MOX(6-10.5/2) (Powder)

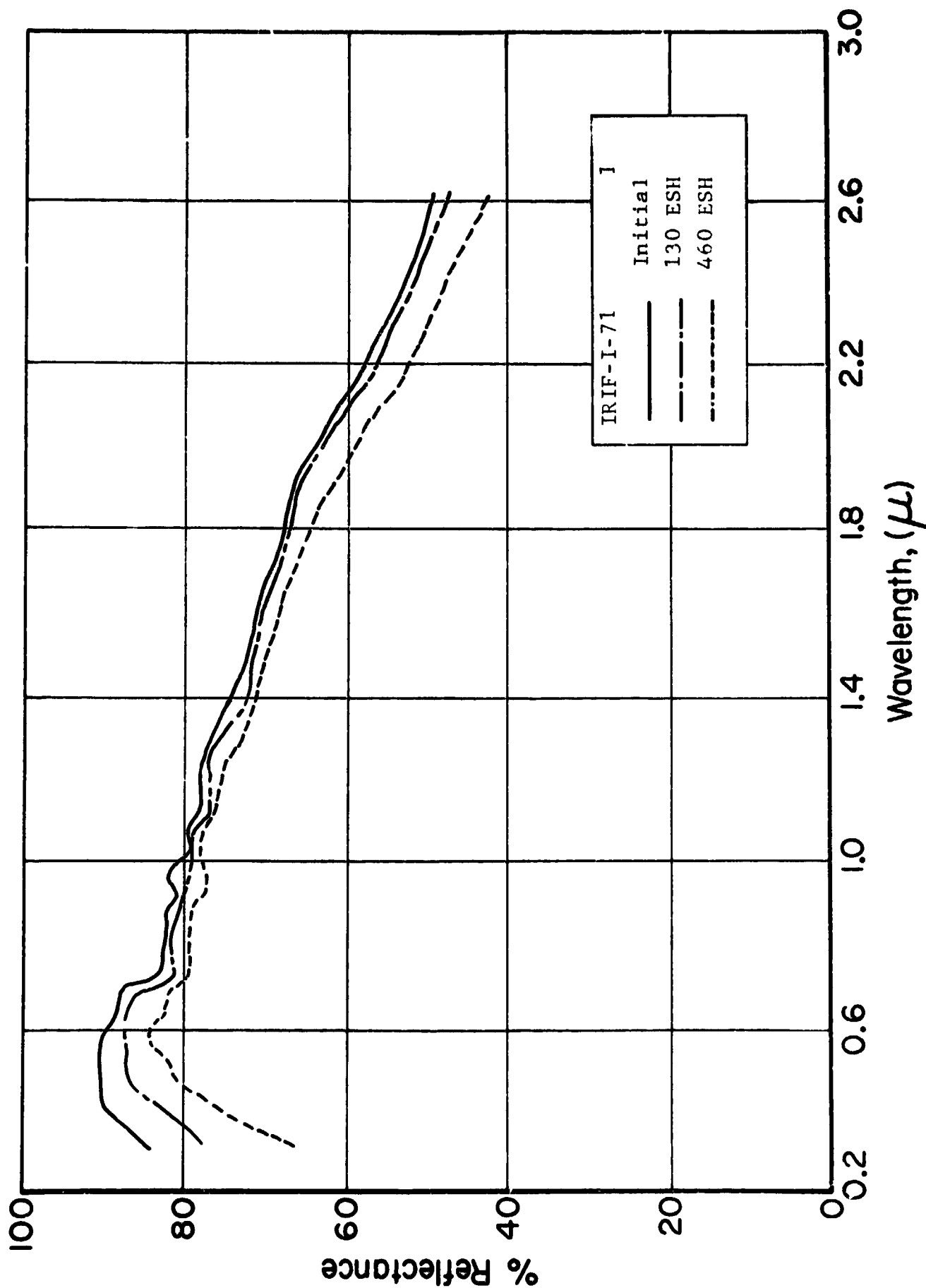


Figure 4.119 REFLECTANCE SPECTRA OF Si_3N_4 (Powder)

4.5.8.4 Analyses

Table 4.22A contains some data which may relate to the anomalous lack of S-band development. We associate low values of R_k with fundamental absorption due to excess ZnO or of TiO_2 . We therefore expect that R_k would be much lower in the case of MOX-A, than in the case of either "MOX" or LH-103. MOX-A, relative to the stoichiometry of Zn_2TiO_4 , contains a 25 mole % excess of Ti while the latter pigments contain approximately 2 mole % excess of Zn. Significantly, the R_k values of the MOX-A pigments differ substantially from one another but, rather than being lower, R_k of the MOX-A pigment is higher than that of the others, thus evidencing no free TiO_2 .

The influence of temperature and time on the properties and performance of MOX-A pigments is shown in Table 4.22B. The improvement of R_k with increasing calcination temperature and time stands out clearly. Generally, while the effect of temperature is as expected, it considerably surpasses that of time at temperature, but the net effect of time may be either beneficial or adverse. The adverse effects of time at temperature on S-band damage (ΔR_{900}) in the 6-10.5 series contrasts with its desirable effects in the (6-12) series.

In summary, IRIF-I-71 test results, primarily those of $\Delta\alpha_s$, clearly demonstrate the instability of MOX-A pigments. The properties and performance of these pigments, whose Zn/Ti mole ratio is at substantial variance from the theoretically necessary stoichiometry of Zn_2TiO_4 , raise fundamental questions about the true nature of the precursor oxalates, the chemistry of their conversion to titanates, and the sensitivity of optical properties and environmental stability to pigment stoichiometry. We address these questions in subsequent investigations.

Table 4-23

IRRADIATION TEST RESULTS CREF-16

Sample Description*	Solar Absorptance Values				$\Delta \alpha_s^{**}$
	Initial	335 ESH	900 ESH	2750 ESH	4720 ESH
(6-12):K ₂ SiO ₃	.224	.246	.245	.253	.267
(6-12):K ₂ SiF ₆	.208	.230	.244	.254	.267
(6-12):Li ₂ SiO ₃	.208	.241	.238	.248	.251
(6-12-A-10)	.182	.225	.236	.236	.246
(6-12-A-10):K ₂ SiO ₃	.197	.214	.240	.258	.253
(6-12-A-10):Li ₂ SiO ₃	.217	.232	.241	.242	.245
(6-12-10):Li ₂ SiO ₃	.181	.200	.202	.221	.224
(6-12-10):K ₂ SiF ₆	.226	.247	.251	.267	.266

*All samples are OI-650G paints with COP LH-106 Zn₂TiO₄ pigments.

** $\Delta \alpha_s$ after 4720 ESH; samples 5 and 12 also received approximately 10^{15} p⁺/cm².

Table 4-24

DATA COMPARISON: CREF TEST No. 16 VS IRIF I-70

No.	(I)	Sample No. (C)	Description	R_k		α_s		$\Delta\alpha_s$		
				(I)*	(C)*	(I)*	(C)*	1060(I)*	900(C)*	Exposure (ESH) 3130(I)
1		10	(6-12):K ₂ SiO ₃	73.5	73.0	.232	.225	.010	.020	.012
10		11	(6-12):K ₂ SiF ₆	73.6	73.0	.192	.208	.015	.036	.021
4		7	(6-12):Li ₂ SiO ₃	72	72.5	.203	.208	.008	.030	.021
3		6	(6-12-A-10)	72	72.5	.213	.182	.008	.054	.030
9		5	(6-12-A-10):K ₂ SiO ₃	76.5	76.5	.210	.197	.010	.043	.015
6		9	(6-12-A-10):Li ₂ SiO ₃	74.5	73.0	.180	.217	.010	.024	.014
5		8	(6-12-10):Li ₂ SiO ₃	74	74.0	.194	.181	.015	.021	.018
11		12	(6-12-10):K ₂ SiF ₆	73.5	71.5	.215	.226	.015	.025	.016

Notation: I - IRIF-I-70; C = CREF Test No. 16

4.5.9 CREF Test No. 16

4.5.9.1 Purpose/Description

Duplicate samples of materials previously irradiated in IRIF Test No. I-70 were irradiated in CREF Test No. 16 (ref. 4.10) in order to extend our knowledge of the more stable COP Zn_2TiO_4 paint systems. (The purpose was not to compare the degradation data obtained in CREF-16 with those in IRIF-I-70).

All of the pigments in this test are Zn_2TiO_4 prepared from IITRI batch LH-106 COP Zn_2TiO_4 . IITRI batches LH-103 (~19%), LH-104 (~39%) and LH-105 (~42%) were blended to make LH-106. All samples are OI-650G paints cured at 325°F for 16hrs. The descriptions of the pigments involved are given in Table 4.23 along with their relevant test data.

4.5.9.2 Sequence

Diffuse reflectance measurements were performed on each sample before irradiation and after exposure to 335 ESH, 900 ESH, 2750 ESH and 4720 ESH. A post-irradiation oxygen bleaching experiment was not conducted. Two of the samples (Nos. 5 and 12) were exposed to a flux of 1.2 KeV proton radiation, estimated to be approximately 10^{15} p/cm².

4.5.9.3 Test Results

The reflectance spectra of the paints are shown in Figures 4.120-125. It should be noted that these paints are duplicates of those irradiated in IRIF Test No. I-70 thus providing data directly comparable to those obtained in IRIF Test No. I-70. Table 4.24 presents the data which can be compared; where it is most apparent that degradation in this CREF test greatly exceeds that in the previous IRIF test.

In the present case, the largest increment in $\Delta\alpha_s$ occurred in the first 335 ESH. After 4720 ESH, maximum $\Delta\alpha_s$ (.064) was exhibited by the (6-12-A-10) system; the least (.028), by the (6-12-A-10): Li_2SiO_3 system. The exposure corresponds to approximately one-half year of continuous exposure to the sun (at 1 A.U.).

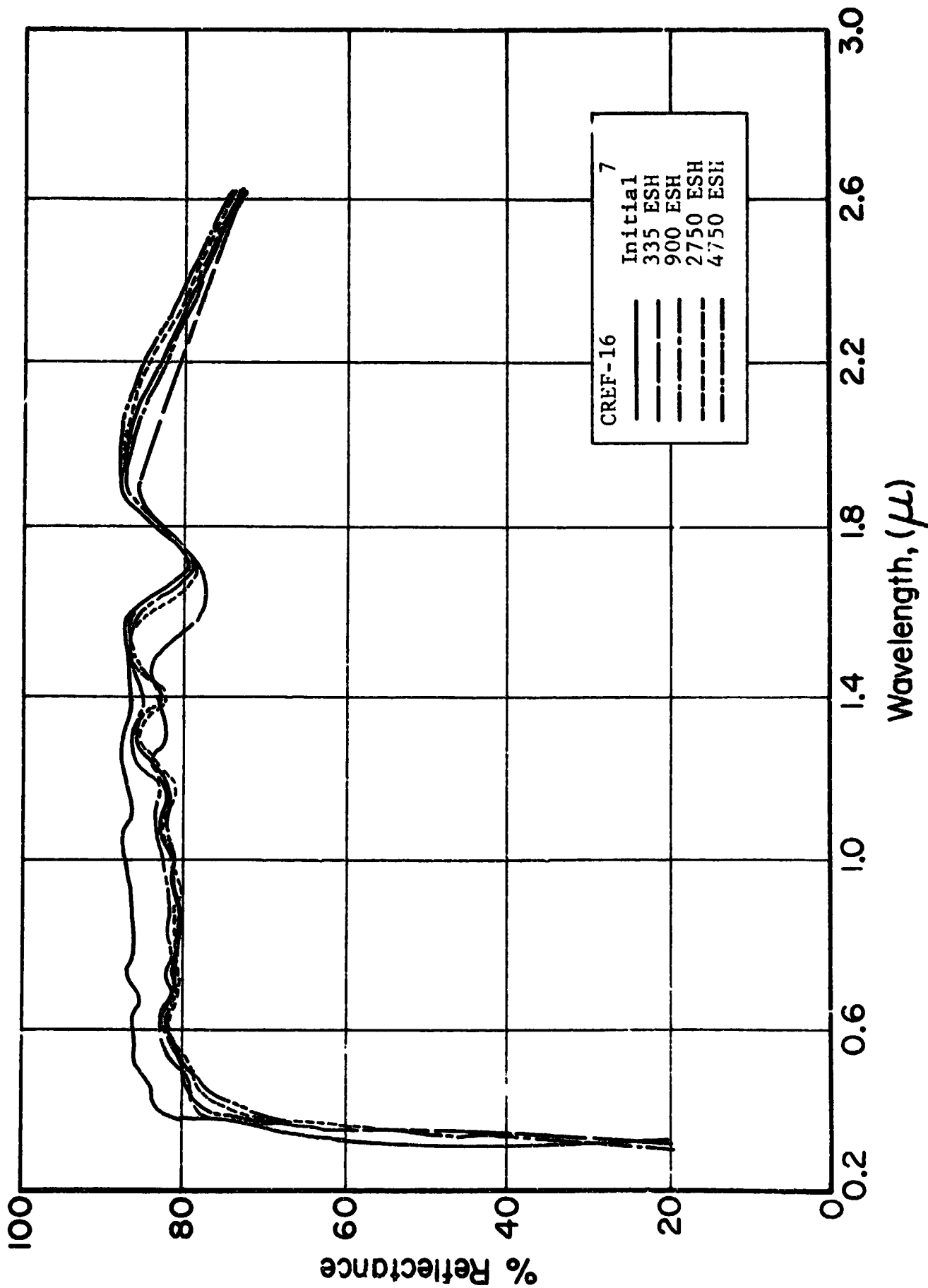


Figure 4.120 REFLECTANCE SPECTRA OF $\text{Li}_7\text{SiO}_3/\text{C}$

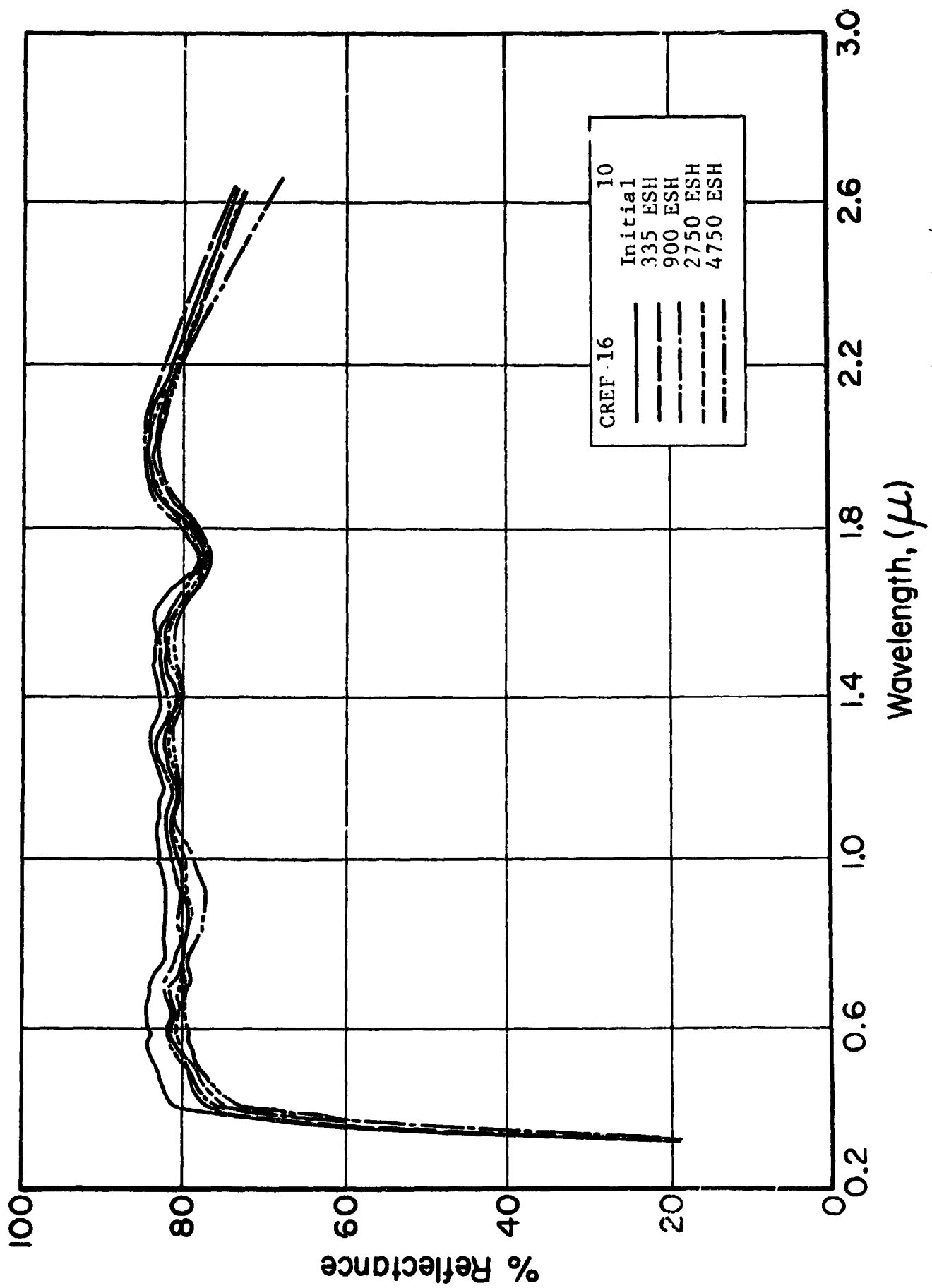


Figure 4.121 REFLECTANCE SPECTRA OF LH-106 (6-12):K₂SiO₃/G

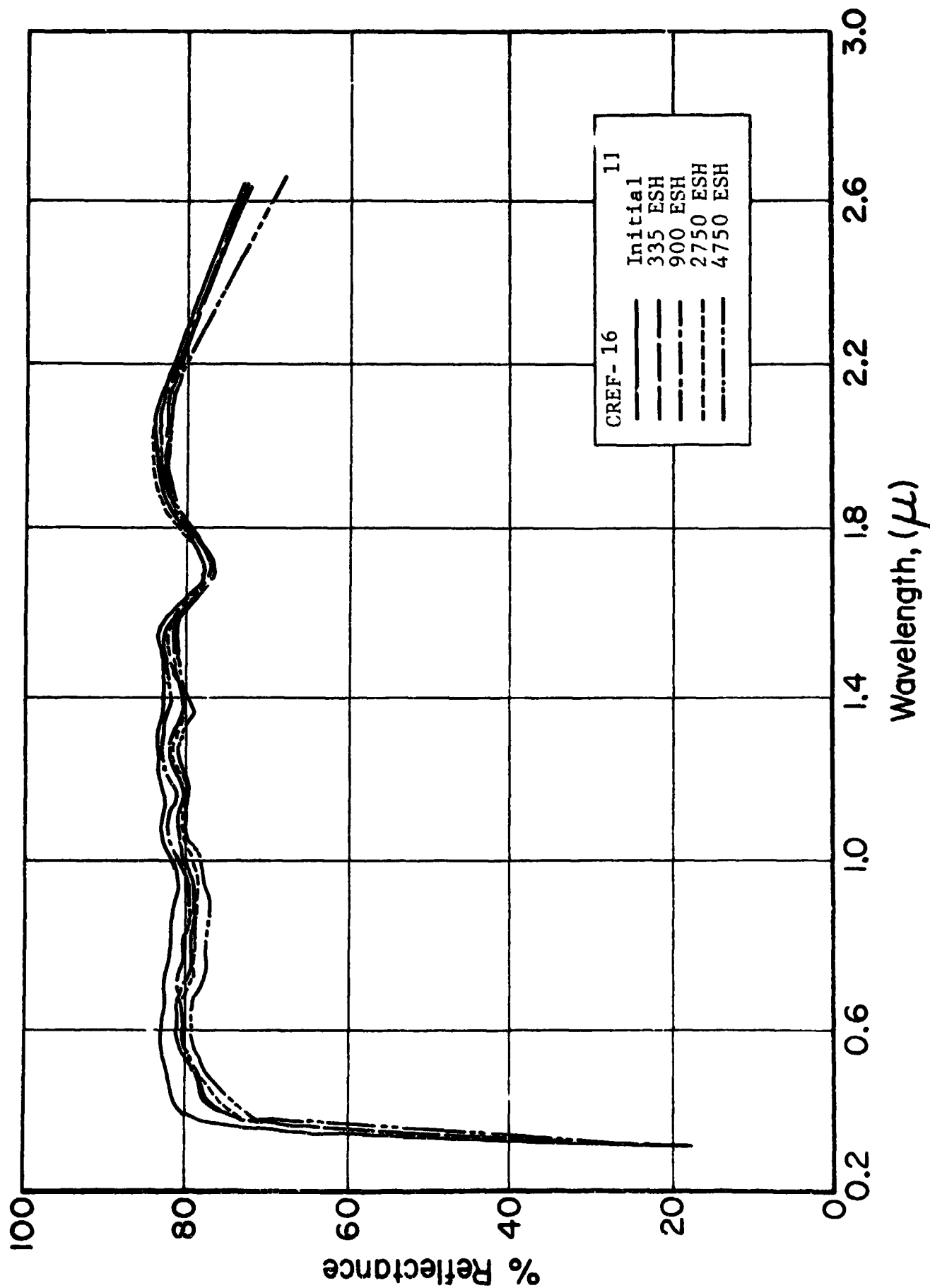


Figure 4.122 REFLECTANCE SPECTRA OF LHI-106(6-12):K₂SiF₆

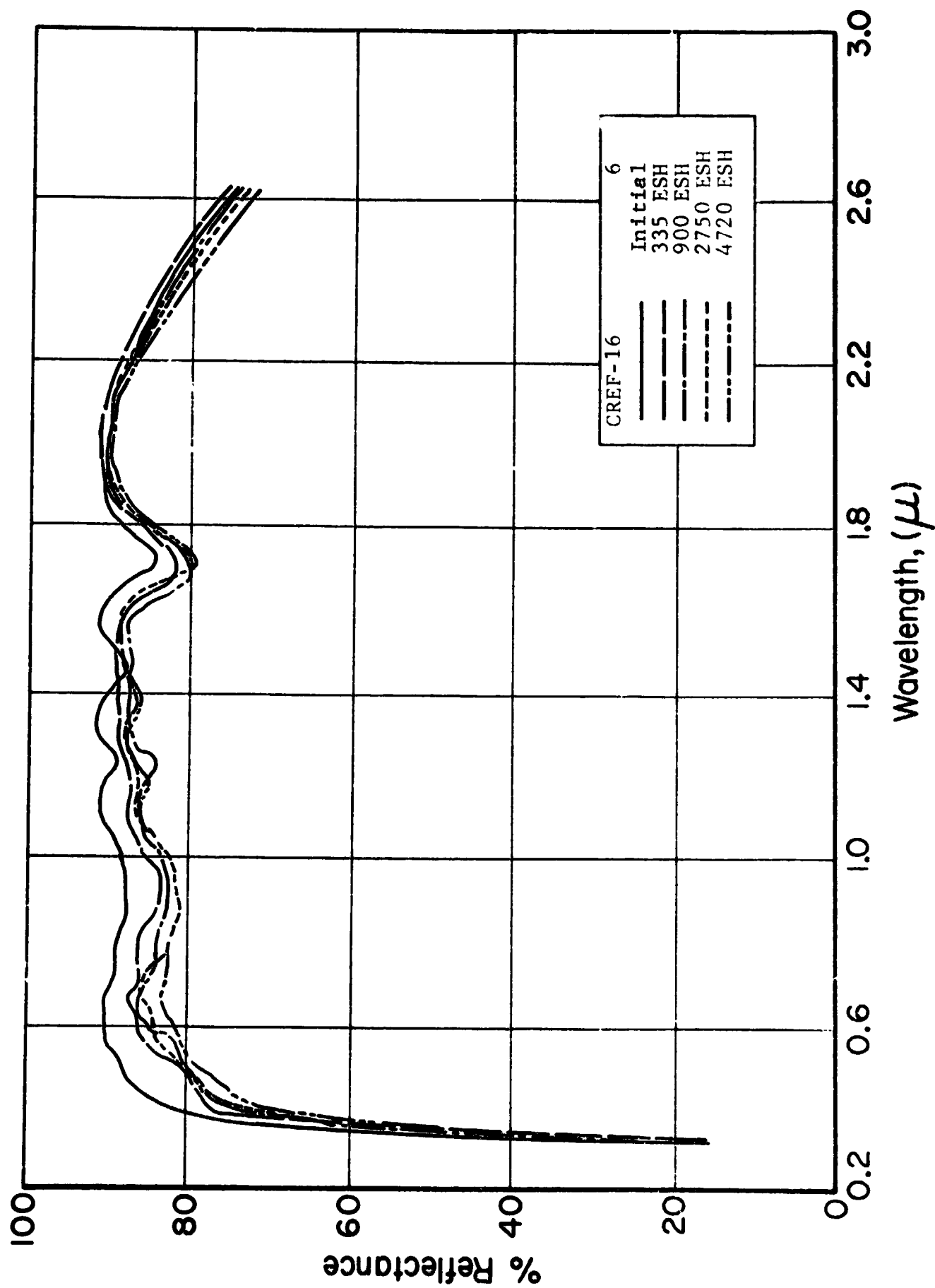


Figure 4.123 REFLECTANCE SPECTRA OF LH-106(6-12-A-10)/G

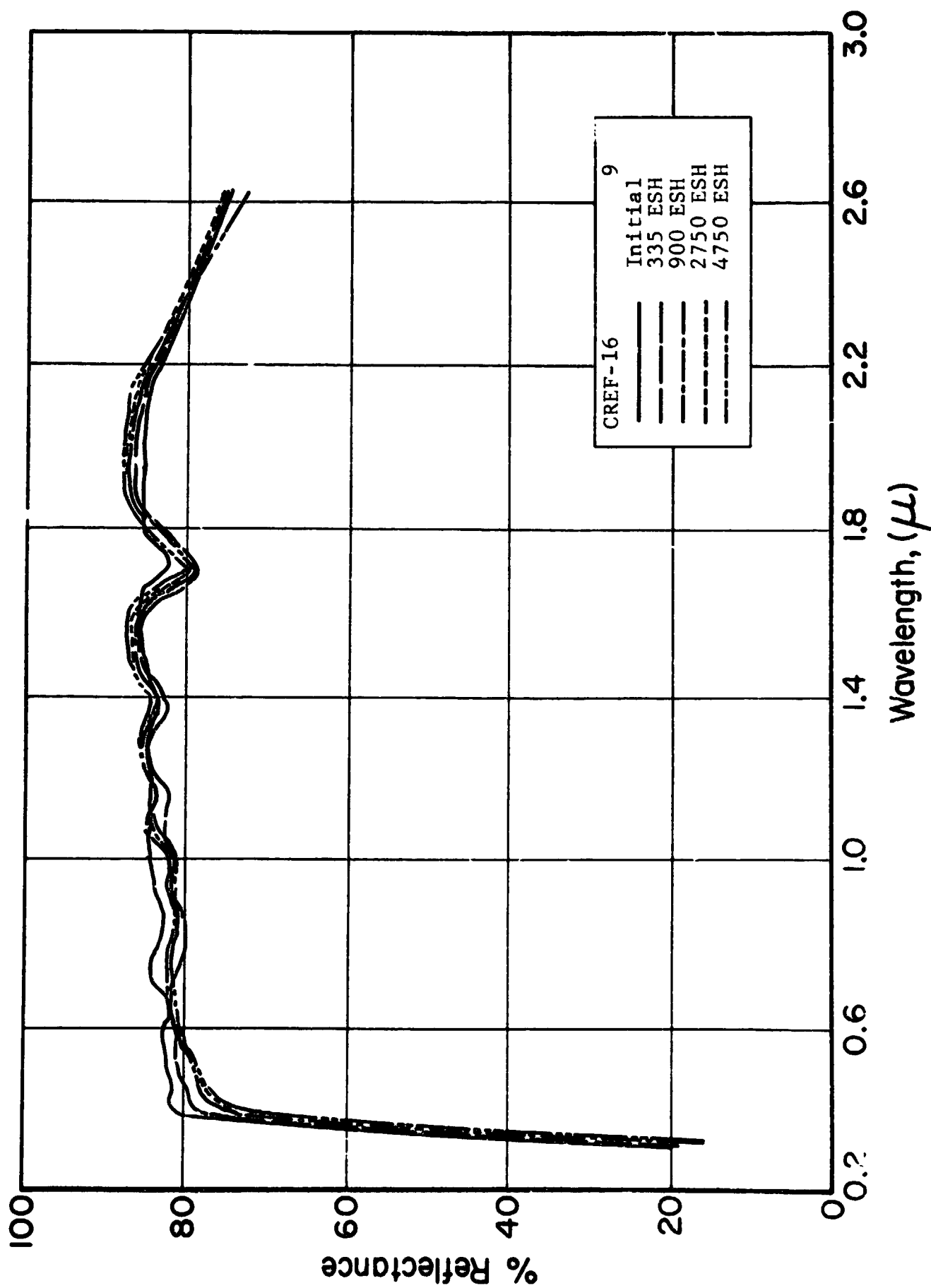


Figure 4.124 REFLECTANCE SPECTRA OF LH-106 (6-12-A-10):Li₇SiO₃/C

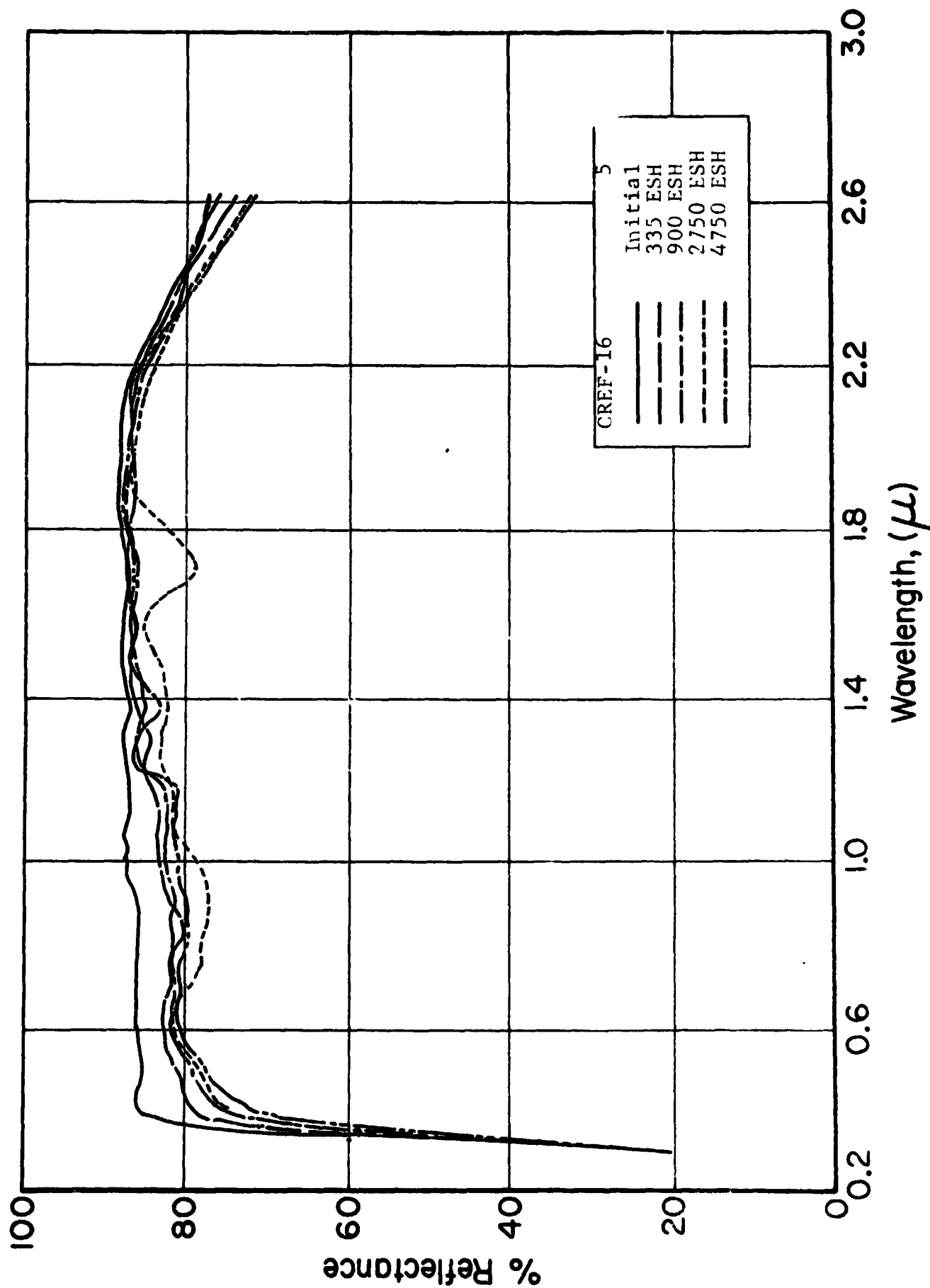


Figure 4.125 REFLECTANCE SPECTRA OF LH-106(6-12-A-10):K₂SiO₃/G

All of the paints performed quite well, even though the data differ. It should be noted that the differences between CREF and IRIF test data are of the order of 1-2% in reflectance for samples 7-10; that samples 5 and 12 definitely overlap the proton beam, and that samples 6 and 11 may have "seen" some stray proton radiation. Those samples which display the greatest differences were also more strongly affected by the combined (UV + p^+) radiation flux. In any event CREF-16 degradation consistently exceeds that in I-70.

4.5.9.4 Analyses and Conclusions

Several possible explanations exist for the CREF-16/I-70 discrepancies. The difference in solar factor (6X in IRIF vs 3X in CREF) can be significant, particularly since the degradation mechanism for S-band development is of second order. It is unlikely, however, that this explanation is sufficient, since much of the degradation occurred outside the S-band. Contamination is another possibility; the four other samples, (1-4 in this test), experimental clear films being subjected to combined UV and proton irradiation, may have undergone decomposition and outgassing. Still another possibility, briefly mentioned in the discussion of I-70 test results, is the loss of short wavelength UV radiation as a result of contamination of the irradiation source cooling water.

Before either I-70 or CREF-16 test results can be fully evaluated, their differences must be explained. We believe that the I-70 samples were indeed under-exposed, and that C-16 samples were contaminated; previous tests have resulted in data midway between their respective results. In the case of I-70 intra-test comparisons are valid, except with respect to binder degradation. C-16 data, however, are much more questionable because of the unknown effects of contamination, especially in those samples exposed to p^+ irradiation. C-16 data, consequently, should be accepted only qualitatively, except that unirradiated

properties data are entirely representative and valid. Finally, C-16 test data, regardless of their anomalous differences, lead to the same conclusions as were obtained in I-70.

4.5.10 Summary and Conclusions

In the case of OI-650 paints, an encapsulant serves two purposes - first, as a physical barrier to photodesorption from the pigment surface, and secondly, as an electronic barrier to interactions of electrons or free radicals in the silicone with the pigment surface, such as discussed in Ref. 4.16. The appearance of the S-band in OI-650 paints with otherwise stable pigments suggests either that the encapsulant is not intrinsically effective in preventing the pigment-vehicle interactions or that its surface coverage is incomplete, or both. O_2 bleach results show higher initial S-band absorption, almost certainly attributable to a pigment-encapsulant interaction. The S-band degradation due to irradiation has been at least partly O_2 -bleachable, suggesting incomplete coverage. From observations of UV-induced S-band development and post-irradiation O_2 bleaching behavior, we conclude that potassium silicate is the most effective encapsulant, because complete coverage is apparently easily obtained and because it does not cause directly, nor predispose the pigment to, excessive S-band absorption.

With minor exceptions the COP pigments and the paints prepared from them exhibit greater stability than those derived from the "MOX" method. In the series of tests, from IRIF I-70 to CREF-16, it is also evident that encapsulation will be required for most pigments and that K_2SiO_3 represents the best choice of encapsulants. Very clearly, the use of acid-washing, when indicated by low R_k values, must be followed by re-calcination. A recalcination by itself proves to be of no advantage or disadvantage.

Pigments prepared via the MOX method exhibit properties which can be controlled by setting appropriate preparative conditions. The added flexibility of the MOX method (over the COP method), however, has not been fully explored; nor have the properties of MOX pigments vs Zn/Ti stoichiometry been sufficiently pursued and understood. The unexpected properties and performance of the MOX-A pigments ended the notion that titanium atom excesses were responsible for the degradation of Zn_2TiO_4 , or at least the S-band in it. They certainly made it clear that the phase relationships, and the chemistry, of Zn-Ti compounds in the formation of Zn_2TiO_4 are poorly known.

In general, the effects of various calcination parameters, chemical treatments and other processing parameters are relatively predictable. Moreover, the overall results of environmental testing point up the inherent stability of Zn_2TiO_4 pigments. The COP method of Zn_2TiO_4 production leads to a better all-around pigment than does the MOX method, although the latter holds some definite and worthwhile advantages.

With reference to paint stability the basic problem is one of electronically isolating a stable pigment from the binder, thus preventing their mutual interaction. Determining pigment production parameters and conditions that lead to reduced pigment surface activity, e.g., via encapsulation, will solve this problem.

4.6 ENVIRONMENTAL TEST REPORTS - PART III

Part III test reports pertain to "MOX" Zn_2TiO_4 pigments. These have been prepared from oxalate precursors which have been separately precipitated.

4.6.1 IRIF Test I-72 (Ref. 4.10)

4.6.1.1 Purpose/Description

The unusually high reflectance of "MOX" Zn_2TiO_4 pigments along with an appreciation of the stoichiometric deficiencies of MOX-A Zn_2TiO_4 pigments prompted the production and testing of another "MOX" pigment batch, in this case designated MOX-B. We distinguish the meaning of the terms "MOX" and MOX: "MOX" refers to the preparation method, and MOX, to the designation of the first batch of pigment made by the "MOX" method. IRIF-I-72 was conducted to evaluate "MOX" pigments with a Zn/Ti ratio of 2.05:1.0, prepared as powders and OI-650G paints, and also to compare their properties and performance with an earlier "MOX" pigment, in this case, designated MOX.

4.6.1.2 Sequence

Diffuse hemispherical reflectance measurements were made in-situ on each sample prior to irradiation, after exposures to 175 ESH, 560 ESH, 1560 ESH and to 2630 ESH, and subsequently after exposure to 760 Torr of pure O_2 .

4.6.1.3 Test Results

The MOX-B pigments precursors were calcined at different calcination schedules of three temperatures each and at different calcination times. The majority of the samples, as Table 4.25 shows, are OI-650G paints. The remainder are MOX-B powder films, a MOX (original "MOX") pigment, and a sample of S-13G paint. Reflectance spectra of the "MOX" samples are given in figures 4.126-136. Pertinent data are summarized in Table 4.25. The results confirm the fact that OI-650G paints are always less stable than the pigments from which they are made and always inferior to them in reflectance properties as well. Also evident is the better stability of the 6-12 pigments. The stability of MOX-B paints, however, is only moderate.

The various properties and environmental performance indices compiled in Table 4.26 support the above conclusions and several others of importance. The earlier statement regarding the superior properties of pigments vs paints made from them is shown to be

Table 4-25
IRIF TEST I-72
ULTRAVIOLET RADIATION TEST RESULTS

Sample No.	Description	Solar Absorbance Values						
		Initial	175 ESH	560 ESH	560 ESH	2630 ESH	O ₂ Bleach	α _s 2630
2	MOX-B(6-9/4)/G*	.235	.305	.328	.357	.362	.288	.127
3	MOX-B(6-9/16)/G	.198	.273	.294	.333	.336	.264	.133
9	MOX-B(6-9/16)	.174	.183	.186	.192	.200	.174	.025
4	MOX-B(6-10.5/1)/G	.204	.260	.276	.311	.315	.252	.111
5	MOX-B(6-10.5/4)/G	.212	.257	.279	.308	.310	.253	.098
6	MOX-B(6-10.5/8)/G	.214	.242	.267	.287	.279	.231	.065
10	MOX(6-10.5/2)	.111	.118	.125	.126	.134	.111	.023
11	MOX-B(6-10.5/8)	.207	.228	.229	.233	.237	.215	.030
7	MOX-B(6-12/0.5)/G	.228	.261	.282	.297	.302	.252	.074
8	MOX-B(6-12/2)/G	.216	.245	.260	.267	.276	.240	.060
12	MOX-B(6-12/2)	.141	.168	.194	.188	.190	.155	.049
1	S-13G (D-375)	.191	.221	.242	.267	.276	.246	.085

*Designates Paint Binder is OI-650C

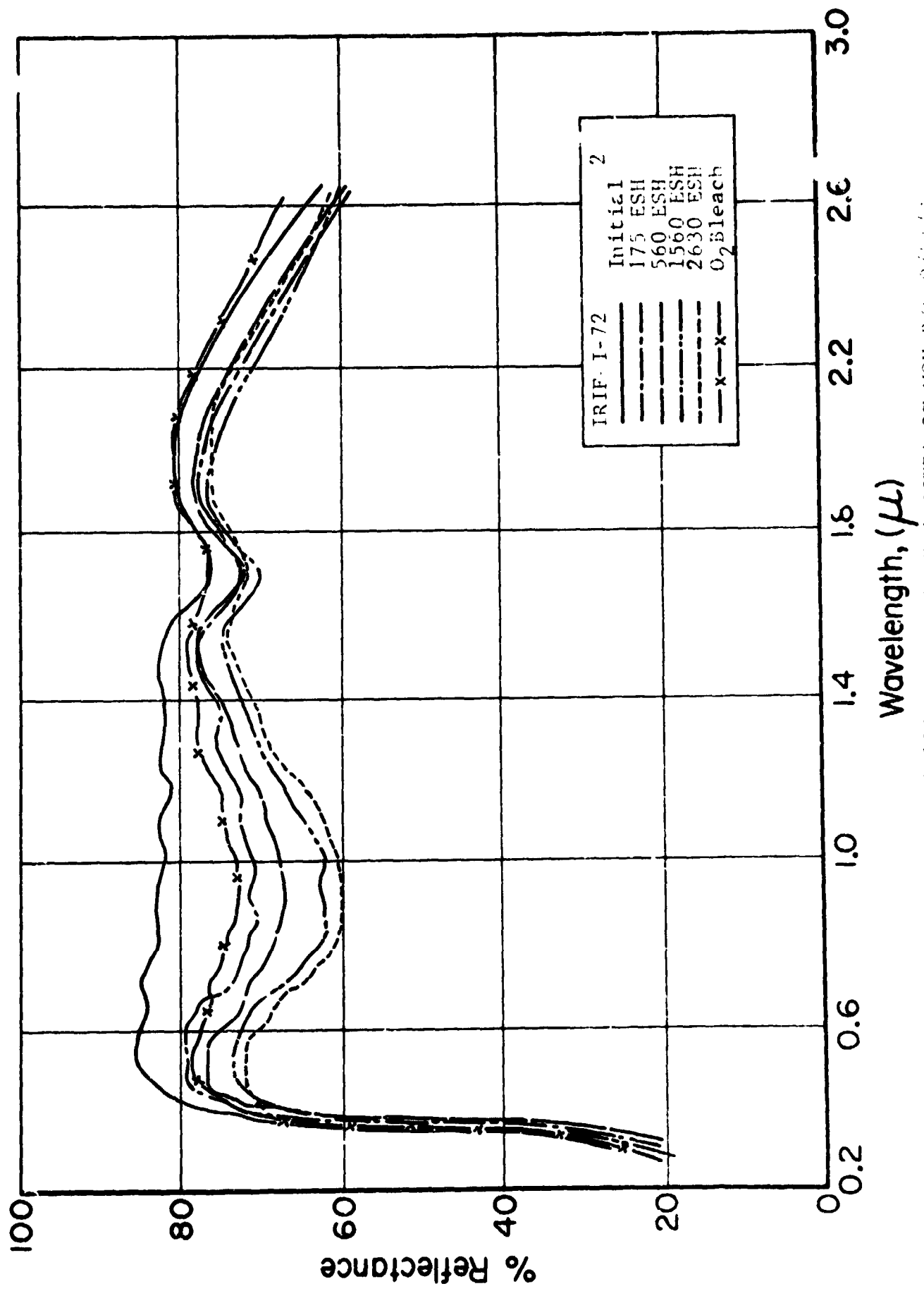


Figure 4.126 REFLECTANCE SPECTRA OF NOX-B(6-9/414)

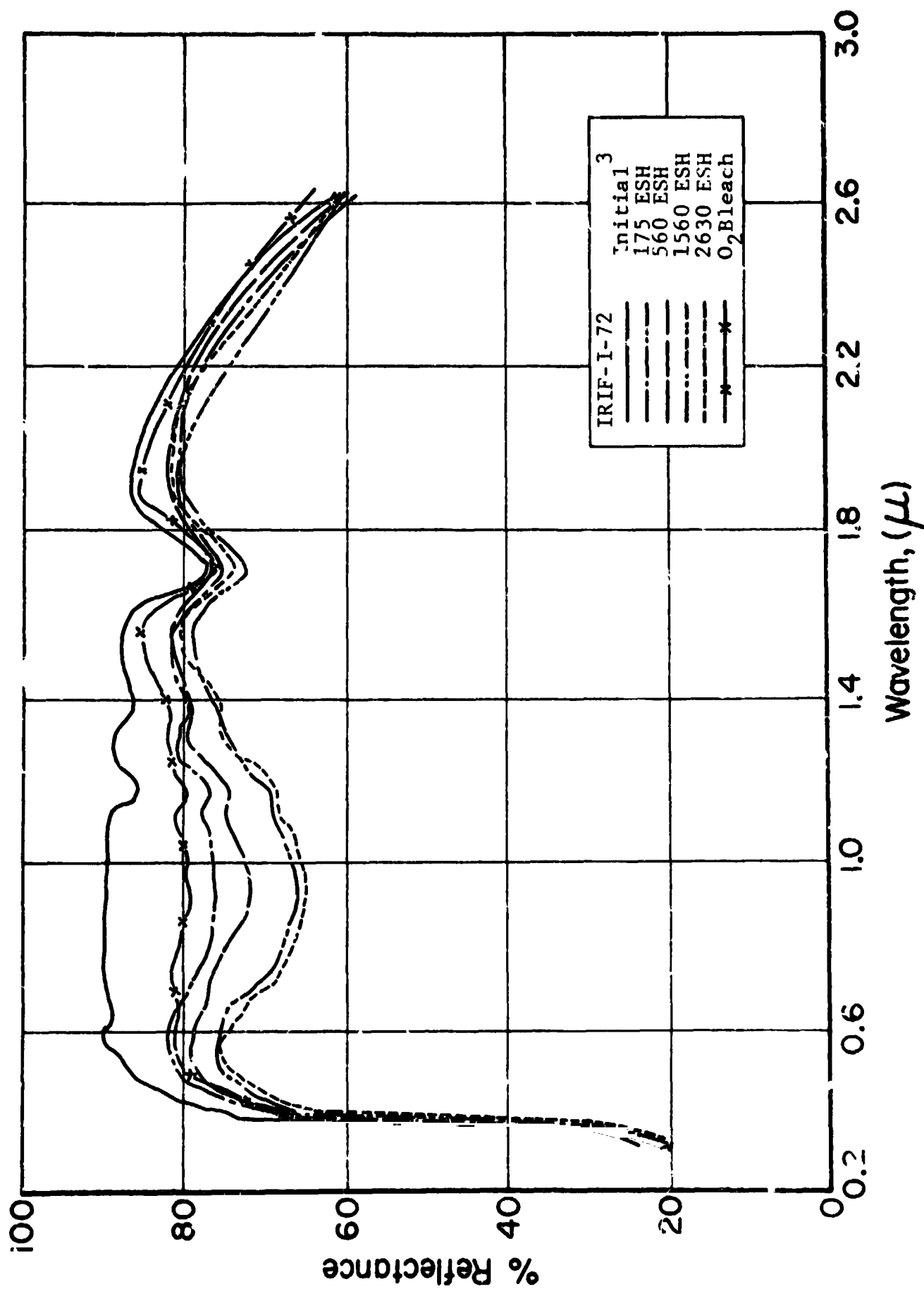


Figure 4.127 REFLECTANCE SPECTRA OF MOX-B(6-9/16)/G

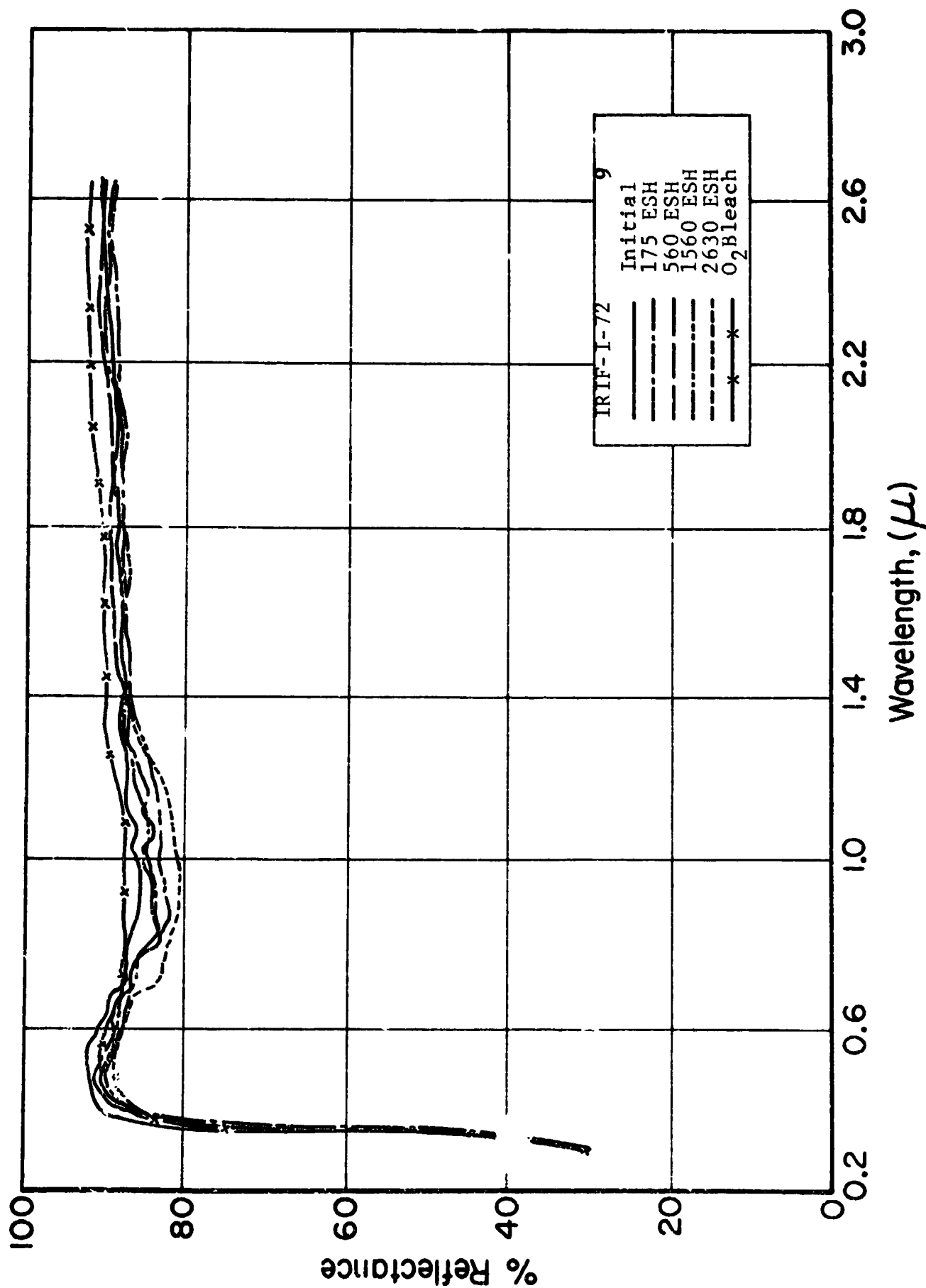


Figure 4.128 REFLECTANCE SPECTRA OF MOX-B (6-9/16) (Powder)

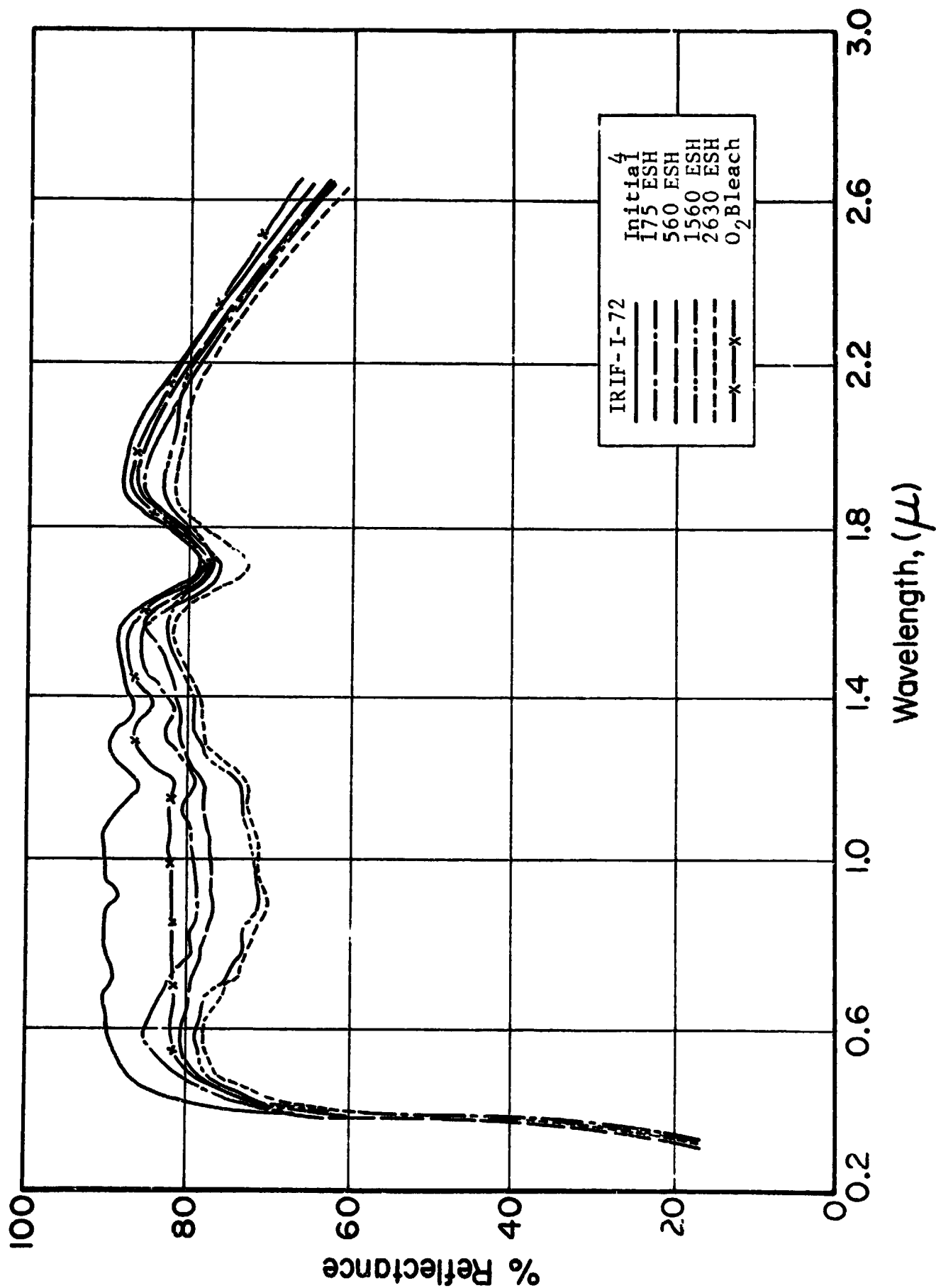


Figure 4.129 REFLECTANCE SPECTRA OF MOX-B(6-10.5/1)/G

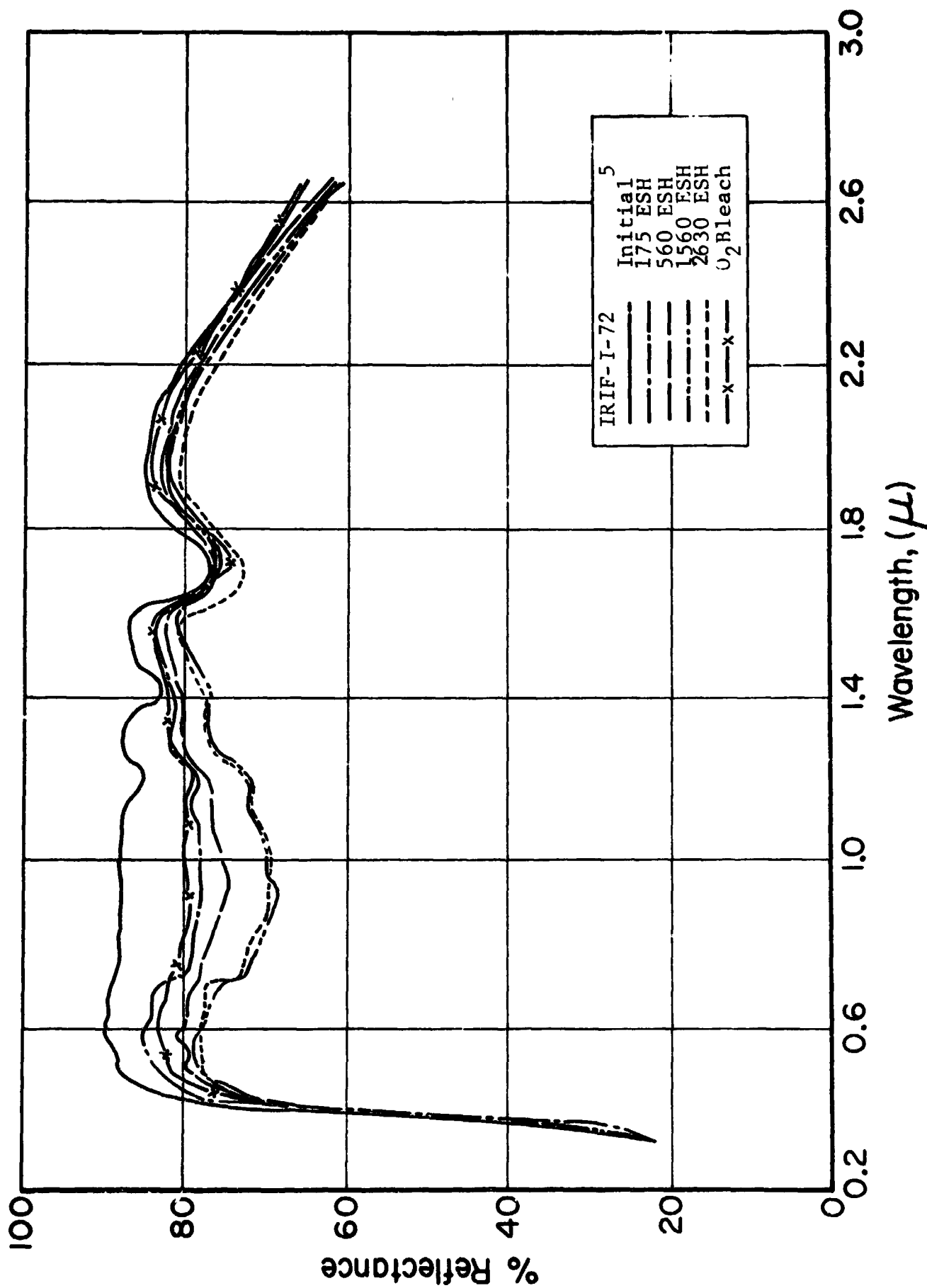


Figure 4.130 REFLECTANCE SPECTRA OF MOX-B(6-10.5/4)/G

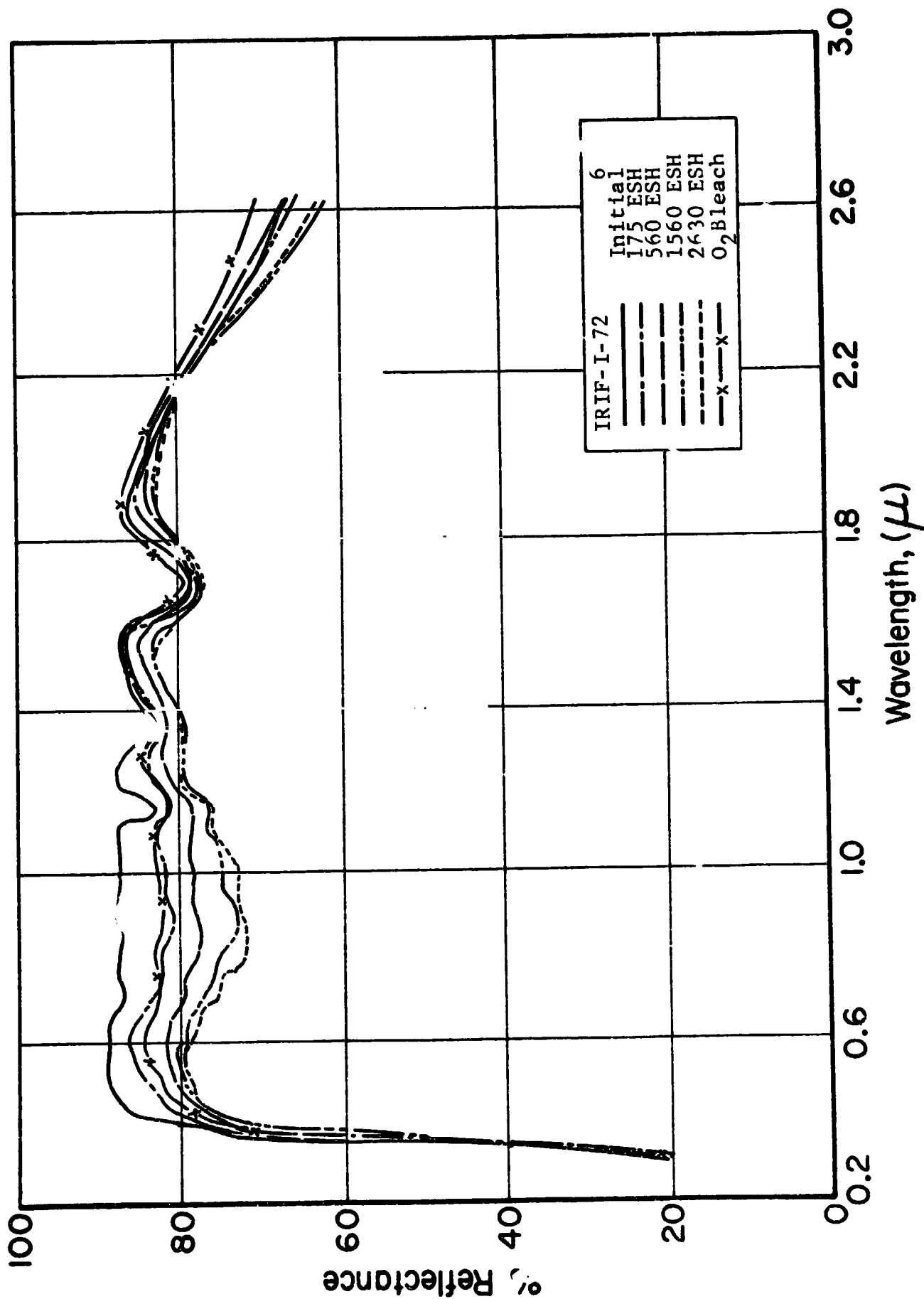


Figure 4.131 REFLECTANCE SPECTRA OF MOX-B(6-10.5/8)/C

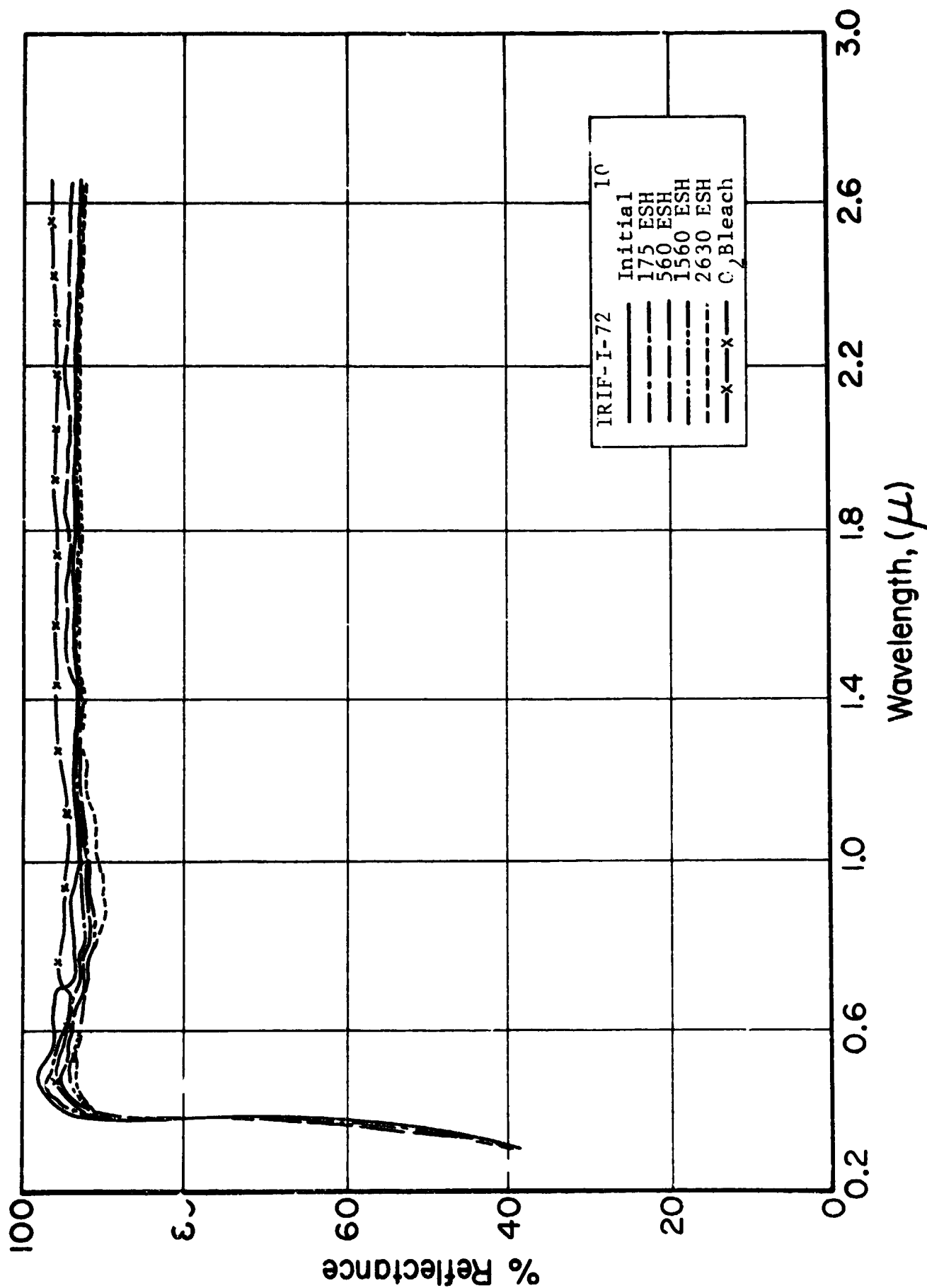


Figure 4.132 REFLECTANCE SPECTRA OF MOX(6-10.5/2) (Powder)

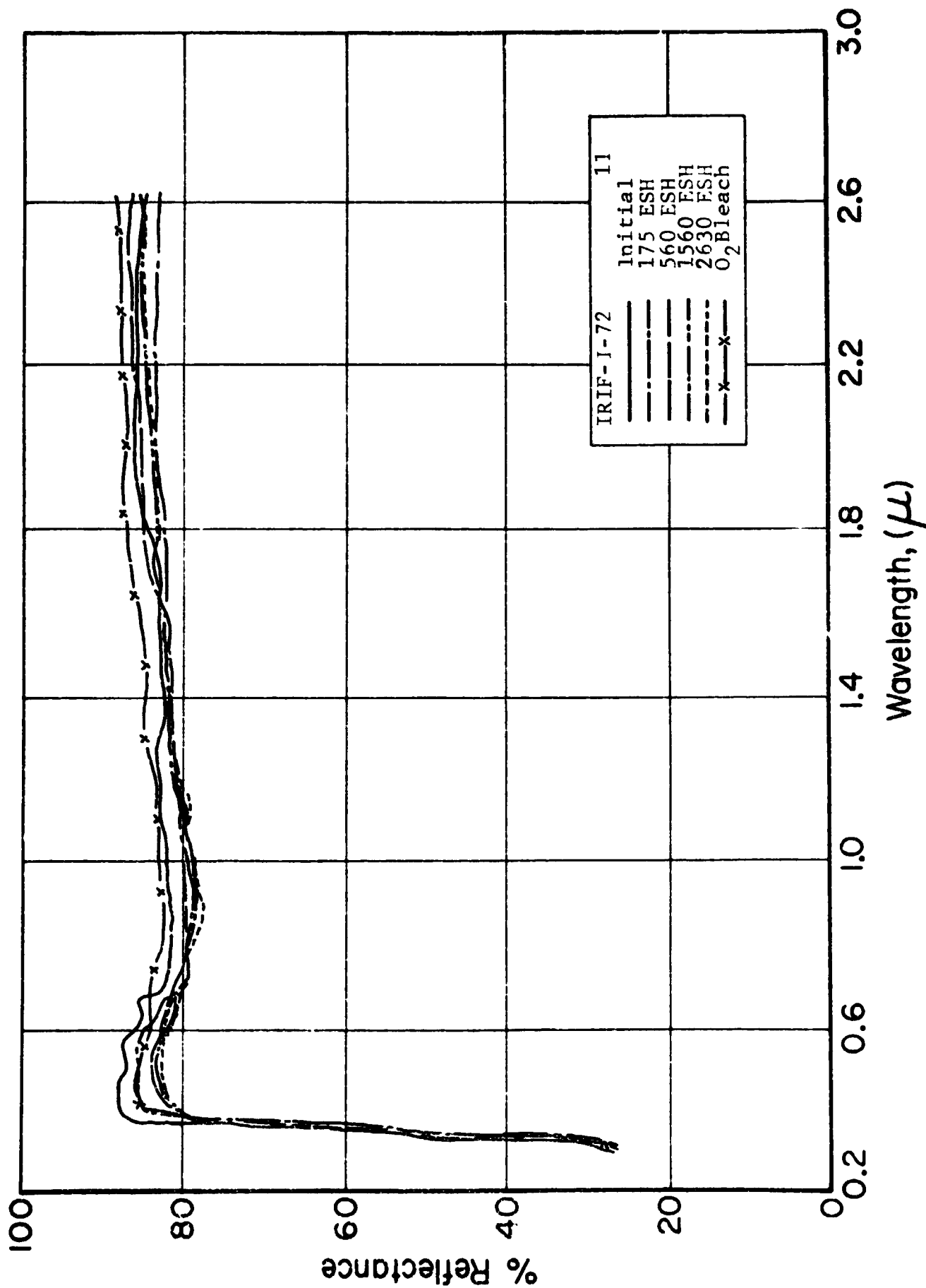


Figure 4.133 REFLECTANCE SPECTRA OF MOX-B(6-10.5/8) (Powder)

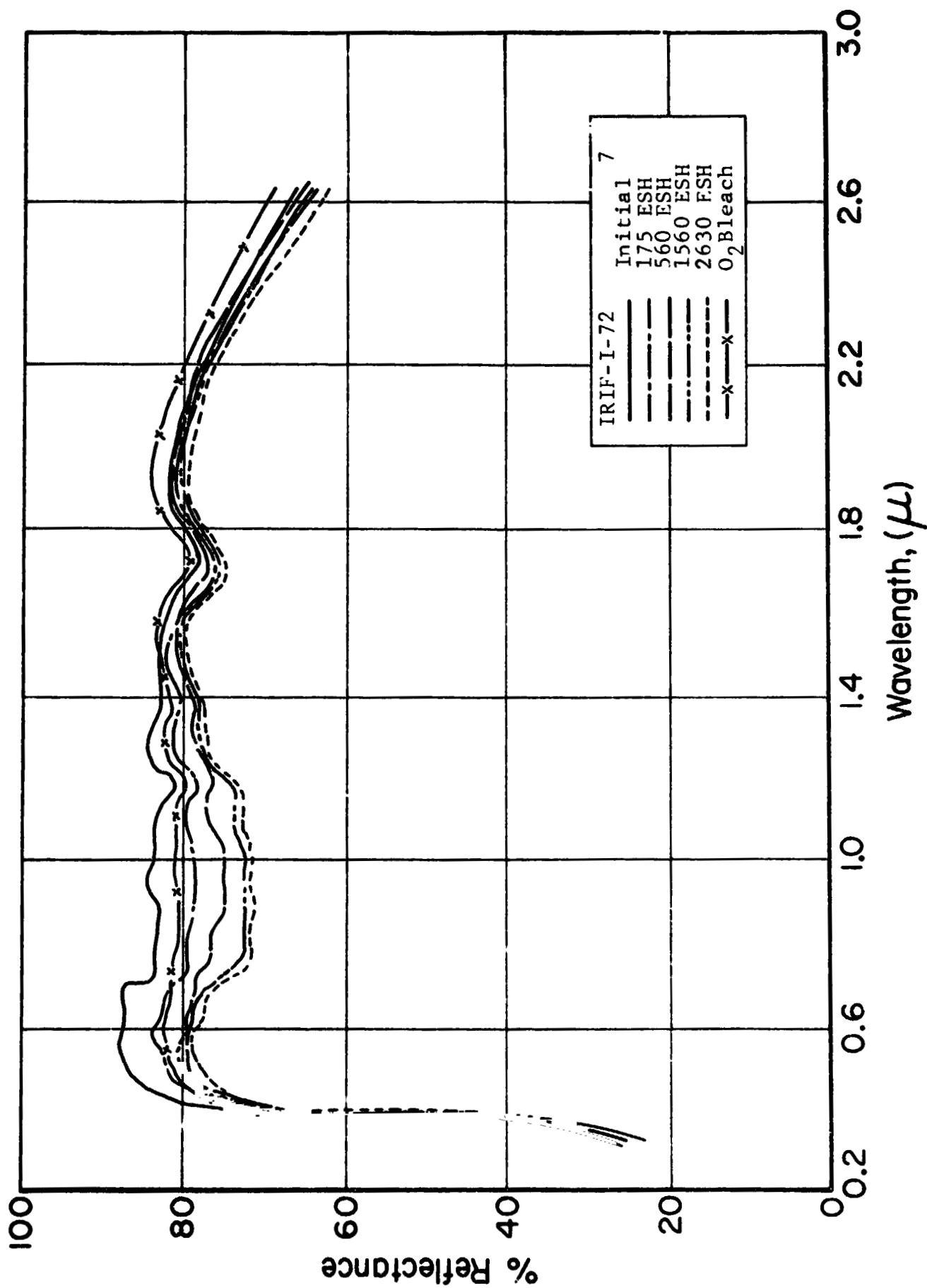


Figure 4.134 REFLECTANCE SPECTRA OF MOX-B(6-12/0.5)/G

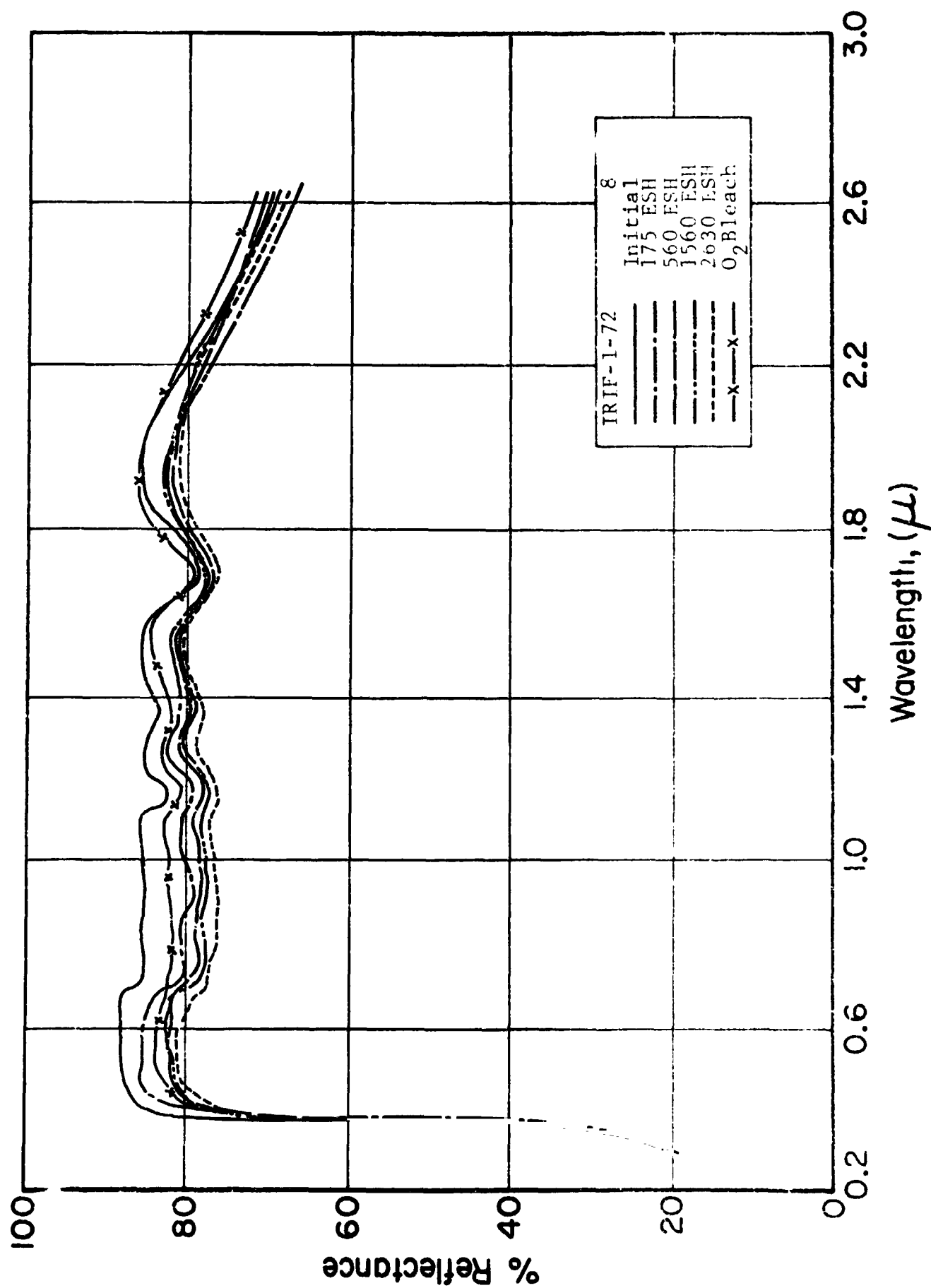


FIGURE 4-135 REFLECTANCE SPECTRA OF MOX-B (6-12/2) /C

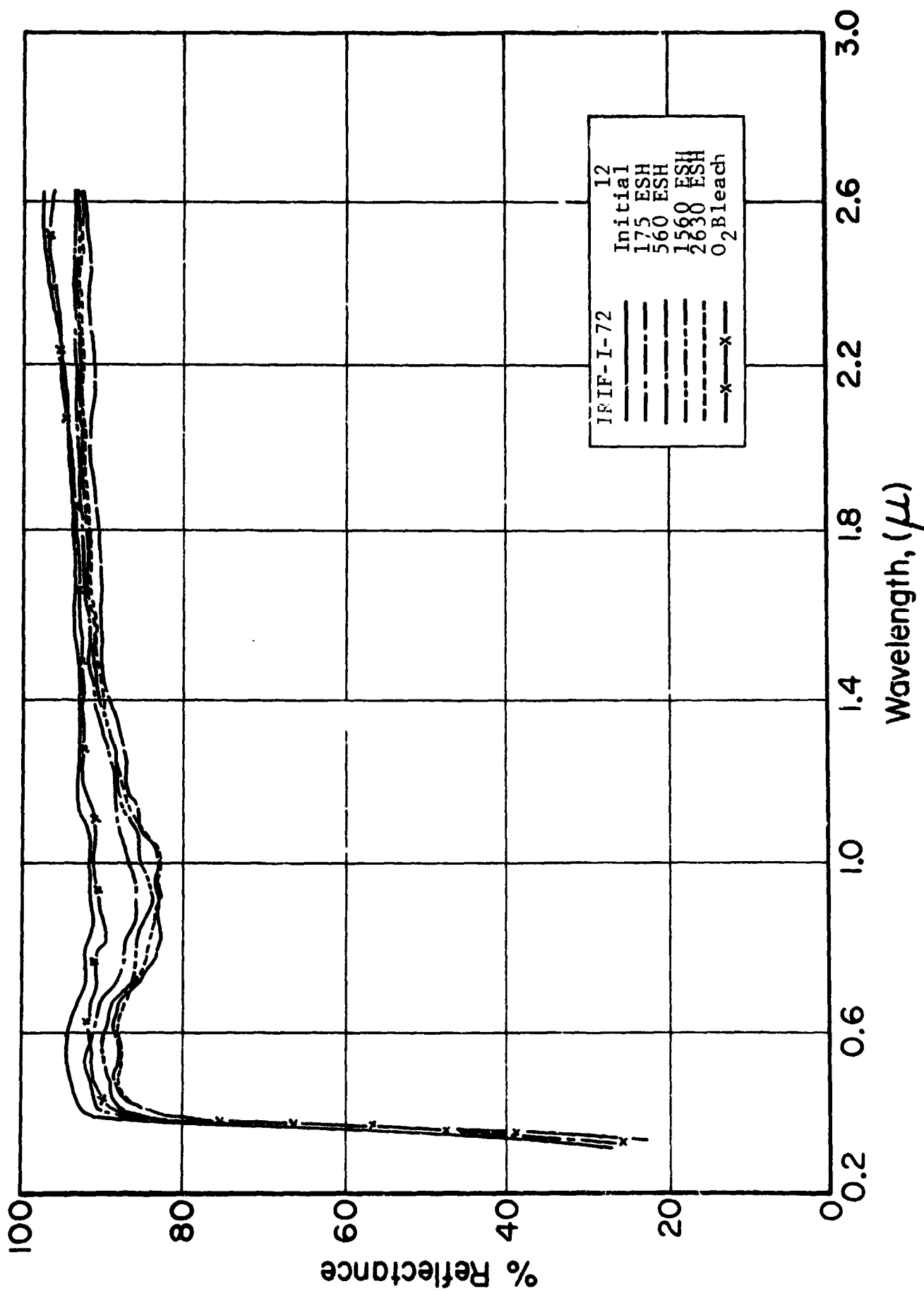


Figure 4.136 REFLECTANCE SPECTRA OF MOX-B(6-12/2) (Powder)

valid on several bases. R_k , the "knee" reflectance, of powders tends to remain rather independent of temperature and time, contrasting rather sharply with the MOX-A behavior. However, the differential between the greater degradation of the paint and the lesser degradation of its pigment (when irradiated separately) tends to decrease with increasing calcination temperature (table 4.26B). The improvement of ΔR_{400} , ΔR_{900} , and of $\Delta \alpha_s$ with increasing temperature clearly exhibit similar trends. Though $\Delta \alpha_s$ of powders increases mildly with increasing calcination temperature, that of corresponding paints decreases substantially. The factors which tend to amplify the absorption effect when a MOX-B pigment is dispersed in OI-650G quite obviously diminish with increasing calcination temperature. These dependencies should not be attributed to temperature alone, because time at temperature, though a weaker influence, also has significant effects. The $\Delta \alpha_s$ values of the two powders in the 6-10.5 series (Table 4.26A) exemplify this point; in this instance the effect of time is to increase $\Delta \alpha_s$ of the powder and, generally to decrease it in the paints (Table 4.26C). A very notable effect is, of course, the decreasing ΔR_{900} with increasing calcination time. Less obvious, but quite important, the full effect of time at temperature for all three temperatures has not been attained. Thus, it would seem that longer calcinations would be desirable. Such, however, may be contra-indicated by other factors, such as particle size growth.

4.6.1.4 Conclusions

The MOX-B paints display poor to moderate stability, definitely not that generally observed in Zn_2TiO_4 paints. The stability of these systems, however, clearly depends upon calcination temperature and time. While the pigments alone demonstrate good performance, the binder "sensitizes" the pigment, causing much stronger S-band absorption to develop than in the pigment alone. The chemical nature of the pigment surface, and quite possibly of the pigment bulk, differs appreciably with calcination temperature, with time at temperature, and also with Zn/Ti stoichiometry.

Table 4-26
SELECTED IRIF-I-72 DATA

Table 4 26A
COMPARISON OF MOX-B POWDERS AND PAINTS
Powder/Paint Properties

Index	6-9/16	6-10.5/2*	6-10.5/8	6-12/2
R_k	55.5/32	57/33.5	56/36	51/34
R_{max}	89/89	96/89	86/87.5	95/87
ΔR_{400}	.045/.130	.030/.115	.040/.089	.055/.050
ΔR_{900}	.040/.124	.035/.182	.032/.124	.070/.095
α_s	.174/.198	.111/.204	.207/.214	.141/.216
$\Delta \alpha_s$.026/.138	.023/.111	.030/0.65	.049/.060

*First column/Second column relate in this case to: 6-10.5/2 powder vs 6-10.5/1 paint.

Table 4-26B
POWDER/PAINT RATIOS
Ratios of Powder/Paint Indices For:

Series	R_k	ΔR_{400}	ΔR_{900}	$\Delta \alpha_s$
6-9/16	1.73	0.35	0.18	0.19
6-10.5/2*	1.70	0.26	0.17	0.21
6-10.5/8	1.56	0.45	0.26	0.45
6-12/2	1.50	1.10	0.74	0.82

*Relates in this case to: 6-10.5/2 powder vs 6-10.5/1 paint.

Table 4 26C
TEMPERATURE AND TIME EFFECTS IN PAINTS
(6-9) (6-10.5) (6-12)

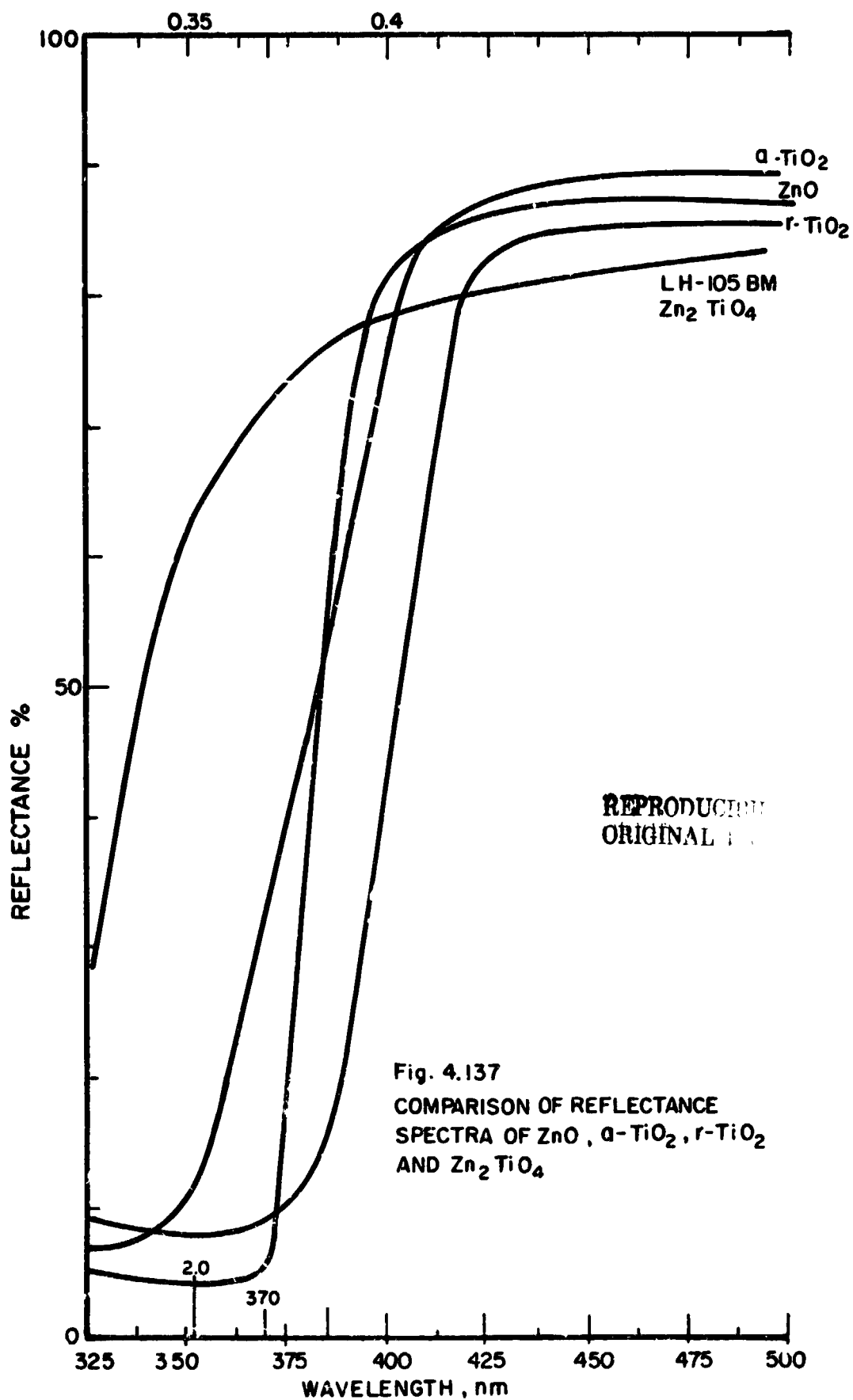
Series: Times:	4hrs	16hrs	1hr	4hrs	8hrs	0.5hrs	2hrs
Index							
R_k	32.5	32	33.5	36	36	37.5	34
R_{max}	85	89	89	88	87.5	86	87
ΔR_{400}	.130	.130	.115	.082	.089	.070	.050
ΔR_{900}	.230	.224	.182	.169	.125	.130	.095
α_s	.235	.298	.204	.212	.214	.228	.216
$\Delta \alpha_s$.127	.138	.111	.098	.065	.074	.060

4.7 STOICHIOMETRIC PIGMENT CHARACTERIZATION STUDIES

4.7.1 INTRODUCTION

The intrinsic stability of Zn_2TiO_4 pigments may not be achievable in practice unless the effects of variations in production process parameters and conditions can be discerned. The primary criterion, of course, is the environmental stability of the paint; how the variable conditions and parameters involved in the various preparative methods affect it is thus of major concern. One critical problem is that the exact Zn/Ti ratio in the final pigment to attain environmental stability is not easily determined, nor is the relationship between it and that in the precursor mixture. We have also assumed that the Zn/Ti ratio affects both the bulk and the surface properties and thus are faced with the possibility that stabilization of bulk properties may require a different Zn/Ti ratio than that which would confer surface (S-band) stability. We are reasonably certain that the MOX precursor components (ZnOx and " TiOX ") are chemically identical to those in the COP precursor mixture. The assumption, however, that, at least above some minimum temperature, Zn_2TiO_4 is the major (or even only) product of the calcination of those precursors has raised some serious questions.

To address the central questions in the relationship of pigment stability to Zn/Ti ratio, we must examine the theoretical background and experimental practice involved in the manufacture of Zn_2TiO_4 . Our basic belief holds that Zn_2TiO_4 is indeed a true compound rather than a solid solution of compounds; Zn_2TiO_4 is not $\text{ZnO} \cdot \text{TiO}_2 \cdot \text{ZnO}$ or a similar compound. Fig. 4.137 displays the reflectance spectra in the optical band gap regions of ZnO , of anatase and rutile TiO_2 and of the 1.95:1.0 (Zn/Ti) product of COP oxalate precursors; it is clear that each is distinctly different from the others. Because the fundamental optical band gaps of materials are intrinsic characteristics, the significance of their reflectance spectra in the fundamental absorption region becomes central to the interpretation of all of our stoichiometry



experiments. The essential point is that the band gap wavelength of a material is characteristic and thus indicative of the material creating the absorption involved. Though X-ray, SEM, gravimetric and other analyses are available, analyzing the effects of Zn/Ti stoichiometry in terms of optical spectra provides a high degree of relevance with respect to our primary application.

4.7.2 Process Chemistry

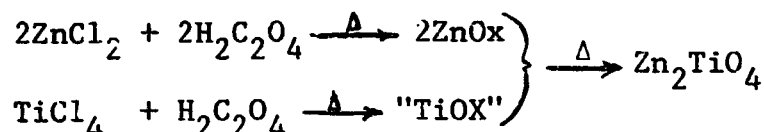
4.7.2.1 Background

The underlying basis for the production of zinc orthotitanate, Zn_2TiO_4 , from oxalate precursors resides in their instability when heated and in the eventual reaction of the "oxalates" or their reduction products to form Zn_2TiO_4 . The chemistry of the reactions, however, has not been well understood. In previous studies of Zn_2TiO_4 pigments, it had been established that an excess of ZnO in the Zn_2TiO_4 product is necessary (Ref. 4.7). The rationale was that a ZnO excess could be removed by appropriate chemical treatment, whereas a TiO_2 excess could not, and that a ZnO excess would not promote Zn_2TiO_4 degradation, whereas TiO_2 would.

4.7.2.2 Chemistry

In light of the questions raised in regard to the proper Zn/Ti ratio and their implications, we believe it necessary to establish conclusively the chemical nature of the products of the precipitation process, and the chemical reactions involved in their high temperature conversion to oxides. Although a specific test was not made to assure that the Zn and Ti compounds produced in the coprecipitation process are identical to those produced when precipitated separately, there is much indirect evidence, including SEM photomicrographs, to suggest that they are.

The precipitation and subsequent calcination processes have been described in the reaction(s):



In the coprecipitation (COP) process, the chlorides of Zn and Ti in the mole ratio of 2.05 Zn/Ti are added simultaneously to an aqueous oxalic acid solution. The resultant precipitate presumably also contains a 2.05 Zn/Ti mole ratio. In the "MOX" process the precipitates obtained from chloride addition are obtained individually; the resulting precipitates, i.e. "ZnOx" and "TiOX", are mixed to obtain a 2.05 Zn/Ti mole ratio, then ball-milled to ensure adequate mixing. In both cases the resulting mixture is calcined to obtain Zn_2TiO_4 pigment.

4.7.2.3 Oxalate Molecular Weight Determinations

4.7.2.3.1 Zinc Oxalate

An obvious requirement in achieving a specific Zn/Ti mole ratio is that the molecular weights of the ZnOx and "TiOX" compounds must be known. Because of the uncertainty in the actual effect on stoichiometry inherent in the MOX-A irradiation test results (IRIF Test No. I-71), we undertook a complete review of the bases for process chemical calculations. Purposely, we have avoided up to this point any reference to the actual chemical nature of "TiOX" (the solid reaction product of TiCl_4 with $\text{H}_2\text{C}_2\text{O}_4$).

Samples of "ZnOx" and of "TiOX" were individually subjected to SEM and x-ray analyses, and were calcined at various temperatures. From mass loss, SEM and x-ray data and analyses of reflectance spectra of the precursors and their products, we have conclusively shown that "ZnOx" is $\text{ZnC}_2\text{O}_4 \cdot 2\text{H}_2\text{O}$. We are thus very certain of this assignment.

4.7.2.3.2 "TiOX" Molecular Weight

The chemical formula of "TiOX", and thus its true molecular weight, can not be obtained as simply. It depends upon temperature-induced mass-loss data corroborated by other evidence. Literature references are sketchy at best and not directly applicable. Tables 4.27 and 4.28 present the available data on static and TGA mass loss of "TiOX"; Fig. 4.138 shows residual mass vs time for the TGA test. The reaction at sufficiently high temperature leads to the production of anatase titanium dioxide; thus,

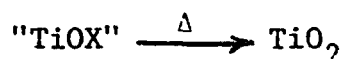


Table 4-27
Mass Loss Data
Static Calcination Data

<u>Temp (°C)</u>	<u>Time (Hr)</u>	<u>Weight Loss, %</u>	<u>FML* Conversion</u>	<u>Yield**</u>
150	1	6.96	.1491	.0242
	4	8.07	.1729	.0512
	48	8.46	.1813	.0606
230	.083	17.44	.3737	.2791
	1	39.92	.8555	.8261
	4	44.34	.9503	.9336
340	.083	43.73	.9372	.9188
	1	44.43	.9522	.9358
	4	44.89	.9621	.9470
500	1	45.56	.9764	.9633
	4	45.52	.9756	.9623
700	1	46.66	1.0000	.9901
	4	46.37	.9938	.9830

*FML - Fractional Mass Loss (= % mass loss / maximum % mass loss), relates to overall reaction completion.

**Yield - Mole fraction of TiO₂ formed/mole of "TiOX".

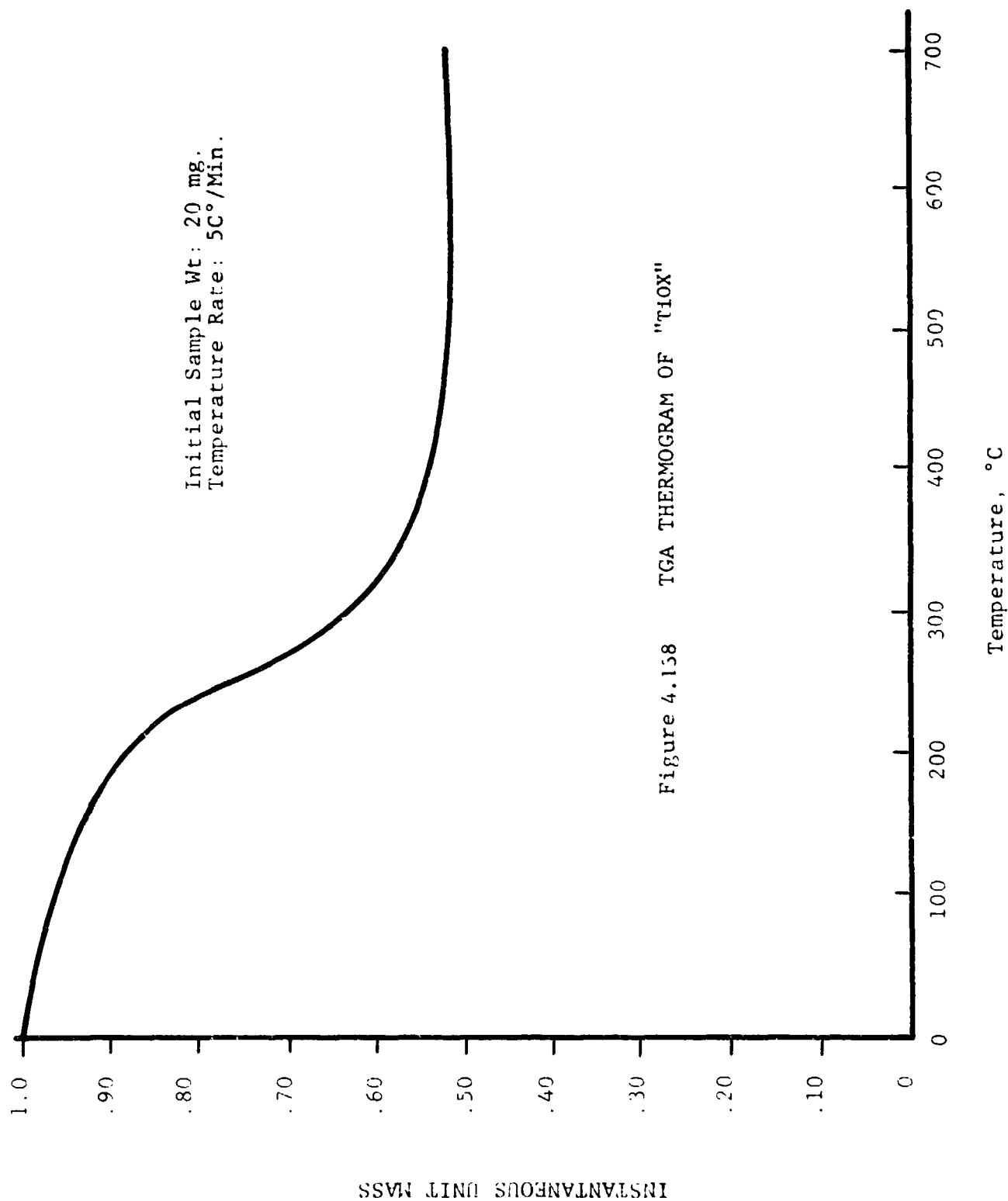


Table 4-28
TGA Data

Temp (°C)	FMR*	FML*	Yield**
25	1.000	0.000	.0000
75	.982	.0373	.0000
100	.969	.0642	.0000
150	.937	.0130	.0081
200	.894	.2195	.11271
250	.785	.4451	.3779
300	.625	.7764	.7672
350	.568	.8944	.9059
400	.553	.9255	.9424
450	.522	.9896	1.000
500	.517	1.000	1.000
600	.517	1.000	1.000
700	.517	1.000	1.000

*FMR = Fraction of original mass remaining;

FML = Wt. loss/max. wt. loss; e.g., $(1.0 - 0.785) / (1.0 - 0.517) = 0.4451$

**Yield - mole fraction of TiO_2 formed/mole of "TiOX"

The highest yield obtained (in terms of mass loss) is 46.66%, or 53.34% conversion of "TiOX" to TiO_2 . The molecular weight of TiO_2 is 79.90. Therefore, the inferred molecular weight of "TiOX" is $79.90 / 0.5334 = 149.79$ (the last decimal place is not significant). TGA data (see Table 4.28) confirm this calculation. This value is in fact the one used in preparing MOX pigments. The only literature available (e.g., Ref. 4.12) lists $\text{Ti}_2(\text{C}_2\text{O}_4)_3 \cdot 10\text{H}_2\text{O}$ with a molecular weight of 540.01. Clearly, this is not the product obtained in the precipitation process.

The mass loss data of tables 4.27 and 4.28 are shown in Fig. 4.139, where the log of the conversion (of the "TiOX" precursor to TiO_2) is plotted vs $1/T(^{\circ}\text{K})$. This method of presenting the mass loss data will be examined subsequently in greater detail. The conversion is determined as the ratio of the product mass at any given temperature and time conditions to the ultimate (or maximum) product mass.

REPRODUCED
ORIGINAL

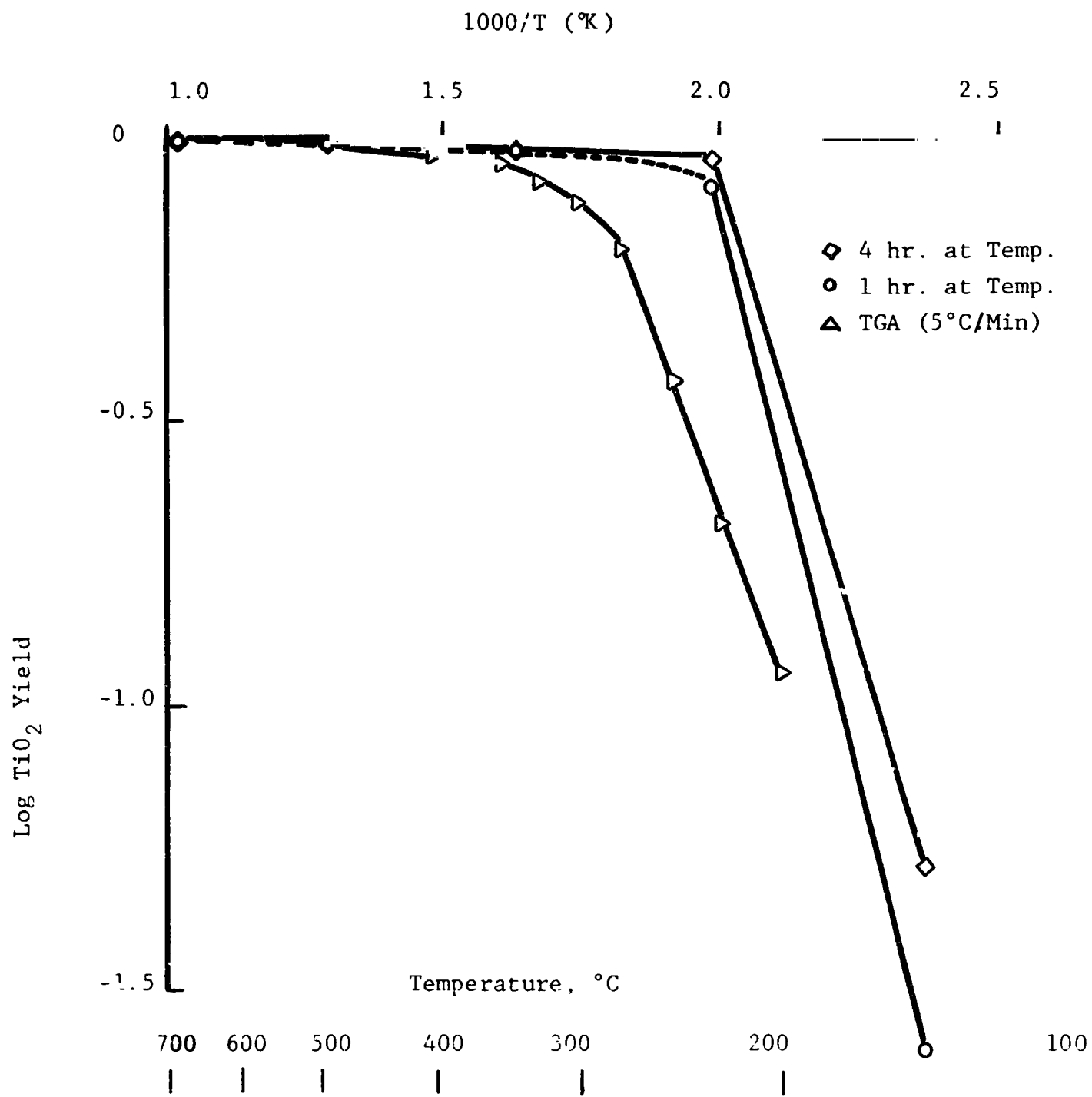


Figure 4.139 "TiO_x" CONVERSION VS RECIPROCAL TEMPERATURE

In the extant case, calcination beyond 500°C produces no additional mass loss, and the ultimate fractional mass loss is 0.5334 from static data and 0.517 from TGA data. The difference (about 1-1/2%) may be due to batch-to-batch variations or slightly different pre-treatment conditions. The extrapolation of the conversion data in the low temperature region in Fig. 4.13⁹ to 0.0 (100% completion) intersects at a temperature of 235°C for the static data and at 300°C for the TGA data. The difference arises because static data represent equilibrium conditions, TGA data very likely do not, although they exhibit consistency.

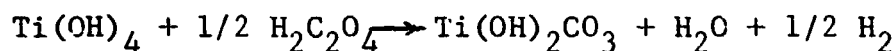
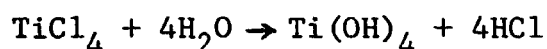
The true minimum molecular weight of "TiOX" can be inferred from the static data by correcting its molecular weight by the weight loss below 235°C, thus, by the factor $(1 - 0.0846)$, i.e., 0.9154. The minimum molecular weight of the true "TiOX" is then $(149.79) \cdot (0.9154) = 137.12$. Hence, for clarification, we have "wet" TiOX, i.e., $\text{TiOX} \cdot n\text{H}_2\text{O}$, with an actual (effective) molecular weight of 149.79 and "dry" TiOX with a minimum molecular weight of 137.12. In practice only the "wet" TiOX is used, and the term "TiOX", unless otherwise noted will refer to $\text{TiOX} \cdot n\text{H}_2\text{O}$.

The molecular weight of 149.79 is easily within an accuracy of $\pm 5\%$; thus it clearly rules out any possibility that "TiOX" is a double oxalate, since $\text{Ti}(\text{C}_2\text{O}_4)_2$ has a molecular weight of 223.94. The radical $\text{TiC}_2\text{O}_4^{++}$, however, has a molecular weight of 135.92. This suggests that "dry" "TiOX" may be $\text{H}_2\text{TiC}_2\text{O}_4$ and that "wet" "TiOX" is $\text{H}_2\text{TiC}_2\text{O}_4 \cdot 0.7 \text{H}_2\text{O}$. Chemical analyses of "wet" "TiOX" have shown that the carbon content is in the range 9.3 - 9.7 w/o and that its hydrogen content is approximately 2.5 w/o. The carbon content would argue strongly against "TiOX" being an oxalate since the two oxalate carbons in "TiOX" would contribute in excess of 16 w/o.

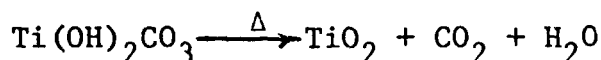
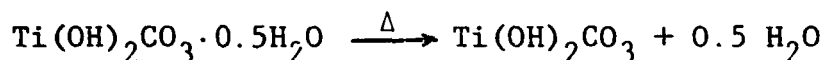
A more likely formula is $\text{Ti}(\text{OH})_2\text{CO}_3$ with a molecular weight of 141.94; with a half mole of water of hydration, the mol wt. becomes 150.95 (very close to the value of 149.79, and within experimental error). With this formula the theoretical values

of carbon and hydrogen content also lie well within experimental error for the physical test values. The justification for this selection follows from the fact that the data from Fig. 4.139 only set an upper limit to water content; the shape of the curve at values of higher mass loss may, and very probably do, reflect some oxalate decomposition rather than, as we have assumed, only water evolution. The opposite, however, is not true. Further, the reaction of TiCl_4 with water is known (Ref. 4.13) to produce a stable tetravalent hydroxide.

In an aqueous solution of oxalic acid, there would be a competition between the H_2O and the oxalic acid for reaction with the TiCl_4 . We assume that the following reaction scheme prevails in the precipitation process:



From our analyses of the mass data, it is reasonable then to postulate that the reactions of "TiOX" when heated are.



4.5.3 "TiOX" Energetics

A further analysis of the data in Tables 4.27 and 4.28 was carried out to establish the reaction kinetics of the "TiOX" calcination. The Clausius-Clapeyron equation was used to calculate the heat of reaction. From the reduced static and TGA data, which are plotted in Fig. 4.139, it is quite obvious that different reactions occur as a function of temperature. In the temperature range below 230°C the heat of activation is very high (11814 cal/mole), close to that expected from the description of water of hydration (9729 cal/mole). The abrupt change in slope at about 1.98×10^{-3} ($\sim 225^\circ\text{C}$) occurs also in the TGA spectrum. A close comparison between these and TGA data

should not necessarily be expected, since these data were obtained under essentially static conditions (by subjecting "TiO₂" to specific temperatures for pre-determined times) while the TGA data reflect an instantaneous, not necessarily an equilibrium, weight loss. Fig. 4.139 is based on the Arrhenius equation:

$$K = \frac{k_1}{k_2} = S \cdot \exp(-\Delta H_A/RT) \quad (4.1)$$

In logarithmic form, eq. 1 becomes

$$\log K = \log S - \Delta H_A/RT \quad (4.2)$$

These equations provide a powerful analytical tool, especially when the reactions involved are in, or very nearly approach, equilibrium. Eq. 4.2 may be re-written in the form

$$y = A - Bx, \quad (4.3)$$

where $y = \log k$

$A = \log S$ (a constant)

$B = \Delta H_A/R$ (a constant)

$x = 1/T$

A chemical reaction whose rate exhibits a temperature dependence can be analyzed to determine ΔH_A . Note that in Fig. 4.139, the slope of $\log k$ vs $1/T$, and thus the heat of reaction, changes abruptly. This signifies that the nature of the reaction is very different at temperatures above $\sim 225^\circ\text{C}$. Other points to note in Fig. 4.139 are the close similarity of the 1 hr and 4 hr static data in the low temperature region and the apparent discrepancy between static and TGA data.

The slope of the TGA data is very close to those of the static data. From the displacement between static and TGA curves we infer a significant time-dependence of the reactions; the TGA reaction at a constantly increasing temperature does not have sufficient time to reach completion. This is further evidenced by the fact that the displacement in the low temperature region, as expected, remains relatively constant with increasing temperature. Significantly, however, both the TGA and static data show a close correspondence above 225°C . The

The reason, of course, is that the heat of reaction is considerably smaller (approximately 1575 cal/mole) and the time dependence, likewise, is much less. The static and TGA data are consistent in predicting a heat of reaction of about 1550 cal/mole for the conversion of "TiOX" to TiO_2 . This would tend to indicate that the oxalate precursors do not react differently as a function of temperature - at least not in terms of the reaction energy.

4.7.4 Conclusions

Our analyses show rather conclusively that the zinc precursor is $\text{Zn}_2\text{C}_2\text{O}_4 \cdot 2\text{H}_2\text{O}$. Less certain, however, is the formula for "TiOX", the titanium precursor. Mass loss data indicate that its molecular weight is approximately 149.8 (137.1 in the "dry" state). The formula inferred from these and other data is $\text{Ti}(\text{OH})_2\text{CO}_3 \cdot 5\text{H}_2\text{O}$. It is certain that "TiOX" is not an oxalate. A Clausius-Clapeyron analysis shows two distinct regimes; a low temperature region (100-250°C) in which thermal desorption of water occurs, and a high temperature region in which "TiOX" converts to TiO_2 with a heat of reaction of about 1575 cal/mole.

4.7.5 Reflectance Spectra Analyses

4.7.5.1 Materials Descriptions

The Reflectance Spectra of Pigments Prepared at Various Zn/Ti Ratios

The effects of stoichiometry on the optical properties of Zn_2TiO_4 pigments were determined from reflectance measurements made on four series of samples, designated "stoichiometry series". The first of this series was prepared from oxalate precursors and covered the range of Zn/Ti ratios from 0.5:1.0 to 2.5:1.0. The second and third series were also of MOX origin and covered a range of Zn/Ti ratios from 1.90:1.0 to 2.05:1.0; they were prepared as 6-9 and 6-12 pigments, respectively. The fourth series was prepared from New Jersey Zinc Co's SP-500 ZnO and DuPont FF anatase TiO_2 under 6/2 - 9/14 thermal conditions.

The spectra for each series are presented in Figs. 4.140-144; these reflectance data will be used subsequently to analyze the trends.

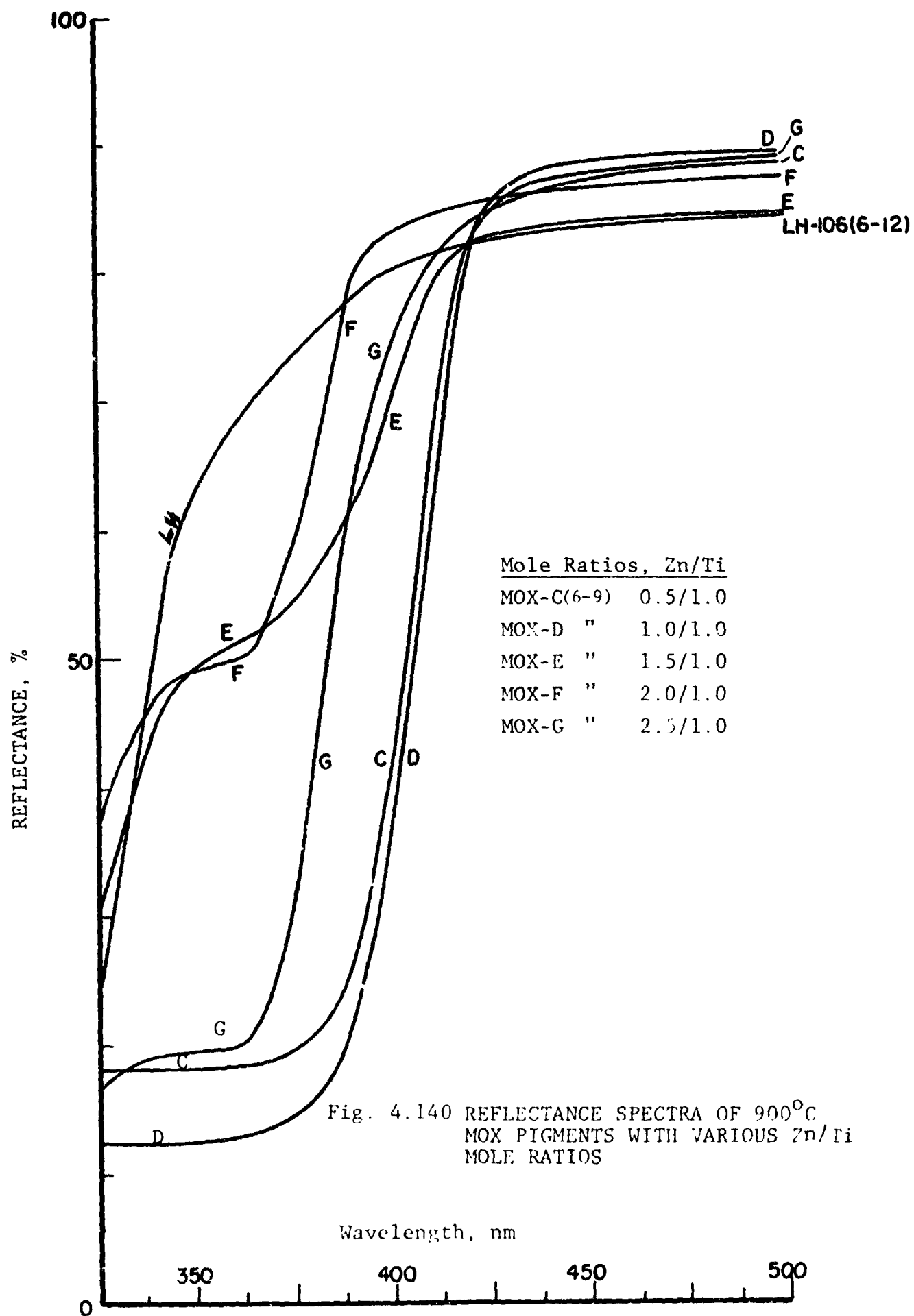
In every case the last three series include pigments with Zn/Ti ratios of 1.90, 1.95, 2.00 and 2.05. The fourth series, the SS pigments, include pigments prepared at a Zn/Ti ratio of 1.82. The pigment designated 1.82K was prepared as noted above except that New Jersey Zinc Co.'s Kadox 25 ZnO was used in place of SP-500 ZnO. Its reflectance spectrum reveals its high impurity level. For comparison with the remainder of the SS stoichiometry series, the 1.82K pigment should not be considered. It is interesting to note, however, that the difference in the "knee" reflectance of the 1.82 and 1.82K pigments is of the same magnitude as that in the MOX pigments with Zn/Ti ratios of 2.00 and less.

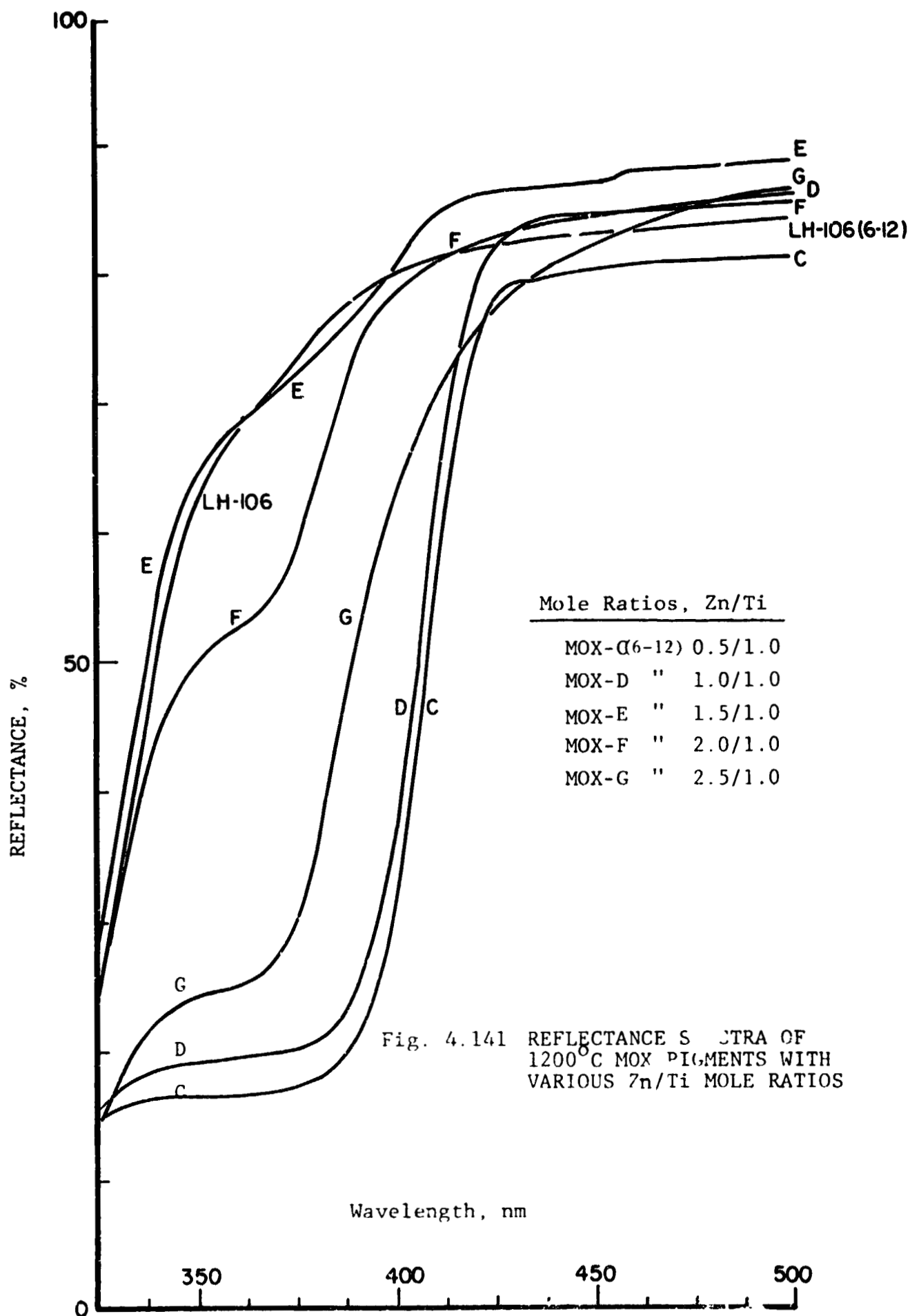
These pigment powders were deposited on IRIF sample coupons from water slurries. After the samples were dried, their diffuse reflectance spectra were measured in the spectral region from 325nm to 2600nm. The spectra in the region from 500 to 2600nm are not particularly significant, and thus have been omitted.

4.7.5.2 Optical Analyses: Zn/Ti Ratios 0.5:1 - 2.5:1.0

The diffuse reflectance spectra (325 to 500nm) for the 900°C and 1200°C samples of MOX-C through MOX-G are exhibited in Figures 4.140 and 4.141. Also included, for comparison, are the curves for LH-106(6-12) which, judging from the band edge, evidently possesses exact Zn_2TiO_4 stoichiometry.

These spectra reveal some important similarities. In both the 900°C and 1200°C cases, the band edge shifts with increasing Zn/Ti ratio toward shorter wavelengths until a pigment with a Zn excess is produced (MOX-G). The shapes of the band edges provide deeper insight. The MOX-G samples (2.5:1.0) show a "knee" which is much more flat than that exhibited by





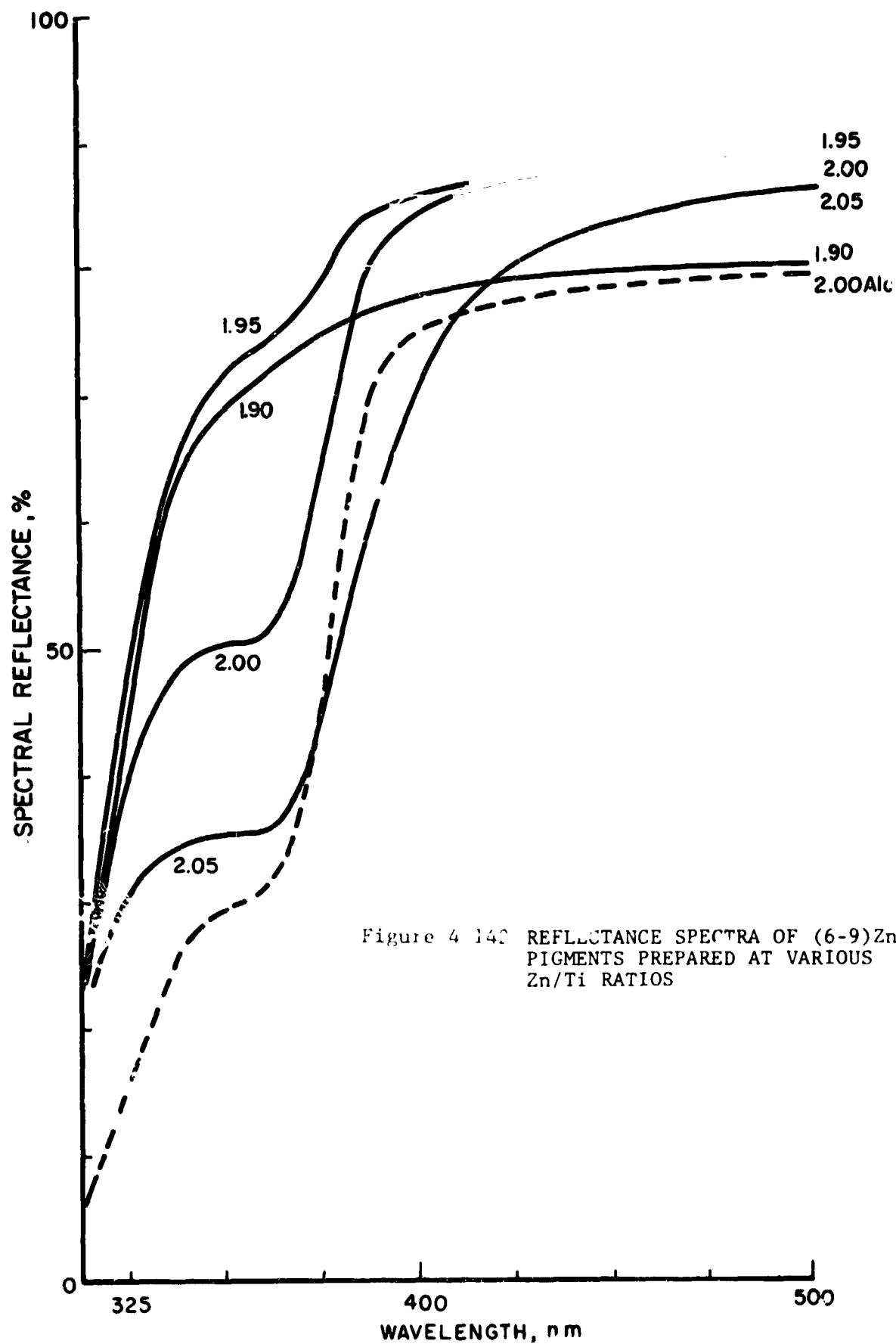


Figure 4 140 REFLECTANCE SPECTRA OF (6-9) Zn_2TiO_4
PIGMENTS PREPARED AT VARIOUS
Zn/Ti RATIOS

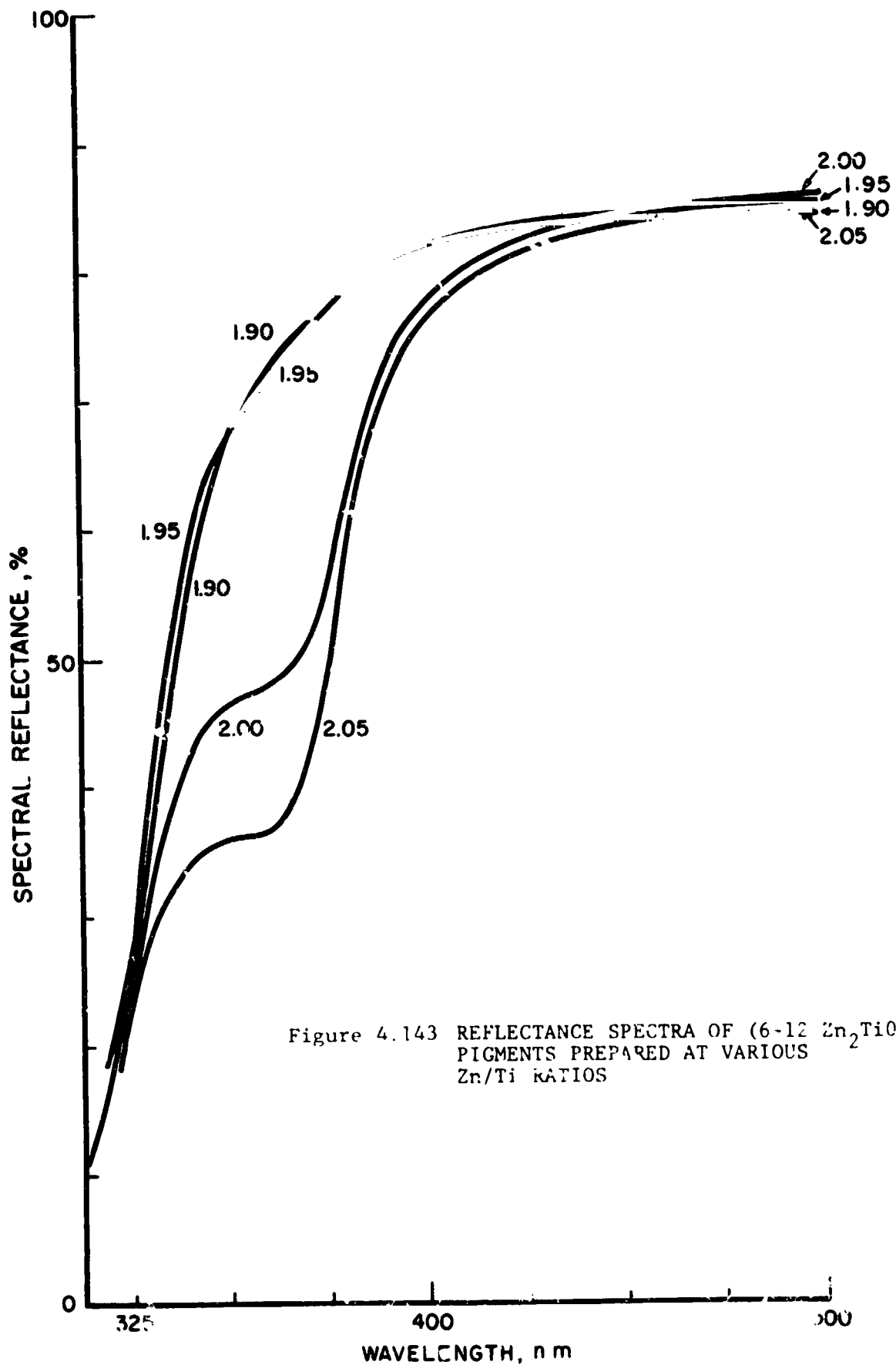


Figure 4.143 REFLECTANCE SPECTRA OF (6-12 Zn_2TiO_4 PIGMENTS PREPARED AT VARIOUS Zn/Ti RATIOS

C-5

REFLECTANCE

SAMPLE DATA

<u>Zn / Ti</u>	<u>COATING Wt.(gm)</u>
2.05	.0465
2.00	.0575
1.95	.0641
1.90	.0586
1.82	.0779
1.82 K	.0676

Fig. 4.144 REFLECTANCE SPECTRA OF $Zn_2 Ti O_4$ PIGMENTS PREPARED AT VARIOUS Zn / Ti RATIOS FROM SOLID STATE PRECURSORS

325

400

500

WAVELENGTH, λ (nm)

other samples; this is the UV signature of free ZnO. It reveals itself in this way because of its sharp fundamental absorption spectrum and its very intense absorption below 375nm (see Fig. 4.139). By contrast the spectrum of fundamental electronic absorption in both rutile and anatase TiO_2 is more gentle; the absorption constant is approximately an order of magnitude less than that of ZnO (below 375nm). The curvature (the shape) of the knee for the Zn-deficient samples obviously is much greater than that in the Zn-rich pigments. The spectra also show that the fundamental band gap of Zn_2TiO_4 lies at 3.60 eV (340nm).

As shown in Table 4.29 the visible and infra-red reflectance values of the 900°C pigments, except in the case of the E-Series pigments, are higher than those of the 1200°C pigments; the extinction coefficients, however, show conclusively that the 900°C pigments have higher reflectance values than 1200°C pigments. It should be noted that the effect of different coating weights is accounted for in calculating the extinction coefficients.

The K_{350} values (Table 4.29) exhibit a definite minimum in the 1.5:1.0 - 2.0:1.0 range of the Zn/Ti ratio for both the 900°C and 1200°C pigments. This series clearly establishes the fact that pigments whose Zn/Ti ratio is in this range possess the best reflectance values.

Comparing the spectra of the various MOX pigments with one another indicates their relative reflectance properties, but comparing each of them directly with the spectral reflectance curves for rutile titania, (r-TiO_2), anatase titania (a-TiO_2) and zinc oxide (ZnO) provides us with considerable insight. In the spectra of MOX-C(9) the fundamental band edge absorption matches that of r-TiO_2 very closely both in slope and cutoff wavelength; that of MOX-C(12) has the same slope as r-TiO_2 but occurs at a longer wavelength. This suggests that the impurity absorption may be due to a metatitanate or other Zn-Ti-O complex. Both

Table 4-29
MOX Pigment Stoichiometry Series Results

Pigment	Reflectance Values			Coating Weight (gms)	Extinction Values			Band Edge Properties			
	R ₃₅₀	R ₄₅₀	R _{i-r}		K ₃₅₀	K ₄₅₀	K _{i-r}	R _g	λ _g	E _g	E _g
MOX-C(9)	18	87	91.5	.0297	42.19	36.18	111.2	53	404	3.07	-
MOX-C(12)	17	80	84	.0266	49.25	30.13	81.06	49	407	3.07	-
MOX-D(9)	12	89.5	91.2	.0291	56.99	42.52	110.6	50.5	406	3.05	-
MOX-D(12)	19	89.5	89	.0705	17.01	13.56	39.27	42.7	407	3.04	-
MOX-E(9)	49	83.5	85	.0515	4.88	17.81	43.71	69.5	399	3.10	3.57
MOX-E(12)	64	87	90.5	.1248	0.00	8.61	24.43	80.5	399	3.10	3.62
MOX-F(9)	49	89	89	.0665	3.78	41.54	41.53	69.5	383	3.23	3.65
MOX-F(12)	50	84	87	.0690	3.35	13.57	35.87	70.5	387	3.20	3.57
MOX-G(9)	19.5	87	92	.1071	10.95	10.03	32.26	54.5	386	3.21	-
MOX-G(12)	24	82	78	.1388	6.95	6.22	12.40	55.5	393	3.15	-
LH-106(12)	63	83	88	.0403	0.00	22.29	64.72				3.63

MOX-D(9) and MOX-D(12) have absorption bands which closely match that of $r\text{-TiO}_2$. MOX-E(9) and MOX-E(12) spectra contain no evidence of $r\text{-TiO}_2$ but do indicate the presence of ZnO; in the MOX-E(12) pigment, however, the amount of ZnO is very small. MOX-F(9) and MOX-F(12) pigments also contain a slight amount of ZnO. The certainty in identifying the impurity improves when, as in the case of the MOX-G pigments, the "knee" has the classic ZnO shape: the band slope matches that of ZnO, and the spectral locations of the slope changes are characteristic of ZnO. In some cases E_g is close to that of ZnO (3.297 eV). Both the spectral and K_{350} values for the MOX-G pigments indicate that the 1200°C pigment, MOX-G(12), contains less ZnO than the 900°C pigment, MOX-G(9). The same observation may also be made in the E and F series.

This experiment strongly suggests the need to maintain the Zn/Ti ratio at or slightly below 2.0:1.0 to achieve maximum reflectance. It also suggests that, on the basis of initial reflectance, the 900°C pigments are best. Most importantly, it demonstrates that ZnO is formed in preference to TiO_2 and therefore that close stoichiometry control is necessary in the preparation of Zn_2TiO_4 pigments from oxalate precursors.

The reflectance spectra confirm and extend the results of X-ray analyses regarding formation of TiO_2 . It is clear that TiO_2 is not formed when Zn/Ti ratios are 1.5:1.0 or greater, even though Zn_2TiO_4 is formed and the titanium excess should theoretically be observable as TiO_2 . At the temperatures involved here, only the rutile form of TiO_2 would be expected. The TiO_2 in many of the MOX materials is definitely of the rutile form which is found in such materials when prepared at temperatures exceeding 700°C.

The most significant finding in these first two series, therefore, is that, both optically and via X-ray analyses, no TiO_2 is evident in pigments with Zn/Ti ratios of 1.5:1.0 or greater. The MOX-A pigments (with a Zn/Ti ratio of 1.149:1.0),

equivalent to the MOX-E pigments of this test, exhibited excellent optical properties (but poor stability) - just as the MOX-E pigments exhibit good properties.

4.7.5.3 Optical Analyses - Zn/Ti Ratios 1.8:1.0 - 2.05:1.0

In Figures 4.142-144 are presented the spectra for pigments with Zn/Ti ratios ranging from 1.82:1.0 to 2.05:1.0. The trend in each case is clear and consistent. As the Zn/Ti ratio increases, the tendency to form ZnO increases also.

Other significant observations are that the spectra of materials with Zn/Ti ratios of 1.90 and 1.95 do not differ substantially. In Table 4.30 we have listed some of the reflectance properties and extinction coefficients derived from them (according to the procedures explained subsequently). Note that the 6-9 materials have very much lower K_{350} values at Zn/Ti ratios of 1.90 and 1.95 than do the 6-12 materials. Comparing the spectra of 6-9 materials directly with those of the 6-12 materials discloses a substantial difference between their effective band gap energies (i.e. E_g); 6-9 materials have a larger band gap and the nature of their spectra suggests that higher temperatures lead to different compounds (possibly sesquitanates) whose absorption in the 325-350nm region is noticeably higher than that for zinc orthititanate.

The design of this experiment anticipated one of the effects evident in the trend of effective E_g with Zn/Ti ratio. The spectra show characteristic ZnO absorption at a Zn/Ti ratio of 2.0, and especially at 2.05, in all the pigments. In preparing the MOX materials the ZnOx material is assumed to be $ZnC_2O_4 \cdot 2H_2O$ with a molecular weight of 189.432. The molecular weight of "TiOX" is taken to be 150.00, based on gravimetric studies of the thermal conversion of "TiOX" to TiO_2 . The spectra reveal very definite evidence of ZnO at Zn/Ti ratios of 2.0 and 2.05.

Table 4-30

Selected Properties of Stoichiometry Series Pigments

<u>Zn/Ti Ratio</u> <u>SS Series Pigments</u>	<u>Coating</u> <u>wt., gms.</u>	<u>R₃₅₀</u>	<u>K₃₅₀</u>	<u>R₄₅₀</u>	<u>K₄₅₀</u>	<u>R_{i-r}</u>	<u>K_{i-r}</u>
1.82	.0779	59.5	2.247	91	37.13	94.00	58.46
1.82K	.0676	45.6	6.341	89.5	42.78	92.0	51.12
1.90	.0586	65.0	1.265	89	49.35	91.0	54.06
1.95	.0641	52.5	4.488	89.5	45.12	92.0	53.91
2.00	.0575	39.5	9.953	90.0	50.30	93.0	67.16
2.05	.0465	34.8	15.029	89.7	62.20	92.0	74.32
<u>MOX Series Pigments</u>							
1.90(6-9)	.0440	69.0	.3271	79.5	17.69	87	24.15
1.95(6-9)	.0780	71.5	-	88.0	14.50	93	21.64
2.00(6-9)	.0780	50.2	4.263	87.8	14.44	93	21.64
2.05(6-9)	.0510	35.5	10.155	83.6	18.23	89	23.60
1.90(6-12)	.0650	67.2	.6289	83.9	14.35	90	19.77
1.95(6-12)	.0665	67.0	.6594	84.7	14.52	89	18.10
2.00(6-12)	.0750	47.1	5.284	84.1	15.08	88	12.52
2.05(6-12)	.0550	36.1	12.042	83.2	16.43	88	20.55
2.05(6-12)Alc	.1500	29.9	5.665	78.8	5.12	87	7.55

While we would expect this at 2.05, the finding of a significant amount of ZnO at 2.0 implies that the effective Zn/Ti ratio is greater than 2.0, and that, if indeed the ZnOx mol. weight is 189.432, the molecular weight of "TiOx" must therefore be greater than 150. This, of course, is consistent with our earlier finding that "TiOx" is $\text{Ti}(\text{OH})_2\text{CO}_3 \cdot 0.5\text{H}_2\text{O}$ (whose mol. wt. is 150.934). This conclusion assumes also, however, that the titanium components were not preferentially retained in mixing equipment or otherwise selectively removed from the zinc-titanium mixture in the process of preparing the various samples. A subsequent argument will show that this assumption is substantiated by experimental data.

The intense absorption of ZnO below 360nm ($>10^6 \text{cm}^{-1}$) would suggest that very small amounts (of the order of several tens of ppm) would be necessary to cause a significant reduction in the reflectance in the 325 - 360nm region. In other words the reflectance in this region is highly sensitive to the concentration of ZnO.

Another comparison which may be made is that between the 2.05 MOX (6-12)Alc sample and the others. This sample pigment was prepared from oxalate precursors which had been precipitated in alcohol solutions (as opposed to aqueous solutions, which are normally used). The spectra are shown in Figure 4.142 and the appropriate data have been listed in Table 4.30. Note that the spectra and properties of the alcohol sample differ markedly from those of the aqueous samples. The nature and shape of the spectra are indicative of a large particle size, larger than those of the aqueous materials. The shape of the reflectance spectrum below 400nm is also very interesting. The sharper absorption in the 376nm region suggests that the material has much more ZnO in it than an equivalent material prepared by aqueous precipitation.

Of the many data examined in the stoichiometry series investigations, those shown in Fig. 4.145 are the most important. In that figure are plotted the K_{350} values of the stoichiometry series pigments in the Zn/Ti ratio range of 1.90:1.0 to 2.05:1.0. K_{350} is defined as

$$K_{350} = \ln\left(\frac{70}{R_{350}}\right)/t_f \quad (4.4)$$

where 70 = an optimum reflectance value at $\lambda = 350\text{nm}$

R_{350} = reflectance value at $\lambda = 350\text{nm}$

t_f = film thickness, cm

The importance of Figure 4.145 resides in several critical characteristics of the data. First, all the curves display minima at Zn/Ti ratios less than 2.0:1.0. Second, all curves show a very strong dependence of K_{350} on ZnO content, i.e. on Zn/Ti ratios above the minima, and a rather weak dependence below them. Third, the K_{350} minima for MOX pigments occurs at Zn/Ti = 1.95, while that for SS pigments, at Zn/Ti = 1.90:1.0. Fourth, the slopes at Zn/Ti ratios above these minima are almost identical.

The conclusions from these observations are that the most reflective pigment is not one with exact Zn_2TiO_4 stoichiometry; both SS and MOX data agree on this point. If we accept that the molecular weights of SS pigment precursors are not subject to challenge, then these data strongly suggest that the molecular weight of "TiOX" must be 153.95 rather than the estimated 150, i.e., higher by the ratio of 1.95/1.90 the ratio of the minima of K_{350} values of MOX vs SS pigments. Quite obviously, they also imply that a Zn/Ti ratio above 1.90 has a much more serious effect than one less than 1.90. The implications of Fig. 4.145 are very important but we must point out, even emphasize, that these data pertain to unirradiated pigments and thus should be regarded as tentative, particularly with respect to their stability in paint systems. UV irradiation test data are summarized in Table 4.31 and graphically presented in Fig. 4.146 as a function of Zn/Ti ratio. The trends in the 6-9 pigments

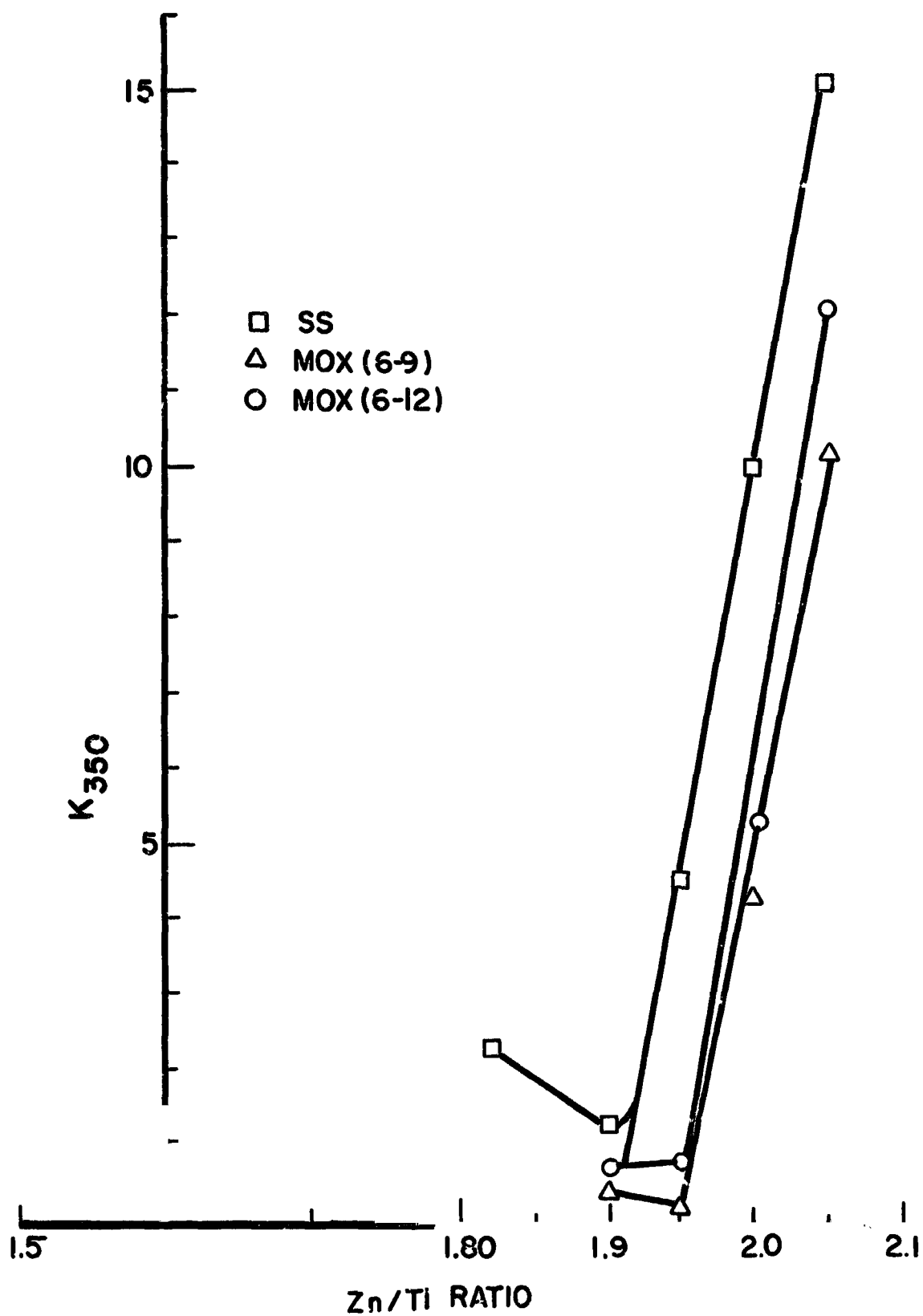


Fig. 4.145 RELATIVE ABSORPTION COEFFICIENT AT $\lambda = 350\text{nm}$ VS Zn/Ti RATIO IN Zn_2TiO_4 PIGMENTS

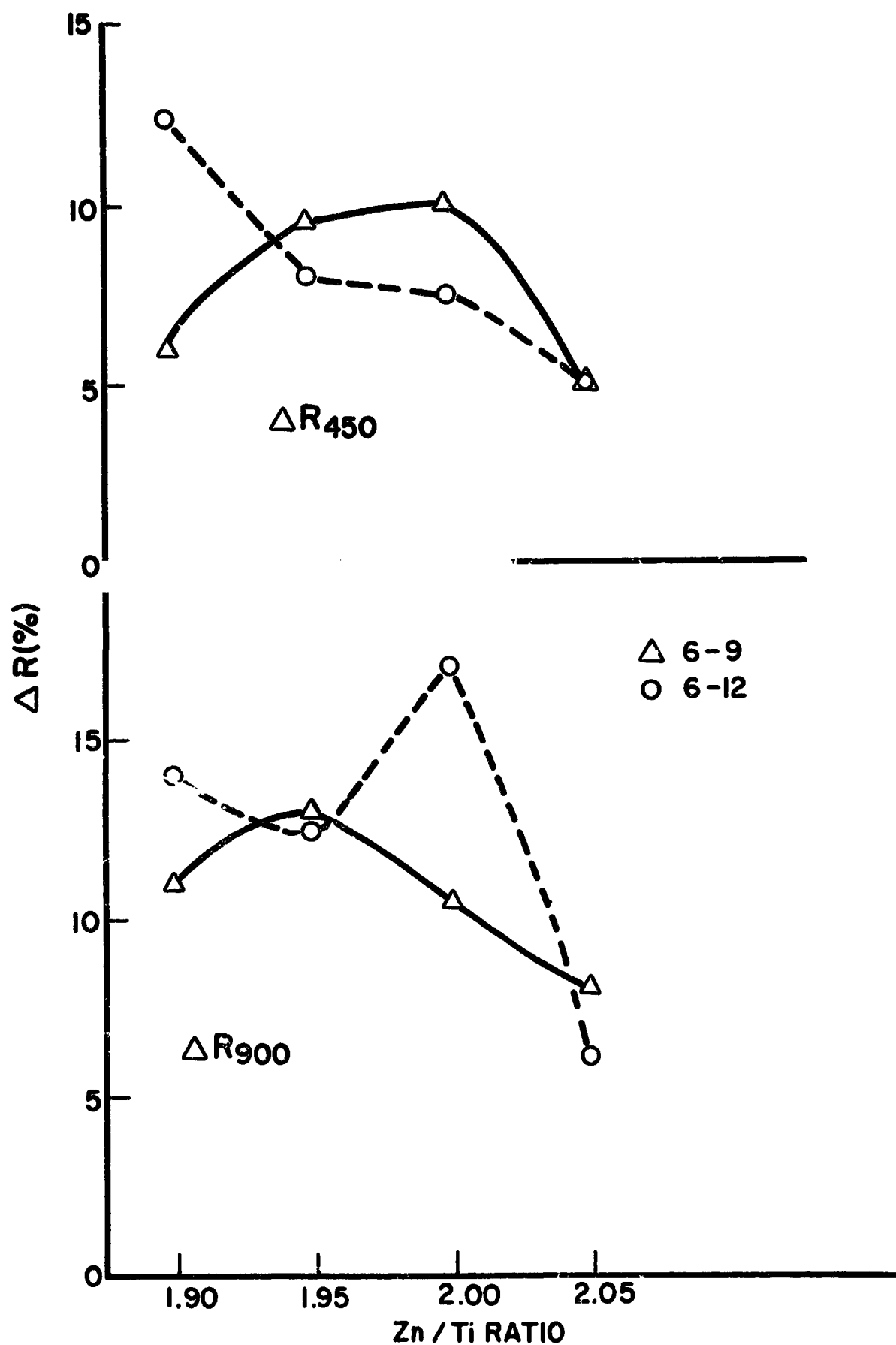


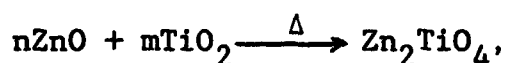
Fig. 4.146 UV SPECTRAL STABILITY VS Zn / Ti RATIO

indicate that damage tends to be greatest at a Zn/Ti ratio between 1.95 and 2.0. The behavior of the 6-12 pigment with a Zn/Ti ratio of 2.0 may be anomalous, because the trends, otherwise, are quite consistent.

4.7.6 Summary

The stoichiometry series pigments have led to several very significant observations: TiO_2 is not formed even at Zn/Ti ratios as low as 1.5:1.0; the most "pure" Zn_2TiO_4 has a Zn/Ti ratio in the range of approximately 1.90:1.0 - 1.95:1.0; and UV stability of the pigment does depend upon pigment stoichiometry. The slopes of the steep portions of the curves in Fig. 4.145 are as expected for small concentrations of a strong absorber (viz., ZnO). The fact that they all have nearly the same slope is further evidence, and suggests that the amount of ZnO formed is independent of the calcination temperature.

The assumption that Zn_2TiO_4 is a pure compound has pervaded this entire program. We speak of Zn-rich Zn_2TiO_4 and of Ti-rich Zn_2TiO_4 . The reaction,



is said to be exactly stoichiometric when $n/m = 2.00$. When $n/m > 2.00$, the resultant Zn_2TiO_4 is Zn-rich. However, when $n/m < 2.00$, it is not possible to claim that the resultant Zn_2TiO_4 is Ti-rich. This is probably because of competing reactions of the precursors to form ZnTiO_3 (metatitanate), $\text{Zn}_2\text{Ti}_3\text{O}_8$ (sesquititanate), Zn_2TiO_4 (orthotitanate), and perhaps other Zn-Ti-O complexes. Finally, it is significant that the impurity in pigments with Zn/Ti ratio > 2 is ZnO, while the impurities in those with Zn/Ti ratios of less than 2.0 are obviously neither ZnO, nor TiO_2 .

4.8 REFERENCES

1. NASA Marshall Space Flight Center, Contract No. NAS8-5379, 20 May 1963 to 8 Oct. 1971; see also G.A. Zerlaut with J.E. Gilligan and N.A. Ashford, "Investigation of Environmental Effects on Coatings for Thermal Control of Large Space Vehicles", IITRI Report No. U6002-97 (Final Report), 8 Oct. 1971; see also G.A. Zerlaut, J.E. Gilligan and N.A. Ashford, "Space Radiation Environmental Effects in Reactively Encapsulated Zinc Orthotitanates and their Faints", AIAA Paper No. 71-449, presented to AIAA 6th Thermophysics Conference, Tullahoma, Tenn. Apr. 26-28, 1971.
 2. D.K. Edwards, et. al., J.O.S.A. 51, p. 1279, 1961.
 3. J.E. Gilligan and R.F. Boutin, "Development of Space Stable Thermal Control Coatings for Use on Large Space vehicles", IITRI Report No. C6233-12 (Triannual Report), Jan. 1972.
- N.B. The following reports, except where noted, are triannual reports and have the same title as Ref. 3 above; they were prepared under NASA-Marshall Space Flight Center Contract No. NAS8-26791.
4. J.E. Gilligan, IITRI Report No. C6233-16, 25 May, 1972.
 5. J.E. Gilligan, et al., IITRI Report No. C6233-20, 25 Sept. 1972.
 6. J.E. Gilligan and Y. Harada, IITRI Report No. C6233-24, 25 Jan. 1973.
 7. G.A. Zerlaut with J.E. Gilligan and N.A. Ashford, IITRI Report No. U6002-97 (Final Report), see Ref. 1.
 8. G.A. Zerlaut and J.E. Gilligan, "Study of In-Situ Degradation of Thermal Control Surfaces", NASA Contract No. NAS8-21074, IITRI Report No. U6061-17 (Interim Summary Report), March 7, 1969, and IITRI Report No. U6061-29 (Final Summary Report), Feb. 20, 1970.
 9. J.E. Gilligan and Y. Harada, IITRI Report No. C6233-32, Nov. 1973.
 10. J.E. Gilligan and Y. Harada, IITRI Report No. C6233-44, Oct. 1974.
 11. J.E. Gilligan and Y. Harada, IITRI Report No. C6233-40, Aug. 1974.

REFERENCES (Cont'd)

12. N.A. Lange, "Handbook of Chemistry," 6th Ed., Handbook Publishers, Inc., Sandusky, Ohio, 1946; CRC Handbook of Physics and Chemistry", 50th Edition, R.C. Weast, (Ed.); Publ., Chemical Rubber Co., Cleveland, Ohio, 1969.
13. S.F.W. Grundall, "A Process for Preparing Basic Titanic Oxalate", U.S. Patent No. 2,027,812, Jan. 1936.

5.0 BINDER DEVELOPMENT

5.1 INTRODUCTION

The fact that binders also must be stable when exposed to ultraviolet radiation can perhaps best be understood in terms of their transmission spectra relative to those of the pigments used with them. The pigment and binder compete for the absorption of ultraviolet photons. Since inorganic pigments, from a pragmatic point of view, are far more stable than organic or semi-organic binders, the paints made from pigments with fundamental absorption edges occurring at wavelengths longer than those of the binders in which they are dispersed will in general be more stable; semi-conductor pigments (e.g. ZnO) absorb so strongly in the ultraviolet that they afford very good protection to the binder. To achieve very low solar absorptance coatings, however, the fundamental absorption edge must be at shorter wavelengths than those of the more common semiconductor pigments. This, of course "exposes" the binder to more ultraviolet radiation and therefore, potentially to substantially increased binder damage.

5.2 OWENS-ILLINOIS 650 "GLASS RESIN" IMPROVEMENT STUDY

Owens Illinois 650 "Glass Resin", even unprotected, has displayed very good ultraviolet stability and, accordingly, is considered with great interest. The principal reason for its not being used in its commercially available form is that it has poor physical properties. Because of its double-chain structure and its high residual functionality, coatings made of this resin become very brittle and craze on aging. This effect is called "coasting" and reflects an ongoing curing process. OI-650 glass resin is produced by polymerization of a trifunctional monomer; the completely cured material thus lacks molecular flexibility.

We have studied the possibility of improving the properties of OI-650 by end group blocking, and by copolymerization of the B-staged resin with a linear polydimethylsiloxane before curing.

5.2.1 Internal Plasticizing of OI-650 Glass Resin by Copolymerization

This approach is based on the concept that introduction of linear polydimethylsiloxane segments in the OI-650 structure should increase the flexibility of the resin. The procedure employed involves (a) preparation of polydimethylsiloxane by polymerization of dimethyldichlorosilane; (b) copolymerization with OI-650.

Dimethyldichlorosilane was added to a mixture of methylene chloride and water under stirring. The resin obtained dissolves in the organic phase. The organic layer was separated and thoroughly washed with water until neutral to eliminate all traces of HCl. This solution was added to a solution of the OI resin in absolute ethanol at the ratio desired, and a clear mixture is obtained. On curing, the hydroxyl-terminated polydimethylsiloxane acts as an internal plasticizer.

Variable amounts of polydimethylsiloxane have been used (1% to 10% by wt.). Unpigmented coatings of various thicknesses were cast on aluminum plates, and cured at room temperature, at 80°C, and at 170°C. The flexibility of the coatings is noticeably improved by the presence of polydimethylsiloxane at concentrations between 1 and 5% by wt.

A composition of OI-650 was prepared containing 4.8% (by weight) polydimethylsiloxane. Paints were formulated from standard OI-650 and from the "modified" OI-650, using zinc orthotitanate as the pigment.

Tests of 41% PVC films indicate a lowered adhesion of both standard and modified films. The "modified" film, however, when baked at 200°F overnight displays a better gloss (implying less binder demand) than the standard film; and it forms a much tougher film than that of the standard paint. Films baked at

350°F are not improved, and in fact become somewhat brittle. Since the product of hydrolysis of dimethyldichlorosilane has a broad molecular weight distribution which includes cyclic oligomers, (that is, low molecular weight components that may cause outgassing problems), it was thought that an improved composition could be obtained by further polymerizing the product of hydrolysis of dimethyldichlorosilane to a higher molecular weight, fully linear polymethylsiloxane. This product could then be used for the modification of the OI-650 resin. The following procedure was employed for the synthesis of an hydroxyl-terminated, linear polydimethylsiloxane:

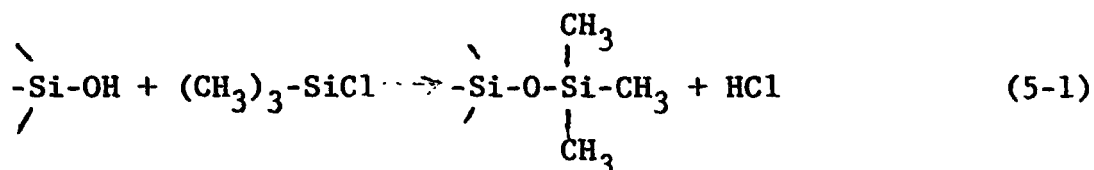
Dimethyldichlorosilane (100cc) was added slowly from a dropping funnel to vigorously stirred water (300cc) maintained at 20-25°C with an ice bath. When the addition was completed, the organic layer was taken up in ethyl ether (75cc) separated from the water phase and dried over magnesium sulfate. The ether solution was filtered and the ether removed by evaporation. The product obtained (33g) was placed in a bottle with concentrated sulfuric acid (6.1cc) and ethyl ether (16cc). The mixture was stirred at room temperature for one day and became very viscous. Then 33cc of ether and 16cc of water were added and the mixture was shaken for another hour. The aqueous layer was drawn off and the solution washed three times with water and then dried over anhydrous potassium carbonate. The ether was distilled by using a water pump. The clear viscous oil obtained is a hydroxyl-terminated, linear polydimethylsiloxane, soluble in various hydrocarbon and other solvents.

This material was added in various ratios to the OI-650 resin in solution. It was found that tetrahydrofuran (THF) can be used as a common solvent for the two resins. However, poor compatibility (that is, mutual solubility of the linear siloxane and OI-650), was observed. On evaporation of the solvent, phase separation occurs, resulting in the formation of droplets of polydimethylsiloxane in the OI-650 matrix.

5.2.2 Modification of OI-650 Resin by Partial End-Blocking With Trimethylchlorosilane

This approach is based on the consideration that the high functionality of OI-650 resin is responsible for the highly cross-linked nature and rigidity of the cured polymer. By partial end-blocking of reactive functional (i.e. silanol) groups, the extent of cross-linking of the resin could be reduced and flexibility could be improved.

Blocking of the silanol groups of the resin was accomplished by reacting it with trimethylchlorosilane:



This reaction was studied under various conditions. If the resin is reacted with an excess of trimethylchlorosilane in the absence of a solvent, a vigorous reaction occurs and hydrochloric acid is evolved, but the reaction occurs predominantly on the surface of the resin. Better results are obtained in the presence of a solvent. It was found that the best solvents for this reaction are weakly basic amides such as dimethyl formamide (DMF). In non-basic solvents, such as acetone, little or no reaction occurs and hydroxyl groups are still present at high concentration after reaction. In basic solvents, such as pyridine, a highly exothermic reaction occurs with formation of a complex pyridine-trimethylchlorosilane. In weakly basic amides, such as DMF, a moderately exothermic reaction occurs and blocking of hydroxyl groups can be obtained. In preliminary experiments, an excess of trimethylchlorosilane was used and complete blocking of hydroxyl groups was obtained, as indicated by infrared analysis of the resin after reaction. In subsequent work, a calculated amount of trimethylchlorosilane was utilized in order to obtain a resin having the desired level of residual hydroxyl groups.

5.3 ENGINEERING EVALUATIONS

Two samples of the OI-650 resin modified by partial end-blocking with trimethylchlorosilane, designated OI-650G, were submitted to the paint laboratory for preliminary evaluations, each sample being approximately 23 grams.

Extensive solubility tests were conducted, the results of which are summarized in Table 5.1. The procedure involves the following steps: the resin was dispersed in the test solvent and its solution properties noted; and the films cast from these solutions were then checked for appearance and physical properties. The symbols in Table 5.1 are identified in the key. In general the hydrocarbons are the best solvents for OI-650G.

Two different thinner formulae were used and evaluated for making a 50% solution of the resin.

"Mix α "

Benzene	75% by volume
Isopropyl Acetate	15%
Isopropyl Alcohol	10%

"Mix β "

Toluene	75% by volume
Butyl Acetate	15%
Butanol	10%

Pours of each solution were made over tin strips, one of which was air-cured overnight, the other cured at 212°F overnight. The air cured pours are much more tacky than the baked ones, and the "mix α " pours are tackier than the "mix β " pours. This latter finding shows that the use of a slower (less volatile) solvent kept the coating open longer for a better final dry.

Table 5.1

LIST OF SOLVENTS

<u>Hydrocarbons</u>	<u>Solution</u>	<u>Film</u>
Petroleum ether	±*	++
Benzene	+	+
Toluene	+	+
Xylene	+	+
Ethyl benzene	+	±
<u>Alcohols</u>		
Methyl alcohol	p	i
190p Ethyl Alcohol	p	i
200p Ethyl Alcohol	±	±
150p Isopropyl Alcohol	±	+
Butyl Alcohol	+	+
Methyl Isobutyl Carbinol	+	+
<u>Esters</u>		
Ethyl Acetate	±	±
180p Isopropyl Acetate	+	+
n-Butyl Acetate	+	+
Methyl Amyl Acetate	+	+
Cellosolve Acetate	+	+
(poor solvent release)		
<u>Ketones</u>		
Acetone	±	±
Methyl-ethyl Ketone	±	±
Methyl Isobutyl Ketone	+	+
Diacetone	p	p
Cyclohexanone	p	p
<u>Cellosolves</u>		
Methyl Cellosolve	p	p
Ethyl Cellosolve	p	p
Butyl Cellosolve	p	p
<u>Nitro Compounds</u>		
2-Nitropropane	p	p

*Key: + = soluble clear
 ± = soluble hazy
 i = insoluble
 p = precipitate forms

Using "mix β ", two grinds were made of zinc orthotitanate pigment (lithium silico fluoride treated and flash re-calcined), one at 26% Pigment Volume Concentration (PVC) and the other at 35% PVC. Both grinds were sprayed on clean aluminum and the panels baked overnight at 212°F. The 26% PVC coating, while not tacky to the touch, exhibits some evidence of dirt collection under pressure, particularly when making conical mandrel and 10-inch pound reverse impact tests. The 35% PVC coating gave better results. Both panels passed the conical mandrel and 10 in-pound reverse impact tests.

Baking for 16 hr at 212°F is required to provide a coating not readily soluble in the original solvent. Paints, pigmented at 35% PVC with S-13G pigment (potassium silicate treated SP500 ZnO), possess excellent shelf-life. (Note that unmodified OI-650 resin cannot usefully be pigmented with silicated zinc oxide: the mixture gels almost instantly). A series of paint films employing S-13G and zinc orthotitanate pigments were prepared in order to establish the cure conditions. One series (designated A-429M) is S-13G pigment in OI-650G; second, in zinc orthotitanate in OI-650, and Zn_2TiO_4 in OI-650G. Out of each series, one film was air dried, one was cured at 250°F/16 hr, and a third cured at 350°F/16hr. All of the unmodified films showed evidence of cracking, while the OI-650G films did not. The modified films definitely require a heat cure. Although, 250°F produces a satisfactory cure, the 350°F treatment, at least from the standpoint of outgassing, is preferable as will be shown below. All of the films which were heat cured displayed excellent adhesion and film toughness. Their general appearance was also very good.

A study of the outgassing of modified OI-650 has been performed by using isothermal TGA in conjunction with a diffusion pump (10^{-5} mm Hg). This apparatus allows continuous recording of the weight of the sample. For the purpose of determining the effect of curing temperature on outgassing, two paint samples of

A-429M have been tested, one cured at 325°F, the other at 400°F. A-429M designates the system: $\text{ZnO}:\text{K}_2\text{SiO}_3/\text{OI-650G}$. The samples were maintained under vacuum at ambient temperature, then heated at 125°C for 25 hr. As expected, the total weight loss due to outgassing decreases with increasing curing temperature. The weight loss from a sample cured at 325°F was 1.05% at room temperature (in vacuo) and 1.25% after subsequently heating it under vacuum at 125°C (total loss, 2.33%). The weight loss of the sample cured at 400°F averaged 0.59% at room temperature (in vacuo) and 0.39% after heating in vacuum at 235°C (total loss, 0.98%). Outgassing tests on three different batches of OI-650G have also been performed by J.P.L. The following results indicate increasingly poor outgassing characteristics:

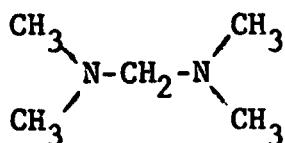
<u>Batch No.</u>	<u>TWL</u>	<u>VCM</u>
M-97	0.17	0.05
	0.15	0.04
M-102	0.89	0.64
	0.55	0.41
M-126	1.53	0.95
	1.10	0.75

The outgassing acceptance criteria (ref. 5.1) are: TWL <1%; VCM <0.1%.

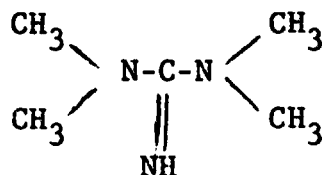
5.4 FUTURE BINDER STUDIES

The two current problem areas with OI-650G are its poor outgassing characteristics and the need for a relatively high curing temperature (350°F). Outgassing may be caused by the presence of low molecular weight components formed by excessive end-blocking of resin. It is recommended that in future work the extent of end-blocking be reduced and that the effect of the degree of end-blocking on the outgassing characteristics of the resin be investigated. A lower degree of end-blocking is also expected to increase the reactivity of the modified resin and to allow the use of a curing temperature lower than the one currently

employed. It is also conceivable that a room temperature curing 0I-650G could be obtained by using catalytic amounts of a tertiary amine. In order to maximize UV radiation stability, an ultra-violet transparent catalyst should be selected. The use of tetramethyl-methanedi-amine is recommended. This compound is expected to be superior to tetramethylguanidine (commonly used for curing RTV silicones) because of the absence of UV-absorbing double bonds:



Tetramethylmethanedi-amine



Tetramethylguanidine

5.5 REFERENCES

1. R.F. Muraca et. al., "Polymers for Spacecraft Hardware: Materials Characterization," JPL Contract No. 950745, Stanford Research Institute Interim Report No. 3 - Part I, Dec. 9, 1966.

6.0 ELECTRON PARAMAGNETIC RESONANCE INVESTIGATIONS

The primary and ultimate test of any pigment is its environmental stability. As we have seen, a considerable amount of information can be gleaned from the reflectance spectra of experimental materials which have been exposed to simulated space environment tests. In addition to these and to the other usual analyses accompanying the development of space-stable pigments, e.g. SEM and x-ray, we initiated several intensive investigations to elicit additional information affecting the development and characterization of Zn_2TiO_4 pigment. They have supported various aspects of the pigment development efforts at various stages. One of the first supporting investigations was the effort to characterize the electron paramagnetic resonance (EPR) properties of experimental Zn_2TiO_4 pigments, before and after UV irradiation. These investigations have produced several conclusions important to the successful development of stable Zn_2TiO_4 pigments.

6.1 BACKGROUND

The intent of the EPR studies is, basically, to provide an analytical tool for characterization of defects in Zn_2TiO_4 pigments. It would be useful to detect and discriminate between those "defects" which are intrinsic, created in the manufacturing process, or are induced by simulated space environmental influences. These studies were initiated early in the program and carried out over an 18 month period. The Zn_2TiO_4 pigment referred to in these studies was produced by the solid state method; the reference pigment for these studies was B-229 (defined in ref. 6.1). EPR studies included not only Zn_2TiO_4 pigments but their precursors. Of special interest in the latter studies were the EPR spectra of individual precursors before and after thermal treatments identical to those used in converting their mixtures to Zn_2TiO_4 pigments.

The EPR research efforts primarily utilized an high-vacuum in situ irradiation facility mated to the EPR spectrometer. They confirm in part some of the results of earlier work, in which the conclusions were considered tentative due to poorer vacuum conditions (Refs. 6.1-3).

In particular, the purposes of these investigations have been:

- the rationalization of the differences in optical damage in differently treated zinc orthotitanate pigments both in terms of intrinsic defect structure and in terms of the presence of precursor-type oxides;
- the elucidation of the various EPR-active species in Zn_2TiO_4 and of the importance of metastable species;
- the identification and characterization of the species responsible for the optical damage at ~ 0.9 microns (S-band);
- the clarification of the relationship of residual paramagnetic centers in ZnO to damage at $\sim 363\text{nm}$ and in the infrared; and, most importantly,
- the correlation of centers detected by EPR spectroscopy with those which are optically important.

A comprehensive summary of previous EPR work is provided in Reference 6.1. and should be consulted for completeness.

6.1.1 Experimental-Equipment and Procedures

A Varian Model 4500 EPR Spectrometer System with a model V-4012-3B 12" electro magnet and model V2100B regulated power supply was used. An NMR magnetometer was used for precise calibration of the magnetic field strength while the Klystron frequency was monitored by a Hewlett-Packard Model 5255A frequency converter. The spectrometer, equipped with high vacuum irradiation and gas adsorbate equipment, appears in Figure 6.1. The in-situ equipment consists of a mounting structure (on the right in the photograph), a 20 liter/sec. ion pump (middle right), and valving and vacuum connections (middle left). The EPR tube (lower left) is mated to

this equipment through an "O-ring" connection. The mounting structure, which is suspended from the ceiling, is movable vertically so that the EPR tube may be raised and lowered into the Varian EPR spectrometer cavity between the pole pieces of the magnet. The latter lies below the table and is not visible in the photograph.

The samples are placed in suprasil EPR tubes and subjected to unfiltered radiation from an Osram 500 watt, point source Mercury Arc lamp collimated with a four-inch diameter fused silica lens (focal-length four inches). The lens is placed at approximately twice the focal length from the lamp providing a one-to-one magnification of the point-source arc whose image is contained entirely within the sample area. Overnight irradiation with this collimated source provides the equivalent of 500 ESH of AH-6 radiation. Irradiations were carried out at 77°K (LN₂) and at ambient temperatures both inside and outside the dewar and cavity. Several irradiations of samples at room temperature were conducted using AH-6 radiation.

In all cases the samples were under high-vacuum in Varian suprasil EPR tubes with approximate 3mm ID. EPR measurements were carried out at liquid nitrogen temperatures, with the exception of an experiment in which metastable species were investigated.

In some experiments, the admission of air or O₂ to the samples in EPR tubes upon completion of post-irradiation EPR measurements was accomplished, in all cases with the samples at room temperature. This usually necessitated removing the sample from an LN₂ dewar, admitting the gas, re-pumping and then re-cooling to 77°K for EPR measurements. (The bleaching experiments performed were preliminary and served more of a diagnostic purpose than a detailed dynamic gas adsorbate EPR investigation). The way in which some of the bleaching experiments were performed thus necessitated an investigation of temperature effects and the role of metastable species to distinguish those effects from true adsorbate phenomena.

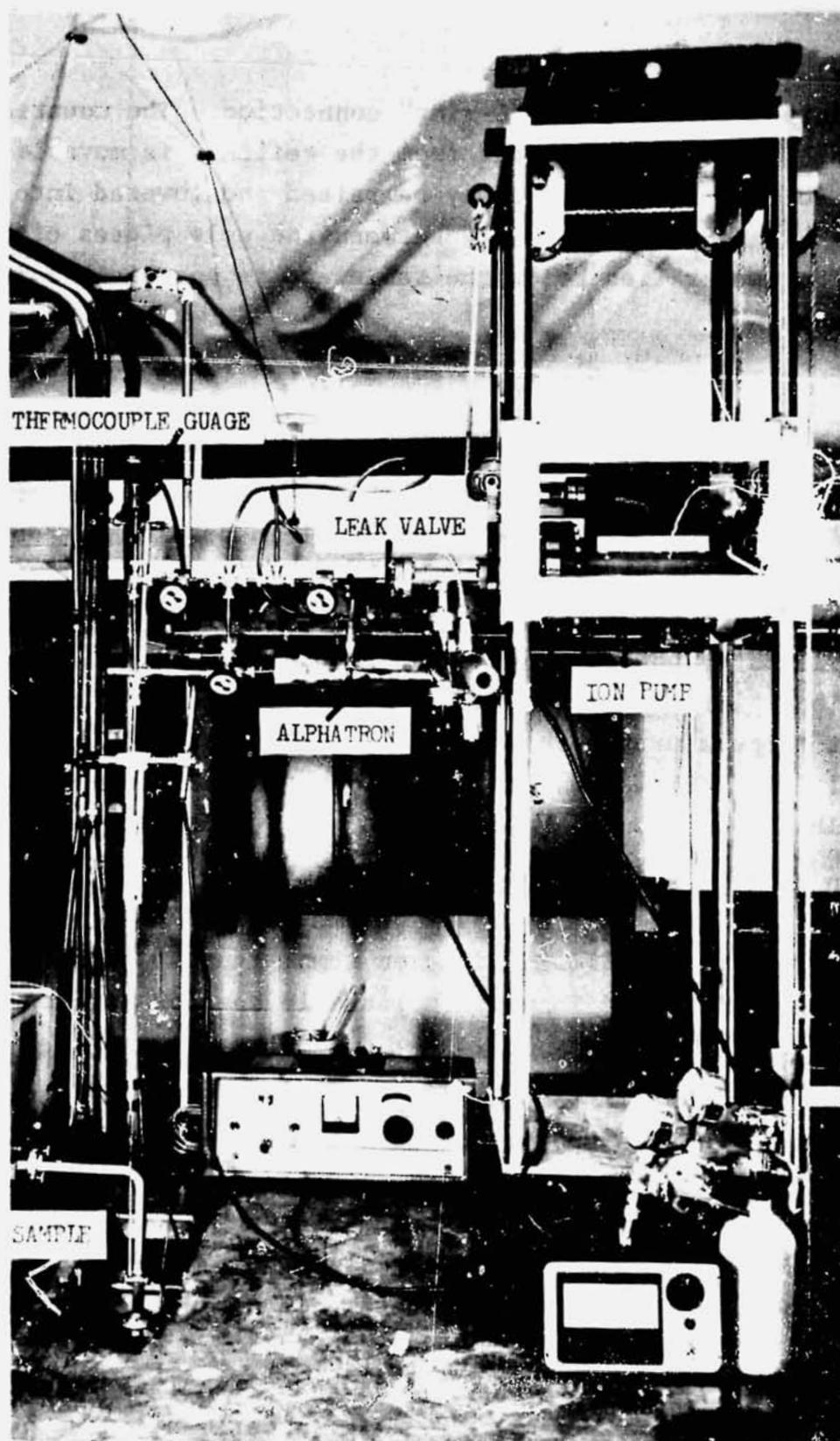


Figure 6.1 EPR FACILITY WITH IN-SITU SAMPLE HANDLING CAPABILITY

6.1.2 Experimental Results

6.1.2.1 ZnO

Untreated SP-500 ZnO gives a weak EPR signal as shown in Figure 6.2a. After 30 minutes of in situ irradiation at 77°K at a vacuum of 10^{-7} , the intensity is greatly increased as is shown in Figure 6.2b. Figure 6.3a shows the intensity of the $g = 1.9565$ signal after warming the irradiated material to, and holding it at, room temperature for 45 minutes (while under high vacuum); after then re-cooling to 77°K (for an EPR measurement), the signal intensity had decreased by about one-half (Figure 6.3b). Re-irradiation for 30 minutes at 77°K restored the previous (irradiation-produced) intensity (Figure 6.3c). Warming the sample to room temperature again and admitting ~ 0.1 torr O_2 resulted in a large decrease in the EPR signal (at 77°K). The pre-irradiation signal is shown in Figure 6.4a; after O_2 bleaching as Figure 6.4b indicates, the signal is actually smaller than the original signal.

6.1.2.2 Anatase Titanium Dioxide Converted to Rutile

The EPR spectrum in Figure 6.5 is that of DuPont FF-anatase converted to rutile by a thermal treatment identical to that given the oxide mixture (ZnO and TiO_2) in the solid state method of preparation of Zn_2TiO_4 ; it was prepared in a water slurry, dried and heated at 925°C in air and annealed. A paramagnetic center with $g_{\perp} = 2.0037$ and $g_{\parallel} = 2.0005$ (most likely an oxygen species) is the only center observed prior to high vacuum treatment. After the formation of rutile in this manner, the material was heated at (500/6) at 10^{-6} - 10^{-7} torr. An intense asymmetric signal attributed to Ti^{+3} with $g_{\perp} = 1.9864$ and $g_{\parallel} = 1.9469$ was observed. (See Figure 6.6). Comparison of this latter spectrum with that of a secondary standard of Mn^{++} in $CaCO_3$ yielded a spin concentration of 2.0×10^{14} spins in a sample of approximately 0.2 gram. The spectrum of LW anatase heat treated in high vacuum is shown in Figure 6.7 for comparison. No additional centers were produced or destroyed by: (a) in-situ irradiation for 30 minutes at 77°K, (b) irradiation for 39 hours at ambient temperatures, or (c) admission of air.

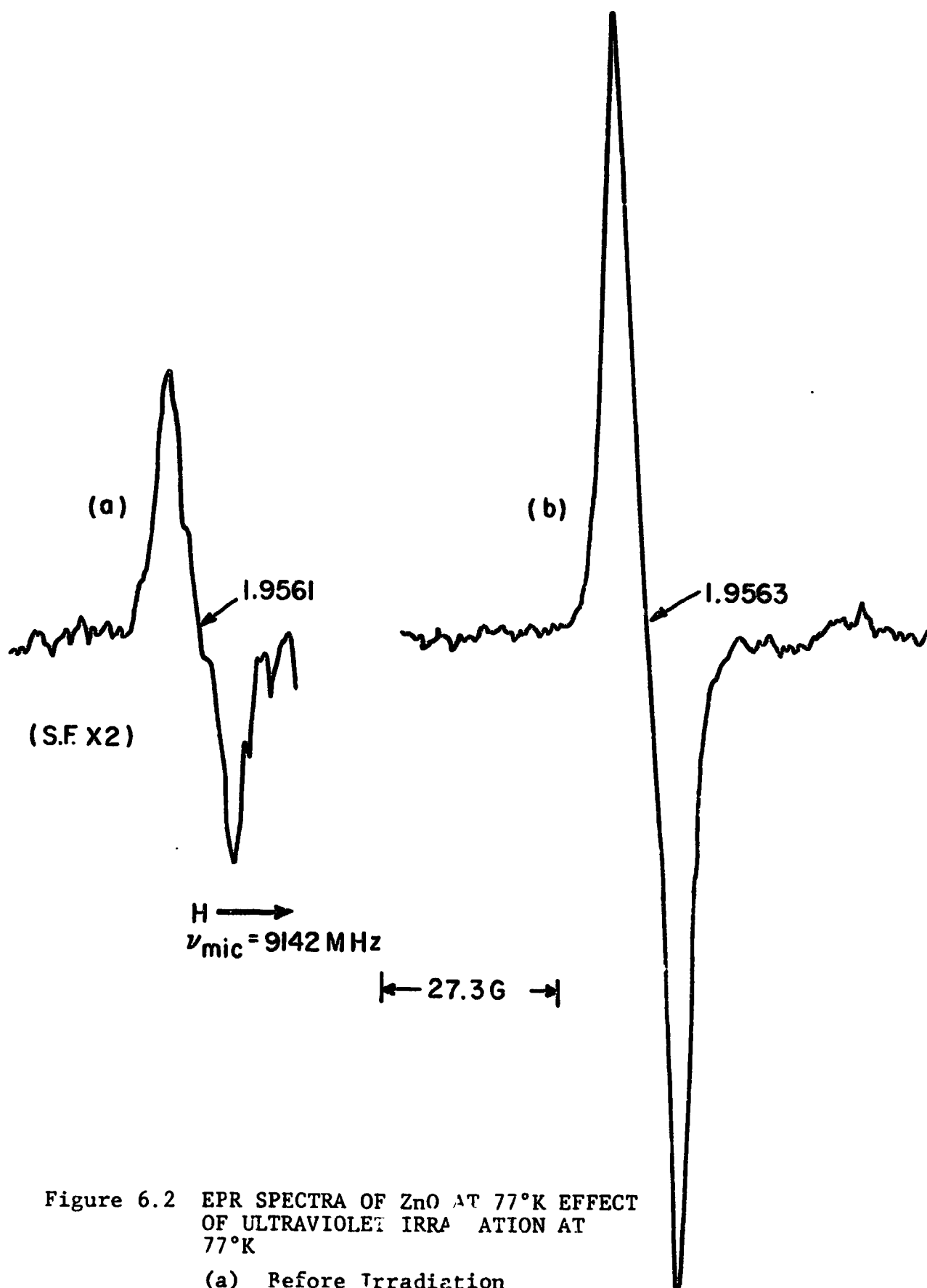


Figure 6.2 EPR SPECTRA OF ZnO AT 77°K EFFECT OF ULTRAVIOLET IRRADIATION AT 77°K

(a) Before Irradiation

(b) After Irradiation

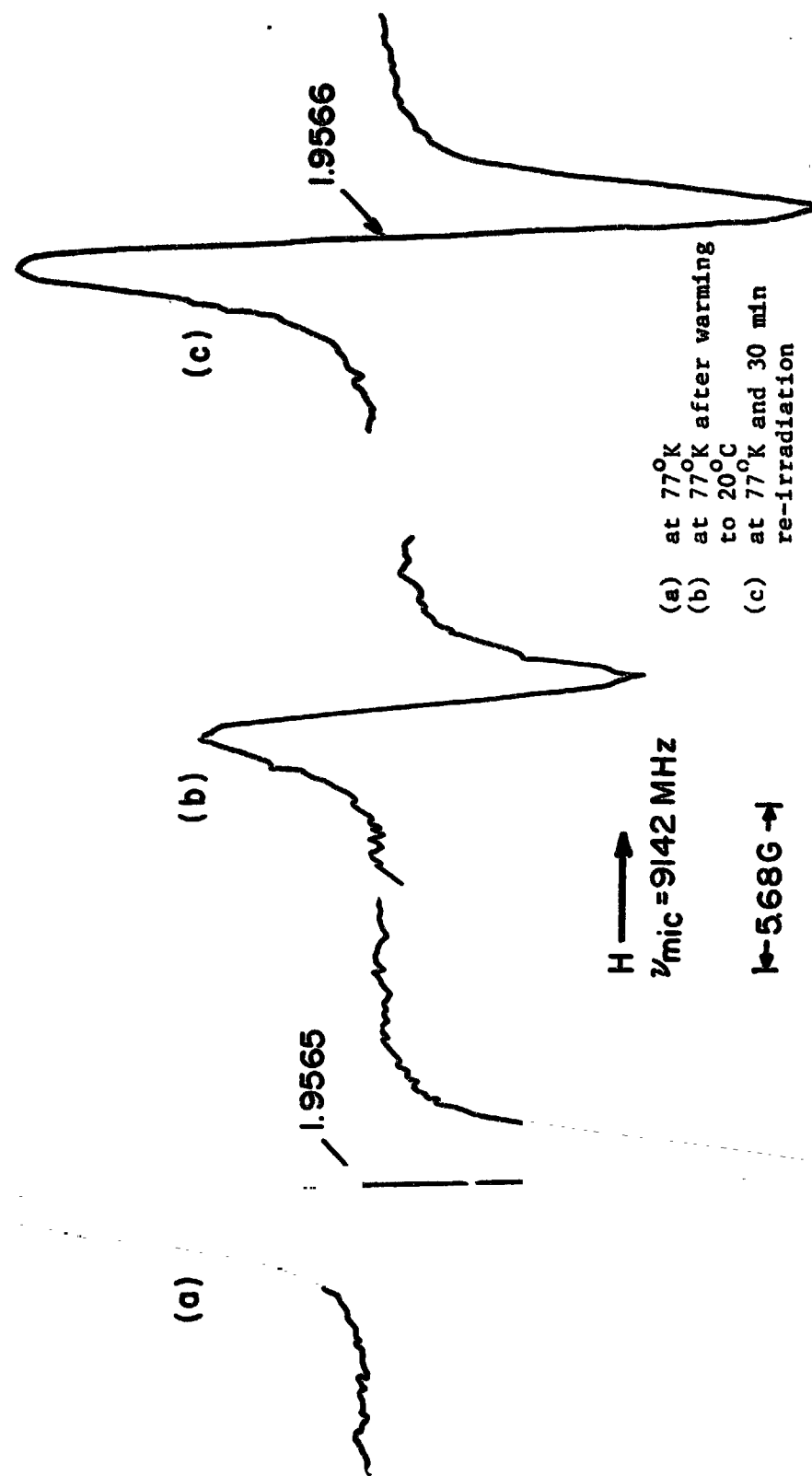


Figure 6.3 EPR OF ZnO AT 77°K
 EFFECT OF WARMING UV-CREATED
 CENTER TO ROOM TEMPERATURE

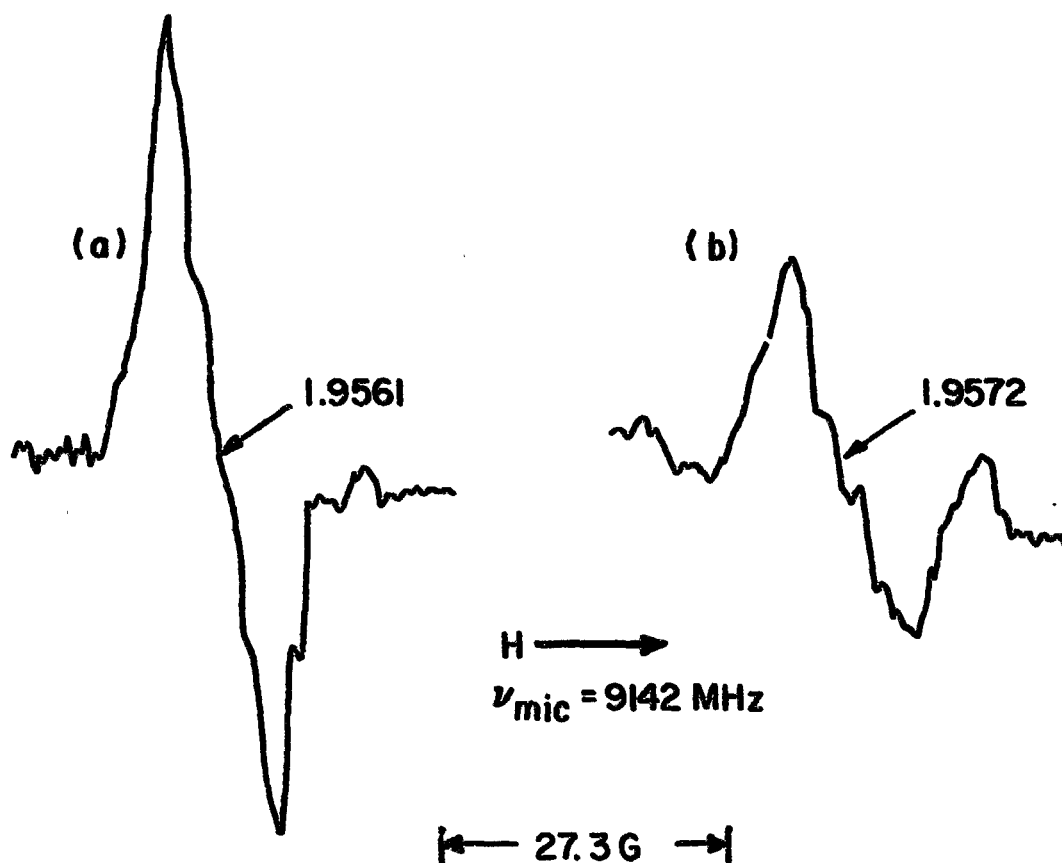


Figure 6.4 EPR SPECTRA OF ZnO AT 77°K EFFECT OF O₂ (ONE TORR) ON ULTRAVIOLET-CREATED CENTER
 (a) Original, before irradiation and O₂ bleaching
 (b) After irradiation and O₂ bleaching

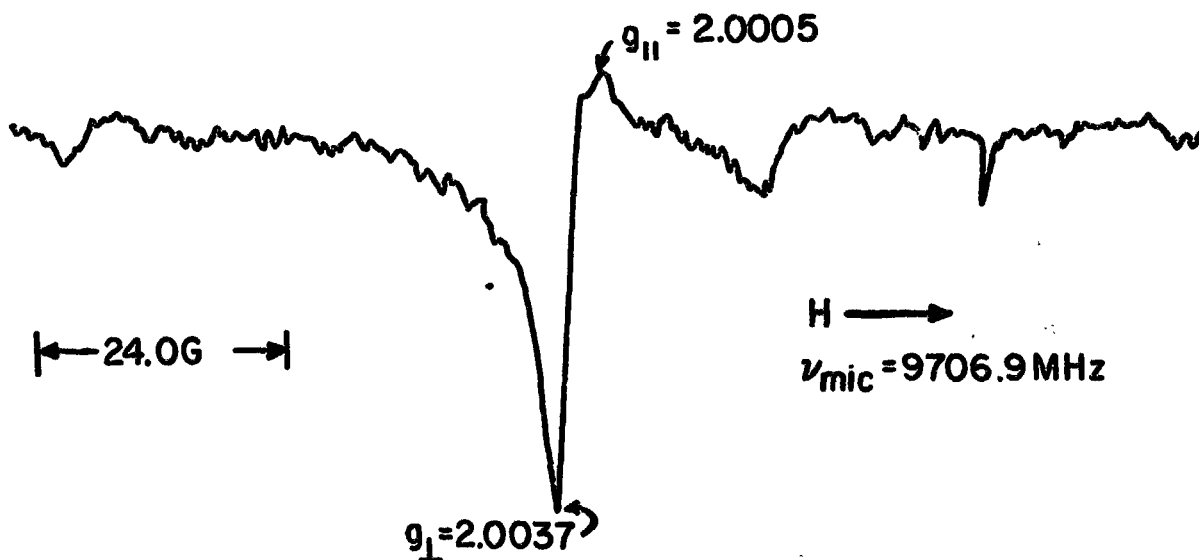


Figure 6.5 EPR AT ~77°K OF F.F. (ANATASE) TiO₂ AT ~10⁻² TORR. MODULATION - 7.4 G

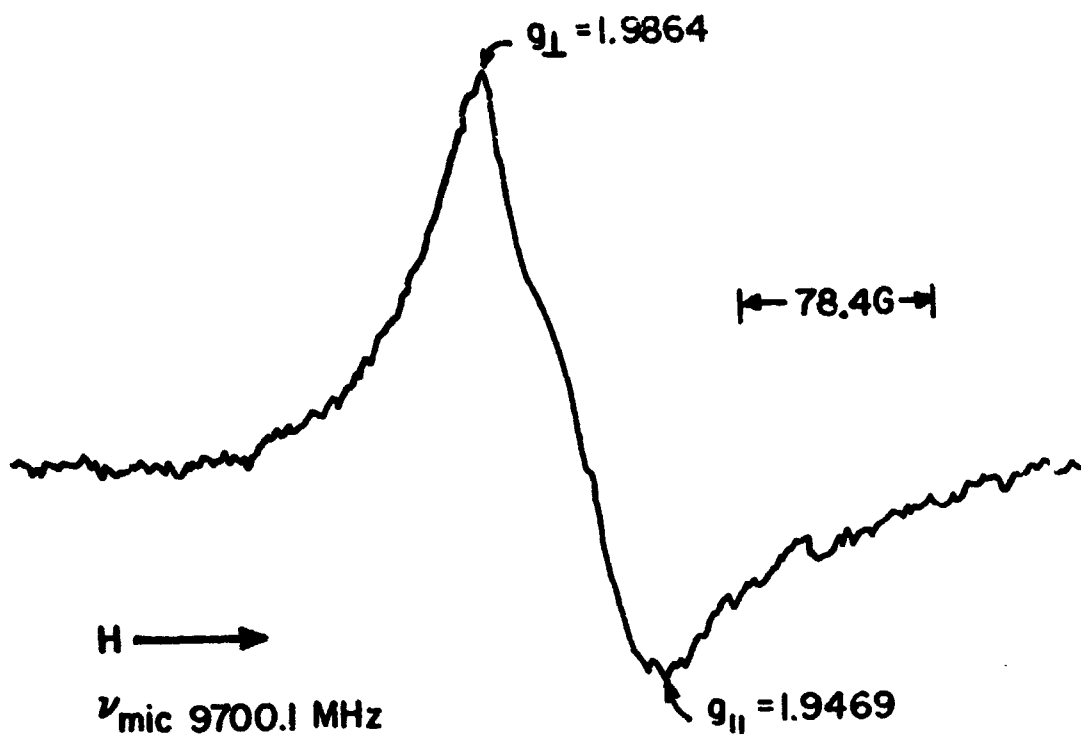


Figure 6.6 EPR AT $\sim 77^{\circ}\text{K}$ OF F.F. (ANATASE) TiO_2 HEATED AT 500°C FOR SIX HOURS AT 10^{-6} TORR. MODULATION - 20.3 G

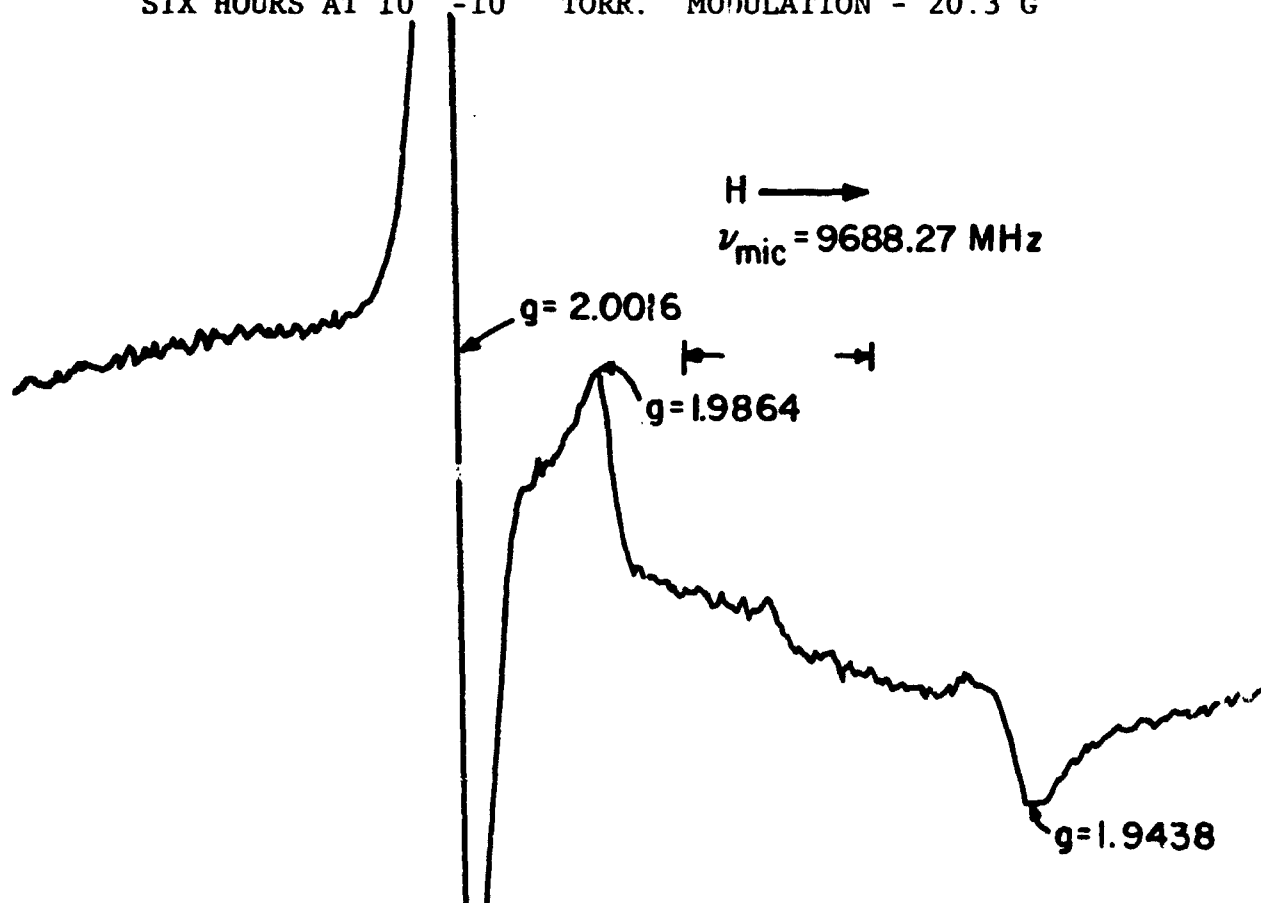


Figure 6.7 EPR AT $\sim 77^{\circ}\text{K}$ OF LW ANATASE HEATED AT 500°C FOR FOUR HOURS AT 10^{-6} TORR. MODULATION - 2.67 G

6.1.2.3 Zinc Orthotitanate (B-229)

A control of sample of Zn_2TiO_4 material (IITRI Batch No. B-229) was heated for four hours at 10^{-6} - 10^{-7} torr. An intense EPR signal with $g_1 = 1.9796$ was observed as well as at a $g_1 = 1.9864$ and the resonance "y", tentatively assigned to conduction electrons in ZnO . The spectra are shown in Figure 6.8. The spin concentration was 2.1×10^{14} in a sample of approximately 0.2g.

The sample B-229 Zn_2TiO_4 with 1% excess ZnO was irradiated in the EPR cavity in a vacuum of 10^{-7} torr at room temperature; the EPR spectrum was observed simultaneously. The spectrum was noisy, but it was apparent that two signals not present in the ground state were created, one at $g = 2.00$ and one at $g = 1.98$. Liquid nitrogen was added to the dewar during irradiation and the signal-to-noise improved (as expected). Warming the sample to room temperature for ~15 minutes and re-cooling resulted in the disappearance of the $g = 1.98$; the spectra are shown in Figure 6.9a. After rewarming the sample to room temperature for ~22 minutes and recooling, both photo-created signals had disappeared as is shown in Figure 6.9b. The large signal in both spectra is the y' center(s) in ZnO .

The sample was evacuated to 10^{-7} torr and EPR spectra was obtained initially (Figure 6.10a), and after one hour room temperature irradiation (Figure 6.10b), 20 hours room temperature irradiation (Figure 6.10c), and after admission of air at 760 torr (Figure 6.10d). A new signal at $g = 4.25$, which seemed to be affected by irradiation was detected but not fully investigated. Only after extensive irradiation was the center "x" detected, and it did not alter even after three days in air. On the other hand the signal "y", attributed to centers in ZnO , did indicate a photo-created, air bleachable component.

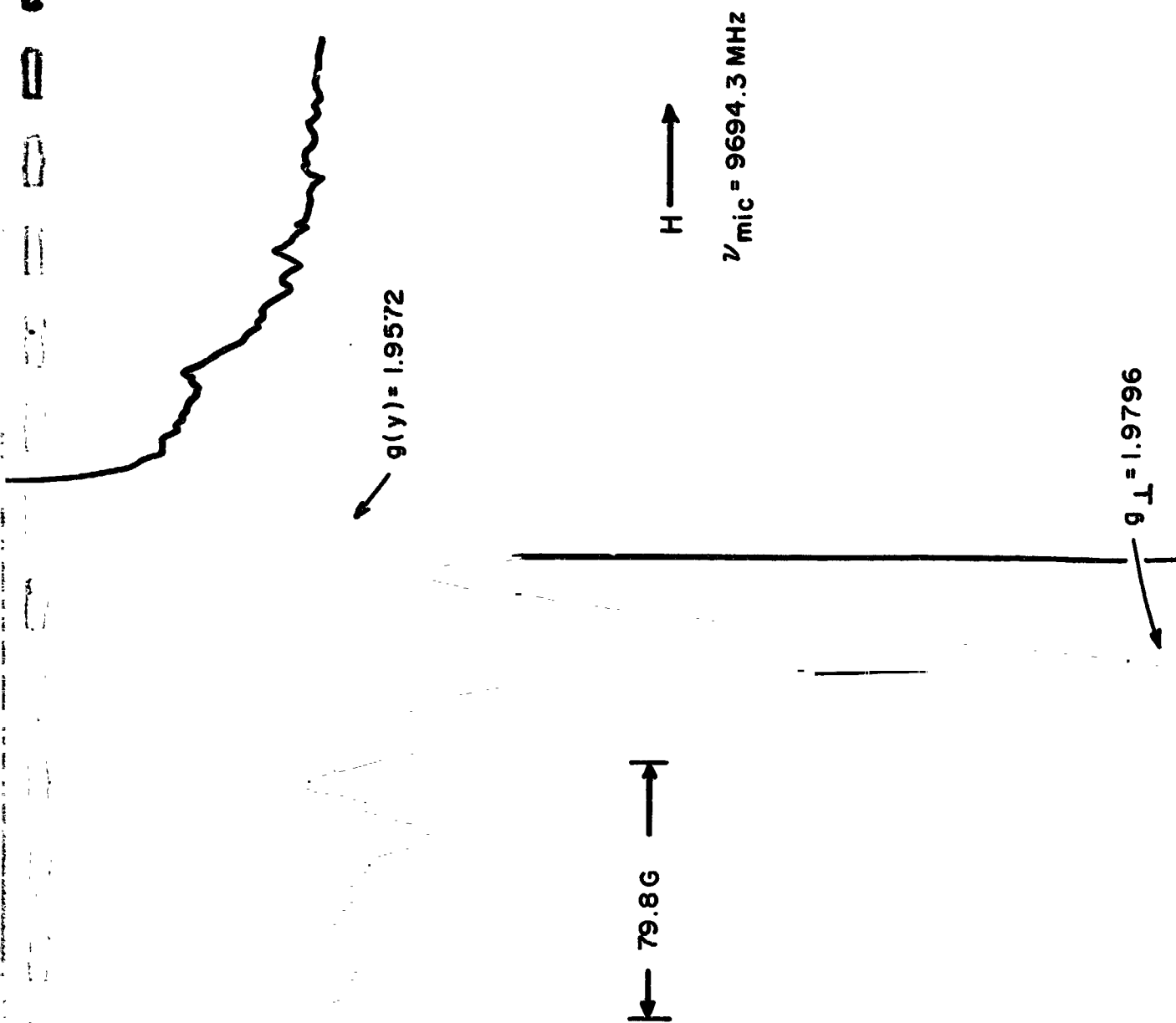


Figure 6.8 EPR AT $\sim 77^\circ\text{K}$ OF SAMPLE B-229, Zn_2TiO PIGMENT, HEATED AT 500°C FOR FOUR HOURS AT 10 TORR MODULATION - 2.67G

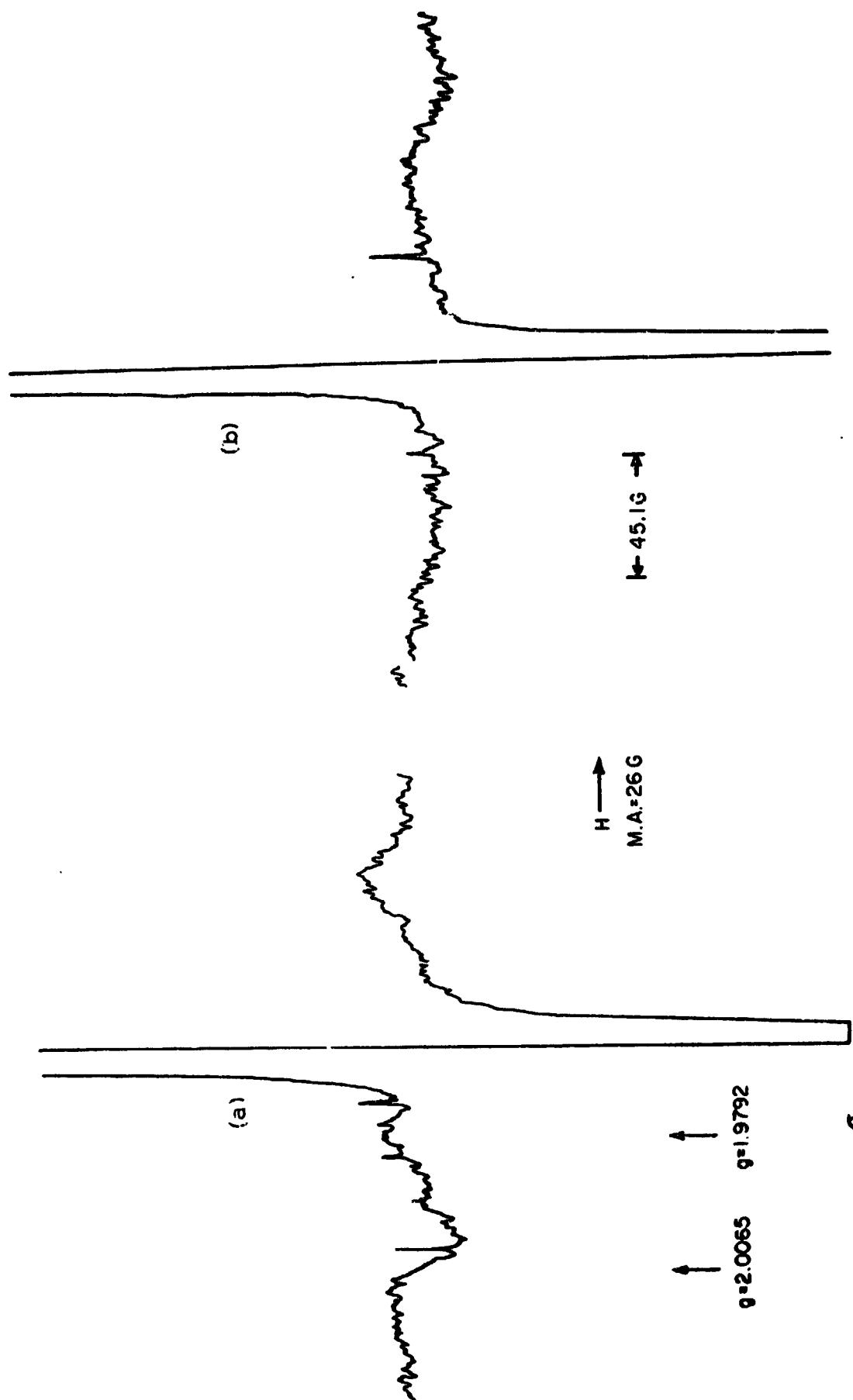


Figure 6.9 EPR SPECTRA OF ZnO EXCESS PRODUCED Zn_2TiO_4 INVESTIGATION OF METASTABLE CENTERS (a) AFTER IRRADIATION (b) AFTER RE-WARMING TO $\sim 20^\circ\text{C}$ AND RE-COLLING TO 77°K .

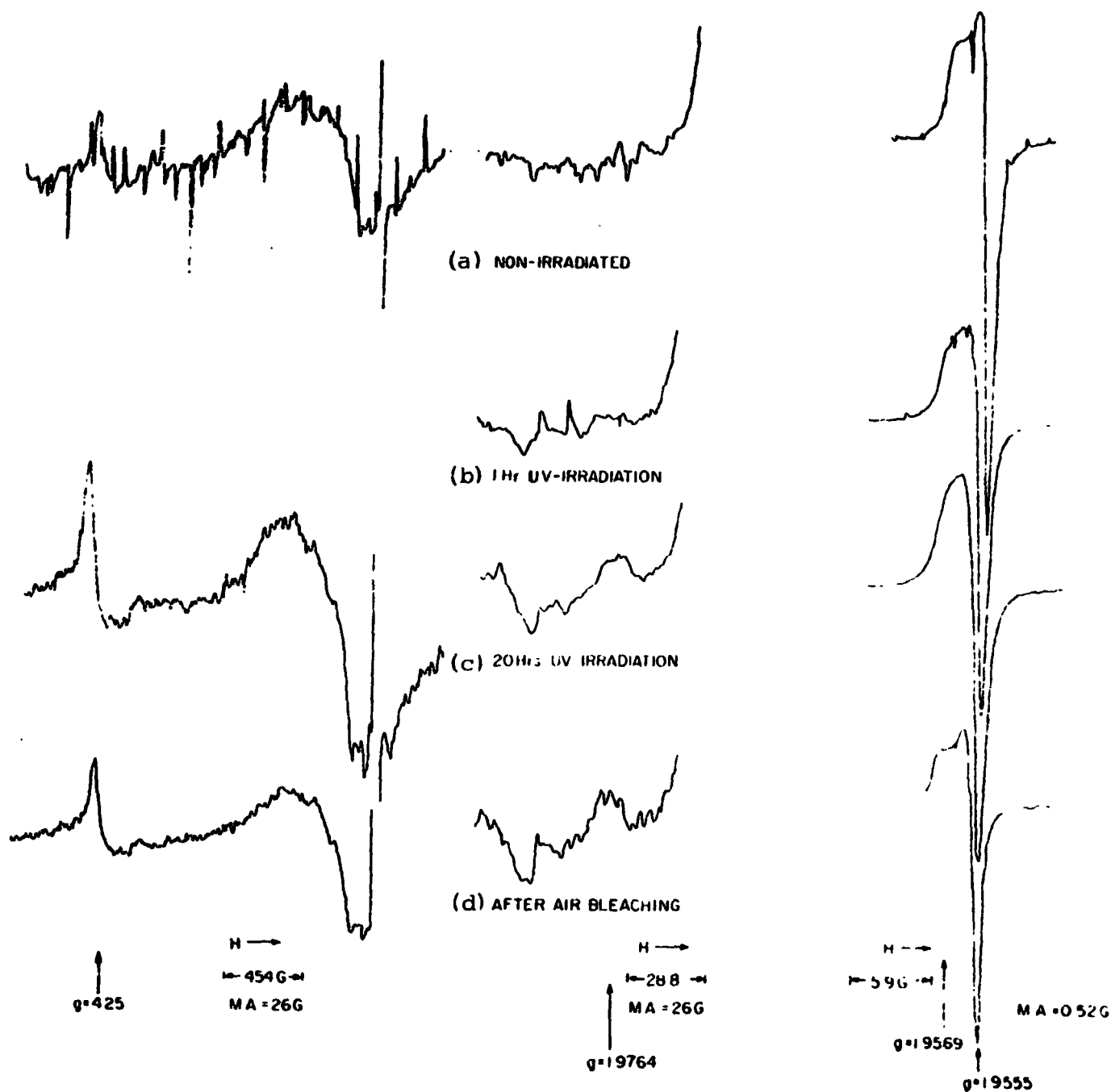


Figure 6.10 EPR SPECTRA OF Zn_2TiO_4 WITH EXCESS ZnO

6.1.2.4 B-454, Zn_2TiO_4 (B-229): Li_2SiF_6

In contrast to the above results, this sample contains no centers attributed to ZnO and after 14 hours of irradiation at room temperature, no new centers are created. Four unidentified centers (shown in Figure 6.11) are observed with mean g values of 2.0840, 2.0664, 2.0018 and 1.9572. An EPR signal at $g = 4.25$ was observed but was weaker than that found in irradiated, untreated zinc orthotitanate.

6.1.2.5 Zn_2TiO_4 with Excess TiO_2

The sample was evacuated to less than 10^{-7} torr and subjected to room temperature irradiation and subsequent air bleaching at one torr for 51 minutes. The spectra are shown in Figure 6.12. Figure 6.12a shows the spectrum of the sample prior to irradiation. In contrast to the results obtained in irradiation Zn_2TiO_4 with an excess of ZnO, 2 hour room temperature irradiation of this material created the signal at $g = 1.98$ (Figure 6.12b) and 19 more hours of irradiation further increased the signal (Figure 6.12c). Additionally, the center was partly bleached (Figure 6.12d) by exposure to air for 51 minutes at a pressure of one torr. Centers attributable to ZnO were not detected in Sample 3, but the center at $g = 4.25$ was intense.

6.2 Discussion of Results

6.2.1 ZnO

Unirradiated SP-500 ZnO exhibits only a weak EPR signal at $g = 1.9561$, which is identified by Geisler and Simmons (Ref. 6.3) as the ultraviolet-sensitive center in non-heat treated ZnO. This signal is increased by ultraviolet irradiation and is oxygen bleachable, thus suggesting that it is associated with the bleachable infrared damage in ZnO. We are reasonably certain that the center itself is not the infrared absorbing species but rather is a localized surface paramagnetic center (trap) that is produced simultaneously with the promotion of electrons to the conduction

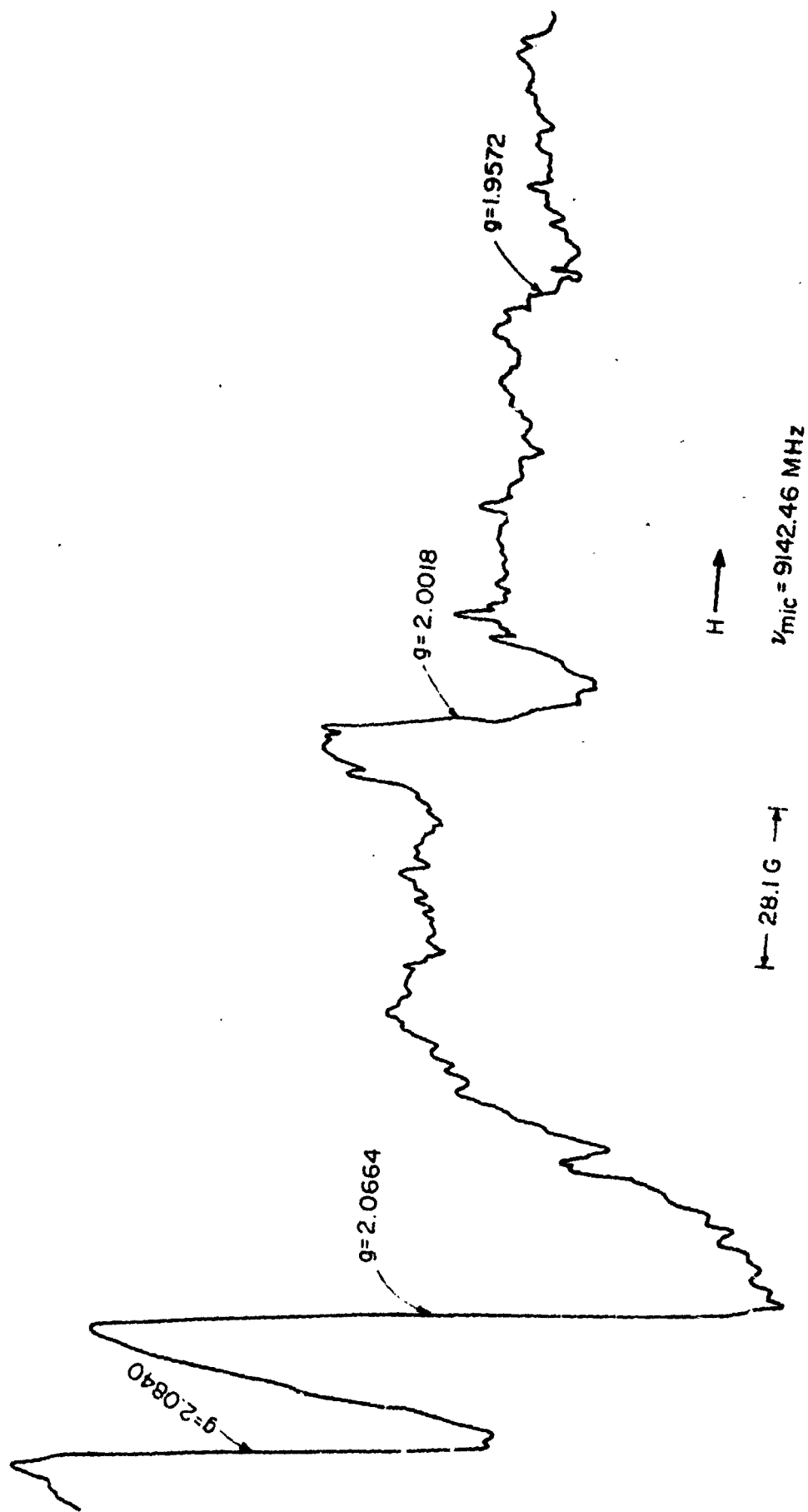


Figure No. 6 11 EPR AT 77°K OF $\text{Zn}_2\text{TiO}_4:\text{Li}_2\text{SiF}_6\text{O}$

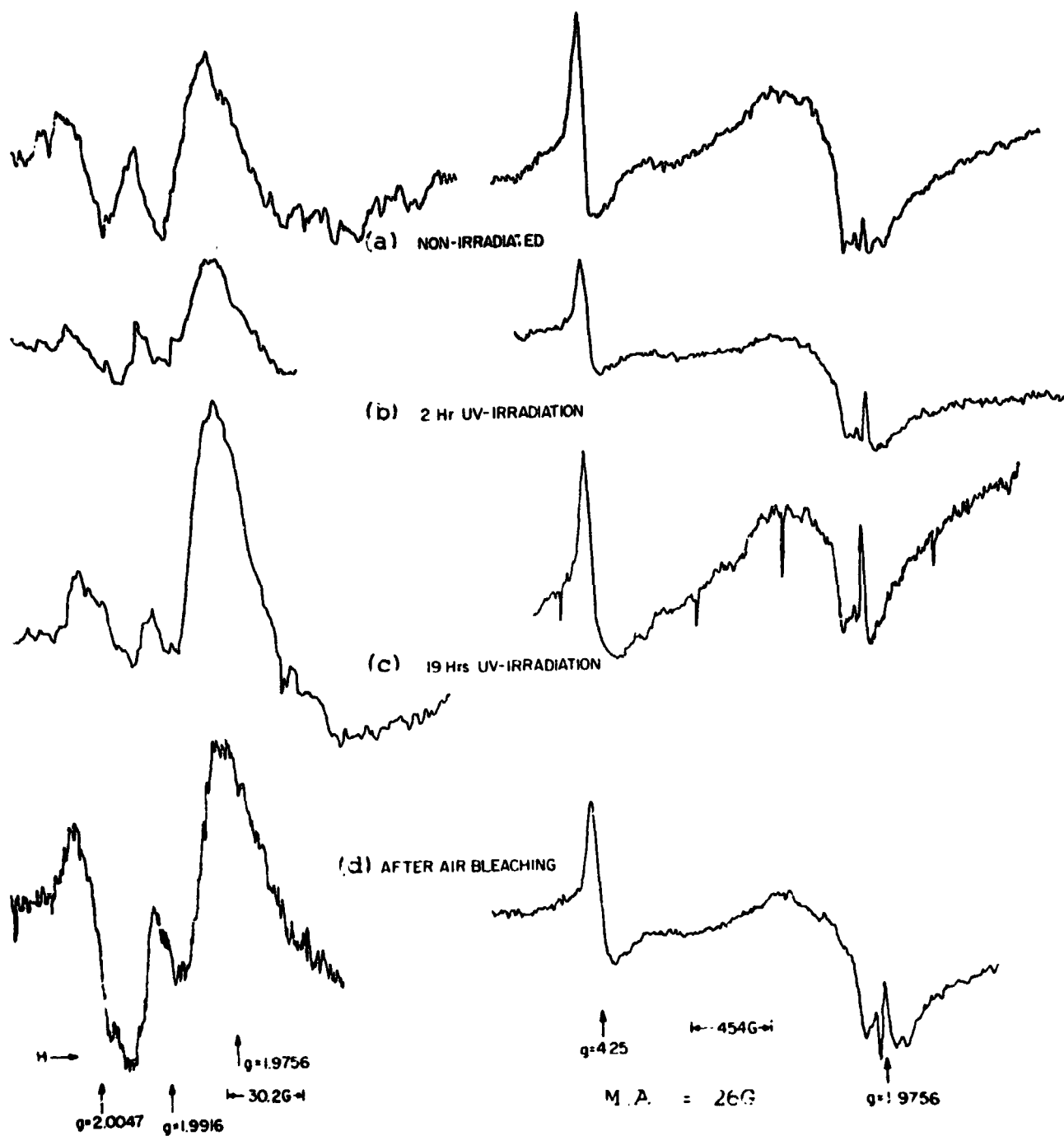


Figure 6.12 EPR SPECTRUM OF Zn_2TiO_4 ISTH EXCESS TiO_2

band. A summary of some of the centers found in ZnO by us and also by other is listed in Table 6-1. Since the sample that we investigated had not been subjected to high temperature heat-treatment, the center with a mean $g = 1.960$ (which we call "y") and the center whose g components are $g_{\perp} = 1.9556$ and $g_{\parallel} = 1.9569$ were not found in ZnO.

Table 6-1

PARAMAGNETIC CENTERS IN ZnO

Center	How Created	Identification of Center
$g = 1.960^*$	(donor-heat created)	Substitutional halogen
$g = 1.9569^*$	Heat created	Electrons in oxygen
$g = 1.9556^*$		Anion vacancies
$g = 1.9561^{**}$	Ultraviolet created	Shallow surface trap

*Found by Kasai (ref. 6.4) (as well as IITRI and others)

**Found by Geisler and Simmons (ref. 6.3).

In previous reports and publications we have postulated that infrared damage in zinc oxide is due to absorption by electrons trapped in the conduction band (Ref.'s 6.5-7). The possibility certainly exists that a trap lying a few hundredths of an eV below the conduction band also contributes, but we have claimed that such a trap, would be filled very rapidly and that nearly all of the induced absorption would result from conduction electrons. The ultraviolet sensitivity of the $g = 1.9561$ center and the fact that it is oxygen bleachable, together with our strong conviction that the EPR of conduction (free) electrons would be extremely difficult to detect at 77°K, make it apparent that this signal is associated with the shallow trap. Thus, the effect of O_2 bleaching is to remove electrons from the conduction band and, consistent with earlier models, to re-oxidize the localized surface trap at $g = 1.9561$, with the ultimate formation of negatively charged oxygen species at the surface.

6.2.2 TiO₂

The EPR spectra of the DuPont FF anatase which was partially converted to rutile seems to be unaffected by ultraviolet irradiation, and the EPR centers found in both irradiated and unirradiated materials resemble those found in the unirradiated precursor anatase (cf Figure 15, Ref. 6.7). These findings, if verified, would rule out any important effect of residual TiO₂ in zinc orthotitanate - at least insofar as Ti⁺³ species (in TiO₂) might contribute to S-band damage. An x-ray diffraction pattern of this sample indicated the presence of both forms. Anatase appeared to be predominant, but the rutile form was present to the extent of 30-40%.

6.2.3 Metastable Species

The term metastable implies that the species is very short-lived, especially at room temperature. Hence it is very important to correlate ultraviolet-induced magnetic resonance changes with the stable optical changes. To achieve the high level of sensitivity required, EPR measurements are normally made at 77°K disappears upon warming the sample, then it is almost certainly not related to any optical damage which persists unaltered through the same temperature change.

Zinc orthotitanate, like ZnO and TiO₂, is a large band gap semiconductor; very likely its band structure resembles that of TiO₂ more than that of ZnO. The upward curvature of the valence and conduction bands near the surface would lead us to suspect that any given type of defect would have different properties depending upon its distance from the surface compared to the band curvature. Oxygen bleaching experiments (Ref. 6.6) have in fact conclusively shown that in both TiO₂ and Zn₂TiO₄ the visible-near infrared damage is only partly bleachable, yet the EPR spectra suggest that the same species, in this case Ti⁺³, are responsible for both the bleachable and unbleachable optical absorption, surface and bulk Ti⁺³, respectively.

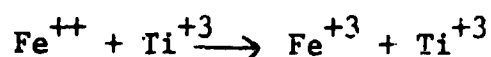
It has now been demonstrated that a form of Ti^{+3} which is metastable can be produced by irradiation at 77°K; and that a different Ti^{+3} species is produced only after extensive irradiation at room temperature. This confirmation of metastable species clarifies some of the EPR results previously reported (Ref. 6.2); long-time room temperature irradiation-produced Ti^{+3} is the species which must be correlated with reflectance damage. In essence we have distinguished centers which are not optically significant from those which may be. In previous 77°K irradiation studies (Ref. 6.2) we found no essential EPR difference between Zn_2TiO_4 powder and Owens-Illinois paint made from it, yet a great deal of difference in the reflectance spectra was noted.

6.2.4 ZnO in Untreated Zn_2TiO_4 (B-229)

The ZnO remaining in Zn_2TiO_4 (B-229) after high-temperature (925°C) reaction exhibits not only the ultraviolet-sensitive center, but also the heat-created center reported by Kasai (Ref. 6.4). These two centers comprise what we have called y' (Ref.'s 6.2 and 6.8). The ultraviolet sensitivity and effect of air-bleaching is observed in the low-field side of the signal in the right hand part of Figure 6.10. We believe that the permanent non-bleachable damage at 363 nm may be associated with the high field component of y' . Note that the center we called y found in high temperature (2400°C) plasma-annealed material at $g = 1.960$, is not found in our non-plasma-annealed materials.

6.2.5 Zn_2TiO_4 (B-229)

The signal at $g = 4.25$ is most likely due to Fe^{+3} (Ref. 6.9). The observation that irradiation of the material increases the intensity of this signal suggests that the Fe^{++} form of iron may be contributing electrons which cause permanent Ti^{+3} damage according to



The presence of iron in orthotitanate may produce another complicating feature in that Fe^{++} is known to absorb at 875 nm (Ref. 6.10).

6.2.6 Li₂SiF₆ Treated Zn₂TiO₄ (B-454)

The Li₂SiF₆-treated B-229 exhibits a less intense signal at $g = 4.25$ (less Fe⁺³) than its (untreated) precursor (B-229) and also exhibits no ZnO-type centers. This supports our earlier thesis (Ref. 6.5) that the surface treatment provides either an electron scavenging effect or prevents primary ionization processes from occurring by providing an electron-rich surface. Stable Ti⁺³ was not found in these materials and the optical reflectance showed no S-band damage.

6.2.7 Zn₂TiO₄ with Excess TiO₂

Here, the creation of partially-bleachable Ti⁺³ is apparent and is corroborating evidence for a Ti⁺³ species being responsible for S-band damage.

6.2.8 Zinc Orthotitanate in OI-650 "Glass Resin"

Extended irradiations of B-229 zinc orthotitanate in Owens-Illinois 650 vehicle have resulted in the observations listed in Table 6.1, where we provide a comparison of the results obtained on the pigment alone (Ref. 6.8) vs those obtained on an Owens-Illinois paint made from this pigment.

The basic findings in this test are that: Ti⁺³ is produced in much greater concentration in the paint; the Ti⁺³ is mostly (but not entirely) oxygen- or air-bleachable; the Fe⁺³ form of iron, a natural impurity in the pigment, follows a different concentration history when the pigment is irradiated as a paint than when irradiated as a pigment alone; and the signal y' responds differently to irradiation in the pigment alone versus that in the paint.

The correlation of the EPR centers with optical damage is by no means complete, but differences in the optical spectra of the pigment and paint are explicable in terms of the centers observed.

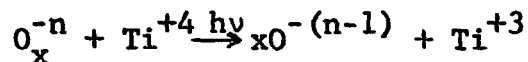
Table 1

COMPARISON OF EPR CENTERS IN ZINC ORTHOTITANATE: PIGMENT VS OWENS-ILLINOIS PAINT

Treatment	Center	Pigment (B-229)	Owens-Illinois Paint (B-415)
Unirradiated	y'	$g_1 = 1.9555$ $g_{ } = 1.9569$	Slightly less signal asymmetry than in pigment with $g = 1.9555$.
1 hr UV-irradiation	x	None observed	None observed
	Fe ⁺⁺⁺	Moderate amount	None observed
	y'	Additional UV-created component	Smaller, more symmetrical signal ($g = 1.95565$)
4 hrs irradiation	x	None observed	Moderate amount
	Fe ⁺⁺⁺	Not examined	Moderate amount
	y'	Not examined	Still smaller signal
	x Fe ⁺⁺⁺	Not examined	Large amount
20 hrs irradiation	Fe ⁺⁺⁺	Not examined	Large amount
	y'	As with 1 hr irradiation	Not much change
	x Fe ⁺⁺⁺	Moderate amount	Very large amount
O ₂ bleaching 850 μ	Fe ⁺⁺⁺	Large amount	Small amount
	y'	Not examined	Increase in intensity, slightly greater than after 4 hrs irradiation.
	x	Not examined	Decrease in intensity, slightly greater than after 4 hrs irradiation
	y'	UV-created component bleached, return to unirradiated spectra	Return of signal asymmetry, $g_1 = 1.9553$, $g_{ } = 1.9567$
	x Fe ⁺⁺⁺	No bleaching; moderate amount remains	Further bleaching (decrease) to moderate amount.
	Fe ⁺⁺⁺	No change; large amount remains.	Increase to moderate - large amount

6.3 PRELIMINARY MODEL FOR DAMAGE IN Zn_2TiO_4

A model of the S-band damage in Zn_2TiO_4 is not a simple one because part of the optical damage is oxygen stable and part (the long wavelength side) is oxygen-bleachable. A model suggested earlier was based on the equation:



where O_x^{-n} stands e.g., for O_2^- , O^- , O^{-2} .

As we stated earlier, Ti^{+3} defects on or near the surface of a particle will behave differently than those closer to its interior. Thus a different donor-acceptor scheme will be important for each. The table below lists a few of the more likely donors and acceptors active in the zinc orthotitanate photolysis scheme.

Table 6-2
LIKELY DONORS AND ACCEPTORS IN Zn_2TiO_4 PHOTOLYSIS

Donors	Acceptors
$\text{Cl}^- = \text{Cl}^\cdot + e^-$	$\text{Ti}^{+4} + e^- = \text{Ti}^{+3}$
$\text{O}_x^{-n} = x\text{O}^{-(n-1)} + e^-$	$\text{O}_2 + e^- = \text{O}_2^-$
$\text{Fe}^{++} = \text{Fe}^{+++} + e^-$	$\text{Fe}^{+++} + e^- = \text{Fe}^{++}$

However complex the solid-state and surface chemistry of this material is, it is obvious that gaseous oxygen plays an important role as a "shuttle" for electrons - and this role can be drastically affected by surface treatment or plasma-treatment alteration, causing a suppression or enhancement of primary ionization processes.

6.4 CONCLUSIONS

From the basic findings noted above we can definitely ascribe the instability of certain zinc orthotitanate pigments to an interaction with the silicone binder. EPR confirms what is observed in the reflectance spectra: the silicone binder obviously predisposes some zinc orthotitanate pigments to S-band damage.

The fact that two distinctly different Ti^{+3} signals are detected is consistent with the above observation because large band-gap semiconductors display strong surface effects. Environmentally created Ti^{+3} may have different electronic environments, wherein it may have different EPR spectra, depending upon where it resides - in the bulk or in the depletion zone (the band-bending region).

From the reflectance spectra we have clearly established the fact that the instability resides with the zinc orthotitanate pigment rather than with the OI-650 vehicle. This interaction has caused catastrophic damage in certain pigments which may not have been completely stabilized by surface treatments. Thus, the preparative stoichiometry is very important, for two reasons - to regulate the ZnO excess and to control the surface defect density which may be predisposed to the photocreation of Ti^{+3} .

The discovery of a spin density of $2.1 \times 10^{14}/0.2$ gm is a significant finding as it raises a strong inference that the Ti^{+3} in Zn_2TiO_4 (B-229) is not mainly Ti^{+3} in residual TiO_2 , but rather is intrinsic. It can not be unequivocally stated, however, that residual TiO_2 remaining in the Zn_2TiO_4 is not much more susceptible to Ti^{+3} formation in Zn_2TiO_4 ; but the propensity for that formation would have to be increased 100-500 times to account for the spin concentration observed.

The different values found for g in the two materials, viz, 1.9864 and 1.9796, also lend support to the thesis that the center arises from two different crystalline environments (possibly a sesqui-titanate). Thus, the problems of stabilizing Zn_2TiO_4 relate to Zn_2TiO_4 intrinsically, rather than to TiO_2 or ZnO impurities.

One of the major objectives of the EPR investigations was to establish a correlation between EPR spectra and optical degradation. Irradiations and EPR measurements carried out in-situ were followed by EPR measurements in an oxygen (adsorbate) environment. Since neither the intensities of EPR spectra nor their disappearance rates in O_2 could be correlated with induced spectral optical degradation or with bleaching rates of the S-band in O_2 , we must conclude that EPR activity and UV induced defect concentrations in Zn_2TiO_4 are not correlatable. This, of course, is not unexpected since EPR transitions are many orders of magnitude less energetic than the optical transitions to which they might relate.

6.5 REFERENCES

1. G.A. Zerlaut, with J.E. Gilligan and N.A. Ashford, "Development of Space Stable Thermal Control Coatings for Use on Large Space Vehicles", IITRI Report No. U6002-97 (Final Report).
2. J.E. Gilligan, "Development of Space Stable Thermal Control Coatings for Use on Large Space Vehicles," IITRI Report No. C6233-4 (Triannual Report) May 15, 1971.
3. C.H. Geisler, and G.L. Simmons, Phys. Ltrs. 11, p. 111 (1964).
4. P.M., Kasai, Phys., Rev. 130, 989 (1963).
5. G.A. Zerlaut, J.E. Gilligan and N.A. Ashford, "Space Radiation Environmental Effects in Reactively Encapsulated Zinc Orthotitanates and Their Paints," AIAA Paper No. 71-449, Presented to the AIAA 5th Thermophysics Conference, Tullahoma, Tennessee, April 26-28, 1971.
6. J.E. Gilligan, "Study of In-Situ Degradation of Thermal Control Surfaces," Report No. IITRI U6061-29 (Final Summary Report), February 20, 1970.
7. J.E. Gilligan, "The Induced Optical Properties of Zinc Oxide," AIAA Paper No. 67-214, presented to AIAA 5th Aerospace Sciences Meeting, New York, New York, January 1967.

References (Cont'd)

8. N.A. Ashford, and G.A. Zerlaut, "Development of Space-Stable Thermal Control Coatings", Report No. IITRI U6002-83 (Triannual Report), Nov. 30, 1970.
9. C. Hirayama, J.G. Castle Jr., and M. Kuriyama, Phys. and Chem. of Glasses, 9, 109 (1968).
10. G. Lehmann, and H. Harder, The American Mineralogist 55, 98 (1970).

7.0 GENERAL COATINGS INVESTIGATIONS

7.1 INTRODUCTORY REMARKS

Three investigations which fall in the category of general coatings investigations were undertaken. The first was the development of a highly stable paint system based on S-13G pigment and the IITRI-modified Owens-Illinois 650 "Glass Resin". A second study attempted to identify satisfactory, commercially available strippable protective coatings to be used on sensitive spacecraft thermal control surfaces during pre-launch storage. In a third study, we investigated the effects of a simulated salt/spray environment on S-13G thermal control paints.

7.2 FORMULATION AND EVALUATION OF A-429M

A-429 is an Owens-Illinois 650 resin pigmented with potassium silicate treated zinc oxide (S-13G pigment). The successful end-blocking of Owens-Illinois 650 resin (described in a proceeding section) permitted the reformulation (see table 7.1) of this paint using the modified resin, designated OI-650G. The paint was, therefore, re-designated A-429M. Although this coating does not exhibit "coasting," it does require baking to optimize its cure. It is adherent, resistant to wide temperature variations (including LN₂ thermal shock), possesses exceptional optical stability (equal to A-429), and has adequate shelf-life.

Table 7-1

FORMULATION OF A-429M THERMAL-CONTROL PAINT

<u>Ingredients</u>	<u>Composition (pbw*)</u>
Silicated ZnO	36
Owens-Illinois 650G	18
Solvent T-26	36
<hr/>	
T-26	
Toluene	75 w/o
n-Butyl Acetate	15 w/o
n-Butyl Alcohol	10 w/o

*parts by weight

7.2.1 Evaluation

Specimens of Batch C-406 of A-429M were prepared using the three different curing schedules shown in Table 7.2, where the physical properties of the resultant coatings are also noted.

Table 7-2
A-429M COATINGS - EFFECTS OF CURE SCHEDULE

<u>Coating No. and Cure</u>	<u>Physical Properties</u>
(A) 24 hr room temperature	Printable, glossy coating
(B) 16 hr at 250°F	Moderately-hard, semi-glossy enamel
(C) 16 hr at 250°F plus 2 hr at 350°F	Hard, dead-flat enamel

IRIF Coupons of the baked coatings were irradiated in both IRIF-I (1500 ESH at 150°F for both (B) and (C) and in the CREF (IRIF-II) (3000 ESH at 50°F for (B)).

7.2.2 Irradiation Tests

7.2.2.1 Sample Description

Test I-57 involved three A-429M samples of an early experimental formulation. The test temperature was maintained in the range 150-155°F. Two of the three samples were cured at 250°F/15 hr; the third, at 350°F/4 hr. The samples were irradiated at an intensity of five (5) equivalent suns. Spectral reflectance measurements were made before irradiation (in air and in vacuum), after 100, 500, 1000, 1500 and 2000 ESH at a pressure of less than 5×10^{-7} Torr, and finally in air.

In CREF Test No. 9, the A-429M sample was irradiated at room temperature at four (4) suns. Spectral reflectance measurements were made initially and after exposures of 575, 2000 and 3000 ESH. In this test the sample is from a more recent formulation of A-429M.

7.2.2.2 Test Results

The spectral reflectance curves for one of two 250°F/15 hr A-429M samples are shown in Figure 7.1; the spectra for the 350°F-4 hr sample are similar, but indicative of even greater stability. The CREF curves are shown in Figure 7.2.

The extraordinary performance of this paint system is markedly evident, especially in I-57 where an unusually severe temperature environment is maintained. Furthermore, despite the fact that these coatings have not been optimized, their reflectance values are quite good. These two statements can be summarized quantitatively by noting that the solar absorptance in I-57 increased by only 0.018 that is, from 0.204 to 0.222 in 2000 ESH.

In the CREF test, an A-429M sample demonstrates very similar stability. In more than 3000 ESH, the solar absorptance has increased by only 0.014. The spectra suggest that the damage has saturated and that the solar reflectance has thus stabilized.

7.2.3 Conclusions

A-429M is undoubtedly the most stable paint system ever developed by IITRI and available in quantity. Its stability considerably exceeds that of S-13G and is superior even to that of Z-93. Its optical and engineering properties have yet to be optimized, but its performance patently qualifies it as ultra-stable paint system. The high outgassing characteristics of the resin, however, may limit its use to applications in which contamination is not a major concern.

7.3 STRIPPABLE PRE-LAUNCH PROTECTION COATINGS EVALUATIONS

7.3.1 Introductory Remarks

Thermal control surfaces for spacecraft are only as reliable as the protective means taken to assure and maintain their cleanliness while in storage, because all surfaces and surface coatings, even the most stable, are susceptible to contamination. Following

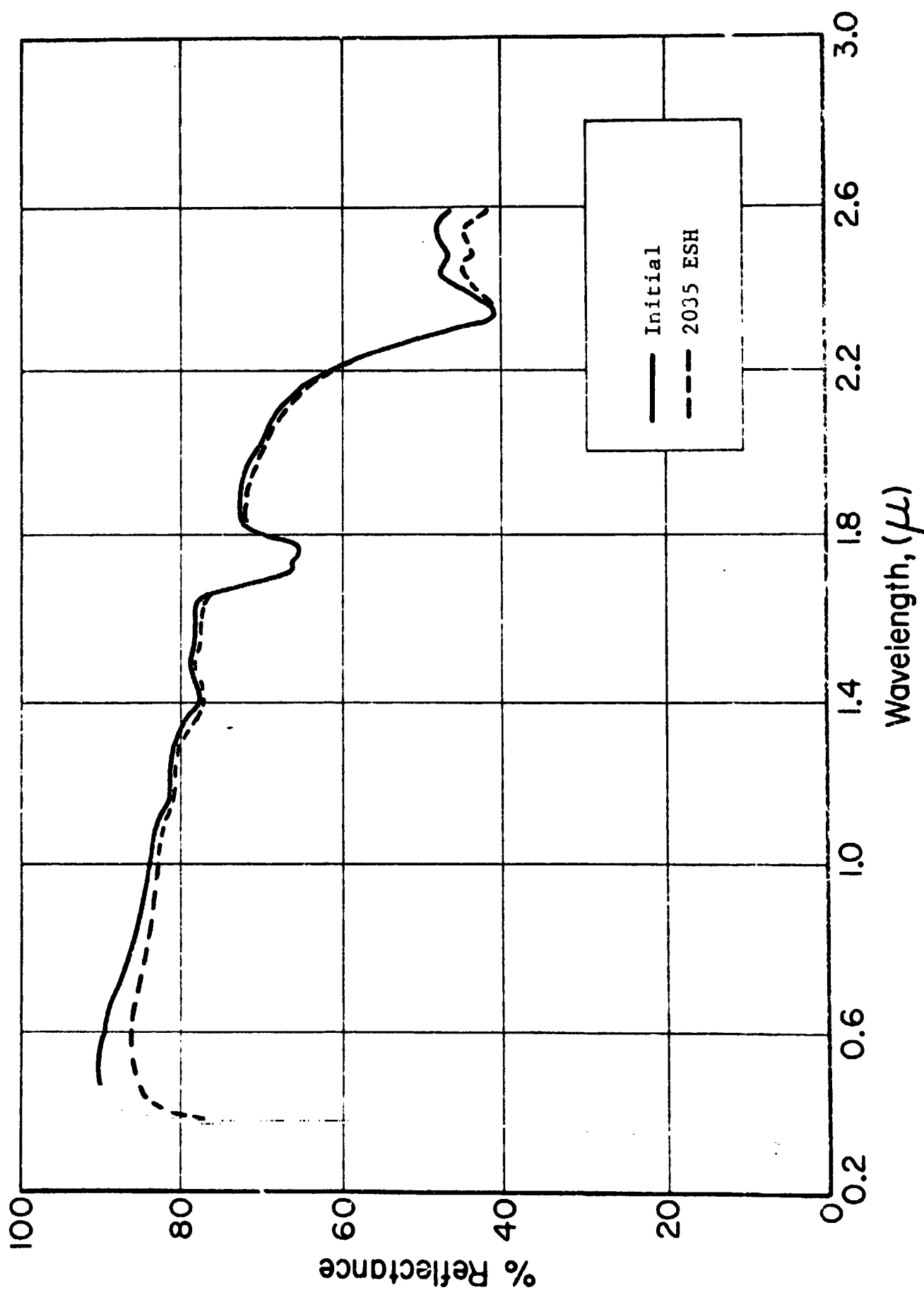


Figure No. 7.1 SPECTRAL REFLECTANCE OF ITRI'S A-429M: ZnO:SiO₃/CI-650G

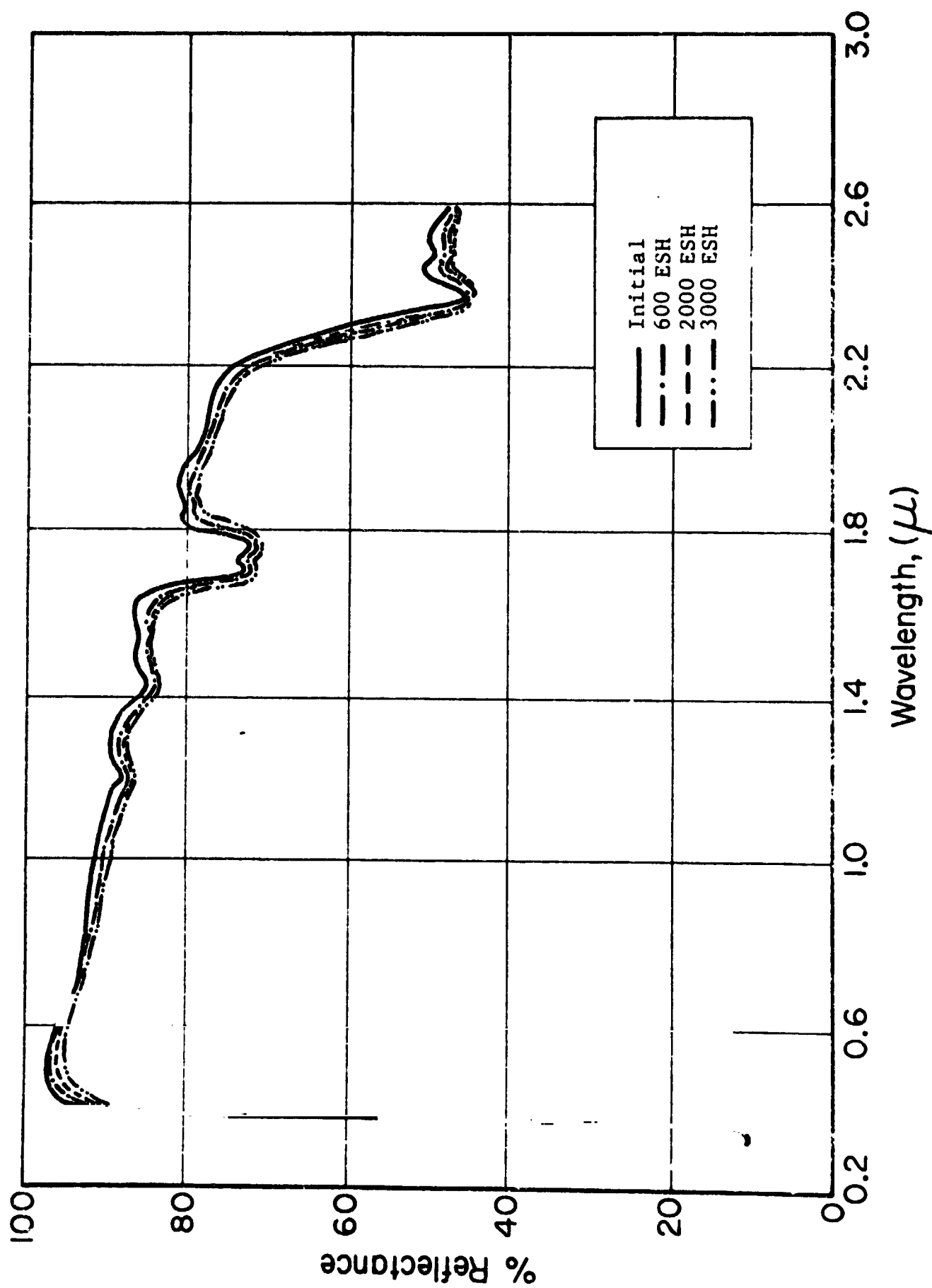


Figure No. 7.2 SPECTRAL REFLECTANCE OF IITRI's A-429M: ZnO:SiO₃/OI-650G

the application of paint, spacecraft surfaces will be exposed to numerous environments, human handling and storage to name but two. The types of contamination are legion; the effects, however, are of two general kinds. The first is due to the increased initial optical absorption and subsequent degradation and increase in α_s . The second effect is the potential accelerated ultraviolet radiation damage in the paint. The effect of ultraviolet radiation on an oil-contaminated white paint, for example, is to accelerate the normal degradation rate of solar absorptance. We are certain that the reported poor - and often-times erratic - performance in space of many white coatings has been the direct result of contamination. Accordingly, the timely application of a protective coating to all exposed, critical thermal control surfaces, to be removed immediately prior to launch, should be made standard procedure. From the time that a coating is applied until the time of launch, the opportunities for contamination are virtually limitless.

Contamination and its effects have been receiving a great deal of attention. Large vehicle sizes and the increasing degree of sophistication in flight experiments and scientific instrumentation place strong demands upon the cleanliness of spacecraft and spacecraft components. A wide array of environments will be experienced by the spacecraft on its way from the various manufacturers and assemblers of its components, to the launch site, and eventually into its space mission.

7.3.2 Objectives

The intent of this effort was to develop protective coatings for thermal control surfaces. We have chosen four representative surfaces: S-13G, Z-93, polished aluminum and suprasil quartz. While largely arbitrary, these choices cover a large spectrum of actually used materials - from the silicones to the inorganic paint systems and from the metals to the dielectric surfaces. The ideal protective coating would be an universal one; it would

be water-based, impermeable, adherent to all surfaces, easily stripped even after long periods of outdoor exposure, readily identifiable as a protective coating, and, of course, would leave no contamination.

7.3.3 Coatings Evaluations

A total of twelve (12) strippable coatings formulations were obtained from commercial sources. These coatings represent both water and hydrocarbon solvent types. The strippable coatings evaluated are listed in Table 7.3

7.3.3.1 Strippability Investigations

Fifteen (15) aluminum panels (3" x 6") were given 0.1-0.3 mil (dry film thickness) application of G.E. SS-4044 primer, followed by 8-10 mils (dry) S-13G. The panels air dried for ten days after which they were sprayed with the strippable coatings. Spraying viscosity, thickness of film, etc., were in accordance with the manufacturer's suggestions. Around one end of each panel, between the protected (S-13G) and the protective films, a layer of 1" masking tape was wrapped. Likewise, 15 aluminum panels were "break free" cleaned and coated with 4-5 mils (dry) Z-93. They also air dried for ten days before being covered with the strippable coatings.

The strippable coatings were then applied to each set. After ten (10) days, each coating was removed by pulling the tape. Notations were made as to the ease of removal and the degree of contamination left on the "protected" thermal control coatings. Comparisons were made with panels of Z-93 and S-13G sprayed with the original sets. The results appear in Table 7.4.

Since weatherometer exposure might radically change the adhesion of the strippable coatings, it was decided to submit five of the most promising of these to this test. Formulas 2, 8 and 9 were tested over Z-93. Formulas 1, 2, 8, 9 and 12 were tested over S-13G, polished aluminum, and suprasil quartz. The panels

Table 7-3

LIST OF STRIPPABLE COATINGS

Company	Name	Thinner
1. Potter Paint	Peel-Astic, ZM-11	Ketones & Hydrocarbons
2. Glidden	Booth Coating, No. 150W900	Ketones & Hydrocarbons
3. DuPont	No. 200-82565	Ketones & Hydrocarbons
4. B.F. Goodrich	Geon 460 x 1 } Hycar 1572 x 45 } 1:1 by wt.	Water
5. B.F. Goodrich	Geon 460 x 1 } Hycar 1572 x 45 } 60% by wt. 40% by wt.	Water
6. B.F. Goodrich	Geon 460 x 1 } Hycar 1572 x 45 } 40% by wt. 60% by wt.	Water
7. B.F. Goodrich	Hycar 2679 } Hycar 2600 x 138 } 1:1 by wt.	Water
8. B.F. Goodrich	Hycar 2679 } Hycar 2600 x 138 } 60% by wt. 40% by wt.	Water
9. B.F. Goodrich	Hycar 2679 } Hycar 2600 x 138 } 40% by wt. 60% by wt.	Water
10. Union Carbide	Latex 799-112	Water
11. Union Carbide	MP-2441	Ketones & Hydrocarbons
12. De Soto	843L001-910L731	Ketones & Hydrocarbons

Table 7-4
EVALUATION OF STRIPPABLE COATINGS/FILMS

Coatings	Over S-13G		Over 293	
	Ease of Removal	Contamination*	Ease of Removal	Contamination*
1. Potter Paint Peel-Astic	Comes off easily; but still has enought adhesion.	None	Too much adhesion. Would tear before it would come loose. Would have to be scraped off.	---
2. Glidden Booth Crating	Comes loose too easily. Slightest jar causes film to start curling.	None	Excellent. Adhesion enough not to come loose but pulled off easily.	None
3. Du Pont No. 200-82565	Comes off easily; but still has adhesion.	None	Too much adhesion. Would have to be scraped off.	---
4. B.F. Goodrich Geon 460 x 1 1:1 Hycar 1572	Comes off easily but still has some adhesion.	None	On fairly tight but would pull off without tearing. Has a light yellow caste.	Very slight yellowing
5. B.F. Goodrich	Film comes off easily; but leaves small areas that stick.	very small areas of coating	Sticks too close in spots.	Considerable yellowing
6. B.F. Goodrich Geon 460 x 1 - 40% Hycar 1572 - 60%	Comes off easily and still has some adhesion.	None	Would not come off without tearing. Too much adhesion.	Considerable yellowing
7. B.F. Goodrich Hycar 2679 1:1 Hycar 2600	Same as number six.	None	sticks a little too well, particularly at panel edges.	None
8. B.F. Goodrich Hycar 2679 - 60% Hycar 2600 - 40%	Same as number six.	None	Sticks at edges but can be pulled away from middle without breaking.	None
9. B.F. Goodrich Hycar 2679 - 40% Hycar 2600 - 60%	Same as number six.	None	Same as number eight.	None
10. Union Carbide Latex 799-112	Same as number six.	None	Breaks before it will pull off. Too much adhesion	--
11. Union Carbide MP-2441	Very little adhesion: (black pigment).	None, in spite of Black pigment	Sticks on much too tightly; would before it would come loose.	Considerable (black pigment)
12. De Soto 8431001-910L731	Slight adhesion yellow pigmentation does not appear to contaminate S-13G.	None, in spite of yellow pigment	Adhesion much too great. Film would not come loose at all.	--

*Contamination remaining on surface, as determined by visual inspection.

were placed in the Atlas Weatherometer for a total of 139 hours, corresponding roughly to six months of exterior exposure.

In order to determine the effects of weathering on strippability and visual contamination, the four most promising formulations were applied on the four basic substrates. After the weatherometer exposure the strippable coatings were peeled back and notations made of stripping ease and visual contamination remaining on the substrate. Table 7.5 contains detailed results.

In general the weatherometer exposure caused no changes in the adhesion of the strippable coatings. The fact that Glidden's formula adhered tightly to Z-93 was not due to the weathering but was caused by the film being only 3 mils (dry). This was proven by preparing a ladder of varying thicknesses of Glidden's strippable coating over Z93. It was found that the film must be in the 7 to 11 mils (dry) range to attain the proper degree of adhesion. Glidden's formula was disqualified, however, because of the film contamination it leaves on the quartz and aluminum surfaces. This same residue is probably left on the Z-93 substrate but is not visible because of the white background.

With respect to the performance over all four substrates, only Potter Paint's Peel-Astic and DeSoto's 843L001-910L731 appeared promising. Both did well over every substrate except Z-93. The B.F. Goodrich formulations were also disqualified because they appear to actually lift a layer of the vapor deposited aluminum and because they adhere too tightly to the quartz. The quality of the vapor deposited aluminum film, however, was later shown to be inferior. Tests of this material were then resumed. Neither the DeSoto and Potter Paint formulas were tried over Z-93 in the weatherometer because they failed in the initial peel tests. On checking the original test panels the Potter Paint film was found to be only 3 mils. The DeSoto coating was 12 mils. Working further with Potter Paint resulted in the discovery that it will peel off Z-93 satisfactorily if a minimum of 7 mils is applied. No visible residue is left.

Table 7-5
EVALUATION OF STRIPPABLE COATINGS/
FILMS AFTER 139 HOURS IN ATLAS WEATHEROMETER

<u>Coatings</u>	<u>Ease of Removal</u> <u>Over Z93</u>	<u>Visual Contamination</u>
Glidden Booth Coating	Adhered too tightly. Cannot be pulled off without tearing.	--
B.F. Goodrich Hycar 2679 - 60% Hycar 2600 - 40%	Adhered too tightly. Pulls, some Z93 came off with it.	none
B.F. Goodrich Hycar 2679 - 40% Hycar 2600 - 60%	Adhesion about right, but spots of Z93 came off with strip.	none
<u>Over S-13G</u>		
Potter Paint Peel-Astic	Too loose except at edges.	none
Glidden Booth Coating	No adhesion. Discarded.	
B.F. Goodrich Hycar 2679 - 60% Hycar 2600 - 40%	Adhesion about right.	none
B.F. Goodrich Hycar 2679 - 40% Hycar 2600 - 60%	Too loose.	none
DeSoto 843L001-910731	Adhesion almost right. Two small spots of of S-13G came off with strip.	none
<u>Over Polished Aluminum</u>		
Potter Paint Peel-Astic	Adhesion about right. Did not remove any aluminum with strip.	none
Glidden Booth Coating	Slight adhesion, except at edges. Does not take aluminum off with strip.	cloudy film
B.F. Goodrich Hycar 2679 - 40% Hycar 2600 - 60%	Pulled aluminum off with strip; otherwise adhesion about right.	--
DeSoto 543L001-910L731	Slight adhesion, except at edges, but does not take aluminum off.	none
<u>Over Suprasil Quartz</u>		
Potter Paint Peel-Astic	Adhesion excellent.	none
Glidden Booth Coating	Very loose; only sticks at edges.	cloudy film
B.F. Goodrich Hycar 2679 - 60% Hycar 2600 - 40%	Adhesion too tight.	none
B.F. Goodrich Hycar 2679 - 40% Hycar 2600 - 50%	Adhesion too tight.	none
DeSoto 843L001-910L731	Adhesion excellent.	none

Potter Paint's formula strips well from S-13G in the range of 4-7 mils dry thickness and from Z-93 in the range of 6-11 mils. These thickness tolerances are critical and specific for each "protected" material. No visual contamination was evident after stripping from the four test substrates.

Another good candidate was DeSoto's 843L001-910L731, which has stripped cleanly from S-13G, polished aluminum and suprasil quartz. It could not be used over Z93, however, because, like most other coatings, it adheres to it too strongly.

7.3.3.2 Ultraviolet Irradiation Tests

The efficacy of the protective coatings was tested in several different ways, all of which, however, involved coating the substrate (S-13G, Z-93, etc.) with the protective coating, removing the latter after a predetermined period of contact, and then exposing the substrate to ultraviolet irradiation. If the "protected" substrate degraded more than normal, the particular strippable coating would be disqualified. All samples were exposed in duplicate in the Weather-O-Meter test for a period of 335 hours, equivalent to approximately one year's atmospheric exposure.

Because of its excellent stripping characteristics Potter Paint's No. ZM-11-CC, "Peel-astic" was applied to a series of Z93 and S-13G coupons for ultraviolet radiation testing. The protective coating was removed from the Z93 and the S-13G surfaces just prior to installation in the IRIF. At that time the coatings had been in contact with their respective substrates a total of 37 days. Half of the coupons had been subjected to 7 days in the Atlas Weatherometer during this period of contact. Spectral reflectance values at three visible wavelengths before and after 501 ESH of ultraviolet radiation are listed in Table 7.6. It is obvious that the strippable coating left considerable contamination on the Z-93 surface; it definitely was not apparent upon visual examination. The S-13G series shows little difference

Table 7-6
EFFECTS OF POTTER ON
"PEELASTIC" STRIPPABLE COATING III. ULTRAVIOLET
STABILITY OF S-13G* AND Z-93*

Test Coatings**	400nm		500nm		600nm	
	Before	After	Before	After	Before	After
<u>Z-93</u>						
a	73.0	68.0	94.0	93.0	95.5	95.0
b	68.5	68.5	93.4	93.0	95.0	95.0
c	60.0	47.0	81.0	73.0	87.0	84.0
d	63.0	55.0	81.0	79.0	87.0	86.0
e	66.0	50.0	89.5	79.0	93.0	89.0
f	40.5	37.0	90.0	87.0	93.0	92.5
<u>S-13G</u>						
a	66.5	----	91.0	----	91.8	----
b	66.0	65.0	90.1	88.8	92.3	91.3
c	57.0	55.0	93.0	92.0	95.0	95.0
d	75.0	66.5	93.1	90.0	94.0	91.8
e	50.0	50.0	93.5	93.0	94.5	94.5
f	76.0	71.0	93.9	92.0	93.9	92.9

*Strippable coating was removed immediately prior to IRIF ultraviolet test.

**a,b controls, no strippable coatings applied
c,d coatings to which strippable coating was applied for 5 weeks before UV testing.
e,f same as c,d, except includes 1 week in Atlas Weather-O-meter.

between the controls and the test coupons. This tentatively indicates that Potter Paint's product ZM-11-CC is a satisfactory protective coating for three of the four substrates, Z93 being the exception. Peel-astic leaves a residue only on Z93, which, even though not apparent to the unaided eye, caused serious damage to its reflectance. S-13G was not affected.

The results of all tests indicate that Potter Paint's Peel-astic would be satisfactory over three of the four substrates used in these tests, viz., Suprasil Quartz, Polished Aluminum and S-13G. The most promising protective coating for Z93 is B.F. Goodrich's formula No. 8, which is water dispersible. Since the Goodrich No. 8 formula is transparent, a red iron oxide shading base was prepared to give it a slight reddish cast, and thus to assure complete coverage and removal. The base was prepared by pebble milling a synthetic red iron oxide, Pfizer's R-2199, in Hycar 2679, a constituent of the Goodrich formula. Potter's Peel-astic has an off-white pigmentation which we believe offers sufficient contrast to S-13G that addition of a shading base is not necessary.

After the Weather-0-Meter test, two IRIF tests of Z-93 and S-13G coatings previously protected with strippable coatings were conducted. Four samples of Z-93 and four of S-13G were exposed to ~1300 ESH of ultraviolet radiation in IRIF Test I-47 and I-48. The sample schedule, which was the same in both tests, was as follows: one unprotected sample was retained as a control (a protective coating was not applied, and the sample was stored in the lab); a second sample was coated with a protective coating and was also exposed only to the lab environment; a third sample was not given a protective coating but was exposed in the Weather-0-Meter (for 335 hrs); and the fourth sample was coated with a protective coating and exposed in the Weather-0-Meter (335 hrs). In all cases Potter Paint's Formula No. ZM-11-CC was used over S-13G, and Goodrich #8 over Z-93. Goodrich #8 is an IITRI designation for the mixture of Goodrich products: 60% Hycar 2679 and 40% Hycar 2600x138.

The damage in test IRIF-I-47 was so severe that contamination was strongly suspected. In Table 7.7 we present for both IRIF-I-47 and IRIF-I-48 the induced spectral reflectance changes at 0.3875μ (which for both S-13G and Z93 is the wavelength at which there appears a maximum UV-induced spectral damage). From this table one can easily observe several trends. First, and most important, coatings which were "protected" suffer much greater damage than those not protected. Second, the ultraviolet stability is not affected by a Weather-O-Meter exposure. Third, the time of contact between the strippable coating and the "protected" coating obviously affects the latter's ultraviolet stability. (Previous IRIF tests of surfaces with much less contact time did not exhibit unusual damage).

Table 7-7
ULTRAVIOLET-INDUCED CHANGES IN SPECTRAL
REFLECTANCE OF "PROTECTED" PAINT FILMS

		<u>S-13G</u>	
		Induced Spectral Reflectance Changes, ΔR_{λ}	
<u>Protective Coating</u>	<u>Weather Exposure</u>	<u>I-47 (1300 ESH)</u>	<u>I-48 (1350 ESH)</u>
None	None	23.5	25.5
Potter	None	65.0(0.4)*	65.0(0.39)
None	335 hrs	21.5	25.0
Potter	335 hrs	39.0	59.5
Contact Time**		40	84
		<u>Z-93</u>	
None	None	7.5	4.5
Goodrich-8	None	14.0	10.5
None	335 hrs	7.5	4.0
Goodrich-8	335 hrs	13.0	---
Contact Time		40	84

*The peak of the curve of ΔR_{λ} vs λ usually occurs at $\lambda = 0.3875\mu$; the number in parentheses is the wavelength (μ) at which the peak actually occurs (when different from 0.3875μ).

**Contact time, number of days protective films were in contact with "protected" surfaces before being stripped for irradiation test.

These tests have shown that the long term contact between the strippable coating and the surface it protects has a degrading effect. Earlier tests showed that contact times of lesser duration did not affect the ultraviolet stability of S-13G.

A mitigating effect of the Weather-O-Meter exposure was noted. The degradation of "unprotected" samples exposed to the Weather-O-Meter was usually less than a "protected" but otherwise identically treated sample.

7.3.4 Conclusions

None of the protective coatings tested can be used with either Z-93 or S-13G. It may be possible to adjust formulations to achieve better initial adhesion characteristics, but the environmental stability of the "protected" surface will inevitably be a critical problem. We discovered that coating contact times of less than ~30 days result in no degradation, while greater contact times pre-disposed the "protected" coating to unusually severe ultraviolet radiation damage.

7.4 SALT SPRAY EFFECTS ON S-13G

To gain some idea of what might happen to S-13G exposed over a long period of time to a salt-spray environment, we put a thick layer of simulated salt water (a saline solution containing representative amounts of the major constituents of ocean water) on the surface of several S-13G coatings and allowed them to evaporate to dryness. Four (4) S-13G coupons were prepared (from IITRI batch C-076); two were untreated and the other two treated as indicated above. The solar absorptance values before and after exposure to 1800 ESH in IRIF Test I-41 are shown in Table 7.8.

Table 7-8
RESULTS OF SIMULATED SALT SPRAY EXPOSURE
EFFECTS ON S-13G UV DEGRADATION

No.	Sample Description	Solar Absorptance		
		Initial	Final*	$\Delta\alpha_s$
1	S-13G Control	0.204	0.248	0.044
2	S-13G with Salt Spray	0.202	0.256	0.054
3	S-13G Control	0.204	0.238	0.034
4	S-13G with Salt Spray	0.205	0.243	0.039

*After exposure to 1800 ESH of AH-6 radiation.

In general, the salt spray samples degrade only slightly more than standard S-13G. Surprisingly, the S-13G with visiaully noticeable amounts of salt water deposits did not degrade as much as might be expected. The spectral data (see Figure 7.3) indicate that the spectral degradation is characteristic of S-13G. It thus appears that a salt spray environment only slightly increases the susceptibility to solar radiation damage - at least, for S-13G. The same results were obtained when essentially the same test was repeated in IRIF-I-44, in which the exposure was 342 ESH. The $\Delta\alpha_s$ values for the control and salt-spray S-13G samples were 0.024 and 0.015, respectively. The control sample degradation is higher than expected, making these particular data somewhat questionable. Nevertheless the effect of a build-up of simulated ocean spray is minimal, if not within the nominal range of degradation.

Very nearly the same conclusion was reached in an irradiation test (ref. 7.1) of S-13G samples which had been exposed to a salt spray enviornment at NASA-Kennedy SFC.

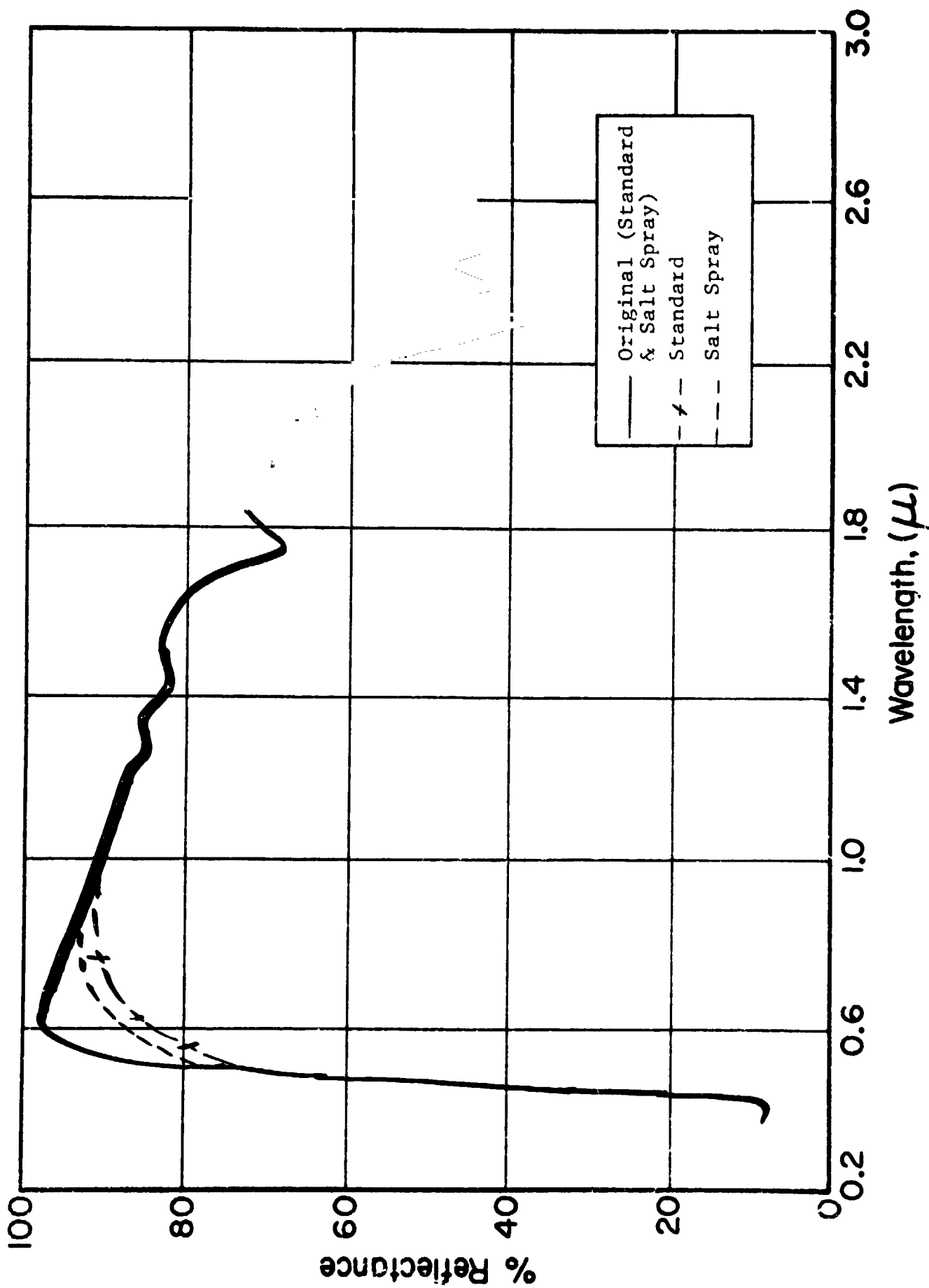


Figure 7.3 UV DEGRADATION OF STANDARD AND SALT SPRAY TREATED S-13G

7.5 REFERENCES

1. J.E. Gilligan, "Testing to Determine the Vacuum-Ultraviolet Degradation Rate of Thermal Control Coatings", NASA Contract No. NAS8-28765, IITRI Report No. C6258-5 (Final Report), Nov. 27, 1972; see also J.E. Gilligan and H.M. King, "The Vacuum-Ultraviolet Degradation of Salt-Spray-Contaminated Thermal Control Coatings" pp. 637-644, in Proceedings of Seventh Conference on Space Simulation, NASA SP-336, 1973.

8.0 PROGRAM SUMMARY - CONCLUSIONS AND RECOMMENDATIONS

In the brief presentation which follows, we highlight the principal accomplishments of the program, establish a perspective for its evaluation, and offer recommendations for continued research and development in the field of materials for thermal control of large space vehicles.

The potential that zinc orthotitanate possesses as a pigment for spacecraft thermal control applications has been thoroughly demonstrated. The practical realization of this potential hinges most importantly on pigment stoichiometry and also on the production process and optimized preparative conditions associated with it. Pigment compatibility with a stable binder also may be a serious impediment to full realization of the pigment's intrinsic stability.

Many of the conclusions reached during the course of the program will undoubtedly require modification because of the discovery of the substantial dependence of optical properties and environmental stability on pigment stoichiometry. This very dependence, however, establishes a proper perspective for understanding the nature of the problem: 1) The composition of " Zn_2TiO_4 ," as a function of Zn/Ti ratio, 2) the determination of the chemical identity of " TiOX ", and 3) the complete elucidation of spectral reflectance values and their stability vs. Zn/Ti ratio (where the true molecular weights of precursors are known) become the primary goals of a continued research and development effort. The important process conditions and parameters have been identified and their effects on pigment properties and performance reasonably well determined. Thus, the basic objectives of the program have been met. Once the three unknowns just noted have been eliminated, the reduction of this technology to practice as described in this document will be mainly an engineering effort.

Comparison of the properties and performance of the pigments prepared by solid state, coprecipitation, and mixed oxalate methods indicates that, while initial properties may vary somewhat from one process to another, none produces a pigment more intrinsically stable than another. Each method retains flexibility in adjustment of the Zn/Ti ratio, and has its associated advantages and disadvantages. The MOX process has the distinctly advantageous property of controlled pigment particle size. The solid state method, on the other hand, is the least complicated.

Environmental testing has, of course, occupied a central role in the program. The methods and techniques that we have used in many instances are highly specialized and sophisticated. The most important elements of environmental testing are test design and interpretation of results. In this regard we must emphasize, without repeating the basics involved, that the interpretation of test results must be accomplished by analyses of spectral reflectance curves. The analyses of spectra of irradiated samples after an oxygen bleach have proved to be invaluable. Environmental testing has, therefore, produced highly significant information regarding the effects of pigment preparative conditions and parameters, calcination variables, chemical treatments, structural modifications and many other factors involved in the development of production processes.

Our attempts to modify Owens-Illinois 650 "Glass Resin" were successful from the standpoint of eliminating "Coasting". The modification process, however, apparently increases the outgassing potential of the modified (CI-650G) resin, seriously reducing its practical potential as a space stable binder. It should be used only in applications tolerant of contamination. The likelihood of developing an alternative process is extremely small. Degassing the modified resin in the B-stage in vacuo holds some promise but could be very expensive. Further

complicating an objective appraisal of its merits are the facts that the modified resin must be thermally cured, that, like the unmodified resin, it too has a tendency to predispose the pigment to extensive S-band degradation, and that the ratio of trimethylchlorosilane/OI-650 must be carefully controlled within a very narrow range. Research on stable binders (References 8.1-3), should be evaluated for acceptable alternatives.

Those activities which have been of a supportive nature have been instructive and rewarding. EPR investigations, while they did not correlate EPR activity with optical degradation, did show that contaminants introduced in the pigment production process could be detected at very low concentrations. The lack of optical vs. EPR correlations - at least for Zn_2TiO_4 - has value, even though negative with respect to our hopes, in defining the most valuable approaches to pigment development.

The protection of spacecraft thermal control surfaces from contamination during pre-launch storage must be a primary objective of spacecraft mission designers. Protective coatings, however, do not appear to represent a viable approach. There may be commercial materials available which do not affect the UV stability of "protected" coatings but the search for them would very probably cost far more than would the alternatives.

IITRI, for many years, has recommended the use of unplasticized plastics for protection of spacecraft components. We very strongly adhere to the axiom that a thermal control surface is an optical surface and that it should be regarded and protected as such. Certain strippable coatings for both Z-93 and S-13G were found to be useful provided that the time of application was less than 30 days. UV irradiation tests clearly showed that thermal control surfaces degraded more than would be expected when the strippable coatings were not removed for 30 days or more.

9.0 GLOSSARY

<u>Term</u>	<u>Definition</u>
Equivalent Sun-Hour (ESH)	An equivalent sun-hour is the total amount of incident ultraviolet ($\lambda < 400\text{nm}$) radiation per unit area in the extraterrestrial solar intensity spectrum at a nominal distance of 1 A.U. over a period of one hour. (The term, though arbitrary and somewhat misleading, in that it refers only to the UV portion of the sun's radiant energy spectrum, is widely accepted and used).
Equivalent Wind-Hour (EWH)	An equivalent wind-hour is the total amount of the incident solar wind flux (expressed in protons/cm ² -sec.) at a nominal distance of 1 A.U. over a period of one hour. At 1 A.U. the solar wind flux is approximately 2.5×10^8 protons/cm ² -sec. An E.W.H., therefore, represents a fluence of 9.0×10^{11} protons/cm ² . (In the text these values would be abbreviated to 2.5(8) and 9.0(11), respectively).
Wind	A "wind" is the solar wind flux at a nominal distance from the sun of 1 A.U., and has the approximate value of 2.5×10^8 protons/cm ² -sec.
Sun	A "sun" is the intensity of the ultraviolet ($\lambda < 400\text{nm}$) portion of the extraterrestrial solar intensity spectrum at a distance from the sun of 1 A.U. The solar constant has a nominal value of 0.139 watt/cm ² ; a "sun" therefore, constituting approximately 9% of the solar constant, has a nominal value of 12.5 milliwatts/cm ² .
$\Delta\alpha_s$	The term "delta α " refers to the total change in solar absorptance experienced by a material after exposure to a specified environment.
Solar Absorptance α_s	Solar absorptance is the ratio of the energy absorbed from the extraterrestrial solar intensity spectrum per unit area by a plane normal surface to the total solar energy incident on it.
p^+	The term p^+ designates a proton, an ionized hydrogen ion.
Adsorbate	The term adsorbate refers to a gas or vapor adsorbed on a solid surface, it does not connote chemi-sorption or physi-sorption, specifically.

Oxygen (O ₂) Bleach	This refers to a process in which oxygen interacts with an irradiated surface to restore either fully or in part the pre-irradiation reflectance of that surface.
S-13G	S-13G (and S-13G/LO) are flight qualified, specification thermal control paint systems by IITRI. Both utilize a potassium silicate encapsulated zinc oxide (New Jersey Zinc Co's SP-500) as the pigment, and General Electric Co's RTV602 methyl silicone potting compound as the binder. For S-13G/LO, however, the RTV-602 is vacuum stripped to remove volatile compounds.
Z-93	Z-93 is a flight-qualified specification thermal control paint system consisting of zinc oxide (New Jersey Zinc Co's SP-500) as the pigment and potassium silicate (Sylvania Electric Co's PS-7) as the binder.
Spectrum	A spectrum, in the sense used in this report, refers to the wavelength regions commonly known as nearultraviolet, visible, and nearinfrared. The ultraviolet spectrum extends from about 300nm to 400nm; the visible, from 400nm to 700nm; the near infrared, from 700nm to 2600nm.
Emittance (ε)	The emittance is the ratio of the thermal energy emitted per unit area and time by a real surface at a temperature T to that of a black-body at the same temperature. Spectral emittance is defined similarly except that it refers to a specific wavelength or wavelength interval.
Astronomical Unit (A.U.)	The nominal distance from the sun to the earth's orbit about the sun is termed one astronomical unit.
Reflectance	Reflectance is defined as the ratio of energy reflected by a surface to that incident on it.
Spectral	The term "spectral" is a qualifying one which refers to a particular wavelength or wavelength interval.
Diffuse	This term refers to the properties of a surface (or radiation source) as determined on a hemispherical (2π) basis.

APPENDIX I
REDUCTION OF SPECTRAL REFLECTANCE DATA TO SOLAR ABSORPTANCE
WORK SHEET

REPRODUCE
ORIGINAL PAGE 1

Sample # I-50-4

By _____

Date 2/23/72

Center Wavelength (μ)

Initial 1200 ESH

.295	<u>11.2</u>	<u>9.5</u>		
.330	<u>8.3</u>	<u>7.0</u>		
.354	<u>7.6</u>	<u>6.5</u>		
.377	<u>20.0</u>	<u>18.0</u>		
.398	<u>76.0</u>	<u>55.0</u>		
.415	<u>85.5</u>	<u>63.0</u>		
.430	<u>90.0</u>	<u>67.5</u>		
.444	<u>91.7</u>	<u>71.0</u>		
.457	<u>92.2</u>	<u>73.3</u>		
.470	<u>93.1</u>	<u>75.0</u>		
.483	<u>93.0</u>	<u>76.5</u>		
.497	<u>93.0</u>	<u>78.5</u>		
.511	<u>92.7</u>	<u>79.5</u>		
.525	<u>92.9</u>	<u>80.4</u>		
.540	<u>92.9</u>	<u>82.0</u>		
.554	<u>92.0</u>	<u>83.0</u>		
.569	<u>92.0</u>	<u>83.5</u>		
.584	<u>92.1</u>	<u>84.0</u>		
.599	<u>91.5</u>	<u>85.3</u>		
.614	<u>91.5</u>	<u>86.5</u>		
.630	<u>91.3</u>	<u>87.3</u>		
.647	<u>91.0</u>	<u>86.0</u>		
.665	<u>90.5</u>	<u>87.6</u>		
.682	<u>90.3</u>	<u>87.0</u>		

Totals 1863.3 1612.8

Calculations:

$$\begin{aligned} \% \alpha_s (\text{Initial}) &= 100.00 - \frac{1863.3 + 1993.2}{50} \\ &= 100 - 77.13 = 22.87 \\ \alpha_s (\text{Initial}) &= 0.2287 \end{aligned}$$

Center Wavelength (μ)

Initial 1200 ESH

.700	<u>92.0</u>	<u>86.0</u>		
.721	<u>92.1</u>	<u>85.9</u>		
.743	<u>91.6</u>	<u>85.8</u>		
.764	<u>91.5</u>	<u>86.0</u>		
.788	<u>91.3</u>	<u>86.5</u>		
.812	<u>90.9</u>	<u>86.5</u>		
.840	<u>90.5</u>	<u>86.4</u>		
.868	<u>89.9</u>	<u>86.3</u>		
.898	<u>89.3</u>	<u>85.3</u>		
.929	<u>89.5</u>	<u>85.5</u>		
.966	<u>88.9</u>	<u>85.3</u>		
1.003	<u>88.0</u>	<u>84.5</u>		
1.043	<u>87.6</u>	<u>84.3</u>		
1.085	<u>86.8</u>	<u>83.7</u>		
1.130	<u>85.5</u>	<u>83.0</u>		
1.180	<u>81.3</u>	<u>78.0</u>		
1.240	<u>84.5</u>	<u>81.0</u>		
1.300	<u>83.8</u>	<u>81.0</u>		
1.380	<u>79.0</u>	<u>76.0</u>		
1.470	<u>80.2</u>	<u>76.9</u>		
1.580	<u>79.2</u>	<u>75.1</u>		
1.710	<u>67.8</u>	<u>63.3</u>		
1.900	<u>72.8</u>	<u>68.0</u>		
2.160	<u>62.5</u>	<u>86.5</u>		
2.620	<u>37.1</u>	<u>30.0</u>		

Totals _____

Calculations:

$$\begin{aligned} \% \alpha_s (1200 \text{ ESH}) &= 100.00 - \frac{1612.8 + 1967.3}{50} \\ &= 100.00 - 71.60 = 28.40 \\ \alpha_s (1200 \text{ ESH}) &= 0.2840 \end{aligned}$$

A MODEL FOR ENVIRONMENT-INDUCED DEGRADATION OF SOLAR ABSORPTANCE

We noted previously that zinc orthotitanate as a competitive paint system must possess an initial α_s/ϵ ratio of 0.1 or less, and that this ratio must not degrade by more than ~ 0.02 in 10^5 ESH. This objective is based strictly on UV exposure, but from the results obtained in this program we can expect $\Delta\alpha_s$ not to exceed ~ 0.03 in a combined environment of 10^5 ESH and the equivalent fluence of charged particles. Experience permits certain qualitative projections based on the typical behavior of α_s vs ESH (or time); very generally

$$\Delta\alpha_s = (\Delta\alpha_s)_\infty [1 - \exp(-k \cdot \text{ESH})], \quad (1)$$

where

$(\Delta\alpha_s)_\infty$ is the ultimate environment-induced $\Delta\alpha_s$;

k is a constant; and

ESH is total UV exposure.

This formula reflects the almost universal behavior of many TC materials: the rate of optical damage decreases with increasing exposure. This behavior is well grounded and understood in theory. Very simply it results from the condition that in a unit volume of material (pigment, binder or both) there is an "initial" concentration of defects which can be converted to "color centers," i.e., active optical defects, by interaction with incident radiation. If the original concentration of defects of the i^{th} type, e.g., is C_o^i , then the concentration at any time thereafter will depend upon radiation intensity, I , the instantaneous concentration of i^{th} type defects, C^i , and the quantum efficiency, ν . Thus, the instantaneous rate of disappearance of C^i potential defects is

$$\frac{dC^i}{dt} = -I\nu C^i \quad (2)$$

Rearranging under integral signs gives

$$\int_{C_o^i}^{C^i} \frac{dC^i}{C^i} = -I\nu \int_0^t dt, \quad (3)$$

IIT RESEARCH INSTITUTE

which, upon integration, becomes

$$\ln \frac{C^i}{C_o^i} = -Ivt \quad (4)$$

In exponential form this is

$$C^i = C_o^i \exp(-Ivt) \quad (5)$$

Our original assumption was that C^i is the concentration of "potential" defects. The concentration of converted (or actual) defects is some integral or half-integral multiple of the difference between initial and instantaneous concentrations. The induced reflectance optical density D is then $k \cdot (C_o^i - C^i)$. Making this substitution in the last equation above then gives

$$OD = k \cdot (C_o^i - C^i) = k \cdot C_o^i [1 - \exp(-Ivt)] \quad (6)$$

This analysis can be greatly expanded and sophisticated, but eq. 6 quite capably indicates the nature of the time rate of degradation of photon-irradiated materials. Comparing it to the relationship suggested pragmatically (i.e., eq. 1), we note that the two are remarkably alike. Assuming that $\Delta\alpha_s$ relates mathematically to $k(C_o^i - C^i)$ and $(\Delta\alpha_s)_\infty$ to kC_o^i , we can see that they are nearly identical. Eq. 1 is a form of the reciprocity equation so frequently used in early spacecraft R&D efforts to extrapolate laboratory irradiation data.

There must be a means of translating engineering requirements, expressed in terms of maximum $\Delta\alpha_s$ after exposure to a specified environment, to materials science requirements, expressed in the language of solid state physics. In such a translation not only is the magnitude of an induced spectral reflectance change important but also its spectral location, shape and width compared to the solar intensity spectrum. Specific requirements on α_s and especially on $\Delta\alpha_s$ essentially become constraints on the growth of individual environment-induced absorption bands. A more detailed development of a model to predict $\Delta\alpha_s$ vs space exposure parameters is given by Gilligan and Brzuskiwicz in IITRI Report No. C6166-12 (cf NASA No. CR 66917), Nov. 1969.

APPENDIX III

OUTGASSING CONTAMINATION PARAMETERS

The outgassing potential of TC surfaces must be maintained at a practical minimum, even if this requires processing their components. The most common method for determining gross outgassing characteristics is the so-called "SRI Method" (ref. 5.1). In this method the total weight loss (TWL) of a sample is determined as a percentage of the sample's initial weight after exposure in vacuum at 125°C for 24 hr. In the same test the weight gain of a collector maintained at 25°C is also determined and compared to the original test sample weight. The ratio in percentage units is the "CVCM" - collected volatile condensable material. The criteria for acceptable performance in this method are:

$$\begin{aligned} \text{TWL} &\leq 1.0\% \\ \text{CVCM} &\leq 0.1\% \end{aligned}$$

Even though the temperature parameters of the method and the minimum acceptable performance criteria are somewhat arbitrary, they tend to relate to the long term weight loss of a coating. The choice of $T = 25^{\circ}\text{C}$ as the collector temperature in many spacecraft applications is high, and thus conservative. The CVCM, however, involves much more complex considerations: water content of volatiles, sticking coefficients (and their temperature dependence), volatilization conditions, and many others.

The importance of understanding outgassing data cannot be overstressed. As an example, extensive tests of S-13G and S-13G/L0 standard formulations indicate that the TWL consists of approximately 50% H_2O (not CVCM). The water content of the TWL represents a very important consideration to a designer concerned about the contamination effects resulting from condensation of volatile components.

The outgassing rate of a material depends upon several factors: vaporization energy, the external pressure (actually the molecular mean free path), the instantaneous concentration and the spatial distribution of each volatile species within the material, the material's bulk temperature and the temperature distribution within the material. With respect to the basic material there are three types of species which constitute the TWL: absorbed species, adsorbed species and chemical fragments. Absorbed species consist primarily of solvents, solvency promoters and other "thinner" or "solvent" components which may become absorbed or entrapped in the dry paint film in the curing process. Additives, used by original manufacturers for processing aids or property adjustments are also included. Finally there are the basic species comprising the binder (after cure), and, of course, the various impurities in all of these ingredients. The TWL of most organic and silicone based paint systems consists of all three species; but the CVCM consists almost entirely of the latter two.

The requirements which the weight loss criteria impose upon zinc orthotitanate paint systems have not been addressed in detail in this program. However, much of what we know about silicones, especially methyl silicones (RTV602 and OI-650), can be extended to provide considerable insight into the prevention or mitigation of silicone outgassing. It is essential to identify the various volatile species, their relative concentrations in the cured dry-film paint coatings, and the vaporization parameters, primarily ΔH_A . From such data we can determine optimum processing parameters for devolatilization of components, provide data for direct use in computerized contamination prediction programs, and assess the feasibility of thermal devolatilization procedures following the application of the paint coatings. A vacuum bake-out of S-13G at 250°C/24 hrs, for instance, significantly reduces its TWL and CVCM; the same treatment for S-13G/I.O is far less effective because of its already low outgassing potential.

APPENDIX IV

SPACE CHARGE ACCUMULATION (SCA) AND COATING ELECTRICAL CONDUCTIVITY

The obvious solution to the Space Charge Accumulation (SCA) problem in surface coatings is either to increase the electrical conductivity of surface coatings or to improvise electrical paths from the surface coatings to the spacecraft electrical ground, or both. Other than this statement, there exist few general guidelines for the electrical conductivity of low α_s/ϵ coatings. Such coatings possess conductivity values characteristic of dielectric materials. Electrical conductivity will typically be in the range 10^{-13} - 10^{-15} mho/cm².

In some instances it is possible to greatly increase these values by the addition of metal flakes/powders (e.g. non-leafing Al). The success of this approach, however, depends very strongly on the binder.

Most binders, including methyl silicones, will wet, and thus electrically isolate, the flakes sufficiently to preclude any substantial increase in electrical conductivity.

Methyl silicone based zinc orthotitanate paints will, without any metal additive, possess electrical resistivities equivalent to an electrical insulator - i.e., of the order of 10^{14} ohms per square.